TESE DE DOUTORAMENTO

CHIRAL NANOMATERIALS WITH TUNEABLE CHIROPTICAL PROPERTIES

Manuel Núñez Martínez

ESCOLA DE DOUTORAMENTO INTERNACIONAL DA UNIVERSIDADE DE SANTIAGO DE COMPOSTELA
PROGRAMA DE DOUTORAMENTO EN CIENCIA E TECNOLOXÍA QUÍMICA

SANTIAGO DE COMPOSTELA
2021

USC
UNIVERSIDADE
DE SANTIAGO
DE COMPOSTELA

DECLARACIÓN DO AUTOR/A DA TESE

D./Dna. **Manuel Núñez Martínez**

Título da tese: **Chiral Nanomaterials with Tuneable Chiroptical Properties**

Presento a miña tese, seguindo o procedemento axeitado ao Regulamento, e declaro que:

1) A tese abarca os resultados da elaboración do meu traballo.
2) De ser o caso, na tese faise referencia ás colaboracións que tivo este traballo.
3) Confirmo que a tese non incorre en ningún tipo de plaxio doutros autores nin de traballos presentados por min para a obtención doutros títulos.
4) A tese é a versión definitiva presentada para a súa defensa e coincide a versión impresa coa presentada en formato electrónico

E comprométome a presentar o Compromiso Documental de Supervisión no caso de que o orixinal non estea na Escola.

En **Santiago de Compostela**, **7 de xullo de 2021**.

Sinatura electrónica

AUTORIZACIÓN DO DIRECTOR / TITOR DA TESE

Chiral Nanomaterials with Tuneable Chiroptical Properties

D. Emilio Quiñoá Cabana
D. Félix Freire Iribarne

INFORMAN:

Que a presente tese, correspóndese co traballo realizado por D. Manuel Núñez Martínez, baixo a miña dirección/titorización, e autorizo a súa presentación, considerando que reúne os requisitos esixidos no Regulamento de Estudos de Doutoramento da USC, e que como director desta non incorre nas causas de abstención establecidas na Lei 40/2015.

De acordo co indicado no Regulamento de Estudos de Doutoramento, declara tamén que a presente tese de doutoramento é idónea para ser defendida en base á modalidade de Monográfica con reproducción de publicaciones, nos que a participación do doutorando foi decisiva para a súa elaboración e as publicacións se axustan ao Plan de Investigación.

En Santiago de Compostela, 7 de Xullo de 2021

Contents

Abbreviations and Acronyms

AFM	Atomic Force Microscopy
Aib	α-aminoisobutyric acid
AgNPs	Silver Nanoparticles
ASL	Auxiliary Stabilizing Ligand
AuNPs	Gold Nanoparticles
[α]	Specific Optical Rotation
ap	Antiperiplanar
CD	Circular Dichroism
CuACC	Copper-Catalyzed azide-alkyne coupling
c-c	*Cis-cisoidal*
cod	*Cis-cis*-1,5-cyclooctadiene
CPL	Circular Polarized Luminiscence
CSP	Chiral Stationary Phase
c-t	*Cis-transoidal*
d	Doblet
δ	Chemical shift
D	Diameter
DCM	Dichloromethane
DIPEA	Diisopropyethylamine
DLS	Dynamic Light Scattering
DMF	N,N-Dimethylformamide
DMSO	Dimethyl sulfoxide
DSC	Differential Scanning Calorimetry
EDX	Energy Dispersive X-Ray spectroscopy
equiv	Equivalents
e.g	Latin expression "*exempli gratia*", for example
et Al.	Latin expression "*et Alii*", and others
FSL	Functionalized Stabilizing Ligand
FWt	Formula molecular weight
g	Grams
GPC	Gel Perfomance Chromatography
h	Hour

USC UNIVERSIDADE DE SANTIAGO DE COMPOSTELA

HATU	(2-(7-Aza-1H-benzotriazole-1-yl)-1,1,3,3-tetramethyluronium hexafluorophosphate)
HMPC	Helical Polymer-Metal complex
HOPG	Highly Oriented Pyrolitic Graphite
HOAt	1-hydroxy-7-azabenzotriazole
HPLC	High-Performance Liquid Chromatography
Hz	Hertz
IR	Infrared
KPS	Potassium persulfate
LB	Langmuir-Blodgett
LBL	Layer-by-Layer
LS	Langmuir-Schaefer
LSPR	Localized Surface Plasmon Resonance
M helix	Counterclockwise helix
m	Multiplet
m.r.u.	Monomeric repetition unit
mg	Milligrams
min	Minute
mL	Milliliters
mM	Millimolar
Mmol	Millimol
MPA	α-methoxy-α-phenylacetic acid
MTPA	α-methoxy-α-trifluoromethyl-α-phenylacetic acid
MS	Mass spectroscopy
N_A	Avogadro's Number
N_{Au}	Number of gold atoms per Gold Nanoparticles core
$N_{complex}$	Average number of complexes
nm	Nanometer
M_w	Molecular weight
MNP	Metal Nanoparticle
nbd	2,5-norbornadiene
NMR	Nuclear Magnetic Resonance
^oC	Celsius degree
P helix	Clockwise helix

PA	Poly(acetylene)
PDI	Polydispersion index
PGME	Phenylglycine methyl ester
Prof.	Professor
PPA	Poly(phenylacetylene)
s	Singlet
syn	synperiplanar
sa	Broad signal
SEM	Scanning Electron Microscopy
STM	Scanning Tunneling Microscopy
sp	Synperiplanar
SCAT	Selective Photocyclic Aromatization
SDS	Sodium Dodecyl Sulphate
TEM	Transmission Electron Microscopy
TGA	Thermogravimetric Analysis
THF	Tetrahydrofuran
TMS	Trimethylsilane
TrMA	Triphenylmetracrilate
UV-Vis	Ultraviolet-Visible Spectroscopy
XPS	X-ray Photoelectron spectroscopy

USC UNIVERSIDADE DE SANTIAGO DE COMPOSTELA

List of publications

During the development of this Thesis, the following articles have been published in scientific journals. Furthermore, the results of these articles have been included within this manuscript.

1) Julián Bergueiro[‡], **Manuel Núñez-Martínez**[‡], Sandra Arias, Emilio Quiñoá, Ricardo Riguera and Félix Freire. *Nanoscale Horiz.*, **2020**, *5*, 495-500.

‡ These authors contributed equally to this work.

Impact factor: 10.989

Category: Materials science (Q1).

M. N.-M. has contributed in the experimental part (synthesis and characterization) discussion of results and the manuscript preparation.

2) **Manuel Núñez-Martínez**, Sandra Arias, Emilio Quiñoá, Ricardo Riguera and Félix Freire, *Chem. Mat*er., **2021**, *33*, 4805-4812.

Impact factor: 9.811

Category: Materials science (Q1).

M. N.-M has contributed in the experimental part (synthesis and characterization) discussion of results and the manuscript preparation.

The authorization of the journals can be found in the following links:

https://www.rsc.org/journals-books-databases/journal-authors-reviewers/licences-copyright-permissions/

https://pubs.acs.org/pb-assets/acspubs/Migrated/dissertation.pdf

Chapter I

Introduction

USC
UNIVERSIDADE
DE SANTIAGO
DE COMPOSTELA

Chapter I: Introduction

In the XX century, the studies of biological macromolecules such as proteins, sugars or DNA took a great relevance due to the relationship between the biological function and the secondary structure (Figure 1). In some of these biomolecules, helices are a motive that repeats along the macromolecule. For this reason, the scientific community has shown special interest in the preparation of molecules with helical structure to obtain novel structures with biological applications.

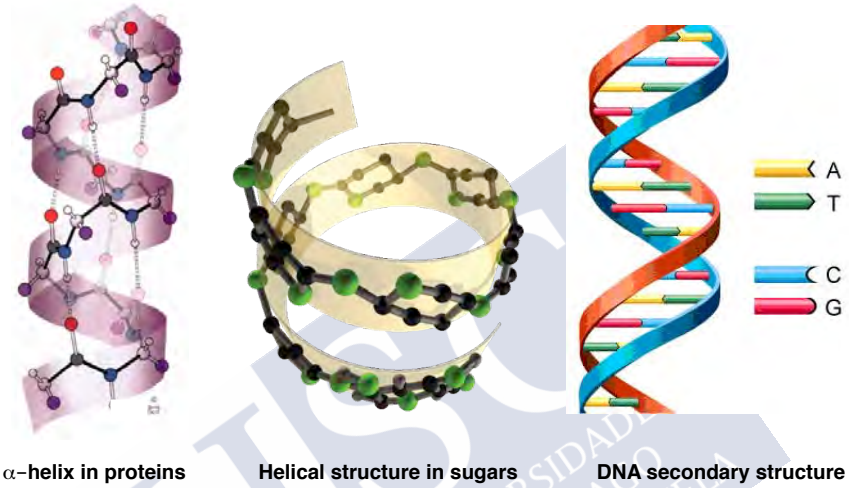

Figure 1. Natural biomacromolecules with helical structure.

In the early 50's, Pauling (1950) proposed the α-helix for proteins[1] and Watson and Crick (1953) discovered one of the most relevant research progresses, the double strand structure of the DNA (Nobel Prize, 1962).[2]

At 1955, Natta reported the first example of a synthetic helical polymer, the isotactic propylene. This polymer shows helical structure in solid state although it adopts a racemic mixture between (*R*) and (*S*) configurations.[3]

Inspired by this work, Pino *et Al.* described the preparation of vinylic polymers with an excess of one helical sense.[4] For this purpose, chiral inductors were used to obtain this excess in the helicity of the polymers. At 1968, Okamoto and co-workers obtained the first helical polymer through the polymerization of an achiral monomer with a chiral catalyst.[5]

[1] Pauling, L.; Corey, R. B.; Branson, H. R. *Proc. Natl. Acad. Sci. U.S.A*. **1951**, *37*, 205.
[2] Watson, J. D.; Crick, F. H. C. *Nature*. **1953**, *171*, 737.
[3] Natta, G.; Pino, P.; Corradini, P.; Danusso, F.; Mantica, E.; Mazzanti, G.; Moraglio, G. *J. Am. Chem. Soc.* **1955**, *77*, 1708.
[4] Pino, P.; Lorenzi, G. P. *J. Am. Chem. Soc.* **1960**, *82*, 4745.
[5] Okamoto, Y.; Suzuki, K.; Ohta, K.; Hatada, K.; Yuki, H. *J. Am. Chem. Soc.* **1979**, *101*, 4763.

In the 80's, Green reported a new class of helical polymers, the poly(isocyanate)s. In this work, Green demonstrated that these polymers are a mixture of left-handed (*M* helices) and right-handed (*P* helices) connected by reversals.[6] This work is the first example of dynamic helical polymers.

1.1 Classification of helical polymers

Helical polymers can be classified mainly into two groups: static and dynamic helical polymers.[7]

I) Static helical polymers

This type of polymers show one preferred helical sense and they are prepared from monomers that contain bulky groups and favour the adoption of one preferred helical sense by steric hindrance. This family of helical polymers presents a high interconversion energetic barrier between the right and left-handed helices and therefore the presence of external stimuli does not affect in the helical sense. Different families of polymers have been prepared as static helical polymers such as poly(methacrylate)s (poly-**1**), poly(methylacrylamide)s (poly-**2**) poly(isocianurate)s (poly-**3**), poly(quinoxaline-2,3-diyl)s (poly-**4**) or poly(guanidine)s (poly-**5**).[8]

II) Dynamic helical polymers

Dynamic helical polymers are defined as those macromolecules that present low interconversion helical barrier energy between the two helical senses (right-handed and left-handed). Thus, the helical sense can be easily modulated by the presence of external stimuli such as: temperature, polarity of solvents or the addition of metal ions (Figure 2). Examples of this type of polymers are poly(isocyanate)s (poly-**6**), poly(silane)s (poly-**7**), poly(acetylene)s (poly-**8**).[9]

III) Foldamers

Foldamers are defined as any polymer with a strong tendency to adopt a specific pack conformation. The helical structure is in equilibrium with unfolded structure and converts them in interesting targets in supramolecular chemistry.[10]

[6] Green, M. M.; Andreola, C.; Munoz, B.; Reidy, M. P.; Zero, K. *J. Am. Chem. Soc.* **1988**, *110*, 4063.

[7] a) Yashima, E.; Maeda, K.; Iida, H.; Furusho, Y.; Nagai, K.; *Chem. Rev.* **2009**, *109*, 6102. b) Cornelissen, J. J. L.; Rowan, A. E.; R. J. M. Nolte, R. J. M.; Sommerdijk, N. A. J. M.; *Chem. Rev.* **2001**, *101*, 4039.

[8] Okamoto, Y.; T. Nakano, T.; *Chem. Rev.* **1994**, *94*, 349

[9] Louzao, I.; Seco, J. M.; Quiñoá, E.; Riguera, R.; *Angew. Chem., Int. Ed.* **2010**, *49*, 1430.

[10] a) Hill, D. J.; Mio, M. J.; Prince, R.B.; Hughes, T.S.; Moore, J.S.; *Chem.Rev*. **2001**, *101*, 3893. b) Appella, D. H.; Christianson, L. A.; Karle, I. L.; Powell, D. R.; Gellman, S. H.; *J. Am. Chem. Soc.* **1996**, *118*, 13071.

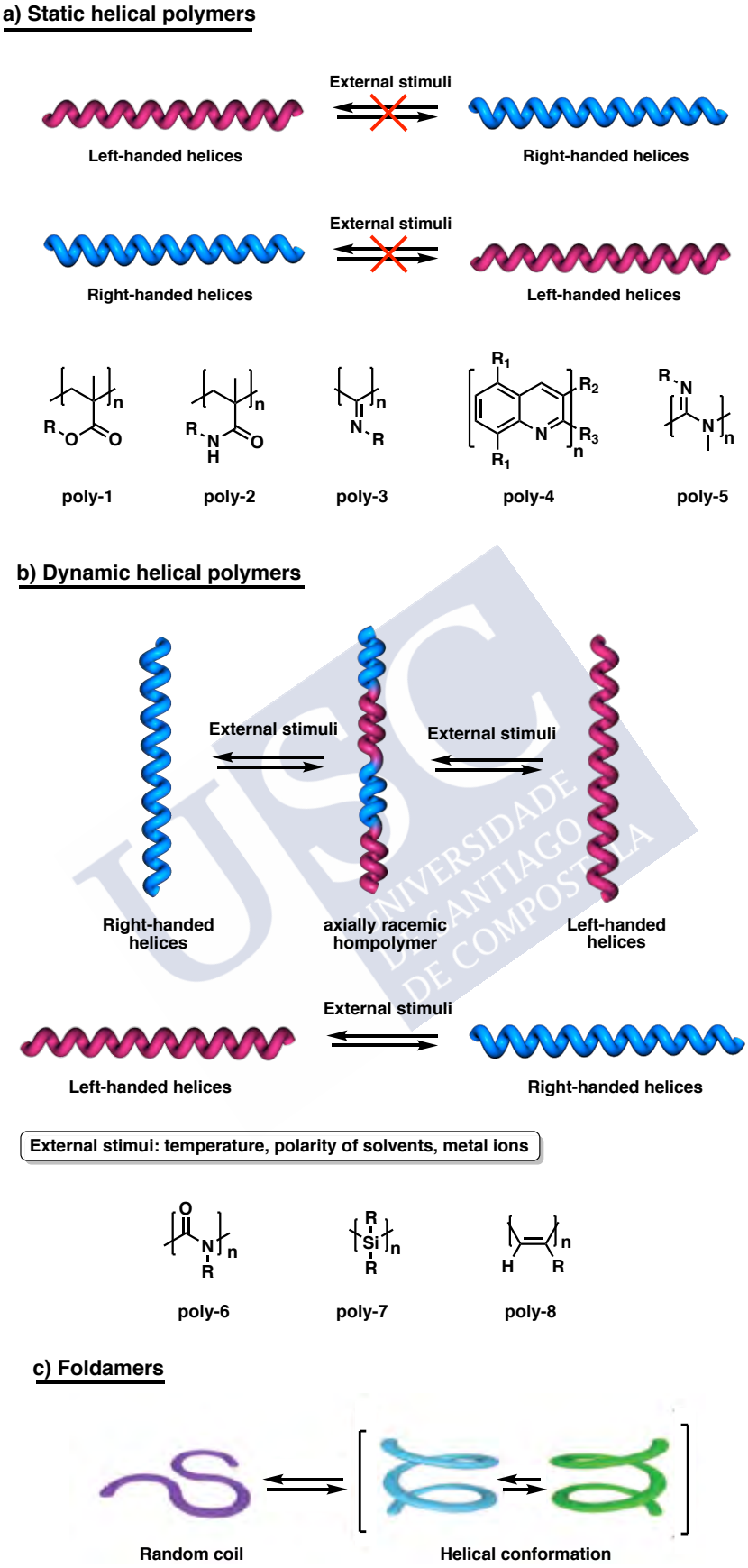

Figure 2. Conceptual representation of the different types of helical polymers.

2. Poly(acetylene)s

Poly(acetylene)s (PAs) are a family of polymers derived from acetylene monomer that presents π-conjugated double bonds. In the last decades, different examples of PAs have been prepared and studied (Figure 3). Thus, Ciardelli *et Al.* prepared a large number of π-conjugated, dynamic poly(acetylene)s (PA)s [11,12] with optical activities by polymerization of optically active phenylacetylenes.

At 1995, professor Yashima developed a new method to obtain dynamic helical polymers. This method consists on non-covalent interactions between the polymers and a chiral substrate after the polymerization to induce an one preferred helical sense. All these novel structures were called poly(phenylacetylene)s (PPAs).[13]

Poly(phenylacetylene)s (PPAs) are a class of poly(acetylene)s (PAs) that have repetition units derived from ethynylbenzene monomers. Moreover, these macromolecules are classified as dynamic helical polymers and therefore its helical sense can be modulated by the addition of different external stimuli such as: temperature, polarity of solvents and metal ions, among others.[14]

To obtain PPAs with helical structure is necessary that the double bonds of the conjugated polyenic skeleton adopt a *cis* configuration [*cis-cisoid* (*c-c*) or *cis-transoid* (*c-t*)]. For this reason, Rh(I) catalysts are used because produce polymers with a high content of *cis* double bonds by a stereospecific living polymerization reaction lead to high molecular weigh helical polymers in high yields (Figure 3).[15]

Different types of Rh(I) catalysts such as $[Rh(nbd)Cl]_2$ (nbd: 2,5-norbornadiene), $[Rh(cod)Cl]_2$ (cod: *cis-cis*-1,5-cyclooctadiene), $[Rh(nbd)BF_4]$ can be used to obtain this polymers in different solvents.

[11] Ciardelli, F.; Benedetii, E.; Pieroni, O.; *Makromol. Chem.* **1967**, *103*, 1.
[12] Ciardelli, F.; Lanzillo, S.; Pieroni, O.; *Macromolecules* **1974**, *7*, 174.
[13] Maeda, K.; Yashima, E.; *Top. Curr. Chem.* **2006**, *265*, 47.
[14] Simonescu, C. I.; Persec, V.; Dumitrescu. S.; *J. Polym. Sci. Polym. Chem.* **1977**, *15,* 2497. (b) Simonescu, C. I.; Percec, V.; *J. Polym. Sci., Part C: Polym. Lett.* **1979**, *17*, 421.
[15] a) Ke, Z.; Abe, S.; Ueno, T.; Morokuma, K.; *J. Am. Chem. Soc.* **2011**, *133*, 7926. b) Hirao, K.; Ishii, Y.; Terao, T.; Kishimoto, Y.; Miyatake, T.; Ikariya, T.; Noyori, R.; *Macromolecules* **1998**, *31*, 3405. (c) Kishimoto, Y.; Eckerle, P.; Miyatake, T.; Ikariya, T.; Noyori, T.; *J. Am. Chem. Soc.* **1994**, *116*, 12131.

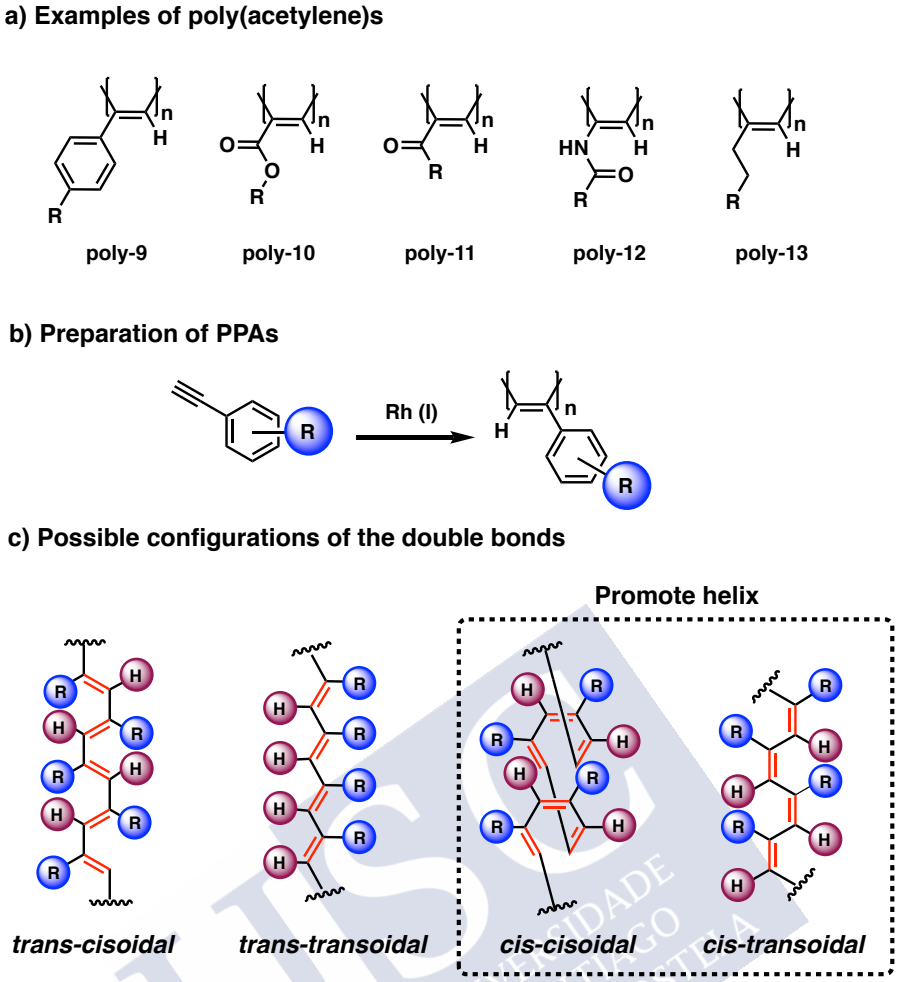

Figure 3. a) Examples of PAs. b) General method for the preparation of PPAs. b) Possible configurations of the conjugated double bonds in PPAs.

The PPAs polymerization mechanism with a Rh(I) catalyst is a 2,1-insertion, with a head to tail stereospecific and regioselective process. This mechanism is produced due to steric repulsion between pendant units (Figure 4).[16]

[16] Ke, Z.; Abe, S.; Ueno, T.; Morokuma, K.; *J. Am. Chem. Soc*. **2011**, *33*, 7926.

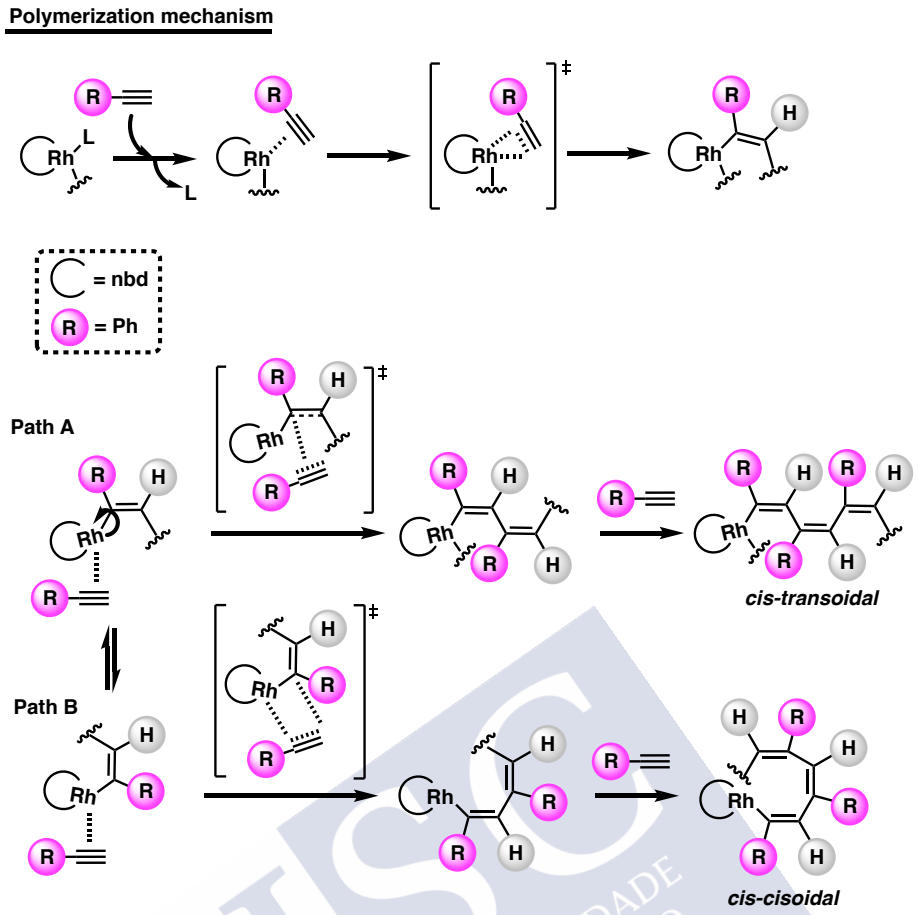

Figure 4. Polymerization mechanism for PPAs using Rh (I) catalyst.

3. Poly(phenylacetylene)s stability

During the last years, PPAs with a *cis-cisoidal* (*c-c*) and *cis-transoidal* (*c-t*) configuration in the conjugated double bonds were studied in detail. This type of materials has a strong potential applications in different fields and the study of their stability is a very important field of knowledge.[17]

Interestingly, Percec *et Al.* studied how the *cis* content of the *c-t* PPAs has a decrease when the polymer is dissolved in chloroform. The reason of that was attributed to a electrocyclization mechanism followed by a disruption of the polymer chain to produce a 1,3,5-triphenylbencene (Figure 5a). This degradation happens both in solid state and solutions and the kinetics of this phenomenon decrease an inert atmosphere and vacuum. On the

[17] a) Liu, l.; Namikoshi, T.; Zang, Y.; Aoki, T.; Hadano, S.; Abe, Y.; Wasuzu, I.; Tsutsuba, T.; Teraguchi, M.; Kaneko, T.; *J. Am. Chem. Soc.* **2013**, *135*, 602. b) Huang, K.; Mawatari, Y.; Miyasaka, A.; Sadahiro, Y.; Tabata, M.; Kashiwaya, Y.; *Polymer* **2007**, *48*, 6366. c) Miyasaka, A.; Mawatari, Y.; Sone, T.; Tabata, M.; *Polym. Degrad. Stab.* **2007**, *92*, 253. d) Percec, V.; Rudick, J. G.; *Macromolecules* **2005**, *38*, 7241.

contrary, the degradation velocity increases at high temperatures demonstrated by ^{1}H NMR experiments. For this reason, these polymers and thermosensitives.[18]

Tabata and co-workers demonstrated the *cis-trans* isomerization in PPAs mediated by heating, pressure or electric field. The isomerization process occurs through a radical mechanism and is supported by electron spin resonance (Figure 5b).

Most recently, Liu *et Al.* described of a highly selective photocyclic aromatization (SCAT) in *cis-cisoidal* PPAs, where the polyene skeleton adopts the require geometry to produce exclusively 1,3,5-trisubstitued benzene derivatives. These products were successfully characterized by Gel Performance Chromatography (GPC), ^{1}H NMR and TOF-MS (Figure 5c).[19]

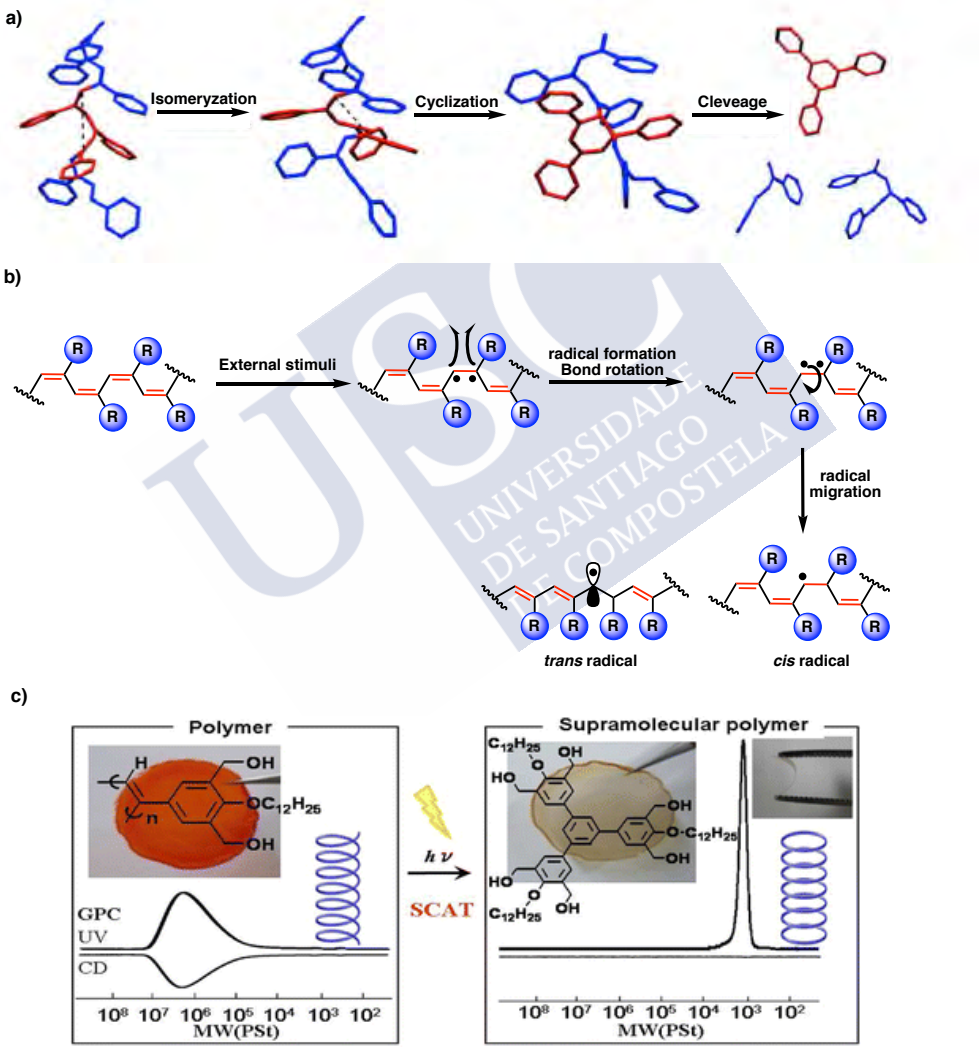

Figure 5. a) Schematic representation for the degradation of PPAs by electrocyclization. b) Isomerization *cis-trans* in PPAs described by Tabata. c) Schematic representation of photocyclic aromatization in *cis-cisoidal* PPAs in solid state.

[18] Vohlidal, J.; Redrova, D.; Pacovska, M.; Sedlacek; *J. Collect Czech Chem. Commun.* **1993**, *58*, 2651.
[19] Miyata, M.; Masahiro, T.; Hiromichi, E.; Takashi, K.; Toshiki, A.; *Chem. Lett.* **2014**, *43*, 1476.

4. Properties of dynamic helical polymers

In the last years, dynamic helical polymers have been widely studied because presents potential applications in fields such as sensing, memory storage, drug delivery, etc. These functions are related to with the helical sense (*P* or *M* helices) and elongation of the polymers. For this reason, the design of the pendant group and the control in the degree of stretch in the polymer are very important parameters to develop new materials with different applications.

In the following sections, the most important properties in dynamic helical polymers will be described in detail.

4.1 Helix induction in dynamic helical polymers

The helix induction takes place in axially racemic polymers where the both helices are present in equilibrium (*P* and *M* helices are in the same population). The interaction of these optically inactive polymers with chiral external stimuli (*e.g.* chiral solvents, chiral molecules) can induce a one preferred helical sense and promotes the formation of optically active helical polymers.

Thus, Yashima and co-workers reported the first example of a helical induction in PPAs using chiral external stimuli. In this work, they used an inactive optically poly-(carboxy)phenylacetylene (poly-**14**) that bears an achiral carboxylic functional group as pendant group. The addition of a chiral amine produces acid-base interactions and also induces one preferred helical sense in the PPAs. Interestingly, the helix induction was demonstrated in solution, gel and solid state (Figure 6).[20,21]

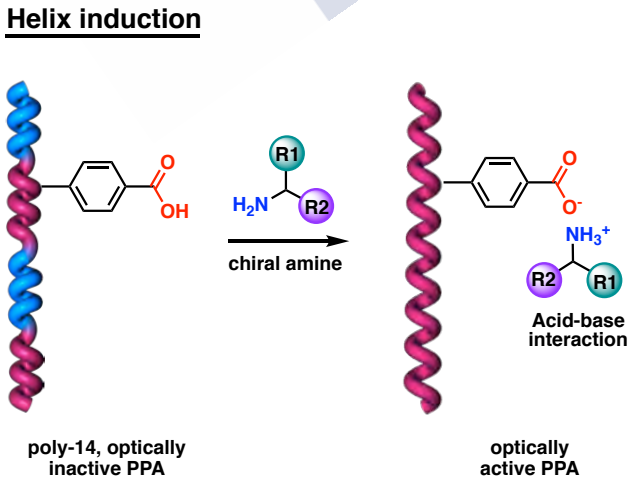

Figure 6. Schematic representation for helix induction phenomena in PPAs.

[20] Yashima, E.; Matsushima, T.; Okamoto, Y.; *J. Am. Chem. Soc.* **1995**, *117*, 11596

[21] Hase, Y.; Nagai, K.; Iida, H.; Maeda, K.; Ochi, N.; Sawabe, K.; Sakajiri, K.; Okoshi, K.; Yashima, E.; *J. Am. Chem. Soc.* **2009**, *131*, 10719.

4.2 Memory effect

Following with the helix induction studies, Yashima's group described a new phenomenon called Memory Effect. This process consists on in the preservation of the helical sense in absence of chiral external stimuli.

In this work, it was demonstrated that when the chiral amine is totally replaced by an achiral amine, the CD signal presents the same intensity indicating the same helical sense in the polymer. The mechanism of this memory effect is very simple, when the chiral amine is replaced by the achiral one, salt bridges are established between the carboxylic group and the achiral amine and the electrostatic repulsions formed maintain the helix (Figure 7).[22]

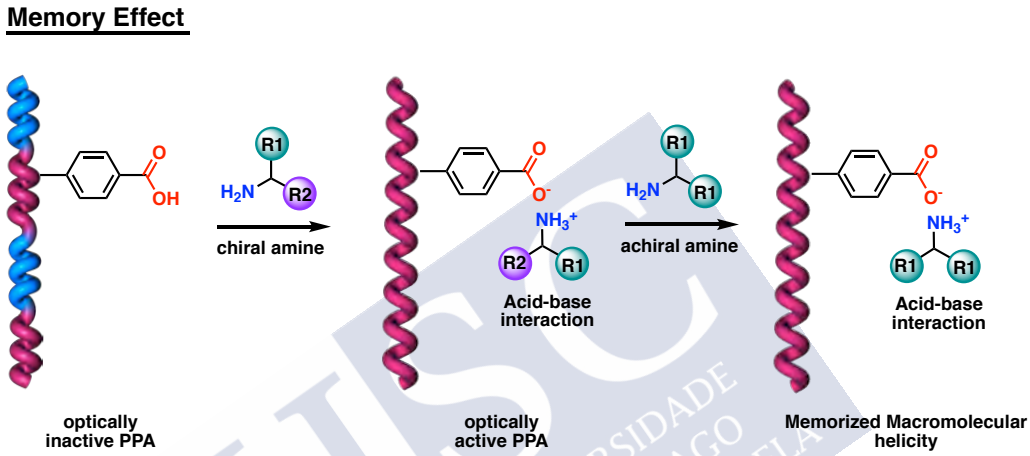

Figure 7. Schematic illustration for the Memory Effect.

4.3 Chiral enhancement in dynamic helical polymers

Chiral enhancement is a very interesting phenomenon in helical polymers because allows increase the chiral content of a starting racemic helical polymer by the addition of a small amount of an external stimuli (*e.g.* temperature, metal ions, polarity of solvents, etc.). The reason of that is the formation of covalent or non-covalent interactions between the polymer and the external stimuli.

Working on this idea, Freire *et Al*. develops a new helical polymer derived from the anilide of α-methoxy-α-phenylacetic acid (poly-**15**) that presents an axially racemic structure due to the presence of a 50% of right and left-handed helices presenting a null CD signal in the vinylic region (CD_{380} = 0). The reason of that is the presence of an equilibrium between two conformations, an antiperiplanar conformation between the carbonyl and the methoxy group [*ap* conformer, dihedral angle for (O-)C—C(=O) 180° ca] and a synperiplanar conformation between these functional groups [*sp* conformer, dihedral angle for (O-)C—C(=O) 0° ca].[23]

[22] Yashima, E.; Maeda, K.; Okamoto, Y.; *Nature*. **1999**, *399*, 449.
[23] Freire, F.; Seco, J. M.; Quiñoá, E.; Riguera, R.; *Angew. Chem. Int. Ed.* **2011**, *50,* 11692.

Interestingly, the addition of a small amount of metal ions (*e.g.* Li^+, Ag^+, Ba^{2+}, etc) to the polymer is able to disrupt the equilibrium due to the formation of a PPA/M^{n+} complex. On the one hand, the addition of monovalent metal ions (*e.g.* Li^+, Na^+ and Ag^+) stabilizes the *ap* conformation in the pendant group due to the chelation of metal ion to the carbonyl and the presence of the cation-π between the cation and the aryl ring. On the other hand, the addition of divalent metal ions (Ba^{2+}, Co^{2+}, Ni^{2+}, etc.) stabilizes the *sp* conformer due to the coordination of the divalent cations to the carbonyl and the methoxy groups (Figure 8). Thus, poly-**15** can act as a metal ion sensor due to its ability to shift the coordination mode depending on the metal ion oxidation state.

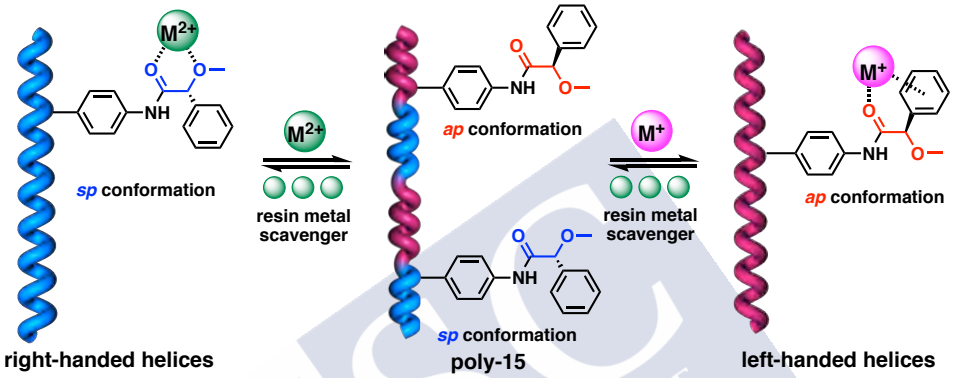

Figure 8. Schematic representation of chiral enhancement with divalent and monovalent metal ions in poly-**15**.

In addition, Arias *et Al*. demonstrated that it is possible to a total control the helical sense in poly-**15** using only monovalent metal ions (Na^+ and Ag^+) by the presence or non-presence of cation-π interactions. Thus, the addition of a small amount of a donor cosolvent (*e.g.* MeOH, MeCN) is able to disrupt the interaction between the metal ion and the aryl ring stabilizing the *sp* conformation in the pendant group (Figure 9).[24]

[24] Arias, S.; Freire, F.; Quiñoá, E.; Riguera, R.; *Polym. Chem*. **2015**, *6*, 4725.

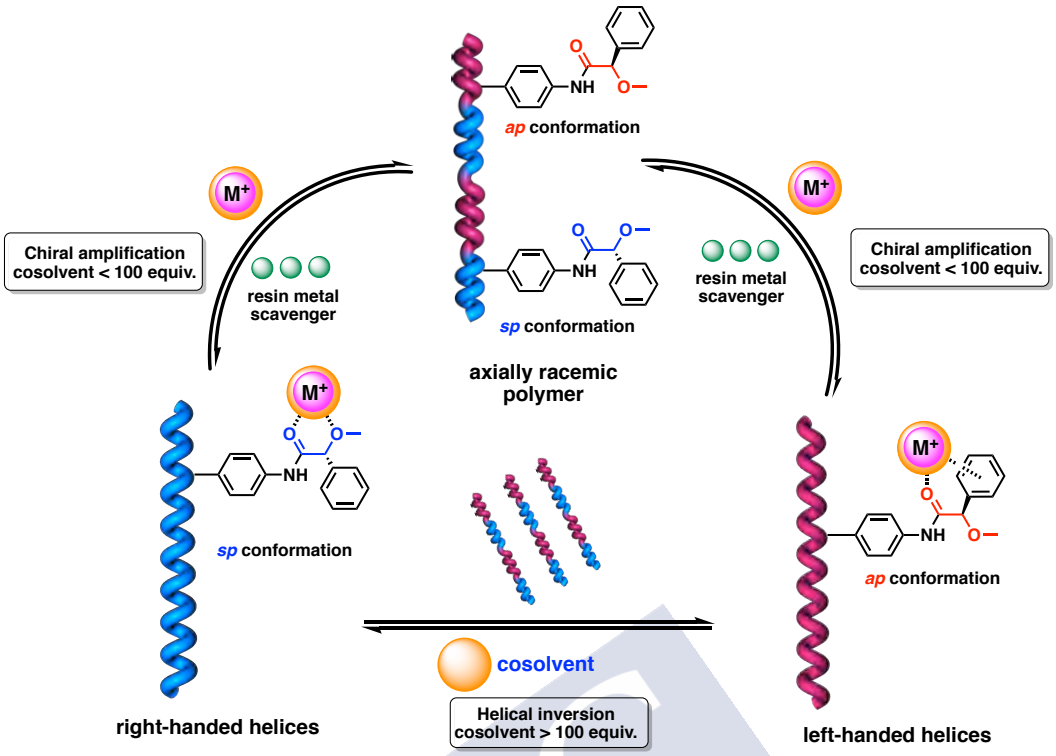

Figure 9. Modulation of the helical sense in poly-**15** by the control of the cation-π interactions.

4.4 Sergeants and Soldiers Effect

The Sergeants and Soldiers Effect is a chiral enhancement phenomenon produced in copolymers composed by chiral and achiral monomers, where chiral counterpart controls the helical sense. It was described by Green and co-workers in poly(isocyanate)s at 1988. In this work, a copolymer consisting on a little amount of chiral units (sergeants) induce a conformational control over the achiral units (soldiers). For this reason, copolymers with a small amount of chiral monomers present the same CD intensity than the parent homopolymers (Figure 10).[25]

[25] a) Green, M. M.; Park, J.-W.; Sato, T.; Teramoto, A.; Lifson, S.; Selinger, R. L. B.; Selinger, J. V. *Angew. Chem. Int. Ed.* **1999**, *38*, 3138. b) Green, M. M.; Peterson, N. C.; Sato, T.; Teramoto, A.; Cook, R.; Lifson, S. *Science* **1995**, *268*, 1860. c) Green, M. M.; Garetz, B. A.; Munoz, B.; Chang, H. P.; Hoke, S.; Cooks, R. G. *J. Am. Chem. Soc.* **1995**, *117*, 4181. d) Green, M. M.; Reidy, M. P.; Johnson, R.D.; Darling, G.; O'Leary, D. J.; Willson, G. *J. Am Chem. Soc.* **1989**, *111*, 6452 .

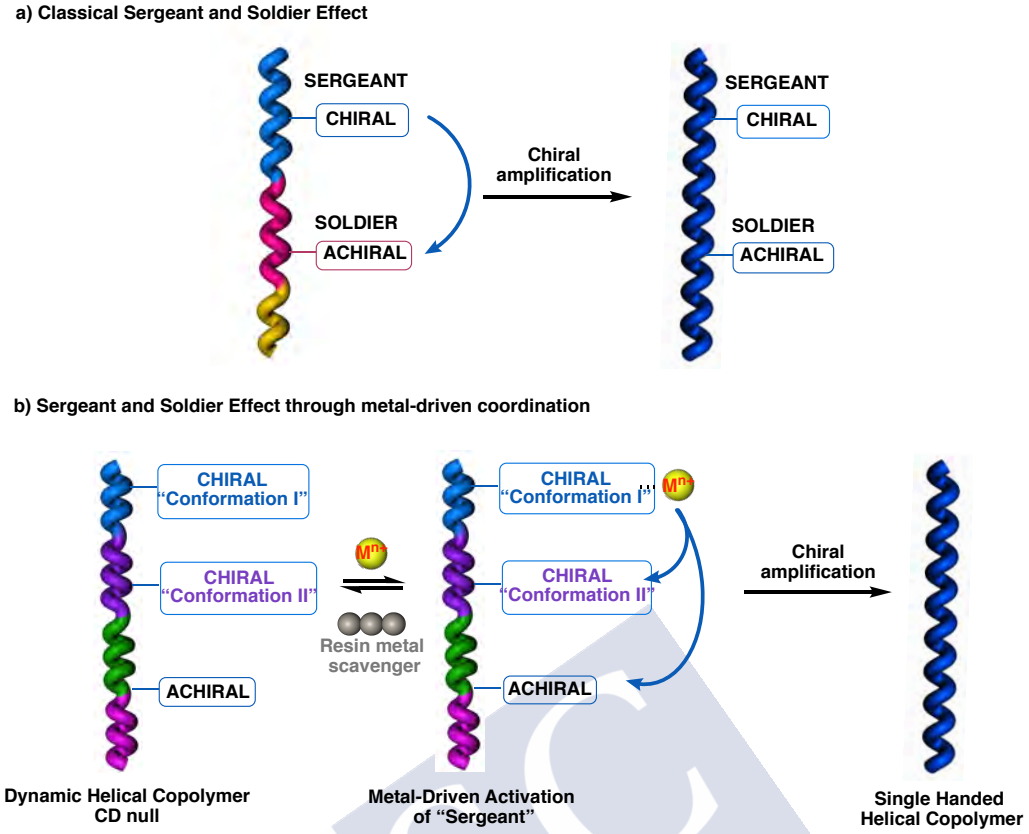

Figure 10. a) Conceptual representation for the classical Sergeants and Soldiers Effect. b) Sergeant and Soldiers Effect mediated metal ion coordination.

At 1997, Meijer *et Al.* described that the Sergeants and Soldiers Effect in supramolecular polymers. To carry out this work, chiral BiPy-BTA and achiral BiPy-BTA were employed derived from aliphatic chains. On the one hand, it was observed that when the chiral BiPy-BTA units are dissolved in non-polar solvents, the formation of helical aggregates is observed. These structures show a strong response in the CD spectra. On the other hand, the achiral units also formed these helical aggregates but did not show CD response. Interestingly, copolymers formed by a 2.5% of chiral monomers and 97.5% of achiral units dissolved in hexane exhibit a strong CD intensity comparable with parent chiral homopolymers.[26]

In this type of supramolecular polymers, the Sergeants and Soldiers Effect is limited by the organization of the system where the design of the different monomer plays an important role.

This problem does not occur in covalent polymers. Taking into account this information, Freire *et Al.* described a new Sergeants and Soldiers Effect based on poly-**15** (sergeant) and achiral units (soldiers). From previous studies, it was demonstrated that poly-**15** presents an axially racemic macroscopic chirality. For this reason, the pendant moiety is in equilibrium

[26] Palmans, A. R. A.; Vekemans, J.; Havinga, E. E.; Meijer, E. W. *Angew. Chem. Int. Ed*. **1997**, *36*, 2648.

between 50% *ap* conformation [dihedral angle for (O-)C—C(=O) 180^{o} ca] and 50% *sp* conformation [dihedral angle for (O-)C—C(=O) 0^{o} ca]. It was also described that poly-**15** can act as metal ions valence sensor where the monovalent metal ions (*e.g.* Na^{+}, Li^{+} and Ag^{+}) stabilize the *ap* due to the presence of the cation-π interaction whereas divalent metal ions (*e.g.* Ba^{2+}, Ca^{2+}, etc.) stabilize the *sp* conformation. On the other hand, as achiral units (soldiers), anilides derived from the phenylacetic and diphenylacetic acid were selected because the parent homopolymers do not show a preferred helical sense (null CD in the vynilic region).[27]

Thus, the formation of copolymers based on anilides derived from MPA monomers and phenylacetic or diphenylacetic acid monomers produce an axially racemic (null CD) highly dynamic polymers. In previous studies, it was demonstrated that poly-**15** can act as a metal ions sensor distinguish between monovalent and divalent metal ions stabilizing one preferred helical sense.

Using this information, small amount of metal ions were added to activate the MPA moiety and produce the Sergeants and Soldiers Effect in the copolymers. Thus, the addition of metal ions stabilizes a specific conformation in the pendant group that induce a specific conformation in the achiral units (Figure 10b).

Moreover, the reversibility of the process was studied removing the metal ions through the addition of metal scavengers resins. Therefore, if the metal ions are removed, the racemic helices are recovered. In this work, it is the first time that a reversibility Sergeants and Soldiers Effect is reported.

Furthermore, the control of the Sergeants and Soldiers Effect were studied by the activation/deactivation of the cation-π interactions in the copolymers. Thus, the addition of monovalent metal ions (*e.g.* Na^{+}) in presence of small amount of donor cosolvent (*e.g.* MeOH) induces an *ap* conformation lead to one preferred helical sense. On the other hand, the presence of high amount of donor cosolvent disrupts the Na^{+}-π stabilizing an *sp* conformation in the pendant group. In this work, an unique external stimulus is able to produce the two helical senses (*P* and *M* helices).[28]

More recently, in our group it was described a novel approach to the classical Sergeant and Soldiers Effect. In this work, it was used chiral Sergeants and chiral Soldiers allowing a control over the external and internal helix in the polymers. In the systems reported here, it is possible to obtain the same helical sense from either the two enantiomers ("chiral soldier", major component, when it faces a single enantiomer of an appropriate "chiral Sergeant", minor component). As a result, this groundbreaking approximation to the Sergeants and

[27] Bergueiro, J.; Freire, F.; Wendler, E. P.; Seco, J. M.; Quiñoá, E.; Riguera, R. *Chem. Sci.* **2014**, *5*, 2170.
[28] Arias, S.; Bergueiro, J.; Freire, F.; Quiñoá, E.; Riguera, R. *Small* **2016**, *12*, 238.

Soldiers Effect allows the preparation of a single-handed helix depending only on the Sergeant's configuration (Figure 11).[29]

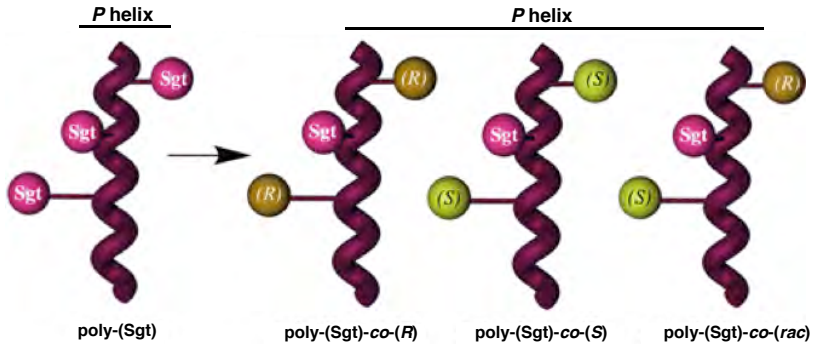

Figure 11. Conceptual representation of the novel chiral to chiral Sergeant and Soldiers Effect.

4.5 Majority rules

Green and co-workers reported another interesting Chiral Enhancement phenomenon in polymers. In this case, they studied poly(isocyanate)s consisting on mixtures of (*R*)- and (*S*)-isocyanate monomers. Interestingly, the presence of a small imbalance in the mixture (*e.g.* copolymer based on 51% of (*R*)-monomer and 49% of (*S*)-monomer) produces one preferred helical sense polymers with a CD intensity identical to the parent polymer. In this effect, the minor component adopts the helical sense of the major component (Figure 12).[30]

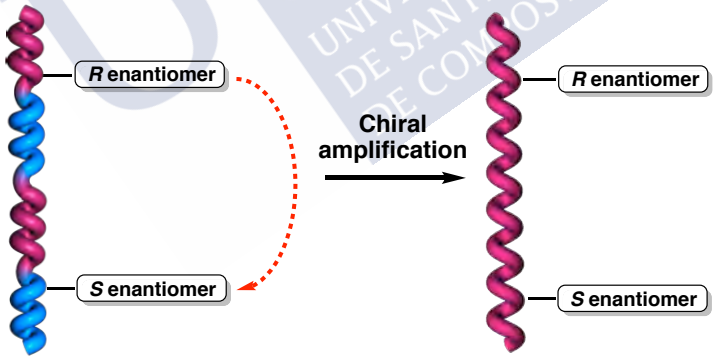

Figure 12. Conceptual representation of majority rules in helical polymers.

4.6 Domino effect

Helix induction is possible in helical polymers and oligomers by covalently[31] or non-covalently interactions incorporating chiral residues at the chain ends. For example, synthetic peptides based on an achiral α-aminoisobutyric acid (Aib) and Z-α,β-dehydrophenylalanine

[29] Cobos, K.; Quiñoá, E.; Riguera, R.; Freire, F.; *J. Am. Chem. Soc.* **2018**, *38*, 12239.
[30] Green, M.; Garetz, B.; Munoz, B.; Chang, H.; Hoke, S.; Graham-Cooks, R.; *J. Am. Chem. Soc.* **1995**, *117*, 4181.
[31] Okamoto, Y.; Matsuda, M.; Nakano, T.; Yashima, E.; *Polym. J.* **1993**, *25*, 391.

(D^{Z}Phe) residues adopt a racemic helical structure.[32] The covalent insertion of chiral α-amino acid residues into the racemic peptides favours a preferred helical sense.[33]

Following these studies, Inai *et Al.* reported an helical induction in optically inactive oligopeptides consisting on an achiral Aib and D^{Z}Phe bearing a *N*-terminal amino group upon interactions with carborxylic acids (Figure 13).[34,35]

The peptides showed a CD active due to the presence of an excess of one helical sense through acid-base interactions with the chiral carbolxylic acids. In this work, the chiral information is transmitted to the peptide via non-covalent interactions at the *N*-terminal amino group.

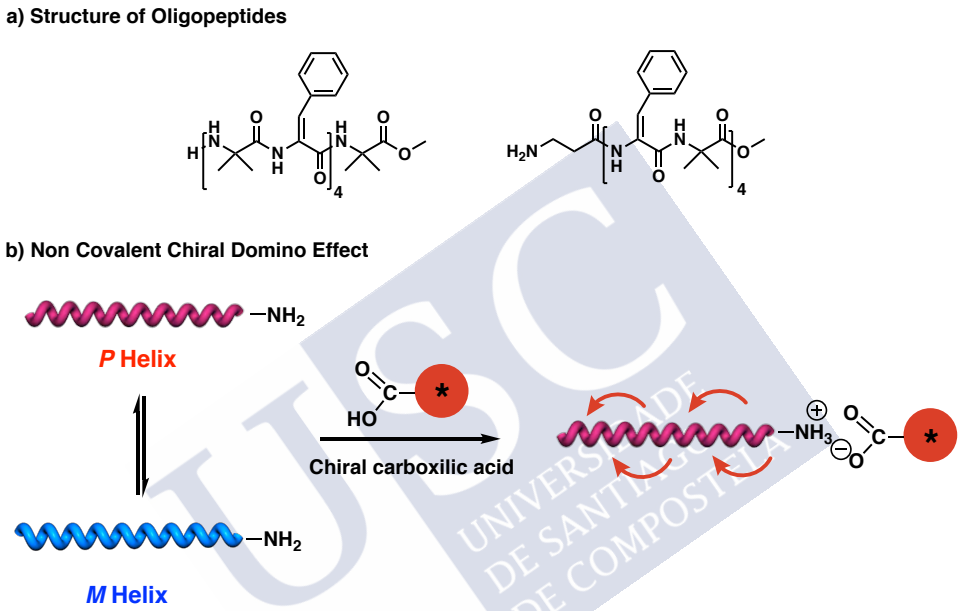

Figure 13. a) Structure of Oligopeptides and b) schematic representation of Domino Effect.

Recently, in our group it was reported a new helical induction phenomenon based on macromolecular gear composed by PPAs, short oligopeptides [$(Aib)_n$ (n = 1-3)] derivatized with MTPA single enantiomers (poly-**16**). In this macromolecular gear phenomenon, the chiral information of the MTPA enantiomer is transmitted along the achiral Aib through chiral teleinduction or/and chiral harvesting to the polyene backbone. Interestingly, the polymers show dynamic behaviour to polarity solvents or modifying the length of the Aib oligopeptide (Figure 14).[36]

[32] Venkatraman, J.; Shankaramma, S. C.; Balaran, P.; *Chem. Rev.* **2001**, *101*, 3131.
[33] Pengo, B.; Formaggio, F.; Crisma, M.; Toniolo, C.; Bonora, G. M.; Broxterman, Q. B.; Kamphuis, J.; Saviano, M.; Iacovino, R.; Rossi, F, Benedetti, E.; *J. Chem. Soc., Perkin Trans.* **1998**, 2, 1651.
[34] Inai, Y.; Komori, H.; Ousaka, N.; *Chem. Rec.* **2007**, *7*, 191.
[35] Ousaka, N.; Inai, Y.; *J. Org. Chem.* **2009**, *74*,1429.
[36] Rodriguez, R.; Suárez-Picado, E.; Quiñoá, E.; Riguera, R.; Freire, F.; *Angew. Chem., Int. Ed.* **2020**, *132*, 8694.

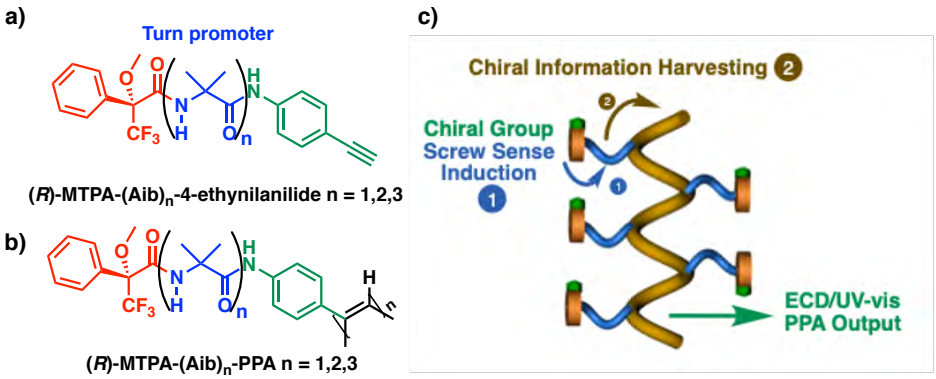

Figure 14. a) Structure of monomers. b) Structure of poly-**16** and c) Conceptual illustration of the chiral information mechanism in a PPA bearing a chiral *N*-terminal Aib oligomer as pendant group.

4.7 Helical inversion

The helical inversion is one of the most interesting properties that present dynamic helical polymers. In this phenomenon, the helical sense of the polymer can switch from *P* to *M* helices and *vice versa* by the addition of external stimuli such as light, temperature, solvents polarity or even metal ions.

In our group, it was described a polymer derived from the (*S*)-pheylglycine methyl ester (poly-**17**). This polymer presents the ability of switch the helical sense with the solvents polarity and with the coordination of metal ions. On the one hand, when the polymer is dissolved in low polar solvents (*e.g.* $CHCl_3$ or THF), the pendant group adopts an *anti* orientation between the two carbonyl groups lead to *M* helices. On the other hand, when poly-**17** is dissolved in high polar solvent (*e.g.* DMSO, DMF), the pendant groups adopt a *syn* orientation between the two carbonyl groups leading to *P* helices. Moreover, the *anti* orientation can be switch by the addition of metal ions (*e.g.* Ba^{2+}) due to the coordination of the cations to both carbonyl groups lead to *P* helices (Figure 15a).[9]

Moreover, in our group it was studied the helical inversion reversibility in polymers derived from *L*-aminoacids methyl ester (*e.g.* Alanine, Isoleucine, leucine methyl ester, among others). These polymers adopt *M* helices in low polar solvents (*e.g.* $CHCl_3$) due the stabilization of the *anti* orientation by hydrogen bonds between neighbouring pendants. This conformation can be changed by the addition of metal ions (*e.g.* Li^+, Ba^{2+}, Ca^{2+}, etc.) due to the coordination of the cations to both carbonyl groups promoting an helical inversion (*P* helices). With the objective to study the reversibility of this process, a donor cosolvent such as MeOH was added. The addition of this cosolvent promotes another helical inversion and the polymer recover the

original helical sense (*M* helices) due to the solvation of the cations by the cosolvent (Figure 15b).[37]

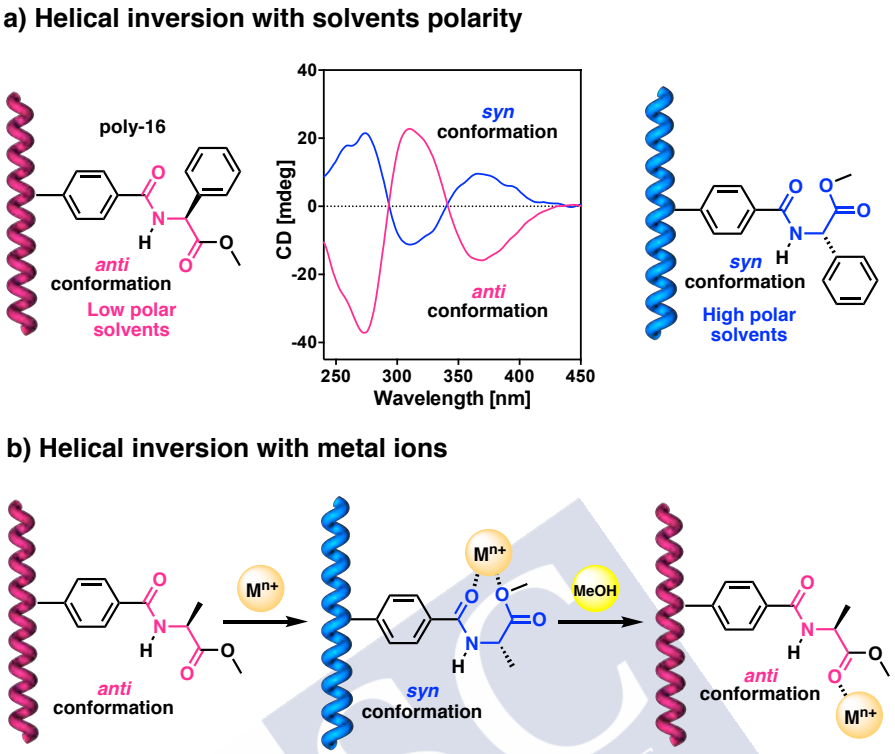

Figure 15. a) Helical inversion mediated by solvents polarity and b) by the addition of metal ions.

4.8 Structural changes in helical polymers

The secondary structure of the PPAs is related to the properties that can present this type of helical polymers. In this family of helical polymers, two parameters can be easily modulated: the helical sense and the elongation.

Yashima *et Al.* have reported that new optically active PPAs with β-cyclodextrins (β-CyD) (poly-**18**) as pendant group (Figure 16). They found that poly-**18** presents a one preferred helical sense in DMSO solution. The addition of increasing amount of water promotes a change in the colour from red to yellow indicating compression in the backbone of the PPA. Interestingly, this change in the elongation of the PPA is accompanied to a helical inversion. In addition, they studied the ability of these PPAs to act as sensor of chiral molecules. For this reason, the polymer was evaluated in presence of (*R*) and (*S*)-1-phenylethylamine. They found that poly-**18** exhibits a positive Cotton Effect in the CD spectra in presence of (*S*)-1-phenylethylamine whereas negative Cotton Effect is observed in the presence of (*R*)-1-phenylethylamine (Figure 16).[38]

[9] Louzao, I.; Seco, J. M.; Quiñoá, E.; Riguera, R.; *Angew. Chem., Int. Ed.* **2010**, *49*, 1430.
[37] Arias, S.; Núñez-Martínez, M.; Quiñoá, E.; Riguera, R.; *Polym. Chem.* **2017**, *8*, 3740.
[38] Maeda, K.; Mochizuki, H.; Osato, K.; Yashima, E.; *Macromolecules* **2011**, *44*, 3217.

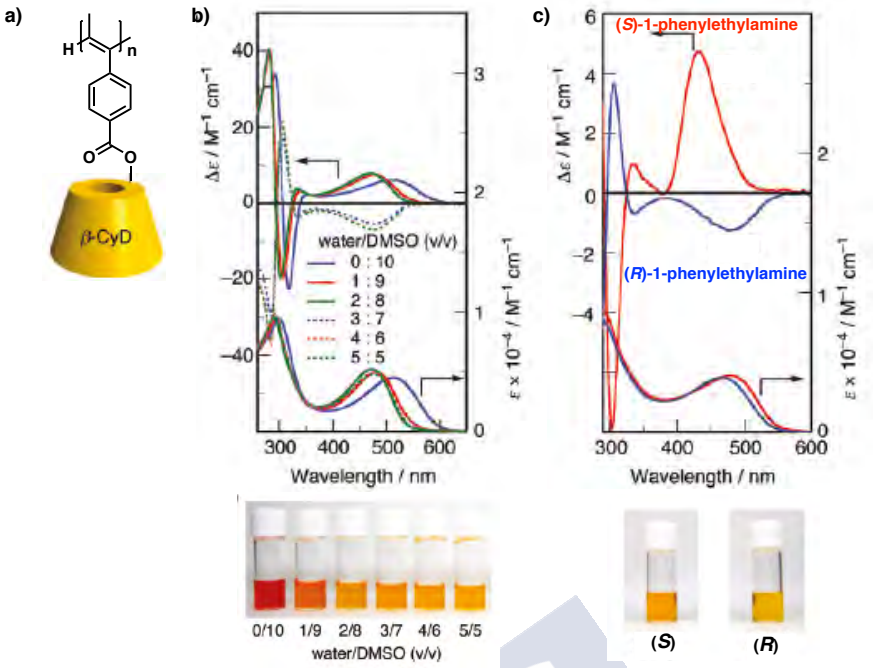

Figure 16. a) Structure of poly-**18**. b) CD spectra for poly-**18** in presence of different mixtures of DMSO/H_2O. c) CD spectra for poly-**18** in presence of (*S*) and (*R*)-1-phenylethylamine.

In our research group, Seila *et al.* prepared a new polymer bears the anilide from (*R*)-α-methoxy-α-trifluoromethyl-α-phenylacetic acid (MTPA) (poly-**19**). This polymer can modulate two parameters: the helical sense and elongation depending on donor/acceptor and polar/non polar character of the solvent.

This PPA presents two bonds that can manipulate the conformation of the pendant group and also the helical sense. The first is the amide bond, this functional group can be tuned from *cis* to *trans* depending on the donor and non-donor character of the solvents. Thus, when poly-**19** is dissolved in donor solvents (*e.g.* DMSO, THF) the amide group adopts a *cis* conformation. On the other hand, when the polymer is dissolved in non-donor solvents (*e.g.* $CHCl_3$, DCM) the amide bond adopts a *trans* conformation (Figure 17).

The second parameter that can be manipulated is the (O-)C—C(=O) bond. On the one hand, in low polar solvents (*e.g.* $CHCl_3$, DCM) the (O-)C—C(=O) bond adopts an *ap* conformation where the carbonyl and methoxy groups are antiperiplanar oriented. On the other hand, when the polymer is dissolved in high polar solvents (*e.g*. DMF and DMSO) the (O-)C—C(=O) bond adopts an *sp* conformation where the carbonyl and methoxy groups are synperiplanar oriented. In this work, it has demonstrated that with the selective manipulation of two bonds in possible to obtain four different helical structures (Figure 17).[39]

[39] Leiras, S.; Freire. F.; Seco, J. M.; Quiñoá, E.; Riguera, R.; *Chem. Sci.* **2013**, *4*, 2735.

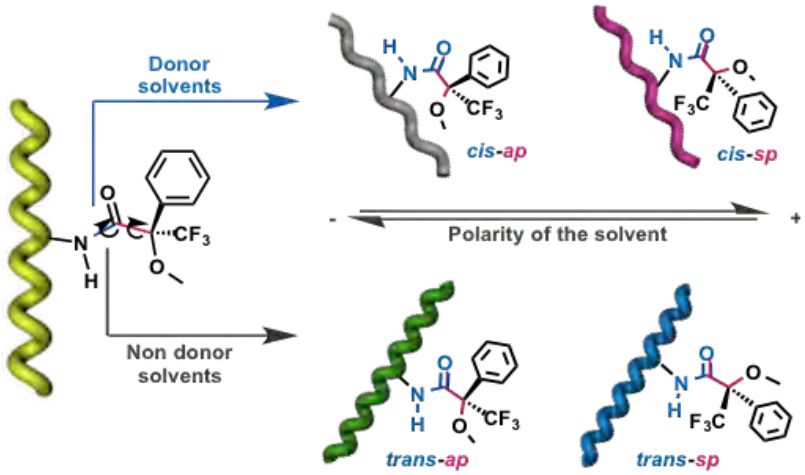

Figure 17. Schematic illustration for the conformation changes in poly-**19** depending on donor/acceptor and high polar/low polar character of the solvent.

Rodriguez *et Al.* carried out another interesting work about structural changes in our group. In this work, it was studied how affect the aromatic substitution pattern (*para-*, *meta-*, *ortho-*) in the dynamic behaviour and elongation in poly-**15**. It was observed that *p*-poly-**15** and *m*-poly-**15** presents the ability to responds at the presence of metal ions. In the case of *meta* substituted poly-**15**, the ability to respond at external stimuli is lower than in the case of *para* substituted polymer due to less dynamic behaviour. Moreover, *m*-poly-**15** presents the combination of two helices, the first one is a *cis-cisoidal* structure similar to the *p*-poly-**15** and the second one is a *cis-transoidal* structure corresponding to more stretched structure. In the case of *ortho-substituted* polymers (*o*-poly-**15**), it was found that does not respond to the presence of external stimuli due to the quasi-static behaviour. Finally, *o*-poly-**15** presents a highly stretched structure with an almost planar structure (Figure 18).[40]

Thus, in this work it was demonstrated that the aromatic substitution pattern in poly-**15** has a strong influence in the dynamic behaviour of the helical polymers. Moreover, it was found that the helical structure is closely related to the substitution aromatic pattern.

[40] Rodríguez, R.; Quiñoá, E.; Riguera, R.; Freire, F.; *J. Am. Chem. Soc.* **2016**, *138*, 9620.

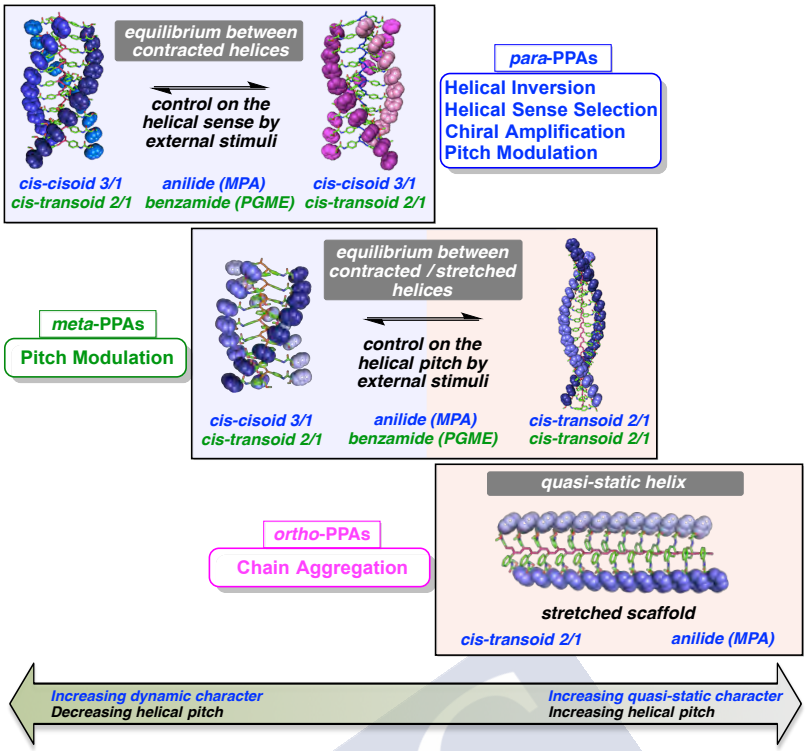

Figure 18. Schematic representation of the effect on aromatic substitution pattern in PPAs.

5. Hybrid materials based on helical polymer and Metal nanoparticles

Hybrid materials are formed from the combination of two different materials. For this reason, they have attracted the attention of the scientific community due to its applications in different fields such as: energy storage,[41] asymmetric catalysis,[42] sensing,[43] or medicine.[44] Interestingly, the properties of these materials are the combination of the components of the system.

In particular, hybrid materials based on Gold Nanoparticles (AuNPs) presents considerable interest because its properties (size and shape) can be easily tuned. AuNPs present a very good stability and they can be obtained from different methodologies. Moreover, the functionalization of these AuNPs with different organic molecules opens new possibilities in the preparation of novel multifunctional materials.[45]

[41] Dubal, P.; Ayyad, O.; Ruiz, V.; Gomez-Romero, P.; *Chem. Soc. Rev.* **2015**, *44*, 1777.
[42] Diaz, U.; Brunel, D.; Corma, A.; *Chem. Soc. Rev.* **2013**, *42*, 4083.
[43] Wang, S.; Kang, Y.; Wang, L.; Zhang, H.; Wang, Y.; *Sens. Actuators, B* **2013**, *182*, 467.
[44] Srinivasan, M.; Rajabi. M.; Mousa, S.; *Nanomaterials* **2015**, *5*, 1690.
[45] Cobley, C.; Chen, J.; Cho, E. C.; Wang, L.; Xia, Y.; *Chem. Soc. Rev.* **2011**, *40*, 44.

5.1 Nanochemistry: Strategies for the preparation of hybrid materials

Normally, hybrid materials are composed with a core-shell composition where the core is consisting on AuNPs and the shell is based on stabilizing ligands such as polymers. Stabilizing ligands plays an important role in the colloidal stability, solubility, charge on the surface and also potential functionalities of the hybrid material.[46]

The ligands of the hybrid materials can be mainly classified in two types: auxiliary stabilizing agents (ASLs) and functionalized stabilizing ligands (FSLs). ASLs are the responsible for the properties such as colloidal stability and solubility. These types of ligands can be used to prepare the AuNPs and then can be easily replaced by FSLs ligands. On the other hand, FSLs ligands are usually used to give other functionalities (*e.g.* Catalytic, luminescent or redox activity) to the material.

Different methods to prepare hybrid materials can be summarized in three protocols: one-phase, two-phase and post-nanoparticle functionalizations.

I) One phase method

This method is commonly called *Turchevich method*,[47] which involves the reduction of a gold solution in the presence of stabilizing agent and a reducing agent (*e.g.* sodium citrate). In this procedure, the reducing agent acts also as stabilizing agent of the nanoparticles. However, this protocol fails to obtain AuNPs with large diameters (d_c > 50 nm) with acceptable low polydispersity. Bastus *et Al.* reported that controlling the reaction conditions (temperature, pH, stirring speed, etc) and the stoichiometry of the reagents, citrated-capped spherical AuNPs (Cit-AuNPs) with different sizes can be obtained.[48]

$$n\cdot HAuCl_4 + n\cdot(^-OCOCH_2)_2C(OH)COO^-)\ (aq)$$
$$\rightarrow 4n\cdot Cl^-\ (aq) + 4n\cdot H^+\ (aq) + Au^0_n + n\cdot(^-OCOCH_2)_2CO\ (aq) + n\cdot CO_2$$

Equation 1. General reaction for the reduction of a gold salt by sodium citrate.

II) Two phase method

Brust and Schiffrin[49] use a phase-transfer agent such as tetraoctylammonium bromide (TOAB) in an organic solvent (*e.g.* Toluene, dichloromethane) to transfer the gold salt (Au^{3+}) from aqueous solution (equation 2).

$$HAuCl_4\,(aq) + N(C_8H_{17})_4^+Br^-\ (tol) \rightarrow N(C_8H_{17})_4^+AuCl_4^-\ (tol) + HBr$$

Equation 2. Phase transfer reaction in Brust-Schiffrin method.

[46] Daniel, M. C.; Astruc, D.; *Chem. Rev.* **2004**, *104*, 293.
[47] Enüstün, B. V.; Turkevich, J.; *J. Am. Chem. Soc.* **1963**, *85*, 3317
[48] Bastus, N. G.; Comenge, J.; Puntes, V.; *Langmuir* **2011**, *27*, 11098.
[49] Brust, M.; Walker, M.; Bethell, D.; Schiffrin, D. J.; Whyman, R.; *J. Chem. Soc., Chem. Commun.* **1994**, 801.

Then, a stabilizing agent (*e.g.* Dodecanethiol or sulphur and amine ligands) is added to the organic solution followed by the addition of a mild reducing agent such as sodium borohydride ($NaBH_4$) (equation 3). The prepared solution of reducing agent must be used immediately after preparation due to the fast decomposition of sodium borohydride (equation 4).[50]

$$n \times Au^{3+}\,(tol) + 3n \times e^{-} \rightarrow Au_n$$

Equation 3. Reduction of gold ions to gold nanoparticles.

$$BH_4^{-}\,(aq) + 3H_2O \rightarrow B(OH)_3\,(aq) + 3H_2 + H^{+} + e^{-}$$

Equation 4. Decomposition reaction of sodium borohydride.

In this method, varying the tiol/gold ratio where a high thiol/gold ratio leads to small AuNPs whereas a high thiol/gold ratio lead to small diameter AuNPs.

III) Post nanoparticle-synthesis methods

Different approaches were developed to modify the core of the AuNPs after of its synthesis.

a) Ligand exchange reaction

This method is a post-nanoparticle surface modification based on the replacement of the auxiliary stabilizing ligands (ASL) by functionalized stabilizing ligands (FSL) on the surface of the nanoparticles (Figure 19). The preparation of AuNPs with this method allows a precise control in the hybrid material and actually it is one of the most common methods employed.[51]

To do that, it is necessary that the ASLs ligands have equal or lower binding affinity than the FSLs ligands. The difference in binding strength and size of the ligands determines the rate reaction and the degree of surface functionalization in the AuNPs.

The degree of functionalization can be controlled by differences in the binding strengths of FSL-Au and ASL-Au, available from scanning tunnelling microscopy (STM) studies of alkyl amines, thiols and carboxylic acids supported of an Au (111) surface.[52]

$$—COOH\ (Au\text{-}O,\ 8.4\ KJ\ mol^{-1}) < —NH_2\ (Au\text{-}N,\ 65\ KJ\ mol^{-1})$$

$$< —SH\ (Au\text{-}S,\ 167\ KJ\ mol^{-1})$$

b) Direct covalent chemistry on the shell

Different functionalities can be introduced at the periphery of the AuNPs shell through chemical reactions. For example, copper-catalyzed azide-alkyne coupling (CuACC) can be employed to incorporate a broad variety of functional groups with biological interest such as

[50] Huhn, J.; Carrillo-Carrion, C.; Soliman, M.; Pfeiffer, C.; Valdeperez, D.; Masood, A.; Chakraborty, I.; Zhu, L.; Gallego, M.; Yue, Z.; Carril, M.; Feliu, N.; Escudero, A.; Alkilany, A.; Pelaz, B.; del Pino, P.; Parak, W. J.; *Chem. Mater.* **2017**, *29*, 399.

[51] Woehrle, G.; Brown, L.; Hutchison, J.; *J. Am. Chem. Soc.* **2015**, *127*, 2172.

[52] Pérez-Mirabet, L.; Surinyach, S.; Ros, J.; Suades, J.; Yáñez, R.; *Mat. Chem. Phys.* **2012**, *137*, 439.

proteins, peptides or DNA to AuNPs. Another example is based on the linkage of ferrocenyl derivatives to AuNPs (Figure 19).[53]

c) Coulombic interactions

Self-assembly of AuNPs functionalized at the periphery (*e.g.* Carboxylates, quaternary amines or ionic counter ions) can be produced with other charged functional groups (Figure 19).[54,55]

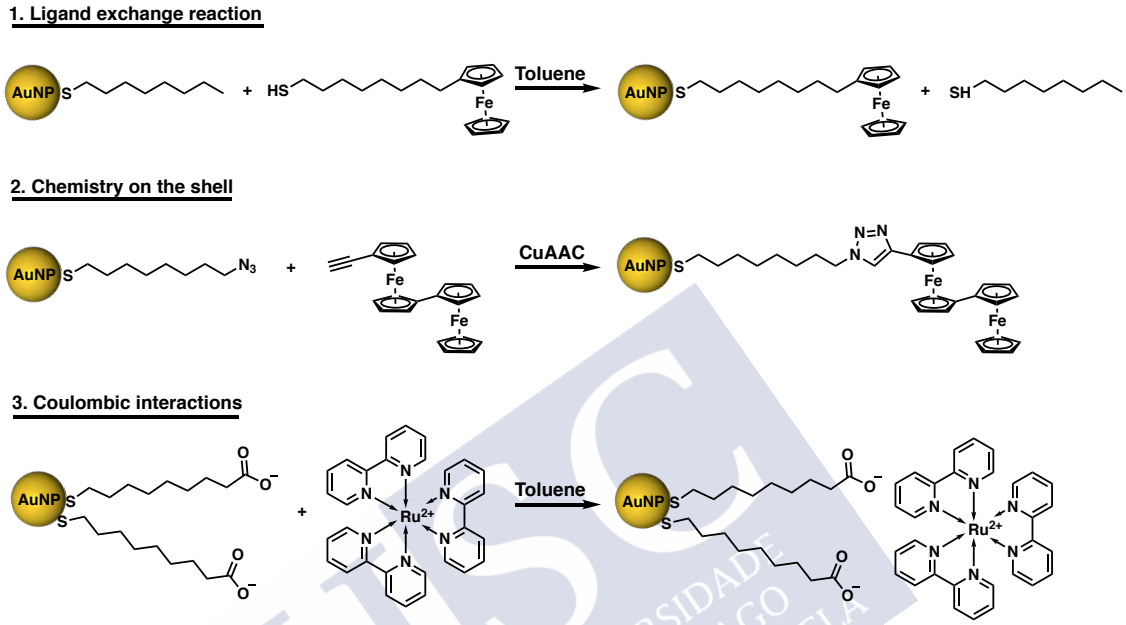

Figure 19. Schematic representation for different examples in post-nanoparticle synthesis.

5.2 Characterization of structural properties of the NPs

As commented before, an inorganic core and an organic shell usually compose the NPs. The total mass of one NP (m_{np}) includes the mass of the inorganic core (m_c) and the mass of the organic shell. Inorganic cores can be visualized by TEM images and the mass of one NP can be easily calculated. Moreover, the NP core volume (V_c) can be estimated using NP dimensions from TEM images [core diameter (d_c)] in the case of spherical NPs.

$$V_c(sphere) = \left(\frac{4}{3}\pi\right) \times \left(\frac{d_c}{2}\right)^3 = \left(\frac{\pi}{6}\right) \times d_c^3$$

Equation 5. Calculation of NP core volume.

In the case the core is composed out of material of density ρ_c, the mass of one NP can be calculated such as:

$$m_c = \rho_c \times V_c$$

Equation 6. Equation to determine the mass of one NP.

[53] Rapakousiou, A.; Djeda, R.; Grillaud, M.; Li, N.; Ruiz, J., Astruc, D.; *Organometallics* **2014**, *33*, 6953.
[54] Huang, T.; Murray, R. W.; *Langmuir* **2002**, *18*, 7077.
[55] Glomm, W.; Moses, S.; Brennaman, M.; Papanikolas, J.; Franzen, S.; *J. Phys. Chem. B.* **2012**, *109*, 804.

For the most of inorganic NPs, the density (ρ) can be found in the literature although in the majority of cases, bulk densities of the materials can be assumed. Interestingly, the molar mass (M_c) of a one NP core can be calculated by:

$$M_c = m_c \times N_A$$

Equation 7. Equation to determine the molar mass of an NP.

- *Transmission Electron microscopy of hybrid materials*

TEM analysis allows obtaining a direct measurement for the size and shape of NPs. Normally, the organic shells do not provide enough contrast to be visible in regular TEM images because they have low electron scattering character. To solve this problem and obtain good images for the organic shell, negative staining with heavily electron-scattering compounds (*e.g.* uranyl acetate, ammonium molibdate, among others) can be employed. In the case of the inorganic core, the NP is usually based on materials such as Ag, Au, Fe_3O_4 and they appear almost black due to the strong electron-scattering character of the material.

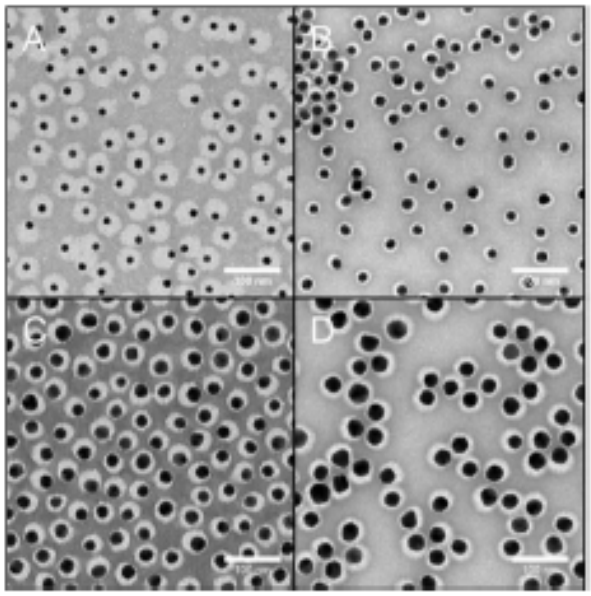

Figure 20. TEM images for PEG-AuNPs using negative staining with uranyl acetate.[56]

- *X-ray Diffraction*

X-ray Diffraction (XRD) can determine the diameter of the crystalline part (d_{crys}) of the NP core. To do that, it has to be recorded a diffractogram. In most of cases, the NPs powder solid is irradiated with a monochromatic X-ray radiation and the diffraction (change in the direction of the elastically scattered radiation) is recorded. In a crystalline sample, diffraction only occurs in some angles, named Bragg's angles (Θ). These angles are associated with crystallographic planes, which depend on the unit cell parameter of the NPs. In classical

[56] Del Pino, P.; Yang, F.; Pelaz, B.; Zhang, Q.; Kantner, K.; Hartmann, R.; Martinez de Baroja, N.; Gallego, M.; Moller, M.; Manshian, B.; Soenen, S. J.; Riedel, R.; Hampp, N.; Parak, W. J.; *Angew. Chem., Int. Ed.* **2016**, *55*, 5483.

representation of XRD, the intensity is plotted with the double of the diffraction angle (2Θ). The number and position of the peaks are characteristic for a crystalline compound.

The intensity of the peaks (*e.g.* The number of counts in the detector for a determined 2Θ) is related to the atomic positions in the crystalline unit cell, and the width of every peak is connected with the crystallite size.

The crystallite size for a crystalline direction, determined by a crystallographic plane and a Bragg's angle (Θ) can be calculated with the Scherrer equation:

$$d_{crys} = \frac{K\,\lambda}{\beta\,cos\Theta}$$

where d_{crys} is the crystallite size. K is the shape factor or Scherrer constant, which varies in the range $0.89 < K < 1$, and usually $K = 0.9$. λ is the wavelength of the X-Ray (*e.g.* for Cu K_λ = 0.15418 nm). β is the line broadening at half the maximum intensity (fwhm). Θ is the Bragg's angle of the analyzed peak.

Normally, for a single crystal of NPs the crystallite size d_{crys} calculated by Scherrer equation must be very similar to the diameter size d_c estimated by TEM analysis.

- *Thermogravimetric Analysis of NPs (TGA)*

This technique measures the mass of the sample while the temperature is increasing. The decomposition of the different parts in the sample allows studying the composition of the material.

- *Infrared Spectroscopy*

Fourier transform infrared spectroscopy (FT-IR) allows identifying different functional groups in the organic shell because each functional group has a specific vibrational fingerprint. For this reason, FT-IR is used to describe the organic shell around the NPs and confirm the functionalization. Furthermore, deviation in the typical vibrations of the functional groups can be used to describe the type of ligand-core interactions.

- *Nuclear Magnetic Resonance (NMR)*

NMR is another technique to determine the chemical structure of the organic shell around the NPs core. This technique is used to give information about the presence and the orientation of the organic ligands. Normally, NMR works very well with small molecules but in the case of large macromolecules is not so good due to the reduced flexibility and the heterogeneity.

- *UV-Vis Absorption Spectroscopy*

This technique allows determining important photophysical properties in colloidal NPs. Until now, several NPs such as quantum dots or plasmonic NPs have been prepared. Each NPs

present particular resonance peaks in their absorption spectra. UV-Vis spectra for NPs provide important information about size, size distribution and shape for the NPs. Interestingly, UV-Vis can be used to determine the concentration of NPs in solution, follow the formation of NPs and their stability.

Plasmonic nanoparticles (such as AuNPs or AgNPs) present characteristic absorption peaks due to the surface plasmon resonance (SPR) in the UV-Vis/NIR region. This nanoparticles can present one or even more SPR peaks depending on the shape of the NPs.[57,58,59] The characteristic number and position of the SPR peaks determine the distinctive colour of NPs solutions (Figure 21).

More precisely, the number of peaks and their position depends on several factors such as NP material, size, size distribution, shape, solvent and aggregation state.[60]

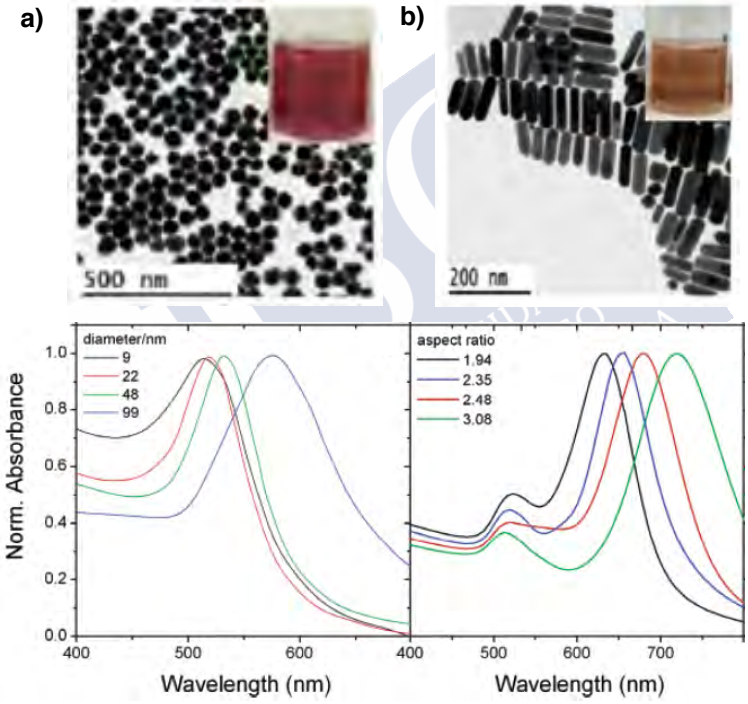

Figure 21. a) TEM image for spherical AuNPs and UV-Vis spectra for spherical AuNPs varying diameters. b) TEM image for Au nanorods and UV-Vis spectra for the nanorods varying the aspect ratio.

- *Dynamic Light Scattering (DLS)*

DLS is a simple, fast, and common technique to determine the hydrodynamic diameter of NPs in solution. DLS is based on in the measurements of temporal fluctuations in scattered light due to the diffusion NPs in solution. Using an autocorrelation function, the diffusion

[57] Liz-Marzán, L. M.; *Langmuir* **2006**, *22*, 32.
[58] Sepulveda, B.; Angelome, P. C.; Lechuga, L. M.; Liz-Marzan, L. M.; *Nano Today* **2009**, *4*, 244.
[59] Barbosa, S.; Agrawal, A.; Rodriguez-Lorenzo, L.; Pastoriza-Santos, I.; Alvarez-Puebla, R. A.; Kornowski, A.; Weller, H.; Liz-Marzan, L. M.; *Langmuir* **2010**, *26*, 14943.
[60] Vial, S.; Pastoriza-Santos, I.; Perez-Juste, J.; Liz-Marzan, L. M.; *Langmuir* **2007**, *23*, 4606.

constant of NPs can be obtained. Finally, applying Einstein-Stokes equation and using the measured diffusion constant value, the NP's hydrodynamic diameter d_h is obtained.

DLS analysis can be carried out plotting distribution of hydrodynamic diameters in terms of number of NPs $N(d_h)$ or the intensity of the scattered light $I(d_h)$. Interestingly, the intensity distribution $I(d_h)$ considers the scattering intensity of NPs fractions. In this way, larger NPs scatter much than smaller NPs and therefore intensity distribution overestimated the value of hydrodynamic diameter.

Applying Mie's theory,[61] the intensity distribution can be transformed in number distributions. For this approximation, several assumptions have to be made, for example that all the NPs are spherical and homogeneous. In the number distribution $N(d_h)$, the contribution of larger NPs is minimal and the hydrodynamic diameter (d_h) are closer to the diameter core (d_c) obtained in TEM analysis.

Occasionally, DLS measurements for hydrodynamic diameters show an increase in the size compared to the structural NPs size (*e.g.* $d_h >> d_c$ for NPs without the presence of organic shells) due to the formation of NPs aggregates. In this case, the DLS measurements give values of NPs agglomerates instead of individual NPs values.

- *Size Exclusion Chromatography (SEC)*

In this technique, a suspension of NPs pass through a porous gel matrix by pressure. The mechanism of the separation is based on the interactions between porous gel and NPs. For this reason, smaller NPs interact stronger with the porous of the gel matrix and therefore they present longer retention times. On the other hand, larger NPs do not interact with the pores and thus pass the gel faster than small NPs. In conclusion, larger NPs are eluted first whereas smaller NPs are eluted later.

In this way, SEC is a technique that can be used to purify NPs from smaller excess molecules such as capping agents or salts.[62]

- *Gel Electrophoresis*

Gel electrophoresis is based on the mobility charge of molecules in a gel matrix under electric field. In this way, molecules with high charges will migrate faster than low charges through the gel.[63] On the other hand, larger molecules can pass through the pore in the gel and in this way, they migrate slower than small molecules.[64] Taking account this information

[61] Bohren, C. F.; Huffman, D. F.; *Absorption and Scattering of Light by Small Particles*, Wiley: New York, **1983**.

[62] Sperling, R. A.; Liedl, T.; Duhr, S.; Kudera, S.; Zanella, M.; Lin, C. –A. J.; Chang, W. H.; Braun, D.; Parak, W. J.; *J. Phys. Chem. C* **2007**, *111*, 11552.

[63] Parak, W. J.; Gerion, D.; Zanchet, D.; Woerz, A. S.; Pellegrino, T.; Micheel, C.; Willians, S. C.; Seitz, M.; Bruehl, R. E.; Bryant, Z.; Bustamante, C.; Betozzi, C. R.; Alivisatos, A. P.; *Chem. Mater.* **2002**, *14*, 2113.

[64] Parak, W. J.; Pellegrino, T.; Micheel, C. M.; Gerion, D.; Williams, S. C.; Alivisatos, A. P.; *Nano Lett.* **2003**, *3*, 33.

and assuming that the NPs have the same charge density, larger NPs will pass through the pore in the gel slower than small NPs.[65]

In the case of charged NPs, they will migrate to the opposite charged pole. In addition, the speed of migration depends on the charged and the hydrodynamic diameter of the nanoparticles. Moreover, longer running time favours better separations. Using all this information, different type of NPs can be separated with this technique.

In summary, electrophoresis can be used to purify NP samples because impurities such as surfactant and molecules typically migrate faster than NPs.

5.3 Examples of hybrid materials based on helical polymers and metal nanoparticles

Nowadays, it can be found several methods for the preparation of hybrid materials based on metal nanoparticles (MNPs) (*e.g.* AuNPs, AgNPs) cover by polymers but in the most of cases the protecting agent of the nanoparticles is not chiral.

In literature, there are few examples of hybrid material formed by helical polymers and metal nanoparticles. Deng *et Al.* reported that the first example of hybrid materials consist on AuNPs and optically active copolymers based on achiral thiol unit and chiral unit poly(*N*-propargylamide) as shell of the nanoparticles. The function of the polymeric shell is act as protecting ligand and a chirality inducer in the AuNPs. Interestingly, the hybrid material shows a different absorption of (*R*)-(+)- and (*S*)-(-)-1-phenylethylamines (Figure 22).[66]

[65] Pellegrino, T.; Sperling, R. A.; Alivisatos, A. P.; Parak, W. J.; *J. Biomed. Biotechnol.* **2007**, 26796.
[66] Zhang, C.; Song, C.; Yang, W.; Deng, J.; *Macromol. Rapid Comm.* **2013**, *34*, 1319.

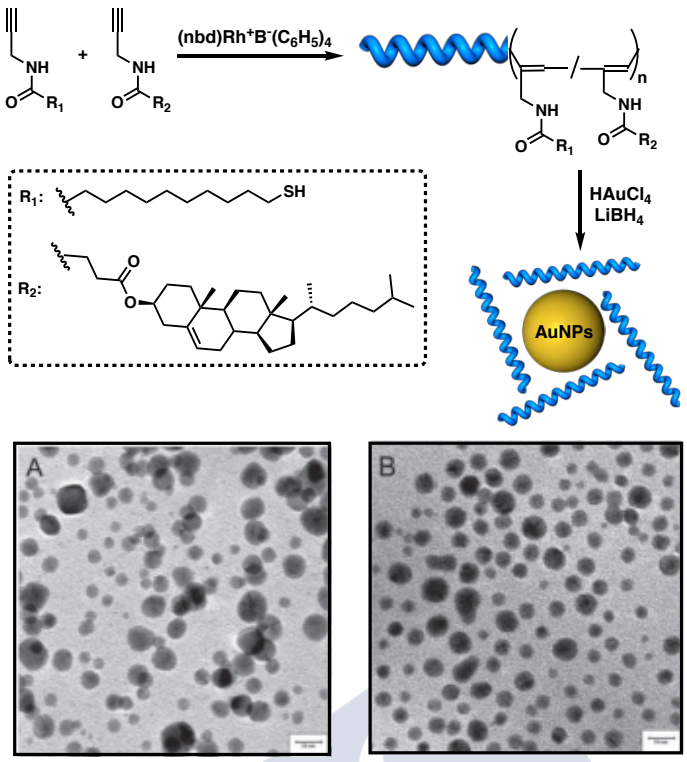

Figure 22. Schematic representation for the preparation of Deng hybrid materials and TEM images for the hybrid material.

Wu *et Al.* described another example for the preparation of hybrid materials. In this work, Fe_3O_4 magnetic nanoparticles with helical poly(phenylisocianide)s was described. To prepare this nanomaterial, two methods were employed: *grafting from* and *grafting onto*. In the first method, *grafting from*, alkyne-Pd(II) catalysts are linked to the surface of the Fe_3O_4 nanoparticles and then, they were polymerized using enantiopure phenyl isocianide bearing alanine ester as pendant. The magnetic and optical active nanomaterials were fully characterized by FT-IR, CD, UV-Vis and DLS measurements (Figure 23).

In the second strategy, *grafting onto*, triethoxysilanyl-terminated single handed helical poly(phenylisocianide)s bearing alanine ester as pendant were prepared. Then, the helical polymers were linked to the magnetic Fe_3O_4 nanoparticles forming a magnetic and optical active nanomaterial. Interestingly, *grafting from* method showed higher nanoparticles density than *grafting to* method. Finally, these hybrid materials materials can be used in enantiomeric crystallization of racemic threonine (Figure 23).[67]

[67] Lin, Y.-L.; Chu, J.-H.; Na, L.; Wu, Z.-Q.; *Macromol. Rapid Commun.* **2018**, *39*, 1700685.

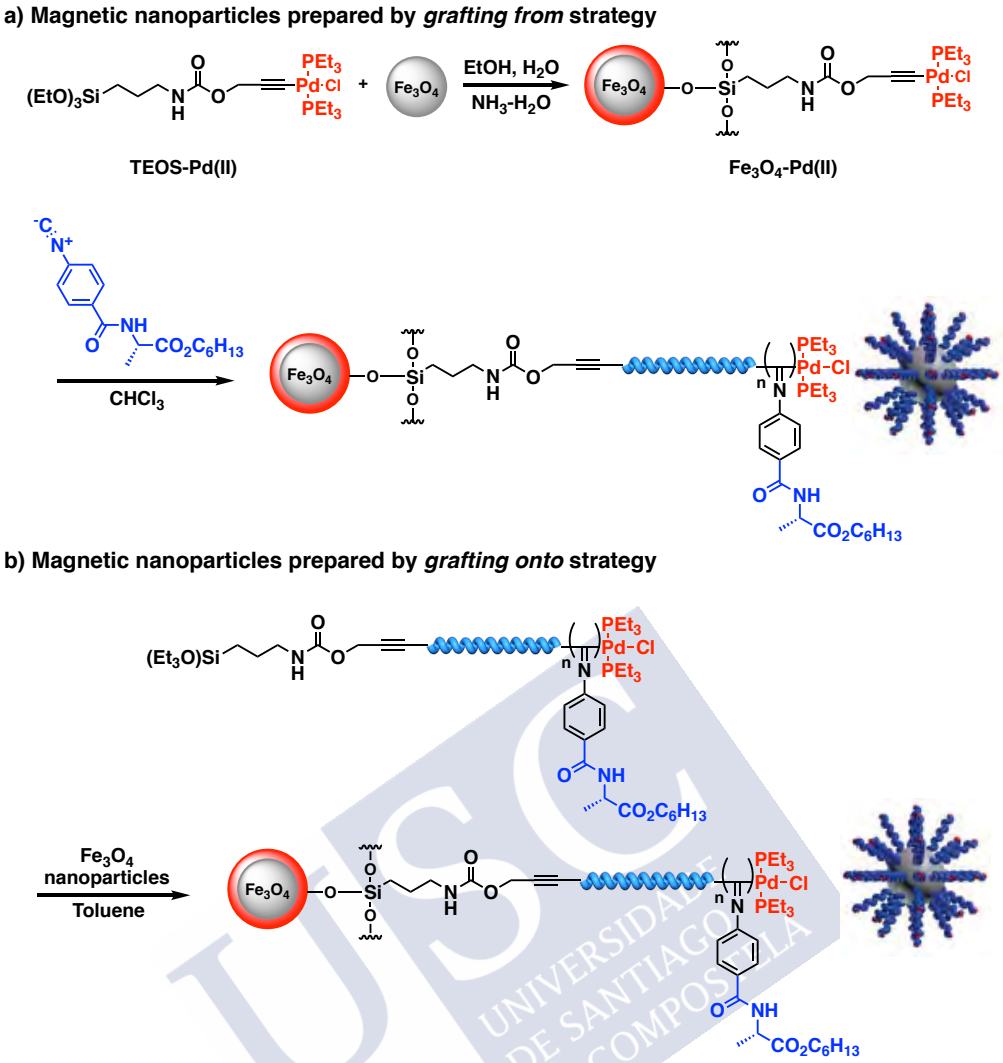

Figure 23. Schematic representation for the preparation of magnetic nanoparticles via a) *grafting from* and b) *grafting onto*.

In another interesting work, Tang and co-workers described the functionalization of achiral PPAs with CdS nanorods. In this work, the method involves the decoration of the thiolated monomers with CdS nanorods and then the polymerization. It is important to note the hybrid material cannot obtain by direct incorporation of the polymer into the CdS nanorods due to the toxicity effect of the thiol group on the Mo, W, Ta and Nb catalyst. On the other hand, when $[Rh(cod)Cl]_2$ is used as catalyst, it was obtained insoluble product probably due to the oxidation on the thiol groups. The hybrid material showed a good solubility in DCM, THF and $CHCl_3$.[68]

This Thesis is focused on the development of hybrid materials based on PPAs and metal nanoparticles.

[68] Xu, H-P.; Xie, B.-Y.; Yuan, W.-Z.; Sun, J.-Z.; Yang, F.; Dong, Y.-Q.; Qin, A.; Zhang, S.; Wang, M.; Tang, B. Z.; *Chem. Commun.* **2007**, 1322.

6. Structural approaches in PPAs

6.1 Determination of the *cis* content in the polyene backbone

The polymerization of the phenylacetylenes monomers using Rh(I) catalysts produces conjugated double bonds in the main chain. These double bonds can adopt a *cis* configuration [*cis-cisoidal* (*c-c*) or *cis-transoidal* (*c-t*)] and form poly(phenylacetylene)s (PPA)s in high yields and low polydispersity.[69,70]

The dihedral angle (ω_1) of the sigma bond σ C (sp^2) can adopt angles between 0^o and 180^o where $\omega_1 < 90^o$ indicates a *cis-cisoidal* configuration and $\omega_1 > 90^o$ form a *cis-transoidal* configuration and the sense of the helix $\omega_1 < 0^o$ *M* helix and $\omega_1 > 0^o$ *P* helix.

Percec *et Al.* carried out studies to distinguish the different four configurations that can adopt the conjugated double bonds in PPAs: *trans-cisoidal* (*t-c*), *trans-transoidal* (*t-t*), *cis-cisoidal* (*c-c*) and *cis-transoidal* (*c-t*). For that, NMR studies and other theoretical studies were carried out.

Interestingly, *trans* PPAs shows the vinylic protons signals between 6.20-7.20 ppm in ^{1}H-NMR. Furthermore, *trans-cisoidal* configuration shows two aromatic protons upfield shifted that the rest of the aromatic protons in the polymer. In the case of *cis-transoidal* configuration, ^{1}H NMR shows all the aromatic resonances in the same region.

The same study was carried out for polymers with *cis* configuration in the conjugated double bonds. ^{1}H-NMR spectra show in all cases the resonances in the vinylic protons around 5.60-5.80 ppm (Figure 24a). In the case of *cis-cisoidal* configurations, one aromatic proton upfield shiffted compared with the aromatic protons of the polymers. On the other hand, *cis-transoidal* polymers shows two aromatic protons shifted upfield.

For example, a *cis-cisoidal* polymer shows in ^{1}H-NMR, the vinylic proton resonances at 5.80 ppm, 1H *ortho*- at 6.70 ppm, 1H *para*- and *meta*- at 6.85 ppm. To calculate the *cis*-content in PPAs, Percec *el Al.* propose the following equation.

$$\%\ cis\text{-content} = [A_{cis}/(A_{total} \times H_{total})] \times 100$$

Equation 8. Equation to determine the % *cis*-content in PPAs.

[69] a) Kishimoto, Y.; Eckerle, P.; Miyatake, T.; Ikariya, T.; Noyori, R.; *J. Am. Chem. Soc.* **1994**, *116*, 12131. b) Tabata, M.; Yang, W.; Yokota, K.; *Polym. J.* **1990**, *22*, 1105. c) Furlani, A.; Napoletano, C.; Russo, M. V.; Feast, W.; *J. Polym. Bull.* **1986**, *16*, 311.

[70] a) Simonescu, C.I.; Percec, V.; *Prog. Polym. Sci.* **1982**, *8*, 133. b) Simonescu, C.I.; Percec, V. J.; *Polym. Sci.: Polymer Symposia* **1980**, *67*, 43. c) Simionescu, C. I.; Percec, V.; J. *Polym. Sci., Polym. Chem. Ed.* **1980**, *18*, 147. d) Simionescu, C. I.; Percec, V.; J. Polym. Sci., *Polym. Lett. Ed.* **1979**, *17*, 421. e) Simionescu, C. I.; Percec, V.; Dumitrescu, S. J. *Polym. Sci., Polym. Chem. Ed*. **1977**, *15*, 2497.

Where A_{cis} is the area of vinylic proton in ^{1}H-NMR (5.60-5.80 ppm), A_{total} is the total area observed in^{1}H-NMR and H_{total} is the number of pendant group protons.

Raman spectroscopy is a very useful technique to extract information about the configuration of the conjugated double bonds in PPAs. In the case of *cis-cisoidal* or *cis-transoidal* presents characteristic resonances bands of the polyene skeleton around 1580 cm^{-1} ($C=C_{cis}$), 1335 cm^{-1} ($C-C_{cis}$) and 965 cm^{-1} ($C-H_{cis}$) (Figure 24b). On the other hand, in the case of *trans-* configuration PPAs, Raman characteristic bands appear around 1475 cm^{-1} ($C=C_{trans}$), 1200 cm^{-1} ($C-C_{trans}$) and 740 cm^{-1} ($C-H_{trans}$).[71] Moreover, IR spectroscopy can give information around 1015 cm^{-1} ($C-H_{trans}$) and 740 cm^{-1} ($C-H_{cis}$) deformation bands.[72]

Using the combination of Raman and ^{1}H-NMR techniques it is possible to determine the configuration of the double bonds (*cis* or *trans*) in PPAs but it is impossible to distinguish between *cis-cisoidal* and *cis-transoidal* configurations. For this reason, another powerful technique such as Differential Scanning Calorimetry (DSC) is employed to determine the configuration of the PPAs.

DSC shows different patterns depending on if the PPAs adopt a *cis-cisoidal* or *cis-transoidal* configuration. Thus, *cis-cisoidal* PPAs just show an exothermic transition peak around 200-240^{o}C due to the isomerization process from *c-c* to *c-t*. On the contrary, *cis-*transoidal thermograms shows two exothermic peaks around 140^{o}C and 240^{o}C corresponding to isomerizations from *c-t* to *c-c* and *c-c* to *t-t* respectively (Figure 24c).[73]

Nevertheless, it is necessary to use other techniques to extract more information about the conjugated double bonds of the PPA. For instance, Ultraviolet-Visible spectroscopy (UV-Vis). From this technique, it is possible to obtain information about of the compression/stretched degree in the polyene backbone. Thus, bathochromic shift in the vinyl region of the PPAs (400 nm) indicates an elongation in the helical structure due to the double bonds are more conjugated. On the other hand, hypsochromic shift indicates that the double bonds are less conjugated and the helical structure is more compressed than in the first case.[74]

---

[71] a) Misayaka, A.; Sone, T.; Mawatari, Y.; Setauesh, S.; Müllen, K.; Tabata, M.; *Macromole. Chem. Phys.* **2006**, *207*, 1938. b) Huang, K.; Mawatari, Y.; Miyasaka, A.; Sadahiro, Y.; Tabata, M.; Kashiwaya, Y.; *Polymer* **2007**, *48*, 6366. c) Miyasaka, A.; Mawatari, Y.; Sone, T.; Tabata, M.; *Polym. Degrad. Stab.* **2007**, *92*, 253.

[72] a) Ito, T.; Shirakawa, H.; Ikeda, S. *J. Polym. Sci., Part A: Polym. Chem.* **1974**, *12*, 11-20. b) Shirakawa, H.; Ikeda, S.; *Polym. J.* **1971**, *2,* 231.

[73] a) Motoshige, A.; Mawatari, Y.; Yoshida, Y.; Motoshige, R.; Tabata, M.; *Polym. Chem.* **2014**, 5, 971. b) Yoshida, Y.; Mawatari, Y.; Motoshige, A.; Motoshige, R.; Hiraoki, T.; Wagner, M.; Müllen , K.; Tabata, M.; *J. Am. Chem. Soc.* **2013**, 135, 4110. c) Motoshige, A.; Mawatari, Y.; Motoshige, R.; Yoshida, Y.; Tabata, M.; J. Polym. Sci., Part A: *Polym. Chem*. **2013**, *51*, 5177.

[74] a) Percec, V.; Peterca, M.; Rudick, J. G.; Aqad, E.; Imam, M. R.; Heiney, P. A.; *Chem. Eur. J.* **2007**, *13*, 9572. b) Percec, V.; Rudick, J. G.; Peterca, M.; Aqad, E.; Imam, M. R.; Heiney, P. A.; *J. Polym. Sci., Part A: Polym. Chem.* **2007**, *45*, 4974. c) Percec, V.; Aqd, E.; Peterca, M.; Rudick, J. G.; Lemon, L.; Ronda, J. C.; De, B. B.; Heiney, P. A.; Meijer, E.

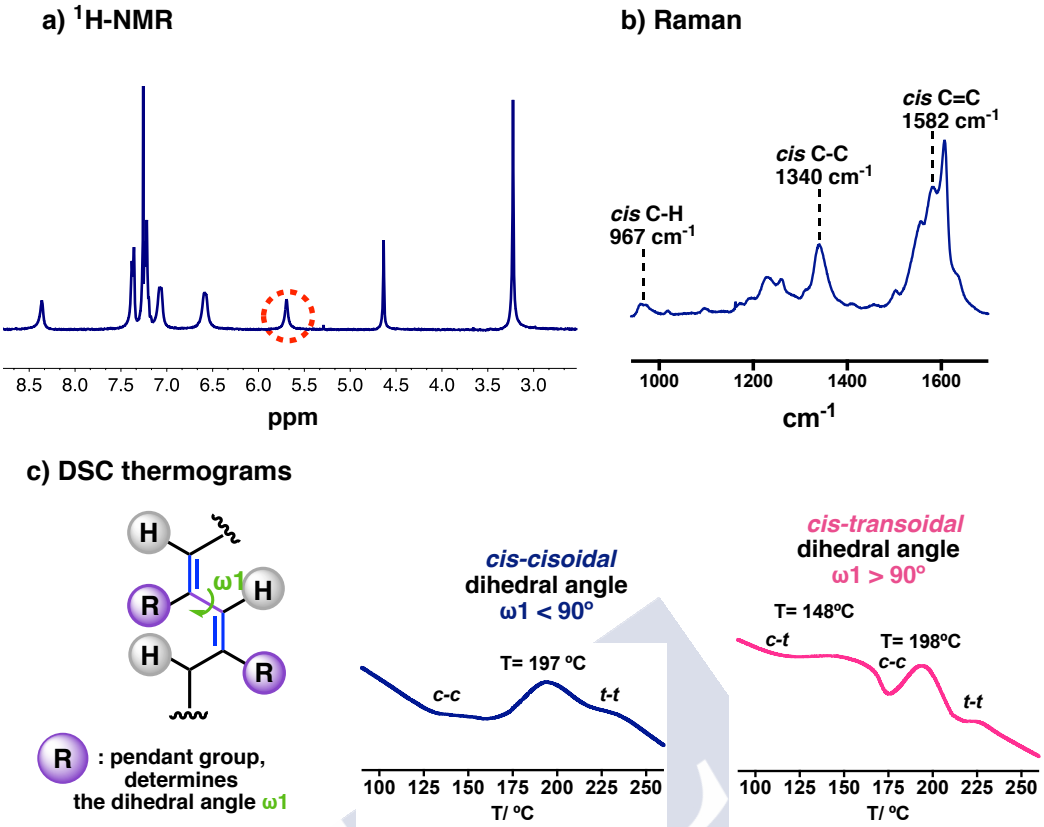

Figure 24. a) ^{1}H-NMR, b) Raman spectra and c) DSC thermograms of PPAs with conjugated double bonds in *cis* configuration.

6.2 Determination of the helical sense in PPAs

To determine the helical sense in PPAs it is necessary to use the combination of several techniques. Normally, techniques with polarized light such as CD and optical rotation are used.

6.2.1 Optical rotation

The observed optical rotation (α) gives values related to the degree of deviation of the polarized light when interacts with chiral molecules in solution. The optical rotation depends on concentration, structure of the molecule, and length of the cubet, solvent and temperature. To avoid ambiguities, It was established a standard value of α, the specific rotation [α]. This value is calculated from equation 9, where *t* is the temperature, λ is the wavelength, α is the observed optical rotation, *l* is the length of the cubet and *c* is the concentration for the solution.[75]

W.; *J. Am. Chem. Soc.* ***2006***, *128*, 16365. d) V. Percec, J. G. Rudick, M. Peterca, M. Wagner, M. Obata, C. M. Mitchell, W. D. Cho, V. S. K. Balagurusamy and P. A. Heiney.; *J. Am. Chem. Soc*. **2005**, *127*, 15257.

[75] Vollhardt, P.; Schore, N.; *Organic Chemistry: Structure and Function.;* 5nd ed., Omega, **2008**, p 174.

$$[\alpha]_{\lambda}^{t} = \frac{\alpha}{l \cdot c}$$

Equation 9. Equation to calculate specific optical rotation [α].

This technique presents some disadvantages compared to CD. For example, it has a low sensitivity due to it is necessary a high amount of sample to obtain α measurement. In helical macromolecules such as PPAs, [α] value is at least one order of magnitude higher when compared with the obtained data for the monomeric unit.

6.2.2 Circular Dichroism

Circular Dichroism (CD) is a very useful technique to determine excess in the helical sense in macromolecules. When Circular Polarised Light (CPL) interacts with the samples, CD gives the differences in the absorption between right-handed circularity polarised light (*R*-CPL) and left-handed circularity polarised light (*S*-CPL) in molecules or macromolecules with chiral chromospheres.

CD spectroscopy allows determining the folding in biomacromolecules such as peptides, showing if they are folded such as α-helix, β-sheet or random coil. Moreover, it is possible to determine different structural, kinetic and thermodynamic parameters.[76,77]

Interestingly, CD spectroscopy can detect changes on the CD traces (helical enhancement or helical inversion) of PPAs due to the interaction of the macromolecules with external stimuli such as temperature, metal ions, pH, among others. In our researcher group, there are published several articles where the external stimuli affect to the secondary structure of the PPAs.

Finally, the amount of sample needed to employ CD spectroscopy is smaller than in the case optical rotation. Less than 1 mg of sample is enough to carried out the experiments.

Using the combination of these techniques (IR, NMR, CD, optical rotation and Raman) is possible to determine the helical sense of the PPAs but it is not possible to built a 3D model of the helical polymer. To do that, it is necessary to obtain other parameters such as packing angle and helical pitch. To solve this problem, X-ray diffraction and Atomic Force Microscopy (AFM) are employed.

[76] a) Hammes, G. G.; Circular Dichroism, Optical Rotatory Dispersion, and Fluorescence Polarization, In *Spectroscopy for the Biological Sciences*, John Wiley & Sons, Inc. **2005**, p 63. b) Bereova, N.; Nakanishi, K., Woody, R. W., *Circular Dichroism: Principles and Applications*, 2nd ed., Wiley-VCH: New York, **2000**, p 912.

[77] a) Nakanishi, K.; Berona, N; Circular Dichroism: Principles and Applications; ed por N. Berova, K. Nakanishi, W. R Woody, **2000**, *Wiley-VCH,* 2nd ed, Cap 13, p 361.b) Harada, N.; Nakanishi, K. *Circular Dichroic Spectroscopy-Exciton Coupling in Organic Stereochemistry*, 2nd ed., University Science Books: Mill Valley, CA, **1983**.

6.2.3 X-ray diffraction

X-ray diffraction can give information related to the secondary structure of PPAs. For this purpose, it is necessary to prepare oriented films of the polymers, being the main difficult the preparation of the sample.

From this technique, information about helical pitch, helix length and interpendant distances can be obtained. Nevertheless, important information about helical sense of PPAs cannot determine with this technique.[78]

6.2.4 Atomic Force Microscopy (AFM)

AFM allows the visualization of the secondary structure of helical PPAs. Using this technique, different parameters such as helical sense, helical pitch or packing angle can be obtained in helical PPAs. To determine this information, the preparation of the samples becomes a very important factor because only well-ordered monolayers are suitable to distinguish the information in the AFM image.[79,80]

Moreover, the monolayer must be form in an adequate substrate. For instance, highly oriented pyrolytic graphite (HOPG) for low polar polymers and mica for polar polymers. The selection of an adequate substrate will allow improving the intermolecular interactions between the helical PPA and the substrate. Different protocols have been developed to obtain well-ordered monolayers and good AFM images.

- **Drop casting**

Yashima *et Al.* studied the structure of PPAs by drop casting in different substrates: mica and highly oriented pyrolytic graphite (HOPG). A copolymer based on two pendants group: an achiral C_{60}-bound and an optically active amine was studied. This copolymer was drop casting on mica and HOPG, and the morphologies of the assemblies were studies by AFM. The AFM images on mica showed isolated spherical aggregates due to the aggregation of C_{60} as consequence of repulsion between hydrophobic C_{60} and hydrophilic mica (Figure 25). On the other hand, AFM images on HOPG showed extended copolymer chains with some isolated particles. From these images, it can be concluded that the attractive force between pendant C_{60} and the substrate plays a critical role in the morphology of this type of copolymers.[81]

[78] Yashima, E.; *Polym. J.* **2010**, *42*, 3.
[79] Kumaki, J.; Sakurai, S.-I.; Yashima, E.; *Chem. Soc. Rev.* **2009**, *38*, 737.
[80] Freire, F.; Quiñoá, E.; Riguera, R.; *Chem. Rev.* **2016**, *116*, 1242.
[81] Nishimura, T.; Takatani, K.; Sakurai, S.; Maeda, K.; Yashima, E.; *Macromolecules* **2002**, *41*, 3602.

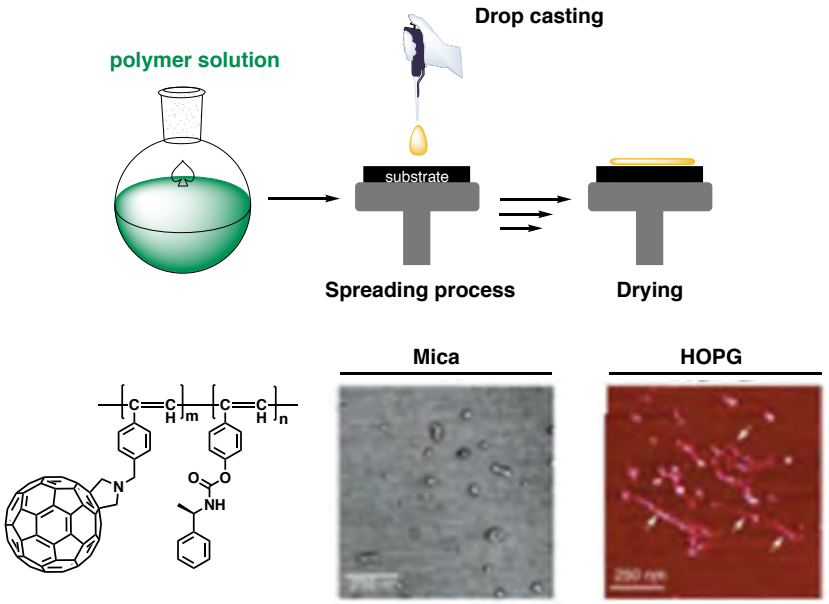

Figure 25. Schematic representation for the drop casting procedure.

- **Spin coating and solvent vapour exposure**

Yashima reasoned another approach, the introduction of long alkyl chains as pendants should favour the self-assembly of PPA chains due to the interdigitation between long chain groups.[82,83,84]

The sample was prepared by spin coating a dilute solution of PPA onto the substrate (mica or HOPG) and kept under a solvent atmosphere overnight to favour the self-assembly of polymer chains.[58] Using this protocol, it can be obtained the helical structure of the PPAs derived from *L* and *D*-alanine decyl ester (Figure 26).[58] AFM images of poly-*L*-alanine decyl ester revealed the presence of a helical pitch of 2.34 nm and a packing angle of 40° where the PPA describes a (external) *M* helix with two residues per turn. Moreover, the internal helix adopts a *c*-*t* configuration and describes the opposite helical sense (*P* helix) (Figure 26).

[82] Okoshi, K.; Sakurai, S.-I.; Ohsawa, j. K.; Kumaki, J.; Yashima, E.; *Angew. Chem. Int. Ed.* **2006**, *45*, 8173.
[83] Sakurai, S.-I.; Okoshi, K.; Kumaki, J.; Yashima, E.; *Angew. Chem. Int. Ed.* **2006**, *45*, 1245.
[84] Sakurai, S.-I.; Okoshi, K.; Kumaki, J.; Yashima, E.; *J. Am. Chem. Soc.* **2006**, *128*, 5650.

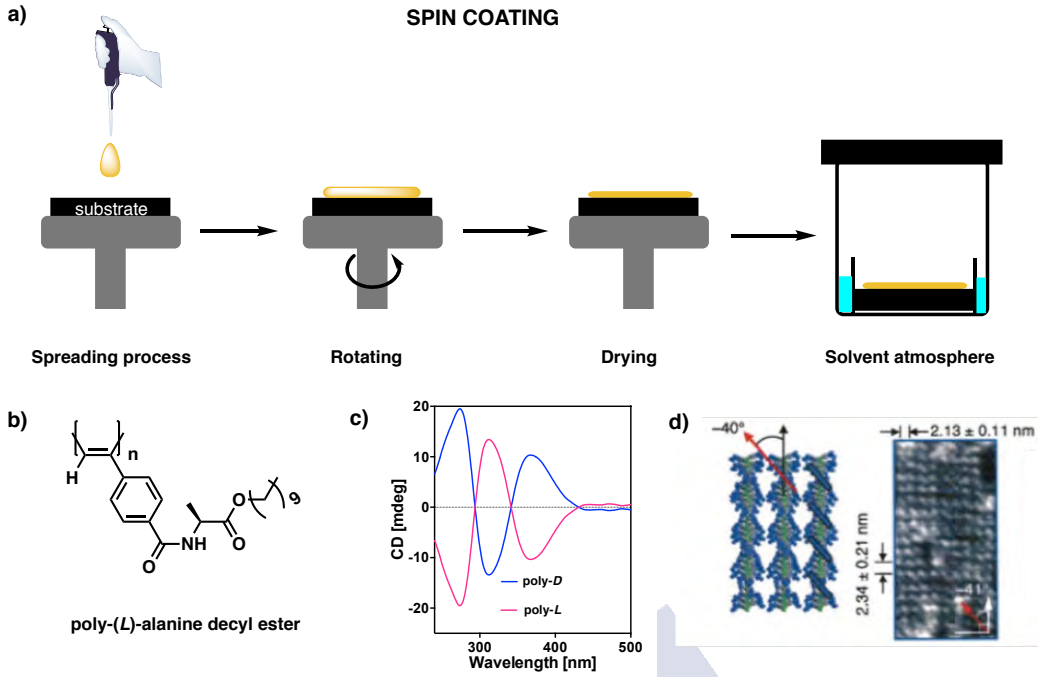

Figure 26. a) Schematic representation for spin coating. b) Structure for poly-(*L*)-alanine decyl ester. c) CD spectra for poly-(*L*)-alanine decyl ester and poly-(*D*)-alanine decyl ester. d) AFM images of 2D crystals self-assembled poly-(*L*)-alanine decyl ester on HOPG.

In our research group, it was applied this protocol to helically racemic poly-(*R*)-**15** on HOPG but it was not observed the presence of 2D crystals due to the dynamic behaviour of this PPA.

The dynamism in the polymer is related to the two possible conformations in the pendant group. This PPA derived from the anilide of (*R*)-α-methoxy-α-phenylacetic acid [poly-(*R*)-**15**] present two conformations in equilibrium (*ap*: carbonyl and methoxy groups antiperiplanar oriented and *sp*: carbonyl and methoxy groups synperiplanar oriented).[23] This conformational equilibrium is transmitted to a 1:1 equilibrium *P/M* helix.

Interestingly, well 2D crystals can be obtained when the 1:1 equilibrium is shifted to *P* or *M* helix by the addition of divalent or monovalent metal ions.[23] Thus, when a diluted solution of helical polymer-metal complex (HMPC) is spin coated onto HOPG and left under a THF atmosphere overnight, it can be obtained well ordered 2D-crystals. This AFM images revealed that the helical pitch is 3.2 nm, the packing angle is 60° and the helical sense depends on the type of metal ions added (*M* helix for monovalent metal ions and *P* helix for divalent metal ions). This information in combination with NMR, Raman, DSC and CD allows knowing the secondary structure of the PPA (Figure 27).

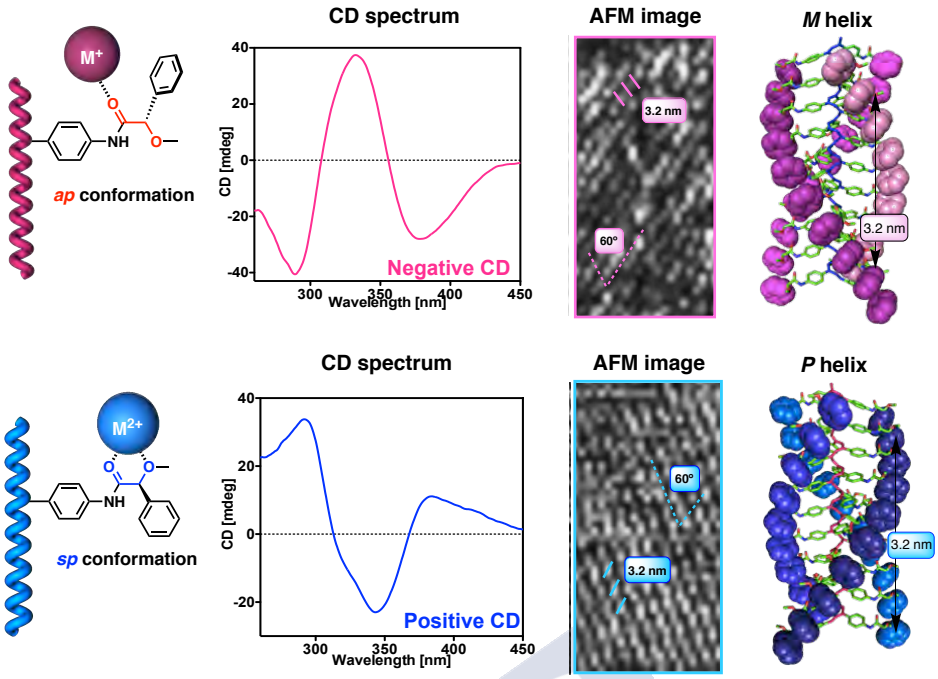

Figure 27. Chiral amplification for poly-(*R*)-**15** in presence of monovalent and divalent metal ions and the corresponding AFM images.

- **Spin coating and thermal annealing**

Percec and co-workers develop a similar protocol based on spin coating procedure, but in this case the sample is also subjected to thermal annealing. This protocol will produce 2D crystals on HOPG and mica and visualize the self-organization of individual dendronized PPAs using AFM. A library of dendronized PPAs with long alkyl chains were prepared for doing those experiments.[85,86]

Thus, *c-t* poly(carbazolyacetylene) (poly-**20**) after spin coating on graphite with thermal annealing at 100°C was observed such as individual polymer chains using AFM. This example shows the high potential of this polymer to obtain well-ordered monolayers (Figure 28).

[23] Freire, F.; Seco, J. M.; Quiñoá, E.; Riguera, R.; *Angew. Chem. Int. Ed.* **2011**, *50,* 11692.

[85] Percec, V.; Obata, M.; Rudick, J. G.; De, B. B.; Glodde, M.; Bera, T. K.; Magonov, S. N.; Balagurusamy, V. S. K.; Heiney, P. A.; *J. Polym. Sci. Part A: Polym. Chem.* **2002**, *40*, 3509.

[86] Percec, V.; Rudick, J. G.; Peterca, M.; Staley, S. R.; Wagner, M.; Obata, M.; Mitchell, C. M.; Cho, W.-D.; Balagurusamy, V. S. K.; Lowe, J. N.; Glodde, M.; Weichold, O.; Chung, K. J.; Ghionni, N.; Magonov, S. N.; Heiney, P. A.; *Chem. Eur. J.* **2006**, *12*, 5731.

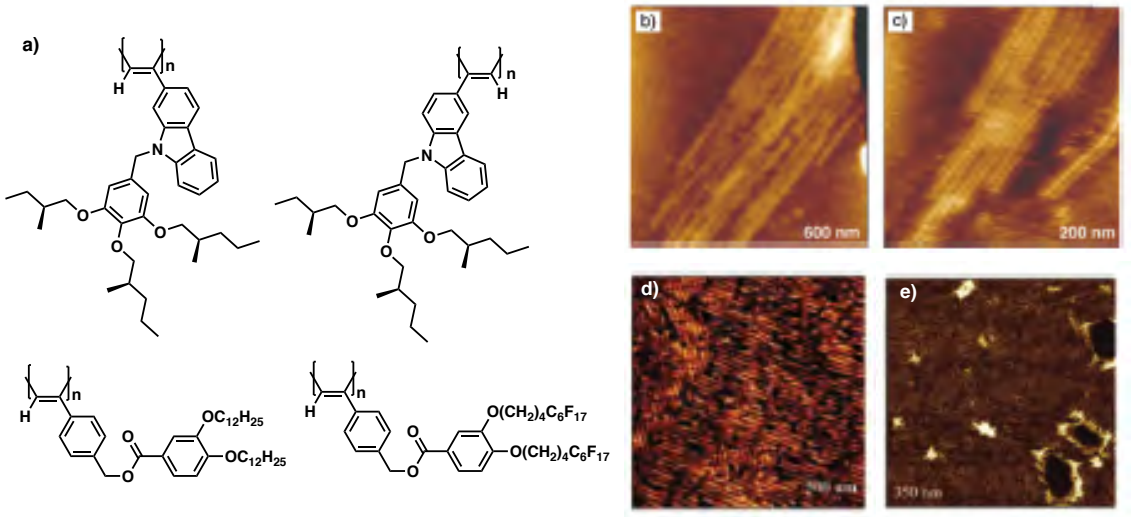

Figure 28. a) Examples of the structure for dendronized PPAs. b), c), d) and e) AFM images on graphite for this type of polymers.

- **Langmuir-Blodgett method**

The previous methods for the preparation of monolayers consist on the evaporation of a solution of the polymer on a solid support, and the monolayer is formed at the air/solid interface. With this protocol plays a very important role, the interactions of the polymer with the support and the evaporation rate of the solvent.

The Langmuir-Blodgett method (LB) is used to prepare monolayers in air/water interphase.[87,88] In this protocol, the hydrophobic/hydrophilic interaction between polymer and support play a special relevance.

Tang *et Al.* reported the formation of monolayers using this method in PPAs with hydrophobic backbone but with hydrophilic pendants groups derived from aminoacids. For that, they prepared PPAs derived from *L*-alanine and *L*-valine methyl ester where the PPA can self-assembly due to their amphiphilic character. To obtain the AFM images, mica was used as substrate where the hydrophilic amino acids residues interact (Figure 29).[89]

[87] Roberts, G. G.; *Langmuir-Blodgett Films*, Plenum, New York, 1990.

[88] Kawauchi, T.; Kumaki, J.; Kitaura, A.; Okoshi, K.; Kusanagi, H.; Kobayashi, K.; Sugai, T.; Shinohara, H.; Yashima, E.; *Angew. Chem. Int. Ed.* **2008**, *47*, 515.

[89] a) Bing, L; Lam, J. W.; Zhen-Qiang, Y.; Tang, B. –Z.; *Langmuir* **2012**, *28*, 5770. b) Li, B.; Kang, Z. K.; Cheuk, K.; Wan, L.; Ling, L.; Bai, C.; Tang, B. Z.; *Langmuir* **2004**, *20*, 7598.

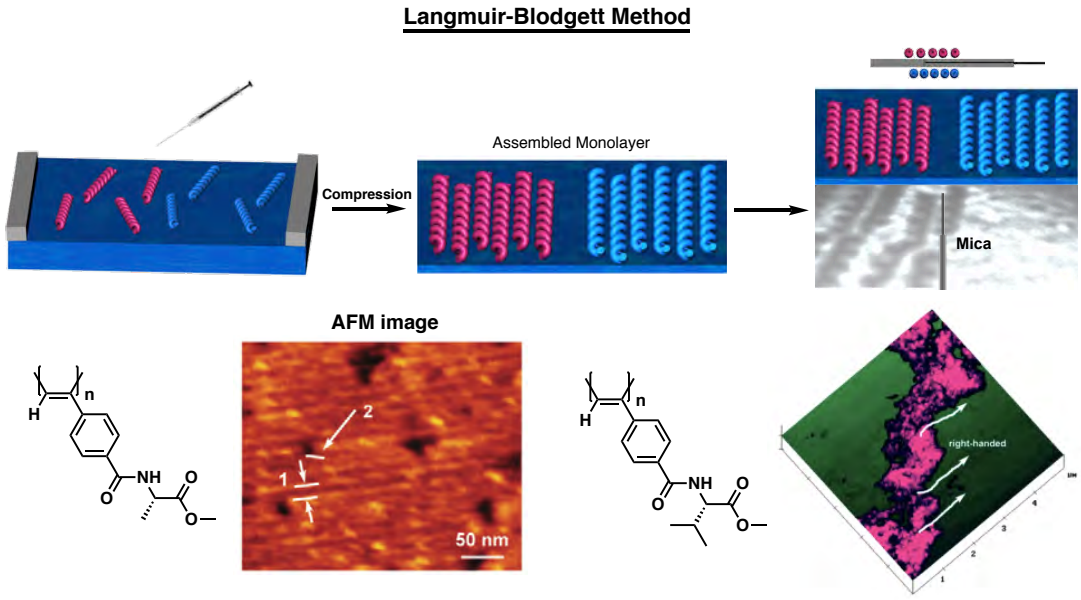

Figure 29. Conceptual representation of Langmuir-Blodgett method.

- **Langmuir-Schaefer method**

In literature, it can be found that the HOPG is the best substrate to obtain AFM images with good quality. This substrate is more hydrophobic than mica and can interact better with the PPAs to form the monolayer. Unfortunately, the HOPG hydrophobic properties are incompatible with its use with LB because the substrate has to be extracted from the water layer.[90]

To prepare good monolayer of PPAs in HOPG, Langmuir-Schaefer[91] approach (LS) is employed, a modification of LB procedure. In this method, the monolayer is expholiated from the interphase allowing its transfer to HOPG.[92]

Following LS protocol, good monolayers were obtained from secondary structure of highly dynamic poly-**15**. For that, a dilute solution of poly-**15** in $CHCl_3$ was spread droplet by droplet onto a pool of water. Then, smooth evaporation of the $CHCl_3$ occurred, followed by a compression of the polymer until compact monolayer was formed.

Finally, the monolayer was transferred from the air/water interphase to HOPG by exfoliation. AFM images showed well-ordered monolayers, with uniform fields composed by right-handed or left-handed helical chains. The good quality of the AFM images allows determining the helical sense as well as the helical pitch (3.2 nm) and the packing angle (±60°). These values are in concordance with those of the polymer complexed with monovalent and divalent metal ions. They indicate that poly-**15** adopts a *c-c* polyene backbone where the

[90] Freire, F.; Quiñoá, E.; Riguera, R.; *Chem. Commun.* **2017**, *53*, 481.
[91] Ulman, A.; *An introduction to Ultrathin, Organic films –From Langumir-Blodgett To Self-Assembly,* Academic Press, New York, 1991.
[92] Rodríguez, R.; Quiñoá, E.; Riguera, R.; Freire, F.; *Nanoscale* **2016**, *8*, 3362.

helices defined by the polyene and the pendant group are in the same direction. Interestingly, AFM images reveal the presence of left- and right-handed oriented superhelices (Figure 30).[93,94,95,96]

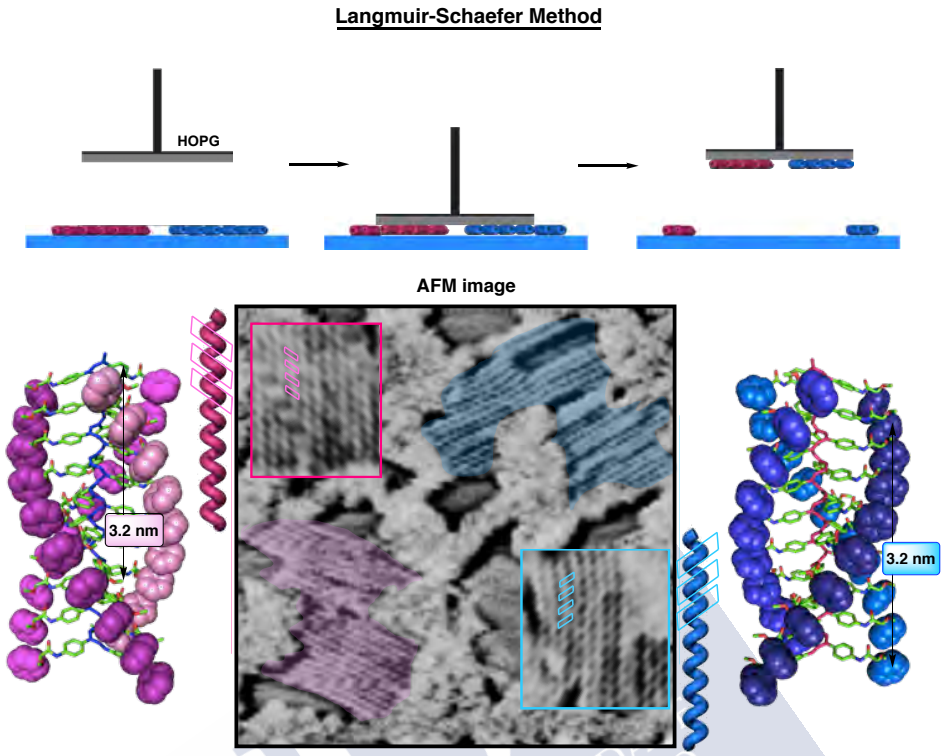

Figure 30. Conceptual representation of Langmuir-Schaefer method.

In another interesting work from our group, LS method was used to study the secondary structure of *meta* substituted PPAs: *m*-poly-**15** bearing the *meta* anilide of (*R*)-α-methoxy-α-phenylacetic acid (MPA) and *m*-poly-**17** bearing the meta benzamide of phenylglycine methyl ester (PGME) as the pendant.[40]

In the case of *m*-poly-**15** (poly-*m*-MPA), the PPA exists in solution in equilibrium between a compressed *c-c* helix (3.2 nm of helical pitch and 60° of packing angle) and a more stretched helix *c-t* helix (5.2 nm of helical pitch and 40° of packing angle). The internal helical senses of the both helices are the same (*P* helices), whereas the external helix described by the pendants rotates in opposite direction (*P* helical sense for the compressed and *M* helical sense for the stretched one) (Figure 31).

[40] Rodríguez, R.; Quiñoá, E.; Riguera, R.; Freire, F. *J. Am. Chem. Soc.* **2016**, *138*, 9620.
[93] Sakurai, S.; Kuroyanagi, K.; Nunokawa, R.; Yashima, E.; *J. Polym. Sci. Part A: Polym. Chem.* **2004**, *42*, 5838.
[94] Matsushita, S.; Azagi,K.; *J. Am. Chem. Soc.* **2015**, *137*, 9077.
[95] Mori, T.; Kyotani, M.; Azagi, K.; *Chem. Sci.* **2011**, *2*, 1389.
[96] Akagi, K.; *Chem. Rev.* **2011**, *109*, 5354.

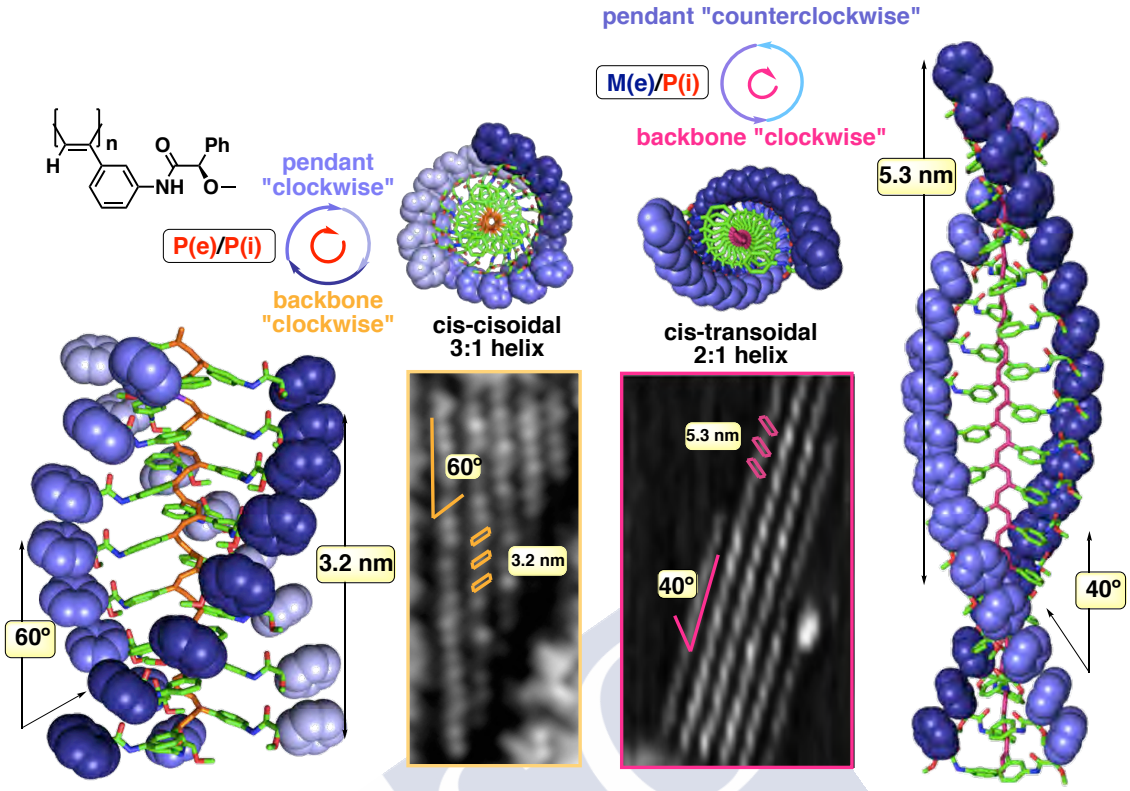

Figure 31. Molecular models for *m*-poly-**15** and and AFM images for the compressed and stretched helices.

In addition, *m*-poly-**17** is composed by two stretched *c-t* helices in equilibrium (one more stretched than the other). AFM images showed 3.8 nm of helical pitch and 60° of packing angle in the less stretched helix. On the contrary, the most stretched helix presents 5.3 nm of helical pitch and 35° of packing angle. The helical senses of internal helix are the same in both cases (*M* helix) whereas the external helix defined by the pendants groups is opposite (*P* helix).

7. Architecture of PPAs

PPAs are a family of dynamic helical polymer that can interconvert the helical sense by addition of external stimuli (*e.g.* Temperature, metal ions, pH, etc). The determination of the secondary structure of PPAs is compolicated due to the dynamic behaviour of the helix of these polymers, which presents variations both in sense and in the chain elongation.

Normally, the structural determination of PPAs is based on the combination of several techniques such as ^{1}H-NMR, Raman spectroscopy, CD, UV-Vis, DSC thermograms and X-ray

It is very important to note here that PPAs are composed by two coaxial helices. The internal one is constituted by the polyenic skeleton, resulting from the positive/negative *c-c* or *c-t* dihedral angle can be studied by CD (Figure 32).

The external one is defined by the orientation of the pendant groups around the axis of the backbone. This helix can be observed using AFM in solid stated when the PPAs is deposited on a solid support.

Interestingly, the helical sense of both helices can be coincident or not, and therefore, the characterization just using CD is not satisfactory. For this reason, solid phase techniques are used to determine the orientation of the external helix (Figure 32). For example, AFM images allow the visualization of the secondary structure of the PPA, giving important information such as packing angle, helical pitch and the helical sense.

From previous studies of the group, it was demonstrated that PPAs with a *c-c* structure show a compressed helices with three residues per turn (3/1). In this case, both helices (internal and external) rotate in the same direction (*e.g.* CD shows a positive Cotton Effect for *P* internal helix and AFM images shows *P* for the external helices). On the other hand, PPAs with a *c-t* structure form a more stretched helix with 2 residues per turn (2/1). Moreover, in this case both helices rotate in opposite directions (*e.g.* CD shows a positive Cotton Effect for *P* internal helix and AFM images shows *M* for the external helices).[40]

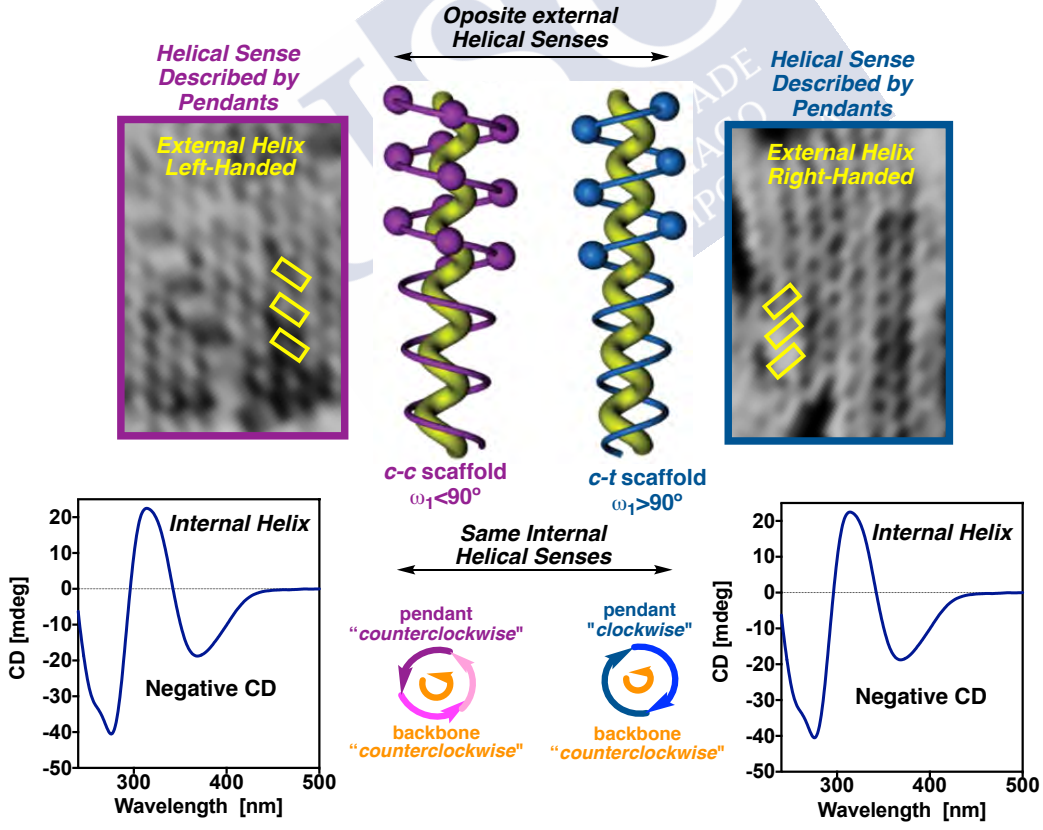

Figure 32. Schematic representation for different helical senses adopted by PPAs. Internal and external helices, CD studies and AFM images.

[40] Rodríguez, R.; Quiñoá, E.; Riguera, R.; Freire, F. *J. Am. Chem. Soc.* **2016**, *138*, 9620.

8. Supramolecular assemblies of PPAs

The evolution of chemistry in the last 60 years can be illustrated by the introduction of just a few new concepts. One is *macromolecule*,[97] whose importance was recognized in the 1953 Nobel Prize to Prof. Staudinger, and the other two are *molecular recognition* and *supramolecular assembly*,[98,99] which gave the 1987 Nobel Prize to Profs. Cram, Lehn and Petersen.

Supramolecular assemblies may present different architectures (films, layers, membranes, spheres, etc.) depending on the type of bonding that binds the molecular components together and how they are spatially arranged. If the components are chiral, the transference of their absolute configuration to the assembly an the presence of supramolecular chirality constitute an especially appaling topic.[100,101,102,103,104]

In this section, it will be summarized the main types of supramolecular assemblies based on PPAs.

8.1 Fibers, superhelices and double helices

PPAs can establish supramolecular interactions between pendants groups and can self-assemble into fiberlike structures. The aggregation requires the presence of adequate functional groups in the pendant as well as complementary between polymer chains. Stereocomplexes are a good example of stereochemically complementary interactions.

One example in the field of PPAs was described by Riguera and co-workers, reporting ther formation of a fiberlike-stereocomplex. The starting PPAs are (*R*)- and (*S*)-α-methoxy-α-trifluoromethyl-α-phenylacetamide (MTPA monomers) pendant groups [poly-(*R*)-**19** and poly-(*S*)-**19**]. These polymer dissolved in THF present the amide groups in *cis* conformation favouring cooperative suparamolecular interactions between enantiomeric helices.[105] These type of stereochemically interactions gives rise to supramolecular fiberlike aggregates at higher concentrations results in gels (Figure 33). The modification of the *cis-trans* by temperature or solvent polarity allows control the formation of the stereocomplex. For

[97] Hierarchical Macrmolecular Structures: 60 years after the Staudinger Nobel Prize I; Percec, V.; Ed.; *Advances in Polymer Science*, Vol. *261*; Springer: New York, **2013.**
[98] Lehn, J.-M.; *Supramolecular Chemistry: Concepts and Perspectives*; Wiley-VCH: Weinheim, Germany, **1995**.
[99] Steed, J. W.; Atwood, J. L.; *Suparamolecular Chemistry*; John Wiley & Sons: West Sussex, U.K., **2005.**
[100] Duan, P.; Cao, H.; Zhang, L.; Liu, M.; *Soft. Matter* **2014**, *10*, 5428.
[101] Zhang, L.; Qin, L.; Wang, X.; Cao, H.; Liu, M.; *Adv. Mater.* **2014**, *26*, 6959.
[102] Yang, Y.; Zhang, Y.; Wei, Z.; *Adv. Mater.* **2013**, *25*, 6039.
[103] Wang, Y.; Xu, J.; Wang, Y.; Chen, H.; *Chem. Soc. Rev.* **2013**, *42*, 2930.
[104] Miyake, H.; Tsukube, H.; *Chem. Soc. Rev.* **2012**, *41*, 6977.
[105] Leiras. S.; Freire, F.; Seco, J. M.; Quiñoá, E.; Riguera, R.; *Chem. Sci.* **2013**, *4*, 2735.

example, the addition of high polar solvents (*e.g.* MeOH) cleavage the intermolecular and intramolecular hydrogen-bonding interaction disrupting the formation of the stereocomplex.

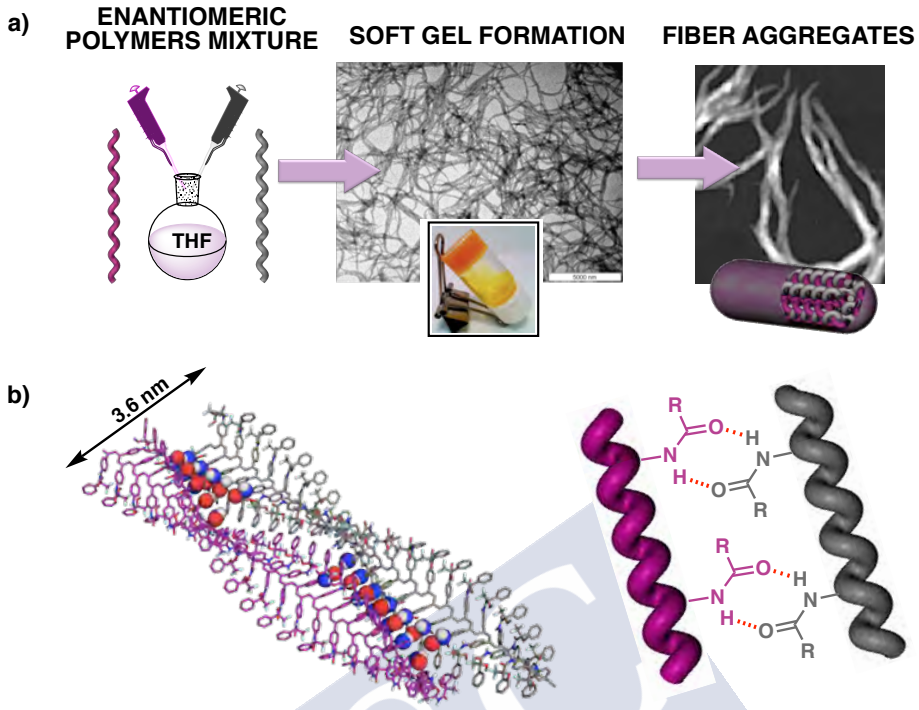

Figure 33. Schematic representation for the formation of stereocmplex with poly-**19**.

Many other examples of fiberlikes aggregates based on PPAs were reported; in some of them the PPA helicity is conserved while in others the aggregation entails the disappearance of the helix. Yashima *et Al.* reported an example of fiberlike aggregates based on poly-(4-carboxyphenylacetylene) where the PPA helicity is conserved. This polymer presents a chiral amplification when a small amount of chiral amine is added. The deposition of this complex to a mica substrate shows in AFM two-helix bundles probably formed by hydrogen bonding between the carboxyl groups of two different helical chains.[106]

Another example was reported by Shinohara, Shigekawa and co-workers. In this case, they observed by Scanning Tunnelling Microscopy (STM) the presence of double helices based on PPAs. The deposition of an optically active PPA derived from menthocarbonylamino groups (poly-**21**) on HOPG shows the formation of double-helical structures. Interestingly, the researcher observed that the molecules of the polymer deposited on HOPG were easy to move by the effect of the probe scanning.[107]

Likewise, Tang's group studied the supramolecular interactions in PPAs containing as pendant groups different aminoacids methyl ester (*e.g.* Alanine, Leucine, valine or

[106] Sakurai, S.I.; Kuroyanagi, K.; Morino, K.; Kunitake, M.; Yashima, E.; *Macromolecules* **2003**, *36*, 9670.
[107] Shinohara, K.; Yasuda, S.; Kato, G.; Fujita, M.; Shigekawa, H.; *J. Am. Chem. Soc.* **2001**, *123*, 3619.

phenylglycine). In this work, NMR analysis of the polymers showed that at high concentrations in low polar solvents, the pendants group interact between intermolecular hydrogen-bonding interactions. Moreover, AFM images showed that when the polymers are dissolved in low polar solvents (*e.g.* THF) and they are slowly evaporated in mica, fiberlike aggregates are formed.[108] All this information suggests that the supramolecular interactions occurs by hydrogen-bonding between amide groups of different chains (C=O···H-N), while in the PPAs with free carbonyl goups at the pendant termini, the aggregations results by association between the amide and carbonyl groups of different helical chains (Figure 34c).

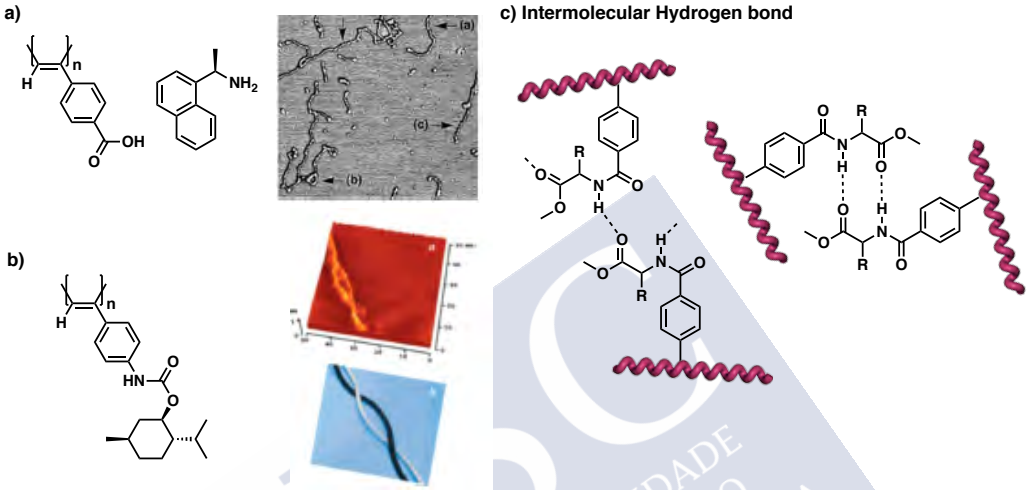

Figure 34. a) AFM images from drop casted procedure. b) STM images on HOPG substrate. c) Intermolecular possible hydrogen bond between helical polymers.

Interestingly, when PPAs containing aminoacids derivatives are dissolved in polar solvents (*e.g.* MeOH) lead to the formation of micellelike aggregates with the backbone in the core and aminoacids pendants in the shell. The reason of that is the amphiphilic character in this type of PPAs (due to non polar backbone and polar pendants).[109] The high number of amino acids residues that decorate the outside of these micelles leads them to stick together by hydrogen-bonding interactions, forming micelles or even larger fiberlike structures.

8.2 Layer-by-Layer assembly of PPAs

The assembly of layer-by-layer (LBL) charged polymers can generate multilayer structures by interaction between polyanions and polycations. Yashima and co-workers published an interesting work about this topic. In this article, they prepared three different LBLs constituted by a) an anionic PPA (with a phosphonate groups as pendants) with a poly(allylamine), b) a cationic PPA (with ammonium groups as pendants) with poly(acrylic

[108] Cheuk, K. K. L.; Li, B. S.; Lam, J. W. Y.; Xie, Y.; Tang, B. Z.; *Macromolecules* **2008**, *41*, 5997.
[109] Li, B.; Cheuk, K. K. L.; Yang, D.; Lam, J. W. Y.; Wan, L. J.; Bai, C.; Tang, B. Z.; *Macromolecules* **2003**, *36*, 5447.

acid), and c) the anionic phosphonate-bearing PPA with the cationic ammonium bearing PPA.[110]

These polymers are optically active but they can induce a specific helical sense by the addition of a chiral sternal stimulus (chiral amine or a chiral carboxilyc acid) that binds to the PPA. The addition of the corresponding counterion polyelectrolyte [poly(allylamine or poly(acrylic acid)] replaces the chiral stimulus agent, generating a LBL assembly with a macromolecular helicity memory.

9. Nanoparticles based on PPAs

Polymer Nanoparticles is commonly defined as nanospheres or nanocapusles made from any type of polymer wich size is in the range of 10-1000 nm. Nanospheres are solid and spherical and they are used to encapsulate molecules inside them or absorb molecules on their surface. Nanocapsules are colloidal particles consisting on hollow core surrounded by the polymeric cover. This type of particles is usually used to encapsulate substances.[111]

To form this type of nanostructures, two main strategies have been described: the emulsification method and the emulsion polymerization.[112,113]

9.1 Emulsification method

Using this method, Deng and co-workers prepared particles of poly(phenylacetylene)s poly-**22** by dropwise addition of a concentrated THF solution of poly-**22** to a solution of the surfactant sodium dodecyl sulphate (SDS) in water. Interestingly, they found that the size is highly dependent of the SDS concentration (Figure 35a).[114]

9.2 Emulsion polymerization

Deng and co-workers also explored the emulsion polymerization method. This methodology requires water, a monomer with low solubility in water, water-soluble initiator and a surfactant. Using this method, Deng *et Al.* used different types of monomers, some of them chiral and therefore, they can obtain chiral particles with sizes around 10^2 nm.

[110] Maeda, K.; Matsushita, Y.; Ezaka, M.; Yashima, E.; *Chem. Commun.* **2005**, 4152.

[111] a) Li, W.; Huang, H.; Li, Y.; Deng J. P. *Polym. Chem*. **2014**, *5*, 1107. b) Song, C.; Liu, X.; Liu, D.; Ren, C.; Yang, W. Deng, J.; P. *Macromol. Rapid Commun.* **2013**, *34*, 1426. c) Zhao, B.; Deng, J.; Deng, J. P. *Macromol. Rapid Commun.* **2016**, *37*, 568. d) Zhang, Y. Y.; Luo, X. F.; Deng, J. P.; Yang, W. T.; *Macromol. Chem. Phys*. **2011**, *212*, 353. e) Rao, J. P.; Geckeler, K. E.; *Prog. Polym. Sci.* **2011**, *36*, 887.

[112] Li, W.; Huang, H.; Li, Y.; Deng, J.; *Polym. Chem* **2014**, *5*, 1107.

[113] Song, C.; Liu, X.; Liu, D.; Ren, C.; Yang, W.; Deng, J.; *Macromol. Rapid Commun.* **2013**, *34*, 1426.

[114] Zhang, Y.; Luo, X.; Deng. J.; *Macromol. Chem. Phys.* **2011**, *212*, 353.

The same group also described the formation of macroscopically racemic poly(phenylacetylene) particles. The formation of the particles is due to the presence of emulsifier such as SDS or Triton X-100 in water. The liquid nature of the phenylacetylene monomer renders unnecessary the use of organic solvent to predissolve it, and in fact, it gets dispersed into the micelles as soon as it is added to the water solution. In this work, [(nbd)-$Rh^{+}B^{-}(C_6H_5)_4$] is used as catalyst and their hydrophobic nature results in its rapid dispersion into the micelles in the aqueous mixture leading after the polymerization small-diameter particles.[115]

D'Amato *et Al.* develop different protocols to obtain nanoparticles with a control size. Thus, they found that when the organometallic catalyst is replaced by a radical initiator such as potassium persulfate (KPS),[116] the polydispersity of the particles decreased due to presence of charged species in the reaction mixture that stabilize the emulsion. Furthermore, the size of the particles can be tuned by modification of the initiator concentration (Figure 35b).

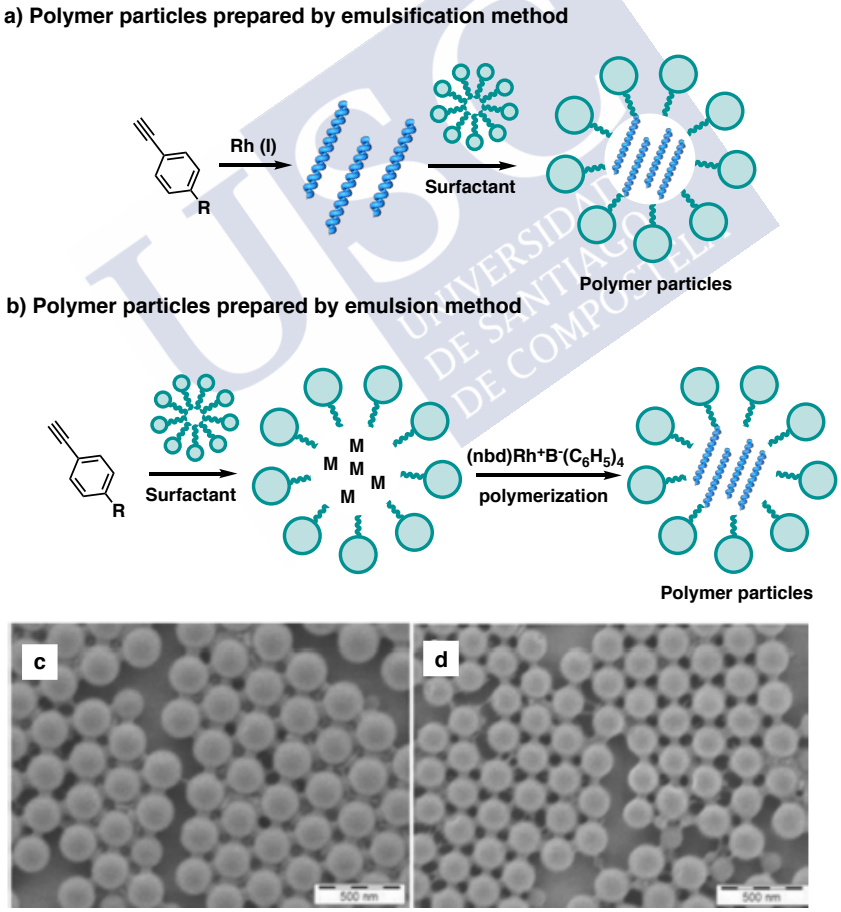

Figure 35. Schematic illustration of a) Emulsification method for polymer particles. b) Emulsion method for polymer particles and c), d) Examples of SEM images for polymer particles.

[115] Chen, B.; Liu, X.; Xu, C.; Song, C.; Luo, X.; Yang, W.; Deng, J.; *Maromol. Chem. Phys.* **2012**, *213*, 603.
[116] Venditti, I.; D'Amato, R.; Russo, M. V.; Falconeri, M.; *Sens. Actuators B* **2007**, *126*, 35.

9.3 PPAs Nanoparticles via non-covalent crosslinking agents

Riguera *et Al.* converted a PPA bearing either (*R*)- or (*S*)-α-methoxy-α-phenylacetic acid (poly-**15**) connected to the phenylacetylene through amide bond, into nanospheres by addition of monovalent or divalent metal ions (perchlorate salts in THF). Poly-**15** dissolved in different organic solvents ($CHCl_3$, THF, DMSO, DMF) presents an equilibrium between left-handed (*M*) and right-handed (*P*) helices showing null CD. Interestingly, the addition of monovalent or divalent metal ions can amplify their left-handed or right-handed helical sense. For example, the left-handed helical sense of poly-(*R*)-**15** when a perchlorate salt of a monovalent metal ion is added, whereas the right-handed helical sense is amplified when a salt of divalent is added to poly-(*R*)-**15**.

The metal ion can act not only as chiral inducer but also as a crosslinking agent between polymer chains forming chiral nanospheres. The size and chiral content of these nanospeheres can be modulated controlling the polymer/metal ratio. Finally, these nanostructures present the ability to encapsulate iron oxide magnetic nanoparticles, quantum dots or organic molecules such as fluorescent dyes (Figure 36).[117]

Moreover, poly-**15** can be converted into other nanostructures (toroids, nanotubes) by variation of the solvent. In the case of nanotubes, they are formed when a cosolvent with a high boling point is added while toroidal nanostructures are obtained upon addition of a solvent in which the polymer is poorly dissolved.[118]

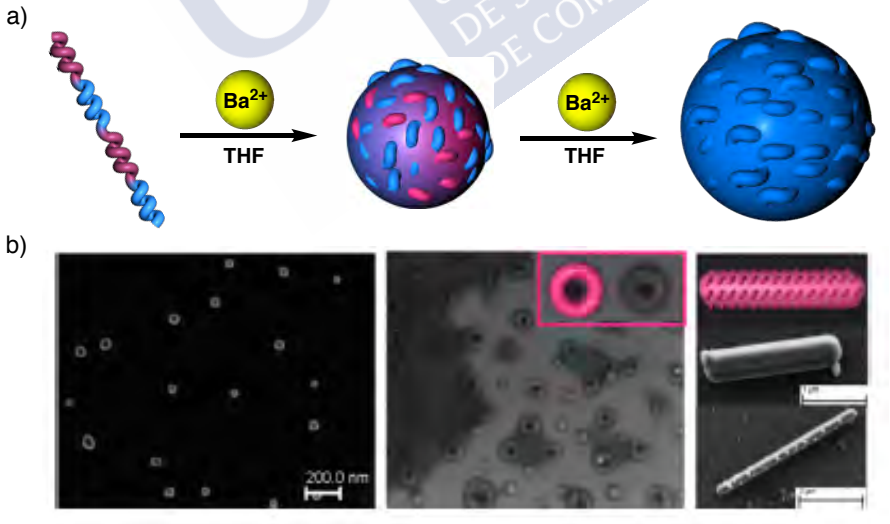

Figure 36. a) Schematic representation for the nanostructuration of poly-**15** with metal ions. b) SEM images of poly-**15** converted into nanospheres, toroids and nanotubes.

[117] Freire, F.; Seco, J. M.; Quiñoá, E.; Riguera. R. *J. Am. Chem. Soc.* **2012**, *134*, 19374.
[118] Arias, S.; Freire, F.; Quiñoá, E.; Riguera, R.; *Angew. Chem. Int. Ed.* **2014**, *53*, 13720.

In another work of our group, PPAs derived from *L*-aminoacids methyl ester (*e.g*. *L*-alanine, *L*-isoleucine, *L*-leucine, etc) can converted into chiral nanospheres (*P* or *M*) varying the polymer/metal/cosolvent ratio. Thus, the addition divalent or monovalent metal ion produce a complex I (chelation of the two carbonyl groups; *sp* conformation) associated to a helical inversion an also the formation of *M* nanospheres. Ulterior addition of a small amount of MeOH transform complex I to complex II and a second inversion is produced leading to the formation of *P* nanospheres.[24]

10. Applications of PPAs

Dynamic helical polymers based on PPAs have several potential applications in fields such as sensing, chiral separation or nanoreactors, among others. This is due to for the possibility to manipulate parameters such as helical sense and elongation. In this section, the main applications of the PPAs with helical structure will be summarized.

10.1 Sensors

In our group, it was prepared the PPA bearing either (*R*)-α-methoxy-α-phenylacetic acid (MPA) (poly-**15**). This polymer present in solution an axially racemic chirality due to the presence of the *M* and *P* helices in the same population showing a null CD. Interestingly, Freire *et Al.* have demonstrated that these polymers are sensitive to the addition of monovalent and divalent metal ions. Thus, the addition of monovalent metal ions (*e.g.* Li^+, Ag^+, Na^+) stabilizes the a*p* conformation in the pendant groups (carbonyl and methoxy groups in antiperiplanar position) showing the CD spectrum a negative Cotton Effect (*M* helices). On the other hand, the addition of divalent metal ions (*e.g.* Ba^{2+}, Ca^{2+}, Co^{2+}) stabilizes the *sp* conformation in the pendant groups (carbonyl and methoxy groups in synperiplanar position) lead to a positive Cotton Effect in the pendant group (*P* helices).

Thus, poly-**15** is able to obtain different helical sense depending on the metal ion valence (*M* helices with monovalent metal ions and *P* helices with divalent metal ions).

In another work of the group, PPAs bearing a *L*-phenylglycine methyl ester as pendant groups were prepared poly-**17**. This polymer showed different behaviour depending on the polarity of the solvents. Thus, low polar solvents (*e.g.* $CHCl_3$, DCM) induce a *syn* conformation in the pendant groups (carbonyl groups in synperiplanar position) leading to *M* helices. Interestingly, high polar solvents (*e.g.* DMSO, DMF) stabilize an *anti* conformation (carbonyl groups in antiperiplanar position) in the pendant group leading to the formation of opposite

[24] Arias, S.; Freire, F.; Quiñoá, E.; Riguera, R.; *Polym. Chem*. **2015**, *6*, 4725.

helical sense. In a different way, poly-**19** is able to act as sensor distinguishing between two parameters in the solvent (the polar/low polar and donor/non donor character). Thus, CD and UV-Vis espectra can detect four different helices depending on the polarity of the solvent and the donor/ non donor character.[105]

10.2 Chiral Recognition

High-Performance Liquid Chromatography (HPLC) with chiral stationary phases (CSP) is one of the most important techniques to separate racemic mixtures.[119] To obtain a good separation between enantiomers in HPLC, the CSP must present a good chiral recognition in the racemate mixture.

Several examples of CSPs were developed but there are still racemates that cannot separate using commercially available CSPs. Thus, helical polymers with one-handed helical sense such as poly(triphenylmethylmethacrylates)s (PTrMA)[120] or polysaccharides[121] were prepared by still present some limitations.

Recently, Yashima and co-workers reported the first example of PPAs as CSP in HPLC. In this work, they prepared a PPA bears bisphenol derivative as pendants (poly-**23**) that presents an axially racemic chirality (*P* and *M* helices in the same population). This PPA suffers chiral amplification in presence of (*S*)- and (*R*)-phenylethanol and the helicity can be memorized in absence of the external stimuli. This polymer was the firs example of a PPA used to separate racemate mixtures (*e.g. trans*-stilbene). Interestingly, the elution order can be easily changed switching the helical sense of the PPA.[122]

More recently, Maeda and Freire. used as CSP in HPLC a helical poly(phenylacetylene) that bears a chiral (*R*)-α-methoxy-α-phenylacetic acid as pendant (poly-**15**). This PPA can tuned the left- and right-handed helical conformations by addition of catalytic amounts of sodium and cesium tetrakis[3,5-bis(triflurometyl)phenyl]borate salts (MBArF), respectively. In this work, it has demonstrated that the changes in the helical structure (right-handed, left-handed

[105] Leiras. S.; Freire, F.; Seco, J. M.; Quiñoá, E.; Riguera, R.; *Chem. Sci.* **2013**, *4*, 2735.

[119] a) Andersson, S.; Allenmark, S. G., *Journal of Biochemical and Biophysical Methods*. **2002**, *54*, 11. b) Liu, Y.; Lantz, A. W.; Armstrong, D. W., *J. Liq. Chromatogr. Relat. Technol.* ***2004****, 27,* 1121.

[120] a) Yuki, H.; Okamoto, Y.; Okamoto, I., *J. Am. Chem. Soc*. **1980**, *102*, 6356. b) Okamoto, Y.; Honda, S.; Okamoto, I.; Yuki, H.; Murata, S.; Noyori, R.; Takaya, H., *J. Am. Chem. Soc*. **1981**, *103*, 6971. c) Nakano, T., *J. Chromatogr. A.* **2001**, *906*, 205-225.

[121] a) Okamoto, Y.; Yashima, E., *Angew. Chem. Int. Ed*. **1998**, *37*, 1020. b) Yashima, E.,*J. Chromatogr. A*, **2001**, *906*, 105. c) Ikai, T.; Okamoto, Y.; *Chem. Rev.* **2009**, *109*, 6077.

[122] Shimomura, K.; Ikai, T.; Kanoh, S.; Yashima, E., *Nat. Chem.* **2014**, *6*, 429.

and racemic mixture) can alter or even invert the elution order of racemic mixtures (Figure 37).[123]

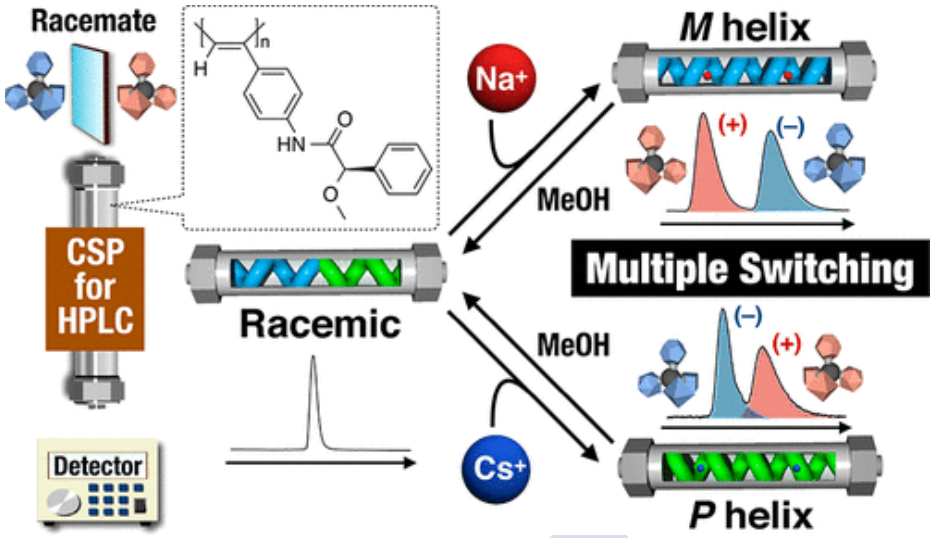

Figure 37. Conceptual representation of three-state switchable CPS consisting on PPAs.

10.3 Asymmetric Catalysis

Optically active polymers can act as asymmetric catalysts. Normally, they are consisting on small molecular chiral ligands covalently attached on achiral polymers where the enantioselectivities are governed by the chiral ligands while the polymers just work as support.[124]

However, helical polymers with one-handed helical sense may have an effect on the enantioselectivity due to helical chirality. Thereby they could be a more efficient asymmetric catalyst than the chiral ligand. Another interesting approach is to employ a rigid-rod one-handed helical polymers that has no stereogenic center except for a macromolecular helicity as a novel scaffold or template spatially organize catalytic active.

Reggelin *et Al.* described the first example of catalytic asymmetric C-C bond forming reaction using helical poly(methacrylate)s (poly-**24**). The polymers were prepared by polymerization with TrMA obtaining a one-handed helical polymer. Moreover, the complexation with palladium catalyst promoted the asymmetric allylic alkylation reaction with a 40-60% *e.e.* (Figure 38a)[125,126]

Yashima and co-workers developed a new helical polymer catalyst consist on 4-carboxyphenyl isocyanide and piperazine units (poly-**25**). This copolymer presents one

[123] Hirose, D.; Isobe, A.; Quiñoá, E.; Freire, F.; Maeda, K.; *J. Am. Chem. Soc.* **2019**, *141*, 8592.
[124] Benaglia, M.; Puglisi, A.; Cozzi, F.; *Chem. Rev.* **2003**, *103*, 3401.
[125] Reggelin, M.; Schultz, M.; Holbach, M.; *Angew. Chem., Int. Ed.* **2002**, *41*, 1614.
[126] Reggelin, M.; Doerr, S.; Klussmann, M.; Schultz, M.; Holbach, M.; *Angew. Chem., Int. Ed.* **2004**, *101*, 5461.

preferred helical sense and enantioselectivity catalyzed a direct aldol reaction between aldehydes and ketones with *e.e* around 12% (Figure 38b).[127]

In another interesting work, Maeda and co-workers prepared series of optically active PPAs bearing oligopeptides (poly-**26**) as pendants in order to know the organocatalytic activities for the epoxidation of chalcone. The studies show the highest enatioselectivites (34% *e.e*) for the PPAs whereas the monomers did not show enantioselectivity (<2% *e.e.*).[128] These results demonstrated that the helical structure of the PPAs is indispensable for the reaction (Figure 38c).

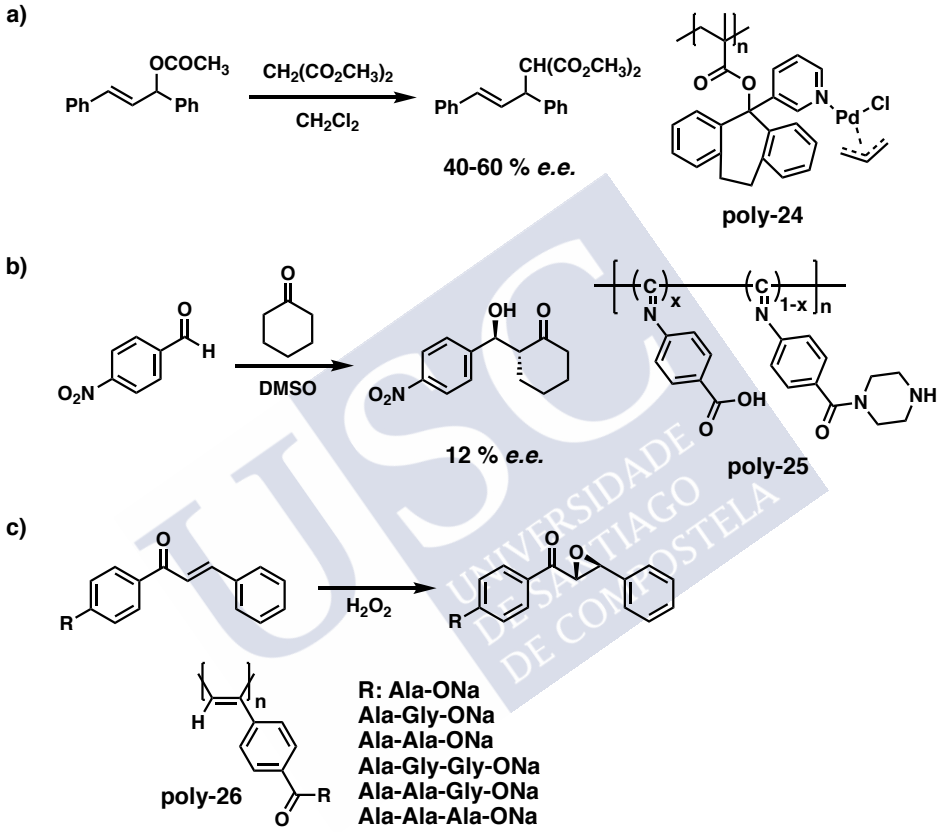

Figure 38. Schematic illustration showing the structure and the reaction of a) poly-**24**, b) poly-**25** and c) poly-**26**.

[127] Miyabe, T.; Hase, Y.; Lida, H.; Maeda, K.; Yashima, E.; *Chirality* **2009**, *21*, 44.
[128] Maeda, K.; Tanaka, K.; Morino, K.; Yashima, E.; *Macromolecules* **2007**, *40*, 6783.

USC
UNIVERSIDADE
DE SANTIAGO
DE COMPOSTELA

Chapter II

Objectives

USC
UNIVERSIDADE
DE SANTIAGO
DE COMPOSTELA

Objectives

Nowadays, hybrid materials have taken a great importance due to their several applications in fields such as catalysis, energy storage, theranostic, etc. The main feature of this type of materials is the combination of the different materials properties.

In many cases, hybrid materials based on metal nanoparticles (MNPs) are formed by a core-shell composition where the core is composed by MNPs and the shell is typically a polymer coating. Thus, this type of hybrid materials composed by MNPs and polymers are very interesting because allows modifying the surface of the MNPs and give them novel functionalities.

For this reasons, an interesting family of polymers to decorate MNPs and prepare new hybrid materials are poly(phenylacetylene)s (PPAs). PPAs are a type of dynamic helical polymers that can modulate their secondary structure (helical sense and/or elongation) by addition of external stimuli such as temperature, metal ions and polarity of solvents, among others. Until now, several examples of PPAs with different pendants groups and functionalities (*e.g.* sensing, asymmetric catalysis, chiral separations) have been prepared.

These properties convert them in excellent candidates to act as chiral protecting agent for MNPs to form novel chiral hybrid materials. However, until now the preparation of this type of materials was not explored in depth.

Taking into account this information, the general objective of this Doctoral thesis is the preparation of novel chiral hybrid materials based on PPA-MNPs (M = Au and Ag). Furthermore, the study of novel properties in these materials associated to the combination of chiral properties of PPAs and plasmonic properties of MNPs.

The main objectives of this Doctoral Thesis can be classified in the next six chapters.

CHAPTER III. Chiral Gold-PPA Nanocomposites with Tunable Helical Sense and Morphology

In literature, it can be found that Brust-Schiffrin methodology is very common methodology to prepare Gold Nanoparticles (AuNPs) in organic media (DCM, $CHCl_3$, toluene, etc.) with an excellent control over the size and the shape.

In this chapter, the main objective is the preparation of novel nanocomposites based on the combination of poly(phenylacetylene)s and AuNPs (PPA-AuNPs) using a variation of the classical Brust-Schiffrin method. Furthermore, the study how affect the presence of AuNPs stabilized by thiolated PPAs in the dynamic properties of the nanocomposites.

Publication associated with this objective: Bergueiro, J.; Núñez-Martínez, M.; Arias, S.; Quiñoá, E.; Riguera, R.; Freire, F.; *Nanoscale Horiz.* **2020**, *5*, 495-500.

CHAPTER IV. Dynamic Chiral PPA-AgNP Nanocomposites: Aligned Silver Nanoparticles Decorating Helical Polymers

The design of suitable organic coatings for the MNPs is a very important factor in the preparation of nanocomposites. The interaction between the organic coating and the MNPs allow obtaining stable MNPs in the nancomposites by steric effects that avoid the natural aggregation tendency of the MNPs along the time. In literature, there are different works where the protection of the MNPs is due to weak supramolecular interactions with the organic coating.

Taking in mind this information, the main objective of this chapter will be the preparation of the first example of PPA-AgNPs nanocomposites using weak supramolecular interactions between the two components of the system. Moreover, the last objective of this chapter will be the study of the AgNPs influence in the dynamic properties of PPAs.

Publication associated with this objective: Núñez-Martínez, M.; Arias, S.; Quiñoá, E.; Riguera, R.; Freire, F.; *Chem. Mater.* **2021**, *33*, 4805.

CHAPTER V. The role of the polymer-AuNP bond in the stimuli-responsive properties of the nanocomposites: Supramolecular vs thiolated PPA-AuNP interactions

Gold nanoparticles (AuNPs) are widely known due to their applications in fields such as sensing, catalysis and hyperthermia, among others.

Taking into account the information of the previous chapter related to the preparation of PPA-AgNP nanocomposites through supramolecular interactions. The main objective of this chapter is the preparation of PPA-AuNPs nanocomposites using this type of non covalent interactions and then, the evaluation of the stimuli-responsive properties of the PPAs after hybridization with AuNPs.

The introduction of AuNPs into the PPA will allow us to study the differences between the nanocomposites (size and/or shape of MNPs, stability, dynamic properties) formed by silver and gold nanoparticles.

CHAPTER VI. Preparation of Helical Polymer-MNPs Nanocomposites via redox driven translocation of Gold or Silver centers: Chiroptical and Colorimetric Switches

It is well known that the surface decoration of MNPs is a powerful tool to develop new materials with applications in different fields such as sensing, catalysis and drug delivery, among others. For instance, helical biomacromolecules such as DNA (*P* helix) or proteins (*e.g.* amylose, *M* helix) have been employed to decorate the surface of the MNPs.

In these cases, the chirality of the nanocomposite is fixed by the secondary structure of the biomacromolecules preventing its modulation by addition of external stimuli.

In this chapter, the main objective is the preparation of chiral tunable helical polymer-MNPs (M = Au and Ag) nanocomposites using PPAs that bears aminoacids methyl ester as pendant group. For this purpose, alanine and methionine methyl ester was chosen to prepare the helical copolymers and act as protecting agents of MNPs.

The design of the copolymers is based on in the functional groups present in the monomeric repeating unit (m.r.u.) where the alanine methyl ester presents two carbonyl groups to modulate the helical sense. Moreover, methionine methyl ester also presents the same carbonyl group and moreover, a thioether group to interact selectively with the MNPs.

CHAPTER VII. ON-OFF Stereocomplexation of Dynamic helical polymer-MNPs (M = Ag, Au) Nanocomposites by Taming the Polymer Helix

Stereocomplexes are supramolecular structures formed by the interaction between two stereoregular and complementary polymers with different properties of parent homopolymers. In previous studies, it was reported that the PPA that bears 4-anilide of (*R*)- and (*S*)-α-methoxy-α-phenylacetic acid (poly-MTPA) can form this type of structures due to the presence of *cis* amide in the periphery of the helix, which produce the formation of fiber-like aggregates by interaction of these two complementary PPAs.

In this chapter, the main objective is the preparation of novel hybrid materials based on poly-(*R*)-MTPA-MNPs and poly-(*R*)-MTPA-MNPs (M = Ag and/or Au). The preparation of these materials allows us to determine the influence of the MNPs in the secondary structure of poly-MTPA.

Finally, the last objective of this chapter will be the preparation of sterecomplexes by the interaction of poly-(*R*)-MTPA-MNPs and poly-(*S*)-MTPA-MNPs (M = Ag or Au) and the study of the stimuli-responsive properties of the sterecomplexes in presence of MNPs.

***CHAPTER VIII*. Effect of the Secondary Structure of PPAs in the Preparation of Polymeric Nanostructures**

The preparation of polymeric nanostructures has attracted the attention of scientific community due to its applications from nanomedicine to nanoelectronics. In this context, many articles related to the preparation of polymeric nanospheres have been published.

Taking into account this information, the objective of this chapter is the development a novel methodology to prepare polymeric nanostructures based on PPAs. Moreover, it is well known that the aromatic substitution pattern takes a strong influence in the dynamic behaviour and stretch/compression of the PPAs. For this reason, another objective of the chapter is the study of the influence of the aromatic substitution pattern of PPAs in the formation of polymeric nanospheres.

Finally, the stability and encapsulation ability of fluorescent dyes of these nanostructures will be studied.

USC UNIVERSIDADE DE SANTIAGO DE COMPOSTELA

Chapter III

Chiral Gold-PPA Nanocomposites with Tunable Helical Sense and Morphology

USC
UNIVERSIDADE
DE SANTIAGO
DE COMPOSTELA

https://pubs.rsc.org/en/content/articlelanding/2020/nh/c9nh00659a#!divAbstract

USC
UNIVERSIDADE
DE SANTIAGO
DE COMPOSTELA

Chapter IV

Dynamic Chiral PPA-AgNP Nanocomposites: Aligned Silver Nanoparticles Decorating Helical Polymers

USC
UNIVERSIDADE
DE SANTIAGO
DE COMPOSTELA

https://pubs.acs.org/doi/10.1021/acs.chemmater.1c00805

USC
UNIVERSIDADE
DE SANTIAGO
DE COMPOSTELA

Chapter V

The Role of the Polymer-AuNP bond in the Stimuli-Responsive Properties of the Nanocomposites: Supramolecular *vs* Thiolated PPA-AuNP Interactions

USC
UNIVERSIDADE
DE SANTIAGO
DE COMPOSTELA

Chapter V: The role of the polymer-AuNP bond in the stimuli-responsive properties of the nanocomposites: Supramolecular vs thiolated PPA-AuNP interactions

Abstract

The chiral amplification effects of a dynamic helical polymer in a helical polymer-metal nanoparticles (MNP) nanocomposite are largely affected by the strength of the polymer-MNPs interaction. Thus, the classical thiol-MNPs bond must be replaced by another weaker. In such way, and for the special case of poly(phenylacetylene)-AgNPs —PPA-AgNPS—, introduction of weak anilide-AgNPs interactions allow to create a stable nanocomposite with of the chiral amplification properties of the helical polymer unaltered.

This protocol based on a direct reduction of the helical polymer silver complex by using $NaBH_4$ cannot be applied to a helical polymer gold complex, because the Au^{3+} ions degrade a polymer containing an anilide group. Thus, to prepare nanocomposites based on PPAs-AuNPs, the previous protocol must be refined. In this case, the gold ions are delivered to the polymer solution as a TOAB complex, conditions where the PPA remains stable. Next, reduction of the Au^{3+} ions is carried out with $NaBH_4$ affording the nanocomposite, where anilide-AuNPs interactions stabilize the nanocomposite. In this hybrid material, 4.2 nm gold nanoparticles are formed and aligned along the polymer chain with a regular distance between particles of 6 nm that corresponds to two helical pitches.

These studies shed light on the preparation of hybrid materials based on helical polymers highlighting the importance of the intramolecular forces used to combine the two components of the hybrid materials, and how these interactions can affect the dynamic behavior of the polymer.

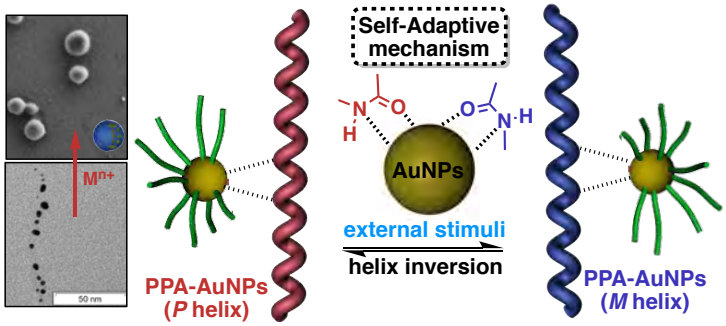

USC
UNIVERSIDADE
DE SANTIAGO
DE COMPOSTELA

1. Introduction

Metal Nanoparticles (MNPs) have been deeply studied during the last decades due to their applications in fields such as sensing,[1] biomedicine,[2,3] and catalysis,[4] among others. MNPs can be prepared by using different protocols that usually affect to their size and shape.[5,6] Moreover, depending on the structural features of the organic molecules used as protecting agents or coatings (small molecules/polymers, charged/neutral, hydrophobic/hydrophilic, etc.) among the particle size or shape, other properties, such as stability, solubility or biocompatibility can be affected.

In the literature, there are several examples of nanocomposites that combine helical macromolecules with relevant biological functions (proteins or DNA) with MNPs.[7-9] In those cases, the helical sense of the biomacromolecules in the composite is fixed and determined by the chirality of the residues used to build up the macromolecule. However, the preparation of more appealing nanocomposites made of dynamic helical polymers[10-26] such as poly(phenylacetylene)s (PPAs) and MNPs, has been scarcely explored.[26-28] These polymers can tune their helical structure (sense and/or elongation) by using different external stimuli such as metal ions, solvent polarity, or temperature, and therefore can provide interesting properties to the nanocomposites.

However, depending on the protocol used to prepare the nanocomposite, the dynamic behavior of the polymer can be largely affected (scheme 1). Thus, the dynamic behavior of PPAs such as poly-(*R*)-**1** that bears the 4-anilide of (*R*)-α-methoxy-α-phenylacetic acid as pendant group (scheme 1a), or poly-(*R*)-**2**, that bears the 4-benzamide of (*S*)-phenylglycine methyl ester as pendant is dramatically reduced when the polymer is attached to a metal nanoparticle by using a thiol-metal bond [*i.e.*, poly-[(*R*)-**1**-*co*-thiol-MNP] nanocomposite (M = Au or Ag)] to form the nanocomposites (scheme 1b).[27]

This problem was surpassed by using supramolecular chemistry to link the PPA to the metal nanoparticle instead of a more "covalent bonds" such as a thiol-Au/Ag linkage.[28] Thus, weak amide-AgNPs interactions between the PPA and the metal nanoparticle, which is found in other polymer-based nanocomposites such as polyvinylpyrrolidone (PVP)-MNPs nanocomposites were employed (Scheme 1c).[28] To prepare this poly-(*R*)-**1**-AgNPs/dodecanethiol nanocomposites, poly-(*R*)-**1** was

complexed to Ag^+ by adding $AgClO_4$ as a source of silver ions, which was further transformed into the poly-(*R*)-**1**-AgNPs/dodecanethiol nanocomposites by using $NaBH_4$ as a reducing agent and the 1-dodecanethiol as co-stabilizing agent.[28]

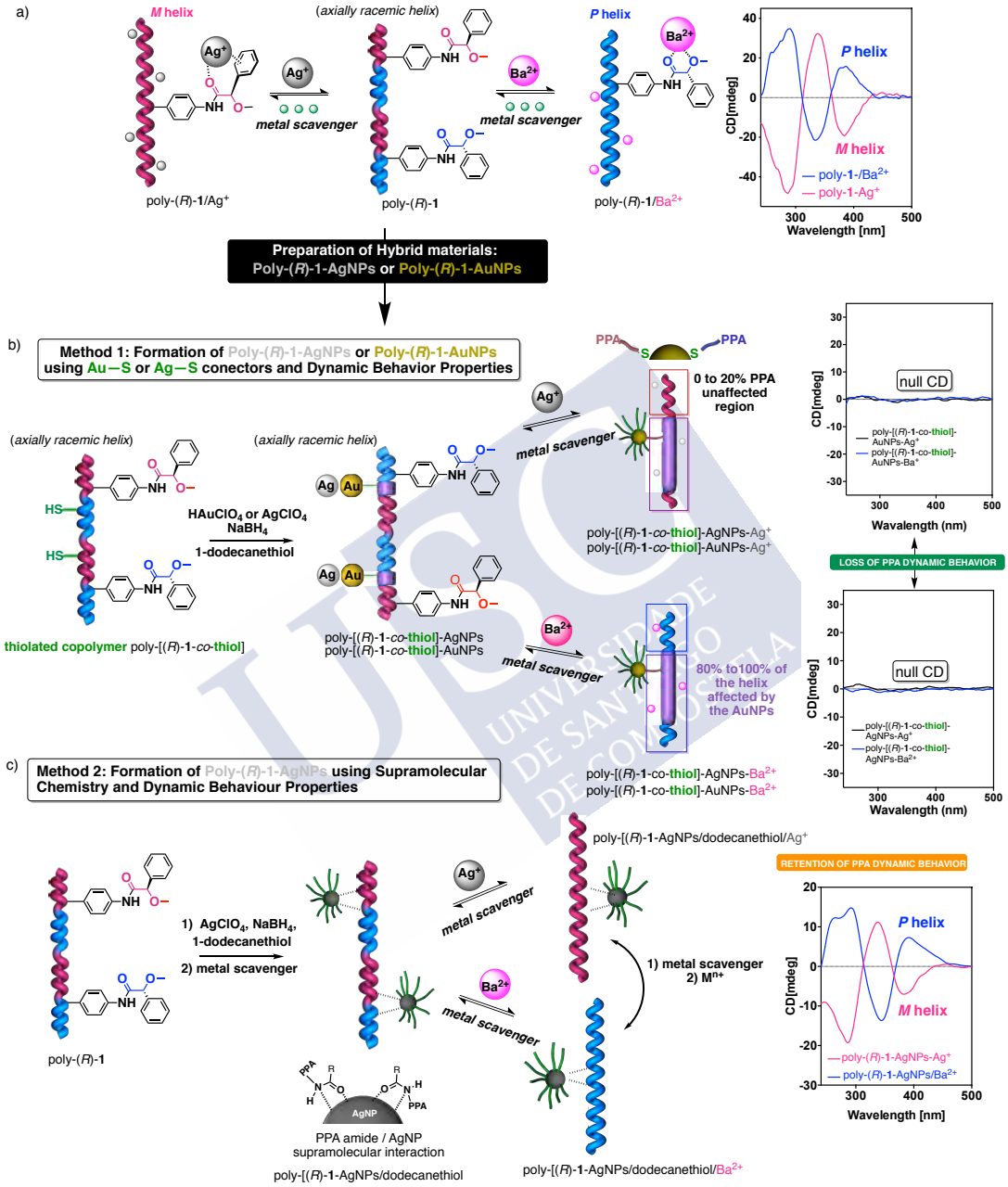

Scheme 1. Schematic representatation of a) dynamic behavior of poly-(*R*)-**1** in presence of divalent and monovalent metal ions. b) Dynamic response of poly-[(*R*)-**1**-*co*-thiol]-AgNPs and poly-[(*R*)-**1**-*co*-thiol]-AuNPs using a thiol-MNPs strong interaction. c) Dynamic response of poly-(*R*)-**1**-AgNPs using amide-AgNPs weak supramolecular interactions.

The resulting nanocomposites show low-polydisperse 2.8 nm AgNPs linearly distributed along the PPA chain. This weak supramolecular interaction between the PPA

and the AgNP allows to preserve the dynamic behavior of poly-(*R*)-**1** within the nanocomposite, where a *P* or *M* helical sense can be effectively induced in the helical polymer by addition of external stimuli.[28] Thus, while strong polymer metal nanoparticles interactions inhibit the dynamic behavior of the nanocomposite,[27] weak supramolecular forces preserve it.[28] Herein, we will explore the formation of poly-(*R*)-**1**-AuNPs/dodecanethiol nanocomposites, where a supramolecular amide-AuNP is used to link both components of the nanocomposite.

2. Results and Discussion

In a first attempt, the preparation of poly-(*R*)-**1**-AuNPs/dodecanethiol nanocomposite was carried out using the protocol developed for poly-(*R*)-**1**-AgNPs/dodecanethiol nanocomposite (scheme 1c). Thus, to a chloroform solution of poly-(*R*)-**1** (0.3 mg mL^{-1}), 0.5 equiv. of a methanolic solution of $HAuCl_4$ were added to form a poly-(*R*)-**1**/Au^{3+} complex (Figure 1a). Once the metal ion is added to the polymer solution a color change from yellow to blue is observed (Figure 1b).

EPR studies revealed the presence of a radical specie in the polymer, which is delocalized along the polyene backbone (Figure 1d) and generated due to a redox process after the addition of the Au^{3+} ions. The generation of these radical species must be avoided in PPAs due to a *cis* to *trans* isomerization of the polyene backbone, that results in a planarization of the polymer, and where non-helical structures can be generated. Moreover, TEM images after addition of $HAuCl_4$ to poly-(*R*)-**1** showed the formation of high polydisperse AuNPs (Figure 1e).

Thus, an alternative protocol must be developed to prepare the poly-(*R*)-**1**-AuNPs/dodecanethiol nanocomposite, avoiding a direct complexation between the polymer and the Au^{3+} ion. From previous studies is known that when a thiolated comonomer was introduced in the polymer chain to form the nanocomposite (method 1, scheme 1b), the polymer was not degraded.[26] This is due to a strong interaction between the thiol group and the Au^{3+} ions, which avoids any further interaction between these ions and the polyene backbone, and therefore the generation of radical species. Thus, we reasoned that instead of using a direct complexation between poly-(*R*)-**1** and the Au^{3+} ions, a variation of the Brust-Schiffrin[30] protocol could be used to prepare the poly-(*R*)-**1**-AuNPs/dodecanethiol nanocomposite.

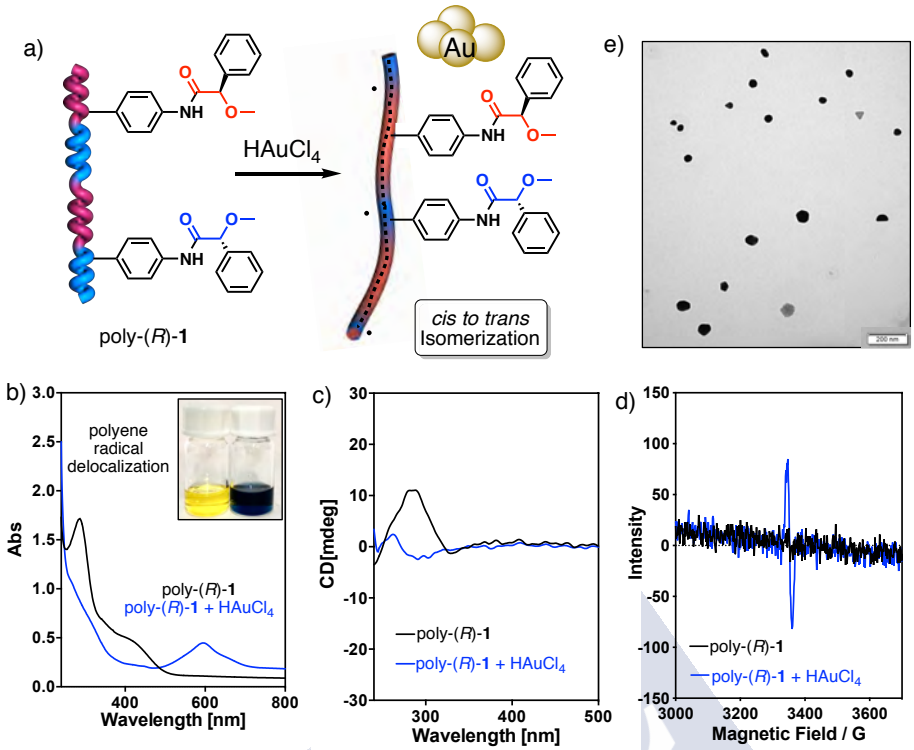

Figure 1. a) Schematic representation for the formation of radicals in poly-(*R*)-**1** in presence of $HAuCl_4$. b) UV-Vis spectra of poly-(*R*)-**1** and poly-(*R*)-**1** in presence of $HAuCl_4$. c) CD studies of poly-(*R*)-**1** and poly-(*R*)-**1** in presence of $HAuCl_4$. d) EPR studies of poly-(*R*)-**1** and poly-(*R*)-**1** in presence of $HAuCl_4$. e) TEM images of poly-(*R*)-1 in presence of $HAuCl_4$.

First, tetraoctylamonium bromide is used to transfer the Au^{3+} ions from a water $HAuCl_4$ solution to an organic solvent, in this case dichloromethane. Next, poly-(*R*)-**1** and 1-dodecanethiol were added to the organic layer and the mixture was stirred until reach -4°C. At this point, no color change was observed in the polymer, indicating that the Au^{3+} ions are complexed to the dodecanethiol and not to the polymer. Next, $NaBH_4$ was added to the dichloromethane solution and the reaction mixture turned from yellow/orange towards brown/black indicating the generation of AuNPs (Figure 2a).

The resulting material was purified by precipitation with toluene and centrifugation (See SI for more details). Further purification of the nanocomposite was carried out by Gel Performance Chromatography (GPC), which showed the presence of a GPC peak (t_R poly-(*R*)-**1**-AuNPs/dodecanethiol = 10 min, Figure 2d) with shorter t_R than those obtained for the starting components (t_R poly-(*R*)-**1** = 21 min; t_R AuNPs = 27 min) (See SI for more details). Moreover, additional GPC studies at two different wavelengths —540 (LSPR absorption) and 380 nm (polymer absorption)—, showed the formation of the nanocomposite, which absorbs at the

two different wavelengths, while the parent components, poly-(*R*)-**1** and AuNPs absorbs at 380 and 540 nm respectively (See SI for more details). Interestingly, the isolated poly-(*R*)-**1**-AuNPs/dodecanethiol nanocomposite exhibits excellent stability and can be stored in solid under argon atmosphere for months.

Characterization of the poly-(*R*)-**1**-AuNPs/dodecanethiol hybrid material was done using different techniques such as Differential Scanning Calorimetry (DSC), ^{1}H-NMR, UV-Vis, and IR studies.

UV-vis measurements showed the UV traces characteristic of poly-(*R*)-**1**, and the presence of an extra UV band at 540 nm which corresponds the localized surface plasmon resonance (LSPR) band of spherical AuNPs (Figure 2b). This fact indicates the presence of the two components in the nanocomposite. Furthermore, ^{1}H-NMR experiments showed the signals corresponding to poly-(*R*)-**1** and 1-dodecanethiol, corroborating therefore the obtention of the nanocomposite (See SI). Interestingly, FT-IR studies showed a strong interaction between the anilide group of poly-(*R*)-**1** and the AuNPs ($\Delta\tilde{\nu}_{CO}$ = 78 cm^{-1}; $\Delta\tilde{\nu}_{NCO}$ = 16 cm^{-1}), fact that indicates as expected the role of the amide at poly-(*R*)-**1** in the stabilization of the AuNPs (Figure 2c). Moreover, poly-(*R*)-**1**-AuNPs/dodecanethiol nanocomposites showed a great stability in solution at different temperatures and with the time (Figure 2d and e).

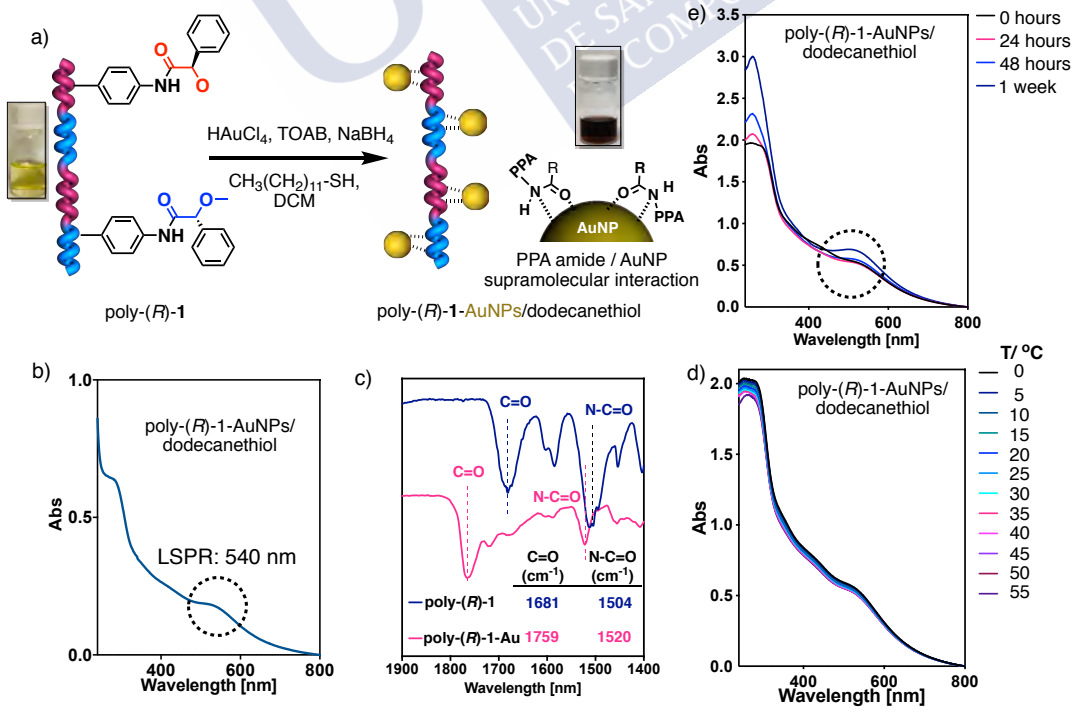

Figure 3. a) TEM images for poly-(*R*)-**1**-AuNPs/dodecanethiol (size: 4.2 ± 1.1 nm) and b) UV-Vis spectrum of poly-(*R*)-**1**-AuNPs. c) FT-IR spectra of poly-(*R*)-**1** and poly-(*R*)-**1**-AuNPs. d) UV-Vis spectra of poly-(*R*)-**1**-AuNPs at different temperatures. e) UV-Vis spectra of poly-(*R*)-**1**-AuNPs at different times.

Once, the presence of the nanocomposite was demonstrated, structural studies on the polymer were carried out to demonstrate that its helical structure remains unaltered during the formation of the hybrid material. Thus, DSC experiments showed a thermogram characteristic for a *cis-cisoidal* structure, like the one obtained for the parent PPA poly-(*R*)-**1** (See SI for details).

To study the morphology of the aggregate Dynamic Light Scattering (DLS), and Electron Microscopy studies were carried out. DLS experiments indicate the formation of large aggregates compared to the parent polymer (poly-(*R*)-**1**) (See SI). On the other hand, Transmission Electron Microscopy (TEM) studies produced images that shown the presence of small, spherical, low-polydisperse AuNPs (4.2 ± 1.1 nm), which are aligned along the polymer chain and regularly separated ca. 6.1 nm, which is coincident with two consecutive helical pitches of poly-(*R*)-**1** (Figure 3 and SI).

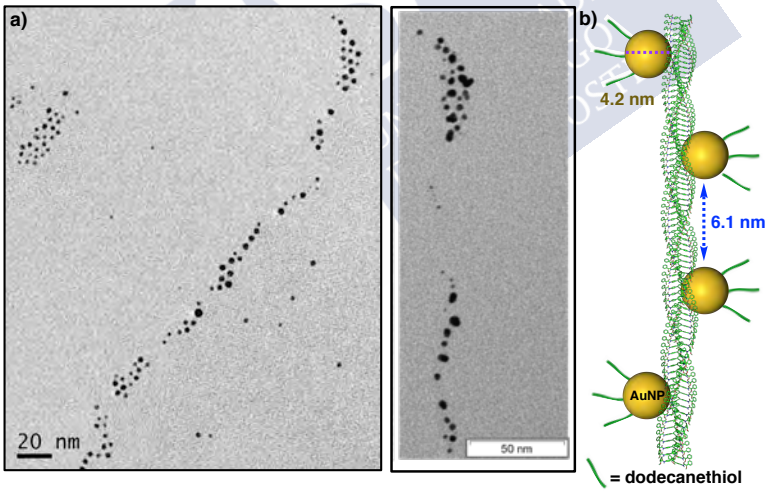

Figure 3. a) TEM images for poly-(*R*)-**1**-AuNPs/dodecanethiol (size: 4.2 ± 1.1 nm) and b) molecular model of poly-(*R*)-**1**-AuNPs/dodecanethiol nanocomposites.

Next, the dynamic behavior of the helical polymer within the nanocomposites was analyzed by Electron Circular Dichroism (ECD) and stimuli responsive studies. These experiments will allow us to determine how the different helical enhancements effects observed in poly-(*R*)-**1**, are affected once the poly-(*R*)-**1**-AuNPs/dodecanethiol is prepared. To do that, ECD experiments of a poly-(*R*)-**1**-AuNPs/dodecanethiol nanocomposites dispersion prepared in chloroform (0.1 mg mL^{-1}) were carried out. As expected, the ECD trace was null in

the 300-500 nm region, which indicates the presence of an axially racemic polymer within the nanocomposite (See SI).

The addition of external stimuli such as monovalent (Li^+) or divalent (Ba^{2+}) metal ions in a poly-(*R*)-**1**-AuNPs/dodecanethiol/M^{n+} 0.5/1.0 mol/mol ratio induce either a *M* (CD_{380} < 0), or *P* (CD_{380} > 0) helix in the PPA similar to those reported previously for poly-(*R*)-**1** (Figure 4b and SI). Comparison of the ECD traces obtained for poly-(*R*)-**1**-AuNPs/dodecanethiol/Ba^{2+} or poly-(*R*)-**1**-AuNPs/dodecanethiol/Li^+ with those obtained for poly-(*R*)-**1**/Ba^{2+} and poly-(*R*)-**1**/Li^+ show that the helical sense induction in the nanocomposite/metal complex is smaller than in the polymer/metal complex (Figure 4b and c). In this case a depletion of ca. 40% of the helix enhancement effect for poly-(*R*)-**1** in the nanocomposite is observed, which is associated to a strong interaction between the anilide groups and the gold nanoparticles.

Finally, the formation of nanospheres based on poly-**1**-AuNPs/dodecanethiol/M^{n+} was explored using the metal ions acting as crosslinking agents. Thus, dispersions of poly-**1**-AuNPs/dodecanethiol/Ba^{2+} complexes (0.1 mg mL^{-1}) at different mol/mol ratios (1/0.2; 1/0.4 and 1/0.6) were prepared and studied by DLS and Surface Electron Microscopy SEM. These studies manifest the presence of nanospheres, whose size and macroscopic chiral content (excess of *P* or *M* helical sense) can be tuned by varying the amount of the metal in the complex (Figure 4d and e and See for more details).

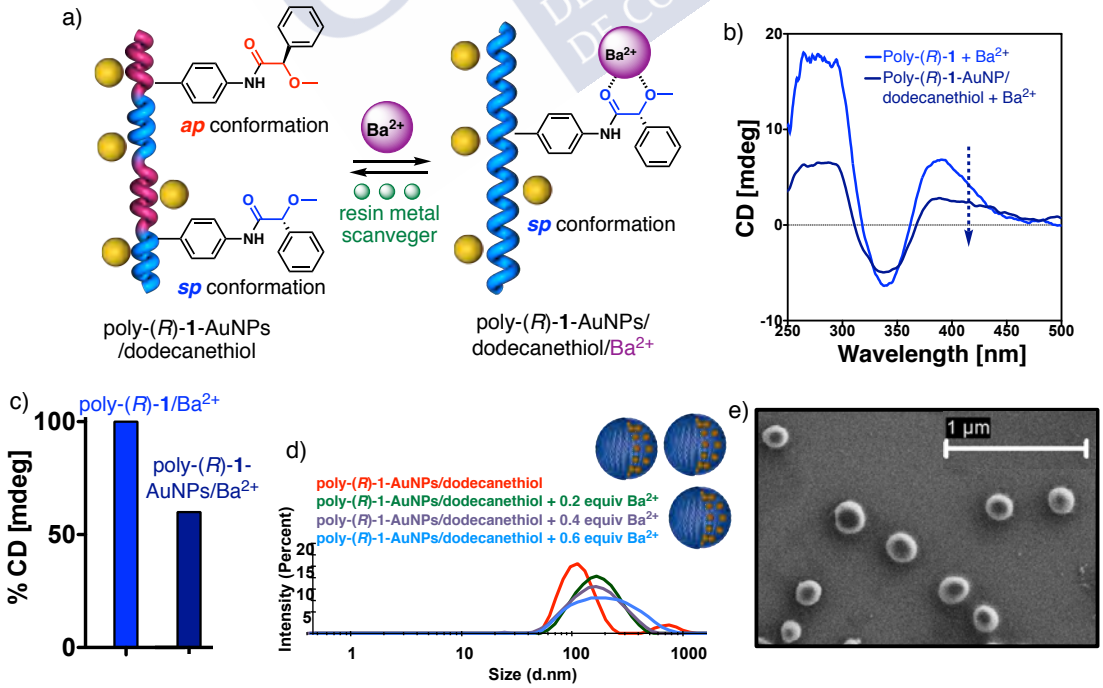

Figure 4. a) Schematic representation of helical induction by the addition of Ba^{2+} over poly-(*R*)-**1**-AuNPs/dodecanethiol nanocomposites. b) CD traces of poly-(*R*)-**1**/Ba^{2+} and poly-(*R*)-**1**-AuNPs/dodecanethiol/Ba^{2+} at 0.1 mg mL^{-1} in $CHCl_3$. c) Representation of % CD intensity at 380 nm for poly-(*R*)-**1**/Ba^{2+} and poly-(*R*)-**1**-AuNPs/dodecanethiol/Ba^{2+}. d) DLS measurements for poly-(*R*)-**1**-AuNPs/dodecanethiol/Ba^{2+} at 0.1 mg mL^{-1} in $CHCl_3$. e) SEM images for poly-(*R*)-**1**-AuNPs/dodecanethiol/Ba^{2+} in solid state (Size: 200 $\pm$ 24 nm).

3. References

1. Zhang, S.; Geryak, R.; Geldmeier, J.; Kim, S.; Tsukruk, V. Synthesis, Assembly, and Applications of Hybrid Nanostructures for Biosensing. *Chem. Rev.*, **2017**, *117*, 12942-13038.

2. Molina, M.; Asadian-Birjand, M.; Balach. J.; Bergueiro, J.; Miceli, E.; Calderon, M. Stimuli-Responsive nanogel composites and their applications in nanomedicine. *Chem. Soc. Rev.* **2015**, *17*, 6161-6186.

3. Carril, M.; Padro, D.; del Pino, P.; Carrillo-Carrion, C.; Gallego, M.; Parak, W. J.; In situ detection of the protein corona in complex environments. *Nat. Commun.* **2017**, *8*, 1542.

4. Zhou, Y.; Sun, H.; Matysiak, S.; Ren, J.; Qu, X.; Mesoporous Encapsulated Chiral Nanogold for Use in Enantioselective Reactions. *Angew. Chem. Int. Ed.,* **2018**, *57*, 16791-16795.

5. Zheng, G.; Bao, Z.; Pérez-Juste, J.; Ruolan, D.; Liu, W.; Dai, J.; Zhang, W.; Lee, L.; Wong, K-Y. Tuning the Morphology and Chiroptical Properties of Discrete Gold Nanorods with Amino Acids. *Angew. Chem. Int. Ed.,* **2018**, *57*, 16452-16457.

6. Sánchez-Iglesias, A.; Zhuo, X.; Albrecht, W.; Bals, S.; Liz-Marzán, L. M.; Tuning Size and Seed Position in Small Silver Nanorods. *ACS Materials Lett.* **2020**, *9*, 1246–1250.

7. Mosquera, J.; Zhao, Y.; Jang, H. –J.; Xie, N.; Xu, C.; Kotov, N. A; Liz-Marzán, L. M.; Plasmonic Nanoparticles with Supramolecular Recognition. *Adv. Funct. Mater.* **2020**, *30*, 1902082.

8. Pigliacelli, C.; Sánchez-Fernández, R.; D. García, M.; Peinador, C.; Pazos, E. Self-assembled peptide-inorganic nanoparticle superstrucutres: from component design to applications. *Chem Commun.* **2020**, *56*, 8000-8014.

9. Lu, J.; Xue, Y.; Bernardino, K.; Zhang, N. –N.; R. Gomes, W.; S. Ramesar, N.; Liu, S.; Hu, Z.; Sun, T.; Farias de Moura, A.; A. Kotov, N.;Liu, K.; Enhanced optical asymmetry in supramolecular chiroplasmonic assemblies with long-range order. *Science*, **2021**, *371*, 1368-1374.

10. Yashima, E.; Maeda, K.; Lida, H.; Furusho, Y.; Nagai, K. Helical Polymers: Synthesis, Structures, and Functions. *Chem. Rev.* **2009**, *109*, 6102-6211.

11. Yashima, E.; Maeda, K. Chirality-Responsive Helical Polymers. *Macromolecules*, **2008**, *41*, 3-12.

12. Rosen, B. M.; Wilson, C. J.; Wilson, D. A.; Peterca, M.; Imam, M. R.; Percec, V. Dendron-Mediated Self-Assembly, Disassembly, and Self-Organization of Complex Systems. *Chem. Rev.* **2009**, *109*, 6275-6540.

13. Freire, F.; Quiñoá, E.; Riguera, R. Supramolecular Assemblies from Poly(phenylacetylene)s. *Chem. Rev.,* **2016**, *116*, 1242-1271.

14. Freire, F.; Seco, J. M.; Quiñoá, E.; Riguera, R. Nanospheres with Tunable Size and Chirality from Helical Polymer–Metal Complexes. *J. Am. Chem. Soc.,* **2012**, *134*, 19374-19383.

15. Guan, X.; Wang, S.; Shi, G.; Zhang, J.; Wan, X.; Thermoswitching of Helical Inversion of Dynamic Polyphenylacetylenes through cis-trans Isomerization of Amide Pendants. *Macromolecules*. **2021**, *54*, 4592-4600.

16. Huang, H.; Duan, H.; Yin, L.; Qi, D.; Xue, J.; Zhang, Y.; Deng, J. Macromolecular Chiral Amplification through a Random Coil to One-Handed Helix Transformation Induced by Metal Ion Coordination in an Aqueous Solution. *Macromolecules*, **2020**, *53*, 6002−6017.

17. Suárez-Picado, E.; Quiñoá, E.; Riguera, R.; Freire, F. Poly(phenylacetylene) Amines: A General Route to Water-Soluble Helical Polyamines. *Chem. Mater. 2018*, *30*, 6908−6914.

18. Arias, S.; Núñez-Martinez, M.; Quiñoá, E.; Riguera, R.; Freire, F. A general route to chiral nanostructures from helical poly-mers: P/M switch via dynamic metal coordination. *Polym. Chem.*, **2017**, *8*, 3740-3745.

19. Echizen, K.; Taniguchi, t.; Tatsuya Nishimura, T.; Maeda, K.; Synthesis of Stereoregular Telechelic Poly(phenylacetylene)s: Facile Terminal Chain-End Functionalization of Poly(phenylacetylene)s by Terminative Coupling with Acrylates and Acrylamides in Rhodium-Catalyzed Living Polymerization of Phenylacetylenes. *J. Am. Chem. Soc.* **2021**, *143*, 9, 3604–3612.

20. Alzubi, M.; Arias, S.; louzao, I.; Quiñoá, E.; Riguera, R.; Freire F. Multipodal dynamic coordination involving cation–π interactions to control the structure of helical polymers. *Chem. Commun.* **2017**, *53*, 8573-8576.

21. Rey-Tarrío, F.; Rodríguez, R.; Quiñoá, E.; Riguera, R.; Freire, F.; Photochemical Electrocyclization of Poly(phenylacetylene)s: Unwinding Helices to Elucidate their 3D Structure in Solution. *Angew. Chem. Int. Ed.* **2021**, *60*, 8095–8103.

22. Fernández, Z.; Fernández, B.; Quiñoá, E.; Riguera, R.; Freire, F.; Chiral Information Harvesting in Helical Poly(acetylene) Derivatives Using Oligo(*p*-phenyleneethynylene)s as Spacers. *Chem. Sci.,* **2020**, *11*, 7182-7187.

23. Arias, S.; Nuñez-Martínez, M.; Quiñoá, E.; Riguera, R.; Freire, F. Simultaneous Adjustment of Size and Helical Sense of Chiral Nanospheres and Nanotubes Derived from an Axially Racemic Poly(phenylacetylene). *Small*, **2017**, *13,* 1602398.

24. Ikai, T.; Kurake, T.; Okuda, S.; Maeda, K.; Yashima, E.; Racemic Monomer-Based One-Handed Helical Polymer Recognizes Enantiomers through Auto-Evolution of Its Helical Handedness Excess. *Angew. Chem. Int*. *Ed.* **2021**, *60*, 4625–4632.

25. Li, Zhou.; Chong-Long, Li.; Run-Tan, Gao.; Shu-Ming, Kang.; Lei, Xu.; Xun-Hui, Xu.; Na, Liu.; Zong-Quan, Wu. Highly Regioselective and Helix-Sense Selective Living Polymerization of Phenyl and Alkoxyallene Using Chiral Nickel(II) Catalysts. *Macromolecules*, **2021**, *54*, 679-686.

26. Rodríguez, R.; Suárez-Picado, E.; Quiñoá, E.; Riguera, R.; Freire, F. Stimuli-responsive Macromolecular Gear: Interlocking Dynamic Helical Polymers with Foldamers. *Angew. Chem. Int. Ed.,* **2020**, *59*, 8616-8622.

27. Bergueiro, J.; Nuñez-Martínez, M.; Arias, S.; Quiñoá, E.; Riguera, R.; Freire, F. Chiral gold–PPA nanocomposites with tunable helical sense and morphology *Nanoscale Horiz.*, **2020**, *5*, 495-500.

28. Nuñez-Martínez, M.; Arias, S.; Quiñoá, E.; Riguera, R.; Freire, F. Dynamic Chiral PPA–AgNP Nanocomposites: Aligned Silver Nanoparticles Decorating Helical Polymers. *Chem. Mater*, **2021**, *33*, 4805–4812.

29. Zhang, C.; Song, C.; Yang, W.; Deng, J. Au@poly(N-propargylamide) Nanoparticles: Preparation and Chiral Recognition. *Macromol. Rapid Commun.* **2013**, *34*, 1319-1324.

30. Brust, M.; Walker, M.; Bethell, D.; Schiffrin, D. J.; Whyman, R. Synthesis of Thiol-derivatised Gold Nanoparticles in a two-phase liquid-liquid system. *J. Chem. Soc., Chem. Commun.* **1994**, 801−802.

Chapter VI

Preparation of Helical Polymer-MNPs Nanocomposites via Redox Driven Translocation of Gold or Silver Centres: Chiroptical and Colorimetric Switches

USC
UNIVERSIDADE
DE SANTIAGO
DE COMPOSTELA

Chapter VI: Preparation of Helical Polymer-MNPs Nanocomposites via Redox Driven Translocation of Gold or Silver Centres: Chiroptical and Colorimetric Switches

Abstract

A helical copoly(phenylacetylene) that follows a dynamic chiral accord effect has been prepared to synthetize dynamic chiral nanocomposites. This copolymer is formed by the 4-benzamide of (*L*)-methionine methyl ester [(*L*)-**1**], used as minor component (20%) to link the polymer to the metal nanoparticles (MNPs) through a thioether —MNP bond (M = Au, Ag)—, in addition to the chirality —helix induction— and stimuli responsive properties helix inversion— contributed by the chiral amino acid. The other comonomer (major component, 80%) is formed by the 4-benzamide of (*L*)-alanine methyl ester, which has the same dynamic behaviour than the (*L*)-methionine methyl ester, stabilizing both the same helical structure under different external stimuli such as solvent polarity or the presence of metal ions. As a result, the copolymer — poly-[(*L*)-$\mathbf{1}_{0.2}$-*co*-(*L*)-$\mathbf{2}_{0.8}$]— adopts a preferred helical sense that can be amplified or inverted by the actuation of a certain stimuli at once in both pendant groups of the copolymer. The formation of the nanocomposite can be followed by the different chiroptical responses of the copolymer once the helical polymer metal complexes are formed —*M* to *P* helix inversion by formation of poly-[(*L*)-$\mathbf{1}_{0.2}$-*co*-(*L*)-$\mathbf{2}_{0.8}$]/Au^{3+} and poly-[(*L*)-$\mathbf{1}_{0.2}$-*co*-(*L*)-$\mathbf{2}_{0.8}$]/Ag^{+}—and further reduced with $NaBH_4$ to generate the corresponding nanocomposites —*P* to *M* helix inversion by formation of poly-[(*L*)-$\mathbf{1}_{0.2}$-*co*-(*L*)-$\mathbf{2}_{0.8}$]-AuNPs (6 nm) and poly-[(*L*)-$\mathbf{1}_{0.2}$-*co*-(*L*)-$\mathbf{2}_{0.8}$]-AgNPs (5 nm)—. These nanocomposites comprise the properties of their components, the chiroptical properties associated to the dynamic helical polymer and the plasmonic properties associated to the MNPs. Thus, while the helical polymer shows a chiroptical response —helix inversion— to the presence of metal ions, the MNPs show their classical colorimetric response due to the formation of nanospheres by addition of the metal ions, which place in the aggregate the MNPs close to each other overlapping their electronic clouds. This fact produces a red shift in the LSPR band, which indicates that they are behaving as larger particles.

USC
UNIVERSIDADE
DE SANTIAGO
DE COMPOSTELA

1. Introduction

In the last decades, metallic nanoparticles (MNPs) have attracted the attention of scientific community due to its several applications in fields such as sensing,[1] theranostic[2,3] and catalysis,[4,5] among others. The success of the material in a certatin fields does not depend only on the MNP but also on the organic molecules used to decorate the nanoparticle surface.[6,7] Thus, several approaches have been described to functionalize and modify the surface of the MNPs.[8]

For example, MNPs have been coated with biomacromolecules such as DNA or proteins to obtain biocompatible nanomaterials, where the helical structure adopted by these macromolecules is neccesary to have a correct function of the biomacromolecule, and the corresponding nanocomposite.[9-10] In such cases, the hybrid material is chiral, formed by nanoparticles decorated with biomacromolecules adopting either *P* or *M* helical structures. In nature, macromolecular helical structures adopt a preferred helical sense —*e. g.* α-helix (*P*), DNA (*P*), amylose (*M*)—, which can not be modified —elongation and/or helical sense— once the biomacromolecule is produced. Nature, although is complex and sophisticated can not generate biomacromolecules with opposite helical sense due to the intrinsic chirality of the building blocks, which is limited in nature to a single (*R*)- or (*S*)-configuration —*e. g. D*-aminoacids—.

Thus, the use of these materials in chiral recognition or asymmetric catalysis is limited. To surpass this obstacle is neccesary to explore other helical macromolecules to decorate the MNPs. In this direction, the stimuli-responsive synthetic helical polymers[11-31] are great candidates to prepare helical polymers-MNPs nanocomposites where the two chiralities of the helix can be explored in different fields.

From literature, it is known that the main limitation of using dynamic helical polymers as coating agents to prepare a helical polymers-MNPs nanocomposites is the functional group used to link the macromolecule to the metal nanoparticles.[32] Thus, if a strong thiol (S—MNP) bond is used (M = Ag or Au) to prepare the nanocomposites, the dynamic behavior and stimuli-responsive properties of the PPA are largely affected when is attached to a metal nanoparticle.[32] In these nanocomposites, the addition of an external stimuli does not trigger a complete helix enhacement or helix inversion in the macromolecule (Scheme 1a). The cooperativity effect between the monomers of the helix is disrupted up by the presence of the MNPs at the helix periphery, which are to heavy to be shifted to another location by a conformational change at the polymer backbone.[32]

To surpass this problem, variations on the connectivity between the MNP and the helical polymer were done such as the use of weak supramolecular anilide-MNP interactions to prepare the helical polymer-MNPs nanocomposites (Scheme 1b).[33] In this case, the addition of external stimuli produce a conformational change in some polymer pendant groups, that through an adaptive mechanim activate/deactivate the supramolecular interactions with the metal nanoparticles and trigger a cooperativity effect along the macromolecular helix to produce a helix inversion or helix enhacenment of the nanocomposites.[33]

These nanocomposites based on supramolecular interactions have the advantage of preserving the dynamic behavior of the helical polymer, but have some other limitations, such as the need to have specific functional groups at the pendant or avoid the use of polar solvents or the presence of polar molecules that can compete with the polymer in the interaction with the MNPs.[33]

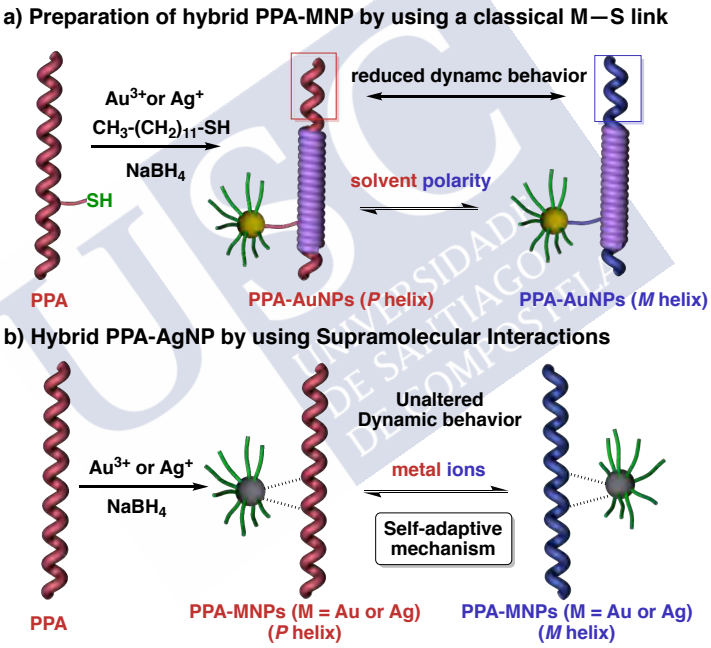

Scheme 1. Dynamic helical polymer-MNPs nanocomposites prepared via (a) classical thiol-MNP interaction and (b) supramolecular interactions.

Herein, we want to do a step forward and prepare a dynamic helical polymer-MNP nanocomposites that comprise both requirements, a strong helical polymer interaction and good stimuli-responsive properties.

Thus, based on our knowledge a nanocomposite formed by a combination of MNPs (M = Au or Ag) and a poly(phenylacetylene) (PPA) that bears the *L*-methionine methyl ester as pendant group was designed. As pendant group we chose this amino acid due to three main reasons: 1) is chiral, and therefore can induce a helical sense in the PPA; 2) contains a thioeter group that produces a strong PPA-MNP interaction and 3) the connecting point —thioeter

group— is separated from the chiral centre by a flexible alkyl chain which can adopt different conformations while conformational changes are being produced in the chiral center that result in changes at the macromolecular *P* or *M* helical structure.

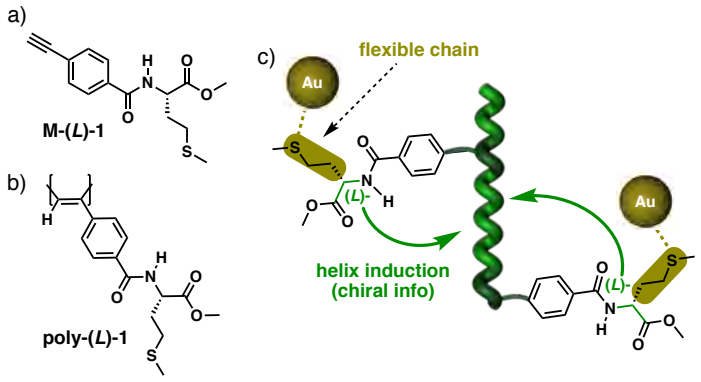

Figure 1. a) Structure of the monomer [M-(*L*)-**1**] and b) the polymer [poly-(*L*)-**1**] designed for this study. c) Illustration of the nanocomposite highlighting the structural features required for its design.

2. Results and Discussion

M-(*L*)-**1** was prepared by coupling the 4-ethynylbenzoic acid with the (*L*)-methionine methyl ester and using 1-Ethyl-3-(3-dimethylaminopropyl)carbodiimide (EDC) and hydroxybenzotriazole (HOBt) as coupling agents. Next, M-(*L*)-**1** was polymerized using $Rh(nbd)Cl]_2$ as catalyst, affording poly-(*L*)-**1** in high yield, high stereoregularity and high content of the *cis* double bonds (See SI for more details).

Next, the helical structure and dynamic behaviour of poly-(*L*)-**1** was analyzed by electronic circular dichroism (ECD) studies. Thus, poly-(*L*)-**1** was dissolved in solvents with different polarity such as $CHCl_3$, CH_2Cl_2, DMF or DMSO. ECD studies reveal that poly-(*L*)-**1** adopts a preferred *M* helix ($CD_{370} < 0$) in low polar solvents, while a *P* helix is obtained when poly-(*L*)-**1** is dissolved in high polar solvents. These results are in agreement with the helical structures induced by other PPAs bearing the 4-ethynilbenzamide of (*L*)-amino acids as pendant groups, and where in low polar solvents —$CHCl_3$, CH_2Cl_2— the two carbonyl groups of the amino acid are *antiperiplanar* (*anti*) oriented, while in high polar solvents —DMSO, DMF— are *synperiplanar* (*syn*) (Figure 2).[18,34,35]

To demostrate the presence of these two conformers in solution, perchlorate salts of metal ions such as $LiClO_4$ or $Ba(ClO_4)_2$ were added to a $CHCl_3$ solution of poly-(*L*)-**1** (0.3 mg mL^{-1}), which should produce an *anti* to *syn* conformational change at the pendant group by chelation with the metal ions and a helix inversion in the PPA. As expected, the addition of a solution of $LiClO_4$ or $Ba(ClO_4)_2$ (10 mg mL^{-1}, MeOH) to a $CHCl_3$ solution of poly-(*L*)-**1** to form the

corresponding helical polymer metal complex (HPMC) —poly-(*L*)-**1**/M^{n+}— in a 1.0/0.5 mol/mol ratio produces a helix inversion in poly-(*L*)-**1**, which confirms the presence of an *syn* conformation at the pendant group in $CHCl_3$.

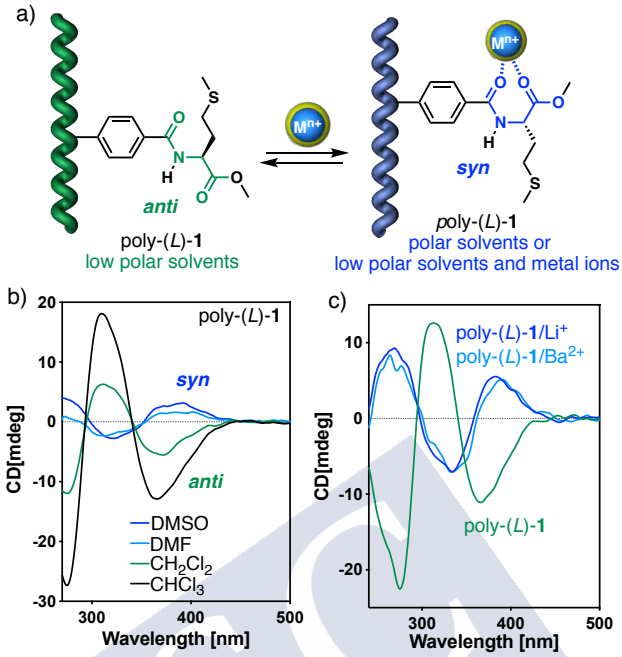

Figure 2. a) Conformational composition of poly-(*L*)-**1** at the pendant group. ECD studies showing a helix inversion effect induced by (b) solvent polarity or (c) metal ions. [poly-(*L*)-**1**] = 0.3 mg mL^{-1}, cuvette length = 0.1 cm.

Next, we proceeed to the preparation of the poly-(*L*)-**1**-MNPs nanocomposites (M = Ag, Au). Thus, a methanolic solution of either $HAuCl_4$ or $AgClO_4$ (10 mg mL^{-1}) were added to a two $CHCl_3$ solutions of poly-(*L*)-**1** (0.3 mg mL^{-1}) in a 0.5/1.0 mol/mol ratio to form either a poly-(*L*)-**1**/Au^{3+} or a poly-(*L*)-**1**/Ag^{+} metal complexes. Unfourtunately, a precipitate was observed in both cases due to the crosslinking ability of the metal ions with the thioether groups of the polymers.

Therefore, an alternative protocol to prepare the nanocomposites must be addressed. The structure of the helical polymer was changed to a copolymer made by two amino acids, the (*L*)-methionine methyl ester —M-(*L*)-**1**— needed to stabilize the metal nanoparticles, and the (*L*)-alanine methyl ester —M-(*L*)-**2**— (Figure 3) that has the same dynamic helix behavior than poly-(*L*)-**1** but lack the thioeter group, responsible for the aggregation of poly-(*L*)-**1**/Au^{3+} and poly-(*L*)-**1**/Ag^{+} metal complexes.

Thus, in the poly-[(*L*)-$\mathbf{1}_r$-*co*-(*L*)-$\mathbf{2}_{1-r}$] (r = 0.2-0.8) copolymer series (Figure 3b) both monomers promote the same helical sense and respond to the external stimuli in the same way —*chiral accord*—. As a result, the dynamic helix behavior and the stimuli-responsive

properties of the poly-[(*L*)-**1**$_r$-*co*-(*L*)-**2**$_{1-r}$] copolymer series is the same than the one obtained for the corresponding homopolymers —*M* helix in low polar solvents ($CHCl_3$, CH_2Cl_2), *P* helix in high polar solvents (DMSO, DMF) and helix inversion from *M* to *P* in $CHCl_3$ by coordination with metal ions (Figure 3c-d)—. The main advantage of using the poly-[(*L*)-**1**$_r$-*co*-(*L*)-**2**$_{1-r}$] copolymer series to prepare the nanocomposite is the possibility of varying the ratio of the two comonomers and determine which copolymer generates the nanocomposite with the best properties.

Before preparing the nanocomposite using the poly-[(*L*)-**1**$_r$-*co*-(*L*)-**2**$_{1-r}$] copolymer series, the role of poly-(*L*)-**2** in the formation of the nanocomposite was analyzed. Poly-(*L*)-**2** has a benzamide group at the pendant which could stabilize the nanocomposite through an benzamide-MNPs supramolecular interactions. From literature it is known that amides or anilides are used to functionalize a MNP with a polymer bearing these functional groups, although no studies have been done with benzamides.

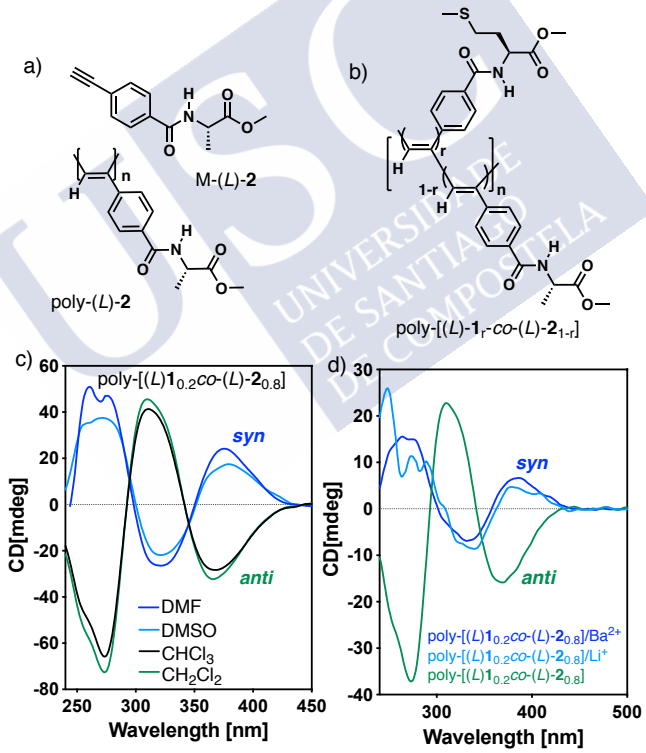

Figure 3. a) Structure of monomer M-(*L*)-**2** and poly-(*L*)-**2**. b) Structure of poly-[(*L*)-**1**$_r$-*co*-(*L*)-**2**$_{1-r}$] (r = 0.2-0.8). ECD studies showing a helix inversion effect induced by c) solvent polarity and c) metal ions in poly-[(*L*)-**1**$_{0.2}$-*co*-(*L*)-**2**$_{0.8}$] (0.3 mg mL^{-1}, cuvette length = 0.1 cm).

Thus to explore the role of a benzamide in a PPA-MNP nanocomposite, $HAuCl_4$ (10 mg mL^{-1}, MeOH) and $AgClO_4$ (10 mg mL^{-1}, MeOH) were added separetely to two different solutions of poly-(*L*)-**2** (0.3 mg mL^{-1}, $CHCl_3$) to form the poly-(*L*)-**2**/Au^{3+} and the poly-(*L*)-**2**/Ag^{+} complexes

in a 1.0/0.5 mol/mol ratio. As expected a helix inversion is observed in both cases by chelation of the alanine methyl ester pendant group with the Au^{3+} or the Ag^{+} ions (See SI). Subsequently, 1 equiv. of a solution of $NaBH_4$ (1 mg mL^{-1}, MeOH) was added to the poly-(*L*)-**2**/Au^{3+} and the poly-(*L*)-**2**/Ag^{+} complexes to form the poly-(*L*)-**2**-AuNP and the poly-(*L*)-**2**-AgNP nanocomposites. A colour change was observed in both solutions due to the formation of the metal nanoparticles, that was confirmed by UV-vis studies where the classical localized surface plasmon resonance (LSPR) band is observed. Unfortunately, TEM images revealed the formation of high polydisperse AuNPs or AgNPs, fact that indicates a poor stabilization of the MNPs by weak supramolecular benzamide-MNPs interactions.

Hence, at this point we know that while both polymers —poly-(*L*)-**1** and poly-(*L*)-**2**— interact with Ag^{+} or Au^{3+} in $CHCl_3$ producing a helix inversion in the polymer, poly-(*L*)-**2** does not stabilize nanoparticles of these metals once they have been reduced. Therefore, the formation of stable poly-[(*L*)-$\mathbf{1}_r$-*co*-(*L*)-$\mathbf{2}_{1-r}$]-AuNPs or poly-[(*L*)-$\mathbf{1}_r$-*co*-(*L*)-$\mathbf{2}_{1-r}$]-AuNPs nanocomposites should be attributed to the thioeter-MNP interactions.

The solubility of the poly-[(*L*)-$\mathbf{1}_r$-*co*-(*L*)-$\mathbf{2}_{1-r}$] (r = 0.2-0.8) copolymer series is directly dependent on the amount of monomer M-(*L*)-**1** in the copolymer. Those copolymers incorporating (*L*)-**1** in a ratio higher than 0.3 show poor solubility in a large variety of solvents. Taking this property into consideration, poly-[(*L*)-$\mathbf{1}_{0.2}$-*co*-(*L*)-$\mathbf{2}_{0.8}$] was chosen as coating agent to carried the formation of the poly-[(*L*)-$\mathbf{1}_{0.2}$-*co*-(*L*)-$\mathbf{2}_{0.8}$]-AuNPs and poly-[(*L*)-$\mathbf{1}_{0.2}$-*co*-(*L*)-$\mathbf{2}_{0.8}$]-AgNPs nanocomposites. Thus, the corresponding helical polymer metal complexes —poly-[(*L*)-$\mathbf{1}_{0.2}$-*co*-(*L*)-$\mathbf{2}_{0.8}$]/Au^{3+} and poly-[(*L*)-$\mathbf{1}_{0.2}$-*co*-(*L*)-$\mathbf{2}_{0.8}$]/Ag^{+} were prepared first. To do that, $HAuCl_4$ (10 mg mL^{-1}, MeOH) or $AgClO_4$ (10mg mL^{-1}, MeOH) were added to two diffferent $CHCl_3$ solutions of poly-[(*L*)-$\mathbf{1}_{0.2}$-*co*-(*L*)-$\mathbf{2}_{0.8}$] (0.3 mg mL^{-1}) in a 0.5/1.0 poly-[(*L*)-$\mathbf{1}_{0.2}$-*co*-(*L*)-$\mathbf{2}_{0.8}$]/M^{n+} mol/mol ratio.

As expected, a helix inversion is observed in both cases due to an *anti* to *syn* conformational change at the pendant groups by chelation with the Au^{3+} (Figure 4a, b) or the Ag^{+} ions (Figure 4e, f). Subsequently, 1 equiv. of a solution of $NaBH_4$ (1 mg mL^{-1}, MeOH) was added to the poly-[(*L*)-$\mathbf{1}_{0.2}$-*co*-(*L*)-$\mathbf{2}_{0.8}$]/Au^{3+} and the poly-[(*L*)-$\mathbf{1}_{0.2}$-*co*-(*L*)-$\mathbf{2}_{0.8}$]/Ag^{+} complexes to form the poly-[(*L*)-$\mathbf{1}_{0.2}$-*co*-(*L*)-$\mathbf{2}_{0.8}$]-AuNP and the poly-[(*L*)-$\mathbf{1}_{0.2}$-*co*-(*L*)-$\mathbf{2}_{0.8}$]-AgNP nanocomposites. A colour change (yellow to red for poly-[(*L*)-$\mathbf{1}_{0.2}$-*co*-(*L*)-$\mathbf{2}_{0.8}$]-AuNPs (Figure 4a) and yellow to orange for poly-[(*L*)-$\mathbf{1}_{0.2}$-*co*-(*L*)-$\mathbf{2}_{0.8}$]-AgNPs) (Figure 4e) was observed in both solutions due to the formation of the metal nanoparticles, that was confirmed by UV-vis studies where the classical LSPR band for either spherical Au (531 nm, Figure 4d) or AgNPs (405 nm, Figure 4h) is present.

Interestingly, TEM imgaes of both nanocomposites show the presence of spherical AuNPs with 6.0 ± 1.6 nm of size in case of poly-[(*L*)-**1**$_{0.2}$-*co*-(*L*)-**2**$_{0.8}$]-AuNPs (Figure 4d) and spherical AgNPs with 5.3 ± 1.8 nm of size in case of poly-[(*L*)-**1**$_{0.2}$-*co*-(*L*)-**2**$_{0.8}$]-AgNPs (Figure 4h). These nanocomposites are stable with time as inferred from UV-vis- studies, which can be stored in solution for days and where no aggregation of the MNPs is observed (see SI for more details).

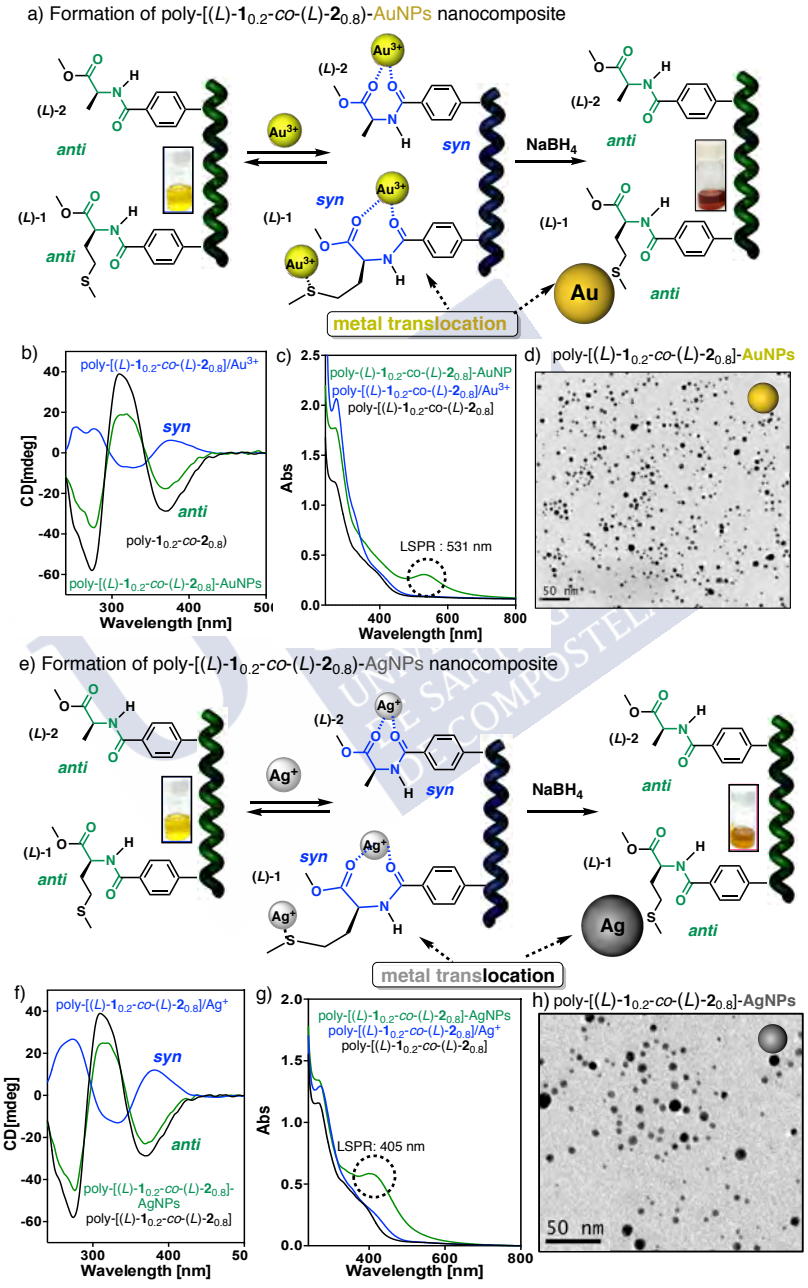

Figure 4. a) Schematic illustration for the preparation of poly-[(*L*)-**1**$_{0.2}$-*co*-(*L*)-**2**$_{0.8}$]-AuNPs and its chiroptical responses associated to a redox driven translocation of a gold metal centre. b) CD and c) UV-vis spectra for poly-[(*L*)-**1**$_{0.2}$-*co*-(*L*)-**2**$_{0.8}$], poly-[(*L*)-**1**$_{0.2}$-*co*-(*L*)-**2**$_{0.8}$]/Au^{3+} and poly-[(*L*)-**1**$_{0.2}$-*co*-(*L*)-**2**$_{0.8}$]-AuNPs. d) TEM image for poly-(**1**$_{0.2}$-*co*-**2**$_{0.8}$)-AuNPs nanocomposites. e) Schematic illustration for the preparation

of poly-[(*L*)-**1**$_{0.2}$-*co*-(*L*)-**2**$_{0.8}$]-AgNPs and its chiroptical responses associated to a redox driven translocation of a silver metal center. f) CD and (g) UV-vis spectra for poly-[(*L*)-**1**$_{0.2}$-*co*-(*L*)-**2**$_{0.8}$], poly-[(*L*)-**1**$_{0.2}$-*co*-(*L*)-**2**$_{0.8}$]/Ag^+ and poly-[(*L*)-**1**$_{0.2}$-*co*-(*L*)-**2**$_{0.8}$]-AgNPs. h) TEM image for poly-[(*L*)-**1**$_{0.2}$-*co*-(*L*)-**2**$_{0.8}$]-AgNPs nanocomposites.

It is worthmentioning the chiropotical responses of poly-[(*L*)-**1**$_{0.2}$-*co*-(*L*)-**2**$_{0.8}$] after complexation with the metal ions —*M* (CD_{370} < 0) to *P* (CD_{370} > 0) helix—and once the poly-[(*L*)-**1**$_{0.2}$-*co*-(*L*)-**2**$_{0.8}$]-MNPs nanocomposites is formed due to a redox driven metal ion translocation process —*P* (CD_{370} > 0) to *M* (CD_{370} < 0) helix—. The helix inversion mechanism produced in poly-[(*L*)-**1**$_{0.2}$-*co*-(*L*)-**2**$_{0.8}$] once a metal ion such as Au^{3+} or Ag^+ is added to form HPMC is identical to that showed by poly-(*L*)-**1** in the presence of metal ions, which can be monitored by IR studie (See SI). The metal ions coordinate the two carbonyls of the pendant group to form a chelate, which results in an to *anti* to *syn* conformational change at the pendant group and a *M* to *P* helix inversion at the helical polymer. Further reduction of the metal ion disrupt the chelate —inferred from IR studies (See SI)— being the MNPs attached to the polymer just through the thioeter group. As a result, the pendant groups recover its preferred *anti* conformation, which produce another helix inversion in the polyene bacbone from *P* to *M*, recovering its initial helical structure. Hence, different chiroptical responses are obtained in the PPA during the complexation with metal ions and ulterior reduction to form the PPA-MNPs nanocomposites.

2.1 Dynamic behavior of Poly-[(*L*)-1$_{0.2}$-co-(*L*)-2$_{0.8}$]-MNPs (M = Au, Ag) nanocomposites

Once the nanocomposites based on a dynamic helical polymer were obtained, their stimuli responsive properties —external stimuli: solvent polarity and metal ions— were tested. As expected, poly-[(*L*)-**1**$_{0.2}$-*co*-(*L*)-**2**$_{0.8}$]-MNPs (M = Au or Ag) nanocomposites show a good stimuli-responsive properties similar to those found for the corresponding materials (See SI). Intriguinly, the addition of metal ions to a dispersion of the poly-[(*L*)-**1**$_{0.2}$-*co*-(*L*)-**2**$_{0.8}$]-MNPs (M = Au or Ag) nanocomposites produced not only a chiroptical response —helix inversion from *M* to *P* due to a chelation of the metal ions with the pendants that result in an *anti* to *syn* conformational change at the pendant group— (See Figure 5a,b and 5e,f for Ag^+ and SI for other metal ions), but also a colorimetric one associated to a bathochromic shift of the LSPR band consequence of the aggregation of the MNPs s by addition of the metal ions —red shift from 405 nm to 425 nm for poly-[(*L*)-**1**$_{0.2}$-*co*-(*L*)-**2**$_{0.8}$]-AgNPs/Ag^+ and from 530 nm to 542 nm poly-[(*L*)-**1**$_{0.2}$-*co*-(*L*)-**2**$_{0.8}$]-AuNPs/Ag^+ — (Figures 5c, 5f and SI). In helical polymer metal complexes such as poly-(*L*)-**1**/M^{n+} is known their ability to form chiral nanospheres due to the

crosslinking ability of the metal ion in non polar solvents such as $CHCl_3$. In case of poly-[(*L*)-**1**$_{0.2}$-*co*-(*L*)-**2**$_{0.8}$]-MNPs (M = Au or Ag) the addition of metal ions such as Ag^+ produce the formation of well defined and low poly-dispersed nanospheres, demonstrated by Dynamic Light Scatering (DLS) and Electron Microscopy studies (SEM and STEM) (Figure 5d and 5h and SI). Interestingly, in this system the formation of nanospheres based on the poly-[(*L*)-**1**$_{0.2}$-*co*-(*L*)-**2**$_{0.8}$]-MNPs (M = Au or Ag) nanocomposites place the MNPs close to each other that results in the overlap of their electronic clouds behaving therefore as larger particles and producing a red shift in the LSPR band.

In the case of the poly-[(*L*)-**1**$_{0.2}$-*co*-(*L*)-**2**$_{0.8}$]-AgNPs/Ag^+ it was found the reversibility o the process by addition of metal scavenger resins, which remove the silver ions from the nanocomposite/metal complex and recovers the initial non-aggregated state of the nanocomposite.

As a result, an hypsochromic shift is produced in the LSPR band recovering the original plasmon band for the nanocomposite. On the contrary, in case of the nanospheres made by poly-[(*L*)-**1**$_{0.2}$-*co*-(*L*)-**2**$_{0.8}$]-AuNPs/Ag^+ complex it was not possible to have a reversible process by addition of metal scavenger resins. In this system, water does not trap the Ag^+ ions and the original form of the nanocomposite is not recovered.

USC UNIVERSIDADE DE SANTIAGO DE COMPOSTELA

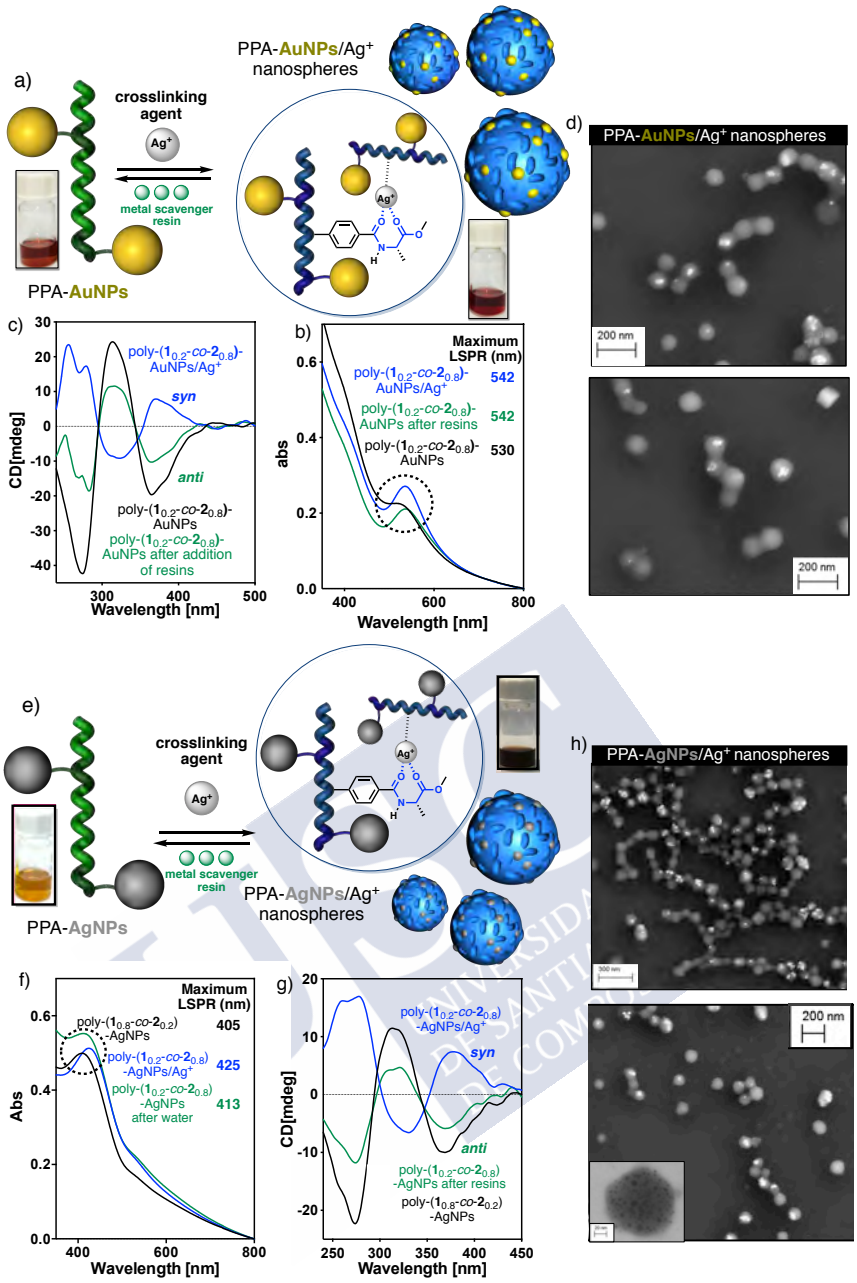

Figure 5. Graphical representation of the controlled aggregation of (a) poly-[(*L*)-**1**$_{0.2}$-*co*-(*L*)-**2**$_{0.8}$]-AuNPs/Ag$^+$ and (d) poly-[(*L*)-**1**$_{0.2}$-*co*-(*L*)-**2**$_{0.8}$]-AgNPs/Ag$^+$. UV and CD studies of the aggregation process for (b,f) poly-[(*L*)-**1**$_{0.2}$-*co*-(*L*)-**2**$_{0.8}$]-AuNPs/Ag$^+$ and (c, g) poly-[(*L*)-**1**$_{0.2}$-*co*-(*L*)-**2**$_{0.8}$]-AuNPs/Ag$^+$. SEM images showing nanospheres of (d) poly-[(*L*)-**1**$_{0.2}$-*co*-(*L*)-**2**$_{0.8}$]-AuNPs/Ag$^+$ and (h) poly-[(*L*)-**1**$_{0.2}$-*co*-(*L*)-**2**$_{0.8}$]-AuNPs/Ag$^+$.

3. References

1. Zhang, S.; Geryak, R.; Geldmeier, J.; Kim, S.; Tsukruk, V. Synthe-sis, Assembly, and Applications of Hybrid Nanostructures for Biosensing. Chem. Rev., **2017**, *117*, 12942-13038.

2. Lin, B.; Wang, Y.; Yang, F.; Huang, L.; Lv, R.; Enhanced Upconversion Luminescence-Guided Synergistic Antitumor Therapy Based on Photodynamic Therapy and Immune Checkpoint Blockade. *Chem. Mater.* **2020**, *32*, 11, 4627–4640.

3. Jaque, D.; Martínez Maestro, L.; del Rosal, B.; Haro-Gonzalez, P.; Benayas, A.; Plaza, J. L.; Martín Rodriguez, E.; García Solé, J. Nanoparticles for photothermal therapies. *Nanoscale*, **2014**, 9494-9530.

4. Moon, H.; Kim, Y.; Photothermal-Mediated Catalytic Reduction of 4-Nitrophenol Using Poly(N-isopropylacrylamide-acrylamide) and Hollow Gold Nanoparticles. *ACS Appl. Polym. Mater.* **2021**, *3*, 2768−2775.

5. Schrinner, M.; Ballauff, M.; Talmon, Y.; Kauffmann, Y.; Thun, J.; Moller, M.; Breu, J. Single Nanocrystals of Platinum Prepared by Partial Dissolution of Au-Pt Nanoalloys. *Science* **2009**, *323*, 617–620.

6. A. Sánchez-Iglesias, X. Zhuo, W. Albrecht, S. Bals, L.M. Liz-Marzán, Tuning Size and Seed Position in Small Silver Nanorods. *ACS Mater. Lett.* **2020**, *2*, 1246-1250.

7. Pastoriza-Santos, I.; Liz-Marzán, L. M. N,N-Dimethylformamide as a Reaction Medium for Metal Nanoparticle Synthesis. *Adv. Func. Mater.* **2009**, *19*, 679-688.

8. Coelho, J. P.; Mayoral, M. J.; Camacho, L.; Martín-Romero, M. T.; Tardajos, G.; López-Montero, I.; Sanz, E.; Ávila-Brande, D.; Giner-Casares, J.; Fernández, G.; Guerrero-Martínez, A.; Mechanosensitive Gold Colloidal Membranes Mediated by Supramolecular Interfacial Self-Assembly. *J. Am. Chem. Soc.* **2017**, *139*, 3, 1120–1128.

9. Mosquera, J.; Zhao, Y.; Hee-Jeong, Y.; Xie, N.; Xu, C.; Kotov, N.; Liz-Marzán, L. M.; Plasmonic Nanoparticles with Supramolecular Recognition. *Adv. Funct. Mater.* **2020**, *30*, 1902082.

10. Pigliacelli, C.; Sánchez-Fernández, R.; D. García, M.; Peinador, C.; Pazos, E. Self-assembled peptide-inorganic nanoparticle superstrucutres: from component design to applications. *Chem Commun.* **2020**, *56*, 8000-8014.

11. Van Leeuwen, T.; Heideman, H. G.; Zhao, D.; Wezenberg, S. J. ; Feringa, B. L. *In situ* control of polymer helicity with a non-covalently bound photoresponsive molecular motor dopant. *Chem. Commun*., **2017**, *53*, 6393-6396.

12. Wang, S.; Chen, J.; Feng, X.; Shi, G.; Zhang, J.; Wan, X. Conformation Shift Switches the Chiral Amplification of Helical Copoly(phenylacetylene)s from Abnormal to Normal "Sergeants-and-Soldiers" Effect. *Macromolecules*, **2017***, 50,* 4610-4615.

13. Freire, F.; Quiñoá, E.; Riguera, R. Supramolecular Assemblies from Poly(phenylacetylene)s. *Chem. Rev*., **2016**, *116*, 1242-1271.

14. Freire, F.; Seco, J. M.; Quiñoá, E.; Riguera, R. Helical Polymer–Metal Complexes: The Role of Metal Ions on the Helicity and the Supramolecular Architecture of Poly(phenylacetylene)s. *Adv. Polym. Sci*., **2013**, *262*, 123-140.

15. Yashima, E. Synthesis and structure determination of helical polymers. *Polymer Journal*, **2010**, *42*, 3-16.

16. Yashima, E.; Maeda, K. Chirality-Responsive Helical Polymers. *Macromolecules*, **2008**, *41*, 3-12.

17. Percec, V.; Rudick, J. G.; Peterca, M.; Heiney, P. A. Nanomechanical Function from Self-Organizable Dendronized Helical Polyphenylacetylenes. *J. Am. Chem. Soc.*, **2008**, *130*, 7503-7508.

18. Arias, S.; Núñez-Martinez, M.; Quiñoá, E.; Riguera, R.; Freire, F. A general route to chiral nanostructures from helical polymers: *P*/*M* switch *via* dynamic metal coordination. *Polym. Chem.,* **2017**, *8*, 3740-3745.

19. Rodríguez, R.; Arias, S.; Quiñoá, E.; Riguera, R.; Freire, F. The role of the secondary structure of helical poly(phenylacetylene)s in the formation of nanoparticles from polymer–metal complexes (HPMCs). *Nanoscale*, **2017**, *8*, 17752-17757.

20. Suárez-Picado, E.; Quiñoá, E.; Riguera, R.; Freire, F. Poly(phenylacetylene) Amines: A General Route to Water-Soluble Helical Polyamines. *Chem. Mater.* **2018**, *30*, 6908−6914.

21. Rodríguez, R.; Suárez-Picado, E.; Quiñoá, E.; Riguera, R.; Freire, F. Stimuli-responsive Macromolecular Gear: Interlocking Dynamic Helical Polymers with Foldamers *Angew. Chem. Int. Ed.,* **2020**, *59*, 8616-8622

22. Suárez-Picado, E.; Quiñoá, E.; Riguera, R.; Freire, F. Chiral Overpass Induction in Dynamic Helical Polymers Bearing Pendant Groups with Two Chiral Centers. *Angew. Chem. Int. Ed.*, **2020**, *59*, 4537-4543.

23. Fernández, Z.; Fernández, B.; Quiñoá, E.; Riguera, R.; Freire, F.; Chiral Information Harvesting in Helical Poly(acetylene) Derivatives Using Oligo(p-phenyleneethynylene)s as Spacers. *Chemical Science*, **2020**, *11*, 7182-7187.

24. Rodríguez, R.; Quiñoá, E.; Riguera, R.; Freire, F. Multistate Chiroptical Switch Triggered by Stimuli-Responsive Chiral Teleinduction, *Chem. Mater.* **2018**, *30*, 2493−2497.

25. Rodríguez, R.; Quiñoá, E.; Riguera, R.; Freire, F. Architecture of Chiral Poly(phenyl acetylene)s: From Compressed/Highly Dynamic to Stretched/Quasi-Static Helices. *J. Am. Chem. Soc.,* **2016,** *138,* 9260-9268.

26. Freire, F.; Seco, J. M.; Quiñoá, E.; Riguera, R. Nanospheres with Tunable Size and Chirality from Helical Polymer–Metal Complexes. *J. Am. Chem. Soc.*, **2012**, *134*, 19374-19383.

27. Yoshinaga, Y.; Yamamoto, T.;Suginome, M.; Enantioconvergent Cu-Catalyzed Intramolecular C–C Coupling at Boron-Bound C(sp3) Atoms of α-Aminoalkylboronates Using a *C*1-Symmetrical 2,2'-Bipyridyl Ligand Attached to a Helically Chiral Macromolecular Scaffold. *J. Am. Chem. Soc.*, **2020**, *142*, 18317–18323.

28. Nagata, Y.; Takeda, R.; Suginome, M.; Asymmetric Catalysis in Chiral Solvents: Chirality Transfer with Amplification of Homochirality through a Helical Macromolecular Scaffold. *ACS Cent. Sci.*, **2019**, *5*, 1235-1240.

29. Li, Yan-Xiang.; Xu, Lei.; Kang, Shu-Ming.; Zhou, Li.; Liu, Na.; Wu, Zong-Quan. Helicity- and Molecular-Weight-Driven Self-Sorting and Assembly of Helical Polymers towards Two-Dimensional Smectic Architectures and Selectively Adhesive Gels. *Angew. Chem. Int. Ed.*, **2021**, *60*, 7174-7179.

30. Li, Zhou.; Chong-Long, Li.; Run-Tan, Gao.; Shu-Ming, Kang.; Lei, Xu.; Xun-Hui, Xu.; Na, Liu.; Zong-Quan, Wu. Highly Regioselective and Helix-Sense Selective Living Polymerization of Phenyl and Alkoxyallene Using Chiral Nickel(II) Catalysts. *Macromolecules*, **2021**, *54*, 679-686.

31. Li, Zhou.; Xun-Hui, Xu.; Zhi-Qiang, Jiang.; Lei, Xu.; Ben-Fa, Chu.; Na, Liu.; Zong-Quan, Wu. Selective Synthesis of Single-Handed Helical Polymers from Achiral Monomer and a Mechanism Study on Helix-Sense-Selective Polymerization. *Angew. Chem. Int. Ed.*, **2021**, *60*, 806-812.

32. Bergueiro, J.; Nuñez-Martínez, M.; Arias, S.; Quiñoá, E.; Riguera, R.; Freire, F. Chiral gold–PPA nanocomposites with tunable helical sense and morphology *Nanoscale Horiz.*, **2020**, *5*, 495-500.

33. Nuñez-Martínez, M.; Arias, S.; Quiñoá, E.; Riguera, R.; Freire, F. Dynamic Chiral PPA-AgNPs Nanocomposites: Aligned Silver Nanoparticles Decorating Helical Polymers. *Chem. Mater.* **2021**, *33*, 4805–4812.

34. Li, B. S.; Lam, J. W. Y.; Yu, Z. –Q.; Tang, B. Z.; Tunable Helical Assemblies of L-Alanine Methyl Ester-Containing Polyphenylacetylene. *Langmuir*, **2012**, *28*, 5770.

35. Li, B. S.; Kang, S. Z.; Cheuk, K. L.; Wan, L.; Ling, L.; Bai, C.; Tang, B. Z.; Self-assembling of Helical Poly(Phenylacetylene) Carrying L-Valine Pendants in Solution, on Mica Substrate, and on Water Surface. *Langmuir*, **2004**, *20*, 7598.

USC
UNIVERSIDADE
DE SANTIAGO
DE COMPOSTELA

USC
UNIVERSIDADE
DE SANTIAGO
DE COMPOSTELA

Chapter VII

ON-OFF Stereocomplexation of Dynamic Helical Polymer-MNPs (M = Ag, Au) Nanocomposites by Taming the Polymer Helix

USC
UNIVERSIDADE
DE SANTIAGO
DE COMPOSTELA

Chapter VII: ON-OFF Stereocomplexation of Dynamic Helical Polymer-MNPs (M = Ag, Au) Nanocomposites by Taming the Polymer Helix

Abstract

Controlled ON/OFF stereocomplexation of dynamic helical polymers-metal nanoparticles nanocomposites —poly(phenylacetylene)-MNPs nanocomposites (M = Au or Ag)— is presented as a novel hybrid material that can be appears either as well dispersed MNPs (stereocomplex OFF) or as fibre-like aggregates (stereocomplex ON) with the metal nanoparticles distributed along the material. The stereocomplex is formed by interaction of two complementary and dynamic helical polymer-MNP nanocomposites. In this case, the use of dynamic helical polymers, *i.e.* poly(phenylacetylene)s (PPAs), as coating agents of the metal nanoparticles makes possible to tune the secondary structure of the polymer —elongation and/or compression— by playing with solvents, fact that trigger or deactivate the formation of the stereocomplex. Moreover, because the stereocomplex is also stabilized by a hydrogen bond network between complementary and enantiomeric helices, variations on the environmental conditions used to prepare the nanocomposite, such as temperature, can also affect in a reversible way to the ON/OFF formation of the PPA-MNP (M = Au, Ag) nanocomposites.

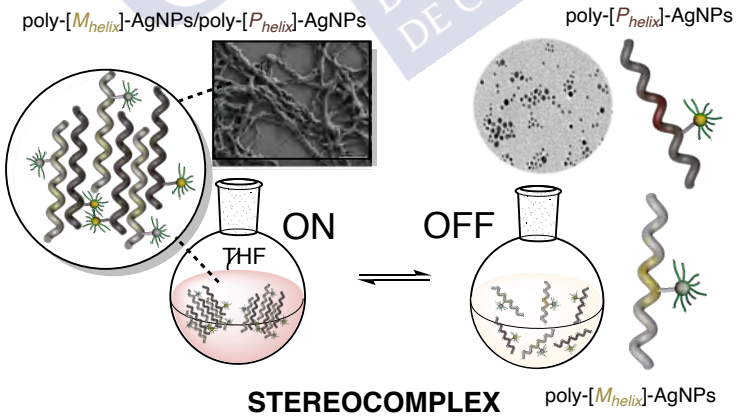

USC
UNIVERSIDADE
DE SANTIAGO
DE COMPOSTELA

1. Introduction

Metal nanoparticles (MNPs) have been exploited during the last decades by the scientific community due to their applications in fields such as theranostic,[1,2] sensing,[3] or catalysis.[4,5] To apply these materials in different fields, and work under different conditions —solvent, temperature, etc—, it is necessary to decorate the NMP surface with an appropriate coating, usually an organic molecule. Thus, in literature is possible to find many research articles dealing with the functionalization and post-functionalization of the MNP surface.[6] Our group has been working lately in the decoration and stabilization of NMPs with dynamic helical polymers such as poly(phenylacetylene)s (PPAs).[7,8]

These polymers have an advantage respect other natural macromolecules such as DNA or proteins. The later, generate water soluble static helical structures that cannot be modified —helix inversion, stretching/compression— once the macromolecule is generated.[9] To do that is necessary to change the absolute configuration of the building blocks (amino acids, nucleotides), which results very expensive. The use of non-natural polymers as coating of MNPs is cheap and allows to work with a large variety of functional groups, introducing some advantages to the material such as working in different conditions such as polar or non-polar solvents, or at different temperatures, light exposure, or pH.[10,11]

Moreover, the introduction of dynamic helical polymers[12-27] as coating agents has an extra property, the possibility of tuning their helical structure once have been prepared. From previous studies it is known that the dynamic behaviour of the helical polymer can be altered by the union strength between the polymer and the MNP (See Chapter III). Thus, in case of using PPAs bearing a thiol or thioether group as linking groups to the MNPs, it is necessary to prepare a copolymer due to the poor solubility of the homopolymers containing thiol or thioether groups in the monomer repeating units (See Chapter I and IV). In case of preparing a copolymer is necessary to consider all the chiral communication mechanisms that can emerge between the two components. Thus, when the copolymer is made by two chiral monomers, a “chiral accord” or chiral coalition effect should occur between monomers to preserve the dynamic behaviour in the copolymer, while if one of the monomers is chiral and the other chiral a Sergeants and Soldiers effect should be triggered within the copolymer series.

On the other hand, if a supramolecular interaction such as an amide—MNP is used to link the two components of the nanocomposite, homopolymers can be used,

although the presence of certain functional groups in the monomer repeating unit or the use of polar solvents can affect to the correct formation of the desired hybrid materials (See Chapter II).

Hence, to design correctly a dynamic chiral nanocomposite, is necessary to consider the functional groups present in the homopolymer/copolymer and the environmental conditions where the nanocomposite will be used.

In this work, our goal is to prepare stereocomplexes from dynamic helical polymers-AuNPs nanocomposites. Stereocomplexes are supramolecular aggregates formed by the interaction of complementary stereoregular polymers with different properties to the parent homopolymers.[28] Attending to the composition of the polymers, two different types of stereocomplexes can be formed: homo-stereocomplexes, formed from enantiomeric homopolymers and hetero-stereocomplexes, generated by the interaction between polymers with structurally different and opposite absolute configuration or different tacticities.

Stereocomplexes made by the interaction of the two enantiomeric Poly-(*D*)- and Poly-(*L*)-(Lactic acid) (PLA), or the interaction between syndiotactic and isotactic Poly(methylmetacrylate)s [*it*- and *st*-PMMA)] have been studied during the last decades.[29] In addition, these studies found that the presence of weak supramolecular interactions such as Van der Waals forces or hydrogen bond interactions are needed for the stabilization of the stereocomplexes.[29] These stereocomplexes have been also employed to prepare nanocomposites with graphene oxide (GO), clay, carbon nanotubes, cellulose nanocrystals, silica, or metal nanoparticles.[30-32]

Our group designed a novel class of stimuli-responsive stereocomplex by interaction of helically complementary poly(phenylacetylene)s (PPAs) obtained from polymerization of the 4-ethynylanilide of (*R*)- and (*S*)-α-methoxy-α-trifluoromethylphenylacetic yielding poly-(*R*)-**1** and poly-(*S*)-**1** respectively (Figure 1a).[33] The stereocomplex is formed by supramolecular interactions between complementary helices bearing *cis* amide bonds on the polymer helix periphery, which produce the formation of supramolecular fibre-like aggregates that at higher concentrations results in gels (Figure 1b-c). Modification of the *cis*-*trans* amide conformation at the pendants by solvent polarity or disrupting the hydrogen bond interactions by increasing temperature or addition of donor solvents (*e.g.* MeOH) allows the controlled formation and cleavage of the stereocomplexes.[33]

Poly-**1** is therefore a great candidate to create a stimuli-responsive stereocomplexes PPA-MNPs (M= Au, Ag) nanocomposite. In a previous work, we found

that poly-**1** does not form stable poly-**1**-MNPs (M = Au, Ag) through supramolecular anilide-MNP interactions (Chapter II).[8] The presence of a CF_3 group at the pendant deactivates the donor behaviour of the anilide and therefore their ability to interact with the MNPs.[8]

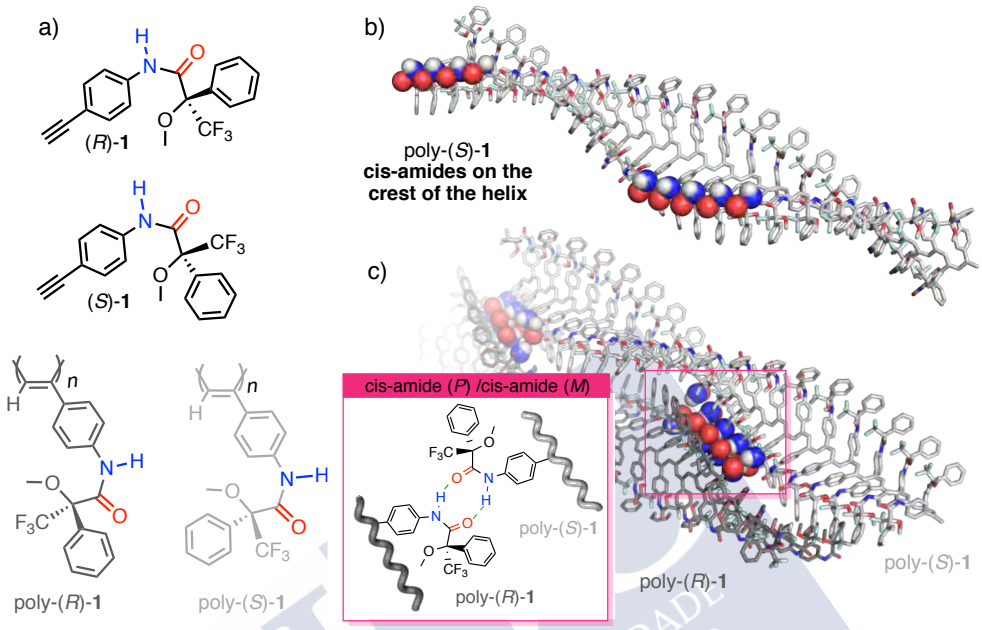

Figure 1. Chemical structure of (a) monomers (*R*)- and (*S*)-**1**; polymers poly-(*R*)- and (*S*)-**1**. b) 3D-model of poly-(*S*)-**1** showing a cis-configuration of the amide groups. c) 3D model of the pol-**1** stereocomplex, highlighting the *cis*-amide/*cis*-amide supramolecular interactions between complementary helices.

2. Results and Discussion

To Hence, if we want to use poly-**1** to prepare the stereocomplexes Poly-(*R*)-**1**/poly(*S*)-**1**/-MNPs (M = Au or Ag) nanocomposite, a thiolated comonomer must be introduced in the poly-**1** chain, which is going to be used to connect the poly-**1** and MNPs. This comonomer can be introduced in the poly-**1** chain in two different ways: 1.- As an achiral monomer, which must follow a Sergeants and Soldiers effect or 2.- as a chiral monomer, where a chiral accord effect must be produced. In both cases, incorporation of an extra monomer to the polymer chain will not disturb the poly-(*R*)-**1** or poly-(*S*)-**1** helices and therefore their complementarity. We opted for the first case, and a copolymer made by a chiral (*R*)- or (*S*)-**1** monomer in combination with an achiral thiolated monomer.

Thiolated PPA copolymers stereocomplexes. Monomer containing the 4-ethynylanilide of 11-mercaptoundecanoic acid (**2**) was prepared (see SI for synthetic details) and copolymerized with either (*R*)- or (*S*)-**1** to form poly-[(*R*)-$\mathbf{1}_{1-r}$-*co*-$\mathbf{2}_r$] and poly-[(*R*)-$\mathbf{1}_{1-r}$-*co*-$\mathbf{2}_r$] with r in a range of 0.01-0.03 (Figure 2). We couldn´t explore other copolymers of this copolymer series with a content of comonomer **2** higher than 3% due to the poor solubility of those copolymers. Hence, three different copolymers were generated for each series —poly-[(*R* or *S*)-$\mathbf{1}_{0.99}$-*co*-$\mathbf{2}_{0.01}$], poly-[(*R* or *S*)-$\mathbf{1}_{0.98}$-*co*-$\mathbf{2}_{0.02}$] and poly-[(*R* or *S*)-$\mathbf{1}_{0.97}$-*co*-$\mathbf{2}_{0.03}$]—. ECD studies show the presence of an effective Sergeants and Soldiers effect (Figure 2a), where the ECD spectra for the different copolymers is very similar to the one obtained for their corresponding parent homopolymers —poly-(*R*)-**1** and poly-(*S*)-**1**—.

From previous studies, we know that comonomer **2** bearing a trans-amide group at the pendant cannot be introduced in a percentage larger than 20% due to the perturbation of the final *cis*-amide content of the copolymer.[33] Thus, it is known that when the percentage of a *trans* amide monomer is increased to reach 20% —poly-[(*R*)-$\mathbf{1}_{0.8}$-*co*-$\mathbf{2}_{0.2}$]—, no stereocomplex is formed by interaction with poly-(*S*)-**1**. Similarly, the 50/50 mixture of the copolymers poly-[(*R*)-$\mathbf{1}_{0.9}$-*co*-$\mathbf{2}_{0.1}$]/poly-[(*S*)-$\mathbf{1}_{0.9}$-*co*-$\mathbf{2}_{0.1}$] (20% *trans* amide content overall) was found not form stereocomplex. In the copolymer series poly-[(*R*)-$\mathbf{1}_{1-r}$-*co*-$\mathbf{2}_r$] and poly-[(*S*-$\mathbf{1}_{1-r}$-*co*-$\mathbf{2}_r$], we must work with copolymers that bear monomer **2** in a percentage below 3% due to solubility problems. In these conditions, the formation of the stereocomplex should be favoured.

Thus, the sterecomplexation of the designed polymers was carried out by mixing solutions of the copolymers with the complementary enantiomeric parent homopolymer, such as poly-[(*R*)-$\mathbf{1}_{0.99}$-*co*-$\mathbf{2}_{0.01}$]/poly-(*S*)-**1** (0.1 mg mL^{-1} in THF) at a 50/50 (v/v) ratio. Following this procedure six different stereocomplexes were prepared poly-[(*R*)-$\mathbf{1}_{0.99}$-*co*-$\mathbf{2}_{0.01}$]/poly-(*S*)-**1**; poly-[(*R*)-$\mathbf{1}_{0.98}$-*co*-$\mathbf{2}_{0.02}$]/poly-(*S*)-**1**; poly-[(*R*)-$\mathbf{1}_{0.97}$-*co*-$\mathbf{2}_{0.03}$]/poly-(*S*)-**1** (Figure 2c), poly-[(*S*)-$\mathbf{1}_{0.99}$-*co*-$\mathbf{2}_{0.01}$]/poly-(*R*)-**1**; poly-[(*S*)-$\mathbf{1}_{0.98}$-*co*-$\mathbf{2}_{0.02}$]/poly-(*R*)-**1**; poly-[(S)-$\mathbf{1}_{0.97}$-*co*-$\mathbf{2}_{0.03}$]/poly-(*R*)-**1** (See SI). Moreover, additional stereocomplexes were prepared by mixing two complementary thiolated copolymers: poly-[(*R*)-$\mathbf{1}_{0.99}$-*co*-$\mathbf{2}_{0.01}$]/poly-[(*S*)-$\mathbf{1}_{0.99}$-*co*-$\mathbf{2}_{0.01}$]; poly-[(*R*)-$\mathbf{1}_{0.98}$-*co*-$\mathbf{2}_{0.02}$]/poly-[(*S*)-$\mathbf{1}_{0.98}$-*co*-$\mathbf{2}_{0.02}$] (Figure 2c).

In all cases, by mixing solutions of complementary and enantiomeric helices the presence of larger aggregates was observed (Figure 2c and SI). DLS studies show that the size of the stereocomplex obtained in a poly-(*R*)-**1**/poly-(*S*)-**1** 50/50 (v/v) mixture (804 nm) is larger than those obtained for poly-[(*R*)-$\mathbf{1}_{1-r}$-*co*-$\mathbf{2}_r$]/poly-(*S*)-**1** mixtures (450nm) (Figure 2b and SI), poly-[(*S*)-$\mathbf{1}_{1-r}$-*co*-$\mathbf{2}_r$]/poly-(*R*)-**1** mixtures (c.a. 350 nm), or even in the stereocomplex formed by the two thiolated copolymers, poly-[(*R*)-$\mathbf{1}_{1-r}$-*co*-$\mathbf{2}_r$]/poly-[(*S*)-$\mathbf{1}_{1-r}$-*co*-$\mathbf{2}_r$] (Figure 2c and SI). The

different size of the aggregates is probably related to the different size of the homopolymers and the copolymers. Thus, whereas homopolymers have a Mw ca. 178058, copolymers poly-[$\mathbf{1}_{1\text{-}r}$-*co*-$\mathbf{2}_r$] (r =0.01-0.03) are smaller than this size.

SEM studies showed the presence of large fibre-like aggregates (Figure 2d and SI), different from the polydisperse particles with a diameter around 45 nm obtained for the solutions containing the complementary helices before mixing them (See SI).

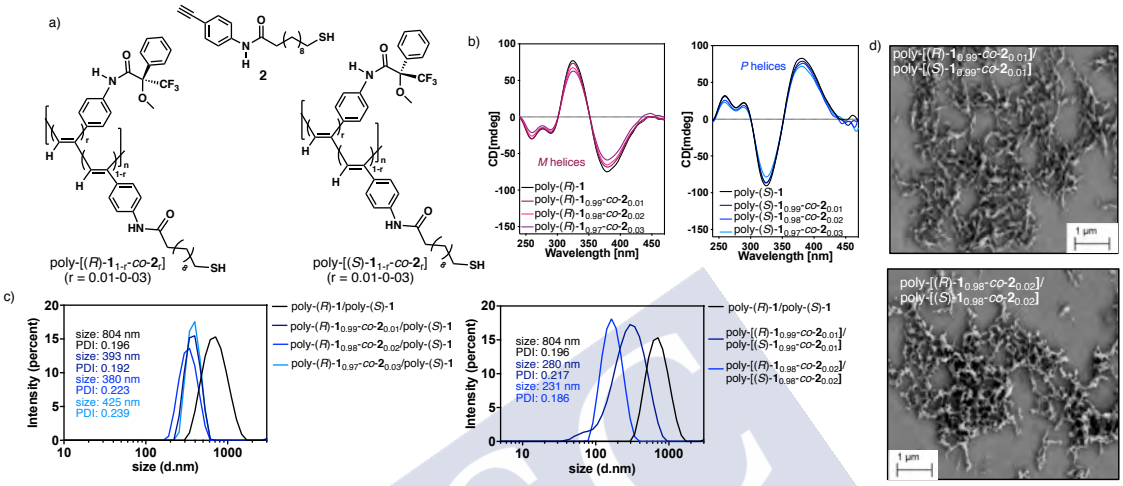

Figure 2. a) Chemical structure of monomer **2**, copolymers poly-[(*R*)-$\mathbf{1}_r$-*co*-$\mathbf{2}_{1\text{-}r}$] and poly-[(*S*)-$\mathbf{1}_r$-*co*-$\mathbf{2}_{1\text{-}r}$] (r = 0.01-0.03). b) CD studies of poly-[(*R*)-$\mathbf{1}_r$-*co*-$\mathbf{2}_{1\text{-}r}$] and poly-[(*S*)-$\mathbf{1}_r$-*co*-$\mathbf{2}_{1\text{-}r}$] (r = 0.01.0-03) in $CHCl_3$. c) DLS studies of poly-(*R*)-**1**/poly-(*S*)-**1** and poly-[(*R*)-$\mathbf{1}_r$-*co*-$\mathbf{2}_{1\text{-}r}$]/poly-[(*S*)-$\mathbf{1}_r$-*co*-$\mathbf{2}_{1\text{-}r}$] mixtures (50/50 in THF). d) SEM images of stereocomplexes formed by poly-[(*R*)-$\mathbf{1}_r$-*co*-$\mathbf{2}_{1\text{-}r}$]/poly-[(*S*)-$\mathbf{1}_r$-*co*-$\mathbf{2}_{1\text{-}r}$] mixtures (50/50 in THF).

As expected, these stereocomplexes show the same stimuli-responsive properties than the parent poly-(*R*)-**1**/poly-(*S*)-**1** stereocomplex. This fact makes possible to control the formation/disruption of the stereocomplex by playing with the donor character of the solvent that affects to the *cis*/*trans* content of the anilide group and therefore to the formation of the stereocomplex —ON (donor solvents, *cis* anilide), OFF (non-donor solvents, *trans* anilide)— (Figure 3).

Moreover, it is also possible to switch ON/OFF the sterecomplexation of these systems by altering the environmental conditions where the stereocomplex is formed and disrupt the *cis*-anilide *M* helix/*cis*-anilide *P* helix supramolecular interactions. Thus, changes on the temperature such as heating up to 60°C can disrupt these supramolecular interactions and therefore the aggregate. The same result is obtained by adding molecules that can interfere in the *cis*-anilide *M* helix/*cis*-anilide *P* helix supramolecular network such as MeOH (Figure 3 and

SI). Interestingly, the addition of MeOH to the stereocompolex promotes a decrease in the size of the aggregates (Figure 3).

Once it was found the ability of the copolymers to form the stereocomplex and retain the dynamic behaviour of the parent homopolymers, we proceeded to the preparation of nanocomposites by hybridization with MNPs (M = Au or Ag).

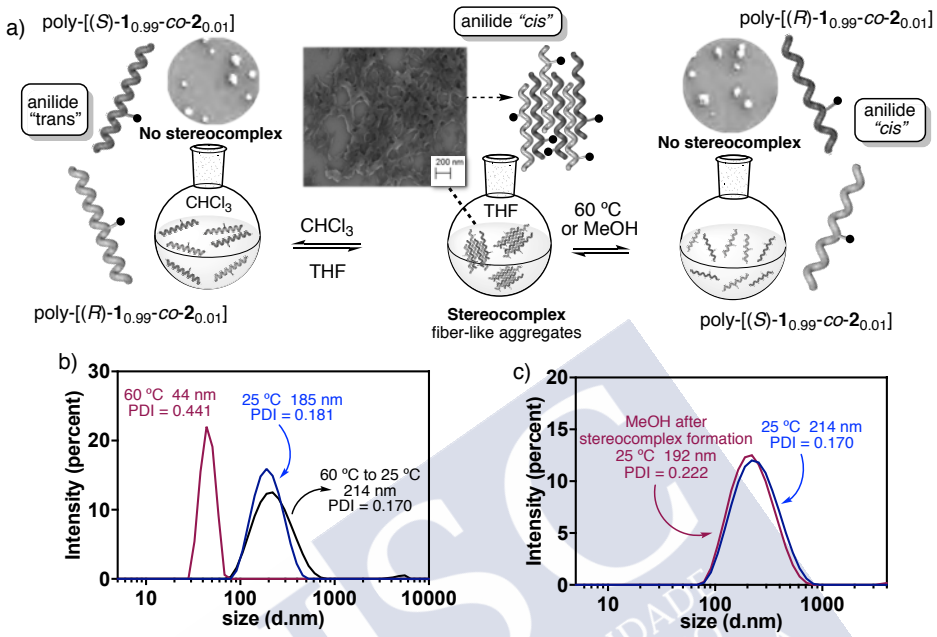

Figure 3. a) Graphical illustration of the ON/OFF stereocomplexation of a 50/50 v/v mixture of poly-[(*R*)-**1**$_{0.98}$-*co*-**2**$_{0.02}$]/ poly-[(*S*)-**1**$_{0.98}$-*co*-**2**$_{0.02}$] in $CHCl_3$ (OFF), THF (ON), THF at 60°C (OFF) and in a THF/MeOH mixture (OFF). DLS studies of the ON/OFF stereocomplexation of a 50/50 (v/v) mixture of poly-[(*R*)-**1**$_{0.98}$-*co*-**2**$_{0.02}$]/ poly-[(*S*)-**1**$_{0.98}$-*co*-**2**$_{0.02}$] in (b) THF, THF at 60°C and (c) in a THF after addition of MeOH.

Poly-[(*R*)-1$_{1-r}$-*co*-2$_r$]-MNPs and poly-[(*S*)-1$_{1-r}$-*co*-2$_r$]-MNPs nanocomposites: Dynamic behaviour studies. Six different poly-[(*R*)-**1**$_{1-r}$-*co*-**2**$_r$]-MNPs and poly-[(*S*)-**1**$_{1-r}$-*co*-**2**$_r$]-MNPs nanocomposites (r = 0.01-0.03; M = Au and Ag) were prepared following a variation of the classical Brust-Schiffrin procedure. ECD studies of THF solutions of poly-[**1**$_{1-r}$-*co*-**2**$_r$]-MNPs (0.3 mg mL^{-1}) showed an active Cotton Effect in the vinylic region (ca. 380 nm) indicating that the nanocomposites retain the helical structure of poly-**1** when the MNPs are hybridated. Moreover, UV-vis studies of the nanocomposites confirmed the formation of MNPs where AuNPs showed the typical LSPR band at 530 nm and the AgNPs at 420 nm.

Interestinlgy, a yellow colour was observed in the THF solutions of poly-[(*R*)-**1**$_{1-r}$-*co*-**2**$_r$]-AgNPs and red colour was observed in the solutions of poly-[(*R*)-**1**$_{1-r}$-*co*-**2**$_r$]-AuNPs. TEM studies were carried out to study the morphology of the MNPs. Thus, TEM images revealed the formation of low polydisperse spherical AuNPs (7.1 ± 3.3 nm) and also the formation of low

polydisperse AgNPs (4.4 ± 1.5 nm). These nanocomposites are stable for several weeks in solution and solid state and therefore confirmed the important role of poly-[(*R*)-**1**$_{1-r}$-*co*-**2**$_r$] (r = 0.01-0.03) in the stabilization of the MNPs.

Moreover, ECD and UV-vis studies of poly-[**1**$_{1-r}$-*co*-**2**$_r$]-MNPs (M = Au or Ag) in different solvents —$CHCl_3$, DCM, DMF and DMSO— showed the formation of dynamic poly-[**1**$_{1-r}$-*co*-**2**$_r$]-MNPs nanocomposites with similar behaviour than the parent homopolymer poly-**1**. Thus, it is possible to obtain nanocomposites with different helical sense by tuning the polar/donor properties of poly-[**1**$_{1-r}$-*co*-**2**$_r$]-MNPs nanocomposites solutions.

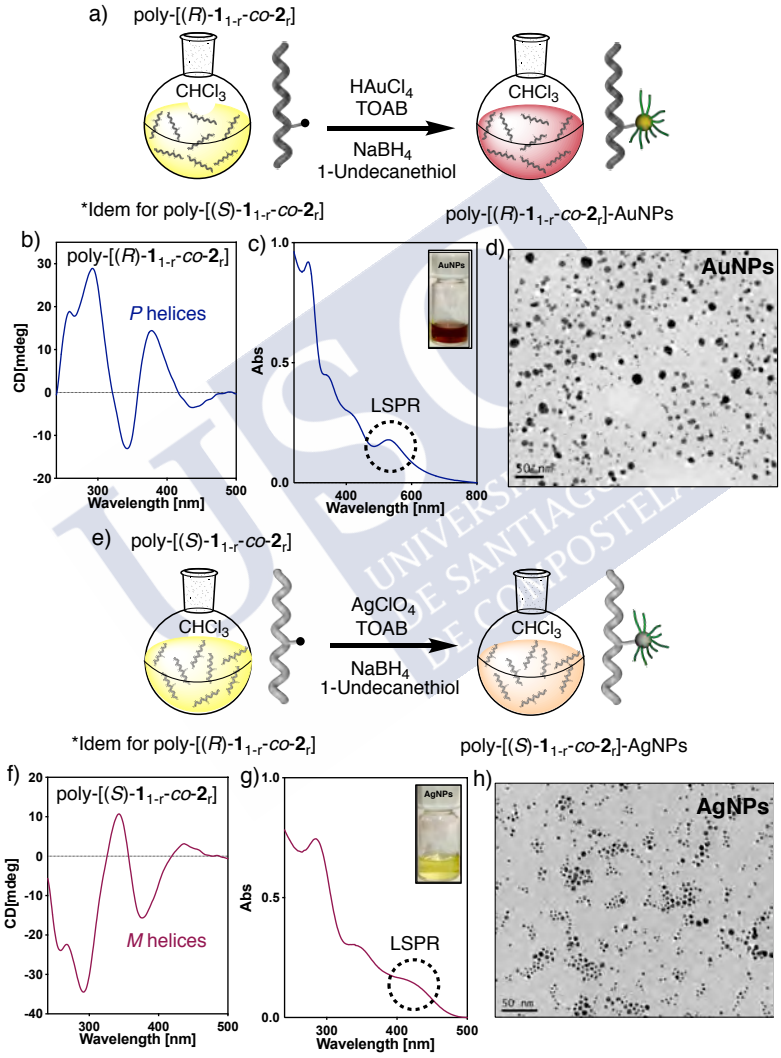

Figure 4. a) Graphic illustration for the preparation of poly-[(*R*)-**1**$_{1-r}$-*co*-**2**$_r$]-AuNPs. b) CD spectrum of poly-[(*R*)-**1**$_{1-r}$-*co*-**2**$_r$]-AuNPs. c) UV-vis spectrum of poly-[(*R*)-**1**$_{1-r}$-*co*-**2**$_r$]-AuNPs. d) TEM image of poly-[(*R*)-**1**$_{1-r}$-*co*-**2**$_r$]-AuNPs. e) Graphic illustration for the preparation of poly-[(*S*)-**1**$_{1-r}$-*co*-**2**$_r$]-AgNPs. f) CD spectrum of poly-[(*S*)-**1**$_{1-r}$-*co*-**2**$_r$]-AgNPs. g) UV-vis spectrum of poly-[(*S*)-**1**$_{1-r}$-*co*-**2**$_r$]-AgNPs. h) TEM image of poly-[(*S*)-**1**$_{1-r}$-*co*-**2**$_r$]-AgNPs.

Stereocomplexation of PPA-nanocomposites: stimuli-responsive properties. Once, it has been demonstrated the formation of the nanocomposites we proceed to the preparation of the stereocomplexes by mixing (50/50 v/v in THF) the hybrid material with the enantiomeric homopolymer (0.3 mg mL^{-1}), i.e. poly-[(*R*)-**1**$_{1-r}$-*co*-**2**$_r$]-AgNPs/poly-(S)-**1**; poly-[(*R*)-**1**$_{1-r}$-*co*-**2**$_r$]-AuNPs/poly-(*S*)-**1**; poly-[(*S*)-**1**$_{1-r}$-*co*-**2**$_r$]-AgNPs/poly-(*R*)-**1**; poly-[(*R*)-**1**$_{1-r}$-*co*-**2**$_r$]-AgNPs/poly-(*R*)-**1** (r = 0.01-0.03), and even by mixing two nanocomposites containing complementary and enantiomeric helical structures and the same or different metal nanoparticle, i. e. poly-[(*R*)-**1**$_{1-r}$-*co*-**2**$_r$]-AuNPs/poly-[(*S*)-**1**$_{1-r}$-*co*-**2**$_r$]-AgNPs (r = 0.01-0.03).

In all cases, the presence of larger aggregates was observed by DLS and electron microscopy studies (Figure 5 and SI). The morphology of these stereocomplexes are fibre-like aggregates where the presence of Ag and AuNPs attached to the copolymer does not affect to the formation of the stereocomplex and their morphology. A combination of SEM and TEM images indicate that the MNPs are distributed all over the fibre structure (Figure 5 and SI).

Stimuli-responsive studies shown that is possible to control the formation/disruption (ON/OFF) of the stereocomplex by altering the secondary structure of the polymer, i.e THF —stretched helix— stereocomplex ON, $CHCl_3$ —compressed helix— stereocomplex OFF. Moreover, by playing with temperature, or by adding molecules that can interfere with the hydrogen bond network that stabilize the stereocomplex is also possible to activate (low temperatures, absence of protic solvents) or deactivate (high temperatures, protic solvents) the stereocomplex.

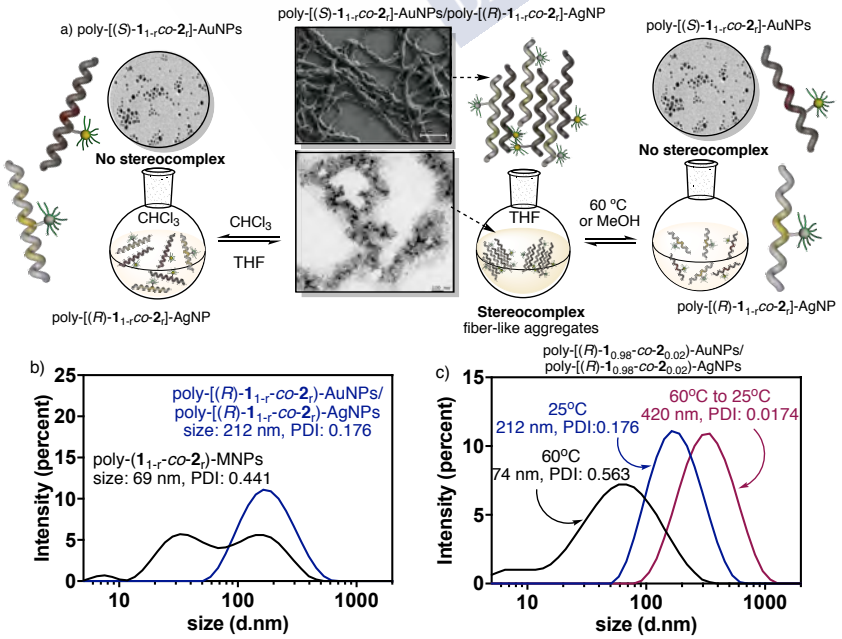

Figure 5. a) Graphical illustration of the ON/OFF stereocomplexation of a 50/50 v/v mixture of poly-[(*R*)-**1**$_{1-r}$-*co*-**2**$_r$]-AgNP/ poly-[(*S*)-**1**$_{1-r}$-*co*-**2**$_r$]-AuNP nanocomposites in $CHCl_3$ (OFF), THF (ON), THF at 60°C (OFF)

and in a THF/MeOH mixture (OFF). DLS studies of the ON/OFF stereocomplexation of a 50/50 (v/v) mixture of poly-[(*R*)-**1**$_{0.98}$-*co*-**2**$_{0.02}$]-AgNP/ poly-[(*S*)-**1**$_{0.98}$-*co*-**2**$_{0.02}$]-AuNP nanocomposites in (b) THF and (c) THF, THF at 25°C and THF at 60°C.

3. References

1. Dreaden, Erik.; Alkilany, A.; Huang, X.; Murphy, C.; El-Sayed, M. The golden age: gold nanoparticles for biomedicine. *Chem. Soc. Rev.*, **2012**, *41*, 2740-2779.

2. Jaque, D.; Martínez Maestro, L.; del Rosal, B.; Haro-Gonzalez, P.; Benayas, A.; Plaza, J. L.; Martín Rodriguez, E.; García Solé, J. Nanoparticles for photothermal therapies. *Nanoscale*, **2014**, 9494-9530.

3. Zhang, S.; Geryak, R.; Geldmeier, J.; Kim, S.; Tsukruk, V. Synthesis, Assembly, and Applications of Hybrid Nanostructures for Biosensing. *Chem. Rev.*, **2017**, *117*, 12942-13038.

4. Moon, H.; Kim, Y.; Photothermal-Mediated Catalytic Reduction of 4-Nitrophenol Using Poly(N-isopropylacrylamide-acrylamide) and Hollow Gold Nanoparticles. *ACS Appl. Polym. Mater.* **2021**, 3, 2768−2775.

5. Schrinner, M.; Ballauff, M.; Talmon, Y.; Kauffmann, Y.; Thun, J.; Moller, M.; Breu, J. Single Nanocrystals of Platinum Prepared by Partial Dissolution of Au-Pt Nanoalloys. *Science*. **2009**, 323, 617–620.

6. González-Rubio, G.; Mosquera, J.; Kumar, V.; Pedrazo-Tardajos, A.; Llombart, P.; Solís, D. M.; Lobato, I.; Noya, E. G.; Guerrero-Martínez, A.; Taboada, J. M.; Obelleiro, F.; MacDowell, L. G.; Bals, S.; Liz-Marzán. L. M.; Micelle-Directed Chiral Seeded Growth on Anisotropic Gold Nanocrystals. *Science*. **2020**, *368*, 1472-1477.

7. Bergueiro, J.; Nuñez-Martínez, M.; Arias, S.; Quiñoá, E.; Riguera, R.; Freire, F. Chiral gold–PPA nanocomposites with tunable helical sense and morphology *Nanoscale Horiz.*, **2020**, *5*, 495-500.

8. Núñez-Martínez, M.; Arias, S.; Quiñoá, E.; Riguera, R.; Freire, F. Dynamic Chiral PPA–AgNP Nanocomposites: Aligned Silver Nanoparticles Decorating Helical Polymers. *Chem. Mat*er., **2021**, *33*, 4805-4812.

9. Fittolani, G.; Seeberger, P.; Delbianco, M.; Helical polysaccharides. *Peptide Science*. **2020**, DOI: 10.1002/pep2.24124.

10. Huang, H.; Ni, X. P.; Loy, G. L.; Chew, C. H.; Tan, K. L.; Loh, Nanoparticles in Poly(*N*-vinylpyrrolidone), *Langmuir*, **1996**, *12*, 909-912.

11. Zhang, Z.; Zhao, B.; Hu, L. PVP protective mechanism of ultrafine silver powder synthesized by chemical reduction processes. *J. Solid State Chem.* **1996**, *121*, 105.

12. Wang, S.; Chen, J.; Feng, X.; Shi, G.; Zhang, J.; Wan, X. Conformation Shift Switches the Chiral Amplification of Helical Copoly(phenylacetylene)s from Abnormal to Normal "Sergeants-and-Soldiers" Effect. *Macromolecules*, **2017***, 50,* 4610-4615.

13. Freire, F.; Quiñoá, E.; Riguera, R. Supramolecular Assemblies from Poly(phenylacetylene)s. *Chem. Rev*., **2016**, *116*, 1242-1271.

14. Freire, F.; Seco, J. M.; Quiñoá, E.; Riguera, R. Helical Polymer–Metal Complexes: The Role of Metal Ions on the Helicity and the Supramolecular Architecture of Poly(phenylacetylene)s. *Adv. Polym. Sci*., **2013**, *262*, 123-140.

15. Yashima, E. Synthesis and structure determination of helical polymers. *Polymer Journal*, **2010**, *42*, 3-16.

16. Yashima, E.; Maeda, K. Chirality-Responsive Helical Polymers. *Macromolecules*, **2008**, *41*, 3-12.

17. Percec, V.; Rudick, J. G.; Peterca, M.; Heiney, P. A. Nanomechanical Function from Self-Organizable Dendronized Helical Polyphenylacetylenes. *J. Am. Chem. Soc.*, **2008**, *130*, 7503-7508.

18. Arias, S.; Núñez-Martinez, M.; Quiñoá, E.; Riguera, R.; Freire, F. A general route to chiral nanostructures from helical polymers: *P*/*M* switch *via* dynamic metal coordination. *Polym. Chem.,* **2017**, *8*, 3740-3745.

19. Rodríguez, R.; Arias, S.; Quiñoá, E.; Riguera, R.; Freire, F. The role of the secondary structure of helical poly(phenylacetylene)s in the formation of nanoparticles from polymer–metal complexes (HPMCs). *Nanoscale*, **2017**, *8*, 17752-17757.

20. Suárez-Picado, E.; Quiñoá, E.; Riguera, R.; Freire, F. Poly(phenylacetylene) Amines: A General Route to Water-Soluble Helical Polyamines. *Chem. Mater.* **2018**, *30*, 6908−6914.

21. Rodríguez, R.; Suárez-Picado, E.; Quiñoá, E.; Riguera, R.; Freire, F. Stimuli-responsive Macromolecular Gear: Interlocking Dynamic Helical Polymers with Foldamers *Angew. Chem. Int. Ed.,* **2020**, *59*, 8616-8622

22. Suárez-Picado, E.; Quiñoá, E.; Riguera, R.; Freire, F. Chiral Overpass Induction in Dynamic Helical Polymers Bearing Pendant Groups with Two Chiral Centers. *Angew. Chem. Int. Ed.*, **2020**, *59*, 4537-4543.

23. Fernández, Z.; Fernández, B.; Quiñoá, E.; Riguera, R.; Freire. F. Chiral Information Harvesting in Helical Poly(acetylene) Derivatives Using Oligo(p-phenyleneethynylene)s as Spacers. *Chem. Sci.* **2020**, *11*, 7182-7187.

24. Rodríguez, R.; Quiñoá, E.; Riguera, R.; Freire, F. Multistate Chiroptical Switch Triggered by Stimuli-Responsive Chiral Teleinduction, *Chem. Mater.* **2018**, *30*, 2493−2497.

25. Rodríguez, R.; Quiñoá, E.; Riguera, R.; Freire, F. Architecture of Chiral Poly(phenyl acetylene)s: From Compressed/Highly Dynamic to Stretched/Quasi-Static Helices. *J. Am. Chem. Soc.,* **2016,** *138***,** 9260-9268.

26. Freire, F.; Seco, J. M.; Quiñoá, E.; Riguera, R. Nanospheres with Tunable Size and Chirality from Helical Polymer–Metal Complexes. *J. Am. Chem. Soc.*, **2012**, *134*, 19374-19383.

27. Arias, S.; Núñez-Martinez, M.; Quiñoá, E.; Riguera, R.; Freire, F. Simultaneous Adjustment of Size and Helical Sense of Chiral Nanospheres and Nanotubes Derived from an Axially Racemic Poly(phenylacetylene). *Small*, **2016**, *13*, 1602398.

28. Slagen, J.; Domb, A.; Biopolymer Stereocomplexes. *Adv. Drug Delivery Rev.*, **2003**, *55*, 549–583.

29. Bertin, A.; Emergence of Polymer Stereocomplexes for Biomedical Applications. *Macromol. Chem. Phys.*, **2012**, *213*, 2329–2352

30. Sun, Y.; He, C.; Synthesis and Stereocomplex Crystallization of Poly(lactide)−Graphene Oxide Nanocomposites. *ACS Macro Lett*. **2012**, *1*, 709−713.

31. Oberhauser, W.; Evangelisti, C.; Jumde, R.; Petrucci, G.; Bartoli, M.; Frediani, M.; Mannini, M.; Capozzoli, M.; Passaglia, E.; Rosi, L.; Palladium-nanoparticles on end-functionalized poly(lactic acid)-based stereocomplexes for the chemoselective cinnamaldehyde hydrogenation: Effect of the end-group. *Journal of Catalysis*. **2015**, *330*, 187-196.

32. Sun, Y.; He, C.; Synthesis, stereocomplex crystallization, morphology and mechanical property of poly(lactide)–carbon nanotube nanocomposites. *RSC Adv.,* **2013**, *3*, 2219-2226.

33. Leiras, S.; Freire, F.; Seco, J. M.; Quiñoá, E.; Riguera, R. Reversible assembly of enantiomeric helical polymers: from fibers to gels. *Chem. Sci.,* **2015**, *6*, 246-253.

USC
UNIVERSIDADE
DE SANTIAGO
DE COMPOSTELA

USC
UNIVERSIDADE
DE SANTIAGO
DE COMPOSTELA

Chapter VIII

Effect of the Secondary Structure of PPAs in the Preparation of Polymeric Nanostructures

USC
UNIVERSIDADE
DE SANTIAGO
DE COMPOSTELA

Chapter VIII: Effect of the Secondary Structure of PPAs in the Preparation of Polymeric Nanostructures

Abstract

In this work, a novel approach for the formation of polymeric nanospheres by a variation of the emulsification method was described. For the preparation of the polymeric nanospheres, it is necessary the combination of a good organic solvent for the PPA (acetone or THF) to dissolve the polymer and water to favor the controlled aggregation of the polymer chains into polymeric nanostructures.

Thus, several PPAs containing anilide or benzamide connection were chosen for the formation of the polymeric nanostructures and test the ability of this methodology to develop a general protocol for the preparation of polymeric nanostructures. Thus, PPAs containing anilide connection and *ortho*, *meta* and *para* aromatic substitution (poly-(*R*)-**1**, poly-(*R*)-**2**, poly-(*R*)-**3**) pattern were evaluated in acetone/water and THF/water mixtures to determine the influence of the secondary structure of the PPAs in the nanostructuration process. In the case of the THF/water system, all the PPAs showed the formation of low polydisperse nanospheres (PDI < 0.2). On the other hand, when the PPA is dissolve in acetone and the water is added to favour the formation of the polymeric nanostructures. The *para* and *meta* PPAs showed the formation of nanospheres whereas the *ortho* PPA showed the formation of longitudinal aggregates.

In the case of the benzamide connection (poly-(*L*)-**5**, poly-(*L*)-**6**, poly-(*L*)-**7**, poly-(*L*)-**8**, poly-(*L*)-**9**), all the PPAs formed low in the polydisperse nanospheres regardless to the system chosen. Interestingly, it was observed that the benzamide-PPAs with bulky groups in the pendant showed an helical inversion/chiral enhancement after the nanostructuration process.

Moreover, the stability of the nanostructures in solution can be enhanced using a poly(vinylalchol) as surfactant. Finally, the encapsulation ability of the polymeric nanostructures was tested with fluorescent dyes.

USC
UNIVERSIDADE
DE SANTIAGO
DE COMPOSTELA

1. Introduction

The combination of chirality and nanoscale has attracted the attention of the scientific community due to their applications in a wide variety of fields such as sensing, catalysis, and biomedical therapy, among others.[1]

During the last years, several examples of nanostructures based on polymers have been reported [*e.g.* micelles, capsules, metal organic frameworks (MOFs)] and in most of them the control of the size and morphology has taken a special relevance because a high number of its properties are related to the control of these parameters.[2]

For these reasons, poly(phenylacetylene)s (PPAs) are an excellent candidates to prepare different types of polymeric nanostructures because can link chirality and nanoscale at the same time. PPAs are a family of dynamic helical polymers where the secondary structure (helical sense and/or elongation) can be tuned in presence of different external stimuli such as polarity of solvents, metal ions, pH, etc. [3-15]

In this field, Prof. Deng is a pioneer in the formation of this kind of nanostructures with helical polymers using different methodologies (*e.g.* emulsification and emulsion). In both cases, the use of surfactants such as poly(vinylpirrolidone) (PVP) as protecting agent of the nanoparticles has taken a essential role in the formation and stabilization of the polymer nanoparticles.[16-17]

For our part, we were centered in the formation of chiral polymeric nanostructures using metal ions as non-covalent crosslinking agents. Using this methodology, it is possible to obtain different PPA nanostructures such as nanospheres, nanotubes or toroids (refs groupr.) but until now this methodology was restricted to organic solvents and the use of metal ions to force the controlled aggregation.[18-20]

Thus, we have a large experience in the preparation of helical polymers based on PPAs with different scaffolds (compressed and stretched), ranging from compressed *cis-cisoidal* structures (ca. 65^{o}) until very stretched *cis-transoidal* polyene scaffolds (ca. 175^{o}).

Herein, we want to explore the effect of the secondary structure of PPAs in the morphology (shape and/or size) of polymeric nanostructures. For that, we chose as methodology the nanoprecipitacion method using the combination of an organic solvent (acetone or THF) to dissolve the PPA and water to favor the controlled aggregation of polymer chains.

First, we will explore *para*-substitued PPAs with different *cis-cisoidal* (poly-(*R*)-**1**, poly-(*R*)-**4**) and *cis-transoidal* polyene scaffolds (poly-(*L*)-**5**, poly-(*L*)-**6**, poly-(*L*)-**7**, poly-(*L*)-**8**, poly-(*L*)-

9) derived from PPAs bearing anilide or benzamides chiral substituents. This study allows us to determine the role of the connectivity of the PPAs in the formation of the polymeric nanostructures (Figure 1b).

Furthermore, we compared poly-(*R*)-**1**, poly-(*R*)-**2** and poly-(*R*)-**3** because present the same connectivity (anilide connection) but different dynamic behavior and stiffness.[21] Thus, it is possible to determine the role of the secondary structure in the formation of the nanostructures by this methodology (Figure 1).

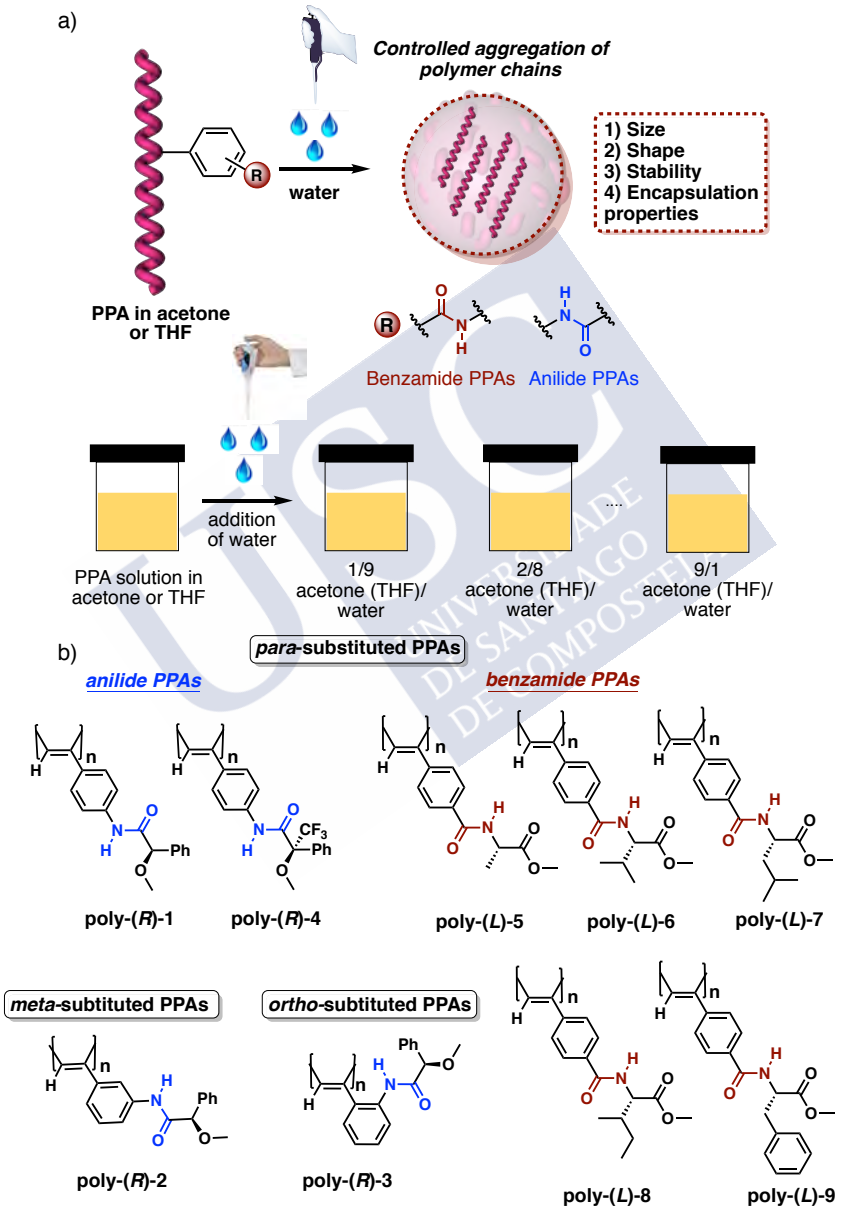

Figure 1. a) Schematic representation for the preparation of polymeric nanospheres. b) Structure of PPAs used in this work.

2. Results and Discussion

To perform these studies we selected the PPAs described above (poly-(*R*)-**1**, poly-(*R*)-**2**, poly-(*R*)-**3**, poly-(*R*)-**4**, poly-(*L*)-**5**, poly-(*L*)-**6**, poly-(*L*)-**7**, poly-(*L*)-**8**, poly-(*L*)-**9**). All the PPAs were prepared according to previous studies using $[Rh(nbd)Cl]_2$ as catalyst and fully characterized by several techniques such as CD, GPC, DSC, TGA and ^{1}H NMR, among others (See SI).

Nanostructuration studies of *para*-substituted PPAs Anilide PPAs

First, the nanostructuration process of *para* substituted PPAs with anilide or benzamide connection (poly-(*R*)-**1**, poly-(*R*)-**4**, poly-(*L*)-**5**, poly-(*L*)-**6**, poly-(*L*)-**7**, poly-(*L*)-**8**, poly-(*L*)-**9**) was studied. These PPAs present in all cases a highly dynamic behavior, where the helical sense can be tuned in presence of different external stimuli such as addition of metal ions or donor/polar character of the solvents.[19,21]

For that, PPAs were dissolved in acetone or THF (0.3 mg mL^{-1}) and then different amounts of water were added to the PPA solution to favour the controlled aggregation of the polymer chain (Scheme 1).

First, the nanostructuration process of PPAs with anilide connection (poly-(*R*)-**1** and poly-(*R*)-**4**) was studied. In the case of poly-(*R*)-**1** it is well known that presents an axially racemic structure where the *P* and *M* helices are in the same population.[9] Moreover, the helical sense of poly-(*R*)-**1** can be tuned by addition of monovalent (*M* helices) and divalent metal ions (*P* helices) indicating the presence of a highly dynamic structure.[9]

Thus, the studies with poly-(*R*)-**1** were carried out following the protocol described in the Figure 1a. Dynamic light scattering (DLS) studies for the different mixtures revealed the formation of low polydisperse nanospheres (PDI < 0.2) using the both combination of solvents (acetone/water or THF/water). Moreover, the size of the nanospheres can be controlled increasing the concentration of poly-(*R*)-**1** in the media (table 1). SEM studies in solid state confirmed the presence of well-defined and low polydisperse spherical nanostructures (Figure 2). As expected, CD studies for the different mixtures (acetone/water and THF/water) of the nanospheres showed the presence of an axially racemic structure (CD_{380} = 0).

Next, we evaluated the dynamic behaviour of the aggregates formed in acetone/water and THF/water mixtures in presence of $Ba(ClO_4)_2$ as external stimuli. For that, over a solution of poly-(*R*)-**1** (v/v, 1/1) was added $Ba(ClO_4)_2$ (10 mg mL^{-1} in MeOH) and the chiroptical response were recorded. The CD spectra for the different mixtures showed in all cases a null Cotton Effect in the vinylic region (CD_{380} = 0) indicating that the Ba^{2+} ions are not coordinated to the pendant group probably due to the solvation of the Ba^{2+} ions by the water (See SI).

In the case of poly-(*R*)-**4**, it was reported that its helical structure (elongation and/or helical sense) can be controlled by the donor/polar character of the solvents. Thus, we can compare two PPAs with anilide connection and different dynamic properties.[22]

As expected, DLS studies of poly-(*R*)-**4** in acetone/water mixtures confirmed the formation of low polydisperse nanostructures (PDI < 0.2) with controlled size. Interestingly, SEM images showed in the case of acetone/water mixtures the presence of well-defined nanospheres (Figure 2). The chiroptical response of the aggregates showed the presence of *M* helices (CD_{380} < 0) leading to the formation of chiral nanospheres with an excess of helical sense.

In the particular case of poly-(*R*)-**4** in THF/water mixtures, the DLS studies suggest the formation of high polydiperse (PDI > 0.2) and bigger aggregates. SEM studies of these mixtures revealed the presence of fiber-like large aggregates (Figure 2). Moreover, the CD studies showed a different chiroptical responses when the water is added to the poly-(*R*)-**4** in THF (See SI).

The formation of these type of nanostructures is probably due to the stabilization of the *cis* amide conformation in the periphery of the helices favouring this type of aggregation.[22]

Table 1. DLS data of poly-(*R*)-**1** and poly-(*R*)-**4** in acetone/water mixtures

Poly-(*L*)-**1** in acetone/water (v/v)			
	1/9 (v/v)	**3/7 (v/v)**	**1/1 (v/v)**
Size/nm	90	296	526
PDI	0.198	0.101	0.151
Poly-(*L*)-**4** in acetone/water (v/v)			
	1/9 (v/v)	**3/7 (v/v)**	**1/1 (v/v)**
Size/nm	55	385	422
PDI	0.122	0.014	0.006

Table 2. DLS data of poly-(*R*)-**1** and poly-(*R*)-**4** in THF/water mixtures

Poly-(*L*)-**1** in THF /water (v/v)			
	1/9 (v/v)	**3/7 (v/v)**	**1/1 (v/v)**
Size/nm	54	1400	1706
PDI	0.242	0.102	0.132
Poly-(*L*)-**4** in THF /water (v/v)			
	1/9 (v/v)	**3/7 (v/v)**	**1/1 (v/v)**
Size/nm	4300	7763	10450
PDI	0.597	0.717	0.487

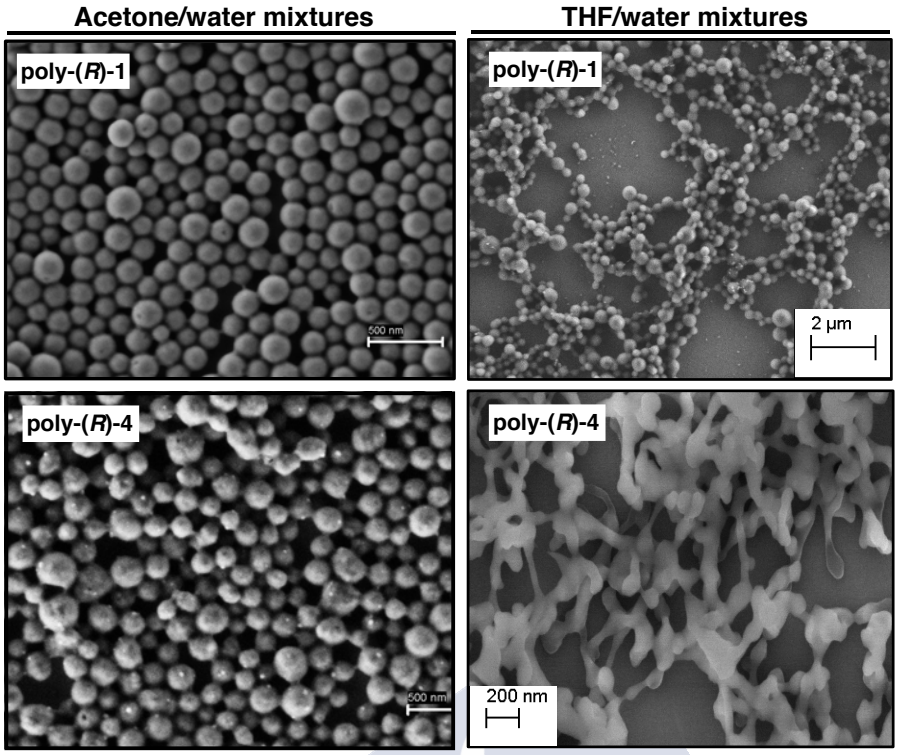

Figure 2. SEM images of poly-(*R*)-**1** and poly-(*R*)-**4** in mixtures acetone/water and THF/water (drop casted and silicon wafer as substrate).

Study of the Nanostructuration of *para* substituted benzamides PPAs

Next, we proceeded with the preparation of polymeric nanostructures with benzamide connection PPAs (poly-(*L*)-**5**, poly-(*L*)-**6**, poly-(*L*)-**7**, poly-(*L*)-**8**, poly-(*L*)-**9**) following the same procedure described previously.

These helical polymers present in low polar solvents (*e.g.* $CHCl_3$, DCM) an *anti* conformation between carbonyl groups in the pendant group leading to the formation of *M* helices. On the other hand, in high polar solvents (*e.g.* DMF, DMSO) these PPAs adopt the contrary helical sense (*P* helices) due to the stabilization of an *anti* conformation between carbonyl groups.[19]

Moreover, the addition perchlorate salts (*e.g.* $LiClO_4$ $Ba(ClO_4)_2$) to a solution of this type of PPAs in low polar solvents promotes an helical inversion due to the coordination of the metal ions to both carbonyl groups.[19] These results in the stimuli-responsive studies revealed that a strong dynamic behaviour and we reasoned that can be good candidates to form polymeric nanostructures.

Thus, DLS studies for the different mixtures (acetone/water and THF/water) showed the formation of low polydisperse aggregates (PDI < 0.2) where the size can be controlled increasing the amount of PPAs in solution.

On the one hand, the chiroptical responses of the different mixtures were evaluated by CD experiments. Thus, in the case of acetone/water mixtures, all the PPAs (poly-(*L*)-**5**, poly-(*L*)-**6**, poly-(*L*)-**7**, poly-(*L*)-**8**, poly-(*L*)-**9**) showed the typical CD signature of these PPAs when they are dissolved in acetone (*P* helices, *syn* conformation) leading to the formation of chiral aggregates (Table 3 and Figure 3a and b). On the other hand, the THF/water mixtures showed a different behavior depending on the type of the PPAs. In the case of poly-(*L*)-**5** and poly-(*L*)-**6**, the PPAs with less steric hindrance, showed the presence of the CD traces of the PPAs in THF when the water is added (Table 4 and Figure 3d, e).

Interestingly, poly-(*L*)-**7**, poly-(*L*)-**8**, poly-(*L*)-**9**, the PPAs with bulkiest groups, the addition of water caused a helical inversion in the case of poly-(*L*)-**7** and a chiral enhancement in poly-(*L*)-**8** and poly-(*L*)-**9** (Figure 3f).

SEM images were obtained to study the morphology of the aggregates in solid state. The images revealed the formation of well-defined nanospheres based on PPAs in both combinations of solvents (Figure 3 c, g and h). As a result, *para* substituted PPAs can form polymeric *P* or *M* nanospheres using this methodology.

Table 3. DLS data of poly-(*L*)-**5**, poly-(*L*)-**6**, poly-(*L*)-**7**, poly-(*L*)-**8**, poly-(*L*)-**9** in acetone/water mixtures

Poly-(*L*)-**5** in acetone/water (v/v)			
	1/9 (v/v)	**3/7 (v/v)**	**1/1 (v/v)**
Size/nm	56	84	230
PDI	0.095	0.098	0.086
Poly-(*L*)-**6** in acetone/water (v/v)			
	1/9 (v/v)	**3/7 (v/v)**	**1/1 (v/v)**
Size/nm	90	173	425
PDI	0.083	0.145	0.067
Poly-(*L*)-***7*** in acetone/water (v/v)			
	1/9(v/v)	**3/7 (v/v)**	**1/1 (v/v)**
Size/nm	68	132	412
PDI	0.130	0.125	0.031
Poly-(*L*)-**8** in acetone/water (v/v)			
	1/9 (v/v)	**3/7 (v/v)**	**1/1 (v/v)**
Size/nm	70	127	413
PDI	0.139	0.140	0.026
Poly-(*L*)-**9** in acetone/water (v/v)			
	1/9 (v/v)	**3/7 (v/v)**	**1/1 (v/v)**
Size/nm	-	7980	7225
PDI	-	0.851	0.453

Table 4. DLS data of poly-(*L*)-**5**, poly-(*L*)-**6**, poly-(*L*)-**7**, poly-(*L*)-**8**, poly-(*L*)-**9** in THF/water mixtures

Poly-(*L*)-**5** in THF/water (v/v)			
	1/9 (v/v)	**3/7 (v/v)**	**1/1 (v/v)**
Size/nm	112	186	433
PDI	0.059	0.065	0.118
Poly-(*L*)-**6** in THF/water (v/v)			
	1/9 (v/v)	**3/7 (v/v)**	**1/1 (v/v)**
Size/nm	126	325	437
PDI	0.056	0.030	0.118
Poly-(*L*)-**7** in THF/water (v/v)			
	1/9 (v/v)	**3/7 (v/v)**	**1/1 (v/v)**
Size/nm	91	297	469
PDI	0.062	0.053	0.041
Poly-(*L*)-**8** in THF/water (v/v)			
	1/9 (v/v)	**3/7 (v/v)**	**1/1 (v/v)**
Size/nm	103	204	1149
PDI	0.086	0.010	0.139
Poly-(*L*)-**9** in THF/water (v/v)			
	1/9 (v/v)	**3/7 (v/v)**	**1/1 (v/v)**
Size/nm	-	415	554
PDI	-	0.121	0.072

Role of the secondary structure of anilide PPAs in the nanostructuration process

In literature, it was reported that the aromatic substitution pattern (*para*, *meta* and *ortho*) takes a great influence in the secondary structure of the anilides that bears (*R*)-α-methoxy-α-phenylacetic acid as pendant group (poly-(*R*)-**1**, poly-(*R*)-**2** and poly-(*R*)-**3**).

Thus, poly-(*R*)-**1** shows the most compressed and dynamic behavior where the helical sense can be modulated in presence of monovalent and divalent metal ions. Poly-(*R*)-**2** exists in a equilibrium of two helices, (compressed and stretched one) and its dynamic behavior is less than poly-(*R*)-**1**. In the case of poly-(*R*)-**3**, this PPA presents the most stretched, rigid and a static structure.[21] The study of these three PPAs allows us to determine the role of the dynamic/stiffness character of the polymers in the nanostructuration process.

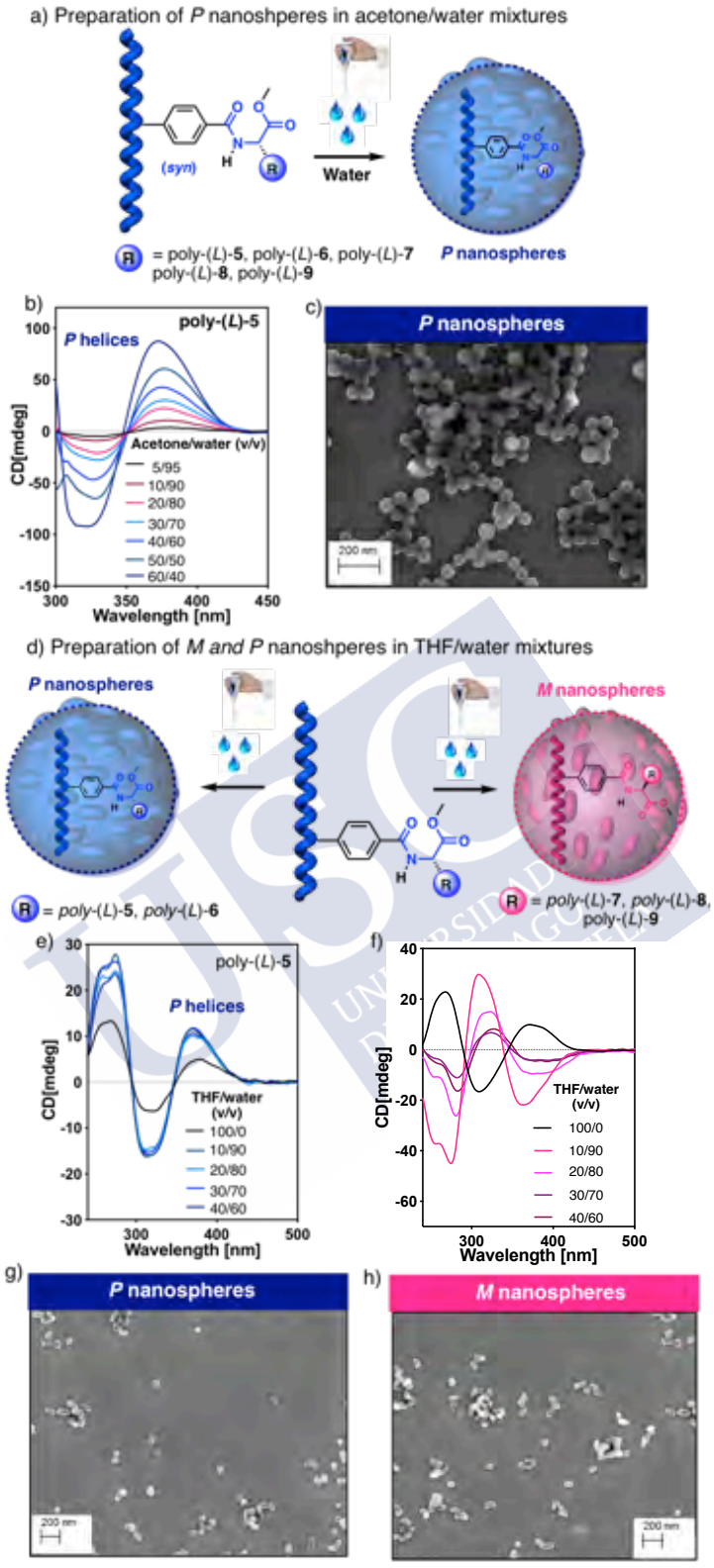

Figure 3. a) Schematic illustration of the formation of PPA nanospheres in acetone/water mixtures. b) CD spectra of poly-(*L*)-**5** in different acetone/water mixtures. c) SEM images of poly-(*L*)-**5** *P* nanospheres. d) Schematic illustration of the formation of PPA nanospheres in THF/water mixtures. e) CD spectra of poly-(*L*)-**5** in THF/water mixtures. f) CD spectra of poly-(*L*)-**7** in THF/water mixtures. g) SEM image of poly-(*L*)-**5** *P* nanospheres. h) SEM image of poly-(*L*)-**7** *M* nanospheres.

As commented before, poly-(*R*)-**1** is able to form well-defined nanospheres when acetone or THF is combined with water and the conditions of the mixture are controlled. As expected, PPAs with a large dynamic behaviour present a great tendency to adopt this type of low polydisperse aggregates.[18]

In the case of poly-(*R*)-**2** (equilibrium of compressed and stretched helices) the nanostructuration is different. In this case, the DLS studies in acetone/water or THF/water showed the formation of low polydisperse aggregates in solution (PDI < 0.2). These studies revealed the ability of poly-(*R*)-**2** to roll up itself to form the nanostructures.

Next, nanostructures were examined by SEM in solid state. These images confirmed the formation of polymeric nanospheres, but in this case the aggregates presented a small coalescence between them. This is attributed to the secondary structure of poly-(*R*)-**2** where two types of helices (compressed and stretched) are present.

In the case of poly-(*R*)-**3** (stretched and quasi static helices), it is possible distinguish two alternatives:

1) Poly-(*R*)-3 acetone/water mixtures:

The DLS studies in solution suggested the formation of high polydisperse aggregates where is not possible to determine the morphology of the aggregates by this technique. Interestingly, SEM images in solid state revealed the formation of longitudinal aggregates with different sizes. This is attributed to poly-(*R*)-**3** tendency to the aggregations and its rigid structure.

2) Poly-(*R*)-3 THF/water mixtures:

On the contrary, DLS studies of poly-(*R*)-**3** in THF/water mixtures showed the formation of low polydisperse aggregates. In this case, SEM images confirmed the presence of low polydisperse nanospheres. Thus, the role of the solvent (THF or acetone) plays an important role in the formation of the polymeric nanostrucutures.

Table 4. DLS data of poly-(*R*)-**2** and poly-(*R*)-**3** in acetone/water mixtures

Poly-(*R*)-**2** in acetone/water (v/v)			
	1/9 (v/v)	**3/7 (v/v)**	**1/1 (v/v)**
Size/nm	78	101	141
PDI	0.170	0.126	0.116
Poly-(*L*)-**3** in acetone/water (v/v)			
	1/9 (v/v)	**3/7 (v/v)**	**1/1 (v/v)**
Size/nm	80	295	494
PDI	0.441	0.427	0.612

Table 5. DLS data of poly-(*R*)-**2** and poly-(*R*)-**3** in THF/water mixtures

Poly-(*R*)-**2** in THF/water (v/v)			
	1/9 (v/v)	**3/7 (v/v)**	**1/1 (v/v)**
Size/nm	324	588	731
PDI	0.043	0.039	0.031
Poly-(*L*)-**3** in THF/water (v/v)			
	1/9 (v/v)	**3/7 (v/v)**	**1/1 (v/v)**
Size/nm	338	449	1161
PDI	0.192	0.159	0.092

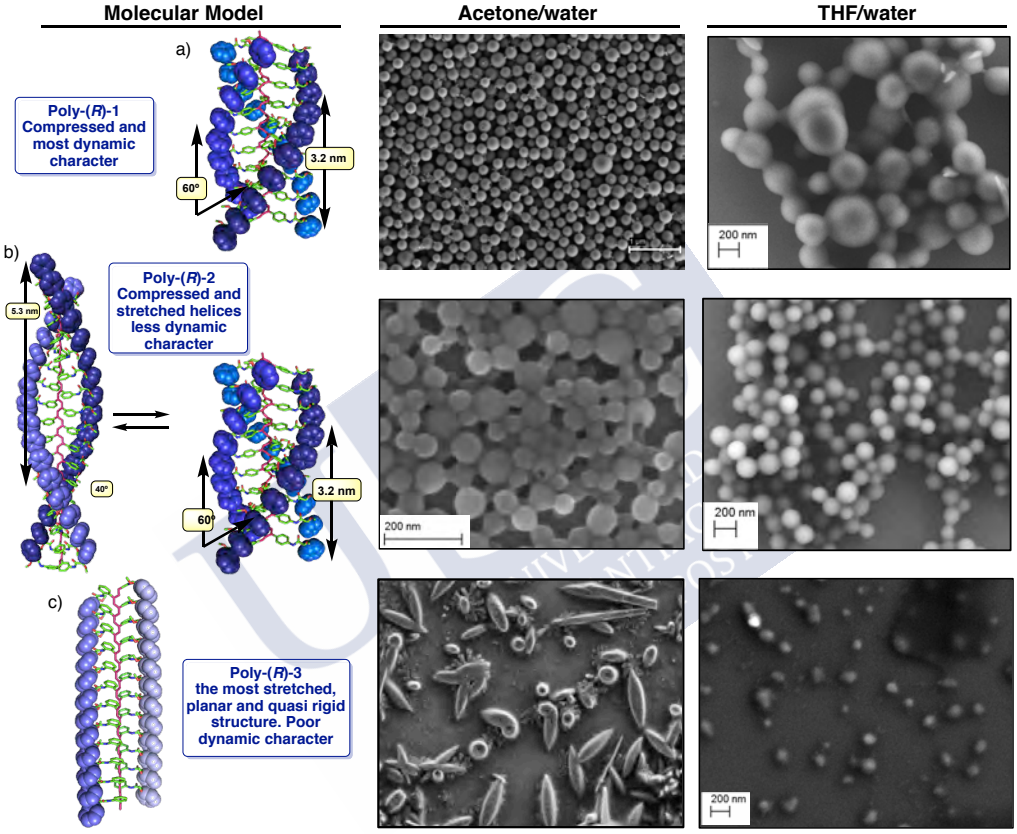

Figure 4. a) Molecular model of poly-(*R*)-**1** and SEM images in acetone/water and THF/water mixtures. b) Molecular model of poly-(*R*)-**2** and SEM images in acetone/water and THF/water mixtures. c) Molecular model of poly-(*R*)-**3** and SEM images in acetone/water and THF/water mixtures.

Encapsulation properties and stability of PPAs nanospheres

Once we obtained the nanospheres, with tunable helical sense and size, we evaluated their ability to encapsulate different compounds such as fluorescent dyes (5,6-carboxyfluorescein, rhodamine B isothiocyanate) and quantum dots.

For that, the chiral nanospheres were formed in presence of the iron oxide or fluorescent dyes and DLS studies were carried out. These studies showed that the encapsulation of the molecules does not affect to the formation of the nanospheres. Confocal microscopy images of the nanospheres in presence of fluorescent dyes and quantum dots

confirmed the encapsulation of the fluorescent molecules in the PPA nanospheres.Therefore, the encapsulation ability of the PPA nanospheres formed via emulsification method has been demonstrated by these experiments.

Finally, we decided to study the stability of the PPAs nanospheres in solution. For that, a model nanospheres prepared with *p*-poly-(*R*)-**1** (1/1, v/v) in acetone/water mixture. DLS measurements at different times showed the coalescence of the nanoparticles due to their poor stability in solution.

To improve the stability of the nanoparticles, poly(vinylalcohol) (PVA) was added as protecting agent to the solution of PPAs nanoparticles. The DLS traces after addition of PVA to poly-(*R*)-**1** showed an increase in the size of the nanospheres. This suggests that the PVA are located in the surface of the poly-(*R*)-**1** acting such as a surfactant. Moreover, the stability of the nanospheres in solution was improved until two days. To confirm the location of PVA in the nanospheres TEM studies were carried out. The images recorded showed the presence of the PVA in the surface of the polymeric nanospheres.

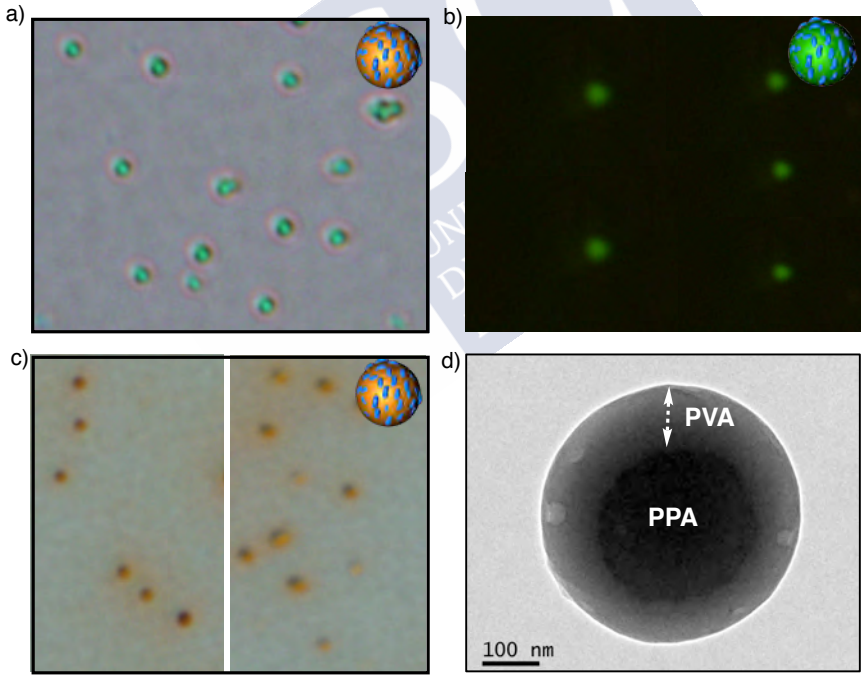

Figure 5. Confocal microscopy images for *p*-poly-(*R*)-**1** in presence of a) quantum dots, b) 5,6-carboxyfluorescein, c) rhodamine B isothiocyanate and TEM images of for poly-(*R*)-**1** in presence of PVA.

3. References

1. Freire, F.; Quiñoá, E.; Riguera, R. Supramolecular Assemblies from Poly(phenylacetylene)s. *Chem. Rev*., **2016**, *116*, 1242-1271.

2. Lefley, J.; Waldron, C.; Remzi Becer, C.; Macromolecular design and preparation of polymersomes. *Polym. Chem.*, **2020**, *11*, 7124.

3. Yashima, E. Synthesis and structure determination of helical polymers. *Polymer Journal*, **2010**, *42*, 3-16.

4. Yashima, E.; Maeda, K. Chirality-Responsive Helical Polymers. *Macromolecules*, **2008**, *41*, 3-12.

5. Percec, V.; Rudick, J. G.; Peterca, M.; Heiney, P. A. Nanomechanical Function from Self-Organizable Dendronized Helical Polyphenylacetylenes. *J. Am. Chem. Soc.*, **2008**, *130*, 7503-7508.

6. Suárez-Picado, E.; Quiñoá, E.; Riguera, R.; Freire, F. Poly(phenylacetylene) Amines: A General Route to Water-Soluble Helical Polyamines. *Chem. Mater.* **2018**, *30*, 6908−6914.

7. Rodríguez, R.; Suárez-Picado, E.; Quiñoá, E.; Riguera, R.; Freire, F. Stimuli-responsive Macromolecular Gear: Interlocking Dynamic Helical Polymers with Foldamers *Angew. Chem. Int. Ed.,* **2020**, *59*, 8616-8622

8. Suárez-Picado, E.; Quiñoá, E.; Riguera, R.; Freire, F. Chiral Overpass Induction in Dynamic Helical Polymers Bearing Pendant Groups with Two Chiral Centers. *Angew. Chem. Int. Ed.*, **2020**, *59*, 4537-4543.

9. Freire, F.; Seco, J. M.; Quiñoá, E.; Riguera, R. Helical Polymer–Metal Complexes: The Role of Metal Ions on the Helicity and the Supramolecular Architecture of Poly(phenylacetylene)s. *Adv. Polym. Sci*., **2013**, *262*, 123-140.

10. Nagata, Y.; Takeda, R.; Suginome, M.; Asymmetric Catalysis in Chiral Solvents: Chirality Transfer with Amplification of Homochirality through a Helical Macromolecular Scaffold. *ACS Cent. Sci.*, **2019**, *5*, 1235-1240.

11. Li, Yan-Xiang.; Xu, Lei.; Kang, Shu-Ming.; Zhou, Li.; Liu, Na.; Wu, Zong-Quan. Helicity- and Molecular-Weight-Driven Self-Sorting and Assembly of Helical Polymers towards Two-Dimensional Smectic Architectures and Selectively Adhesive Gels. *Angew. Chem. Int. Ed.*, **2021**, *60*, 7174-7179.

12. Li, Zhou.; Chong-Long, Li.; Run-Tan, Gao.; Shu-Ming, Kang.; Lei, Xu.; Xun-Hui, Xu.; Na, Liu.; Zong-Quan, Wu. Highly Regioselective and Helix-Sense Selective Living Polymerization of Phenyl and Alkoxyallene Using Chiral Nickel(II) Catalysts. *Macromolecules*, **2021**, *54*, 679-686.

13. Lefley, J.; Waldron, C.; Remzi Becer, C.; Helix-sense-selective co precipitation for preparing optically active helical polymer nanoparticles/graphene oxide hybrid nanocomposites. *Polym. Chem.*, **2020**, *11*, 7124–7136.

14. Bergueiro, J.; Nuñez-Martínez, M.; Arias, S.; Quiñoá, E.; Riguera, R.; Freire, F. Chiral gold–PPA nanocomposites with tunable helical sense and morphology *Nanoscale Horiz.*, **2020**, *5*, 495-500.

15. Nuñez-Martínez, M.; Arias, S.; Quiñoá, E.; Riguera, R.; Freire, F. Dynamic Chiral PPA-AgNPs Nanocomposites: Aligned Silver Nanoparticles Decorating Helical Polymers. *Chem. Mater.* **2021**, *33*, 4805–4812

16. Zhang, Y.; Deng, J.; Pan, K.; Chiral Helical Polymer Nanomaterials with Tunable Morphology: Prepared with Chiral Solvent To Induce Helix-Sense-Selective Precipitation Polymerization. *Macromolecules* **2018**, *51*, 8878−8886.

17. Yong, X.; Wu, Y.; Deng, J.; Chiral helical substituted polyacetylene grafted on hollow polymer particles: preparation and enantioselective adsorption towards cinchona alkaloids. *Polym. Chem.*, **2019**, *10*, 4441-4448.

18. Freire, F.; Seco, J. M.; Quiñoá, E.; Riguera, R. Nanospheres with Tunable Size and Chirality from Helical Polymer–Metal Complexes. *J. Am. Chem. Soc.*, **2012**, *134*, 19374-19383.

19. Arias, S.; Núñez-Martinez, M.; Quiñoá, E.; Riguera, R.; Freire, F. A general route to chiral nanostructures from helical polymers: *P*/*M* switch *via* dynamic metal coordination. *Polym. Chem.,* **2017**, *8*, 3740-3745.

20. Rodríguez, R.; Arias, S.; Quiñoá, E.; Riguera, R.; Freire, F. The role of the secondary structure of helical poly(phenylacetylene)s in the formation of nanoparticles from polymer–metal complexes (HPMCs). *Nanoscale*, **2017**, *8*, 17752-17757.

21. Rodríguez, R.; Quiñoá, E.; Riguera, R.; Freire, F. Architecture of Chiral Poly(phenyl acetylene)s: From Compressed/Highly Dynamic to Stretched/Quasi-Static Helices. *J. Am. Chem. Soc.,* **2016,** *138,* 9260-9268.

22. Leiras, S.; Freire, F.; Seco, J. M.; Quiñoá, E.; Riguera, R. Controlled modulation of the helical sense and the elongation of poly(phenylacetylene)s by polar and donor effect. *Chem. Sci.*, **2013**, *4*, 2735-2743.

USC
UNIVERSIDADE
DE SANTIAGO
DE COMPOSTELA

Chapter IX

Resume

USC
UNIVERSIDADE
DE SANTIAGO
DE COMPOSTELA

Nos últimos anos, a comunidade científica prestou un gran interese no desenrolo de novos materiais híbridos. Este tipo de materiais presentan como característica principal que teñen a combinación das propiedades que posúen por separado os seus compoñentes. Entre os máis estudados están os materias híbridos formados por nanopartículas metálicas e polímeros. O papel dos polímeros é moi importante xa que impiden a agregación das nanopartículas metálicas e ademais poden dotar de novas funcionalidades ao material.

Aínda que existe unha gran variedade deste tipo de materiais formados por polímeros e nanopartículas metálicas, a gran maioría deles non presentan quiralidade. Tendo en conta isto, os poli(fenilacetileno)s (PPAs), que son unha familia de polímeros helicoidais dinámicos son un tipo de macromoléculas moi interesantes para decorar MNPs xa que poden modular a súa estrutura secundaria (sentido de xiro e/ou elongación) mediante a presenza de estímulos externos como poden ser as variacións de temperatura, a adición de ións metálicos, ou o cambio de pH, entre outros. Este control sobre a estrutura secundaria fan que posúan potenciais aplicacións en campos tan diferentes como a catálise, o desenrolo de sensores ou a preparación de fases estacionarias quirais para HPLC.

Esta tese de doutoramento titulada *Chiral Nanomaterials with Tuneable Chiroptical Properties*, posúe seis capítulos no que se estudará a formación de nanomateriais formados por poli(fenilacetileno)s. Nos primeiros cinco capítulos prestarase especial atención á decoración dos polímeros helicoidais con nanopartículas metálicas e á influenza destas na estrutura secundaria do polímero. No último capítulo, abordarase a formación doutro tipo de nanomateriais poliméricos baseados unicamente en poli(fenilacetileno)s.

A continuación farase un resumo dos resultados mais relevantes de cada capítulo:

Captítulo III. Materiais Híbridos Quirais Ouro-PPA con Sentido de Xiro e Morfoloxía axustable

Os materiais híbridos representan unha nova ferramenta para xerar novos materiais con aplicacións en campos tan diferentes coma o desenrolo de sensores, terapias médicas ou en catálise, entre outros.

Aínda que na literatura pódense encontrar moitos traballos que describen a formación de materiais híbridos combinando macromoléculas helicoidais (*e.g.* ADN, proteínas) e nanopartículas metálicas, esta quiralidade axial que presenta o polímero queda fixada e non se pode modular mediante a presenza de estímulos externos.

Tendo en conta esta información, neste capítulo preséntase o primeiro exemplo dun material híbrido formado por polímeros helicoidais dinámicos e nanopartículas de ouro (AuNPs). Para isto, utilizouse como polímero helicoidal un PPA que ten un derivado da (*S*)-fenilglicina metil ester [poli-(*S*)-PGME] no se grupo *pendant*. En traballos previos do grupo de investigación, demostrouse que este PPA pode modular o seu sentido de xiro mediante a

presenza de estímulos externos tales como a polaridade dos disolventes ou a adición de ións metálicos. Desta forma, cando este PPA se disolve en disolventes pouco polares (*e.g.* $CHCl_3$, DCM), o seu grupo *pendant* adopta unha conformación *antiperiplanar* entre os grupos carbonilo do tipo lámina β estabilizando a formación de hélices tipo *M*. Por outra banda, cando se disolve en disolventes máis polares (*e.g.* DMF, DMSO), o PPA adopta o sentido de xiro contrario (hélices tipo *P*) xa que se estabiliza unha conformación *synperiplanar* entre os grupos carbonilo.

Este fenómeno de inversión da helicidade obsérvase tamén mediante a adición de ións metálicos (*e.g.* Li^+, Ag^+, Ba^{2+}) ao PPA. Desta forma, cando se engaden ións metálicos ao poli-(*S*)-PGME disolto en disolventes pouco polares, obsérvarse una inversión da helicidade (hélices tipo *P*) debido a coordinación dos catións aos grupos carbonilo nunha conformación en *synperiplanar.*

Tendo en conta este traballo previo, para a formación do materias híbridos baseados en PPA-AuNPs deseñouse un copolímero formado polo derivados da (*S*)-PGME e outro comonómero tiolado aquiral nun pequeno porcentaxe (do 1 ao 5%). Usando este deseño, as unidades quirais da (*S*)-PGME actuarán como indutoras da helicidade e a unidades tioladas serán os puntos de unión das nanopartículas de ouro.

Unha vez formados os copolímeros descritos anteriormente, procedeuse a formación dos materiais híbridos. Para isto, empregouse unha variación do procedemento descrito por Brust-Schiffrin para a formación de AuNPs en disolvente orgánicos. Neste caso, utilízase o copolímero tiolado como axente protector das AuNPs para formar unha superficie quiral nas nanopartículas de ouro.

O estudos de estímulo-resposta do materials híbridos mostraron un comportamento dinámico do material en disolventes de diferente polaridade, obtendo hélices tipo *P* en disolventes mais polares (DMSO e DMF) e hélices tipo *M* cando se disolve o material en disolventes menos polares ($CHCl_3$ ou DCM). Ademais, fixéronse estudos estímulo-resposta mediante a adición de ións metálicos ao PPA-AuNPs. Estes estudos mostraron unha resposta do material híbrido complemente diferente á do polímero en solitario. Mentres que o PPA respondía a presenza de ións metálicos invertindo o seu sentido de xiro, o PPA-AuNPs no responde a este estímulo indicando a que AuNPs impide esta inversión de helicidade.

Finalmente, procedeuse a caracterización da morfoloxía dos materiais híbridos mediante microscopía electrónica (SEM e TEM). Estes estudos mostraron que a morfoloxía do material esta directamente relacionada coa cantidade de unidades tioladas presente no copolímero. Desta forma, os copolímeros que presenta a menor porcentaxe de unidades

tioladas mostran nanopartículas de ouro illadas mentres que os PPAs con maior cantidade de unidades tioladas mostraron a formación de fibras con AuNPs na súa superficie.

Capítulo IV. Materiais Híbridos Quirais Dinámicos PPA-AgNP: Nanopartículas de Prata Aliñadas Decorando Polímeros Helicoidais

No primeiro capítulo desta tese de doutoramento, fíxose unha primeira aproximación á formación de materiais híbridos baseados en PPA-AuNPs a través da clásica interacción entre un grupo tiol e AuNPs. Usando esta metodoloxía, púidose observar unha perda do carácter dinámico do PPA unha vez se conxugan coas AuNPs. A explicación a isto é a forte unión da AuNP ao PPA que impide ao mesmo tempo a inversión da helicidade.

Na bibliografía aparecen diferentes exemplos onde as MNPs (M = Au ou Ag) están estabilizadas a través de interaccións supramoleculares débiles. Un exemplo deste tipo de materiais son os formados polo polímero poli(vinilpirrrolidona) (PVP) e MNPs, onde a PVP proporciona os grupos funcionais amida necesarios para a estabilización das MNPs.

Tendo en conta esta información, neste capítulo propúxose o uso deste tipo de interaccións non covalentes entre un PPA e AgNPs. Este tipo de estabilización seguirá un mecanismo autoadaptativo que permitirá ao PPA-AgNPs manter as súas propiedades dinámicas tal e como ocorre no PPA illado.

Para a realización destes estudos preparáronse o poli-(*R*)-MPA derivado da 4-anilida do ácido (*R*)-α-metoxi-α-fenilacético e poli-(*R*)-MTPA derivado da 4-anilida do ácido (*R*)-α-metoxitrifluorometilfenilacético. A selección destes dous PPAs baseouse no comportamento helicoidal dinámico que presentan e no diferente carácter dador do seu grupo amida.

Poli-(*R*)-MPA é un PPA cun comportamento altamente dinámico e, que en ausencia de estímulos externos, presenta unha estrutura racémica, onde as hélices tipo *M* e *P* están en igual proporción. Ademais, este PPA pode modular o seu sentido de xiro mediante a adición de catións monovalentes (hélices tipo *M*) ou a adición de catións divalentes (hélices tipo *P*). No caso de poli-(*R*)-MTPA, presenta un grupo funcional, CF_3, fortemente atractor de electróns que debería desactivar o poder dador do grupo amida. Deste forma, poderase estudar a función do grupo funcional amida na estabilización das AgNPs.

Para a obtención do material híbrido, poli-(*R*)-MPA-AgNPs, empregouse un método de redución directa con $NaBH_4$ despois da complexación dos ións Ag^+ ao grupo *pendant* (hélices tipo *M*). A morfoloxía de poli-(*R*)-MPA-AgNPs estudouse mediante microscopía electrónica de transmisión (TEM) e estes estudos mostraron a formación de AgNPs esféricas de 2.8 nm. Ademais, observouse unha disposición lineal entre elas cunha distancia de 3.1 nm que é coincidente co paso de xiro do PPA confirmando o papel de poli-(*R*)-MPA na estabilización das nanopartículas.

Durante o proceso de redución observouse un interesante fenómeno de inversión da helicidade (de hélices tipo *M* a *P*). Co obxectivo de demostrar si os ións de Na^+ existentes no axente redutor ($NaBH_4$) teñen unha influenza no sentido de xiro despois da formación do híbrido fixéronse estudos con resinas atrapa catións. Estes estudos demostraron que os ións Na^+ son os responsables da inversión de helicidade unha vez formado o material híbrido.

Os estudos de resposta dinámica de poli-(*R*)-MPA-AgNPs mostraron se pode modular a seu sentido de xiro mediante a adición de ións monovalentes (hélices tipo *M*) e ións divalentes (hélices tipo *P*) obtendo un comportamento dinámico análogo ao de poli-(*R*)-MPA. Ademais, observouse a formación de nanoesferas poliméricas (tipo *P* ou *M*) con AgNPs na súa periferia debido á capacidade dos ións metálicos de actuar como axentes de entrecruzamento entre cadeas poliméricas.

Por último para a comprobación do papel do grupo amida na estabilización das nanopartículas, preparáronse poli-(*R*)-MTPA-AgNPs seguindo o mesmo protocolo utilizado para o caso anterior. Estes estudos mostraron a formación de AgNPs moi polidispersas confirmando unha menor interacción do grupo amida coas AgNPs.

Capítulo V. Papel da Interaccións Polímero-AuNPs nas Propiedades Estímulo-Resposta dos Materiais Híbridos: Interacciones Supramoleculares vs PPA-AuNPs tiolados

No capítulo anterior, estudouse a formación de materiais híbridos baseados en PPA-AgNPs. Nese caso, utilizouse como axente protector quiral das AgNPs o PPA derivado do ácido (*R*)-α-metoxi-α-fenilacético (poli-(*R*)-MPA) que é un PPA altamente dinámico. Ademais, os grupos amida presentes no seu *pendant* permitiron a estabilización das AgNPs mediante interaccions supramoleculares débiles entre eles.

Tendo en conta esta información, neste capítulo estudouse a combinación entre o poli-(*R*)-MPA e AuNPs aproveitando a interacción non covalente entre os grupos amida e as AuNPs. En primeiro lugar, procedeuse a formación do poli-(*R*)-MPA-AuNPs a través dun procedemento de redución directa despois de coordinación dos ións Au^{3+} ao poli-(*R*)-MPA. Usando este procedemento, observouse como a cor da disolución cambiaba de amarelo a azul despois de engadir os ións Au^{3+} ao poli-(*R*)-MPA.

Co fin de estudar as causas deste cambio de cor realizáronse diferentes experimentos. En primeiro lugar, as medidas de UV-Vis do poli-(*R*)-MPA despois de engadir os ións Au^{3+} mostraron a desaparición da banda vinílica, confirmando a perda da estrutura secundaria do PPA. Experimentos de resonancia paramagnética electrónica (EPR) mostraron a presenza dun radical orgánico en poli-(*R*)-**1** que está deslocalizado a través da cadea polimérica. A xeración desta especie radicalaria atribuíuse a un proceso redox entre o PPA e os ións Au^{3+}. Para confirmar esta hipótese, realizáronse experimentos de espectroscopia fotoelectrónica de raios

X (XPS) para obter información sobre o estado de oxidación do ouro. Estes experimentos demostraron a presenza de Au^0 confirmando ao mesmo tempo o proceso redox na formación da especie radicalaria. Ademais, as imaxes de TEM obtidas mostraron que este proceso redox implica a formación de AuNPs.

Unha vez comprobado que a formación de poli-(*R*)-MPA-AuNPs a través do método de redución directa deu orixe a un proceso redox e a formación de AuNPs e a unha especia radicalaria no PPA, procedeuse a formación deste material híbrido utilizando unha variación do método de Brust-Schiffrin.

Usando esta metodoloxía puidéronse obter poli-(*R*)-MPA-AuNPs perfectamente estables en disolución. Ademais, as imaxes de TEM mostraron a formación de AuNPs cun tamaño de 4.2 $\pm$ 1.1 nm cunha separación de 6.1 nm entre elas que coincide con dous pasos de hélice neste polímero helicoidal.

Para finalizar, realizáronse estudos de estímulo-reposta mediante a adición de ións metálicos monovalentes e divalentes (Li^+ e Ba^{2+}) para obter unha mellora da quiralidade cara hélices tipo *P* ou *M*. Estes experimentos mostraron unha diminución de arredor dun 40% na intensidade do espectro de dicroísmo circular. Esta baixada de intensidade de CD está relacionada coa forza de interacción entre poli-(*R*)-MPA as AuNPs como mostran os experimentos de FT-IR.

Capítulo VI. Preparación de Materiais Híbridos PPA-MNPs via Translocación Redox de Centros de Ouro e Prata: Sensores Quirópticos e Colorimétricos

Como se viu nos capítulos anteriores, os grupos funcionais utilizados para estabilizar as nanopartículas metálicas (MNPs) teñen un papel fundamental no comportamento dinámico dos material híbridos.

Desta maneira, cando se utiliza unha interacción moi forte entre o PPA e as MNPs (*e.g.* S—AuNPs), os polímeros perden a maior parte do seu dinamismo e as súas propiedades estímulo-resposta. Para superar este problema co dinamismo dos PPAs, nos capítulos II e III explorouse o uso de interaccións supramoleculares débiles entre os PPAs e as MNPs. Nestes casos, observouse que o comportamento dinámico dos PPAs non se ve alterado cando se aplican estímulos externos (*e.g.* adición de ións metálicos). Pero estes PPAs están limitados ao uso de grupos funcionais específicos no *pendant* e a evitar o uso de disolventes polares que compitan cos PPAs na interacción coas MNPs.

Tendo en conta todo isto, neste capítulo estudouse a formación de PPAs-MNPs (M = Au ou Ag) que teñan unha forte interacción entre eles e ademais conserven o dinamismo propio do PPA.

Para levar a cabo a preparación deste tipo de materiais híbridos, pensouse no deseño dun PPA que presente a (*L*)-metionina metil éster (poli-(*L*)-MetOMe) como grupo *pendant*. Este PPA presentaría as seguintes características que permitirán obter un material híbrido estable e que ao mesmo tempo conserve as propiedades estímulo-resposta propias dos PPAs.

1) Posúe un centro quiral, desta maneira pode obterse un sentido de xiro maioritario no PPA (hélices tipo *P* ou *M*).

2) Contén un grupo funcional tioéter que pode interaccionar forte e selectivamente coas MNPs.

3) O grupo tioéter está separado por unha cadea alquílica longa e flexible do centro quiral, o que permite que o grupo *pendant* adopte diferentes conformacións dando lugar a hélices tipo *P* ou *M*.

Tendo en conta todo isto, preparouse o poli-(*L*)-MetOMe a través do procedemento clásico de polimerización. Para levar a cabo isto, usouse un catalizador de Rh (I) co obxectivo de obter un PPA cun alto contido *cis* dos seus dobres enlaces, un alto peso molecular e unha baixa polidispersión. Unha vez preparados, procedeuse a realizar os estudos do carácter dinámico dos PPAs utilizando como estímulo externo disolventes de diferente polaridade. Desta maneira, poli-(*L*)-MetOMe presenta un Efecto Cotton negativo na rexión vinílica ($CD_{380} < 0$) cando se disolve en disolventes de baixa polaridade ($CHCl_3$, DCM) dando lugar a estabilización de hélices tipo *M*. Por outra banda, poli-(*L*)-MetOMe presenta un efecto Cotton positivo ($CD_{380} > 0$) dando lugar a formación de hélices tipo *P* en disolventes de polaridade alta (DMSO, DMF). Desta maneira é posible modular o sentido de xiro do PPA a través da polaridade dos disolventes.

A continuación, procedeuse a formación dos materiais hibridos poli-(*L*)-MetOMe-MNPs (M = Ag o Au) a través dun mecanismo de redución directa con $NaBH_4$ despois de coordinar os precursores metálicos ($AgClO_4$ ou $HAuCl_4$) ao PPA. Unha vez engadidos os ións metálicos (Ag^+ ou Au^{3+}) ao poli-(*L*)-MetOMe observouse como o espectro de CD presentaba un Efecto Cotton nulo na rexión viníilca ($CD_{380} = 0$). Isto é debido a habilidade de entrecruzamento dos catións metálicos entre cadeas poliméricas que favorecen a aparición dun precipitado.

Para buscar unha solución a esta perda do sinal de CD, buscouse como método alternativo a preparación dun copolímero baseado en dous derivados de aminoácidos: a (*L*)-metionina metil éster, necesaria para a estabilización das MNPs (M = Ag ou Au), e a (*L*)-alanina metil éster que presenta o mesmo sentido de xiro e ademais non posúe o grupo tioéter responsable da aparición do precipitado. Como resultado, obtivéronse os copolímeros poli-[(*L*)-$MetOMe_r$-*co*-(*L*)-$AlaOMe_{1-r}$] (r = 0.2-0.8) que presentan o mesmo sentido de xiro e as mesmas propiedades dinámicas que os seus correspondentes homopolímeros.

Unha vez estudado o dinamismo dos copolímeros procedeuse a formación dos materiais híbridos poli-[(*L*)-MetOMe$_{0.2}$-*co*-(*L*)-AlaOMe$_{0.8}$]-MNPs (M = Au ou Ag). Para facer isto, empregouse unha metodoloxía de redución directa usando $NaBH_4$ como redutor. Desta maneira, a adición tanto de Au^{3+} como de Ag^{+} aos copolímeros deu lugar a unha inversión de helicidade (hélices tipo *P*, $CD_{380} > 0$) debido á coordinación dos catións metálicos aos grupos carbonilo do *pendant* formando os complexos poli-[(*L*)-MetOMe$_{0.2}$-*co*-(*L*)-AlaOMe$_{0.8}$]/M^{n+} (M^{n+} = Ag^{+} ou Au^{3+}).

A continuación procedeuse á formación dos materiais híbridos poli-[(*L*)-MetOMe$_{0.2}$-*co*-(*L*)-AlaOMe$_{0.8}$]-MNPs (M = Ag ou Au). Os espectros de CD despois da formación dos materiais híbridos mostraron outra inversión de helicidade (hélices tipo *M*, $CD_{380} < 0$) recuperando a sinal de CD de partida do PPA, onde a MNPs interaccionan forte e selectivamente co grupo tioéter. É moi interesante sinalar que o cambio de helicidade débese a un mecanismo de translocación do metal onde os grupos funcionais do *pendant* distinguen o estado de oxidación. Desta maneira, os catións metálicos interaccionan con grupos carbonilo ($CD_{380} > 0$, hélices tipo *P*) mentres que as MNPs só interaccionan co grupo tioéter ($CD_{380} < 0$, hélices tipo *M*) actuando o copolímero como un sensor quiróptico.

Para rematar o capítulo, estudouse as propiedades de estímulo-resposta dos materiais híbridos poli-[(*L*)-MetOMe$_{0.2}$-*co*-(*L*)-AlaOMe$_{0.8}$]-MNPs usando o catión metálico Ag^{+} como estímulo externo. Estes estudos revelaron que a adición do Ag^{+} promove unha inversión helicoidal tanto en poli-[(*L*)-MetOMe$_{0.2}$-*co*-(*L*)-AlaOMe$_{0.8}$]-AuNPs/Ag^{+} como en poli-[(*L*)-MetOMe$_{0.2}$-*co*-(*L*)-AlaOMe$_{0.8}$]-AgNPs/Ag^{+} dando lugar a hélices tipo *P* e mostrando un cambio de cor da disolución. Ademais, os espectros de UV-Vis mostraron un desprazamento da banda do plasmón localizado de superficie que no caso dos poli-[(*L*)-MetOMe$_{0.2}$-*co*-(*L*)-AlaOMe$_{0.8}$]-AgNPs/Ag^{+} é reversible mediante a adición de resinas atrapa catións.

Capítulo VII. Estereocomplexación ON-OFF de Materiais Compostos baseados en Polímeros Helicoidais dinámicos-MNPs (M = Ag e Au) a través do Dominio do Polímero Helicoidal

Denomínase como estereocomplexo a un agregado supramolecular formado por interacción de polímeros estereoregulares e complementarios, dando como resultado un novo material cunhas propiedades diferentes ás dos hompolímeros iniciais.

En estudos previos do grupo de investigación, demostrouse que o polímero derivado da 4-anilida do ácido α-metoxitrifluorometilfenilacético (poli-MTPA) pode formar este tipo de agregados supramoleculares mediante a interacción de poli-(*R*)-MTPA e poli-(*S*)-MTPA cando están disoltos en THF. Este material fórmase por interacción entre hélices complementarias que levan configuracións de amida *cis* na periferia das hélices do polímero, producindo agregados de tipo fibra que poden ser detectados a través de técnicas como DLS e SEM.

Ademais, a modificación da conformación *cis-trans* do grupo amida a través do cambio da polaridade do disolvente ou a ruptura dos enlaces hidróxeno permite modular a formación dos esterecomplexos.

Neste capítulo, procedeuse a formación dun novo tipo de material baseado en PPA-MNPs (M = Ag e Au) para a posterior preparación dos esterecomplexos. Con este obxectivo, deseñouse un copolímero con unidades quirais de MTPA e outro comonómero tiolado para ter puntos de conexión para as MNPs.

En primeiro lugar, procedeuse a preparación dos monómeros (*R*)- e (*S*)-MTPA, xunto cos comonómeros tiolados. Unha vez obtidos, prepáraronse os copolímeros coa utilización dun catalizador de Rh (I) que ten como característica principal a obtención de PPAs cun alto peso molecular e un alto contido *cis* dos seus dobres enlaces, dando como resultado polímeros con estrutura helicoidal. Os copolímeros obtidos presentarán unha parte quiral (unidades de MTPA) que permitirá a formación de esterecomplexos mediante a modulación da conformación *cis-trans* do grupo amida. Ademais, a parte aquiral (unidades tioladas) que permitirá a unión das MNPs dando como resultado un novo tipo de esterecomplexos. Desta maneira, os copolímeros formados son uns bos candidatos para a formación de materiais de tipo estereocomplexo decorados con MNPs.

Como se esperaba, os copolímeros tiolados mostraron a mesma habilidade que os homopolímeros de poli-MTPA para formar os esterecomplexos. Isto confirma que a presenza das unidades tioladas en baixa proporción non inflúe na formación dos agregados. Ademais, os estudos de estímulo-resposta destes esterecomplexos confirmaron que a súa formación pode modularse mediante a polaridade do disolvente ou a ruptura dos enlaces hidróxeno.

Unha vez avaliada a capacidade dos copolímeros para formar os esterecomplexos, procedeuse ao estudo da formación destas estruturas en presenza de MNPs. Para isto, en primeiro lugar formáronse os materiais híbridos PPA-MNPs (M = Ag ou Au) a través dunha variación do procedemento de Brust-Schiffrin. Este procedemento deu como resultado a formación de AuNPs de 7.1 ± 3.3 nm e AgNPs de 4.4 ± 1.5 nm de diámetro estabilizadas cos copolímeros tiolados.

Por último, procedeuse a formación dos esterecomplexos con materiais híbridos descritos anteriormente. Os estudos de DLS e microscopía electrónica mostraron a formación de agregados de tipo fibra dos copolímeros en presenza das MNPs, confirmando que a súa presenza no inflúe na formación dos estereocomplexos. Ademais, os estudos de estímulo-resposta destes materiais demostraron que a súa formación pode controlarse a través da polaridade do disolvente ou a ruptura dos enlaces hidróxeno.

***Capítulo VIII*. Inlfuenza da Estrutura Secundaria dos PPAs na Preparación de Nanoestructuras Poliméricas**

A combinación da nanoescala e quiralidade está a atraer a curiosidade da comunidade científica debido as fortes aplicacións en campos como a catálise, os sensores ou a terapia biomédica, entre outros.

Na bibliografía existe diferentes traballos nos que se forman nanoestruturas poliméricas (*e.g.* nanoesferas, nanotubos, toroides), pero na actualidades existen moi poucos exemplos destas nanoestruturas formadas por PPAs ou as existentes están restrinxidas ao uso de ións metálicos como axentes de entrecruzamento entre cadeas poliméricas.

Neste traballo, presentouse unha nova metodoloxía para a formación de nanoestruturas poliméricas co emprego usando o método de nanoprecipitación. Como polímeros, foron elixidos PPAs con diferentes conexións (benzamida e anilida) e dentro dos PPAs de tipo anilida usáronse polímero con diferente substutición no anel aromático (*para*, *meta* e *orto*). Desta forma, puídose estudar como inflúe o tipo de conexión e a estructura secundaria na formación das nanoestruturas poliméricas.

En primeiro lugar, estudáronse todos os PPAs (anilidas e benzamidas) substituídos en posición *para*. Neste, caso puidose observar a través de experimentos de DLS a formación de nanoesferas poliméricas cunha polidispersión moi baixa (PDI < 0.2). Ademais, as imaxes de microscopía electrónica confirmaron a presenza destas esferas.

A continuación, estudáronse os PPAs con conexión anilida substituídos en posición *orto*, *meta* e *para*. En estudos previos demostrouse que a substitución no anel aromático ten unha forte influenza no carácter dinámico dos PPAs. Así, os PPAs substituídos en *para* e *meta* presentan a estructura máis dinámica respondendo a estímulos externos mentres que o PPA substituído en orto presenta una estrutura casi estática. Tendo en conta isto, procedeuse ao estudos de nanoestructuración. Neste caso, os polímeros máis dinámicos (*para* e *meta*) mostraron a formación de esferas poliméricas, confirmado mediante experimentos de SEM e DLS. No caso do PPA substituído en posición *orto*, observouse a través de imaxes de SEM a formación de agregados lonxitudinais confirmando a influenza da estructura secundaria na agregación das cadeas poliméricas.

Por último, relizáronse estudos de microscopía confocal confirmando a capacidade destas estructuras para encapsular diferentes fluorocromos.

USC
UNIVERSIDADE
DE SANTIAGO
DE COMPOSTELA

Chapter X

Conclusions

USC
UNIVERSIDADE
DE SANTIAGO
DE COMPOSTELA

This thesis is focused on the preparation of novel hybrid materials based on poly(phenylacetilene)s (PPAs) and metal nanoparticles (MNPs). PPAs are a family of dynamic helical polymer where the structural parameters (helical sense and/or elongation) can be tuned by external stimuli such as temperature, polarity of solvents, metal ions, etc. These features make them excellent candidates to act as chiral coverture of MNPs.

Throughout the different chapters, it was demonstrated the ability of the PPAs to act as protecting agent and give a chiral environment in the MNPs. In addition, the study of interaction strength between the MNPs-PPAs, in conjunction with the dynamic properties, took a special relevance during this thesis.

Next, the main conclusions for each chapter are summarized below.

***Chapter III*. Chiral Gold-PPA Nanocomposites with Tunable Helical Sense and Morphology**

We have studied the role of a macromolecular helical structure in the formation of a helical polymer-Au nanocomposite. To perform these studies a poly(phenylacetylene) bearing the benzamide of a phenylglyicine methylester (M**1**) as pendant group was chosen.

This selection was done based on our knowledge in the structure and dynamic behavior of the polymer. To form the nanocomposite, a thiolated monomer was introduced in the polymer chain. This thiolated monomer has a structural effect on the copolymer secondary structure and its dynamic behavior before and after the formation of the hybrid material.

Thus, the introduction of the thiolated comonomer in the copolymer chain destabilize the helical arrangement of the M**1** monomers placed close to this residue. Interestingly, we found that the thiol groups should be located in nearby positions, because the depletion of the helix folding it is not further affected by increasing the amount of the thiol group in a molar fraction range of 0.01-0.05.

Additionally, hybridization of these thiolated copolymers with AuNPs produces another perturbation in the polymeric secondary structure, although its dynamic behavior it is not affected, being possible to modulate the nanocomposite chirality by the action of external stimuli such as solvent polarity.

Next, we found that the morphology of the nanocomposites can be modulated through the thiolated monomer ratio within the copolymer chain. Thus, at the lowest thiolated molar fraction (0.01), the nanocomposite appears as dispersed AuNPs in electron microscopy. Interestingly, at higher molar ratios of the thiolated monomer, the controlled formation of fiber-like structures is produced by combining the crosslinking ability o of the AuNPs with the self-assembly properties of the copolymer.

Finally, a further controlled self-assembly of a nanocomposite was achieved by using metal ions (Ba^{2+}) as crosslinking agents. Thus, in the case of Au-poly-(M**1**$_{0.98}$-*co*-M**2**$_{0.02}$) and Au-poly-(M**1**$_{0.99}$-*co*-M**2**$_{0.01}$) it was possible to generate macroscopically chiral nanospheres, whose size could be controlled by tuning the nanocomposite/Ba^{2+} ratio.

Therefore, a first insight into the control over the chiral dynamicity of plasmonic nanocomposites was demonstrated. Notably, a first controlled assembly into different nanomorphologies was achieved by considering the thiol comonomer content and the helix-to-helix supramolecular interactions. Besides, by using metal ions as crosslinking agents, some of these morphologies are further nanostructured into macroscopically chiral nanospheres with low polydispersity.

Chapter IV. **Dynamic Chiral PPA-AgNP Nanocomposites: Aligned Silver Nanoparticles Decorating Helical Polymers**

A novel approach to obtain PPA-AgNPs nanocomposites without altering the dynamic behavior of the parent polymer is described.

Weak amide-AgNP supramolecular interactions are used to prepare chiral dynamic nanocomposites. To perform these studies, poly-(*R*)-**1**, bearing the 4-anilide of (*R*)-α-methoxy-α-phenylacetic acid was chosen as a protecting agent. First, a poly-(*R*)-**1**/Ag^{+} complex is formed in a 1.0/0.5 mol/mol ratio, which is further reduced to the poly-(*R*)-**1**-AgNPs/dodecanethiol nanocomposite using $NaBH_4$ as the reducing agent. TEM studies of the nanocomposite show that the AgNPs are regularly distributed along the polymer chain. Poly-(*R*)-**1** acts as a template by placing the AgNPs at fixed distances of 3.1 nm, which corresponds to the helical pitch of poly-(*R*)-**1**. Stimuli-responsive studies show that poly-(*R*)-**1**-AgNPs/dodecanethiol nanocomposite responds to monovalent and divalent metal ions just like the parent polymer, poly-(*R*)-**1**, does. Hence, a *P* helix is induced by monovalent metal ions, while an *M* helix is fixed when divalent metal ions are added to a dispersion of the hybrid material. Moreover, during these studies, the ability of the poly-(*R*)-**1**-AgNPs/dodecanethiol/M^{n+} nanocomposite to form other nanostructures such as nanospheres was also demonstrated.

Chapter V. **The role of the polymer-AuNP bond in the stimuli-responsive properties of the nanocomposites: Supramolecular vs thiolated PPA-AuNP interactions**

it was demonstrated that it is possible to prepare a dynamic chiral nanocomposites based on a supramolecular interaction between a PPA and gold nanoparticles (AuNP-anilide interactions). To prepare these nanocomposites, a variation of the Brust-Schiffrin protocol is necessary due to the degradation of the PPA by Au^{3+} ions. In this case, TOAB is first complexed to the Au^{3+} ions, then poly-(*R*)-**1** and the reducing agents are added producing the

nanocomposites which contains small and low polydisperse AuNPs (4.2 ± 1.1 nm) aligned along the polymer chain and regularly displayed at ca. 6 nm that corresponds to two consecutive helical pitches.

These studies confirm that to prepare a dynamic helical polymer-MNP nanocomposite is necessary to consider how the strength of the PPA-MNP interaction affects to its dynamic behavior. Thus, while strong thiol-AuNP interactions reduce dramatically the dynamic behavior of the PPA, weaker supramolecular interactions maintain a good stimuli response property in the nanocomposite.

These studies are of great importance in the development of novel hybrid materials based on dynamic helical polymers, providing us rules about how to attach these polymers to other materials, not only metal nanoparticles without affecting their dynamic behavior.

Chapter VI. **Preparation of Helical Polymer-MNPs Nanocomposites via Redox Driven Translocation of Gold or Silver Centres: Chiroptical and Colorimetric Switches**

In conclusion, dynamic chiral nanocomposites based on stimuli-responsive helical polymers and MNPs has been described taking into account the main limitations of previously described dynamic chiral nanocomposites, which are affected mainly by the connection between the PPA and the MNP. Thus, herein we prepared a dynamic helical poly(pheylacetylene) copolymer formed by the 4-ethynylbenzamides of two natural amino acids such as the (*L*)-alanine [(*L*)-**1**] and the (*L*)-methionine [(*L*)-**2**]. As a result the poly-[(*L*)-$\mathbf{1}_{r}$-*co*-(*L*)-$\mathbf{2}_{1-r}$] (r = 0.2-0.8) copolymer series was prepared. This copolymer series follows a *chiral accord* effect, adopting the same helical sense and the same stimuli responsive properties than the parent homopolymer. Taking into account the poor solubility of the copolymer series, only the copolymer poly-[(*L*)-$\mathbf{1}_{0.2}$-*co*-(*L*)-$\mathbf{2}_{0.8}$] has been used to prepare the nanocomposites. Poly-[(*L*)-$\mathbf{1}_{0.2}$-*co*-(*L*)-$\mathbf{2}_{0.8}$]-AuNPs and poly-[(*L*)-$\mathbf{1}_{0.2}$-*co*-(*L*)-$\mathbf{2}_{0.8}$]-AgNPs were preparing first the corresponding HPMC —Poly-[(*L*)-$\mathbf{1}_{0.2}$-*co*-(*L*)-$\mathbf{2}_{0.8}$]/Au^{3+} and Poly-[(*L*)-$\mathbf{1}_{0.2}$-*co*-(*L*)-$\mathbf{2}_{0.8}$]/Ag^{+}— that were further reduced with $NaBH_4$ to generate the poly-[(*L*)-$\mathbf{1}_{0.2}$-*co*-(*L*)-$\mathbf{2}_{0.8}$]-AuNPs and the poly-[(*L*)-$\mathbf{1}_{0.2}$-*co*-(*L*)-$\mathbf{2}_{0.8}$]-AgNPs nanocomposites.

Interestingly, the formation of the nanocomposite can be monitored by CD, where the copolymer acts as a multistate chiroptical switch. Thus, the formation of the HPMCs produce a helix inversion process —*M* (CD_{370} < 0) to *P* (CD_{370} > 0) helix— due to an *anti* to *syn* conformational change at the pendant groups of poly-[(*L*)-$\mathbf{1}_{0.2}$-*co*-(*L*)-$\mathbf{2}_{0.8}$] by complexation with either Au^{3+} or Ag^{+} ions. Furhter reduction of the metal ions results in another helix inversion —*P* (CD_{370} > 0) to *M* (CD_{370} < 0) helix—induced by a redox driven translocation of either a gold or silver centre. This helix inversion is also accompanied by a solution colour change from yellow

to red in the case of the poly-[(*L*)-**1**$_{0.2}$-*co*-(*L*)-**2**$_{0.8}$]-AuNPs nanocomposite and from yellow to dark orange in case of the poly-[(*L*)-**1**$_{0.2}$-*co*-(*L*)-**2**$_{0.8}$]-AgNPs nanocomposite. This colour change is due to the generation of a LSPR band consequence of the generation of the MNPS.

These nanocomposites showed similar chiroptical stimuli responsive properties to those observed for the parent copolymer poly-[(*L*)-**1**$_{0.2}$-*co*-(*L*)-**2**$_{0.8}$]. In addition the nanocomposites showed a solution colour change in the presence of metal ions. This fact is due to the formation of nanospheres based on the nanocomposites which place the MNPs close to each other overlapping their electronic clouds. This fact produces a red shift in the LSPR band which indicates that they are behaving as larger particles. This colour change is reversible in the poly-[(*L*)-**1**$_{0.2}$-*co*-(*L*)-**2**$_{0.8}$]-AgNPs/Ag^{+} nanocomposite, where the addition of metal scavenger resins trap the metal ions, and the poly-[(*L*)-**1**$_{0.2}$-*co*-(*L*)-**2**$_{0.8}$]-AgNPs recovers its initial state.

Thus, we have developed a novel approach to prepare a chiroptical and colorimetric swtiches based on hybrid materials made by combination of dynamic helical polymers and metal nanoparticles, which open a new horizon in the application of these nanocomposites in fields such as sensing, chiral recognition or asymmetric asynthesis among others.

Chapter VII. **ON-OFF Stereocomplexation of Dynamic helical polymer-MNPs (M = Ag, Au) Nanocomposites by Taming the Polymer Helix**

In this work, it was demonstrated that it is possible to prepare a stimuli-responsive stereocomplexes based on dynamic-helical polymers-MNP (M = Au or Ag) nanocomposites. Thus, two complementary and enantiomeric helical polymers functionalized with Au or Ag nanoparticles interact between them to form fibre like aggregates stabilized by a hydrogen bond network formed by *cis*-amide groups located at the crest of the helical polymers. The possibility of tuning the helical structure of the polymer by external stimuli in combination with the possibility of acting on the hydrogen bond network makes possible to create a stimuli responsive nanocomposite stereocomplex, and where different morphologies can be obtained for the enantiomeric hybrid material mixture.

The creation of the stereocomplex it is not straightforward being necessary to make a previous design of the copolymer to stabilize the metal nanoparticle with the helical polymer without affecting to the stereocomplexation ability of the polymer. This work is pioneering in this topic, and we believe that important applications in both the helical polymers and metal nanoparticle fields can emerge by a correct design of the hybrid materials used to prepare the stereocomplex.

Chapter VIII. **Effect of the Secondary Structure of PPAs in the Preparation of Polymeric Nanostructures**

In this work, we have developed a new simple and fast methodology for the formation of polymeric nanospheres by a nanoprecipitation method in absence of other surfactants. For this purpose, we chose a broad variety of PPAs with anilide and benzamide connections and different aromatic substitution patter (*para*, *meta* and *ortho* anilides).

First, PPAs with para substitution pattern (anilide or benzamide connections) were studied. In the case of poly-(*R*)-**1** and poly-(*R*)-**4** (benzamide connections), the DLS studies confirmed

In the case of anilide connections, we evaluated the aromatic substation pattern (poly-(*R*)-**1**, poly-(*R*)-**2**, *o*-poly-(*R*)-**3**) using two combinations of solvents (acetone/water and THF/water). It was found that the THF/water form in all cases polymeric nanospheres whereas the acetone/water form polymeric nanospheres in the case of *para* and *meta* PPAs. Interestingly, *o*-poly-(*R*)-**1** showed the formation of longitudinal aggregates confirming the influence of the secondary structure of the PPAs in the nanostructuration process.

Next, it was evaluated the benzamide connection PPAs (poly-(*L*)-**5**, poly-(*L*)-**6**, poly-(*L*)-**7**, poly-(*L*)-**8**, poly-(*L*)-**9**). Using these PPAs, it is possible to obtain chiral nanospheres in acetone/water. Interestingly, it was observed in the THF/water system that PPAs with not bulky groups —poly-(*L*)-**3** and poly-(*L*)-**6** showed the corresponding Cotton Effect ($CD_{380} > 0$) for the PPA in THF. On the other hand, PPAs with bulky groups —poly-(*L*)-**4**, poly-(*L*)-**5**, poly-(*L*)-**7**— showed an helical inversion ($CD_{380} < 0$) when the water is added.

Finally, it was demonstrated the ability of the nanospheres to encapsulate different fluorescent dyes such as 5,6-carboxyfluorescein, rhodamine B isothiocyanate.

In our opinion, this work open new possibilities in the rational design of polymeric nanostructures using PPAs. This type of polymeric nanostructures shows potential applications in fields such as nanoreactors, nanocarriers or chiral stationary phases for HPLC.

USC
UNIVERSIDADE
DE SANTIAGO
DE COMPOSTELA

Chapter XI

Experimental Sections and Methodology

USC
UNIVERSIDADE
DE SANTIAGO
DE COMPOSTELA

Experimental Section Chapter III:

1. Materials and methods

Commercially available chemicals have been used as delivered. Solvents were purchased as reagent grade and distilled if necessary. Anhydrous solvents were either purchased as ultra-dry solvent from Acros Organics® or received from solvent purification system. For the coupling and polymerization reactions, dry THF was obtained from MBRAUN SPS 800 solvent purification system. Water was purified by Millipore water purification system.

Coupling reagents (2-(7-Aza-1H-benzotriazole-1-yl)-1,1,3,3-tetramethyluronium hexafluorophosphate) (HATU), 1-ethyl-3-(3-dimethylaminopropyl)carbodiimide hydrochloride (EDC.HCl), hydroxybenzotriazole (HOBt), 1-hydroxy-7-azabenzotriazole (HOAT), 4-ethynylbenzoic acid, and 4-ethynylaniline were purchased from AnaSpec Inc. (*L*)-Phenylglycine methyl ester hydrochloride ((*L*)-PGME), triphenylmethanethiol, 11-bromo-1-undecanol, methylsulfonyl chloride, 2,2-(ethylenedioxy)diethylamine, trifluoroacetic acid (TFA), triisopropylsilane, rhodium norbornadiene chloride dimer {$[Rh(nbd)Cl]_2$}, diisopropyltriethylamine (DIEA), triethylamine (TEA, 99%), tetraoctylamonium bromide (TOAB), dodecanethiol, sodium borohydride ($NaBH_4$) and tetrachloroauric acid ($HAuCl_4$) were purchased from Aldrich.

NMR experiments were carried out in a Varian Inova 250 (250 MHz resonance 1H). Size exclusion chromatography studies were performed on Alliance 2695 HPLC System (Waters) liquid chromatography system equipped with a UV 2489 detector (Waters). The samples were eluted by three Phenogel columns connected to each other with stacionary phases of 10^3, 10^4 and 10^5 Amstrong and packed with a solid support of a cross-linked stiyrene and *p*-divinylbenzene copolymer.

CD measurements were done in a Jasco-720 spectropolarimeter. UV spectra were registered in a Jasco-730 spectrophotometer.

FT-IR measurements were carried out on a Bruker IFS-66v while Raman measurements were carried out in a Renishaw confocal Raman spectrophotometer (Invia Reflex model), equipped with two lasers (diode laser 785 nm and Ar laser 514 nm).

DSC measurements were performed in a DSC Q200 Tzero Technology (TA Instruments, New Castle, UK) equipped with a refrigerated cooling system RCS90 (TA Instruments) using a Tzero low-mass aluminum pan.

TGA experiments were carried out in a Q5000SA instrument (TA Instruments, New Castle, UK) using a platinum pan.

DLS measurements were performed on a Nano-ZS 90 (Malvern) equipped with a He-Ne laser (l = 633 nm) under scattering angle of 173°. The samples were maintained at the designed temperature for 5 min before testing.

SEM samples were performed on a LEO-435VP electron microscope. A drop of polymer solution of 1 mg mL^{-1} in $CHCl_3$ (with 0.5 equivalents of a barium perchlorate solution for assembly experiments with Au-poly-(M**1**$_r$-*co*-M**2**$_{1-r}$) (r = 0.95-0.99) was settled on a silicon wafer chip and allowed to dry at rt for 12 h.

TEM measurements were performed on a Phillips CM-12 electron microscope. A drop of a solution of 1 mg mL^{-1} in $CHCl_3$ (with 0.5 equivalents of a barium perchlorate solution for assembly experiments with Au-poly-(M**1**$_r$-*co*-M**2**$_{1-r}$)) was settled on a carbon grid and allowed to dry at rt for 12 h.

2. Names and codes

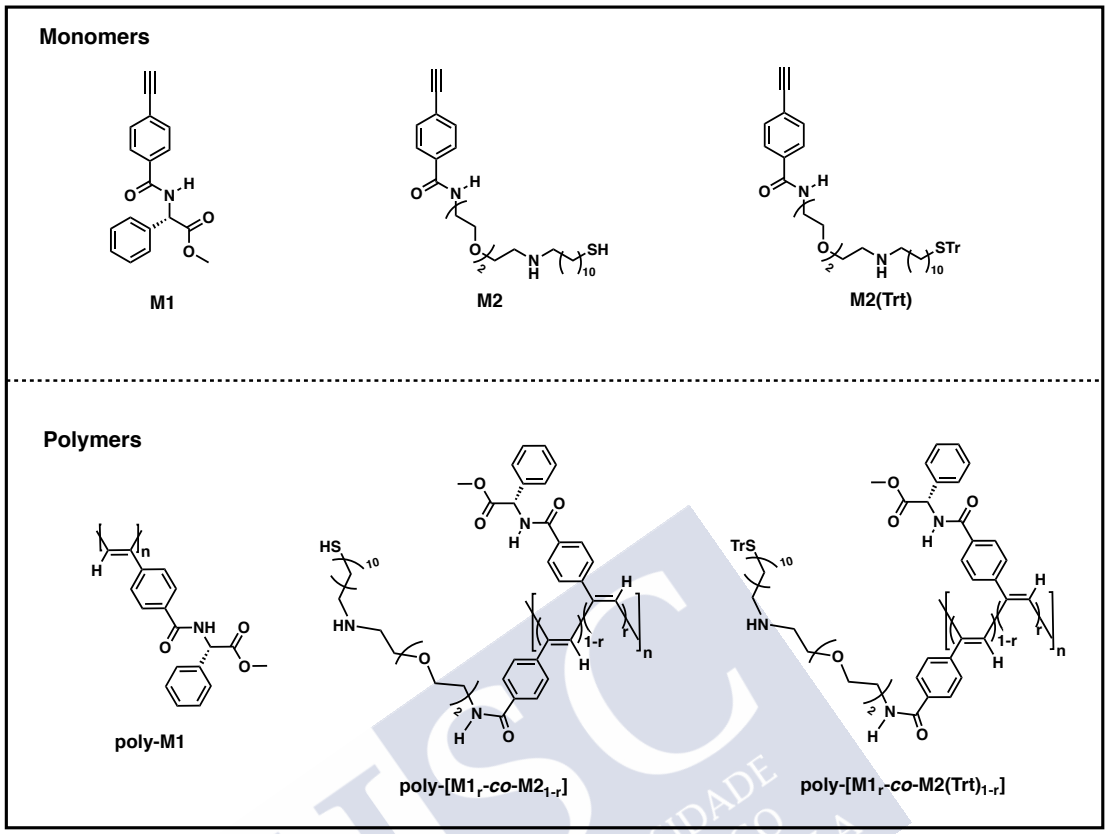

3. Synthesis of Monomers

Synthesis of M1:

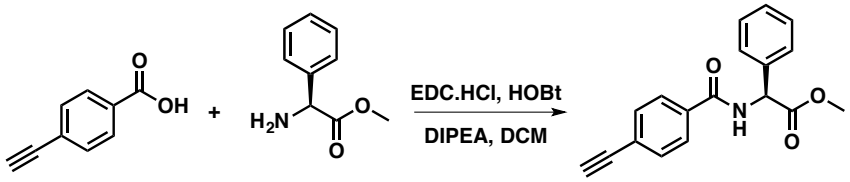

1 **2** **M1**

Monomer M**1** was prepared according to a previous work:[1] (*L*)-Phenylglycine methyl ester hydrochloride **2** (911 mg, 1.2 equiv.) was dissolved in water, basified with a saturated solution of $NaHCO_3$ and extracted with DCM. The aqueous layer was dried over anhydrous Na_2SO_4, filtrated and solvent was evaporated at reduced pressure. Then, the amino ester was dissolved in dried DCM (30 mL) and 1-ethyl-3-(3-dimethylaminopropyl)carbodiimide hydrochloride (EDC·HCl, 867 mg, 1.2 equiv.), 1-hydroxybenzotriazole (HOBt, 608 mg, 1.2 equiv.) and 4-ethynylbenzoic acid (**1**) were added (550 mg, 1.0 equiv.). The resulting suspension was stirred and monitored by TLC. When the reaction was judged as completed, the reaction mixture was washed with water, HCl (1M), water and a saturated solution of $NaHCO_3$. The combined organic layers were dried over anhydrous Na_2SO_4, filtered and the solvent was evaporated at reduced pressure. The crude product was chromatographed on silica gel (70-230 mesh) with hexane/ethyl acetate (4/1) as eluent to obtain 980 mg (89% yield) of pure product.

Spectroscopy data:

^{1}H NMR (250 MHz, $CDCl_3$) δ (ppm): 3.2 (s, 1H), 3.7 (s, 3H), 5.7 (d, 1H), 7.1 (d, 1H), 7.41 (m, 5H), 7.5 (d, 2H), 7.7 (d, 2H).

^{13}C NMR (62.5 MHz, $CDCl_3$) δ (ppm): 52.9, 56.8, 79.7, 82.6, 125.7, 127.1, 127.3, 128.6, 129.0, 132.2, 133.5, 136.5, 165,7, 171.4,

$[a]_D$= +70 (15 mg mL^{-1}, $CHCl_3$).

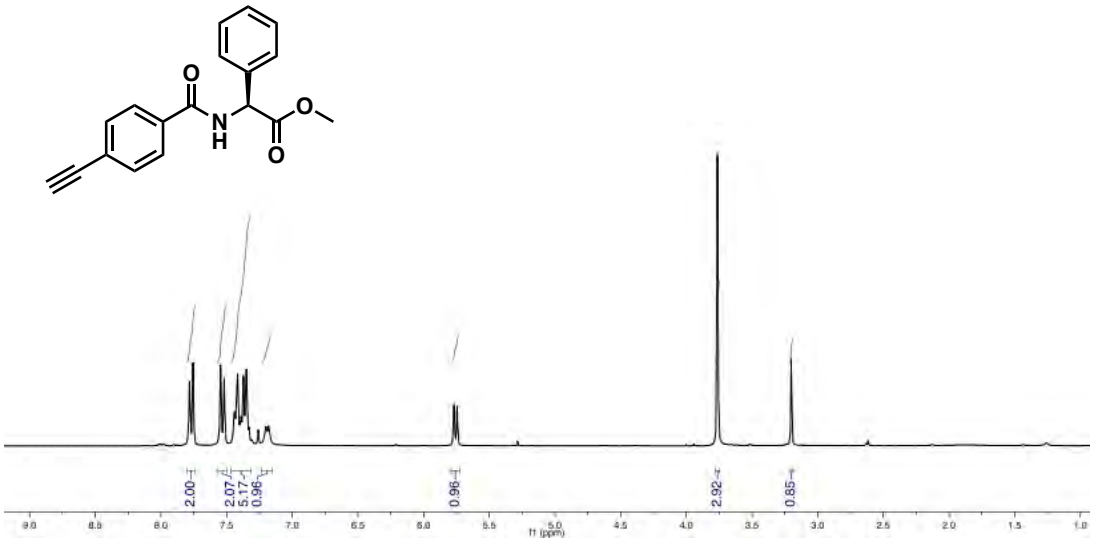

Figure S1. ^{1}H NMR for monomer M**1**.

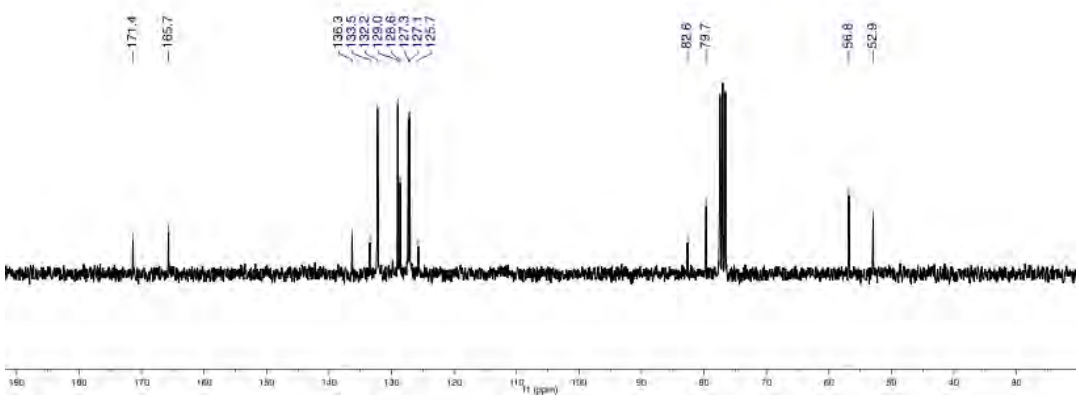

Figure S2. ^{13}C NMR for monomer M**1**.

Synthetic route for M2(Trt) and M2:

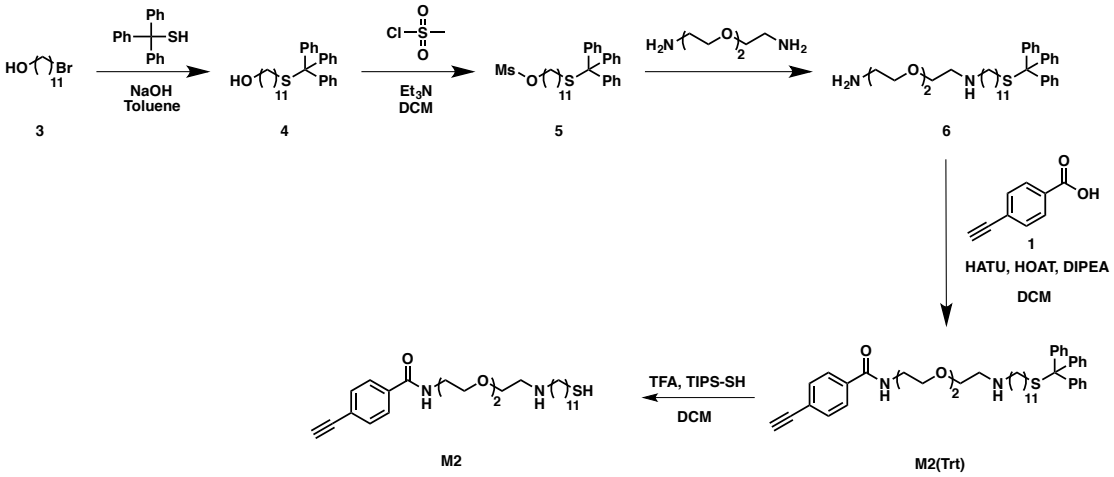

Scheme S1. Synthetic route for M**2**(Trt) and M**2**.

Synthesis of 4:

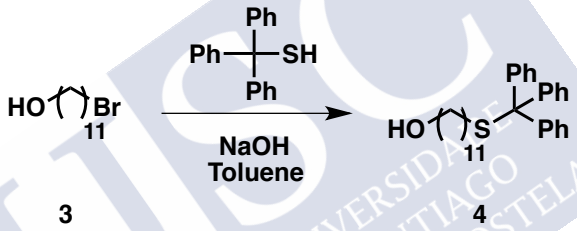

Triphenylmethanethiol (1.32 g, 4.37 mmol) was dissolved in a solution of ethanol/toluene (1:1, 4 mL) and NaOH (0.23 g, 5.97 mmol) in 3 mL of H_2O was added. Then 11-bromo-1-undecanol (**3**, 1.00 g, 3.98 mmol) was also dissolved in a solution of ethanol/toluene (1:1, 4 mL) and added to the triphenylmethanethiol mixture. The new reaction mixture was stirred overnight at room temperature. Once the reaction was completed (checked by TLC) all the mixture was poured into a saturated solution of $NaHCO_3$ and washed three times. The organic layer was separated and added into another solution saturated of NaCl and also washed for three times. Afterward the organic layer was separated, dried (Na_2SO_4) and concentrated. The crude product was purified by column chromatography over silica gel using hexane/ethyl acetate (9:1, 4:1 and 1:1, v/v) as an eluent. The solvent was removed in vacuum to obtain compound **4** as colorless oil (Yield 1.6 g, 95%).

Spectroscopy data:

^{1}H NMR (250 MHz, $CDCl_3$) δ (ppm): 1.0-2.0 (m, 18H), 2.1-2.2 (m, 2H), 3.5-3.7 (m, 2H), 7.0-7.5 (m, 15H).

^{13}C NMR (62.5 MHz, $CDCl_3$) δ (ppm): 25.8, 28.6, 29.0, 29.2, 29.4, 29.5, 29.6, 32.1, 32.8, 63.0, 66.4, 126.5, 127.5, 129.6, 130.1, 154.1.

HRMS (ESI) m/z calculated for $C_{30}H_{38}NO_2$ [M + Na^+]: 469.2536, found: 469.2535.

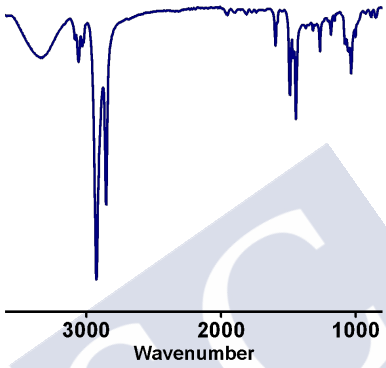

Figure S3. FT-IR spectrum for compound **4**.

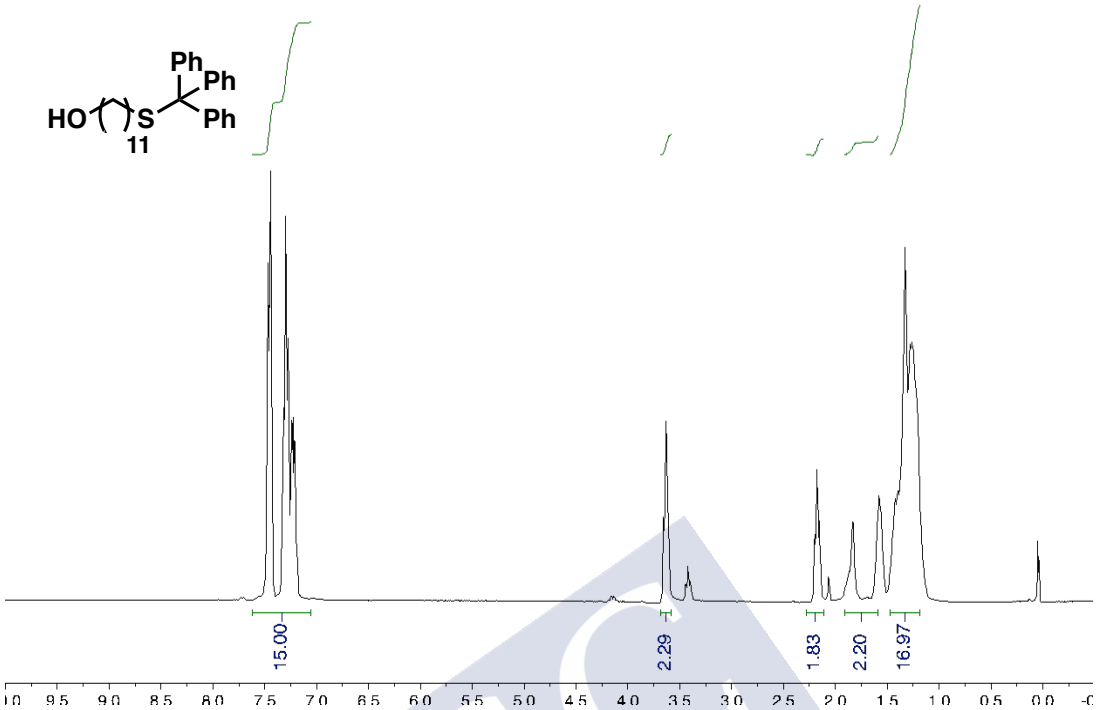

Figure S4. ^{1}H NMR spectrum for compound **4**.

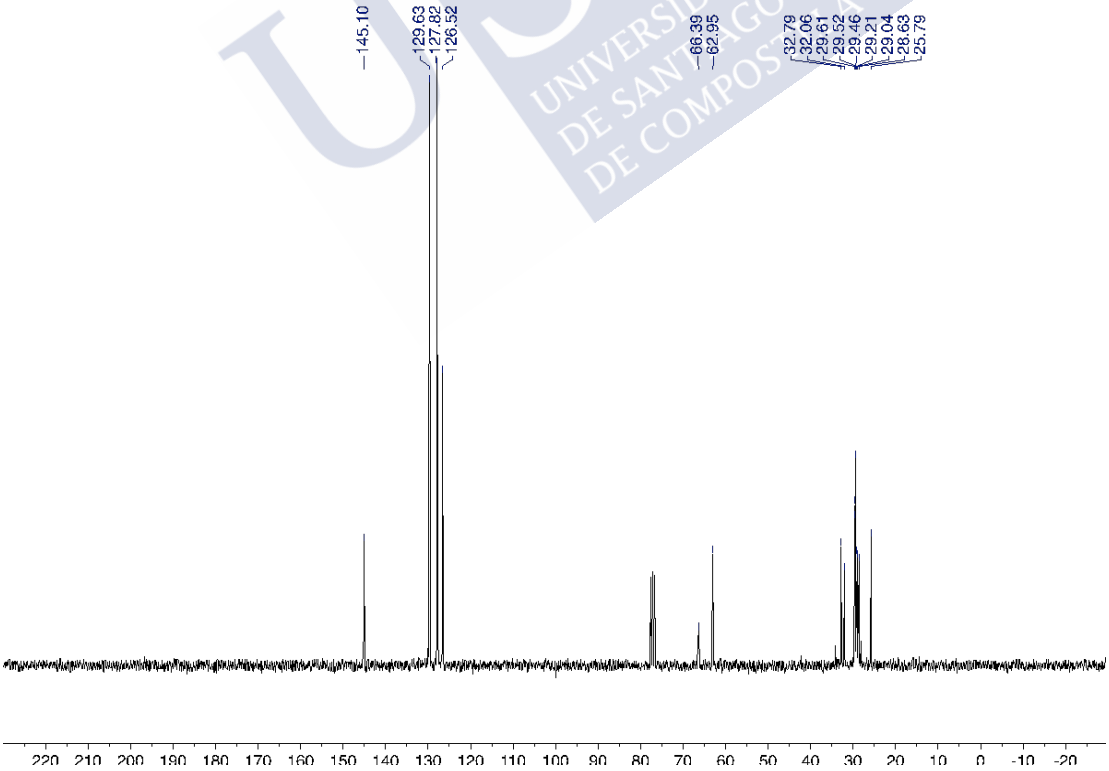

Figure S5. ^{13}C NMR spectrum for compound **4**.

Synthesis of 5:

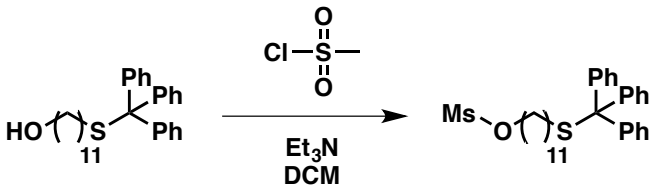

4 **5**

To a solution of compound **4** (1 g, 2.23 mmol) in dry DCM at 4°C, triethylamine (0.45 g, 4.47 mmol) was added. Methylsulfonyl chloride (0.38 g, 3.35 mmol) was injected drop by drop to the solution maintaining the temperature less than 5°C. After 30 minutes the reaction mixture was warmed up to room temperature and stirred for another 30 minutes. Once the reaction was completed (according to TLC), the DCM was evaporated at reduced pressure. The viscous compound was again diluted with DCM and poured into solution of HCl (1 M) and treated twice. Organic layer was poured into a saturated solution of $NaHCO_3$ and washed three times. The organic layer was separated and added into another solution saturated of NaCl and also treated three times. Afterward organic layer was separated, dried (Na_2SO_4) and concentrated at reduced pressure. The crude product was purified by column chromatography over silica gel using hexane/ethyl acetate (1:1, v/v) as an eluent. Solvent was removed in vacuum to afford compound **5** as colorless oil (Yield 1.09 g, 93%).

Spectroscopy data:

^{1}H NMR (250 MHz, $CDCl_3$) δ (ppm): 1.1-1.5 (m, 16H), 1.77 (t, 2H), 2.20 (t, 2H), 2.92 (s, 3H), 3.20 (t, 2H), 7.2-7.6 (m, 15H).

^{13}C NMR (62.5 MHz, $CDCl_3$) δ (ppm): 25.5, 28.6, 29.1, 29.4, 32.0, 32.8, 34.1, 37.3, 66.4, 70.3, 126.6, 127.9, 128.0, 129.6, 145.1.

HRMS (ESI) m/z calculated for $C_{31}H_{40}O_3S_2$ [M + Na^+]: 547.2312, found: 547.2311.

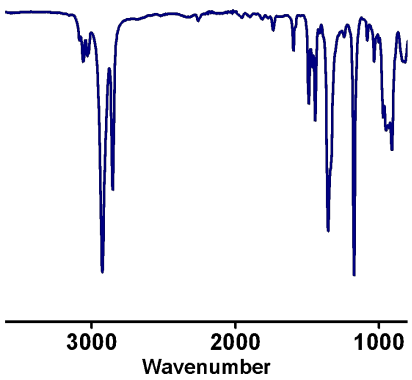

Figure S6. FT-IR spectrum for compound **5**.

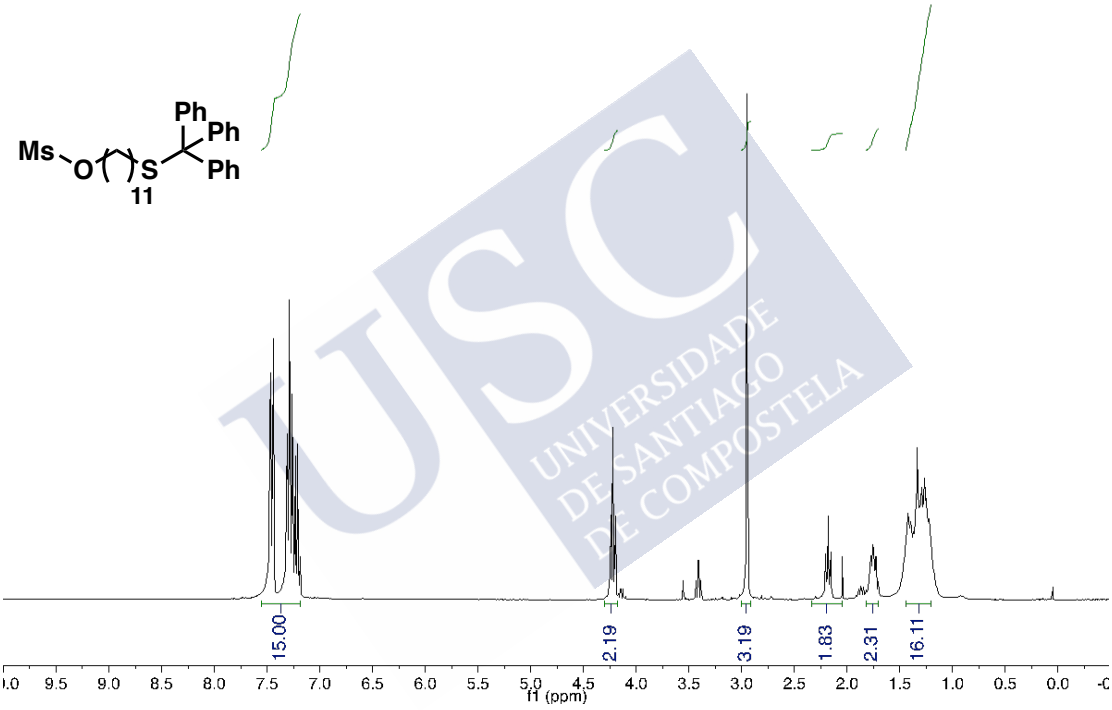

Figure S6. ^{1}H NMR spectrum for compound **5**.

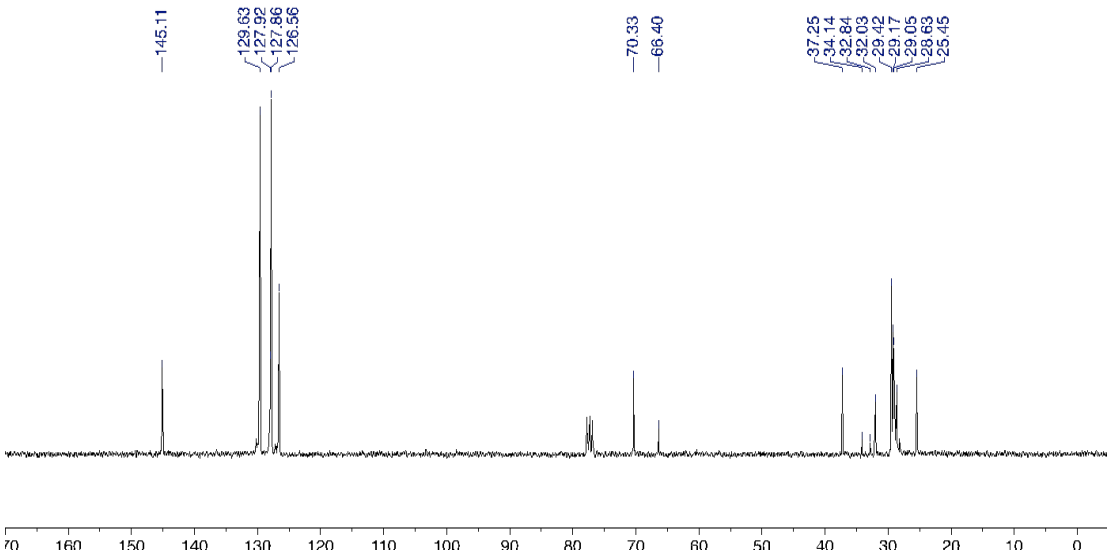

Figure S7. ^{13}C NMR Spectrum for compound **5**.

Synthesis of 6:

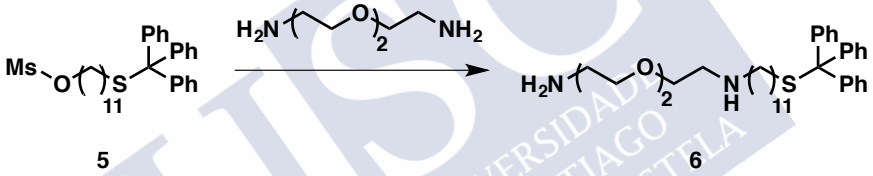

Compound **5** (0.9g, 1.71 mmol) was dissolved in a 2,2-(ethylenedioxy)diethylamine (2.54 g, 17.15 mmol). Once the reaction was completed after 4 hours (according to TLC). The compound was diluted with DCM and poured into a saturated solution of $NaHCO_3$ and washed two times. Afterward organic layer was separated, dried (Na_2SO_4) and concentrated at reduced pressure. Solvent was removed in vacuum to afford compound **6** (Yield 0.89 g, 92%).

Spectroscopy data:

^{1}H NMR (250 MHz, $CDCl_3$) δ (ppm): 1.0-1.6 (m, 22H), 2.15 (t, 2H), 2.62 (t, 2H), 2.75 (t, 2H), 2.82 (t, 2H), 3.51 (t, 2H), 3.63 (t, 2H), 7.0-7.5 (m, 15H).

^{13}C NMR (62.5 MHz, $CDCl_3$) δ (ppm): 27.4, 28.6, 29.0, 29.2, 29.4, 29.6, 30.2, 32.0, 41.8, 49.4, 50.1, 66.3, 70.3, 70.7, 73.4, 126.5, 127.8, 129.6, 145.1.

HRMS (ESI) m/z calculated for $C_{36}H_{52}N_2O_2S$ [M + H]: 577.37, found: 577.3832.

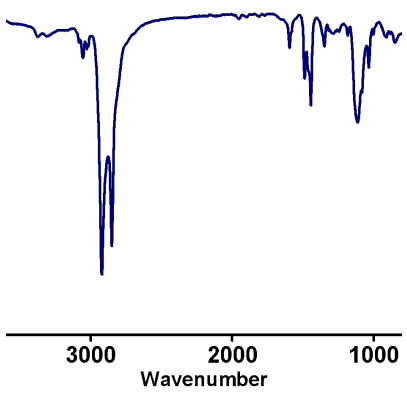

Figure S8. FT-IR spectrum for compound **6**.

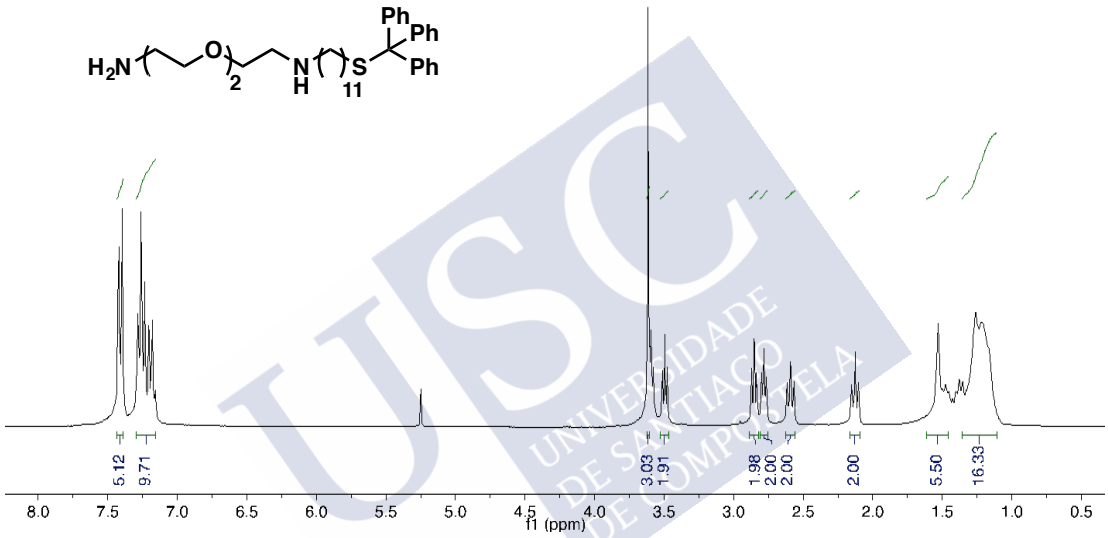

Figure S9. ^{1}H NMR spectrum for compound **6**.

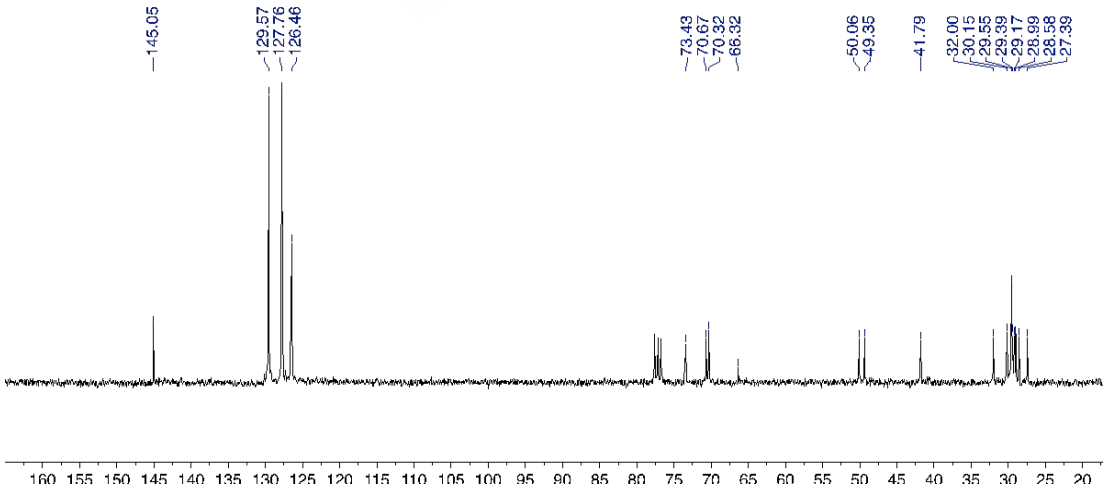

Figure S10. ^{13}C NMR spectrum for compound **6**.

Synthesis of M2(Trt):

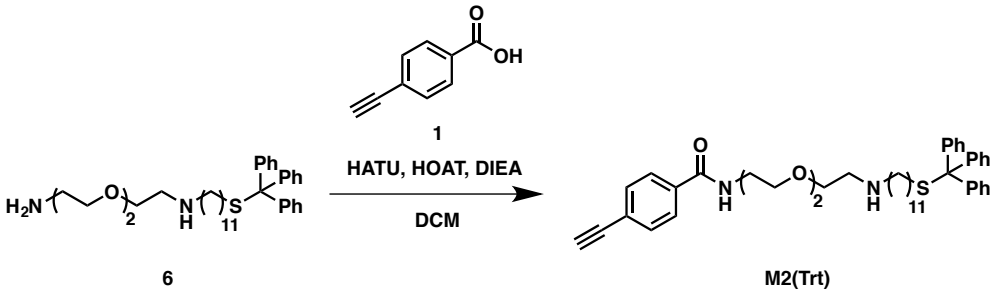

(2-(7-Aza-1H-benzotriazole-1-yl)-1,1,3,3-tetramethyluronium hexafluorophosphate) (HATU, 2.02 g, 5.31mmol) 1-hydroxy-7-azabenzotriazole (HOAt, 0.717, 5.31 mmol), 4-methylbenzoic acid (**1**, 0.78 g, 5.31 mmol) and diisopropyltriethylamine (DIPEA, 0.69 mL, 5.31 mmol) were dissolved in 35 mL of DCM, and the mixture was stirred for 15 min to activate the acid. Then, the compound **6** (2 g, 3.35 mmol) was added and the reaction mixture was stirred overnigth. The organic layer was washed with a saturated solution of $NaHCO_3$ three times. The combined organic layers were dried over anhydrous Na_2SO_4, filtered and the solvent was evaporated at reduced pressure. The crude product was chromatographed on silica gel (70-230 mesh) with hexane/ethyl acetate (1/1) as eluent obtaining compound M**2**(Trt) in a 90% yield (2.25 g).

Spectroscopy data:

^{1}H NMR (250 MHz, $CDCl_3$) δ (ppm): 1.0-1.6 (m, 22H), 2.15 (t, 2H), 3.15 (s, 1H), 3.2-3.6 (m, 17H), 7.1-7.8 (m, 19H).

^{13}C NMR (62.5 MHz, $CDCl_3$) δ (ppm): 25.0, 26.4, 28.6, 28.6, 29.0, 29.4, 31.0, 32.0, 32.0, 36.6, 38.6, 39.9, 66.3, 69.9, 70.5, 79.3, 82.8, 126.5, 127.1, 127.8, 129.6, 129.6, 132.1, 145.1.

HRMS (ESI) m/z calculated for $C_{45}H_{56}N_2O_3S$ [M + H]: 705.01, found: 705.0124.

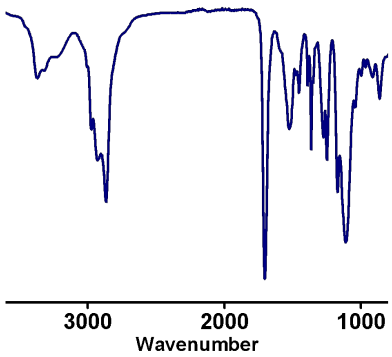

Figure S11. FT-IR spectrum for compound M**2**(Trt).

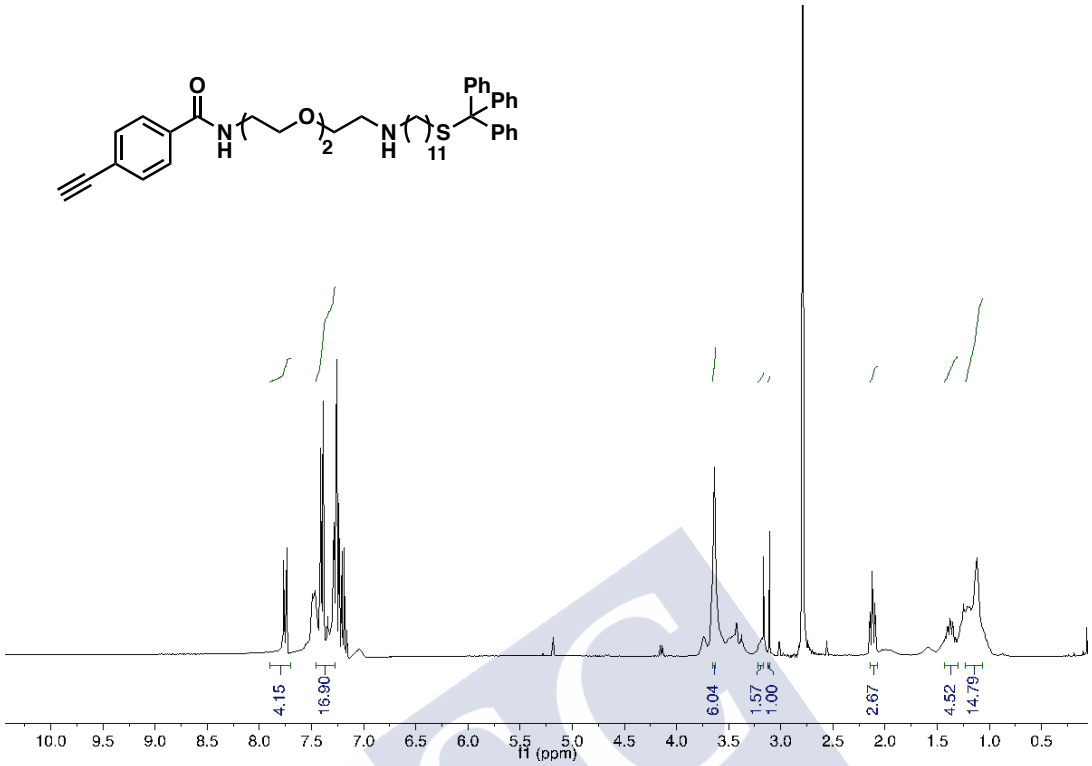

Figure S12. ^{1}H NMR spectrum for compound M**2**(Trt).

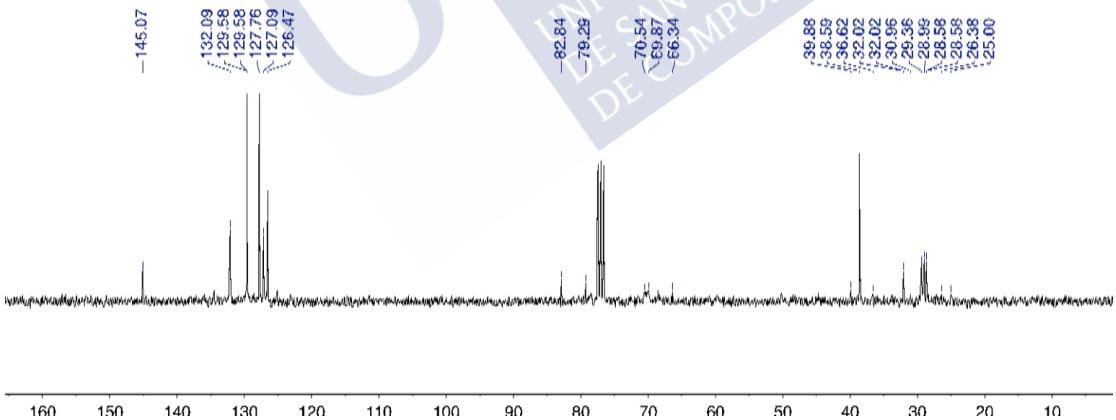

Figure S13. ^{13}C NMR spectrum for monomer M**2**(Trt).

Synthesis of M2:

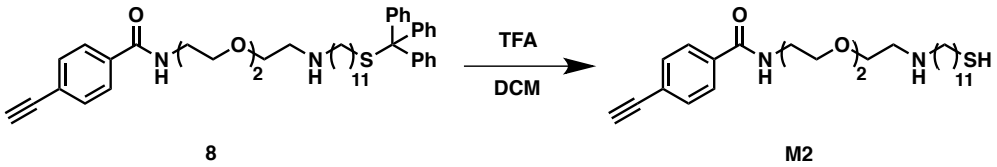

8 M2

Compound **7** (0.4 g, 0.567 mmol) was dissolved in a mixture of equal parts of trifluoroacetic acid, triisopropylsilane and DCM (1/1/1, 2.83 mL). After 2 hours the reaction was completed (according to TLC) and the solvent was evaporated at reduced pressure. The compound was again diluted with DCM and poured into hexane treated twice. Solvent was removed in vacuum to afford monomer M**2** (Yield 0.19 g, 72%).

Spectroscopy data:

^{1}H NMR (250 MHz, $CDCl_3$) δ (ppm): 1.1-1.4 (m, 16H), 1.5-1.8 (m, 10H), 2.30(t, 2H), 2.51 (q, 4H), 2.81 (t, 4H), 3.09 (s, 1H), 7.3-7.6 (m, 4H).

^{13}C NMR (62.5 MHz, $CDCl_3$) δ (ppm): 24.6, 25.5, 25.7, 28.3, 28.8, 29.0, 29.0, 29.3, 34.0, 37.8, 44.1, 83.4, 83.5, 117.4, 119.3, 132.9, 138.5, 171.6.

HRMS (ESI) m/z calculated for $C_{26}H_{42}N_2O_3S$ [M + H]: 462.69, found: 462.2878.

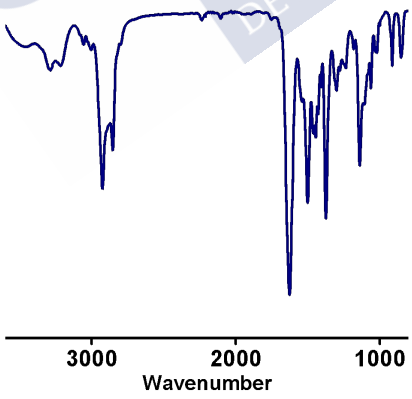

Figure S14. FT-IR spectrum for monomer M**2**.

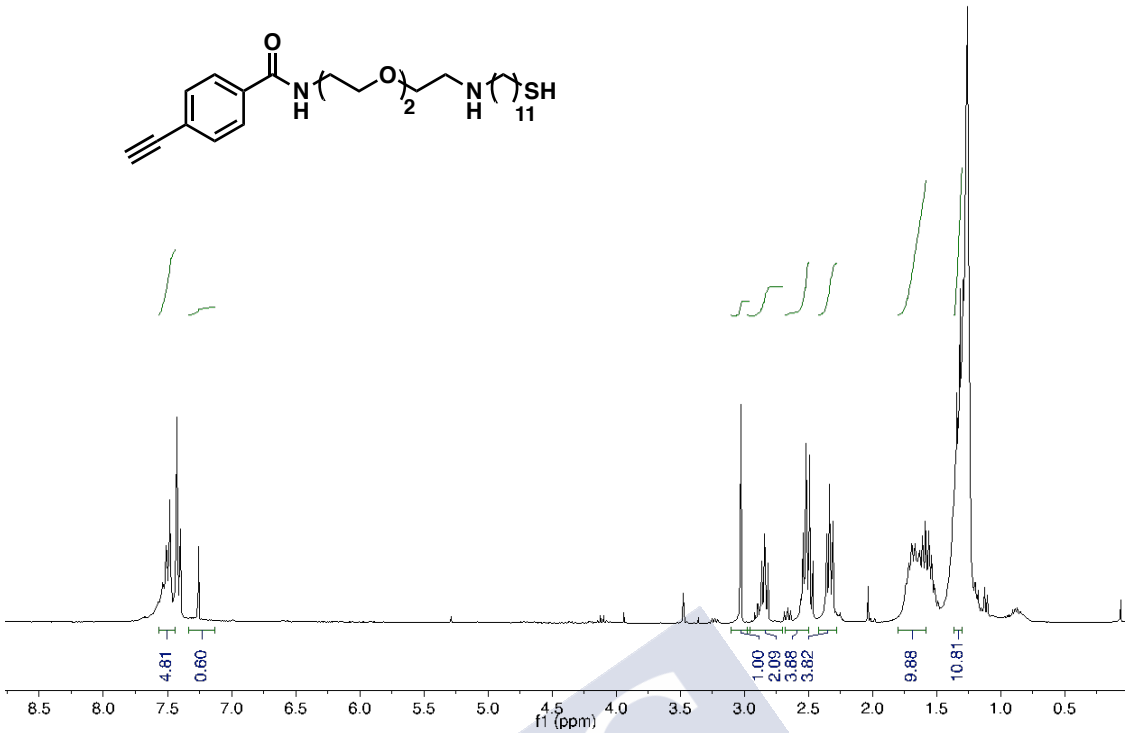

Figure S15. ^{1}H NMR spectrum for monomer M**2**.

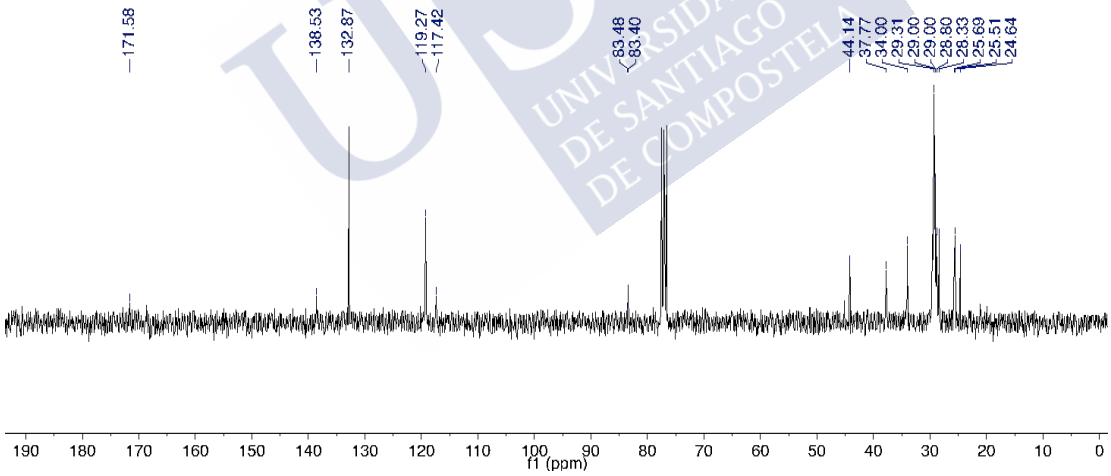

Figure S16: ^{13}C NMR spectrum for monomer M**2**.

4. Synthesis Homo- and Copolymers

General procedure for polymerization: The reaction flask (sealed ampoule) was dried under vacuum and argon flushed for three times before a monomer amount was added as a solid. Then, the flask was evacuated on a vacuum line and flushed with dry argon (three times). Dry THF was added with a syringe and then triethylamine dropwise. A solution of rhodium norbornadiene chloride dimer {$[Rh(nbd)Cl]_2$} in THF was added at 30 ^{o}C. The reaction mixture was stirred at 30 ^{o}C for 6 h. Then, the resulting polymer was diluted in DCM and it was precipitated in a large amount of methanol, centrifuged (2 times), reprecipitated in hexane and centrifuged again.

4.1 Synthesis of Poly-M1

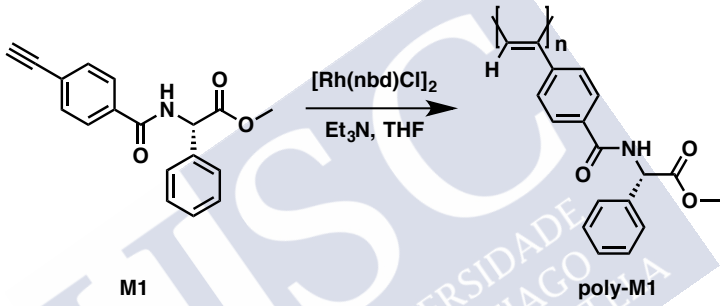

Following the general procedure 73.3 mg (0.250 mmol) of M**1**, 7 mL of Et_3N and 0.576 mg of $[Rh(nbd)Cl]_2$ were employed in 0.75 mL of THF to obtain after purification 67.4 mg of poly-M**1** (Yield 92%).[1] **GPC data:** M_n: 26252, M_w: 47057, M_p: 33670, M_z: 102574, PDI: 1.79.

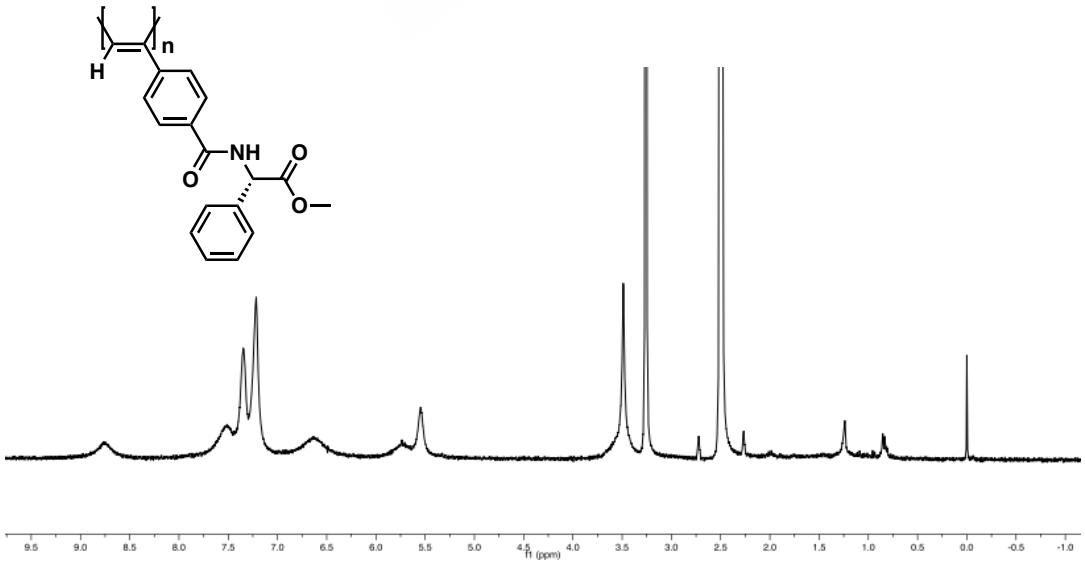

Figure S17. ^{1}H NMR for poly-M**1** in DMSO-d_6.

4.2 Synthesis of copolymers poly-(M1$_r$-*co*-M2(Trt)$_{1-r}$)

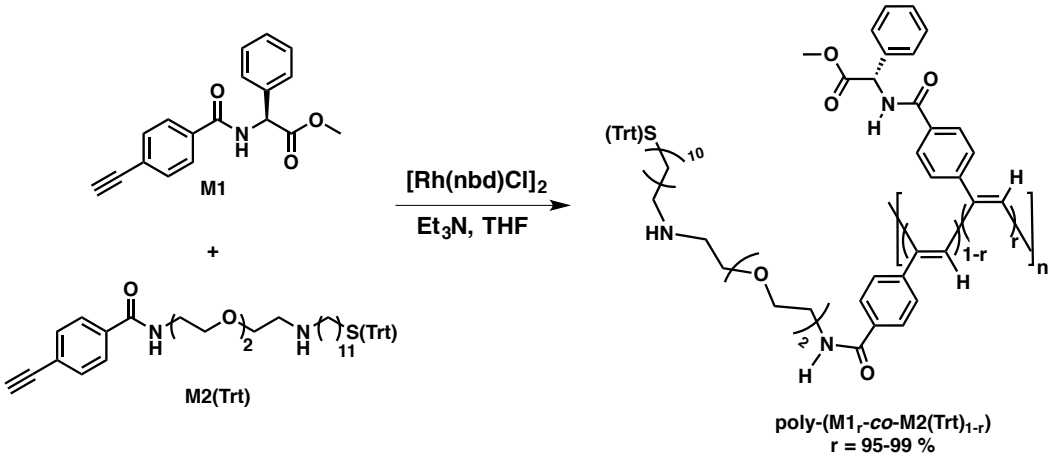

Following the general procedure quantities of M**1**, M**2**(Trt), Et_3N, $[Rh(nbd)Cl]_2$, and THF as shown in Table S1 were employed. Reaction yield is also indicated in the Table S1.

Table S1:

Copolymer	M1 (mg)	M1 (mmol)	M2 (mg)	M2 (mmol)	Cat (mg)	THF (mL)	Et_3N (µL)	poly (mg)	Yield (%)
poly-(M1$_{0.95}$-*co*-M2(Trt)$_{0.05}$)	88.8	0.305	11.1	0.012	1.2	0.70	7	74	74
poly-(M1$_{0.96}$-*co*-M2(Trt)$_{0.04}$)	90.5	0.311	9.1	0.010	1.2	0.70	7	75	75
poly-(M1$_{0.97}$-*co*-M2(Trt)$_{0.03}$)	93.1	0.320	7.0	0.008	1.2	0.70	7	50	50
poly-(M1$_{0.98}$-*co*-M2(Trt)$_{0.02}$)	95.1	0.327	4.6	0.006	1.2	0.70	7	65	76
poly-(M1$_{0.99}$-*co*-M2(Trt)$_{0.01}$)	97.6	0.335	2.3	0.003	1.2	0.70	7	71	71

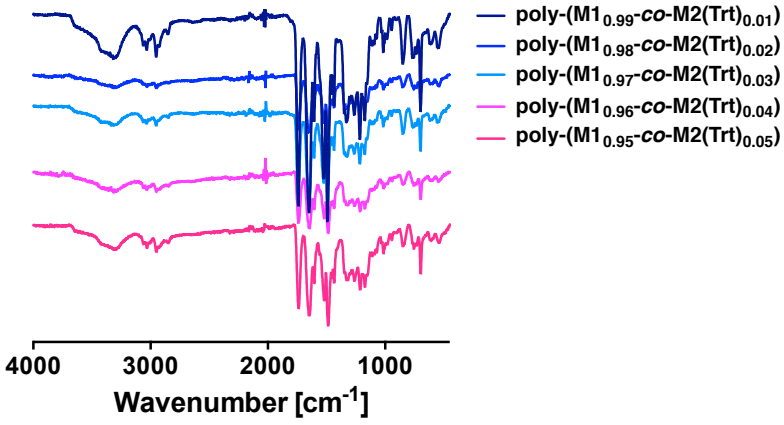

Figure S18. FT-IR spectra for copolymers poly-(M**1**$_r$-*co*-M**2**(Trt)$_{1-r}$) (r = 0.95-0.99).

GPC studies

Table S2. GPC data for copolymers poly-(M**1**$_r$-*co*-M**2**(Trt)$_{1-r}$).

Copolymer	M_n	M_w	M_p	M_z	PDI
poly-(M1$_{0.95}$-*co*-M2(Trt)$_{0.05}$)	13020	28433	33670	49560	2.18
poly-(M1$_{0.96}$-*co*-M2(Trt)$_{0.04}$)	19493	36052	43918	57338	1.84
poly-(M1$_{0.97}$-*co*-M2(Trt)$_{0.03}$)	16004	20473	28176	35683	1.33
poly-(M1$_{0.98}$-*co*-M2(Trt)$_{0.02}$)	6799	16269	19383	24542	2.39
poly-(M1$_{0.99}$-*co*-M2(Trt)$_{0.01}$)	14376	19378	18699	25269	1.34

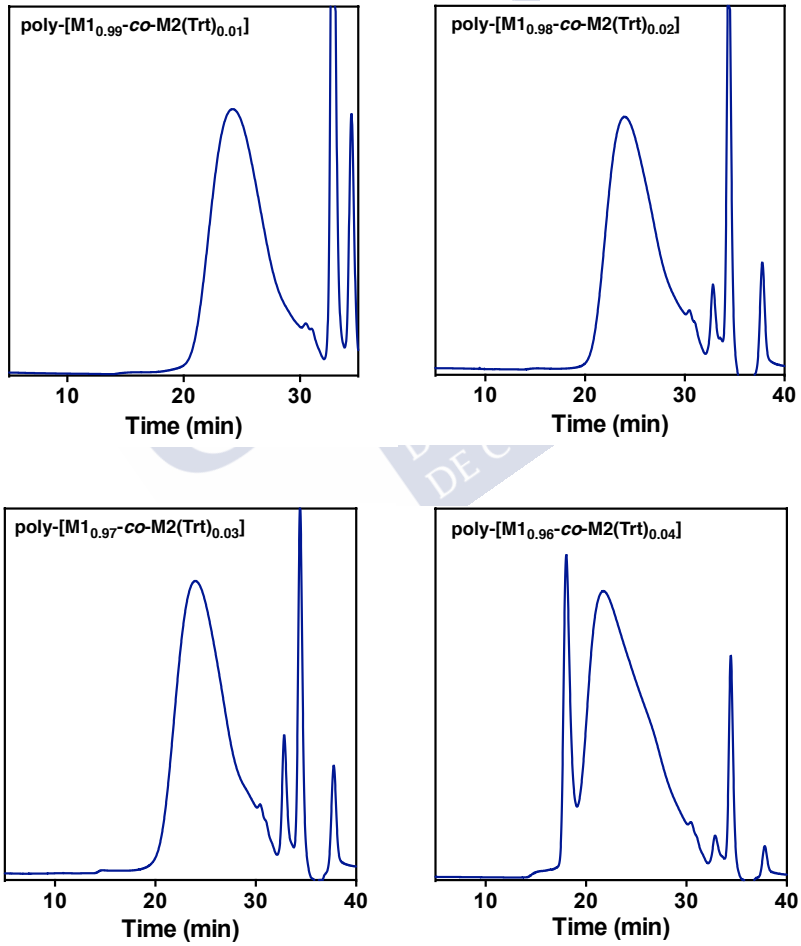

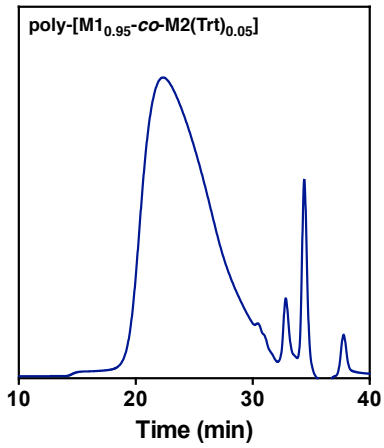

Figure S19. GPC chromatograms for poly-[M**1**$_r$-*co*-M**2**(Trt)$_{1-r}$] series.

The *cis* stereoregularity of the copolymers was determined by ^{1}H NMR spectroscopy where the vinyl proton resonates at 5.8 ppm, and Raman resonances. The peak at 1580 cm^{-1} is assigned to C=C bond stretching in the *cis* poly(acetylene) and overlaps with that of the phenyl ring. The peak at 1340 cm^{-1} is assigned to the *cis* C-C bond coupled with the single bond connecting the main chain and the phenyl ring. The peak at 1004 cm^{-1} is assigned to the C-H bond deformation of the *cis* form.

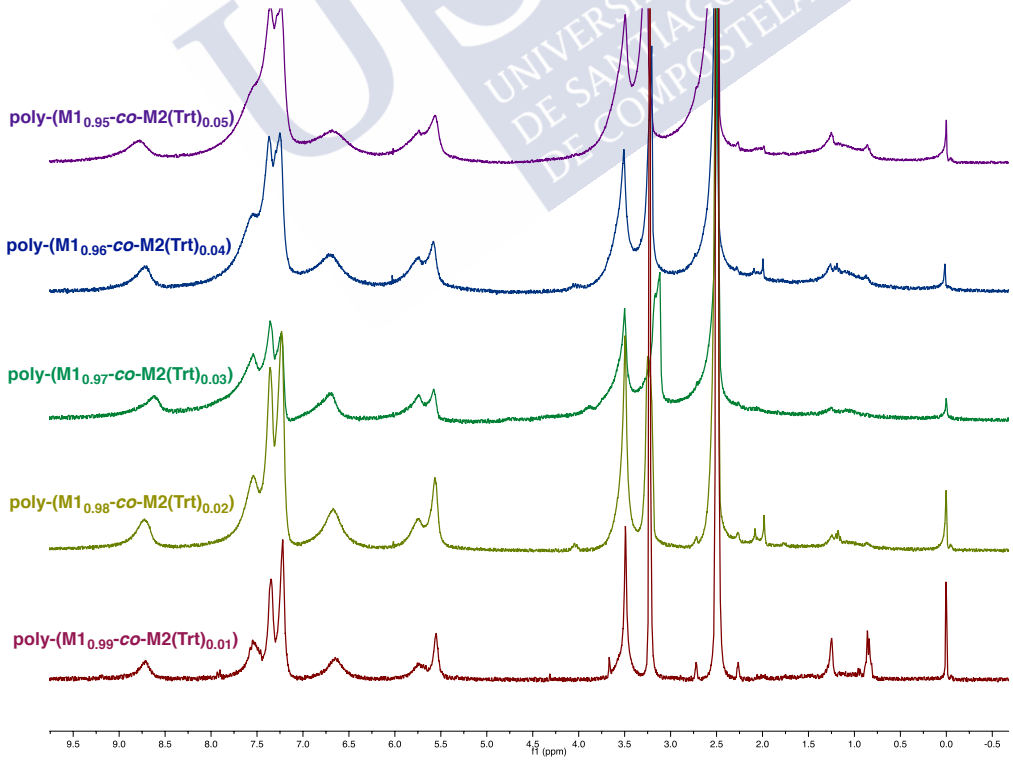

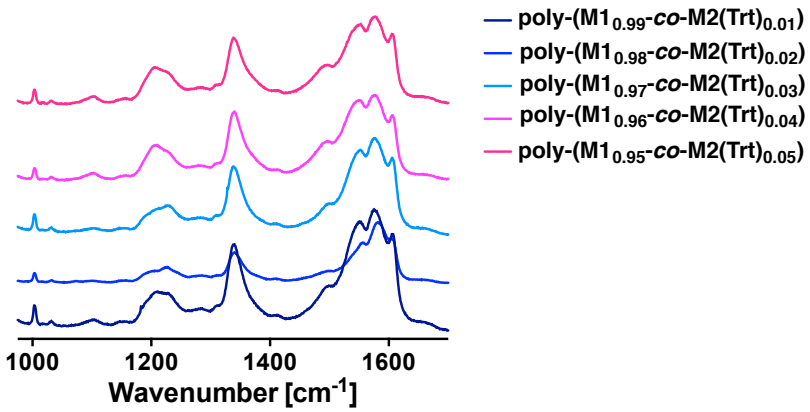

Figure S20. H NMR in DMSO-d_6 and Raman spectra for copolymers poly-(M**1**$_r$-*co*-M**2**(Trt)$_{1-r}$) (r = 0.95-0.99).

5. Thermal studies for copolymers poly-(M1$_r$-*co*-M2(Trt)$_{1-r}$)

5.1 DSC studies for poly-(M1$_r$-*co*-M2(Trt)$_{1-r}$)

DSC studies were carried out in order to determine de geometry of the polymer backbone. As a general protocol, a polymer sample was kept in an aluminum pan and heated from 40 ^{o}C to 350 ^{o}C with a heating rate of 10 ^{o}C/min.

The thermograms of the polymers show typical traces for a *cis-trans* backbone, where two exothermal peaks corresponding to the *c-t* to *c-c* and the *c-c* to *t-t* were observed.

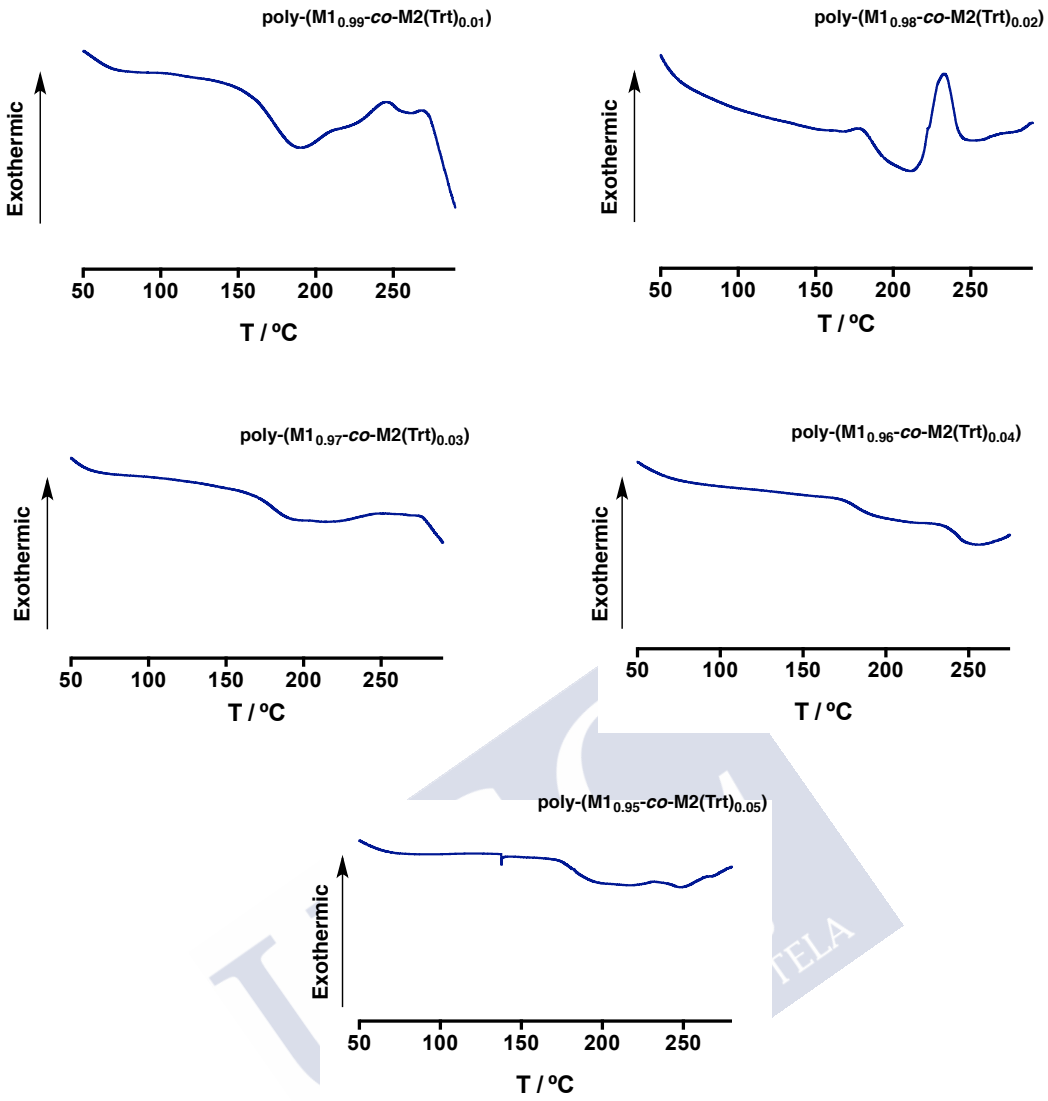

Figure S21. DSC thermograms for copolymers poly-(M**1**$_r$-*co*-M**2**(Trt)$_{1-r}$).

5.2 TGA studies for copolymers poly-(M1$_r$-*co*-M2(Trt)$_{1-r}$)

TGA Studies were carried out in order to determine the thermal stability of the copolymers. As a general protocol, a polymer sample was kept in a platinum pan and heated from 40 ^{o}C to 850 ^{o}C with a heating rate if 10 ^{o}C/min.

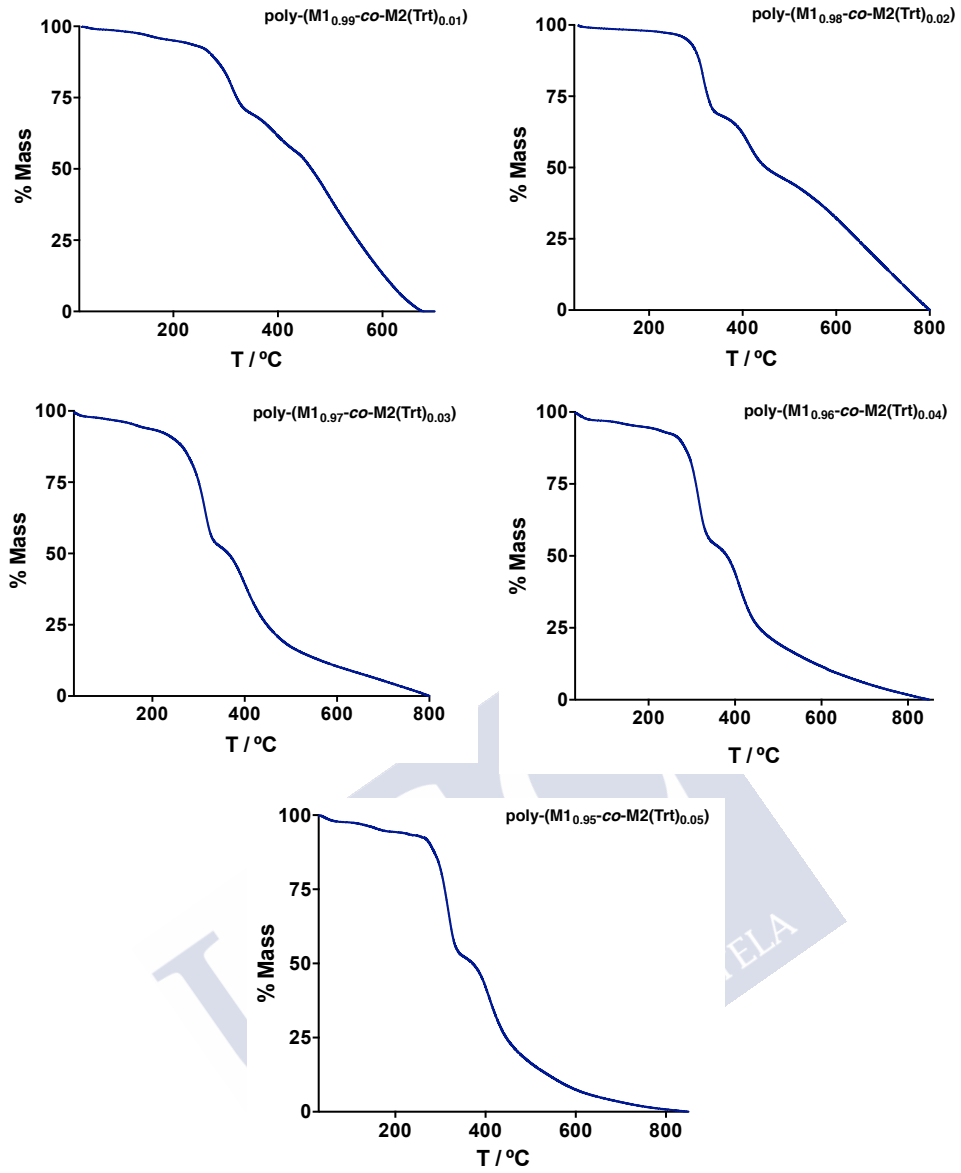

Figure S22. TGA thermograms for copolymers poly-(M**1**$_r$-*co*-M**2**(Trt)$_{1-r}$).

6. CD and UV-Vis studies for poly-(M1$_r$-*co*-M2(Trt)$_{1-r}$) in polar and low polar solvents

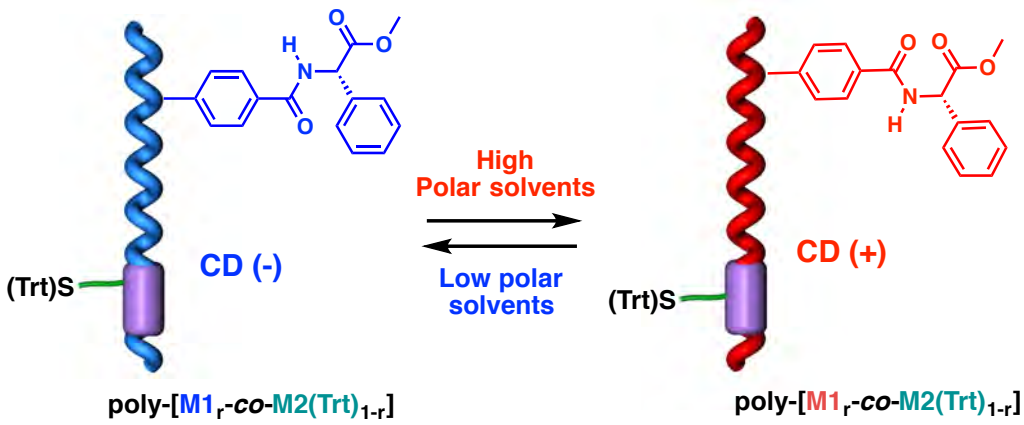

CD and UV-Vis studies were performed with a solution of poly-(M**1**$_r$-*co*-M**2**(Trt)$_{1-r}$) in different high polar (DMSO, DMF) and low polar ($CHCl_3$, THF) solvents which concentration was 0.3 mg mL^{-1}.

Poly-(M**1**$_r$-*co*-M**2**(Trt)$_{1-r}$) dissolved in low polar solvents ($CHCl_3$, THF) presents a negative Cotton effect (*M* helices) in the vinylic region corresponding to a *anti* conformation between carbonyl groups in the pendant group. On the other hand, poly-(M**1**$_r$-*co*-M**2**(Trt)$_{1-r}$) dissolved in high polar solvents (DMF, DMSO) presents a positive Cotton effect (*P* helices) corresponding to a *syn* between carbonyl groups in the pendant group.

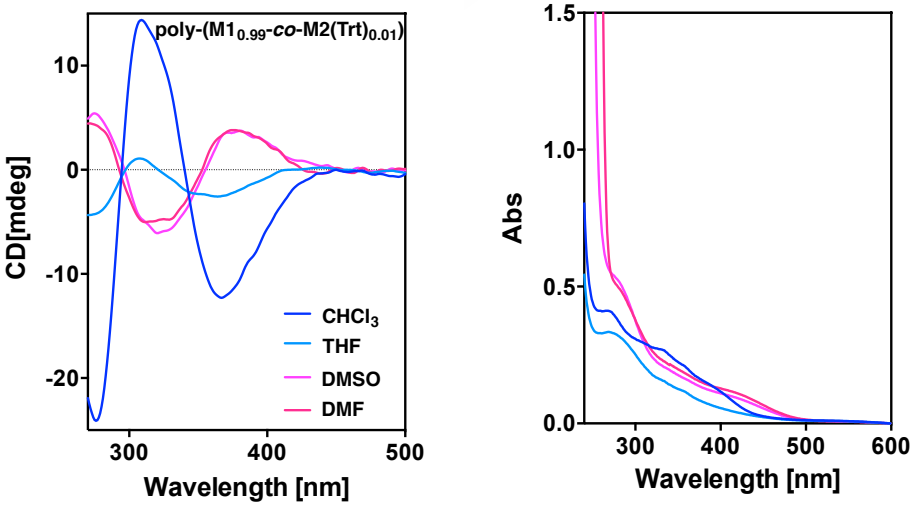

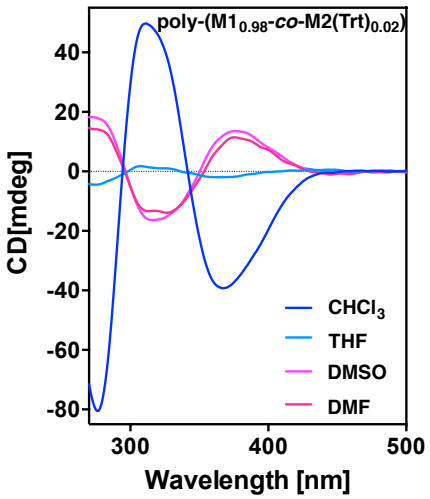
poly-(M1$_{0.98}$-*co*-M2(Trt)$_{0.02}$)
CD[mdeg]
Wavelength [nm]
CHCl$_3$
THF
DMSO
DMF

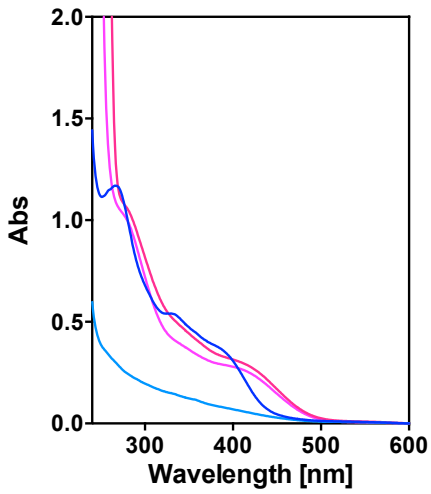
Abs
Wavelength [nm]

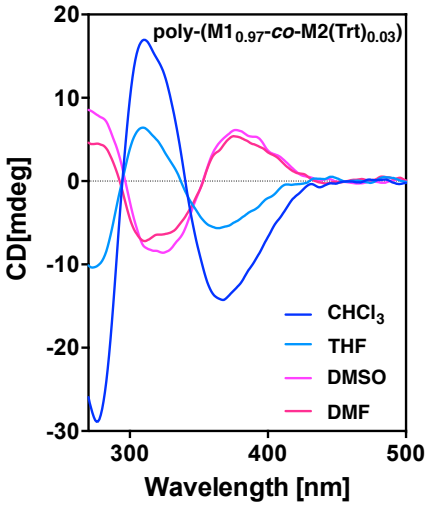
poly-(M1$_{0.97}$-*co*-M2(Trt)$_{0.03}$)
CD[mdeg]
Wavelength [nm]
CHCl$_3$
THF
DMSO
DMF

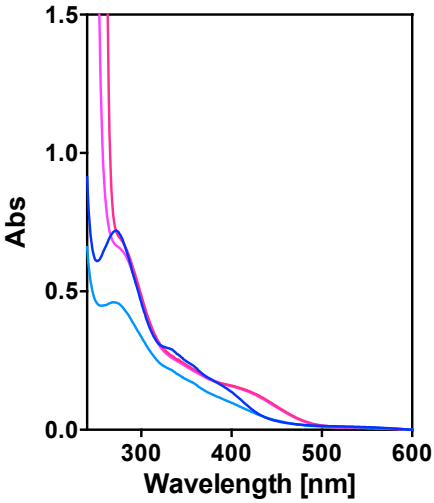
Abs
Wavelength [nm]

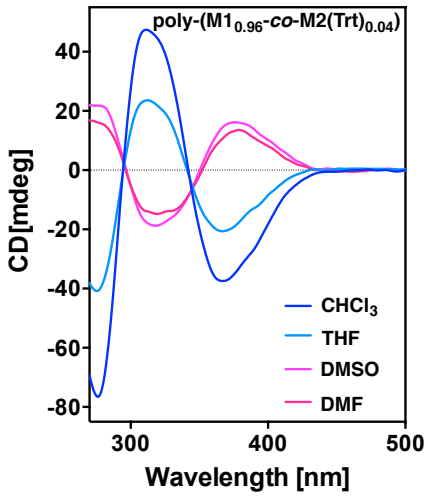
poly-(M1$_{0.96}$-*co*-M2(Trt)$_{0.04}$)
CD[mdeg]
Wavelength [nm]
CHCl$_3$
THF
DMSO
DMF

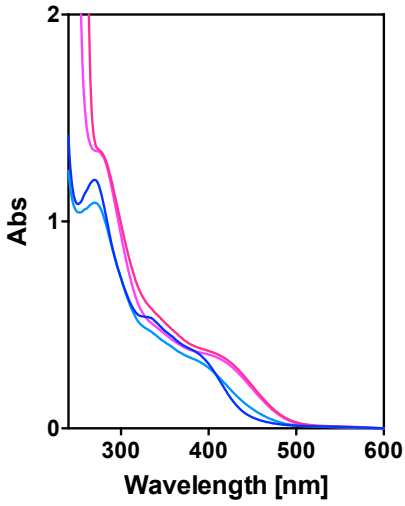
Abs
Wavelength [nm]

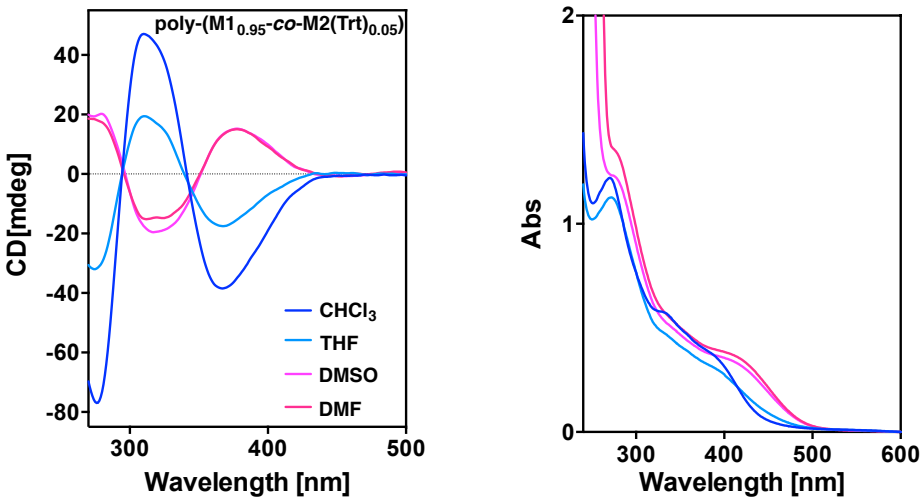

Figure S23. CD and UV-Vis spectra for copolymers poly-(M**1**$_r$-*co*-M**2**(Trt)$_{1-r}$) in polar (DMF, DMSO) and low polar solvents ($CHCl_3$, THF) at 0.3 mg mL^{-1} of concentration.

7. CD and UV-Vis studies of poly-(M1$_r$-*co*-M2(Trt)$_{1-r}$) in presence of $LiClO_4$

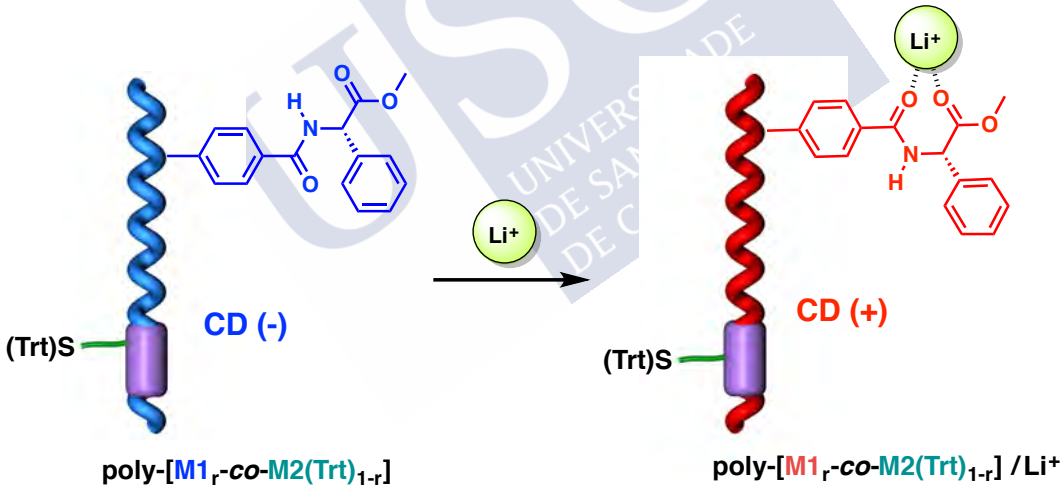

CD and UV-Vis studies were performed with a solution of poly-(M**1**$_r$-*co*-M**2**(Trt)$_{1-r}$) in $CHCl_3$ (0.3 mg mL^{-1}) using $LiClO_4$ dissolved in MeOH which concentration was 10.0 mg mL^{-1}.

Thus, poly-(M**1**$_r$-*co*-M**2**(Trt)$_{1-r}$) dissolved in $CHCl_3$ shows a negative Cotton effect (*M* helices) in the vinylic region corresponding to a *anti* conformation between carbonyl groups. On the other hand, the addition of Li^+ ions promotes a *syn* between carbonyl groups lead to a positive Cotton Effect in the vinylic region (*P* helices).

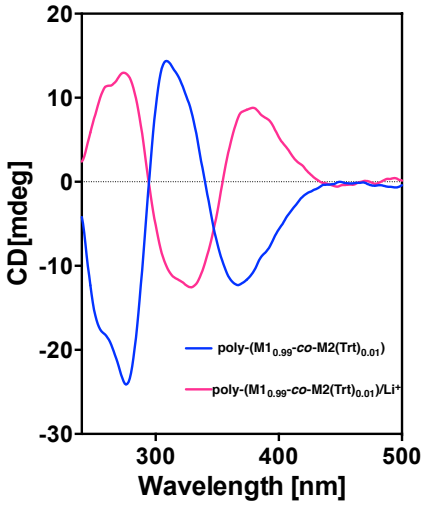
CD[mdeg]
Wavelength [nm]
poly-(M1$_{0.99}$-*co*-M2(Trt)$_{0.01}$)
poly-(M1$_{0.99}$-*co*-M2(Trt)$_{0.01}$)/Li$^+$

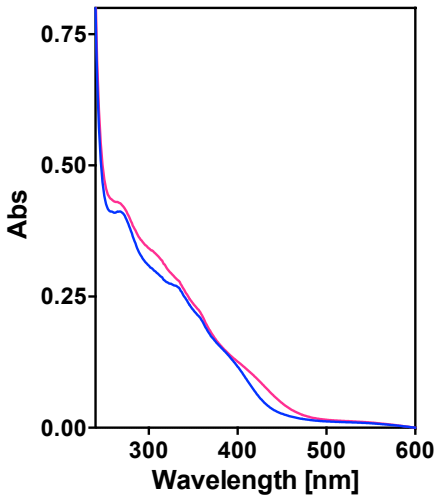
Abs
Wavelength [nm]

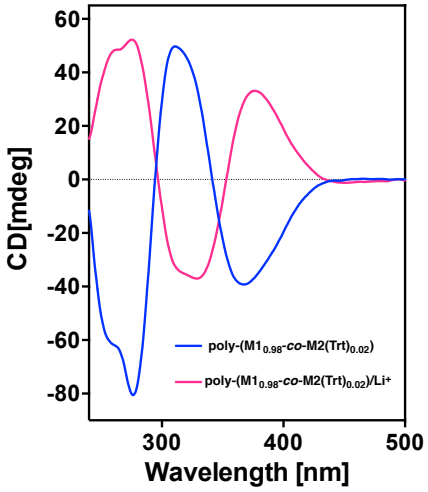
CD[mdeg]
Wavelength [nm]
poly-(M1$_{0.98}$-*co*-M2(Trt)$_{0.02}$)
poly-(M1$_{0.98}$-*co*-M2(Trt)$_{0.02}$)/Li$^+$

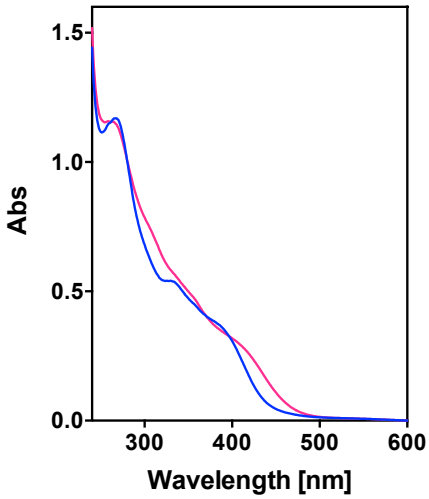
Abs
Wavelength [nm]

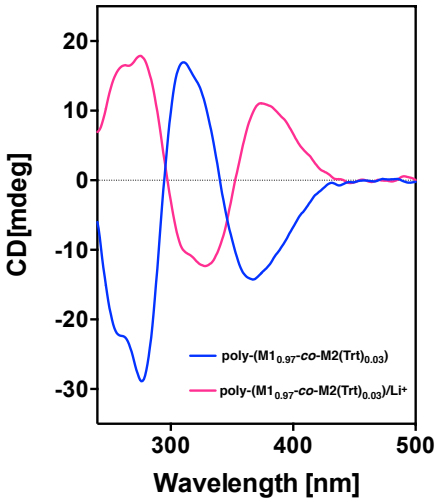
CD[mdeg]
Wavelength [nm]
poly-(M1$_{0.97}$-*co*-M2(Trt)$_{0.03}$)
poly-(M1$_{0.97}$-*co*-M2(Trt)$_{0.03}$)/Li$^+$

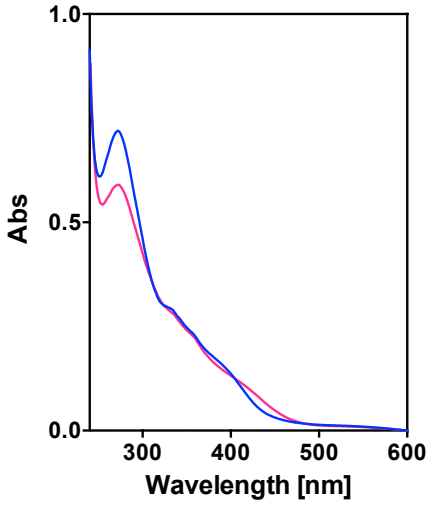
Abs
Wavelength [nm]

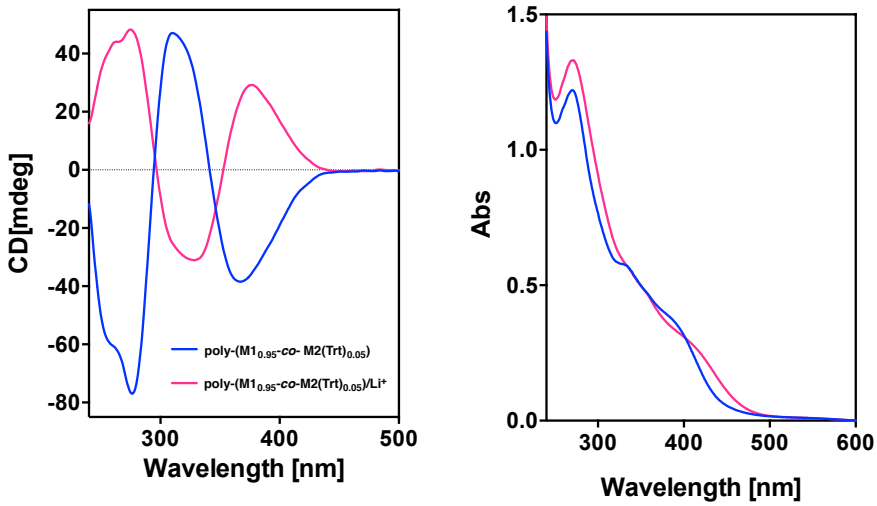

Figure S24. CD and UV-Vis studies for poly-(M**1**$_r$-*co*-M**2**(Trt)$_{1-r}$) in $CHCl_3$ (0.3 mg mL^{-1}) in presence of Li^+ ions.

8. Deprotection of copolymers poly-(M1$_r$-*co*-M2(Trt)$_{1-r}$)

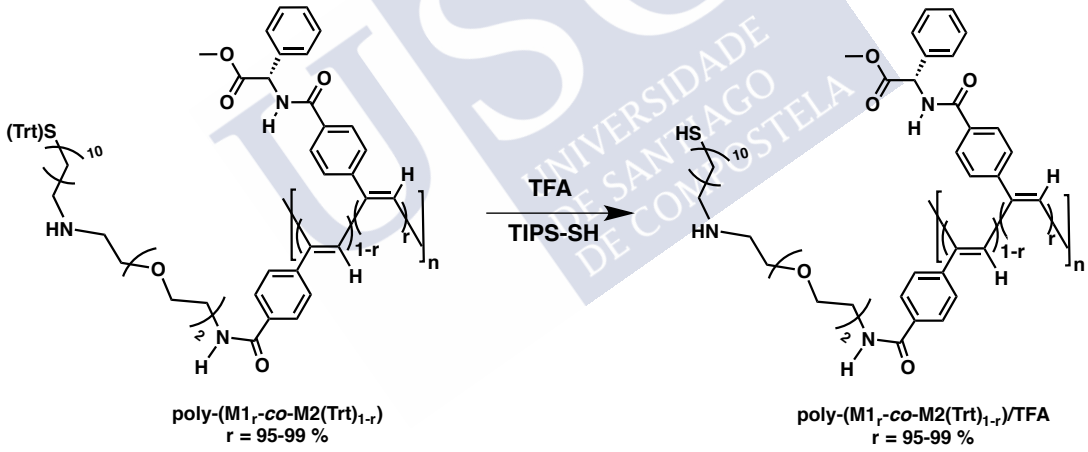

To a solution of copolymers poly-(M**1**$_r$-*co*-M**2**(Trt)$_{1-r}$ (3 mg mL^{-1}, $CHCl_3$) was added a mixture of TFA/TIPS-SH (1% v/v). After 1 hour, the copolymers were precipitated in MeOH and redisolved in a mixture of $CHCl_3$/MeCN. Finally, the solvent was evaporated at reduced pressure and the resulting copolymers were characterized by NMR, CD and UV-Vis.

8.1 ^{1}H NMR for poly-(M1$_r$-*co*-M2$_{1-r}$) and poly-(M1$_r$-*co*-M2$_{1-r}$)/TFA

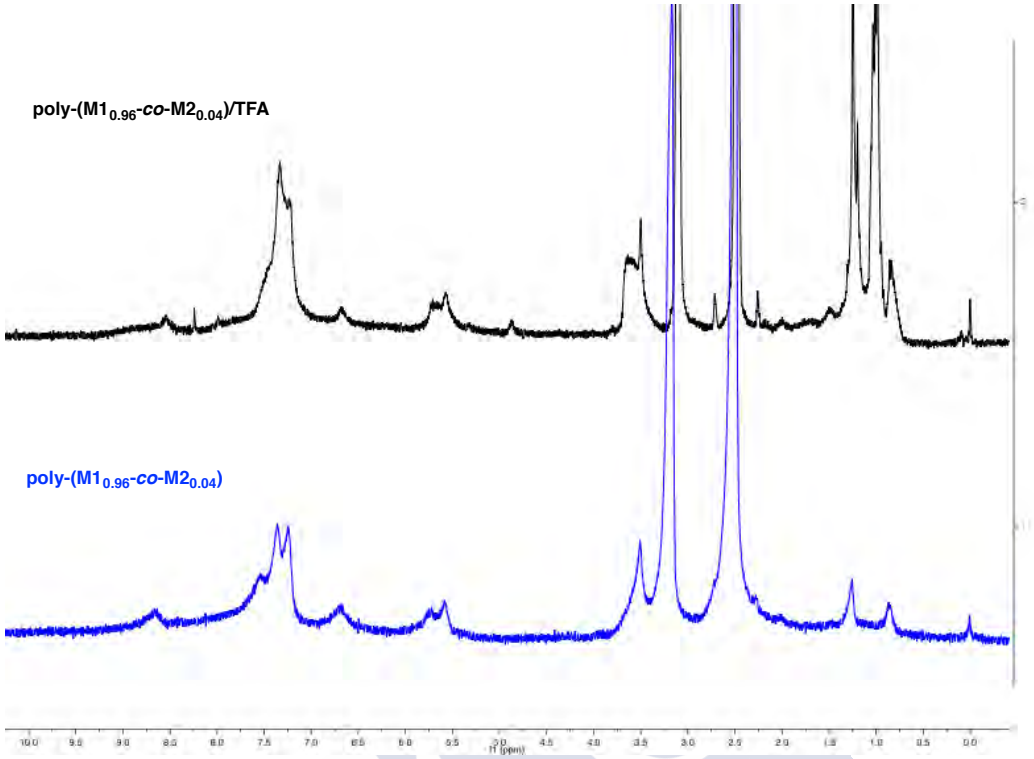

Figure S25. ^{1}H NMR Comparative spectra for copolymers poly-(M1$_{0.96}$-*co*-M2$_{0.04}$) and poly-(M1$_{0.96}$-*co*-M2$_{0.04}$) titrated with TFA.

8.2 CD studies for copolymers poly-(M1$_r$-*co*-M2$_{1-r}$) titrated with TFA

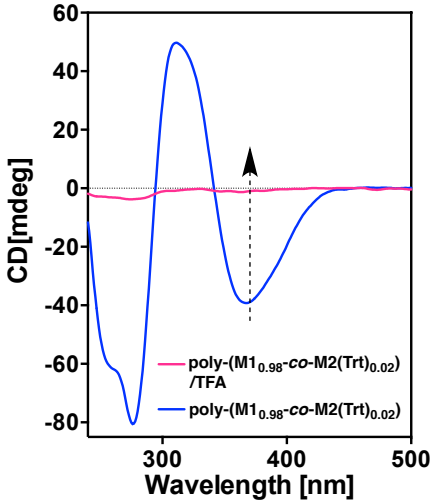

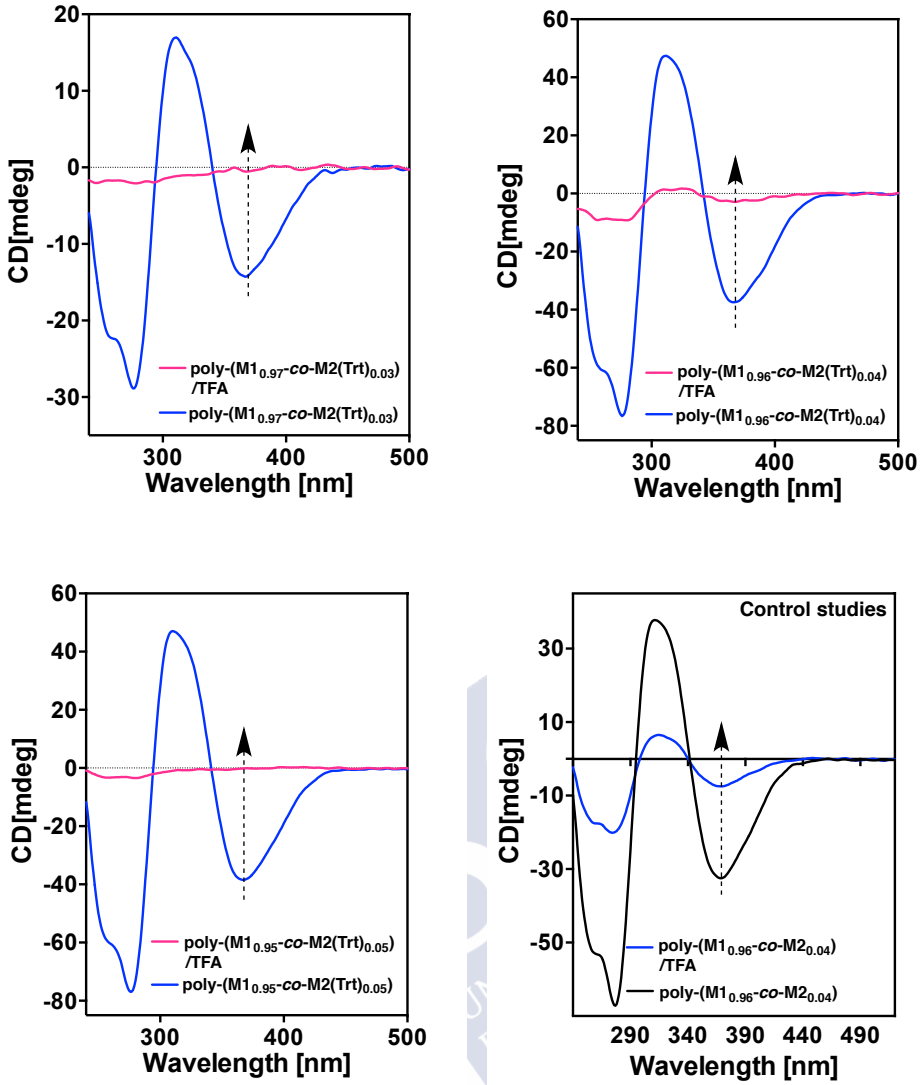

Figure S26. CD and UV-Vis studies for titration of copolymers poly-(M**1**$_r$-*co*-M**2**(Trt)$_{1-r}$) (0.3 mg mL^{-1}, $CHCl_3$) with TFA/TIPS-SH (1% v/v).

9. Synthesis for the co-polymer series poly-(M1$_r$-*co*-M2$_{1-r}$)

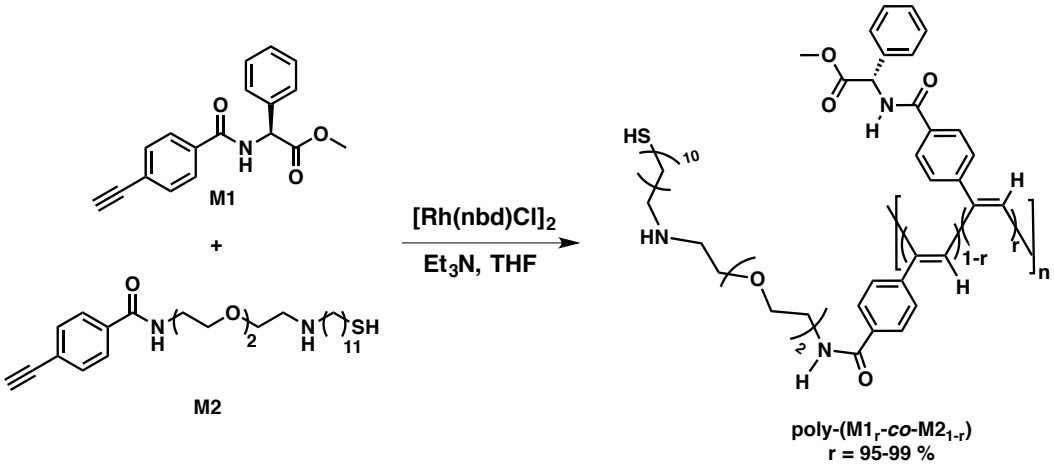

Following the general procedure quantities of M**1**, M**2**, Et_3N, $[Rh(nbd)Cl]_2$, and THF as shown in Table S3 were employed. Reaction yield is also indicated in the Table S3.

Table S3:

Copolymer	M1 (mg)	M1 (mmol)	M2 (mg)	M2 (mmol)	Cat (mg)	THF (mL)	Et_3N (µL)	poly (mg)	Yield (%)
poly-(M1$_{0.95}$-*co*-M2$_{0.05}$)	69.7	0.238	5.7	0.013	0.576	0.75	7	62.0	71
poly-(M1$_{0.96}$-*co*-M2$_{0.04}$)	70.3	0.240	4.6	0.010	0.576	0.75	7	54.7	73
poly-(M1$_{0.97}$-*co*-M2$_{0.03}$)	71.1	0.243	3.4	0.008	0.576	0.75	7	57.7	77
poly-(M1$_{0.98}$-*co*-M2$_{0.02}$)	71.8	0.245	2.3	0.005	0.576	0.75	7	60.7	81
poly-(M1$_{0.99}$-*co*-M2$_{0.01}$)	72.5	0.248	1.1	0.003	0.576	0.75	7	66.0	88

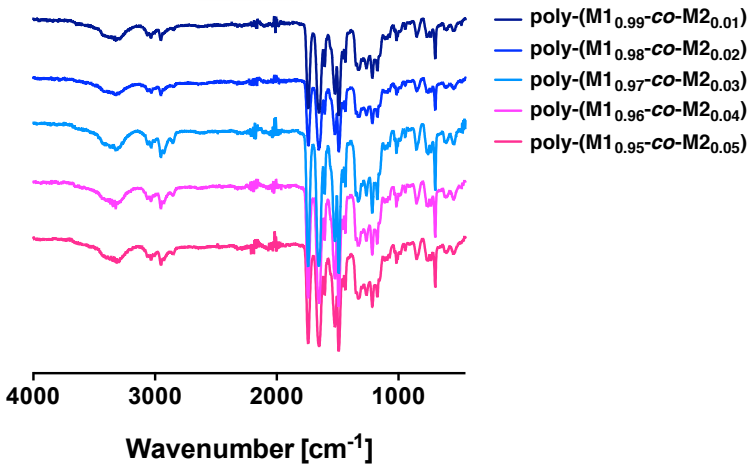

Figure S27. FT-IR spectra for the copolymers poly-(M**1**$_r$-*co*-M**2**$_{1-r}$).

Table S4: GPC data for poly-M**1** and poly-(M**1**$_r$-*co*-M**2**$_{1-r}$).

Copolymer	M_n	M_w	M_p	M_z	PDI
Poly(M1$_{0.99}$-*co*-M2$_{0.01}$)	16024	65822	24020	39072	4.10
Poly(M1$_{0.98}$-*co*-M2$_{0.02}$)	15830	40045	25930	91247	2.53
Poly(M1$_{0.97}$-*co*-M2$_{0.03}$)	16195	38108	32056	78513	2.35
Poly(M1$_{0.96}$-*co*-M2$_{0.04}$)	13462	28799	18798	57885	2.13
Poly(M1$_{0.95}$-*co*-M2$_{0.05}$)	11774	23219	15450	46952	1.97

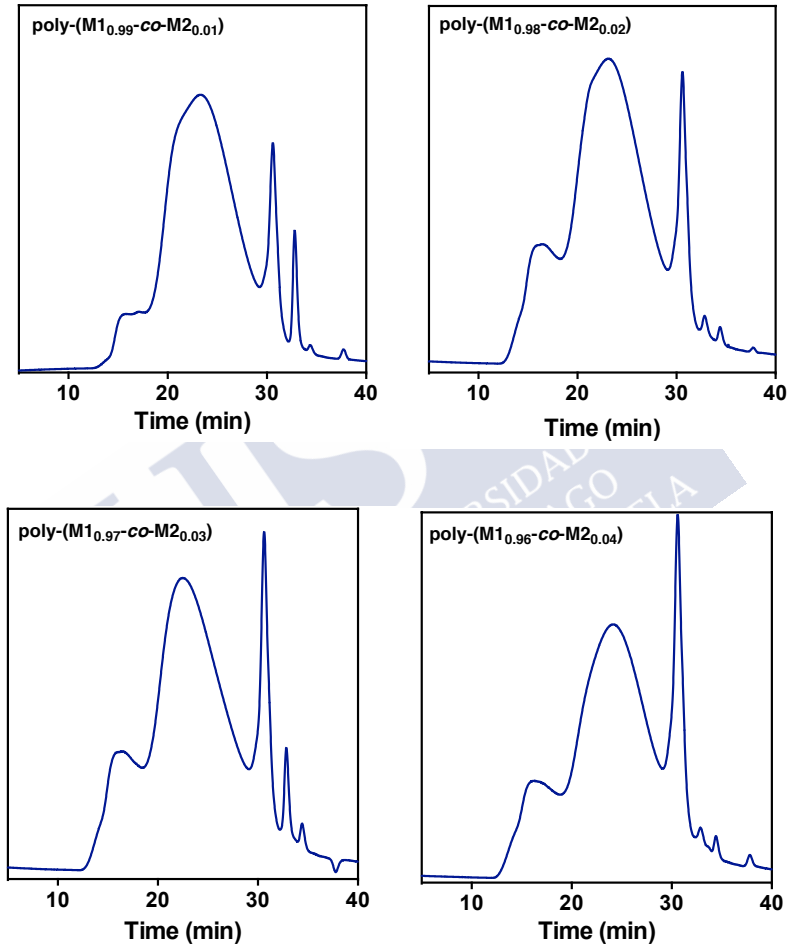

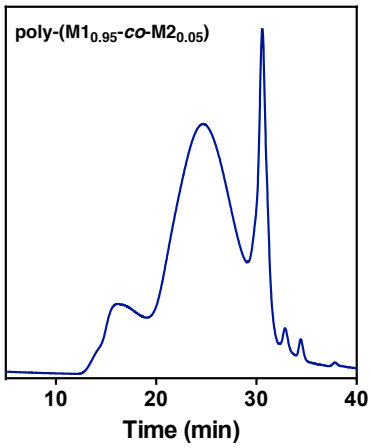

Figure S28. GPC chromatograms for poly-(M**1**$_r$-*co*-M**2**$_{1-r}$) series.

The *cis* stereoregularity of the copolymers was determined by ^{1}H NMR spectroscopy where the vinyl proton resonates at 5.8 ppm, and Raman resonances. The peak at 1585 cm^{-1} is assigned to C=C bond stretching in the *cis* poly(acetylene) and overlaps with that of the phenyl ring. The peak at 1342 cm^{-1} is assigned to the *cis* C-C bond coupled with the single bond connecting the main chain and the phenyl ring. The peak at 1006 cm^{-1} is assigned to the C-H bond deformation of the *cis* form.

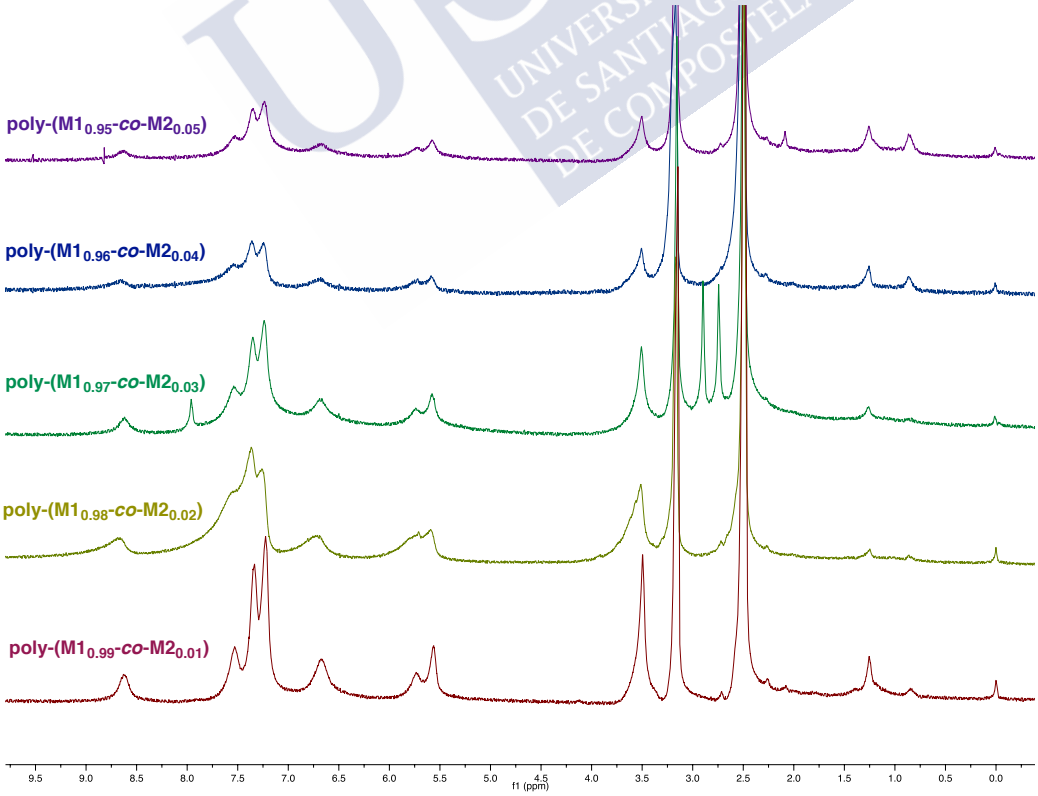

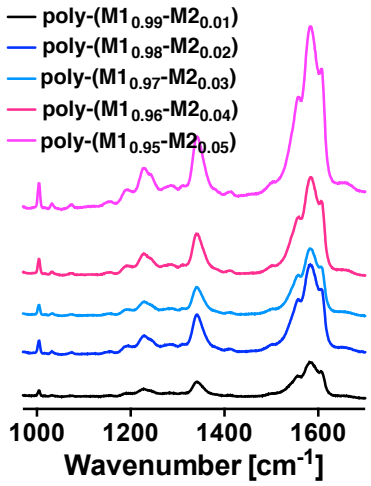

Figure S29. ^{1}H NMR in DMSO-d_6 and Raman spectra for copolymers poly-(M**1**$_r$-*co*-M**2**$_{1-r}$).

10. CD and UV-Vis studies for copolymers poly-(M1$_r$-*co*-M2$_{1-r}$) in high polar and low polar solvents

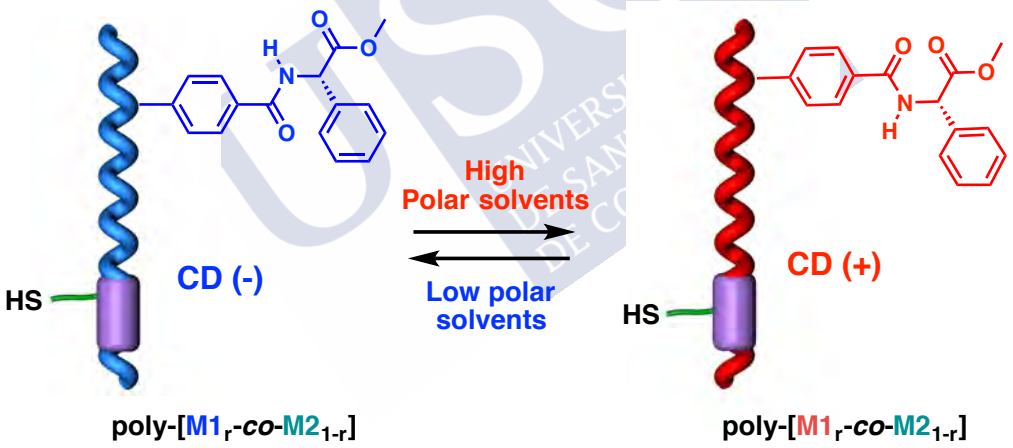

CD and UV-Vis studies were performed with a solution of poly-(M**1**$_r$-*co*-M**2**$_{1-r}$) in different high polar (DMSO, DMF) and low polar ($CHCl_3$, THF) solvents which concentration was 0.3 mg mL^{-1}.

Poly-(M**1**$_r$-*co*-M**2**$_{1-r}$) dissolved in low polar solvents ($CHCl_3$, THF) presents a negative Cotton effect in the vinylic region (*M* helices) corresponding to a *anti* conformation between carbonyl groups in the pendant group whereas poly-(M**1**$_r$-*co*-M**2**$_{1-r}$) dissolved in high polar solvents (DMF, DMSO) presents a positive Cotton effect (*P* helices) corresponding to a *syn* between carbonyl carbonyl groups in the pendant group.

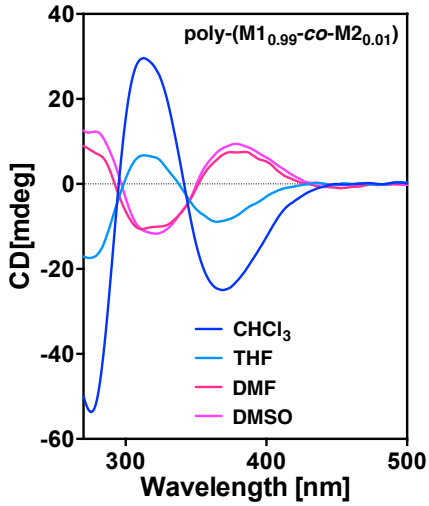
poly-(M1$_{0.99}$-*co*-M2$_{0.01}$)
CD[mdeg]
Wavelength [nm]
CHCl$_3$
THF
DMF
DMSO

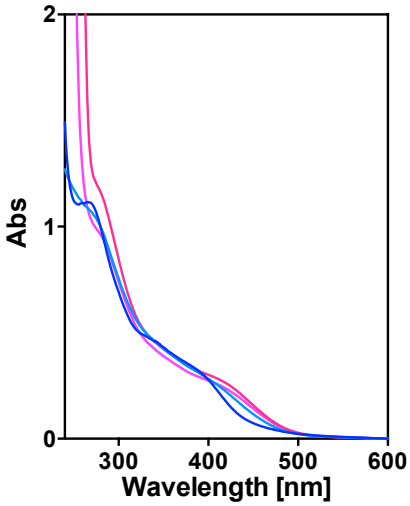
Abs
Wavelength [nm]

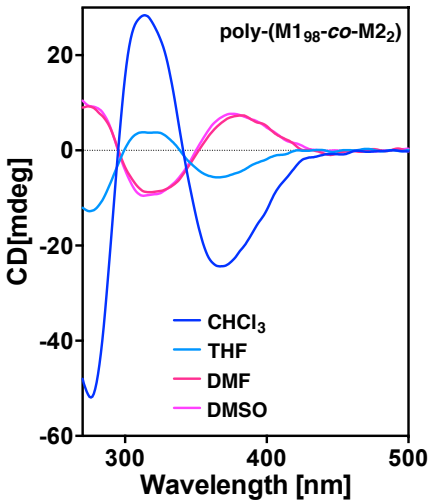
poly-(M1$_{98}$-*co*-M2$_2$)
CD[mdeg]
Wavelength [nm]
CHCl$_3$
THF
DMF
DMSO

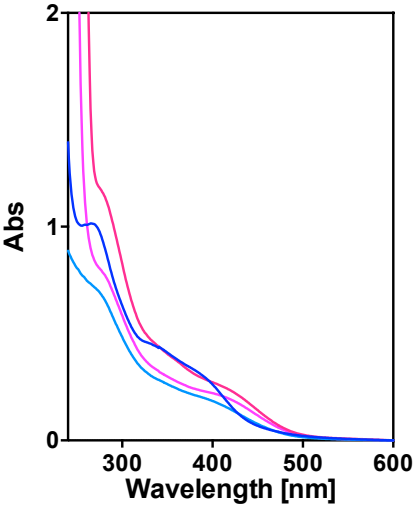
Abs
Wavelength [nm]

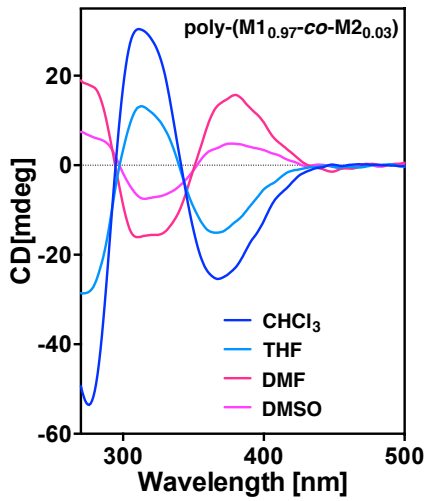
poly-(M1$_{0.97}$-*co*-M2$_{0.03}$)
CD[mdeg]
Wavelength [nm]
CHCl$_3$
THF
DMF
DMSO

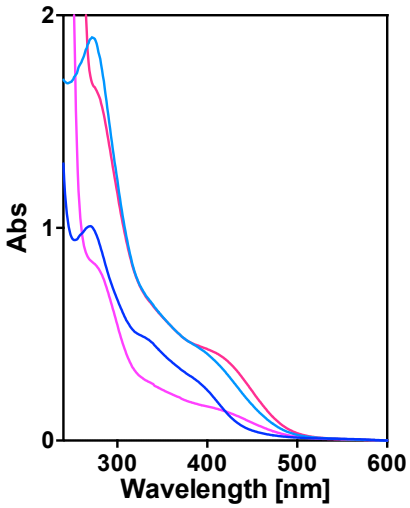
Abs
Wavelength [nm]

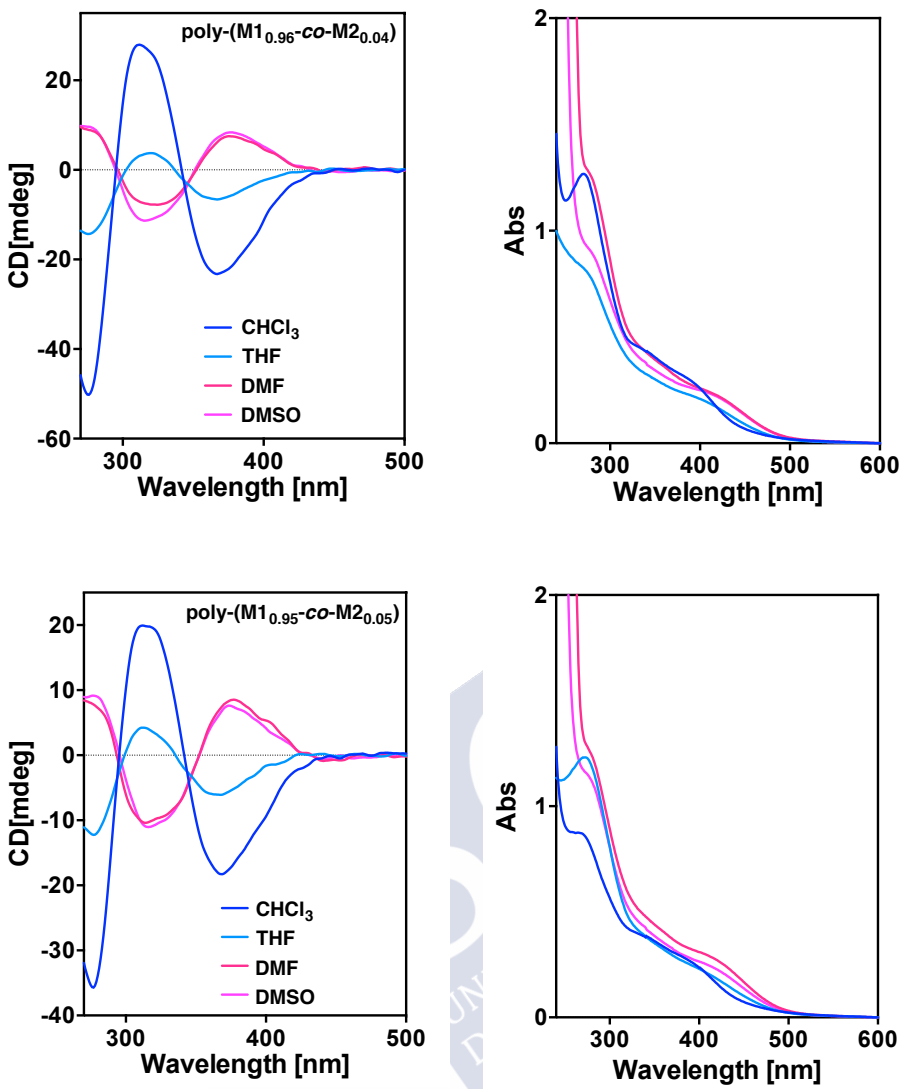

Figure S30. CD and UV-Vis studies for copolymers poly-(M**1**$_r$-*co*-M**2**$_{1-r}$) in polar (DMF, DMSO) and low polar solvents (THF, $CHCl_3$) at 0.3 mg mL^{-1} of concentration.

11. CD and UV-Vis studies for copolymers poly-(M1$_r$-*co*-M2$_{1-r}$) in presence of $LiClO_4$

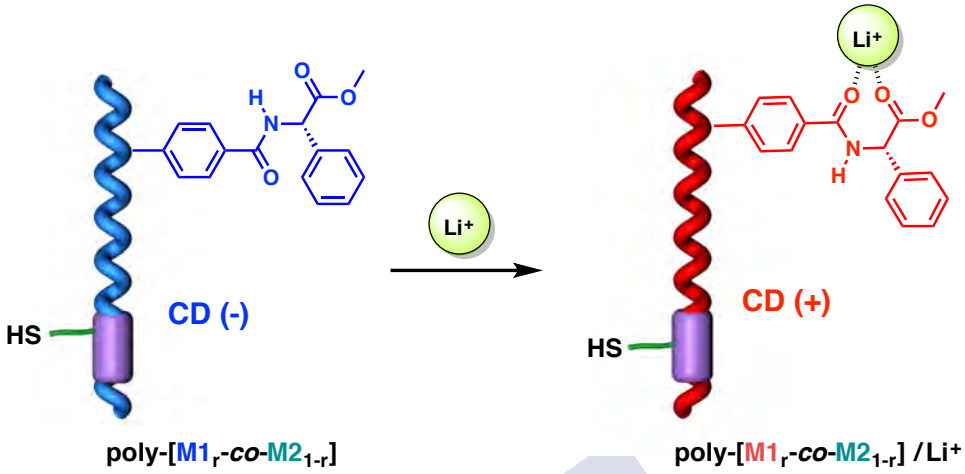

CD and UV-Vis studies were performed with a solution of poly-(M**1**$_r$-co-M**2**$_{1-r}$) in $CHCl_3$ (0.3 mg mL^{-1}) using $LiClO_4$ dissolved in MeOH which concentration was 10.0 mg mL^{-1}.

Thus, poly-(M**1**$_r$-co-M**2**$_{1-r}$) dissolved in $CHCl_3$ shows a negative Cotton effect in the vinylic region (*M* helices) corresponding to a *anti* conformation between carbonyl groups in the pendant group. The addition of Li^+ ions promotes a *syn* between carbonyl groups lead to a positive Cotton Effect in the vinylic region (*P* helices).

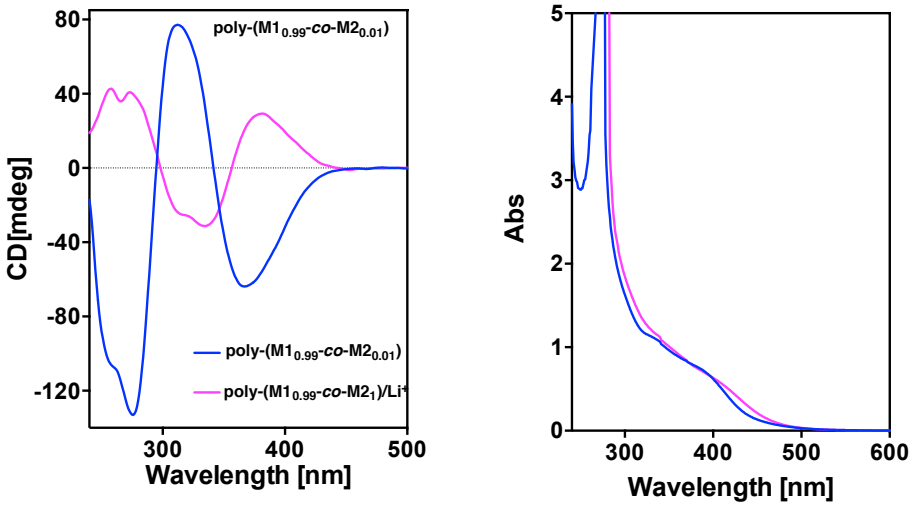

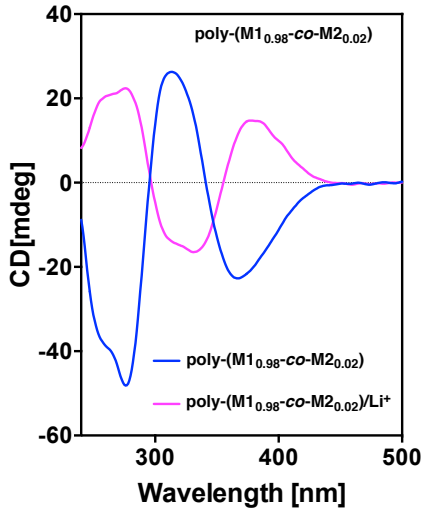
poly-(M1$_{0.98}$-*co*-M2$_{0.02}$)
CD[mdeg]
Wavelength [nm]
poly-(M1$_{0.98}$-*co*-M2$_{0.02}$)
poly-(M1$_{0.98}$-*co*-M2$_{0.02}$)/Li$^+$

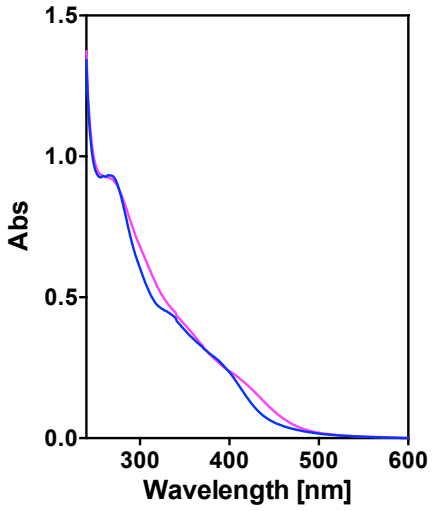
Abs
Wavelength [nm]

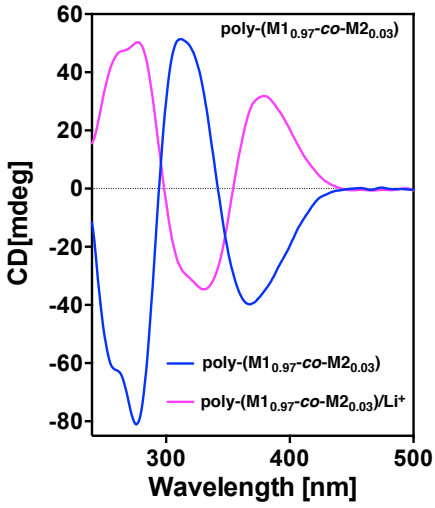
poly-(M1$_{0.97}$-*co*-M2$_{0.03}$)
CD[mdeg]
Wavelength [nm]
poly-(M1$_{0.97}$-*co*-M2$_{0.03}$)
poly-(M1$_{0.97}$-*co*-M2$_{0.03}$)/Li$^+$

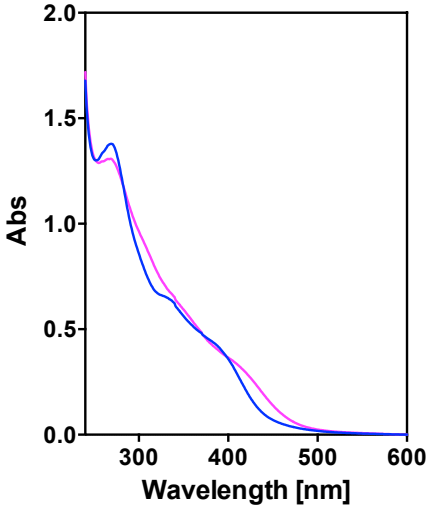
Abs
Wavelength [nm]

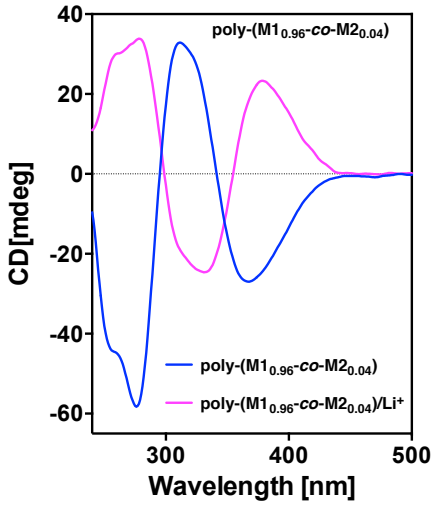
poly-(M1$_{0.96}$-*co*-M2$_{0.04}$)
CD[mdeg]
Wavelength [nm]
poly-(M1$_{0.96}$-*co*-M2$_{0.04}$)
poly-(M1$_{0.96}$-*co*-M2$_{0.04}$)/Li$^+$

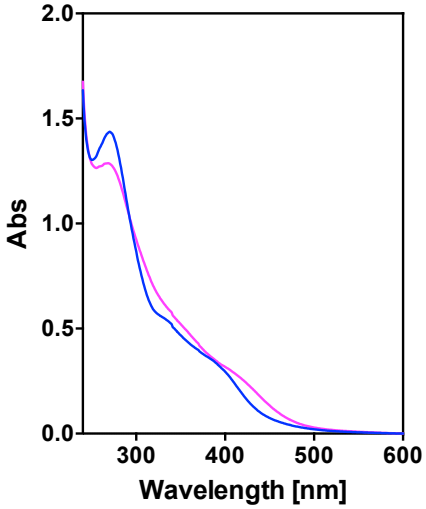
Abs
Wavelength [nm]

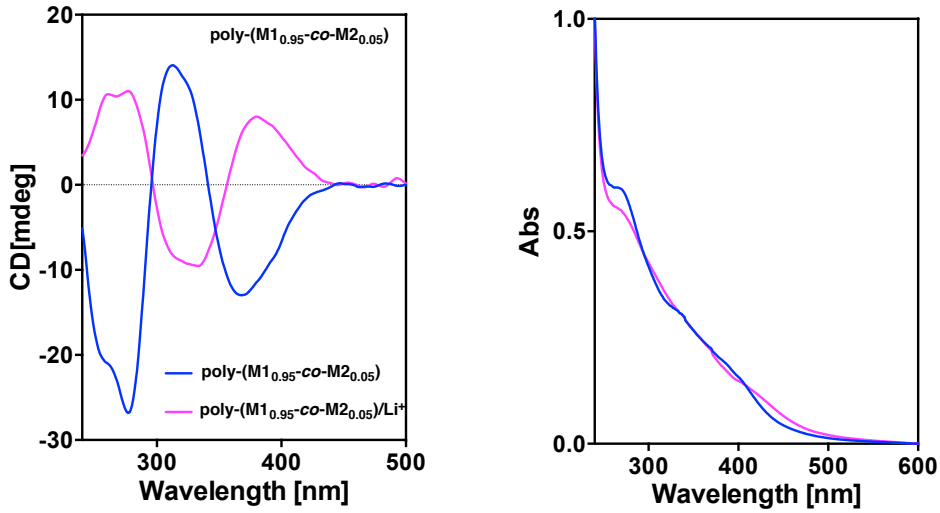

Figure S31. CD and UV-Vis studies for copolymers poly-(M**1**$_r$-*co*-M**2**$_{1-r}$) (r = 0.95-0.99) dissolved in $CHCl_3$ (0.3 mg mL^{-1}) in presence of $LiClO_4$ (10.0 mg mL^{-1}, MeOH).

Table S5: FT IR studies for poly-(M**1**$_r$-*co*-M**2**$_{1-r}$) and poly-(M**1**$_r$-*co*-M**2**$_{1-r}$)/Li$^+$

	C=O$_{(1)}$ (ester)/ (cm^{-1})	C=O$_{(2)}$ (amide)/ (cm^{-1})	OMe/ (cm^{-1})
poly-(M1$_r$-*co*-M2$_{1-r}$)	1741	1646	1090
poly-(M1$_r$-*co*-M2$_{1-r}$)/Li$^+$	1736	1642	1091

12. Thermal studies for copolymer series poly-(M1$_r$-*co*-M2$_{1-r}$)

12.1 DSC studies for poly-(M1$_r$-*co*-M2$_{1-r}$)

DSC studies were carried out in order to determine de geometry of the polymer backbone. As a general protocol, a polymer sample was kept in an aluminium pan and heated from 40 ^oC to 350 ^oC with a heating rate of 10 ^oC/min.

The thermograms of the polymers show typical traces for a *cis-transoidal* backbone, where two exothermal peaks corresponding to the *c-t* to *c-c* and the *c-c* to *t-t* were observed.

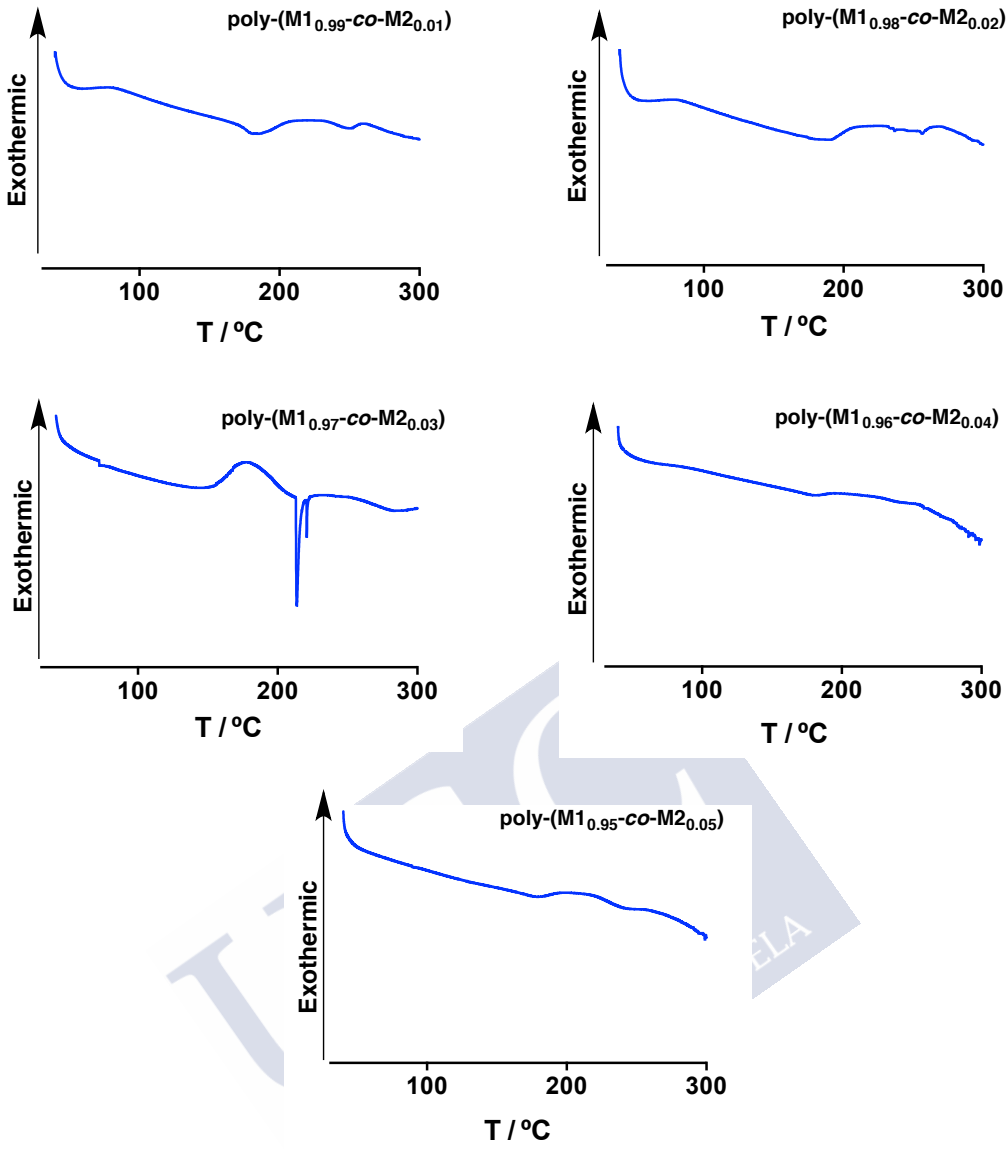

Figure S32. DSC thermograms for copolymers poly-(M**1**$_r$-*co*-M**2**$_{1-r}$) .

12.2 TGA studies for copolymers poly-(M1$_r$-*co*-M2$_{1-r}$)

TGA Studies were carried out in order to determine the thermal stability of the copolymers. As a general protocol, a polymer sample was kept in a platinum pan and heated from 40 °C to 850 °C with a heating rate if 10 °C/min.

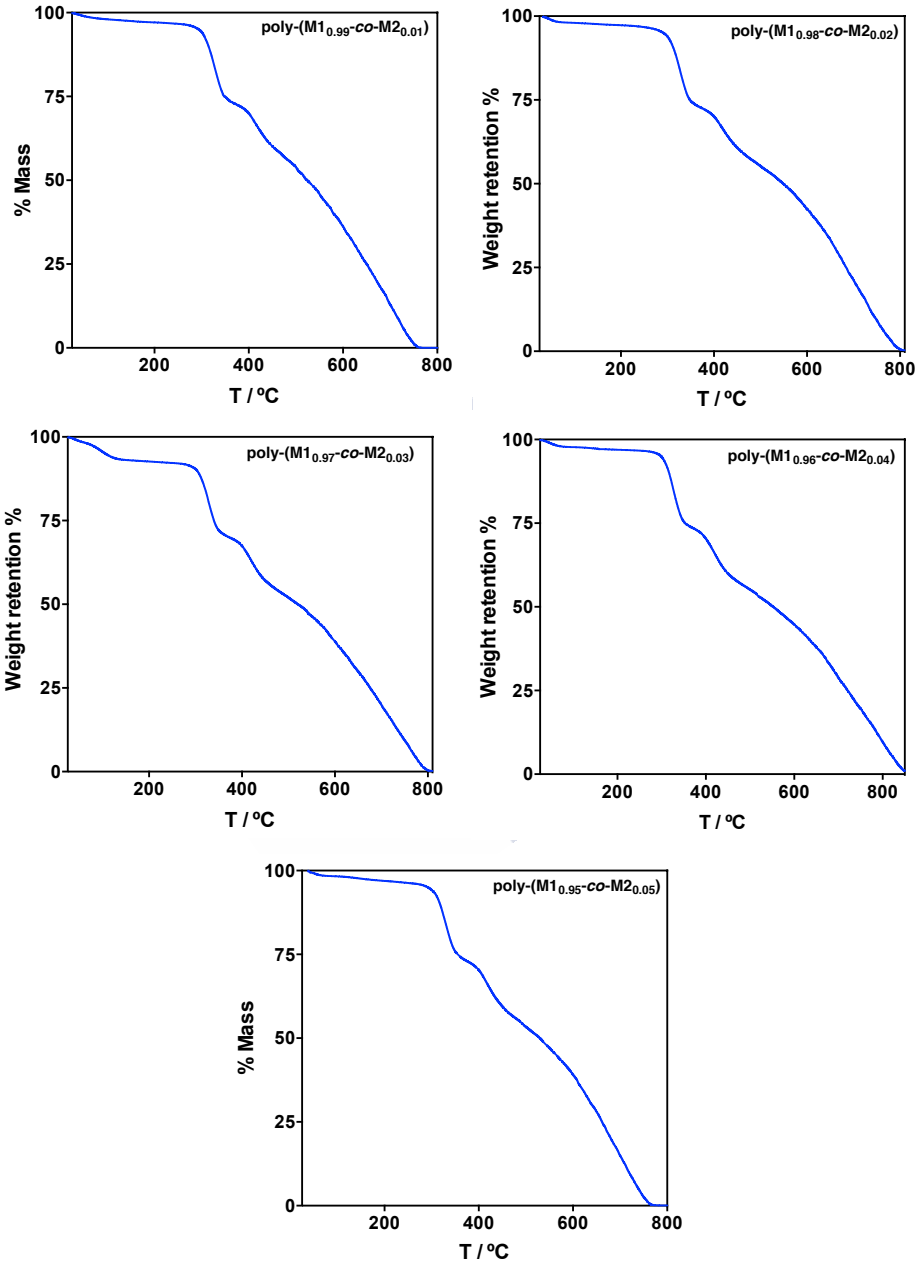

Figure S33. TGA thermograms for copolymers poly-(M**1**$_r$-*co*-M**2**$_{1-r}$) (r = 0.99-0.95).

13. Synthesis of Gold Nanoparticles (AuNPs)

13.1 Synthesis for AuNPs@dodecanethiol

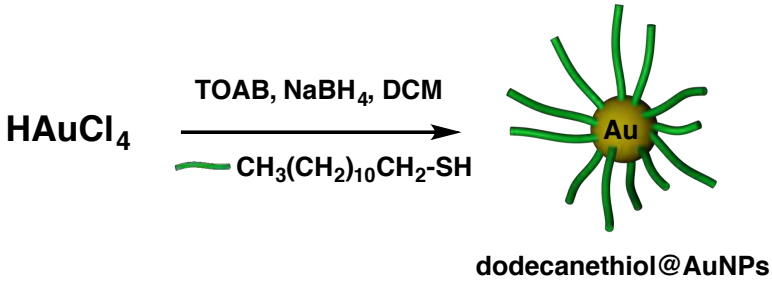

To a solution of tetraoctylamonium bromide (TOAB, 0.444 g, 0.812 mmol) into DCM (20mL) was added a solution of $HAuCl_4$ (0.080 g, 0.202 mmol) in distilled water (1.25 mL) and allowed to stir at rt. After some time, the mixture was washed with DCM (20 mL x 3). A solution of dodecanethiol (40 μL) in DCM (5 mL) were prepared, both solutions were added simultaneously to the reaction mixture and allowed to stir at -4°C for 30 min. After this time was added as a reducing agent, a solution of $NaBH_4$ (76 mg) in distilled water (2 mL). The reaction mixture turns a yellow-orange to brown – black. EtOH (HPLC grade, 50 mL) is added to the solution and left at -4 ° C for 18 h. After this time, the reaction mixture was filtered using a filter plate. The precipitate obtained was dissolved in $CHCl_3$ and a second process was conducted in toluene precipitation using centrifuge (1h, 11000 rpm) and obtaining AuNPs-dodecanethiol in a quantitative yield.

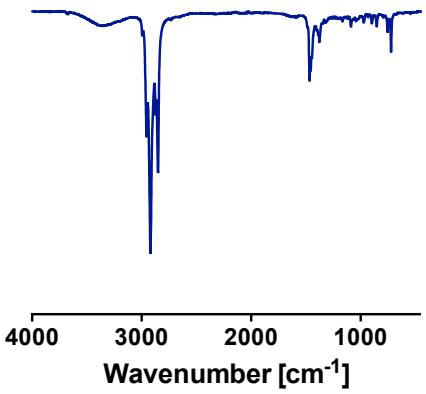

Figure S34. FT-IR spectrum for AuNP@dodecanethiol.

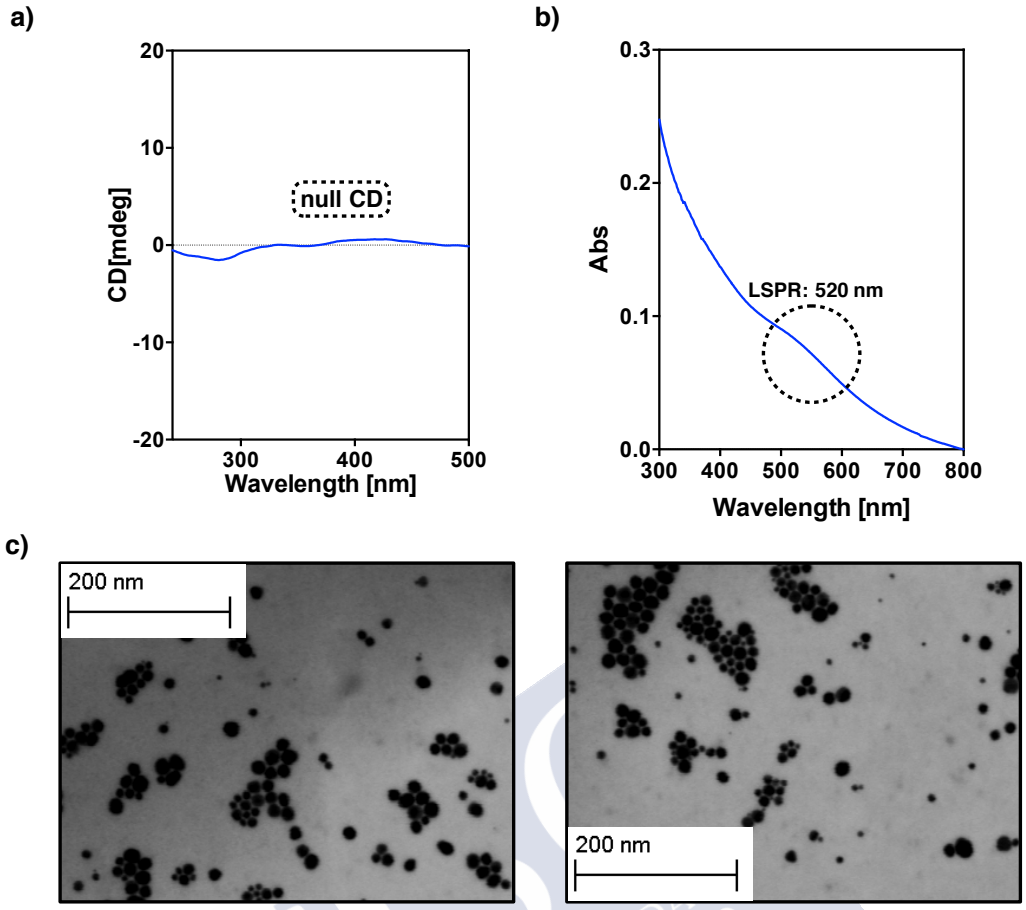

Figure S35. a) CD spectrum for Au@dodecanethiol in $CHCl_3$ at 1.0 mg mL^{-1} of concentration. b) UV-Vis spectrum for Au@dodecanethiol in $CHCl_3$ at 1.0 mg mL^{-1} of concentration. c) TEM images for Au@dodecanethiol (size: 13 nm, SD: 3 nm, scale bar: 200 nm, 255 nanoparticles).

13.2 Synthesis of Au-poly-(M1$_r$-*co*-M2$_{1-r}$) nanocomposites

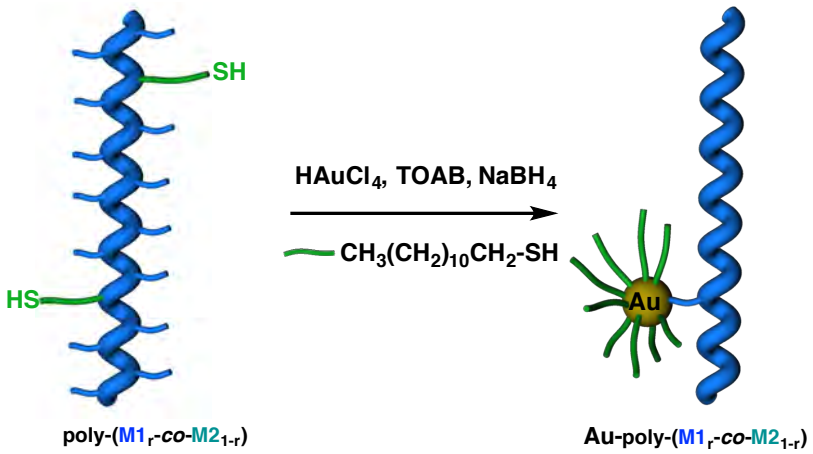

To a solution of tetraoctylamonium bromide (TOAB, 0.444g, 0.812 mmol) into DCM (20mL) was added a solution of $HAuCl_4$ (0.080 g, 0.202 mmol) in distilled water (1.25 mL) and allowed to stir at rt. After some time the mixture was washed with DCM (20 mL x 3). A copolymer (poly-M**1**$_r$-*co*-M**2**$_{1-r}$) solution (0.020 g) in DCM (5 mL) and another solution of dodecanethiol (40 uL) in DCM (5 mL) were prepared, both solutions were added simultaneously to the reaction mixture and allowed to stir at - 4°C for 30 min. After this time was added as a reducing agent, a solution of $NaBH_4$ (0.076 mg) in distilled water (2 mL). The reaction mixture turns a yellow-orange to brown – black. EtOH (HPLC grade, 50 mL) is added to the solution and left at -4 ° C for 18 h. After this time, the reaction mixture was filtered using a filter plate. The precipitate obtained was dissolved in $CHCl_3$ and a second process was conducted in toluene precipitation using centrifuge (1h, 11000 rpm) and obtaining poly-(M**1**$_r$-*co*-M**2**$_{1-r}$)-Au. Extra purification was required for the nanonanocomposites. The peak corresponding to poly-(M**1**$_r$-*co*-M**2**$_{1-r}$)-Au was collected and further analyzed by means of UV, CD and SEM.

13.3 GPC characterization for Au-poly-(M1$_r$-co-M2$_{1-r}$) nanocomposites

Size exclusion chromatography studies were performed on a Alliance 2695 HPLC System (Waters) liquid chromatography system equipped with a UV 2489 detector (Waters) using. The samples were eluted by two Phenogel columns connected to each other with stacionary phases of 10^3 and 10^5 Amstrong and packed with a solid support of a cross-linked stiyrene and *p*-divinylbenzene copolymer. To characterize the hybrid materials Au-poly-(M**1**$_r$-*co*-M**2**$_{1-r}$) GPC chromatograms were recorded at 380 (polymer absorption) and 540 nm (gold nanoparticles absorption).

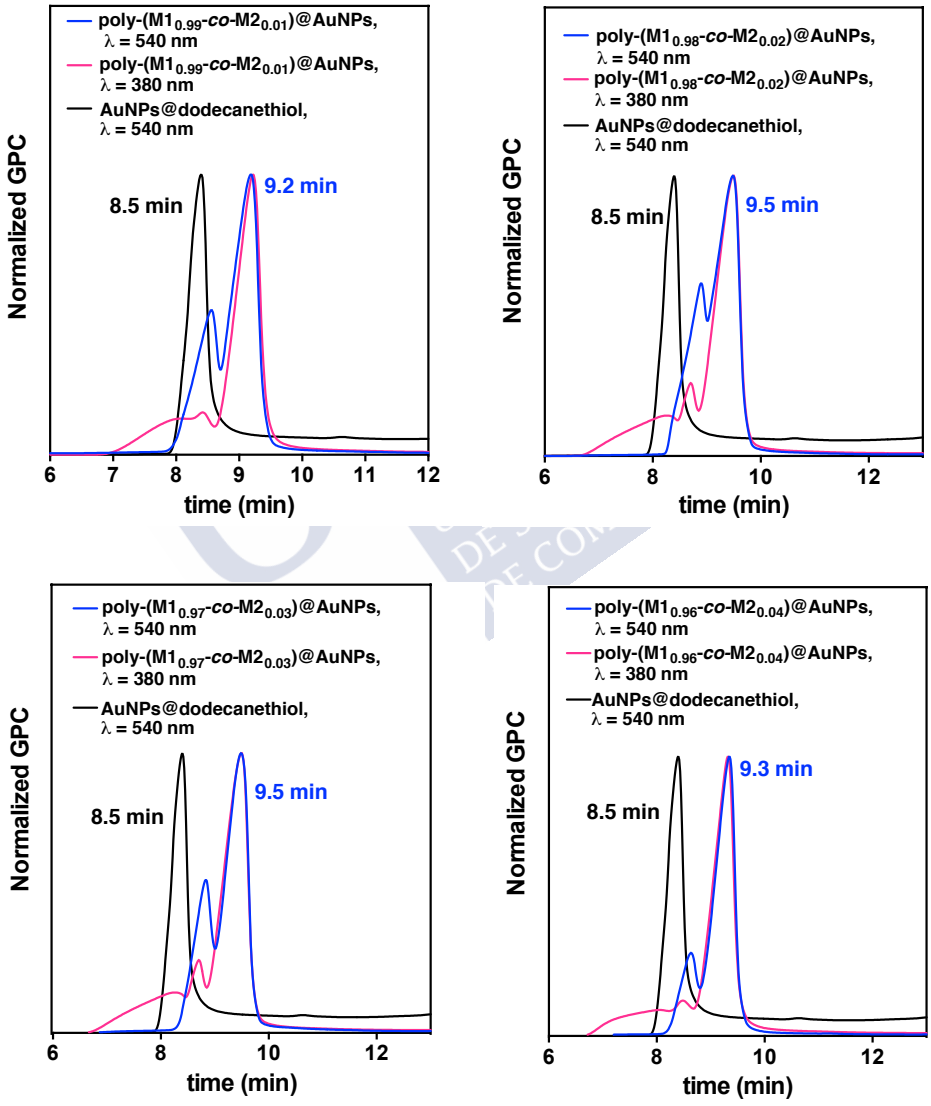

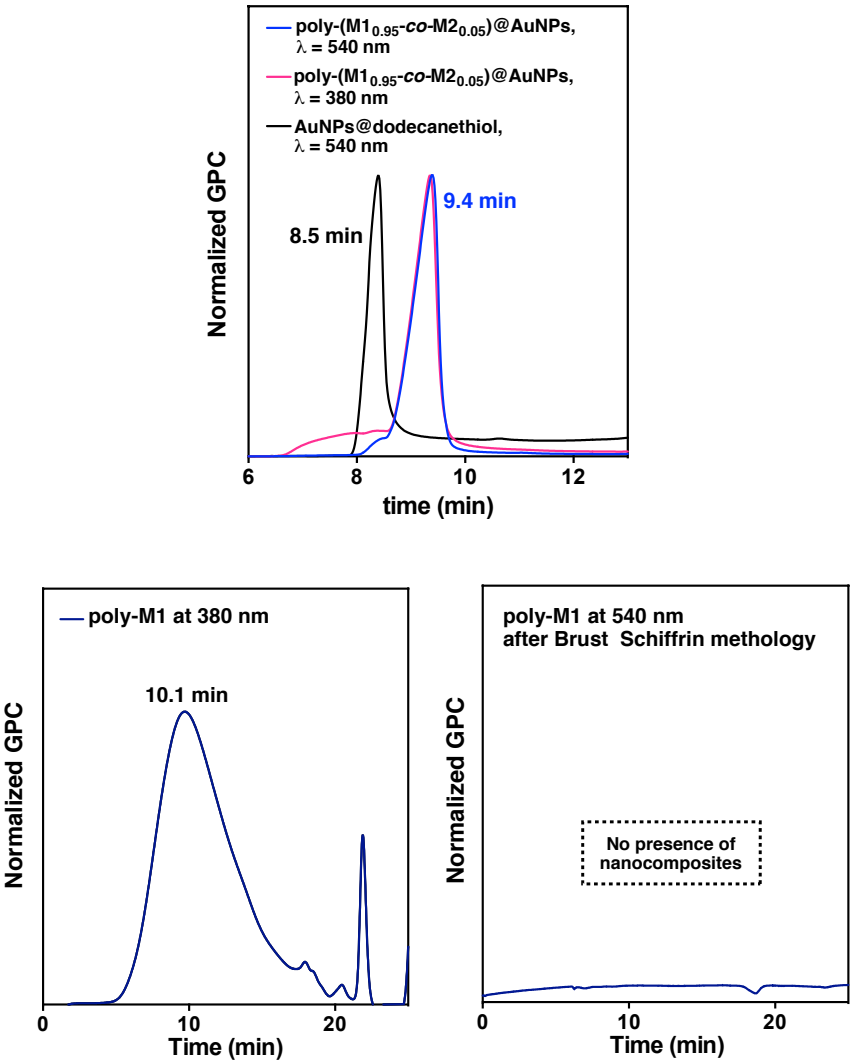

Figure S36. GPC chromatograms for Au-poly-(M**1**$_r$-*co*-M**2**$_{1-r}$) nanocomposites and control studies for poly-M**1**.

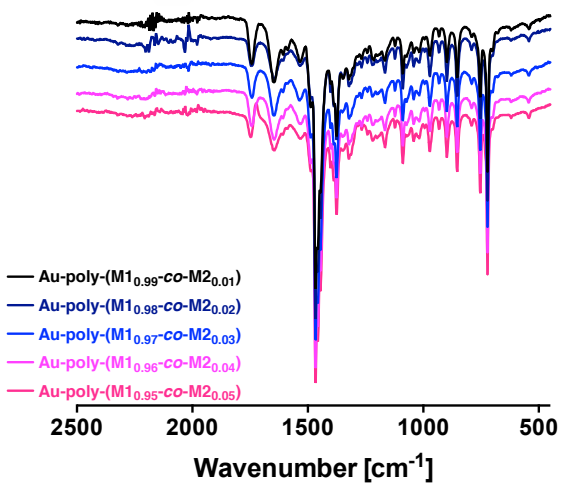

Figure S37. FT-IR spectra for Au-poly-(M**1**$_r$-*co*-M**2**$_{1-r}$) nanocomposites.

14. Thermal studies for Au-poly-(M1$_r$-*co*-M2$_{1-r}$) nanocomposites

14.1 DSC studies for Au-poly-(M1$_r$-*co*-M2$_{1-r}$) nanocomposites

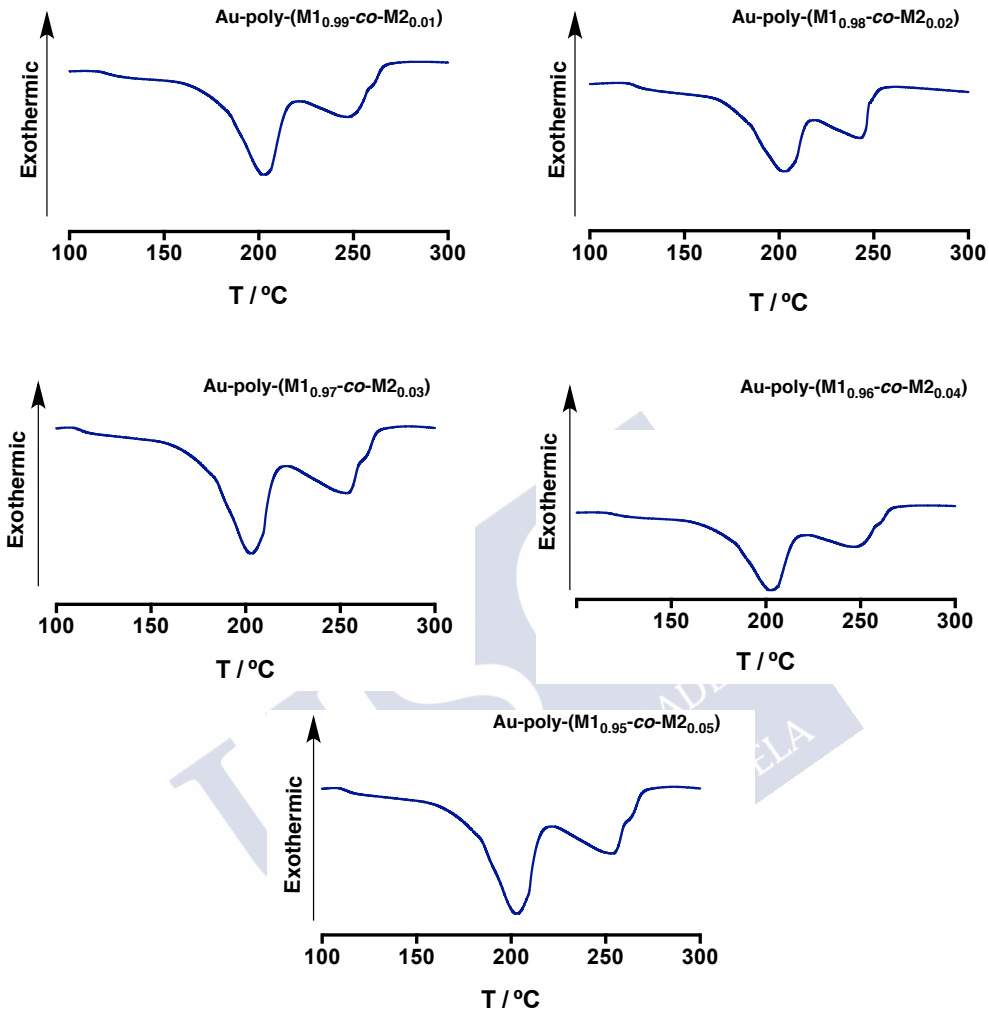

Figure S38. DSC thermograms for Au-poly-(M**1**$_r$-*co*-M**2**$_{1-r}$) nanocomposites.

14.2 TGA studies for Au-poly-(M1$_r$-*co*-M2$_{1-r}$) nanocomposites

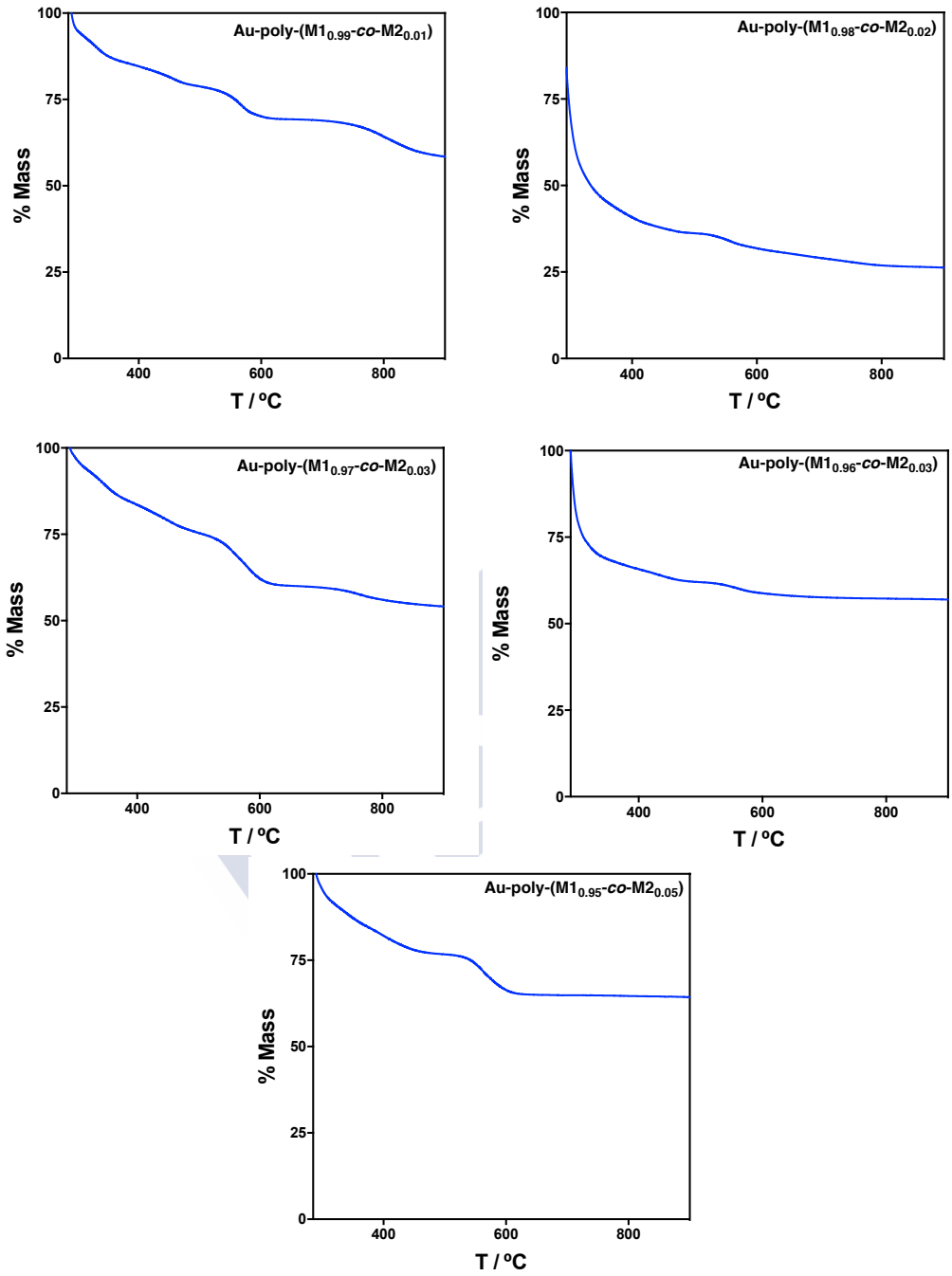

Figure S39. TGA thermograms for Au-poly-(M**1**$_r$-*co*-M**2**$_{1-r}$) nanocomposites.

15. CD and UV-Vis experiments for Au-poly-(M1$_r$-*co*-M2$_{1-r}$) nanocomposites in high polar and low polar solvents

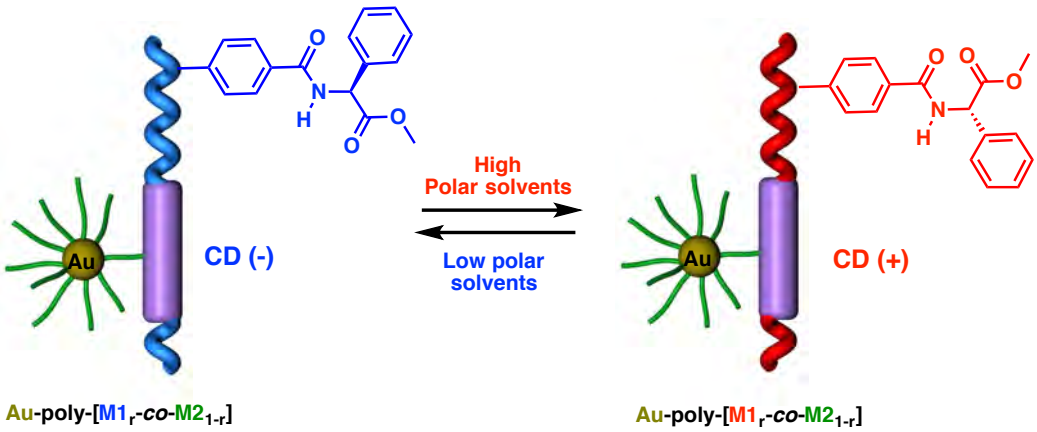

CD and UV-Vis studies were performed with a solution of Au-poly-(M**1**$_r$-*co*-M**2**$_{1-r}$) in high polar (DMSO, DMF) and low polar ($CHCl_3$, THF) solvents.

Au-Poly-(M**1**$_r$-*co*-M**2**$_{1-r}$) dissolved in low polar solvents (0.3 mg mL^{-1}, $CHCl_3$ and THF) presents a negative Cotton effect (*M* helices) in the vinylic region corresponding to a *anti* conformation between carbonyl groups in the pendant group. Differently, Au-poly-(M**1**$_r$-*co*-M**2**$_{1-r}$) dissolved in high polar solvents (0.3 mg mL^{-1}, DMF and DMSO) presents a positive Cotton effect (*P* helices) corresponding to a *syn* conformation between carbonyl groups

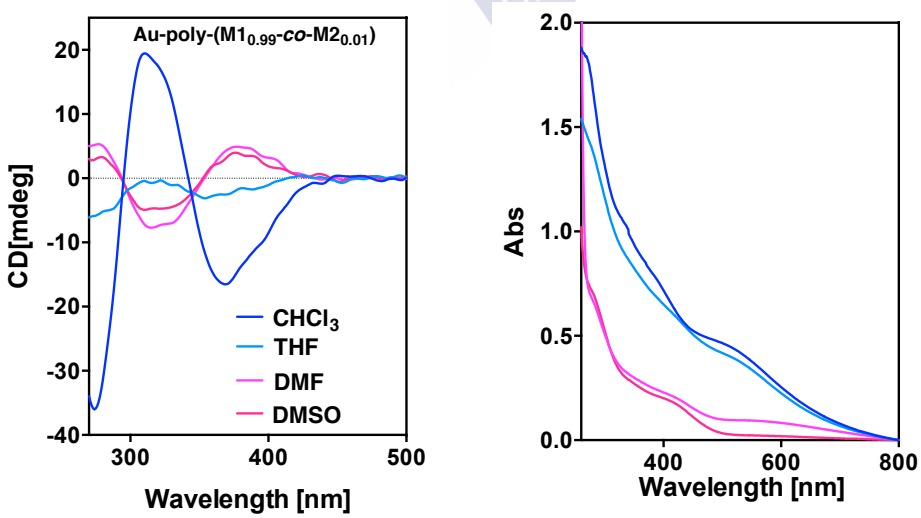

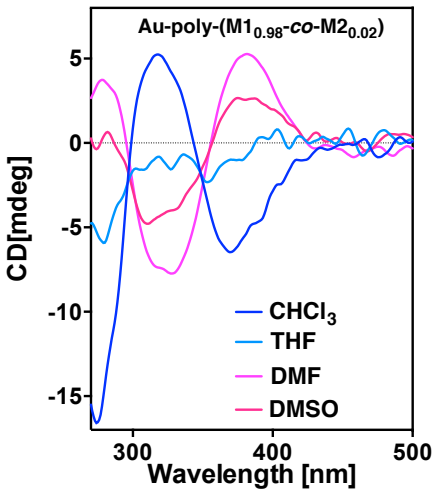
Au-poly-(M1$_{0.98}$-*co*-M2$_{0.02}$)
CD[mdeg]
Wavelength [nm]
CHCl$_3$
THF
DMF
DMSO

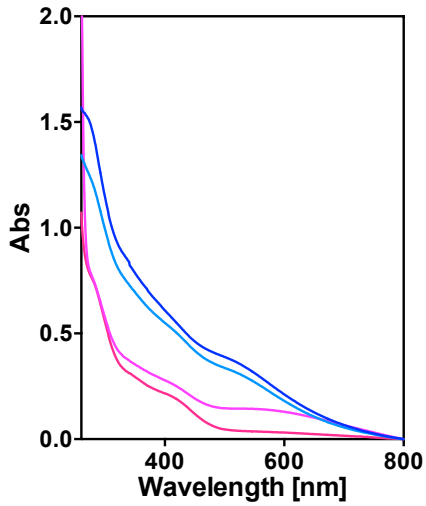
Abs
Wavelength [nm]

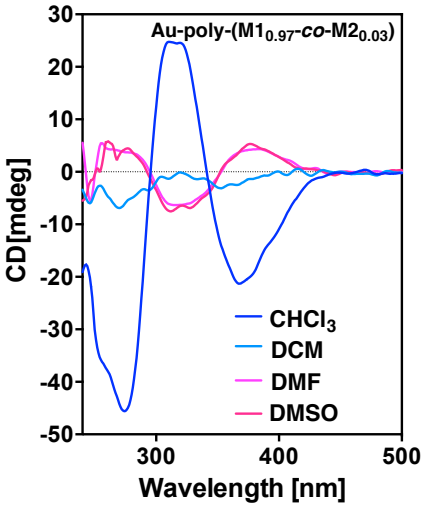
Au-poly-(M1$_{0.97}$-*co*-M2$_{0.03}$)
CD[mdeg]
Wavelength [nm]
CHCl$_3$
DCM
DMF
DMSO

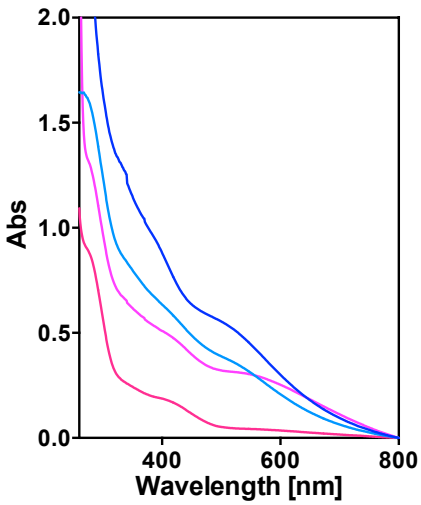
Abs
Wavelength [nm]

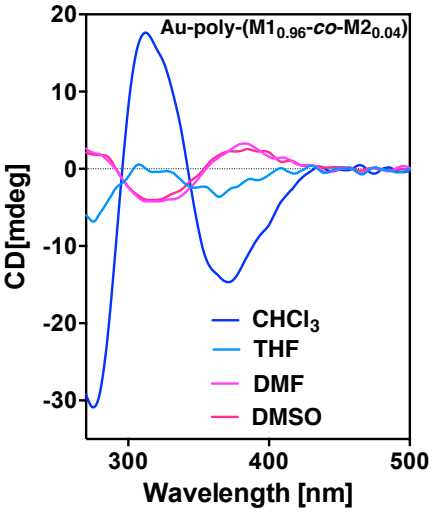
Au-poly-(M1$_{0.96}$-*co*-M2$_{0.04}$)
CD[mdeg]
Wavelength [nm]
CHCl$_3$
THF
DMF
DMSO

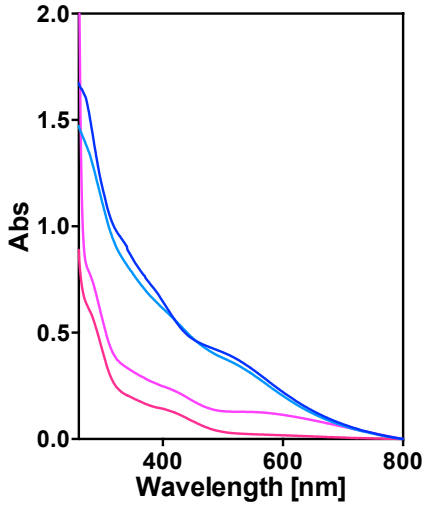
Abs
Wavelength [nm]

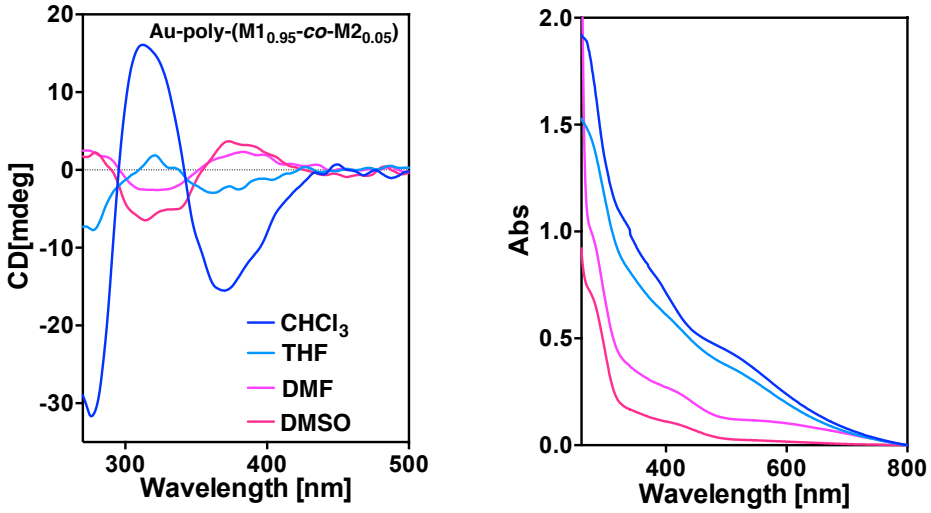

Figure S40. CD and UV-Vis experiments for copolymers Au-poly-(M**1**$_r$-*co*-M**2**$_{1-r}$) in high polar and low polar solvents.

16. CD and UV-Vis experiments for Au-poly-(M1$_r$-co-M2$_{1-r}$) nanocomposites in presence of LiClO$_4$

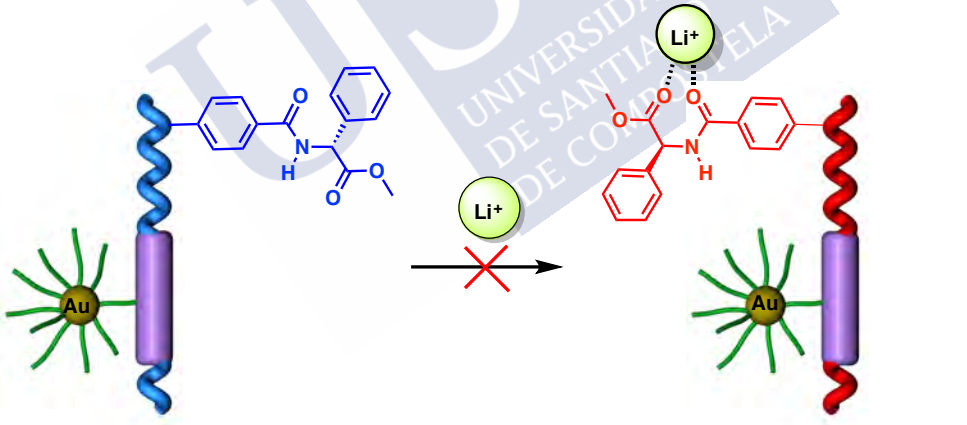

CD and UV-Vis studies were performed with a solution of poly-(M**1**$_r$-*co*-M**2**$_{1-r}$)-AuNPs in $CHCl_3$ (0.3 mg mL^{-1}) using $LiClO_4$ dissolved in MeOH which concentration was 10.0 mg mL^{-1}.

Thus, Au-poly-(M**1**$_r$-*co*-M**2**$_{1-r}$) dissolved in $CHCl_3$ shows a negative Cotton effect (*M* helices) in the vinylic region corresponding to an *anti* conformation between carbonyl groups in the pendant group. The addition of Li^+ ions to Au-poly-(M**1**$_r$-*co*-M**2**$_{1-r}$) cannot promote a helical inversion preserving the same helical sense (*M* helices).

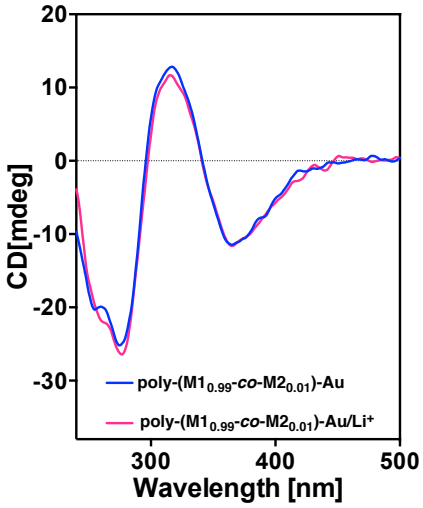
CD[mdeg]
Wavelength [nm]
poly-(M1$_{0.99}$-*co*-M2$_{0.01}$)-Au
poly-(M1$_{0.99}$-*co*-M2$_{0.01}$)-Au/Li$^+$

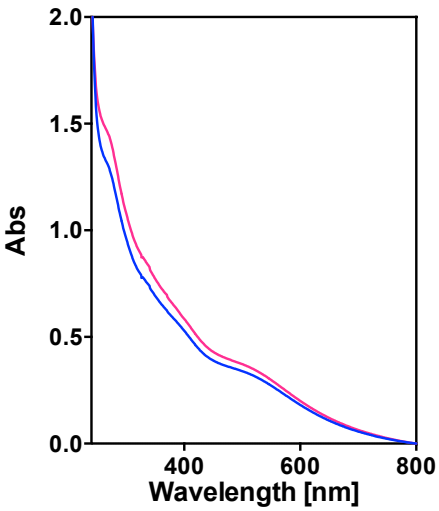
Abs
Wavelength [nm]

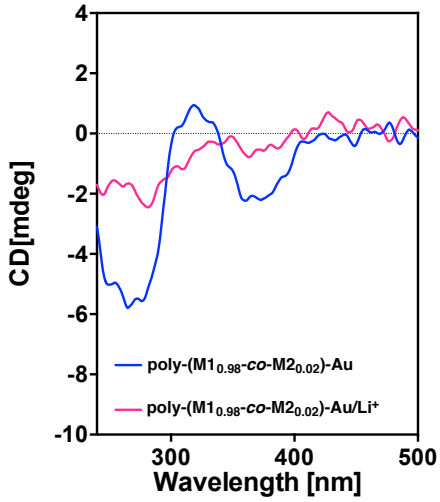
CD[mdeg]
Wavelength [nm]
poly-(M1$_{0.98}$-*co*-M2$_{0.02}$)-Au
poly-(M1$_{0.98}$-*co*-M2$_{0.02}$)-Au/Li$^+$

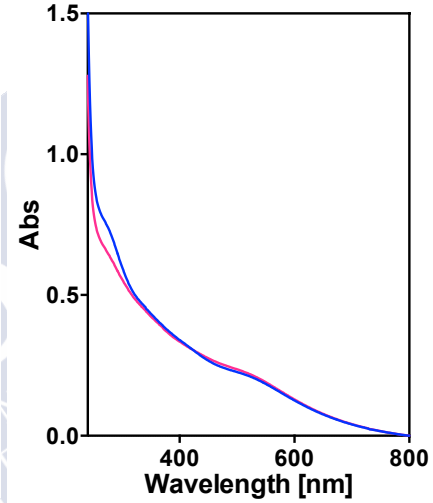
Abs
Wavelength [nm]

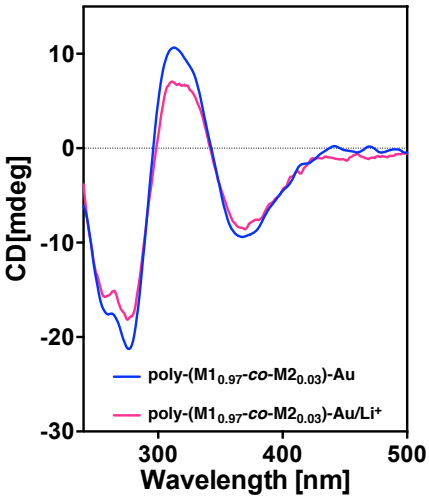
CD[mdeg]
Wavelength [nm]
poly-(M1$_{0.97}$-*co*-M2$_{0.03}$)-Au
poly-(M1$_{0.97}$-*co*-M2$_{0.03}$)-Au/Li$^+$

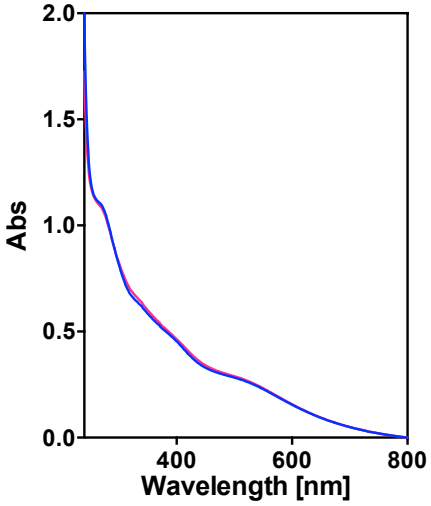
Abs
Wavelength [nm]

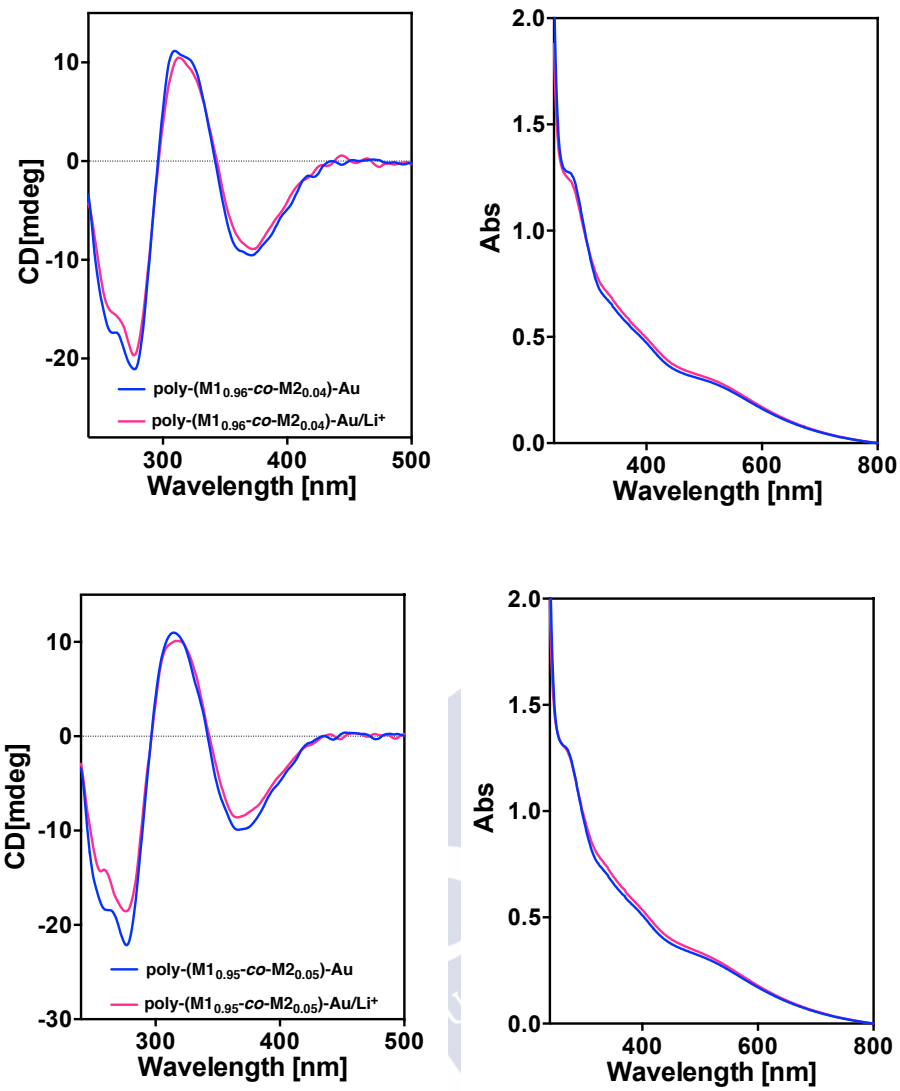

Figure S41. CD and UV-Vis studies for copolymers Au-poly-(M**1**$_r$-*co*-M**2**$_{1-r}$) dissolved in $CHCl_3$ (0.5 mg mL^{-1}) in presence of $LiClO_4$ dissolved in MeOH (10.0 mg mL^{-1}).

17. % Maximum CD signal for poly-M1, poly-(M1$_r$-*co*-M2(STrt)$_{1-r}$), poly-(M1$_r$-*co*-M2$_{1-r}$) and Au-poly-(M1$_r$-*co*-M2$_{1-r}$) nanocomposites

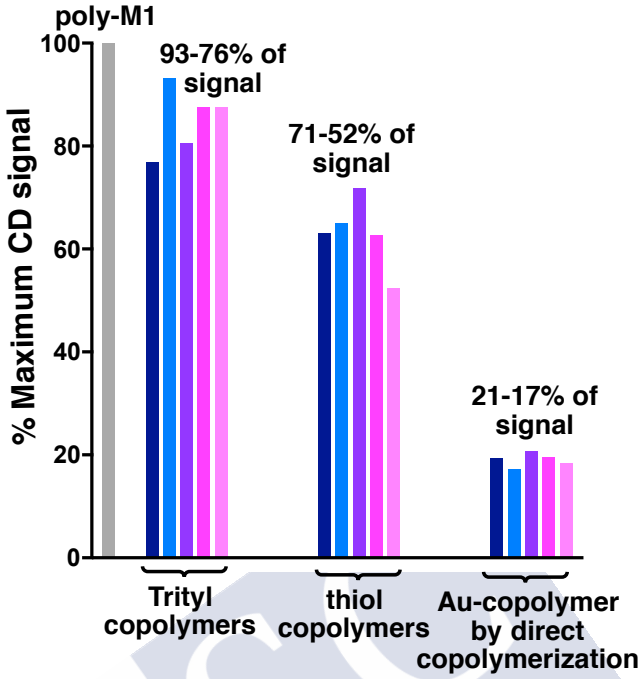

Figure S42. % Maximum CD signal for poly-M**1**, copolymers poly-(M**1**$_r$-*co*-M**2**(Trt)$_{1-r}$), copolymers poly-(M**1**$_r$-*co*-M**2**$_{1-r}$) and Au-poly-(M**1**$_r$-*co*-M**2**$_{1-r}$) nanocomposites.

18. CD and UV-Vis experiments for copolymers Au-poly-(M1$_r$-*co*-M2$_{1-r}$) nanocomposites in solid state

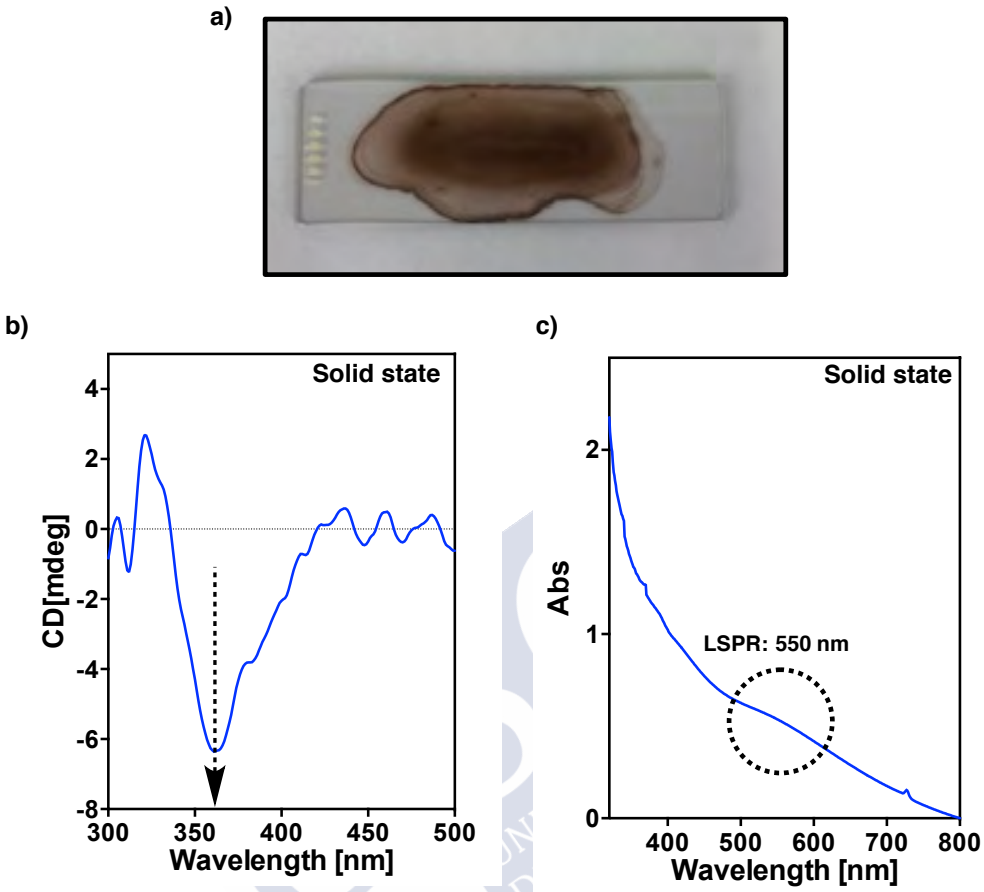

Figure S43. a) Film for Au-Poly-(M**1**$_{0.96}$-*co*-M**2**$_{0.04}$) in solid state. b) CD and c) UV-Vis measurements for Au-poly-(M**1**$_{0.95}$-*co*-M**2**$_{0.05}$) nanocomposites in solid state.

19. Microscopy (SEM and TEM) studies for Au-poly-(M1$_r$-*co*-M2$_{1-r}$) nanocomposites

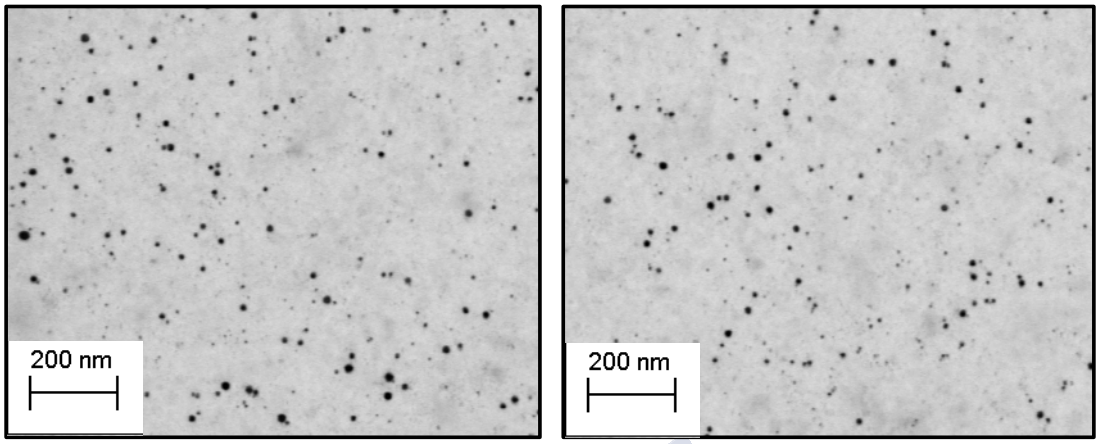

Figure S44. TEM images for Au-poly-(M**1**$_{0.99}$-*co*-M**2**$_{0.01}$) nanocomposites (size: 12 nm, SD: 3 nm, 101 nanoparticles, scale bar: 200 nm).

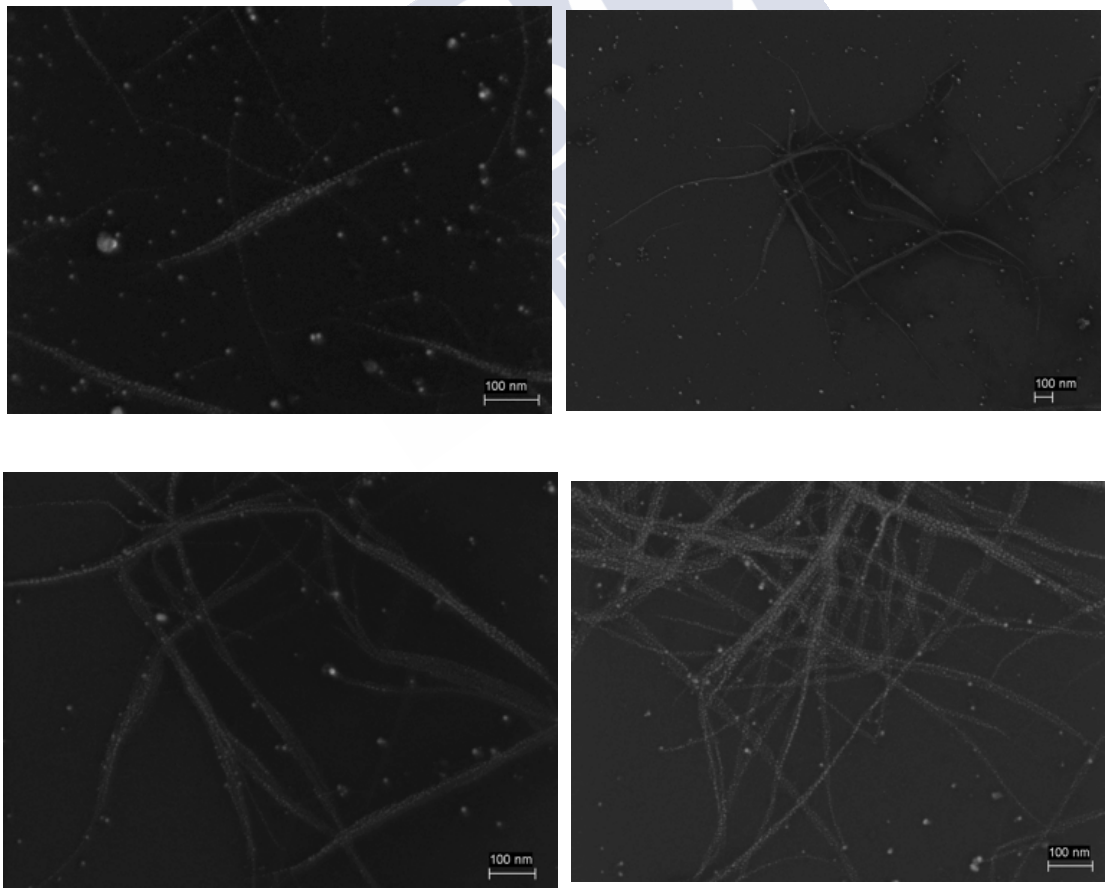

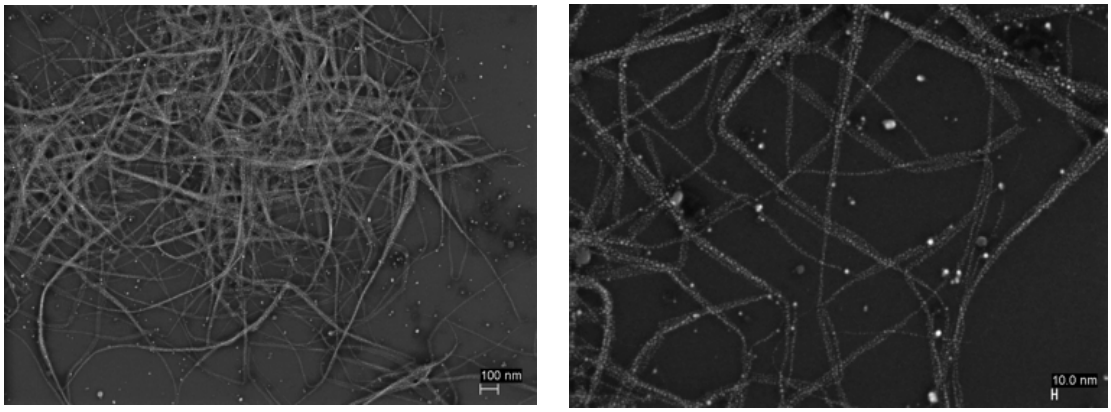

Figure S45: SEM microscopy images for Au-poly-(M**1**$_r$-*co*-M**2**$_{1-r}$) (r = 0.97-0.95) nanocomposites.

20. Nanostructuration studies for Au-poly-(M1$_r$-*co*-M2$_{1-r}$) nanocomposites in presence of $Ba(ClO_4)_2$

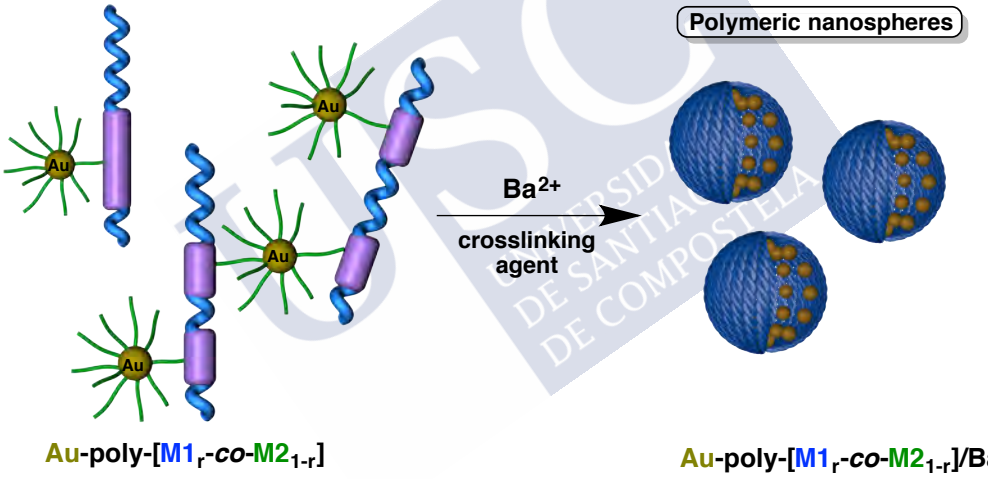

The addition of barium perchlorate (10.0 mg mL^{-1}) in MeOH to a solution of Au-poly-(M**1**$_r$-M**2**$_{1-r}$) (r = 0.99-0.95) nanocomposites (0.3 mg mL^{-1}, $CHCl_3$) produce the formation of chiral polymeric nanospheres due to the ability of Ba^{2+} to act as a crosslinking agent between polymer chains.

poly	Ba^{2+} (mol)	size (nm)	pdi
poly-($M1_{0.99}$-*co*-$M2_{0.01}$)-Au	0	741	0.687
poly-($M1_{0.99}$-*co*-$M2_{0.01}$)-Au	0.2	482	0.213
poly-($M1_{0.99}$-*co*-$M2_{0.01}$)-Au	0.4	534	0.224

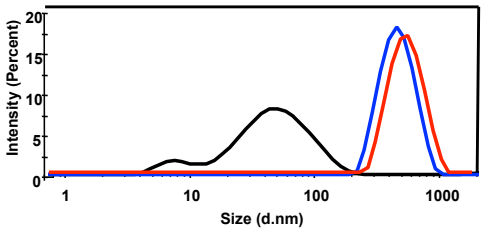

poly	Ba^{2+} (mol)	size (nm)	pdi
poly-($M1_{0.98}$-*co*-$M2_{0.02}$)-Au	0	720	0.433
poly-($M1_{0.98}$-*co*-$M2_{0.02}$)-Au	0.2	366	0.092
poly-($M1_{0.98}$-*co*-$M2_{0.02}$)-Au	0.2	599	0.152

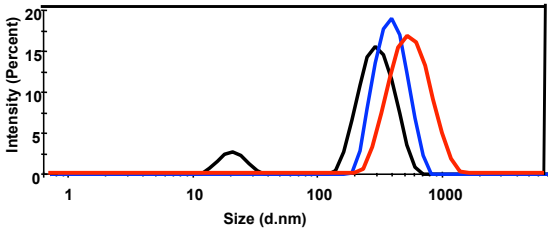

poly	Ba^{2+} (mol)	size (nm)	pdi
poly-($M1_{0.97}$-*co*-$M2_{0.03}$)-Au	0	464	0.656
poly-($M1_{0.97}$-*co*-$M2_{0.03}$)-Au	0.2	418	0.500

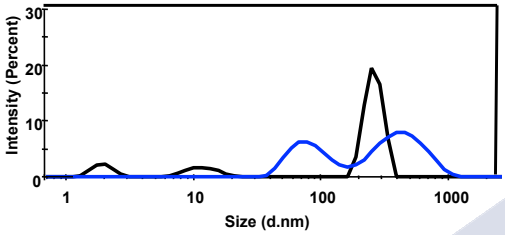

poly	Ba^{2+} (mol)	size (nm)	pdi
poly-($M1_{0.96}$-*co*-$M2_{0.04}$)-Au	0	2891	1.000
poly-($M1_{0.96}$-*co*-$M2_{0.04}$)-Au	0.2	1038	0.381

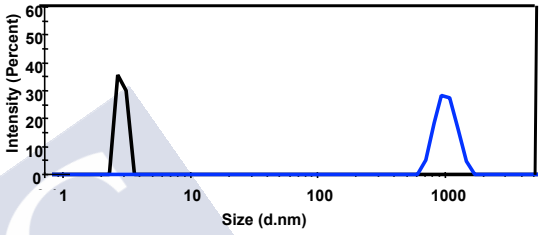

poly	Ba^{2+} (mol)	size (nm)	pdi
poly-($M1_{0.95}$-*co*-$M2_{0.05}$)-Au	0	407	0.851
poly-($M1_{0.95}$-*co*-$M2_{0.05}$)-Au	0.2	705	0.326

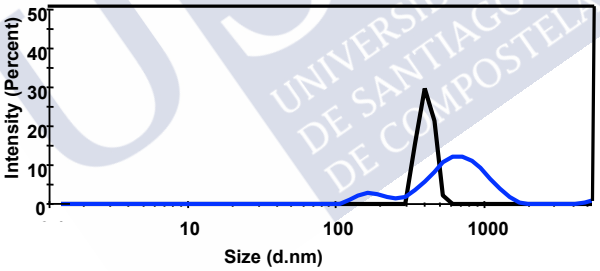

Figure S46. DLS measurements for Au-poly-(M**1**$_r$-*co*-M**2**$_{1-r}$) nanocomposites (0.3 mg mL^{-1} in $CHCl_3$) in presence of $Ba(ClO_4)_2$ (10.0 mg mL^{-1} in MeOH).

21. SEM images for Au-poly-(M1$_r$-*co*-M2$_{1-r}$) nanocomposites in presence of $Ba(ClO_4)_2$

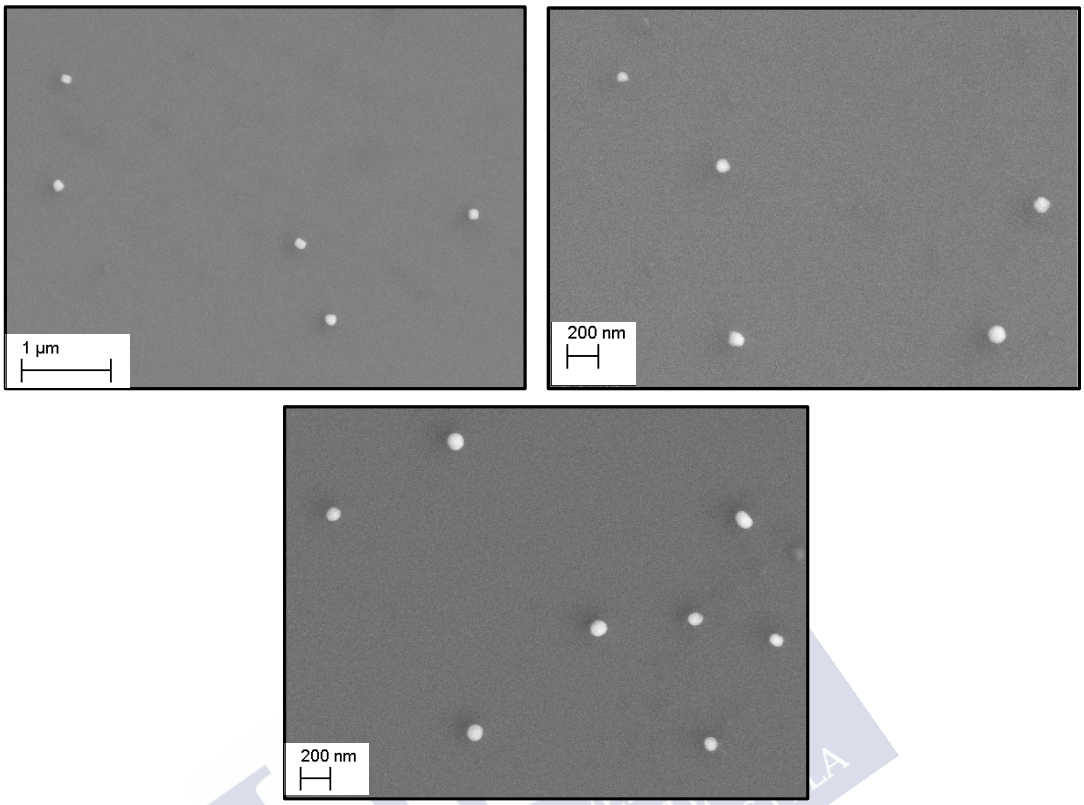

Figure S47. SEM images in solid state prepared from Au-poly-(M**1**$_r$-*co*-M**2**$_{1-r}$) (0.3 mg mL^{-1}, $CHCl_3$) in presence of $Ba(ClO_4)_2$ (10.0 mg mL^{-1} in MeOH).

22. Control studies

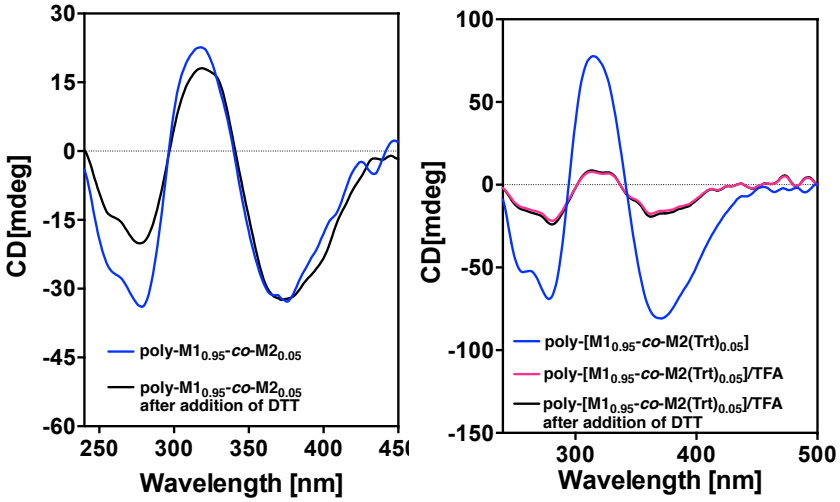

Figure S48. Control studies after addition of DTT for poly-[M**1**$_{0.95}$-*co*-M**2**$_{0.05}$] and poly-[M**1**$_{0.95}$-*co*-M2(Trt)$_{0.05}$].

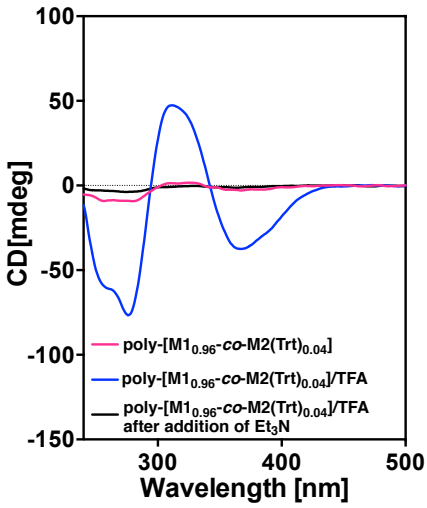

Figure S49. Control studies after addition of Et_3N for poly-[M**1**$_{0.96}$-*co*-M**2**$_{0.04}$]/TFA.

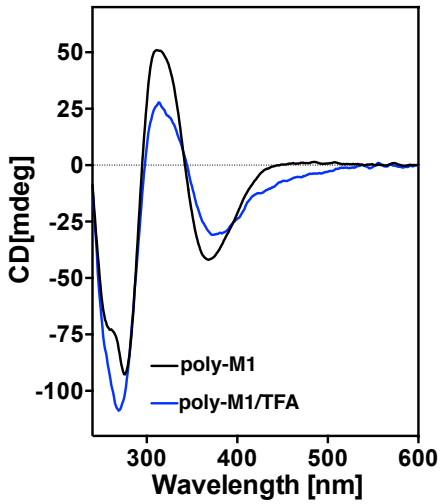

Figure S50. Control studies for poly-M**1** (0.3 mg mL^{-1}, $CHCl_3$) in presence of TFA (1 % v/v).

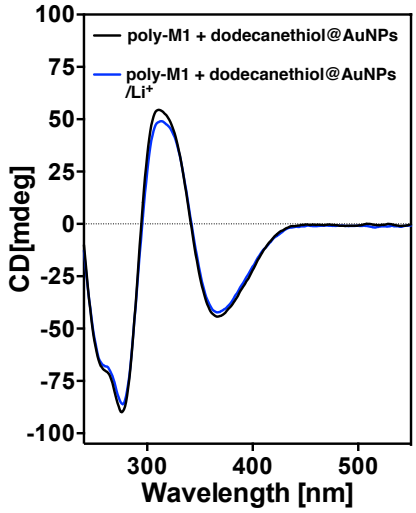

Figure S51. CD studies for a mixture (1:1) of poly-M**1**/dodecanethiol@AuNPs in $CHCl_3$ and poly-M**1**/dodecanethiol@AuNPs ($CHCl_3$) in presence of Li^+ ions (10 mg mL^{-1}, MeOH).

23. Supporting references

S1. M. Alzubi, S. Arias, I. Louzao, E. Quiñoá, R. Riguera, F. Freire, *Chem. Commun.* **2017**, *53*, 8573.

S2. S. Arias, R. Rodríguez, E. Quiñoá, R. Riguera, F. Freire, *J. Am. Chem. Soc.* **2018**, *140,* 667.

S3. F. Freire, J. M. Seco, J. E. Quiñoá, R. Riguera, *J. Am. Chem. Soc.* **2012**, *134*, 19374.

S4. G. Yesilbag, T. Mizuhara, K. Saha, Z. Jiang, S. Hou, R. Das, V. Rotello, *Tetrahedron Letters*, **2015**, *56*, 3653.

S5. M. Brust, M. Walker, D. Bethell, D. J. Schiffrin, R. Whyman, *J. Chem. Soc. Chem. Commun.,* **1994**, 801.

USC UNIVERSIDADE DE SANTIAGO DE COMPOSTELA

Expertimental Section Chapter IV:

1. Materials and methods

Chemicals. Commercially available chemicals have been used as delivered. Solvents were purchased as reagent grade and distilled if necessary. Anhydrous solvents were either purchased as ultra-dry solvent from Acros Organics® or received from solvent purification system. For the coupling and polymerization reactions, dry THF was obtained from MBRAUN SPS 800 solvent purification system. Water was purified by Millipore water purification system. Coupling reagents (2-(7-Aza-1H-benzotriazole-1-yl)-1,1,3,3-tetramethyluronium hexafluorophosphate) (HATU), 1-hydroxy-7-azabenzotriazole (HOAT), 4-ethynylbenzoic acid, and 4-ethynylaniline were purchased from AnaSpec Inc. (*R*)-α-methoxyphenylacetic acid, (*R*)-α-methoxy-α-trifluorophenylacetic acid, oxalyl choride, rhodium norbornadiene chloride dimer {$[Rh(nbd)Cl]_2$}, diisopropylethylamine (DIEA), triethylamine (TEA, 99%), dodecanethiol, sodium borohydride ($NaBH_4$), silver perchlorate ($AgClO_4$) and barium perchlorate [$(Ba(ClO_4)_2$] a were purchased from Aldrich.

Instrumentations and Characterizations. NMR experiments were carried out in a Varian Inova 300 (300 MHz resonance 1H). Size exclusion chromatography studies were performed on Alliance 2695 HPLC System (Waters) liquid chromatography system equipped with a UV 2489 detector (Waters). The samples were eluted by three Phenogel columns connected to each other with stationary phases of 10^3, 10^4 and 10^5 Amstrong and packed with a solid support of a cross-linked styrene and *p*-divinylbenzene copolymer. CD and UV measurements were registered in a Jasco-720 spectropolarimeter and a Jasco-730 spectrophotometer respectively at a nanocomposite concentration of 0.3 mg mL^{-1}. FT-IR measurements were carried out on a Bruker IFS-66v. DLS studies were performed on a Nano-ZS 90 (Malvern) equipped with a He-Ne laser (l = 633 nm) under scattering angle of 173°. The samples were maintained at the designed temperature for 5 min before testing. DLS measurements were carried out in all cases at 0.3 mg·mL^{-1}. SEM measurements were performed on a LEO-435VP electron microscope equipped with an energy dispersive X-ray (EDX) spectrometer. TEM measurements were performed on a JEOL JEM 2010 and 200 KV as a voltage. To study the nanocomposite, or the nanospheres the same protocol was used. A dispersion of the nanocomposite or the nanospheres at a concentration of 0.3 mg mL^{-1} was drop casted onto of silicon wafer chip and allowed to dry at rt for 12h for SEM studies, while in case of TEM studies the dispersed materials were drop-casted onto carbon chip and allowed to dry at rt for 12.h.

2. Synthesis of monomer M1

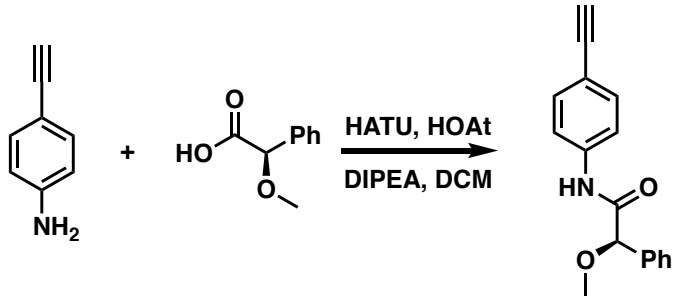

The general procedure of the synthesis of monomer M**1** can be found in the reference [S1].

(2-(7-Aza-1H-benzotriazole-1-yl)-1,1,3,3-tetramethyluronium hexafluorophosphate) (HATU, 971 mg, 2.55 mmol), 1-hydroxy-7-azabenzotriazole (HOAt, 348 mg, 2.55 mmol), (*R*)-α-methoxy-α-phenylacetic acid ((*R*)-MPA, 424 mg, 2.55 mmol), disiisopropyehtylamine (DIPEA) (330 μL, 2.55 mmol) were dissolved in CH_2Cl_2 and the mixture was stirred 15 min to activate the acid. Then, 4-ethynilaniline (250 mg, 2.12 mmol) was added and the mixture was stirred 24 h. The mixture was washed twice with HCl 1M, next with saturated $NaHCO_3$ solution (twice) and finally with saturated NaCl solution. The crude was chromatographed on silica gel (70-230 mesh) with hexane/ethyl acetate (7/3) as eluent (75 % of yield).

Spectroscopic data:

^{1}H NMR (300 MHz, $CDCl_3$) δ(ppm): 3.12 (s, 1H), 3.43 (s, 3H), 4.77 (s, 1H), 7.31 (m, 7H), 7.68 (d, 2H), 8.66 (s, 1H).

^{13}C NMR (70 MHz, $CHCl_3$) δ(ppm): 57.5, 77.0, 83.5, 83.9, 117.9, 119.4, 127.2, 128.8, 133.0, 136.4, 137.9, 168.7.

$[\alpha]_D^{20}$= -15 (10 mg mL^{-1}, $CHCl_3$).

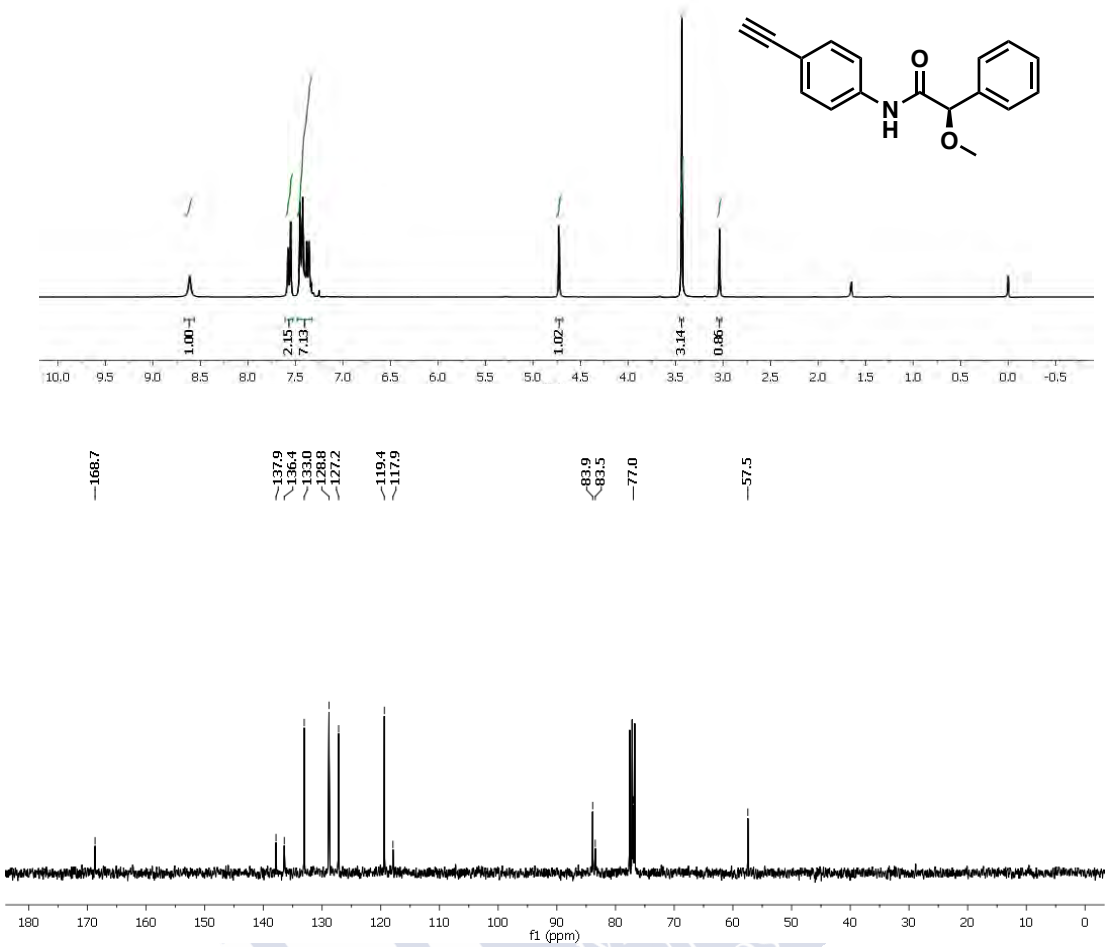

Figure S1. ^{1}H NMR and ^{13}C NMR spectra of monomer M**1** in $CDCl_3$.

3. Synthesis of monomer M2

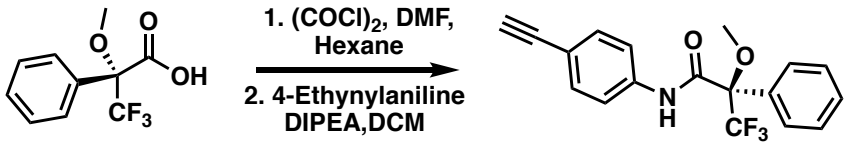

M2

Momomer M**2** was prepared according to reference [S2]:

Oxalyl chloride (260 mL, 1.4 equiv) was added dropwise to a solution of (*R*)-α-methoxy-α-(trifluoromethyl)phenylacetic acid (500 mg, 1.0 equiv) in dry hexane and DMF (300 μL) at 0°C under an Ar atm. After 4 h stirring at rt, the reaction mixture was filtered, and the solution dried under vacuum to give the acetyl chloride as a colorless oil in quantitative yield.

Next, (*R*)-α-methoxy-α-(trifluoromethyl)phenylacetyl chloride was dissolved in DCM (40.0 mL) and diisopropyltriethylamine (DIPEA, 522 μL, 1.4 equiv) and 4-ethynilaniline (300.0 mg, 1.2 equiv) where added to the solution. The reaction mixture was stirred at rt overnight. The residue was diluted, and the organic solution was washed with HCl 1M, saturated $NaHCO_3$ aq. solution and saturated NaCl aq. solution. The solution was evaporated and the residue was chromatographed on silica gel with hexane-AcOEt (7/3, v/v) as eluent [590 mg M**2**, 82% yield of pure product].

Spectroscopic data:

^{1}H NMR (300 MHz, $CDCl_3$) δ (ppm): 3.06 (s, 1H), 3.49 (s, 3H), 7.41-7.49 (m, 5H), 7.55-7.59 (m, 4H), 8.61 (broad s, 1H).

^{13}C NMR (70 MHz, $CDCl_3$) δ (ppm): 55.2, 77.1, 83.1, 118.6, 119.5, 127.7, 128.8, 129.8, 131.9, 133.0, 137.1, 164.3.

^{19}F NMR (282.24 MHz, $CDCl_3$) δ (ppm): -68.57.

$[\alpha]_D^{20}$= +65 (15 mg mL^{-1}, $CHCl_3$)

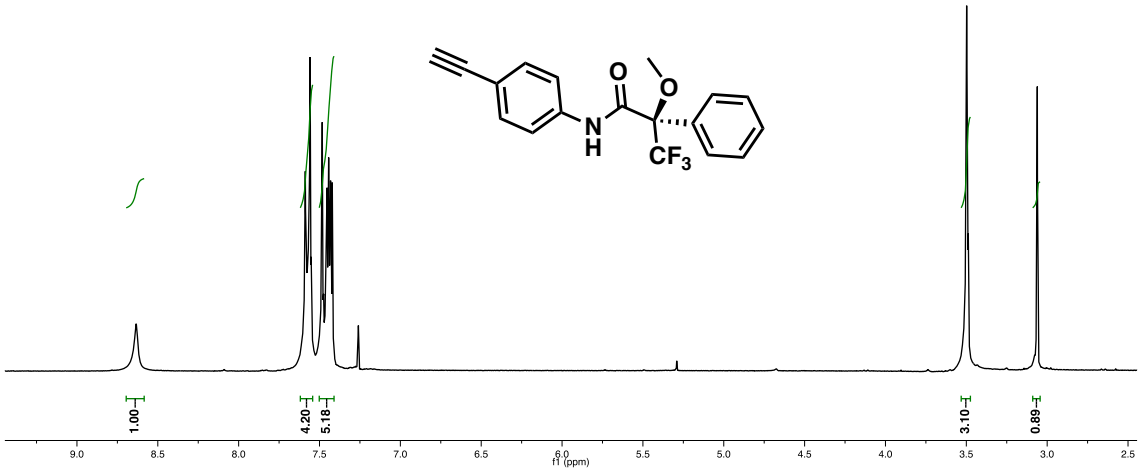

Figure S2. ^{1}H NMR of monomer M**2** in $CDCl_3$.

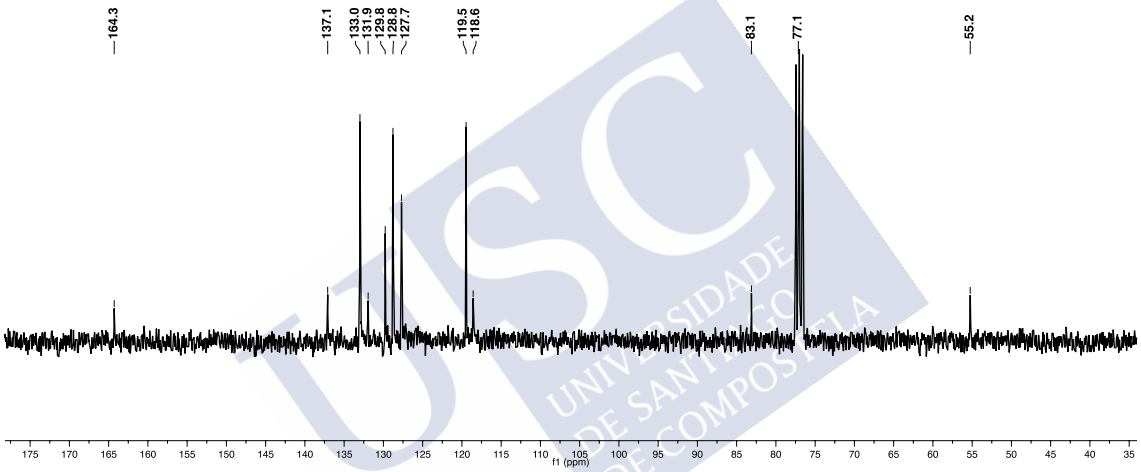

Figure S3. ^{13}C NMR of monomer M**2** in $CDCl_3$.

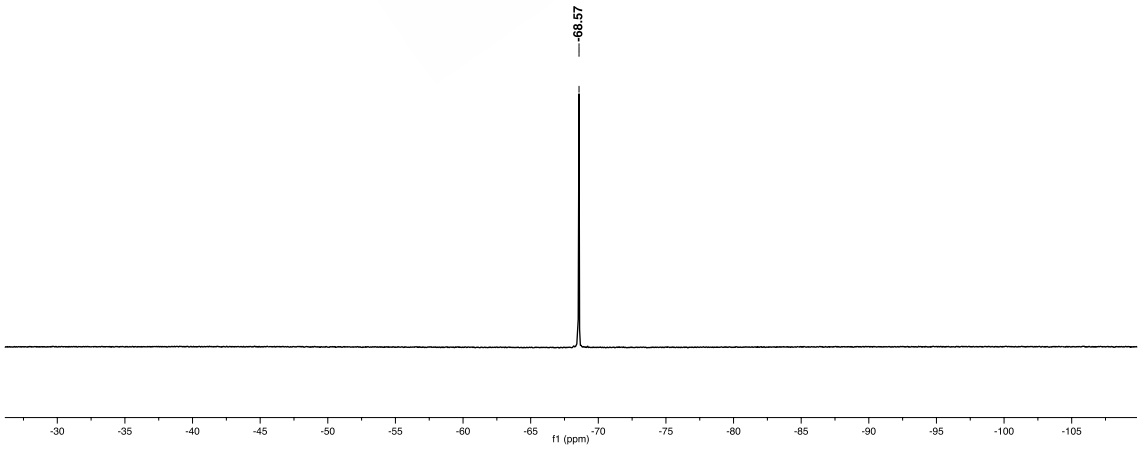

Figure S4. ^{19}F NMR of monomer M**2** in $CDCl_3$.

4. Synthesis of polymer poly-(*R*)-1 and poly-(*R*)-2

- **Synthesis of poly-(*R*)-1**

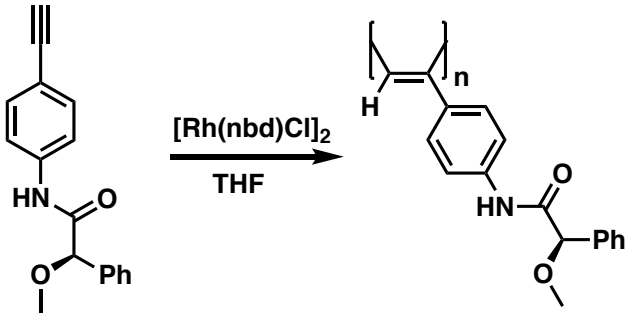

The general procedure for the synthesis of poly-(*R*)-**1** and poly-(*R*)-**2** can be found in references [S1] and [S2].

The reaction flask (sealed ample) was dried under vacuum and Ar flushed for three times before the corresponding monomer M**1** (100 mg) was added as a solid. Then, the flask was dried with a vacuum line and flushed with Ar (three times). Dry THF (0.75 mL) was added with a syringe and Et_3N dropwise. A solution of catalyst, $[Rh(nbd)Cl]_2$ (1.70 mg) was added at 30° C. The reaction mixture was stirred at 30° C for 24 h. The resulting polymer was diluted in CH_2Cl_2 and precipitated in a large amount of MeOH, centrifugated twice and reprecipitated using hexane and centrifugated again (90% of yield).

GPC data of poly-(*R*)-**1**: M_n: 65563, M_w: 150744, M_p: 150264, M_z: 273851, PDI: 2.29.

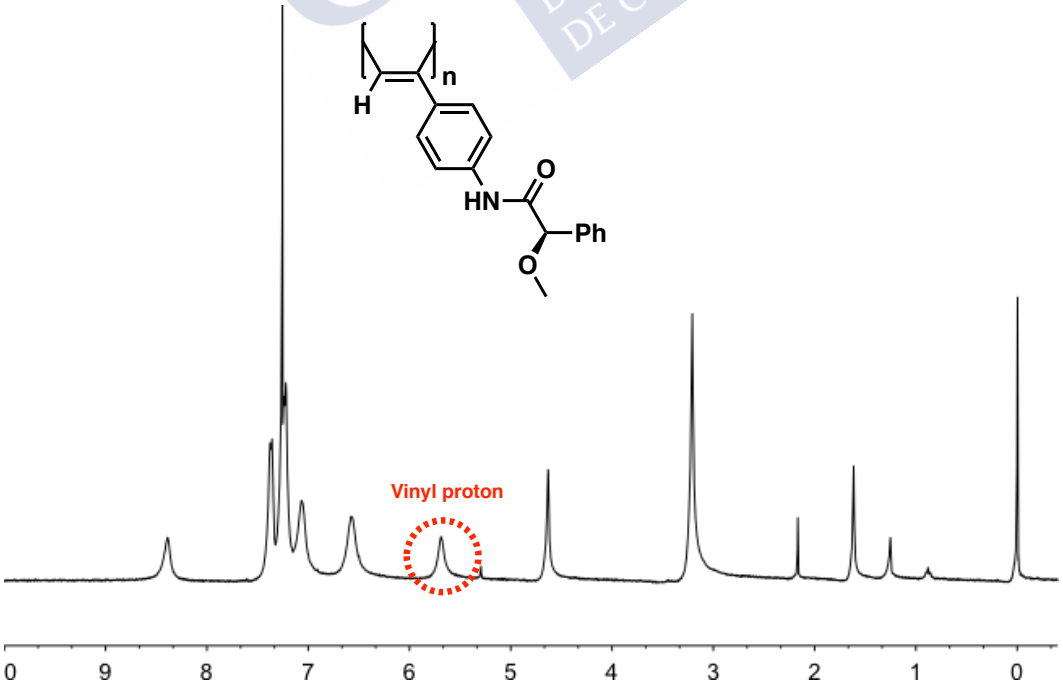

Figure S5. ^1H NMR spectrum of poly-(*R*)-**1** in $CDCl_3$.

- **Synthesis of poly-(*R*)-2**

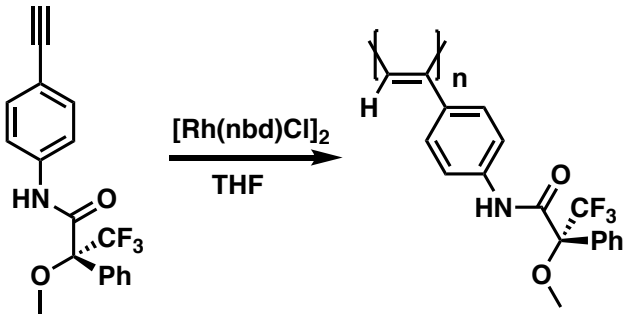

The reaction flask (sealed ample) was dried under vacuum and Ar flushed for three times before the corresponding monomer M**2** (75 mg) was added as a solid. Then, the flask was dried with a vacuum line and flushed with Ar (three times). Dry THF (0.5 mL) was added with a syringe and Et_3N dropwise. A solution of catalyst, $[Rh(nbd)Cl]_2$ (1.15 mg)] was added at 30^o C. The reaction mixture was stirred at 30^o C for 24 h. The resulting polymer was diluted in $CHCl_2$ and precipitated in a large amount of MeOH, centrifugated twice and reprecipitated using hexane and centrifugated again (87% of yield).

GPC data of poly-(*R*)-**2**: M_n: 84737, M_w: 178058, M_p: 182446, M_z: 342353, PDI: 2.10

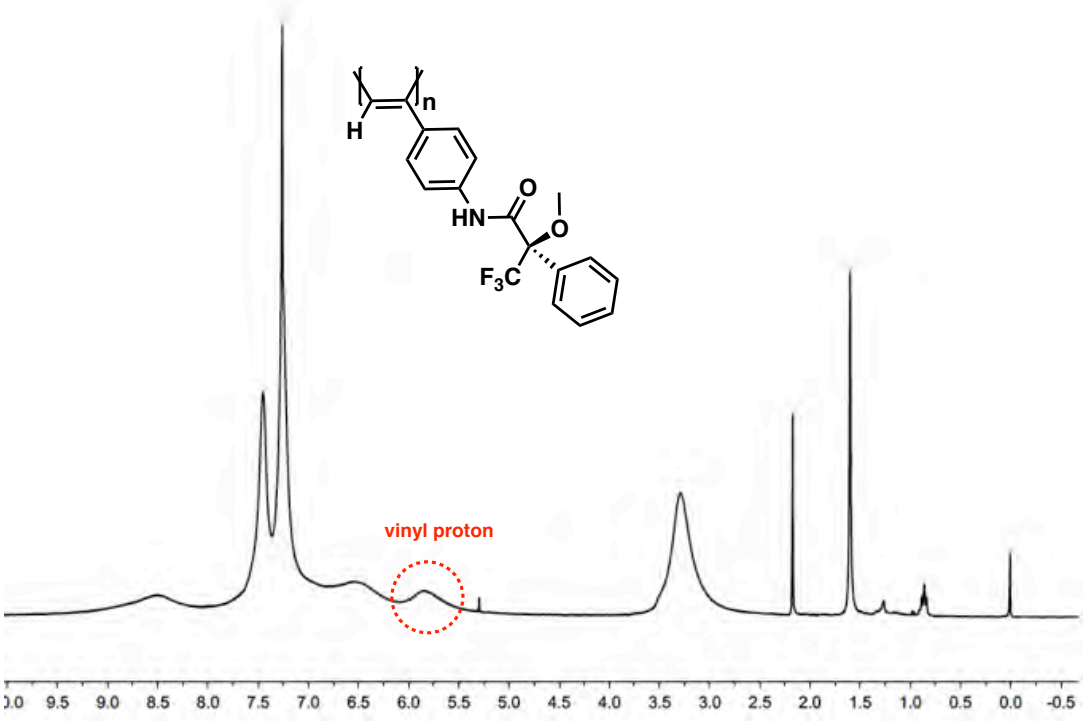

Figure S6. ^{1}H NMR spectrum of poly-(*R*)-**2** in $CDCl_3$.

5. CD and UV-Vis studies of poly-(*R*)-2 with monovalent and divalent metal ions

CD and UV-Vis studies were performed with a solution of poly-(*R*)-**2** $CHCl_3$ (0.3 mg mL^{-1}, $CHCl_3$) using different amounts of $AgClO_4$ (10 mg mL^{-1}, MeOH) as source of monovalent metal ion and $Ba(ClO_4)_2$ (10 mg mL^{-1}, MeOH) as source of divalent metal ion.

It was observed that the additions of Ag^+ and Ba^{2+} ions to poly-(*R*)-**2** do not promote a helical inversion preserving the same helical sense in poly-(*R*)-**2**.

Moreover, UV-Vis experiments have shown a bathochromic effect after addition of 0.5 equiv of Ag^+ (10 mg mL^{-1}, MeOH) ions to poly-(*R*)-**2** (0.3 mg mL^{-1}, $CHCl_3$).

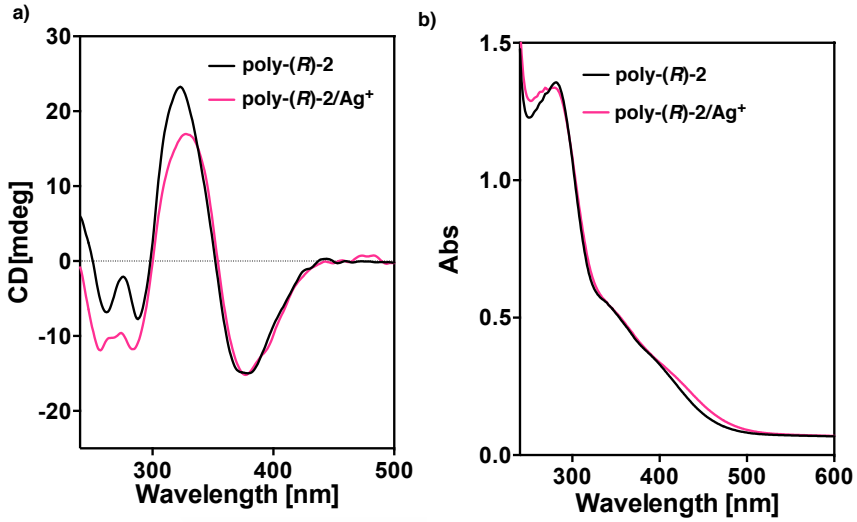

Figure S7. a) CD studies of poly-(*R*)-**2** and poly-(*R*)-**2**/Ag^+ complex. b) UV-Vis studies of poly-(*R*)-**2** and poly-(*R*)-**2**/Ag^+ complex.

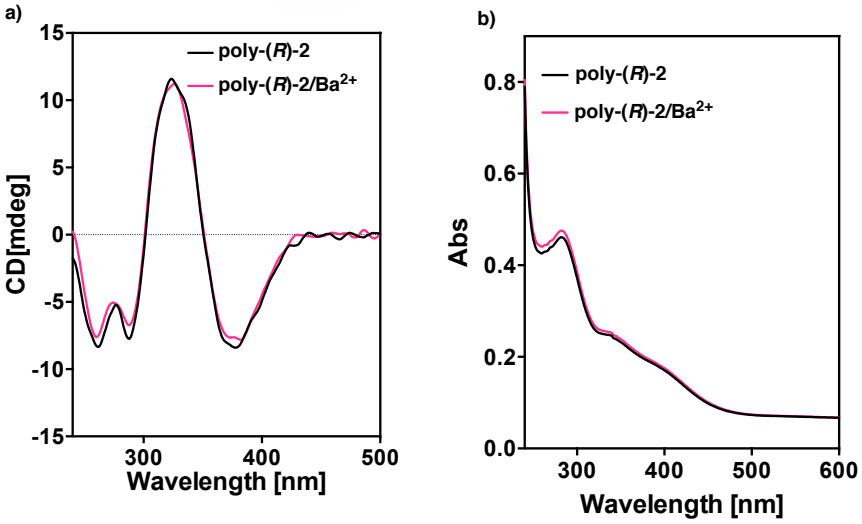

Figure S8. a) CD studies of poly-(*R*)-**2** and poly-(*R*)-**2**/Ba^{2+} complex. b) UV-Vis studies of poly-(*R*)-**2** and poly-(*R*)-**2**/Ba^{2+} complex.

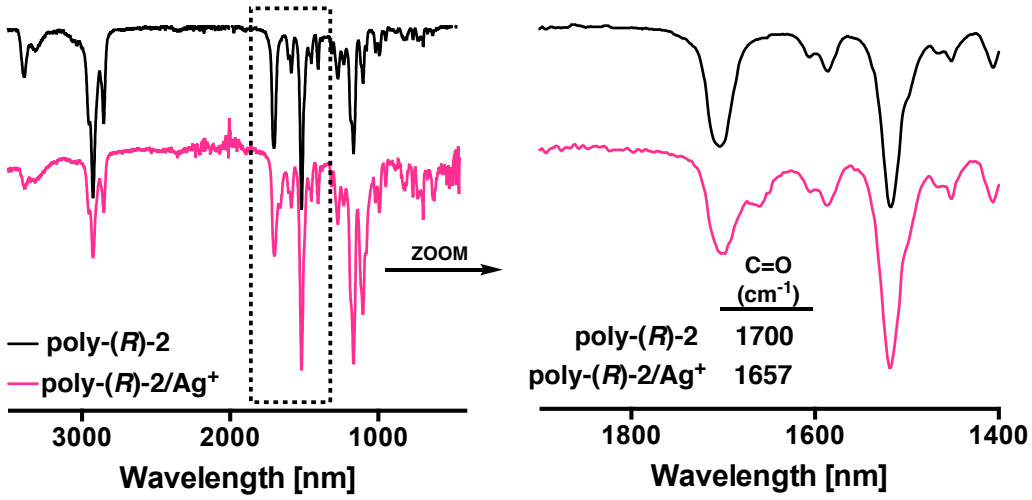

Figure S9. FT-IR studies of poly-(*R*)-**2** and poly-(*R*)-**2**/Ag^+ complex.

6. General procedure for the synthesis of poly-1-AgNPs and poly-(*R*)-2-AgNPs

Poly-(*R*)-**1**-AgNPs and poly-(*R*)-**2**-AgNPs were prepared according to this procedure. First, all the glassware was washed with aqua regia, Milli Q water and acetone. The reactions were carried out at rt and using an Ar atmosphere.

Poly-(*R*)-**1** (or poly-(*R*)-**2**) was dissolved in $CHCl_3$ (0.3 mg mL^{-1}) and then, $AgClO_4$ (0.5 equiv) in MeOH was added to form the poly-(*R*)-**1**/Ag^+ complexes. Next, $NaBH_4$ (1.0 equiv, 1.0 mg mL^{-1}, MeOH) was added to form AgNPs. Finally, 1-dodecanethiol was added to the dispersion of AgNPs.

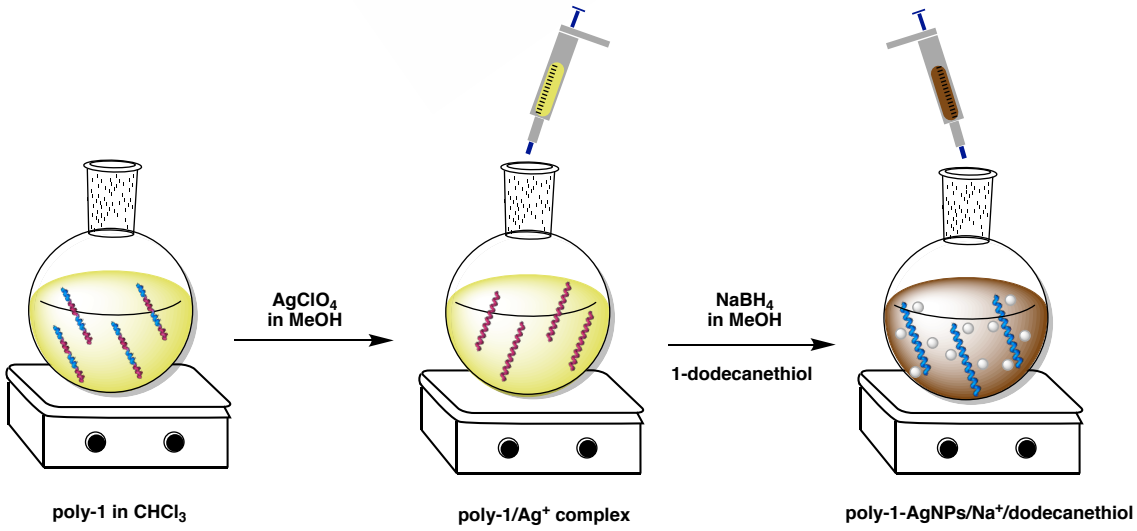

Scheme S1. Schematic representation of the synthesis of poly-**1**-AgNPs or poly-(*R*)-**2**-AgNPs hybrid materials.

7. ^{1}H NMR of poly-1-AgNPs

The *cis* stereoregularity of the poly-(*R*)-**1**-AgNPs was determined by ^{1}H NMR where the vinyl proton resonance appears at 5.7 ppm.

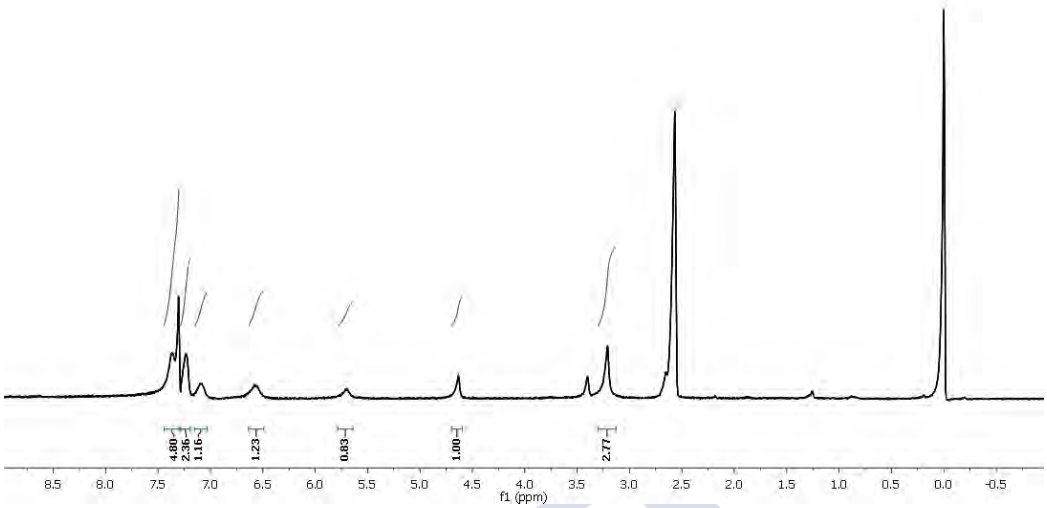

Figure S10. ^{1}H NMR of poly-(*R*)-**1**-AgNPs in $CDCl_3$.

8. FT-IR studies of poly-(*R*)-1-AgNPs and poly-(*R*)-2-AgNPs

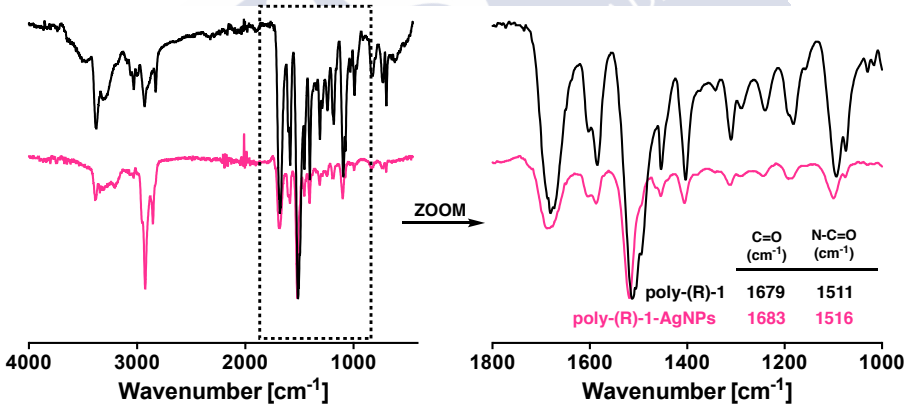

Figure S11. FT-IR spectra of poly-(*R*)-**1** and poly-(*R*)-**1**-AgNPs

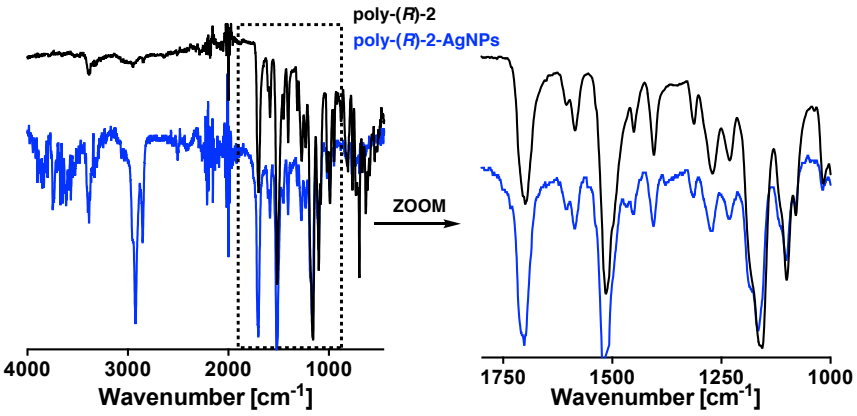

Figure S12. FT-IR spectra of poly-(*R*)-**2** and poly-(*R*)-**2**-AgNPs

9. Synthesis of poly-1-AgNPs in different solvents

Following the general procedure, poly-(*R*)-**1**-AgNPs nanocomposites were prepared using different polar and low-polar solvents.

- **Synthesis in THF**

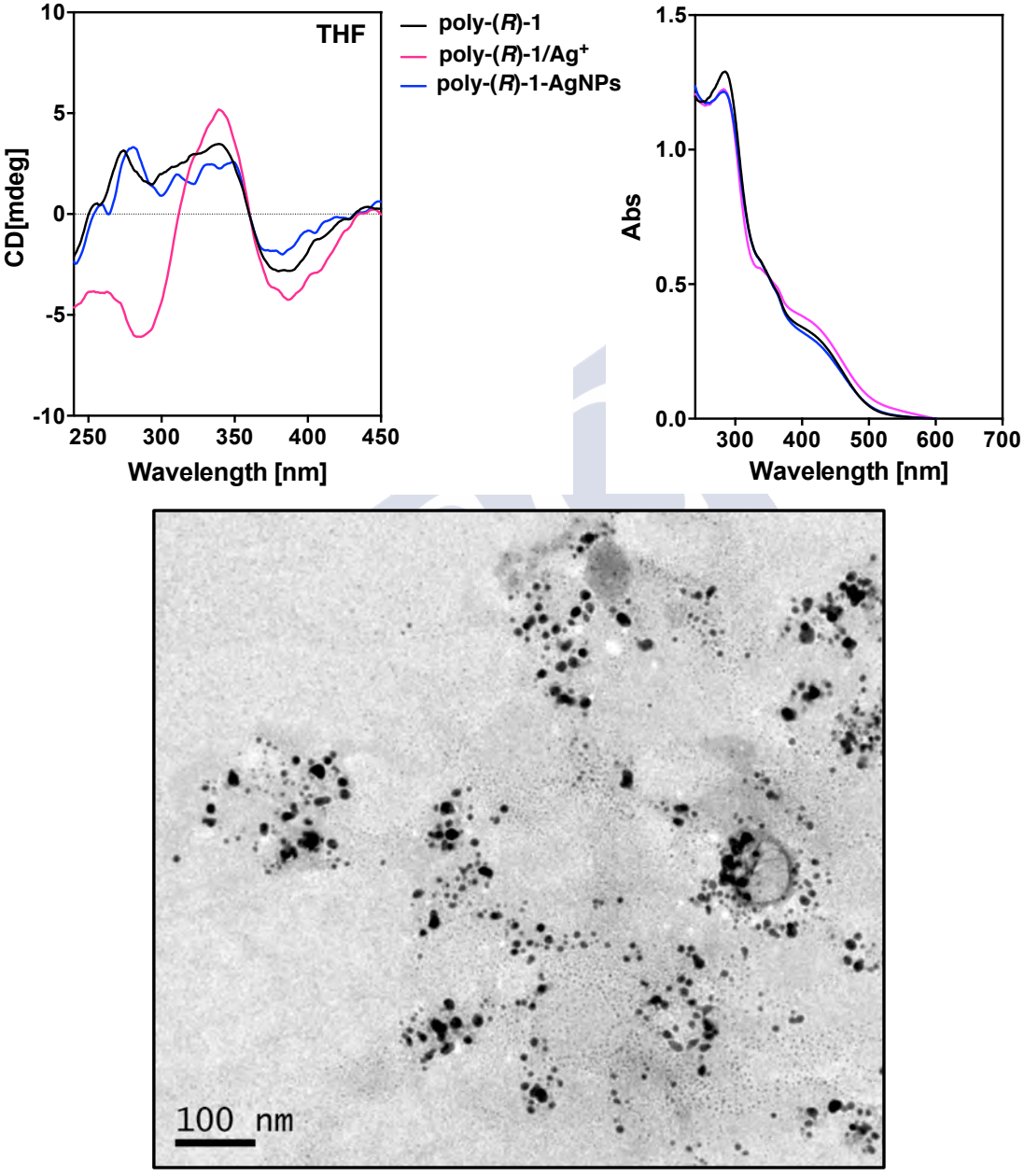

Figure S13. CD, UV-Vis spectra and TEM images of poly-**1**-AgNPs (0.3 mg mL^{-1}) in THF.

- **Synthesis in dioxane**

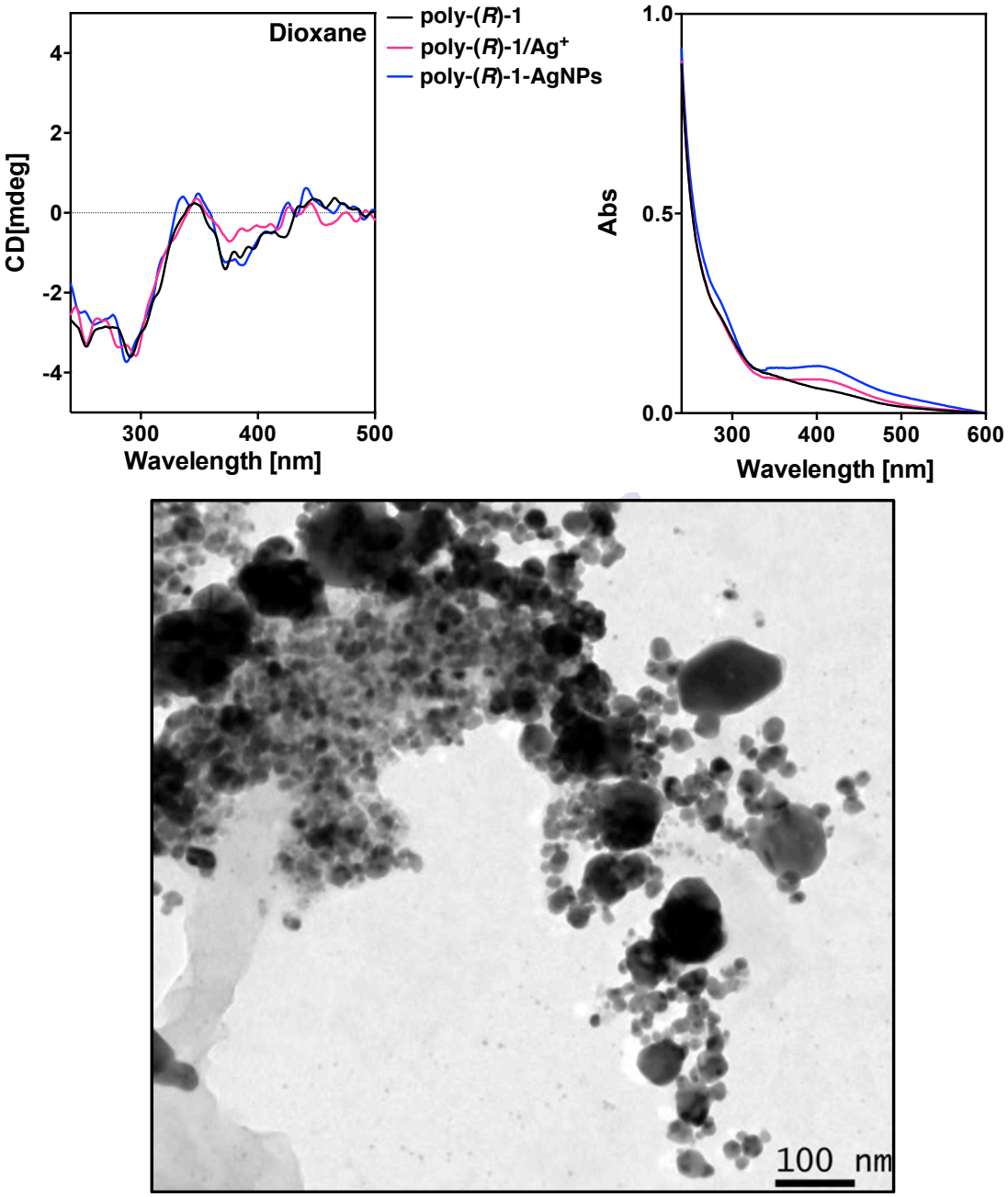

Figure S14. CD, UV-Vis spectra and TEM images of poly-**1**-AgNPs (0.3 mg mL^{-1}) in dioxane.

- **Synthesis in DMSO**

c)

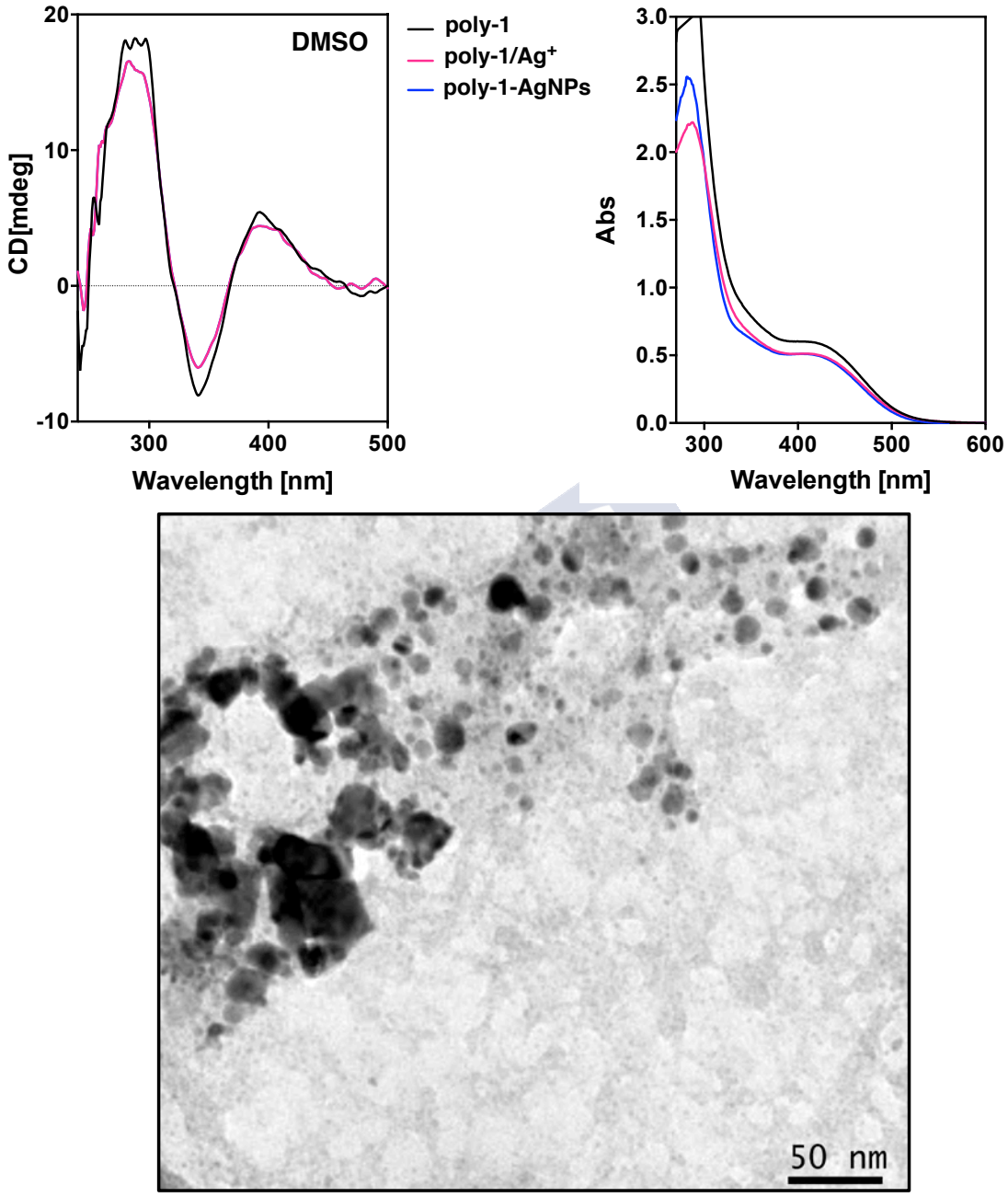

Figure S15. CD, UV-Vis spectra and TEM images of poly-**1**-AgNPs (0.3 mg mL^{-1}) in DMSO.

- **Synthesis in dichloromethane**

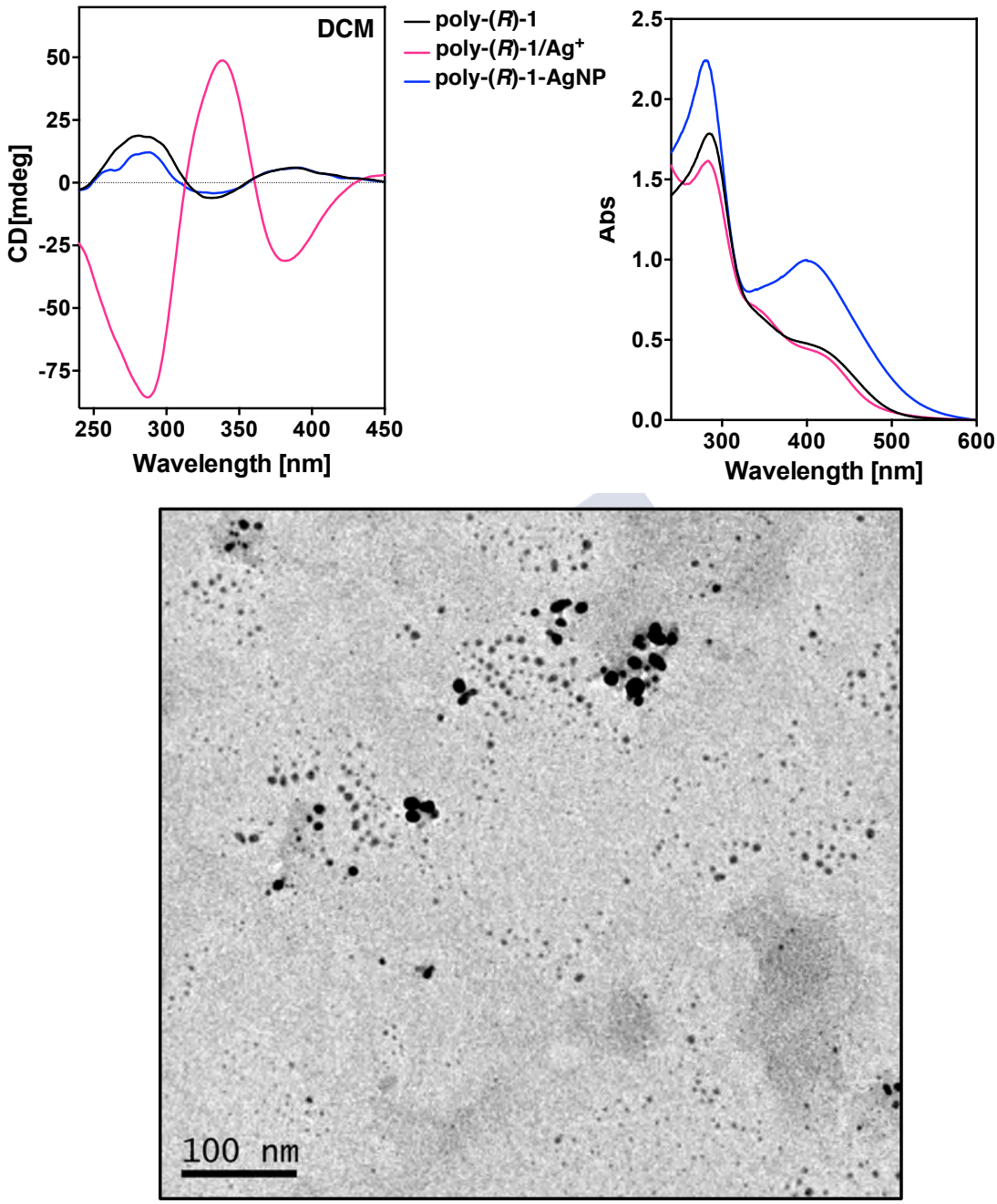

Figure S16. CD, UV-Vis spectra and TEM images of poly-**1**-AgNPs (0.3 mg mL^{-1}) in DCM.

- **Synthesis in acetone**

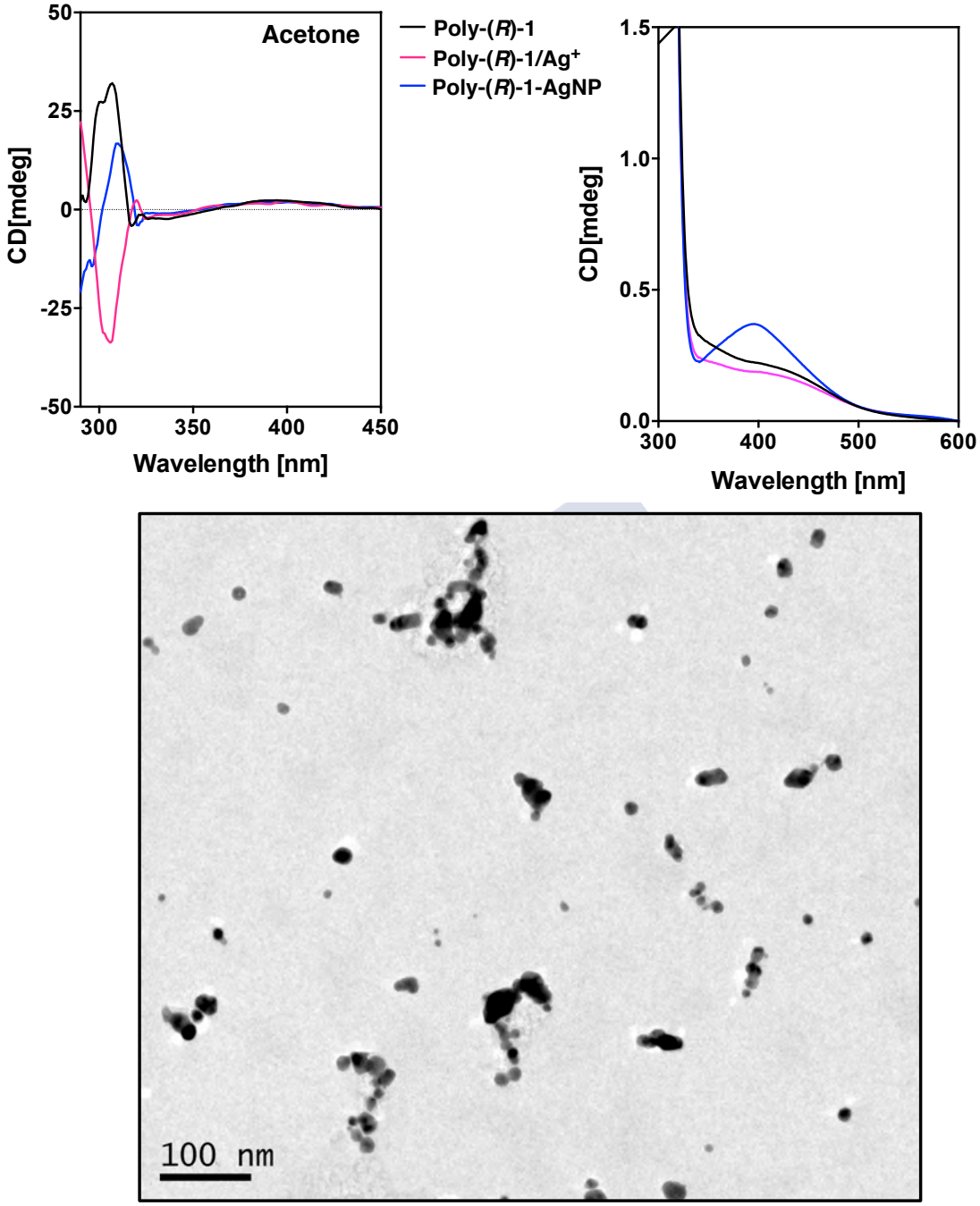

Figure S17. CD, UV-Vis spectra and TEM images of poly-**1**-AgNPs (0.3 mg mL^{-1}) in acetone.

- **Synthesis in DMF**

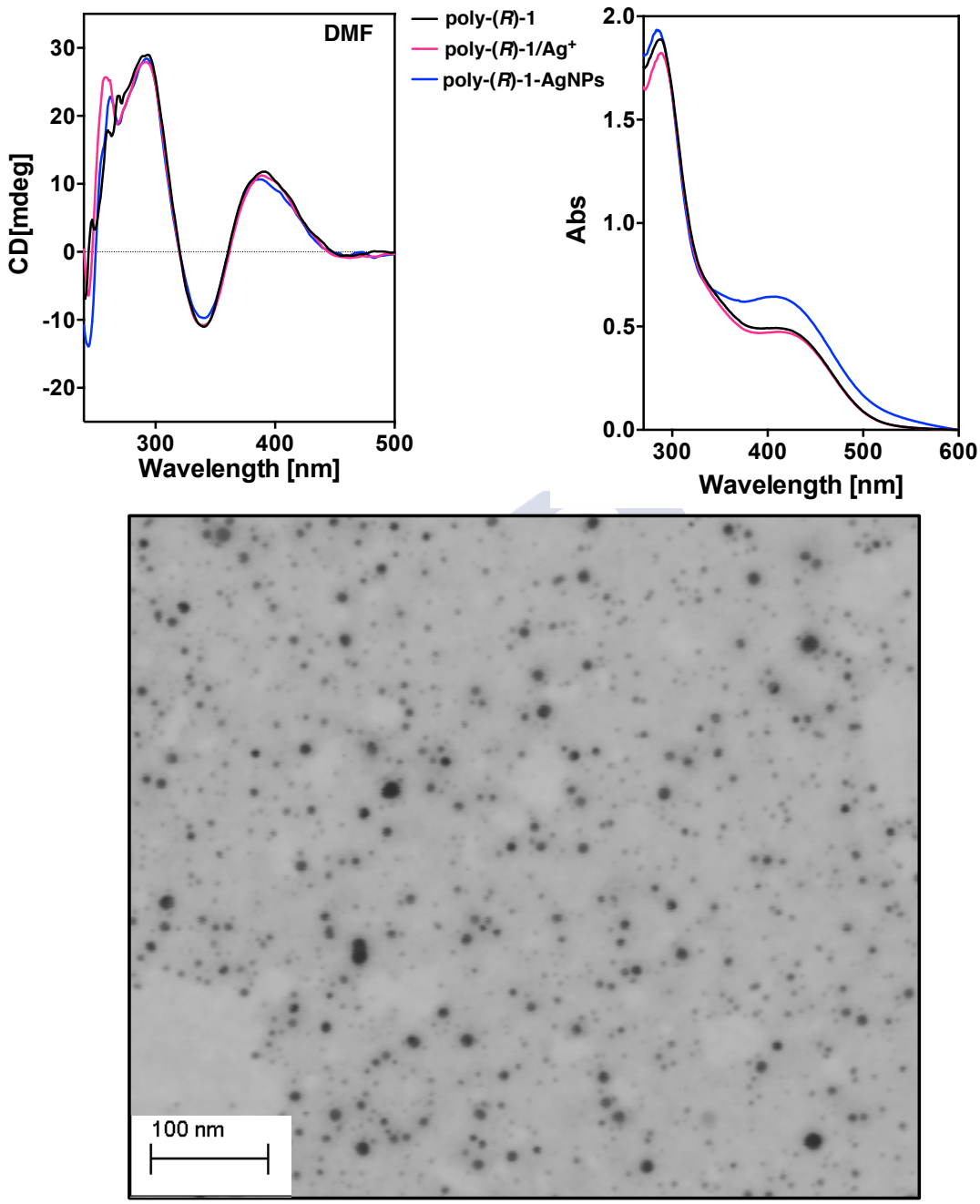

Figure S18. CD, UV-Vis spectra and TEM images of poly-**1**-AgNPs (0.3 mg mL^{-1}) in DMF.

10. CD and UV-Vis studies of poly-1-AgNPs/metal ion interactions

The addition of monovalent metal ions (10.0 mg mL^{-1} in MeOH) to poly-**1**-AgNPs (0.3 mg mL^{-1} in $CHCl_3$) promotes an *ap* conformation [dihedral angle for (C=O—C—OMe) 180° ca] in the pendant group leading to a left-handed helical sense due to the chelation of the monovalent ions to the carbonyl group and the presence of M^+-π interaction.

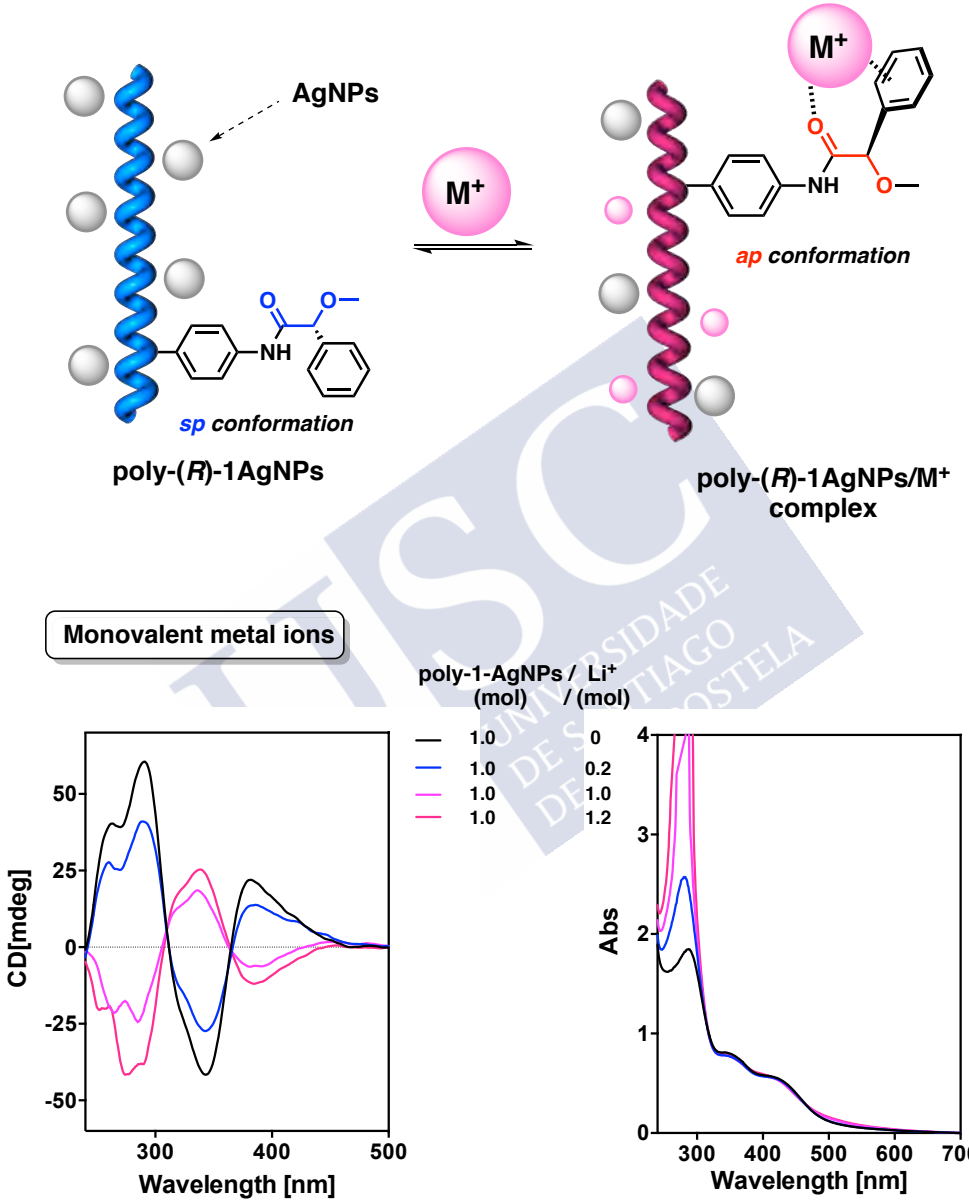

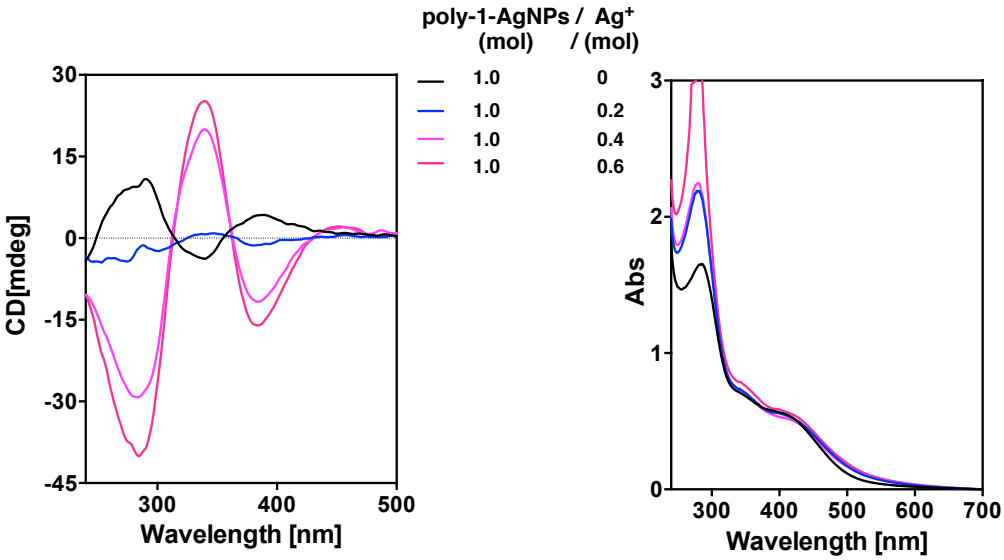

Figure S19. CD and UV-Vis studies of poly-(*R*)-**1**-AgNPs in presence of monovalent metal ions.

The addition of divalent metal ions (10 mg mL^{-1} in MeOH) to poly-**1**-AgNPs (0.3 mg mL^{-1} in $CHCl_3$) promotes a *sp* conformation [dihedral angle for (C=O—C—OMe) 0^{o} ca] in the pendant group leading to a right-handed helical sense due to the coordination of the divalent ions to carbonyl and methoxy groups.

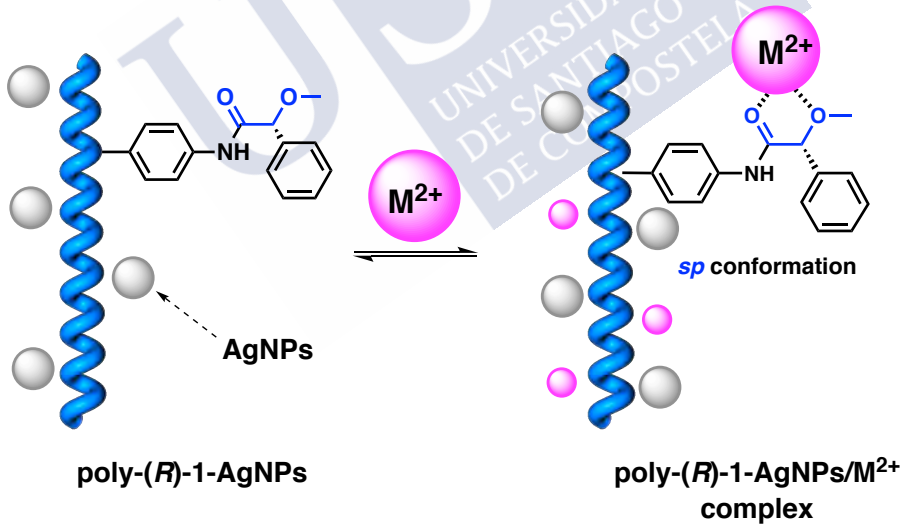

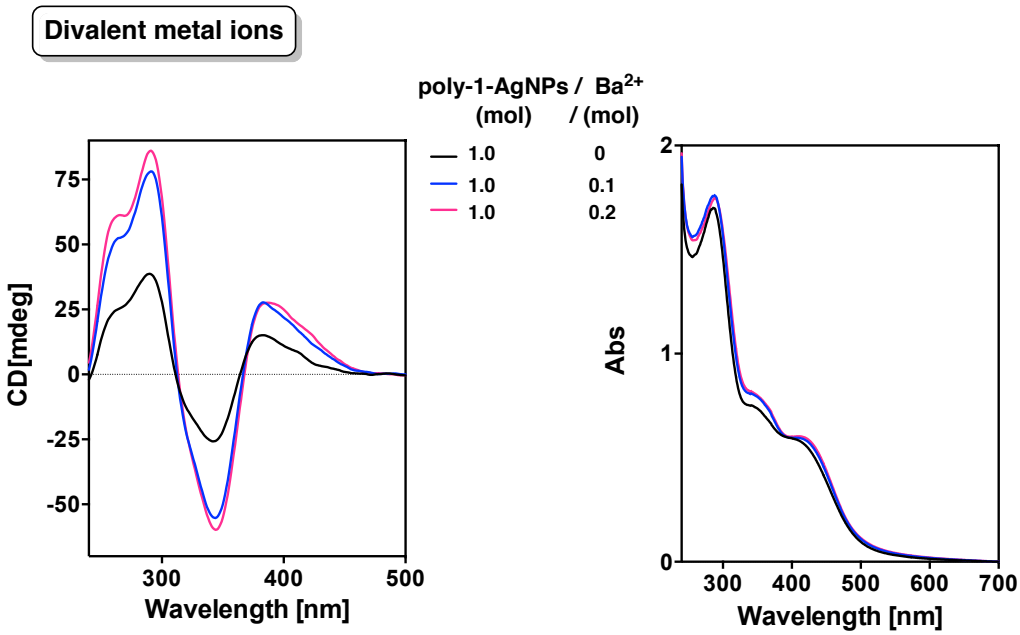

Figure S20. CD and UV-Vis studies of poly-(*R*)-**1**-AgNPs in presence of divalent metal ions.

11. Microscopy studies of poly-1-AgNPs: SEM and TEM images

SEM measurements were performed on a LEO-435VP electron microscope equipped with an energy dispersive X-ray (EDX) spectrometer.

TEM measurements were performed on a JEOL JEM 2010 and 200 KV as a voltage.

A solution of poly-(*R*)-**1**-AgNPs (0.3 mg mL^{-1}) was drop casted onto of silicon wafer chip and allowed to dry at rt for 12h and SEM images was carried out.

For TEM studies, a drop solution of poly-(*R*)-**1**-AgNPs (0.3 mg mL^{-1}) was settled onto carbon chip and allowed to dry at rt for 12 h.

During these studies, the presence of AgNPs (size: 2.8 $\pm$ 0.5 nm) with a lineal distribution was observed.

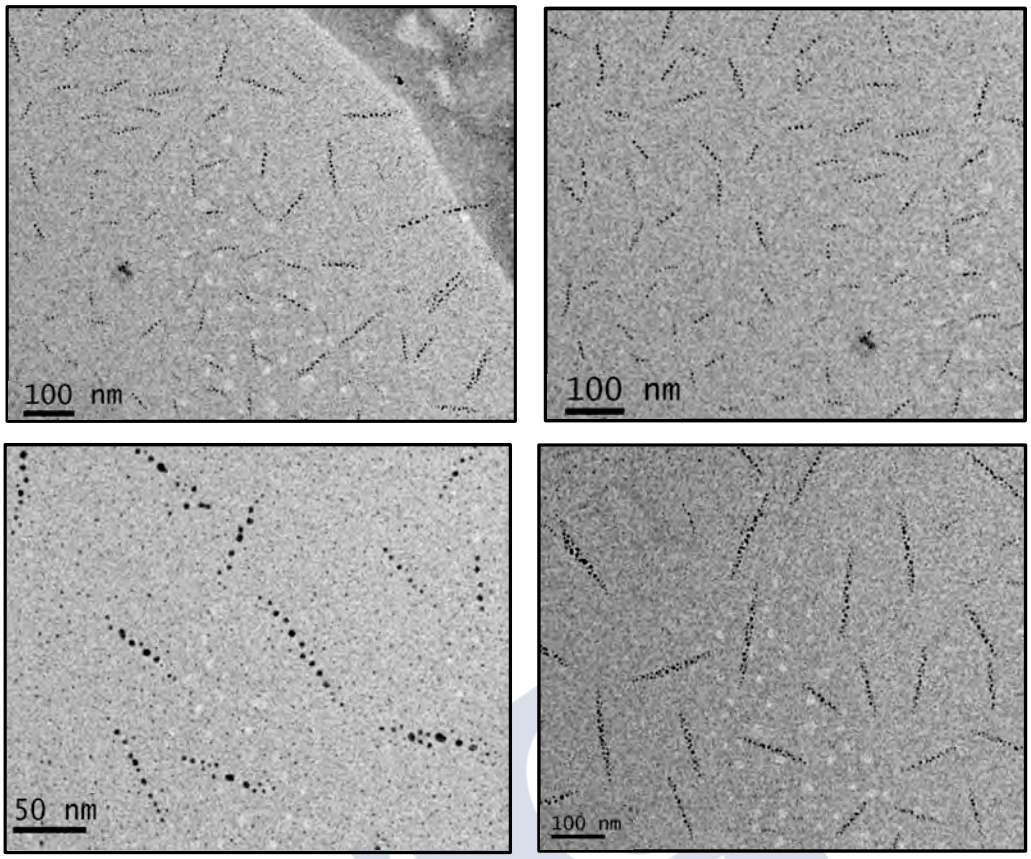

Figure S21. TEM images of poly-(*R*)-**1**-AgNPs with lineal distribution (size: 2.8 ± 0.5 nm)

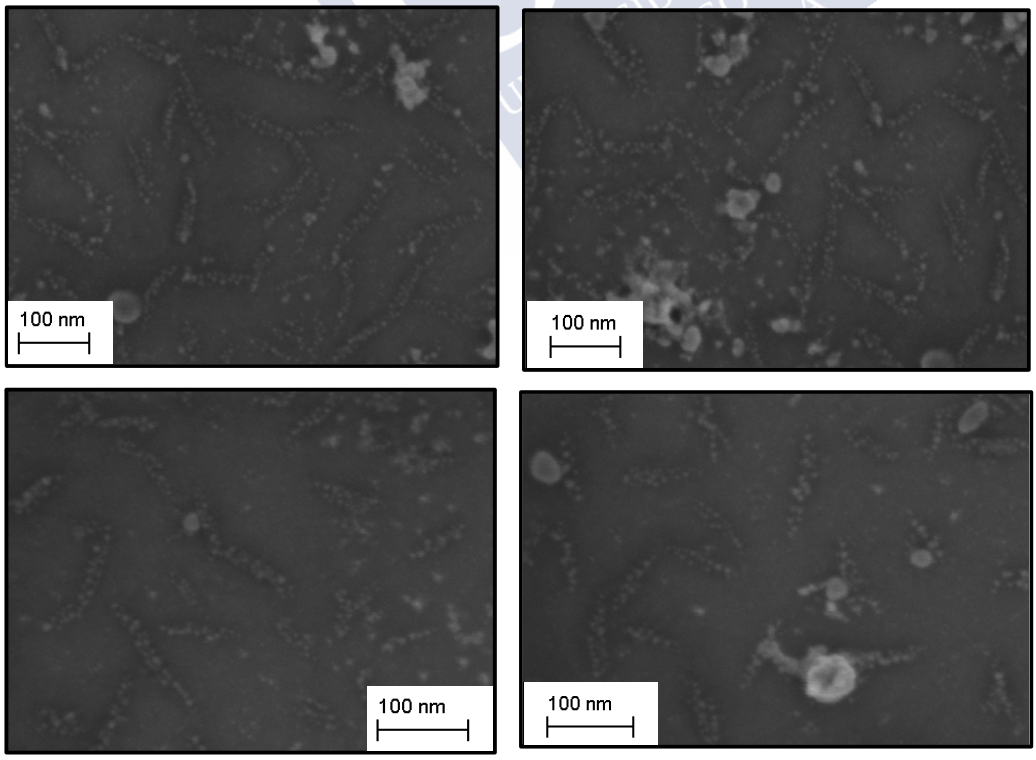

Figure S22. SEM images of poly-**1**-AgNPs with lineal distribution.

12. Stability of poly-(*R*)-1-AgNPs/Na^+ with time

The stability of poly-(*R*)-**1**-AgNPs/Na^+ nanocomposites were studied by UV-Vis experiments at different times. Poly-(*R*)-**1**-AgNPs/Na^+ (0.3 mg mL^{-1}, $CHCl_3$) showed a decrease in the LSPR band intensity indicating that the AgNPs aggregated with time.

The stability of the AgNPs in the nanocomposite was improved by adding 1-dodecanethiol (0.2 equiv) to poly-(*R*)-**1** after formation of AgNPs. UV-Vis spectra recorded at different times showed the same LSPR band intensity.

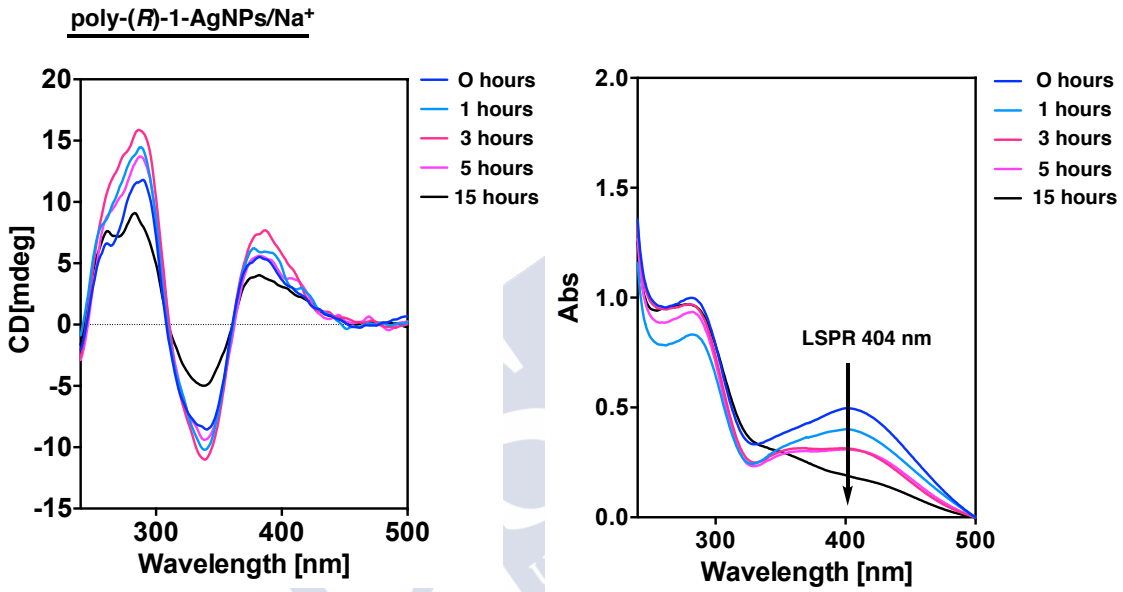

Figure S23. CD and UV-Vis for poly-(*R*)-**1**-AgNPs/Na^+ (0.3 mg mL^{-1}, $CHCl_3$) at different times.

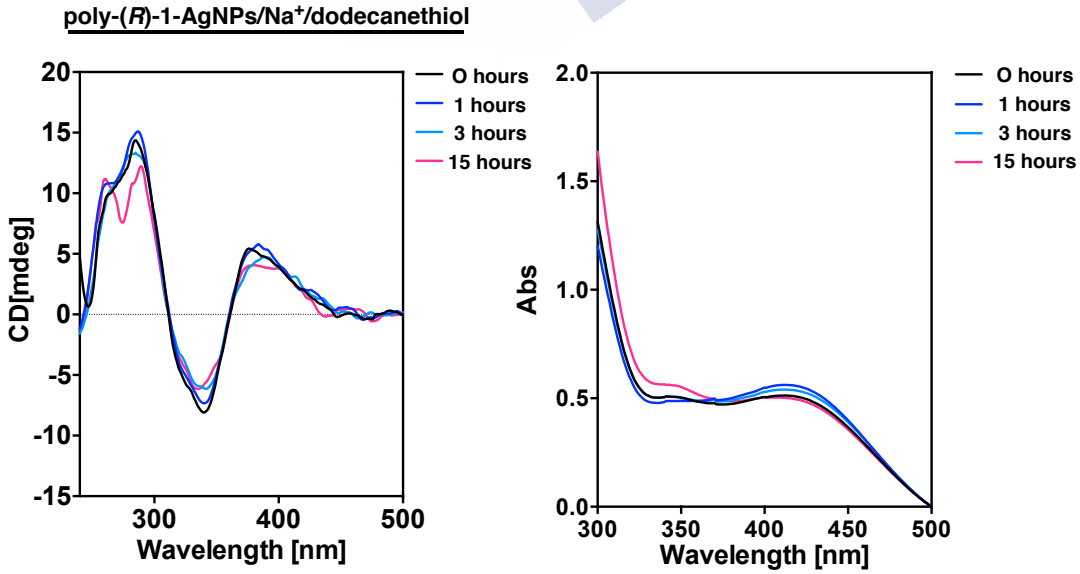

Figure S24. CD and UV-Vis for poly-(*R*)-**1**-AgNPs/Na^+ (0.3 mg mL^{-1}, $CHCl_3$) at different times after addition of 1-dodecanethiol.

13. TEM images of poly-(*R*)-1-AgNPs/Na^+/dodecanethiol

TEM measurements were performed on a JEOL JEM 2010 and 200 KV as a voltage. A drop solution of poly-(*R*)-**1**-AgNPs/Na^+/dodecanethiol (0.3 mg mL^{-1}) was settled onto carbon chip and allowed to dry at rt for 12 h.

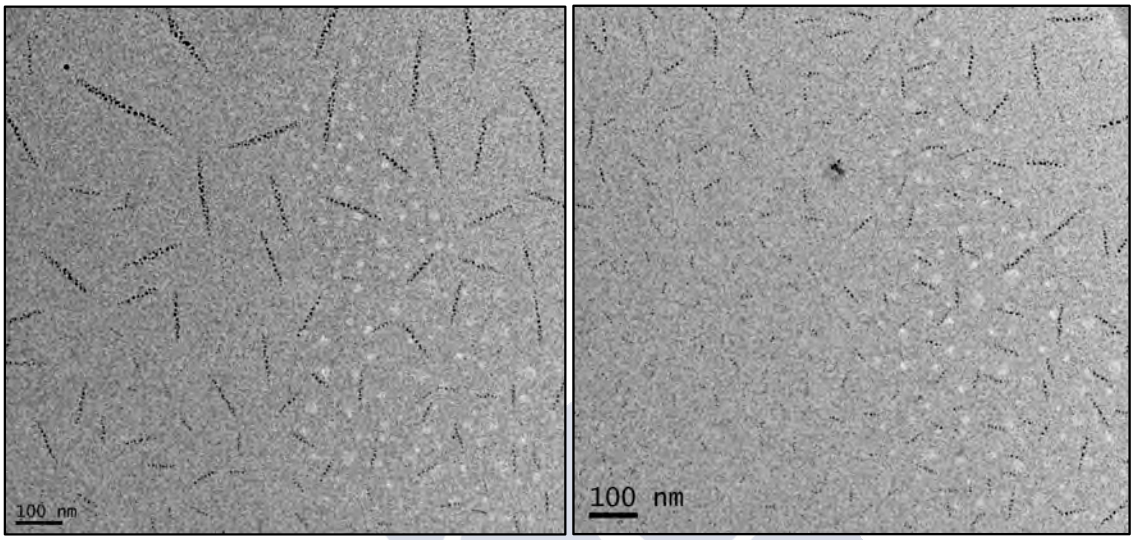

Figure S25. TEM images of poly-(*R*)-**1**-AgNPs/Na^+/dodecanethiol with lineal distribution

14. Microscopy studies of poly-2-AgNPs: TEM images

TEM measurements were performed on a JEOL JEM 2010 and 200 KV as a voltage. A drop solution of poly-**2**-AgNPs (0.3 mg mL^{-1}) was settled onto carbon chip and allowed to dry at rt for 12 h.

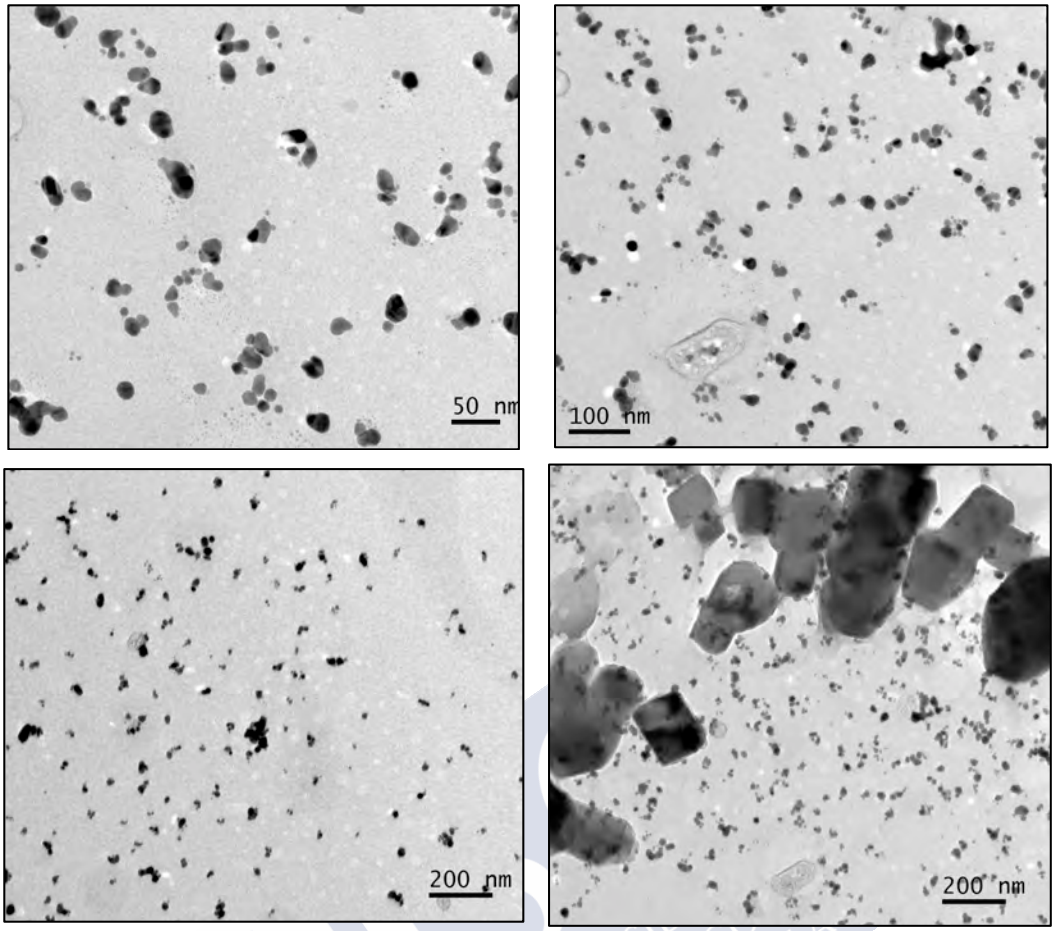

Figure S26. TEM images of poly-(*R*)-**2**-AgNPs

15. Formation of poly-(*R*)-1-AgNPs using $LiBH_4$

Following the general procedure, poly-(*R*)-**1**-AgNPs/Li^+ nanocomposites were prepared using $LiBH_4$ as a reducing agent. First, all the glassware was washed with aqua regia, Milli Q water and acetone. The reaction was carried out at rt under an Ar atmosphere.

Polymer poly-(*R*)-**1** was dissolved in $CHCl_3$ (0.3 mg mL^{-1}) and then, $AgClO_4$ (0.5 equiv) in MeOH was added to form the poly-(*R*)-**1**/Ag^+ complexes where the pendant groups adopt an *ap* conformation due to silver ions complexed with the carbonyl groups. Finally, $LiBH_4$ (1 equiv) in MeOH was added to form AgNPs. In this case, the CD spectra showed a negative Cotton effect indicating the complexation of the Li^+ ions to the carbonyl groups and the presence of Li^+-π interactions.

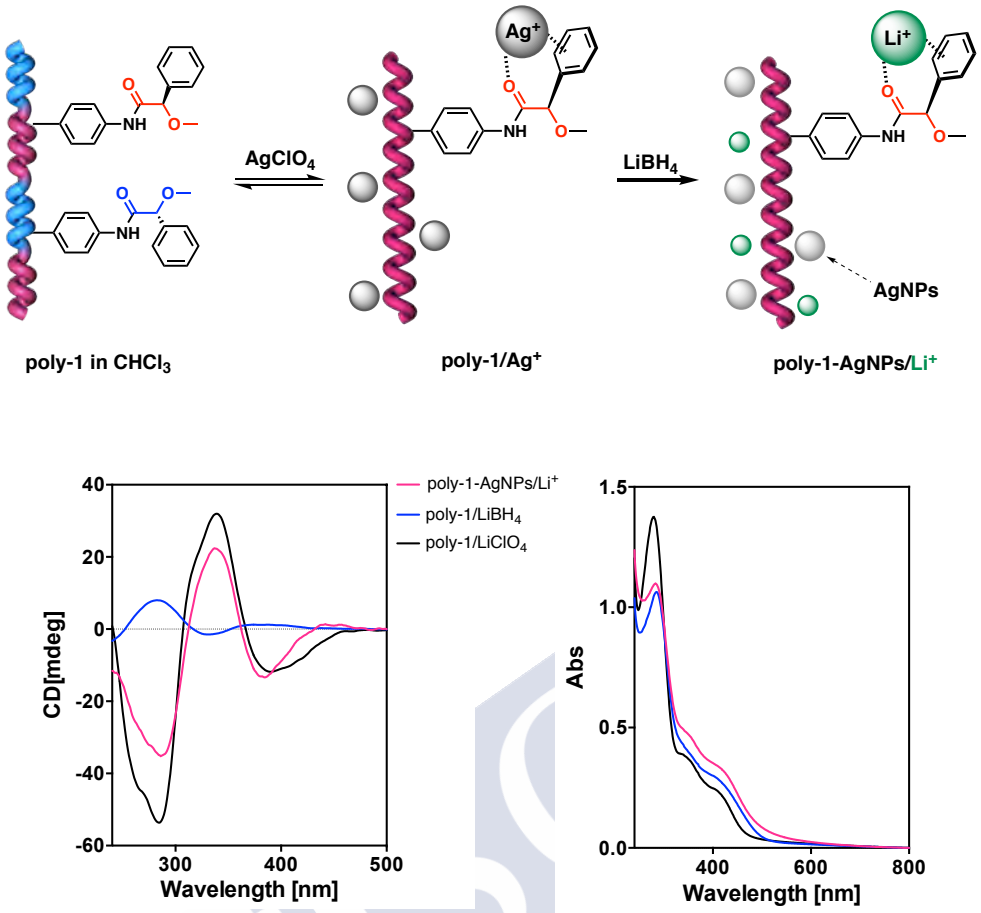

Figure S27. Role of $LiBH_4$ in the helical sense of poly-(*R*)-**1**.

16. Effect of $NaBH_4$ in the helical sense of poly-(*R*)-1-AgNPs/Na^+

The influence of $NaBH_4$ in the helical sense of poly-(*R*)-**1**-AgNPs was studied by CD and UV-Vis experiments. Following the general procedure, poly-(*R*)-**1**-AgNPs/Na^+ were prepared using $NaBH_4$ as a reducing agent. CD experiments shows a positive Cotton effect indicating a *sp* conformation between carbonyl and methoxy group in the *pendant* group.

$NaBH_4$ (1 equiv, 10 mg mL^{-1}) was added to poly-(*R*)-**1** as control experiment. CD experiments showed a null Cotton effect in the vinylic region (380 nm) indicating the absence of interaction between poly-(*R*)-**1** and $NaBH_4$.

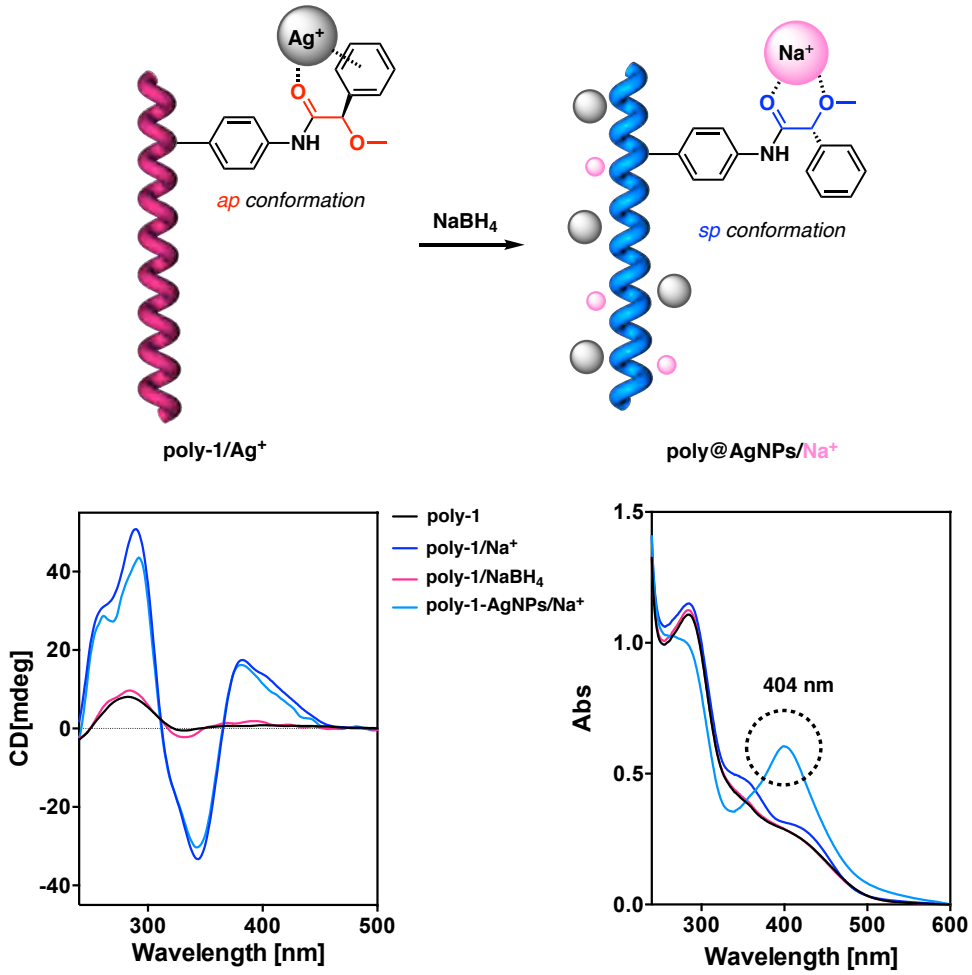

Figure S28. Influence of the $NaBH_4$ in the helical sense of poly-(*R*)-**1**-AgNPs.

17. Role of Na^+ cations in the helicity of poly-(*R*)-1-AgNPs/Na^+

CD experiments showed a negative Cotton Effect when Ag^+ (0.5 equiv, 10 mg mL^{-1}) in MeOH was added to a solution of poly-(*R*)-**1** (0.3 mg mL^{-1}) in $CHCl_3$. These experiments confirmed the presence of left-handed helices due to the chelation of Ag^+ ions to the carbonyl groups and the presence of Ag^+-π interaction.[S3]

On the other hand, CD experiments showed a positive Cotton Effect when $NaBH_4$ (1 equiv, 1 mg mL^{-1}) was added to a solution of poly-(*R*)-**1**/Ag^+ complex (0.3 mg mL^{-1}) to form poly-(*R*)-**1**-AgNPs/Na^+.

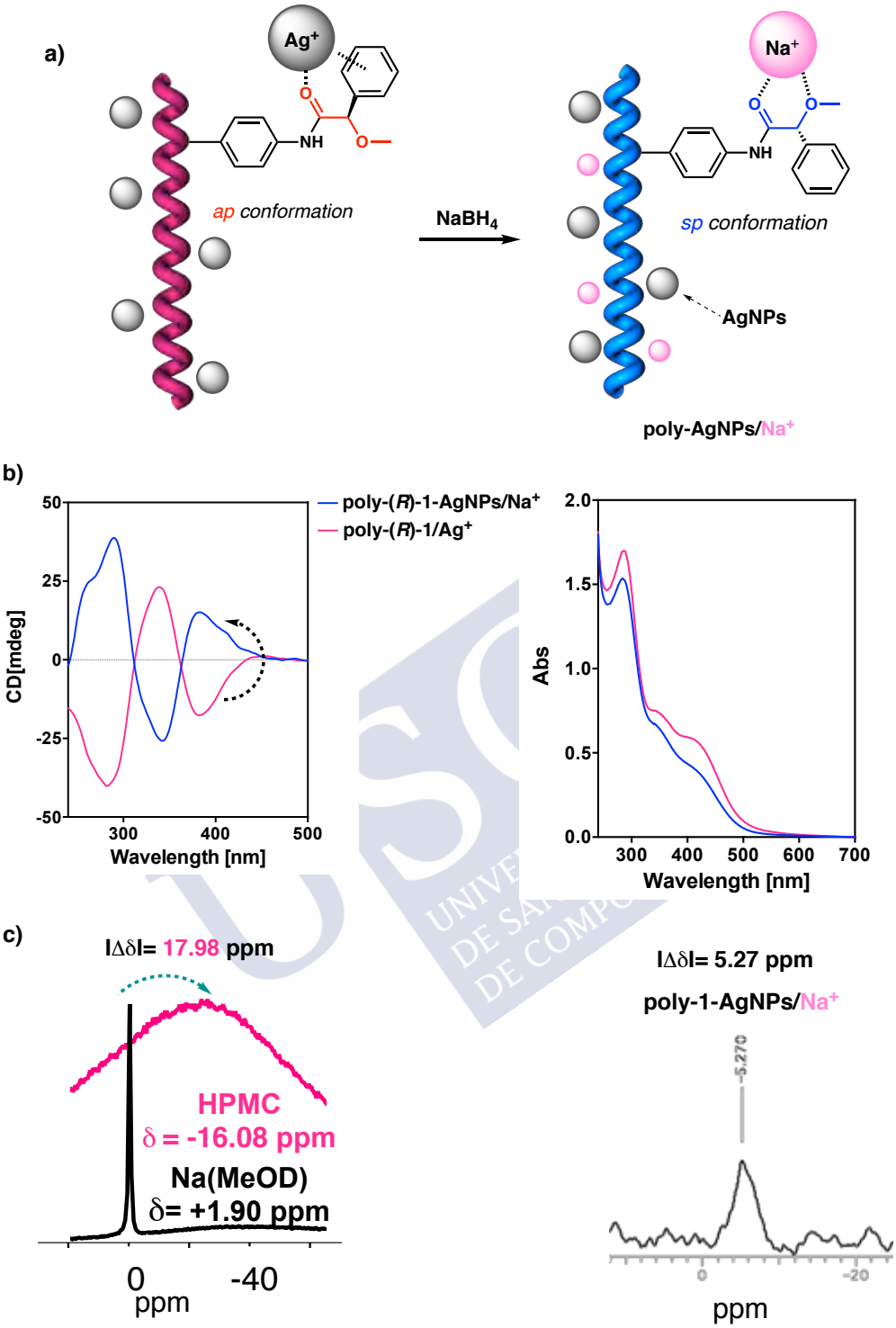

Figure S29. a) Schematic representation of the role of $NaBH_4$ in the helical sense of poly-(*R*)-**1**-AgNPs/Na^+. b) CD and UV-Vis spectra of poly-(*R*)-**1**/Ag^+ and poly-(*R*)-**1**-AgNPs/Na^+. c) ^{23}Na NMR of poly-(*R*)-**1**-AgNPs/Na^+ showing the absence of Na^+-π interaction.

18. Experiments with metal scavenger resins

Commercially available Quadrapure™ (Aldrich) resins (MPA, TU, IDA) were employed as metal scavenger resins. These resins contain different functional groups that interact with metal ions. The TU resin contains a thiourea functional group, IDA possess an imino diacetate group and the MPA resin a mercaptophenyl amino group.

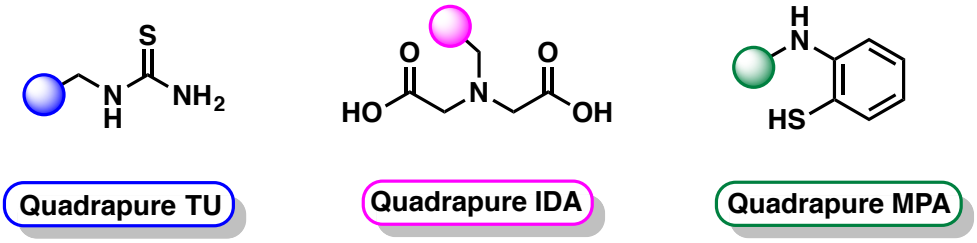

Figure S30. Chemical structure of metal scavenger resins (Quadrapure TU, IDA, MPA).

To carry out these experiments, the resins were swollen in $CHCl_3$ for 1h (0.05 g mL^{-1}). Next, 100 mg of resin were added to a solution of poly-(*R*)-**1**-AgNPs/Na^+ (0.3 mg mL^{-1} in $CHCl_3$). After 30 min, the CD and UV-Vis spectra confirmed that Na^+ ions promoted the helical sense in poly-(*R*)-**1**-AgNPs/Na^+.

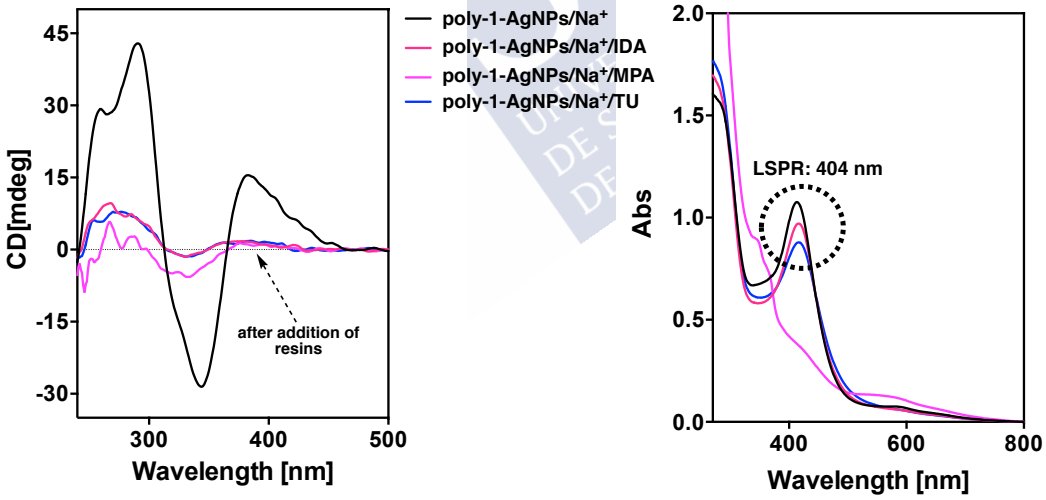

Figure S31. CD and UV-Vis spectra of poly-(*R*)-**1**-AgNPs/Na^+ in presence of resins metal scavengers (MPA, TU and IDA).

19. Formation of chiral nanospheres using poly-(*R*)-1-AgNPs/dodecanethiol and monovalent and divalent metal ions

The addition of Ag^+ (10 mg mL^{-1}) in MeOH to a solution of poly-(*R*)-**1**-AgNPs/dodecanethiol (0.3 mg mL^{-1}) in $CHCl_3$ produces left-handed helices indicating the chelation of Ag^+ ions to the carbonyl group and the presence of Ag^+-π interactions.

SEM measurements showed the formation of low polydisperse polymeric nanospheres due to the ability of the metal ions to act as crosslinking agents between polymer chains.

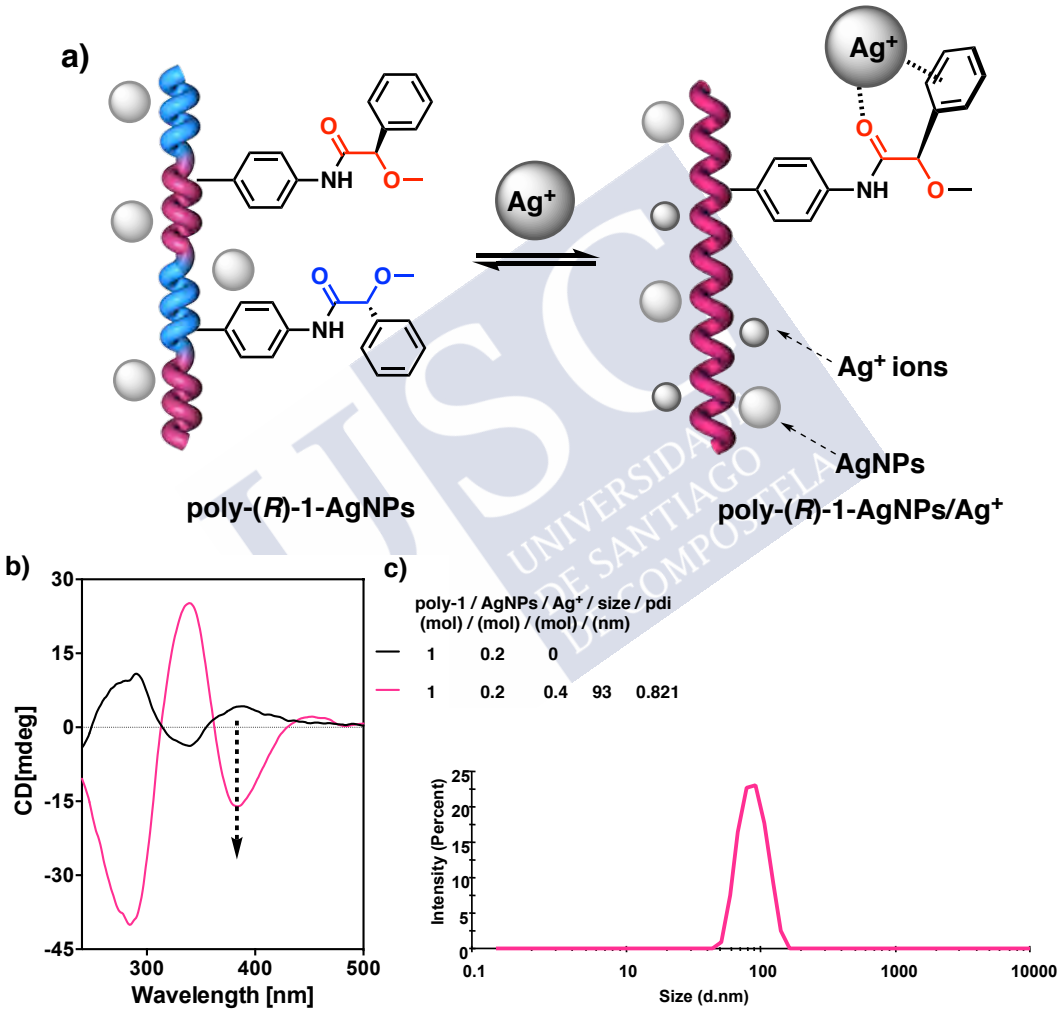

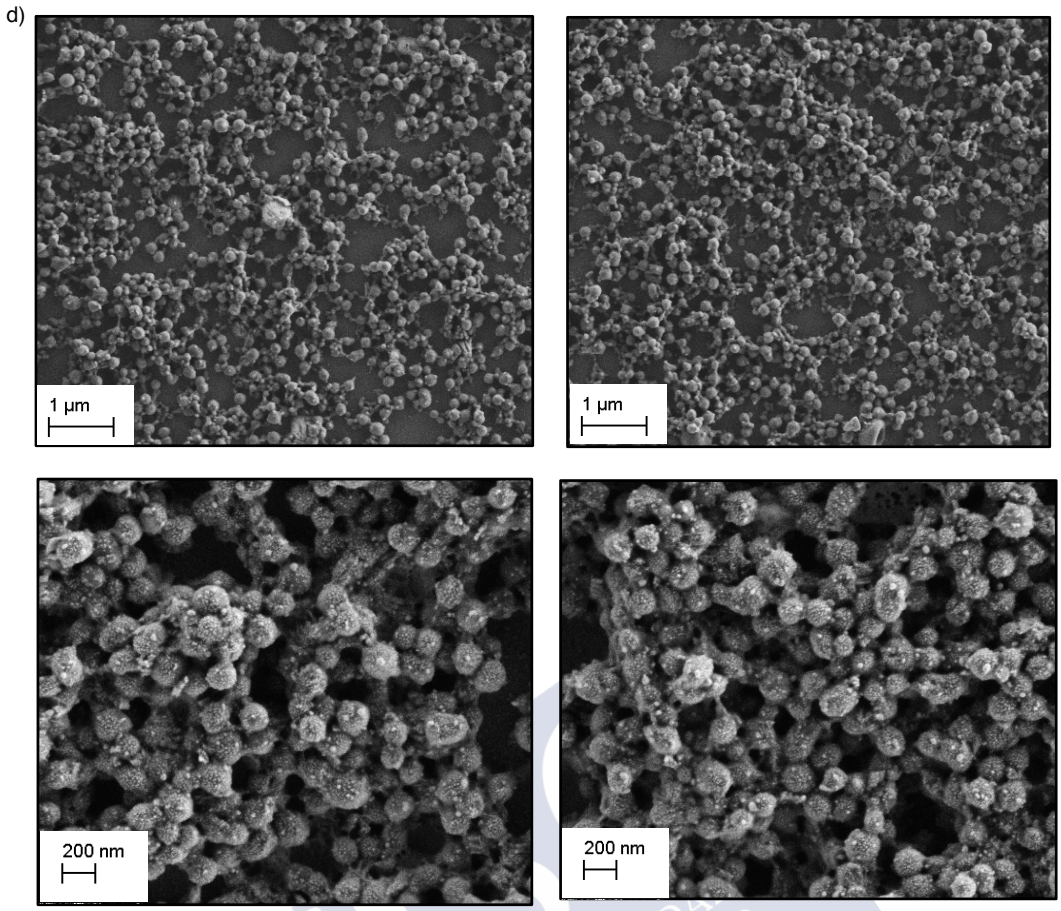

Figure S32. a) Schematic representation for the poly-(*R*)-**1**-AgNPs/dodecanethiol/Ag^+. b) CD traces for poly-(*R*)-**1**-AgNPs/dodecanethiol and poly-(*R*)-**1**-AgNPs/dodecanethiol/Ag^+. c) DLS studies for poly-(*R*)-**1**-AgNPs/dodecanethiol and poly-(*R*)-**1**-AgNPs/dodecanethiol/Ag^+. d) SEM images for poly-(*R*)-**1**-AgNPs/dodecanethiol/Ag^+ nanospheres.

The addition of Ba^{2+} ions (10 mg mL^{-1}) in MeOH to a solution of poly-(*R*)-**1**-AgNPs/dodecanethiol (0.3 mg mL^{-1}) in $CHCl_3$ produces right-handed helices indicating the chelation of Ba^{2+} to carbonyl and methoxy groups.

SEM measurements showed the formation of low polydisperse polymeric nanospheres due to the ability of the metal ions to act as crosslinking agents between polymer chains.

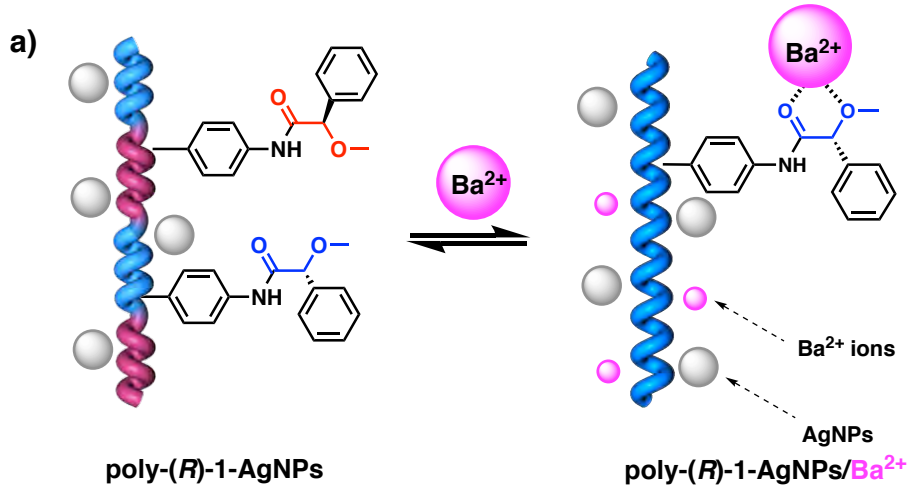
a)
NH
O
O
NH
O
O
Ba2+
Ba2+
NH
O
O
Ba2+ ions
AgNPs
poly-(R)-1-AgNPs
poly-(R)-1-AgNPs/Ba2+

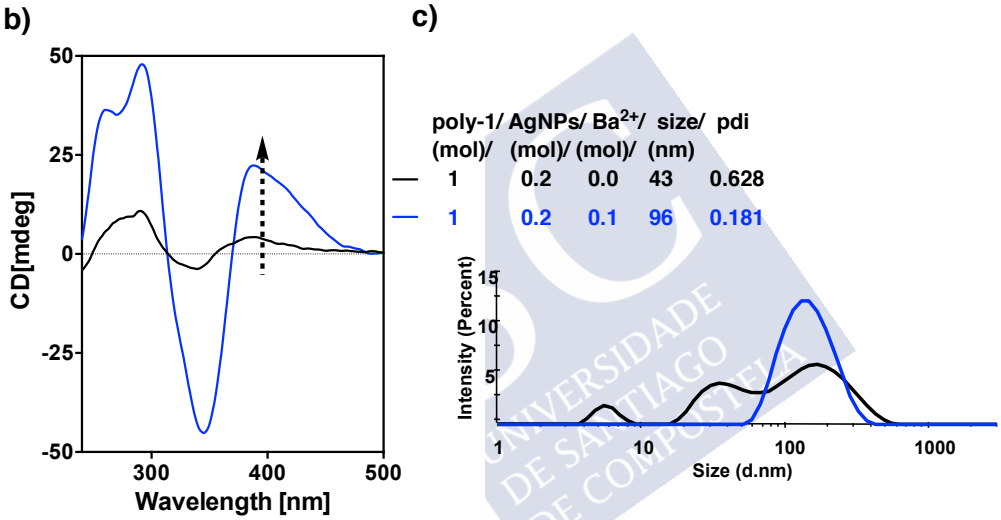
b)
50
25
0
-25
-50
CD[mdeg]
300
400
500
Wavelength [nm]
c)
poly-1/ AgNPs/ Ba2+/ size/ pdi
(mol)/ (mol)/ (mol)/ (nm)
1 0.2 0.0 43 0.628
1 0.2 0.1 96 0.181
Intensity (Percent)
15
10
5
1
10
100
1000
Size (d.nm)

d)

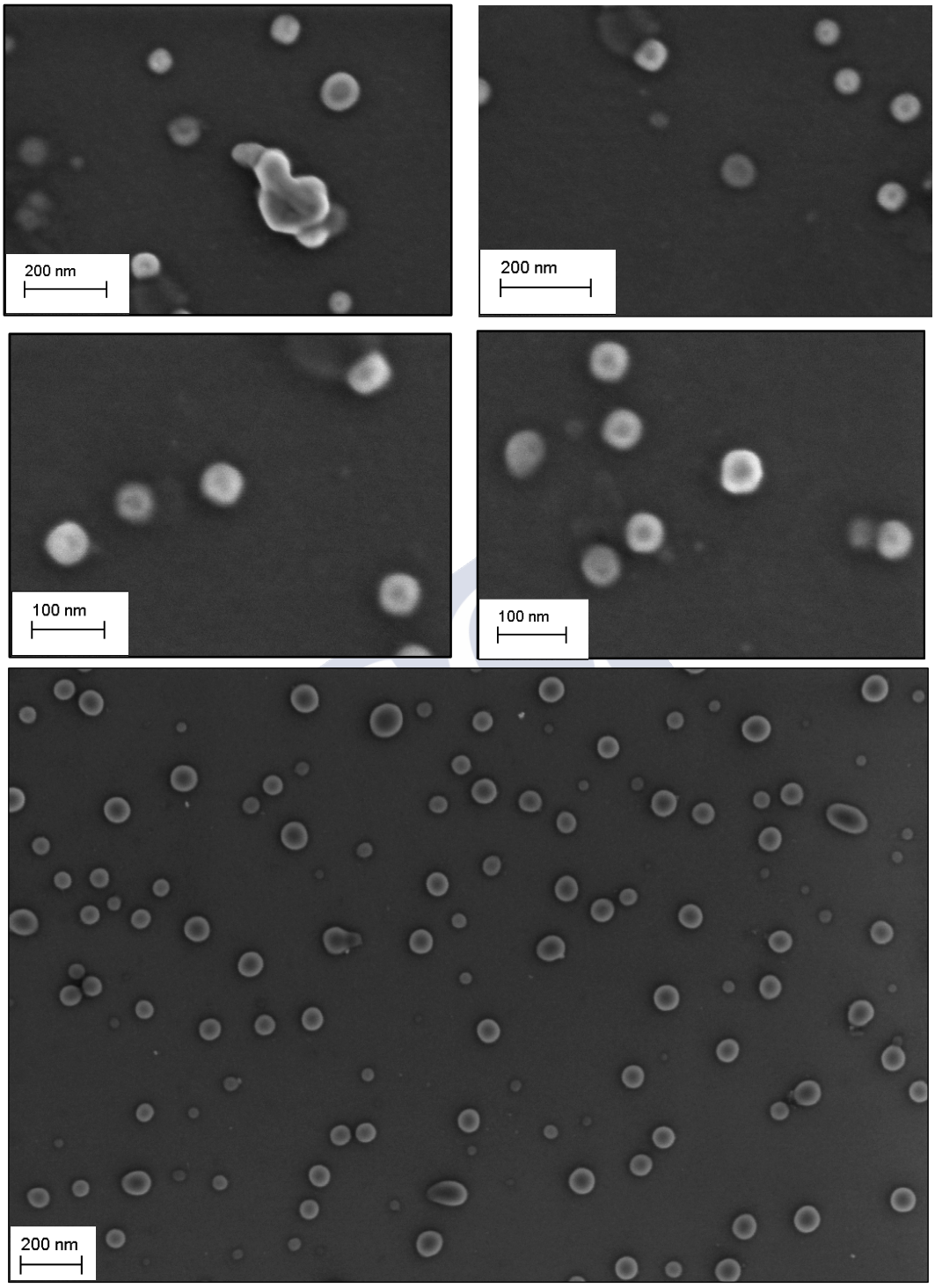

Figure S33. a) Schematic representation for the poly-(*R*)-**1**-AgNPs/dodecanethiol/Ba^{2+}. b) CD traces for poly-(*R*)-**1**-AgNPs/dodecanethiol and poly-(*R*)-**1**-AgNPs/dodecanethiol/Ba^{2+}. c) DLS studies for poly-(*R*)-**1**-AgNPs/dodecanethiol and poly-(*R*)-**1**-AgNPs/dodecanethiol/Ba^{2+}. d) SEM images for poly-(*R*)-**1**-AgNPs/dodecanethiol/Ba^{2+} nanospheres (size: 61 $\pm$ 21 nm, 120 nanoparticles).

20. Control studies: "Enantiomer comparison"

20.1 CD studies of poly-(*R*)-1 and poly-(*S*)-1

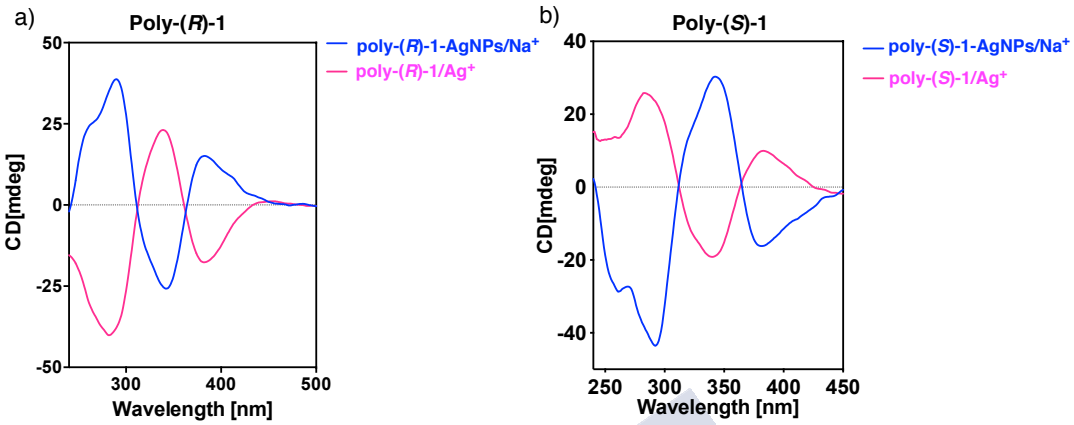

Figure S34. CD studies of a) poly-(*R*)-**1**/Ag^+, poly-(*R*)-**1**-AgNPs/Na^+ and b) poly-(*S*)-**1**/Ag^+, poly-(*S*)-**1**-AgNPs/Na^+.

21. Control studies: "the thiol linkage" poly-[(*R*)-1_r-*co*-3_{1-r}]

21.1 Synthesis of poly-[(*R*)-1_r-*co*-3_{1-r}] (r = 0.01-0.05) series

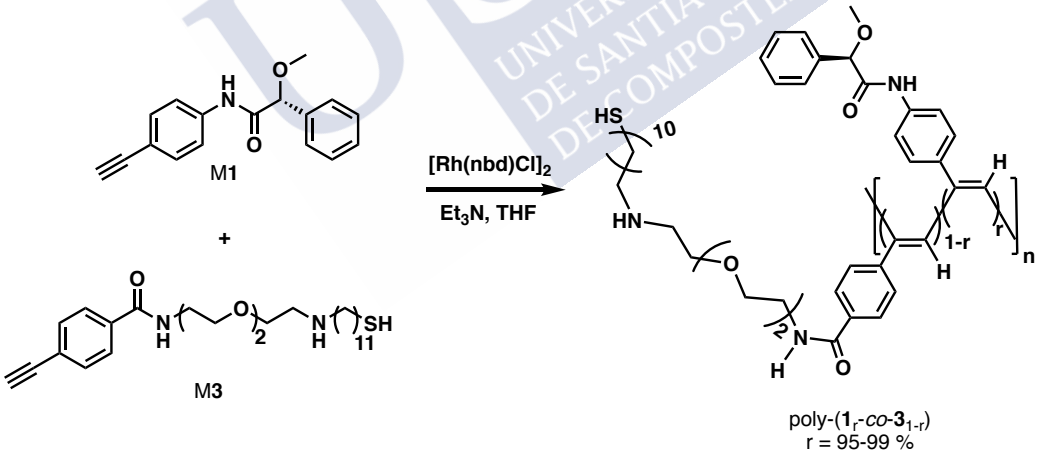

The synthesis of monomer M**3** can be found in the reference [S5].

Following the general procedure quantities of M**1**, M**3**, Et_3N, $[Rh(nbd)Cl]_2$, and THF as shown in Table S4 were employed. Reaction yield is also indicated in the Table S4.

Table S4:

Copolymer	M1 (mg)	M1 (mmol)	M3 (mg)	M3 (mmol)	Cat (mg)	THF (mL)	Et_3N (µL)	Yield (%)
poly-[(*R*)-**1**$_{0.95}$-*co*-**3**$_{0.05}$]	94.9	0.358	5.1	0.018	0.576	0.75	7	82
poly-[(*R*)-**1**$_{0.96}$-*co*-**3**$_{0.04}$]	95.6	0.362	4.1	0.015	0.576	0.75	7	90
poly-[(*R*)-**1**$_{0.97}$-*co*-**3**$_{0.03}$]	96.9	0.366	3.1	0.011	0.576	0.75	7	91
poly-[(*R*)-**1**$_{0.98}$-*co*-**3**$_{0.02}$]	97.7	0.369	2.1	0.008	0.576	0.75	7	75
poly-[(*R*)-**1**$_{0.99}$-*co*-**3**$_{0.01}$]	99.0	0.374	1.0	0.004	0.576	0.75	7	88

Table S5: GPC data

Copolymer	M_p	PDI
poly-[(*R*)-**1**$_{0.95}$-*co*-**3**$_{0.05}$]	15711	3.42
poly-[(*R*)-**1**$_{0.96}$-*co*-**3**$_{0.04}$]	18673	3.01
poly-[(*R*)-**1**$_{0.97}$-*co*-**3**$_{0.03}$]	27050	3.28
poly-[(*R*)-**1**$_{0.98}$-*co*-**3**$_{0.02}$]	28321	2.56
poly-[(*R*)-**1**$_{0.99}$-*co*-**3**$_{0.01}$]	30524	2.87

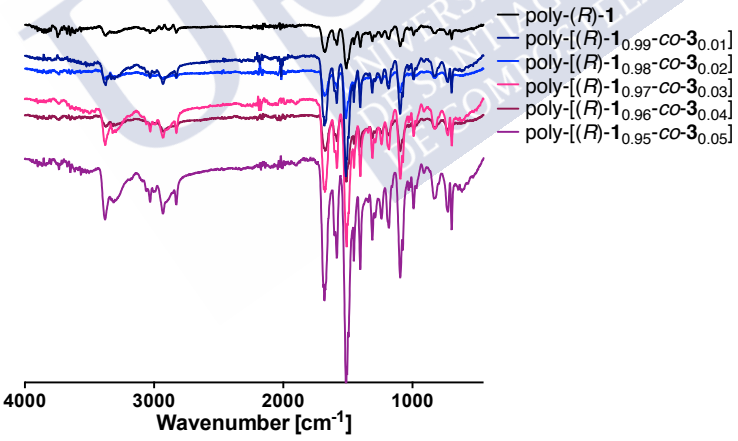

Figure S35. FT-IRs of poly-(*R*)-**1**, poly-[(*R*)-**1**$_{0.99}$-*co*-**3**$_{0.01}$], poly-[(*R*)-**1**$_{0.98}$-*co*-**3**$_{0.02}$], poly-[(*R*)-**1**$_{0.97}$-*co*-**3**$_{0.03}$], poly-[(*R*)-**1**$_{0.96}$-*co*-**3**$_{0.04}$] and poly-[(*R*)-**1**$_{0.95}$-*co*-**3**$_{0.05}$].

The *cis* stereoregularity of the copolymers was determined by ^{1}H NMR where the vinyl proton resonances appears at 5.7 ppm.

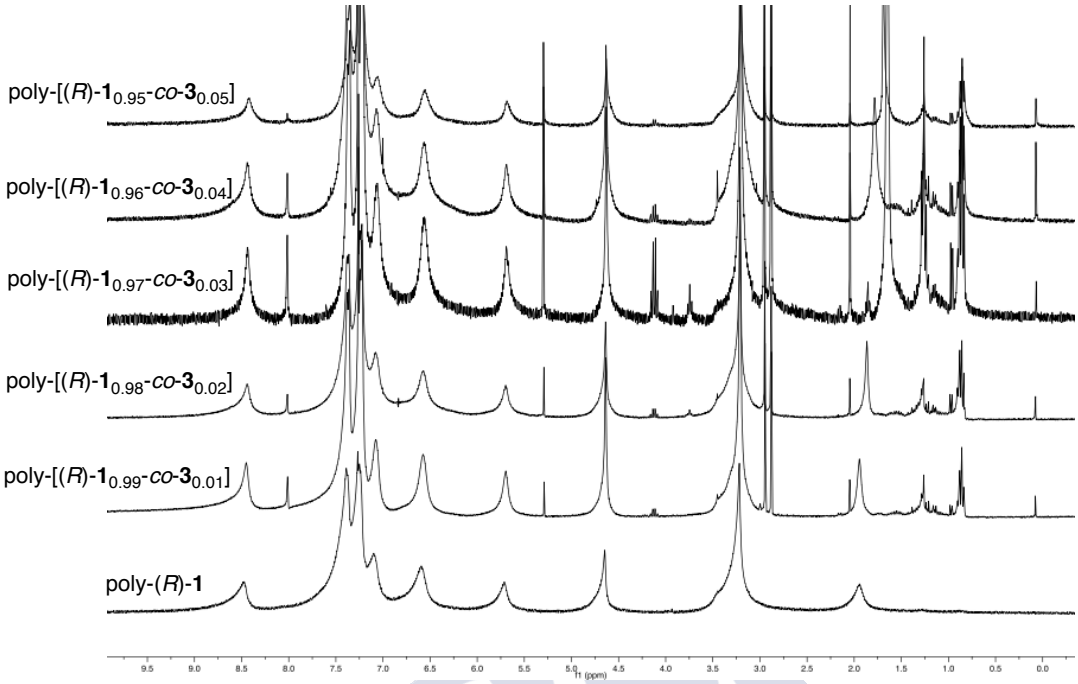

Figure S36. ^{1}H NMR of poly-(*R*)-**1**, poly-[(*R*)-**1**$_{0.99}$-*co*-**3**$_{0.01}$], poly-[(*R*)-**1**$_{0.98}$-*co*-**3**$_{0.02}$], poly-[(*R*)-**1**$_{0.97}$-*co*-**3**$_{0.03}$], poly-[(*R*)-**1**$_{0.96}$-*co*-**3**$_{0.04}$], poly-[(*R*)-**1**$_{0.95}$-*co*-**3**$_{0.05}$] in $CDCl_3$.

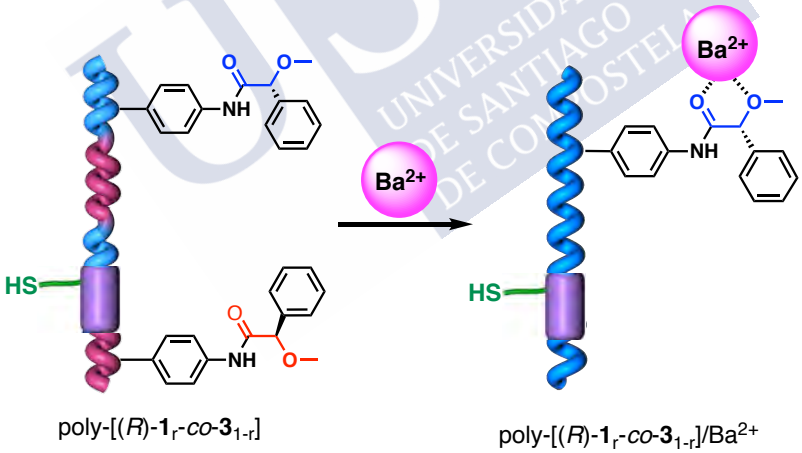

poly-[(*R*)-**1**$_r$-*co*-**3**$_{1-r}$] poly-[(*R*)-**1**$_r$-*co*-**3**$_{1-r}$]/Ba^{2+}

CD studies were performed with a solution of poly-[(*R*)-**1**$_r$-*co*-**3**$_{1-r}$] (r = 0.01-0.05) in $CHCl_3$ (0.3 mg mL^{-1}) using $Ba(ClO_4)_2$ dissolved in MeOH which concentration was 10.0 mg mL^{-1}.

Thus, poly-[(*R*)-**1**$_r$-*co*-**3**$_{1-r}$] dissolved in $CHCl_3$ shows a null Cotton Effect (CD_{380} = 0). The addition of Ba^{2+} ions to poly-[(*R*)-**1**$_r$-*co*-**3**$_{1-r}$] promotes the stabilization of *sp* conformation between carbonyl and methoxy groups lead to *P* helices.

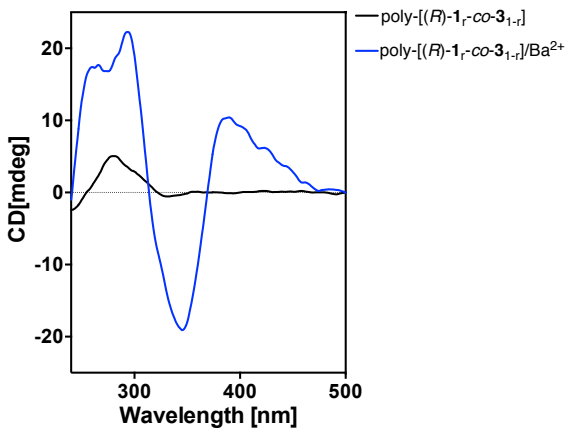

Figure S37. Representative CD studies of poly-[(*R*)-$\mathbf{1}_r$-*co*-$\mathbf{3}_{1\text{-}r}$] in presence of $Ba(ClO_4)_2$.

21.2 Preparation of poly-[(*R*)-1_r-*co*-$3_{1\text{-}r}$]-AgNPs

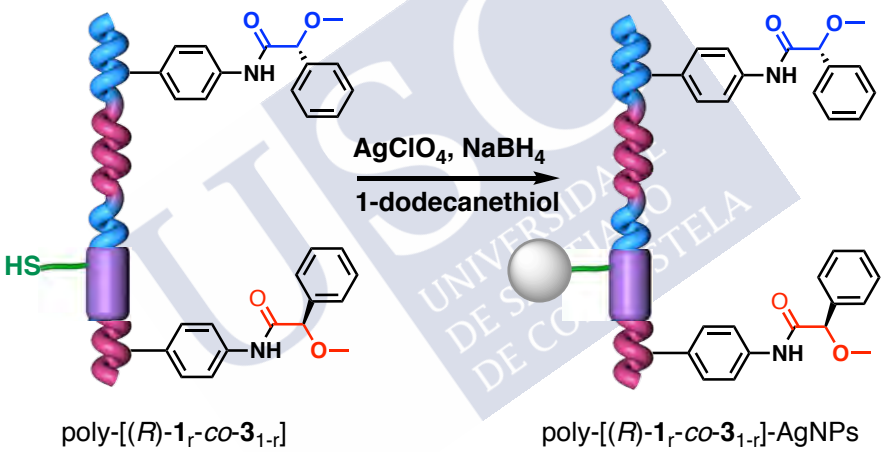

To a solution of tetraoctylamonium bromide (TOAB, 0.444g, 0.812 mmol) into DCM (20mL) was added a solution of $AgClO_4$ (0.041 g, 0.202 mmol) in distilled water (1.25 mL) and allowed to stir at rt. After some time the mixture was washed with DCM (20 mL x 3). A copolymer (poly-[(*R*)-$\mathbf{1}_r$-*co*-$\mathbf{3}_{1\text{-}r}$) solution (0.020 g) in DCM (5 mL) and another solution of dodecanethiol (40 mL) in DCM (5 mL) were prepared, both solutions were added simultaneously to the reaction mixture and allowed to stir at - 4°C for 30 min. After this time was added as a reducing agent, a solution of $NaBH_4$ (0.076 mg) in distilled water (2 mL). The reaction mixture turns a yellow-orange to brown – black. EtOH (HPLC grade, 50 mL) is added to the solution and left at -4 ° C for 18 h. After this time, the reaction mixture was filtered using a filter plate. The precipitate obtained was dissolved in $CHCl_3$ and a second process was conducted in toluene precipitation using centrifuge (1h, 11000 rpm) and obtaining poly-[(*R*)-$\mathbf{1}_r$-*co*-$\mathbf{3}_{1\text{-}r}$]-AgNP. The product was characterized by CD, UV, IR and STEM.

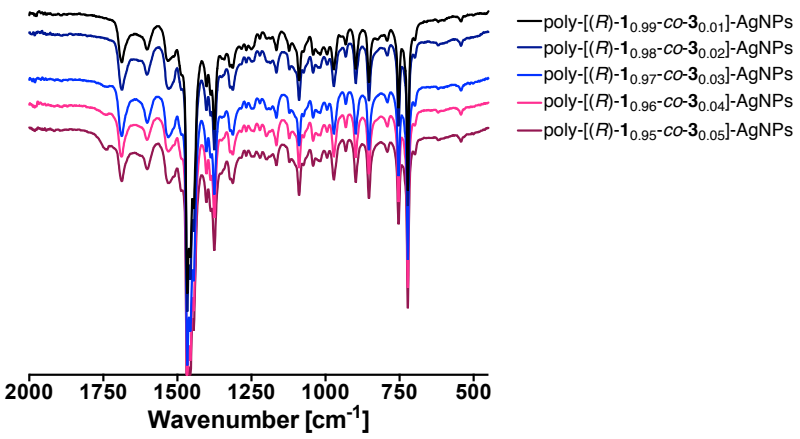

Figure S38. IRs of poly-[(*R*)-**1**$_{0.99}$-*co*-**3**$_{0.01}$]-AgNPs, poly-[(*R*)-**1**$_{0.98}$-*co*-**3**$_{0.02}$]-AgNPs, poly-[(*R*)-**1**$_{0.97}$-*co*-**3**$_{0.03}$]-AgNPs, poly-[(*R*)-**1**$_{0.96}$-*co*-**3**$_{0.04}$]-AgNPs and poly-[(*R*)-**1**$_{0.95}$-*co*-**3**$_{0.05}$]-AgNPs.

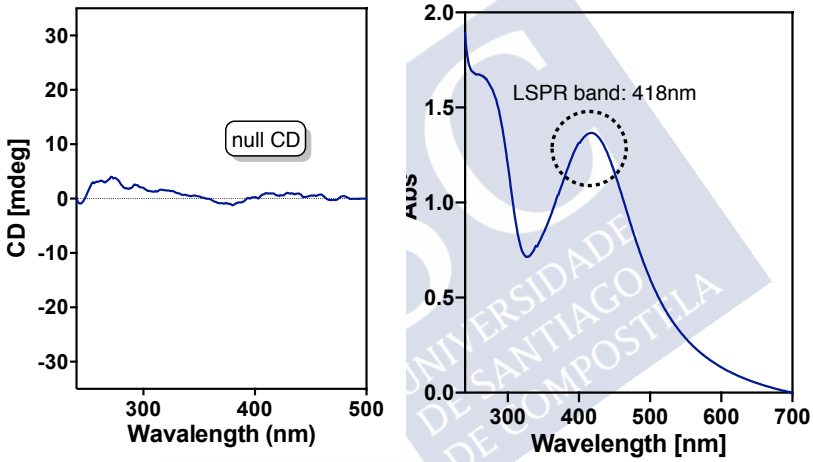

Figure S39. CD and UV-Vis studies of poly-[(*R*)-**1**$_r$-*co*-**3**$_{1-r}$]-AgNPs.

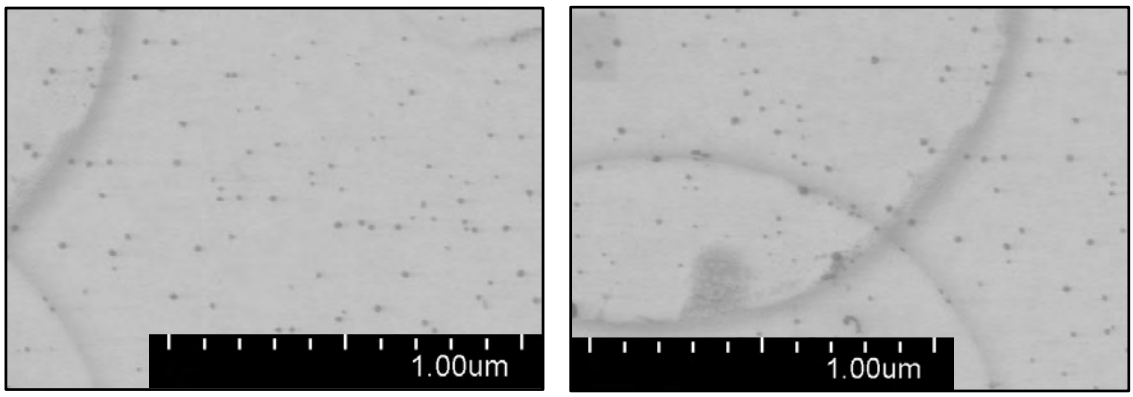

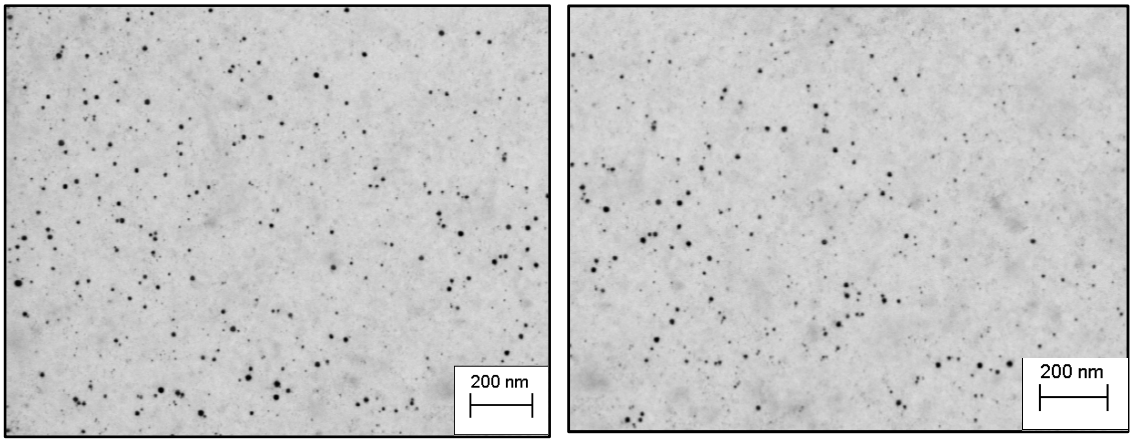

Figure S40. TEM images of poly-[(*R*)-**1**$_r$-*co*-**3**$_{1-r}$]-AgNPs (size: 13.9 ± 2.5 nm).

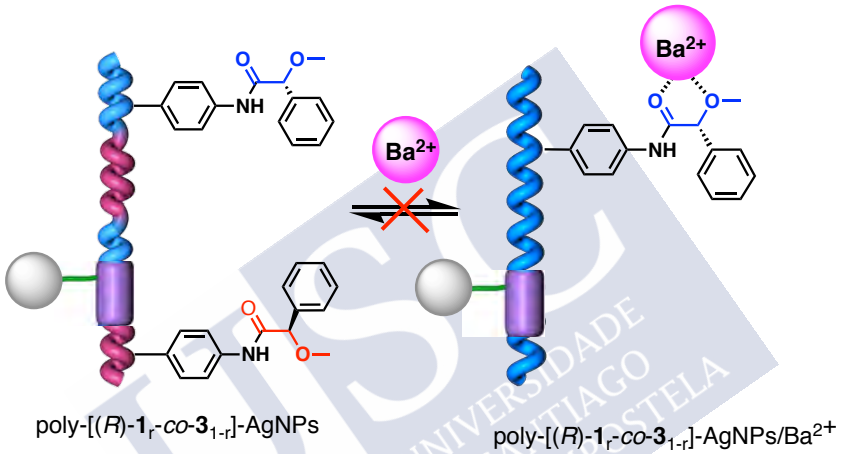

CD studies were performed with a solution of poly-[(*R*)-**1**$_r$-*co*-**3**$_{1-r}$]-AgNPs in $CHCl_3$ (0.3 mg mL^{-1}) using $Ba(ClO_4)_2$ dissolved in MeOH which concentration was 10.0 mg mL^{-1}.

Thus, poly-[(*R*)**1**$_r$-*co*-**3**$_{1-r}$]-AgNPs dissolved in $CHCl_3$ shows a null Cotton Effect (CD_{380}= 0). The addition of Li^+ ions to poly-[(*R*)-**1**$_r$-*co*-**3**$_{1-r}$]-AgNPs cannot promote the stabilization of one preferred helical sense.

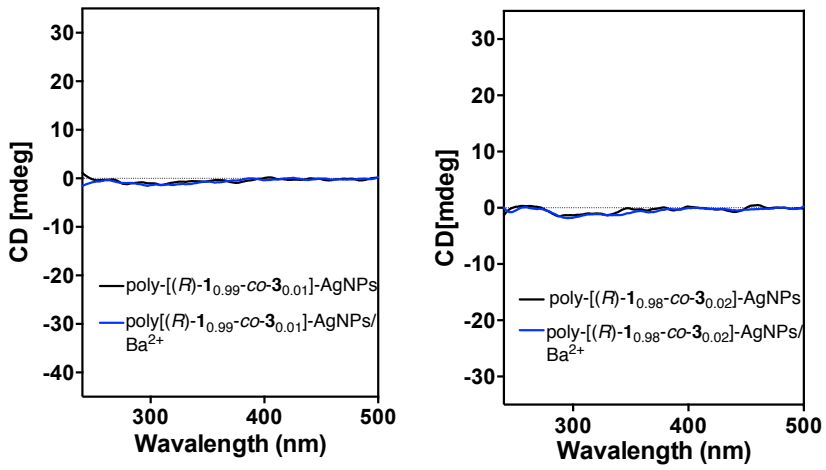

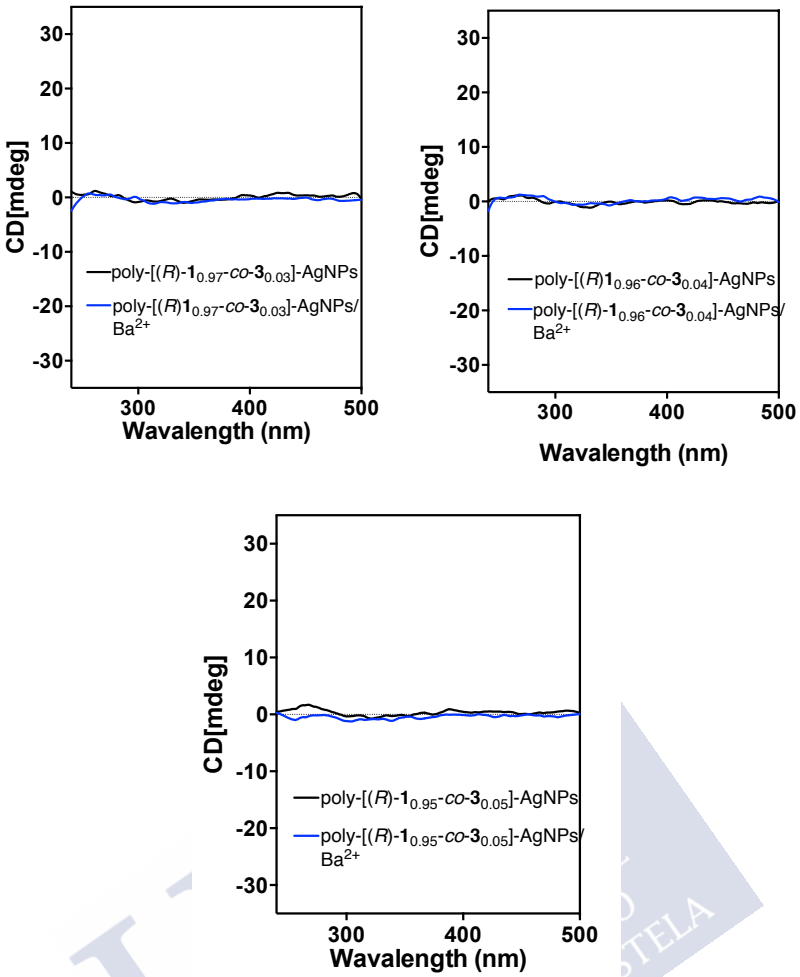

Figure S41. CD studies of poly-[(*R*)-**1**$_r$-*co*-**2**$_{1-r}$]-AgNPs (r = 0.01-0.05) in presence of $Ba(ClO_4)_2$.

22. Chiral enhancement and reversibility of the process with resins metal scavengers in presence of silver nanoparticles

To carry out these experiments, the resins were swollen in $CHCl_3$ for 1h (0.05 g mL^{-1}). Next, 100 mg of resin were added to a solution of poly-(*R*)-**1**-AgNPs/Na^+ (0.3 mg mL^{-1} in $CHCl_3$). After 30 min, the CD and UV-Vis spectra were recorded confirming that Na^+ ions are removed obtaining a null CD.

Next, 0.5 equiv of $AgClO_4$ (10 mg mL^{-1}, MeOH) or 0.5 equiv of $(BaClO_4)_2$ (10 mg mL^{-1}, MeOH) were added to poly-(*R*)-**1**-AgNPs showing a chiral enhancement to *M* or *P* helices respectively.

Examples of the use of scavenger follow next:

REVERSIBILITY AND CHIRAL ENHANCEMENT OF THE PROCESS IN PRESENCE OF SILVER NANOPARTICLES

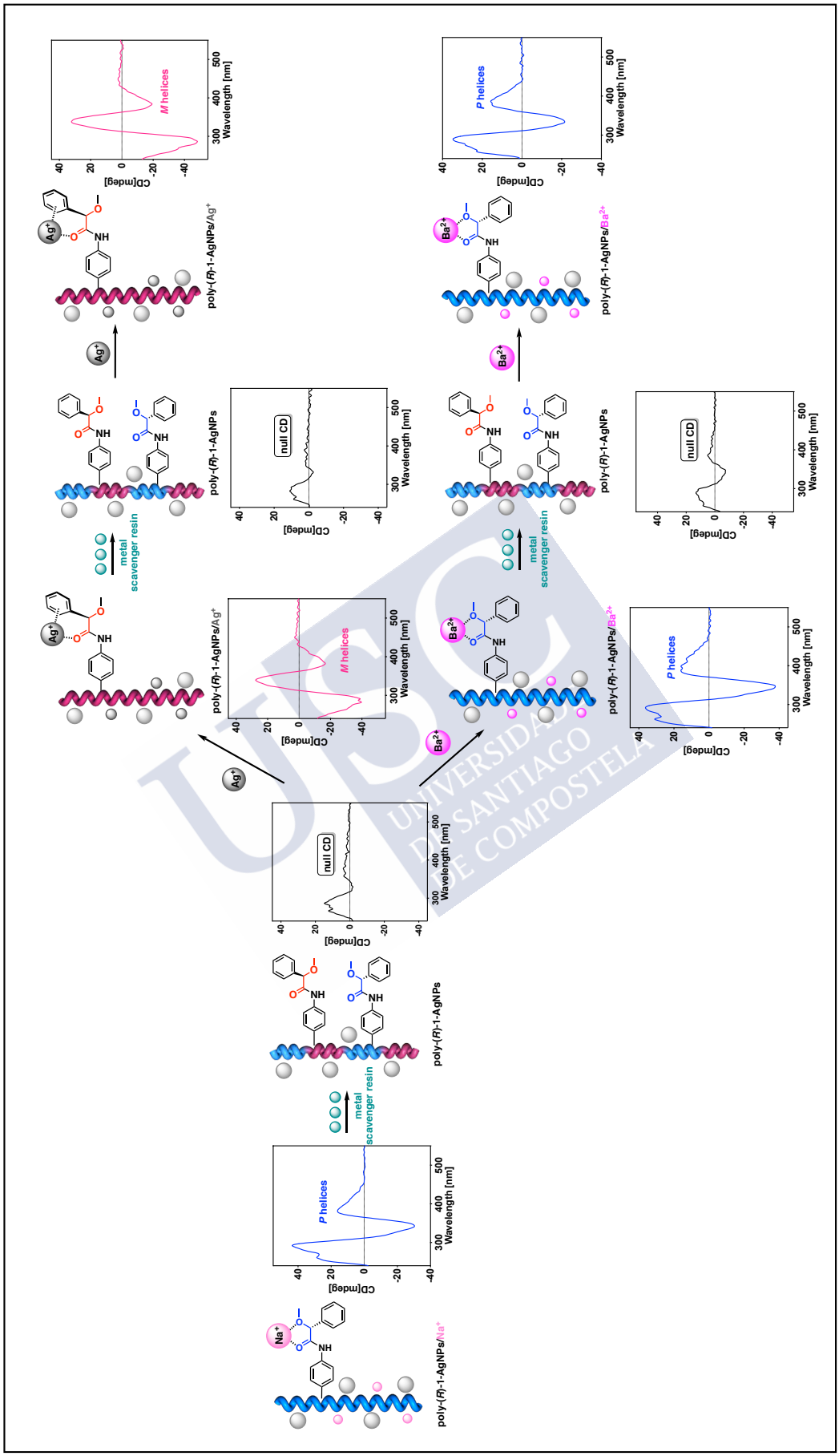

23. Supporting references

S1. Freire. F; Seco, J. M.; Quiñoá, E.; Riguera, R.; Chiral Amplification and Helical Sense Tuning by Mono and Divalent Metals on Dynamic Helical Polymers, *Angew. Chem. Int. Ed.,* **2011**, *50*, 11692-11696.

S2. Leiras, S.; Freire, F.; Seco, J. M.; Quiñoá, E.; Riguera, R. Controlled modulation of the helical sense and the elongation of poly(phenylacetylene)s by polar and donor effect. *Chem. Sci*., **2013**, *4*, 2735-2743.

S3. Arias, S.; Freire, F.; Quiñoá, E.; Riguera, R.; The leading role of cation–π interactions in polymer chemistry: the control of the helical sense in solution, *Polym. Chem*., **2015**, *6*, 4725-4733.

S4. Freire. F; Seco, J. M.; Quiñoá, E.; Riguera, R.; Nanospheres with Tunable Size and Chirality from Helical Polymer–Metal Complexes, *J. Am. Chem. Soc.*, **2012**, *134*, 19374–19383.

S5. Bergueiro, J.; Núñez-Martínez, M.; Arias, S.; Freire, F.; Quiñoá, E.; Riguera, R.; Chiral Gold-PPA Nanocomposites with Tunable Helical Sense and Morphology, *Nanoscale Horiz.,* **2020**, *5*, 495-500.

USC UNIVERSIDADE DE SANTIAGO DE COMPOSTELA

Experimental Section Chapter V:

1. Materials and methods

Chemicals. Commercially available chemicals have been used as delivered. Solvents were purchased as reagent grade and distilled if necessary. Anhydrous solvents were either purchased as ultra-dry solvent from Acros Organics® or received from solvent purification system. For the coupling and polymerization reactions, dry THF was obtained from MBRAUN SPS 800 solvent purification system. Water was purified by Millipore water purification system. Tetraoctylamonium bromide (TOAB, 99%), dodecanethiol, sodium borohydride ($NaBH_4$, 99%) and tetrachloroauric acid ($HAuCl_4$, $\geq$ 99.99% of purity) were purchased from Aldrich.

Instrumentations and Characterizations. NMR experiments were carried out in a Varian Inova 300 (300 MHz resonance 1H). Size exclusion chromatography studies were performed on Alliance 2695 HPLC System (Waters) liquid chromatography system equipped with a UV 2489 detector (Waters). The samples were eluted by three Phenogel columns connected to each other with stationary phases of 10^3, 10^4 and 10^5 Amstrong and packed with a solid support of a cross-linked styrene and *p*-divinylbenzene copolymer. CD and UV measurements were registered in a Jasco-720 spectropolarimeter and a Jasco-730 spectrophotometer respectively at a nanocomposite concentration of 0.3 mg mL^{-1}. FT-IR measurements were carried out on a Bruker IFS-66v. DLS studies were performed on a Nano-ZS 90 (Malvern) equipped with a He-Ne laser (l = 633 nm) under scattering angle of 173°. The samples were maintained at the designed temperature for 5 min before testing. DLS measurements were carried out in all cases at 0.3 mg·mL^{-1}. SEM measurements were performed on a LEO-435VP electron microscope equipped with an energy dispersive X-ray (EDX) spectrometer. TEM measurements were performed on a JEOL JEM 2010 and 200 KV as a voltage. To study the nanocomposite, or the nanospheres the same protocol was used. A dispersion of the nanocomposite or the nanospheres at a concentration of 0.3 mg mL^{-1} was drop casted onto of silicon wafer chip and allowed to dry at rt for 12h for SEM studies, while in case of TEM studies the dispersed materials were drop-casted onto carbon chip and allowed to dry at rt for 12.h. DSC measurements were performed in a DSC Q200 Tzero Technology (TA Instruments, New Castle, UK) equipped with a refrigerated cooling system RCS90 (TA Instruments) using a Tzero low-mass aluminum pan. TGA experiments were carried out in a Q5000SA instrument (TA Instruments, New Castle, UK) using a platinum pan. EPR experiments were carried out in a Bruker EMX with a frequency around 9.443 GHz and using perylene in H_2SO_4 as internal

reference. XPS analysis of the samples was performed using a Thermo Scientific K-Alpha ESCA instrument equipped with aluminium Kα monochromatized radiation at 1486.6 eV X-ray source. Due the no conductor nature of samples was necessary to use an electron flood gun to minimize surface charging. Neutralization of the surface charge was performed by using both a low energy flood gun (electrons in the range 0 to 14 eV) and a low energy Argon ions gun.

The XPS measurements were carried out using monochromatic Al-Ka radiation (hn = 1486.6 eV). Photoelectrons were collected from a take-off angle of 90º relative to the sample surface. The measurement was done in a Constant Analyser Energy mode (CAE) with a 100 eV pass energy for survey spectra and 20eV pass energy for high resolution spectra. Charge referencing was done by setting the lower binding energy C 1s photo peak at 284.8.0 eV C1s hydrocarbon peak. Surface elemental composition was determined using the standard Scofield photoemission cross sections.

2. Monomer M1 and polymer poly-(*R*)-1

The general procedure for the synthesis of monomer M**1** and polymer poly-(*R*)-**1** (Figure S1) can be found in reference [S1].

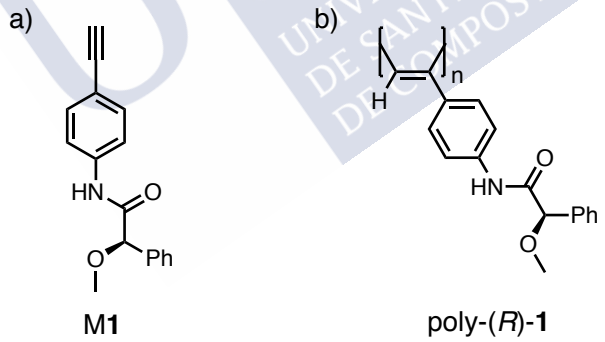

Figure S1. Structure for a) monomer M**1** and b) poly-(*R*)-**1.**

3. CD and UV-Vis for poly-(*R*)-1 in presence of $HAuCl_4$

A solution of poly-(*R*)-**1** (0.3 mg mL^{-1}) in $CHCl_3$ was titrated with 0.5 equiv of $HAuCl_4$ (10 mg mL^{-1}) in MeOH. Immediately, the colour solution turns from yellow to blue and CD and UV-Vis experiments were recorded.

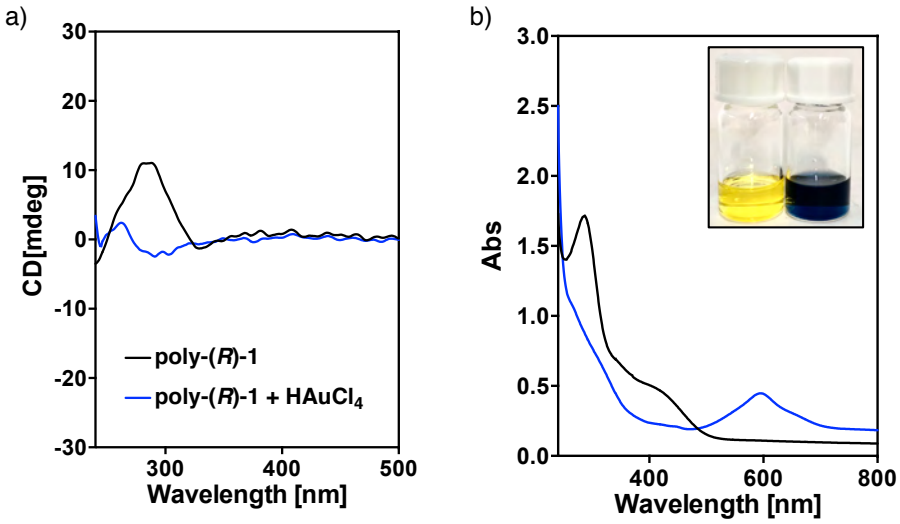

Figure S2. a) CD and b) UV-Vis measurements for poly-(*R*)-**1** and poly-(*R*)-**1** after addition of $HAuCl_4$.

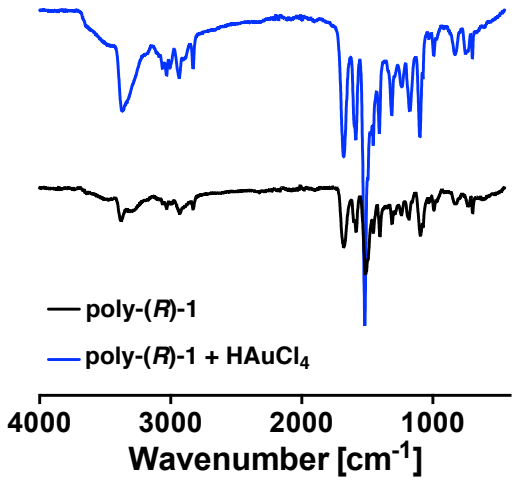

Figure S3. FT-IR spectra for poly-(*R*)-**1** and poly-(*R*)-**1** after addition of $HAuCl_4$.

4. XPS experiments

XPS experiments were carried out to determine the oxidation state of the gold when is added to poly-(*R*)-**1**. For this purpose, 0.3 mg of poly-(*R*)-**1** were dissolved in 1 mL of $CHCl_3$, and 0.5 equiv of $HAuCl_4$ (10 mg mL^{-1}, MeOH) were added. Next, the sample was dried and XPS spectra were recorded.

Table S1. Gold Au4f Binding Energy BE (eV) / Relative Percent (Rel. %).

Sample	Au4f7/2 Au (0)	Au4f7/2 Au (1+)	Au4f7/2 Au (3+)
Poly-(*R*)-1	-	-	-
Poly-(*R*)-1 + $HAuCl_4$	84.0/31.64%	-	86.37/68.36

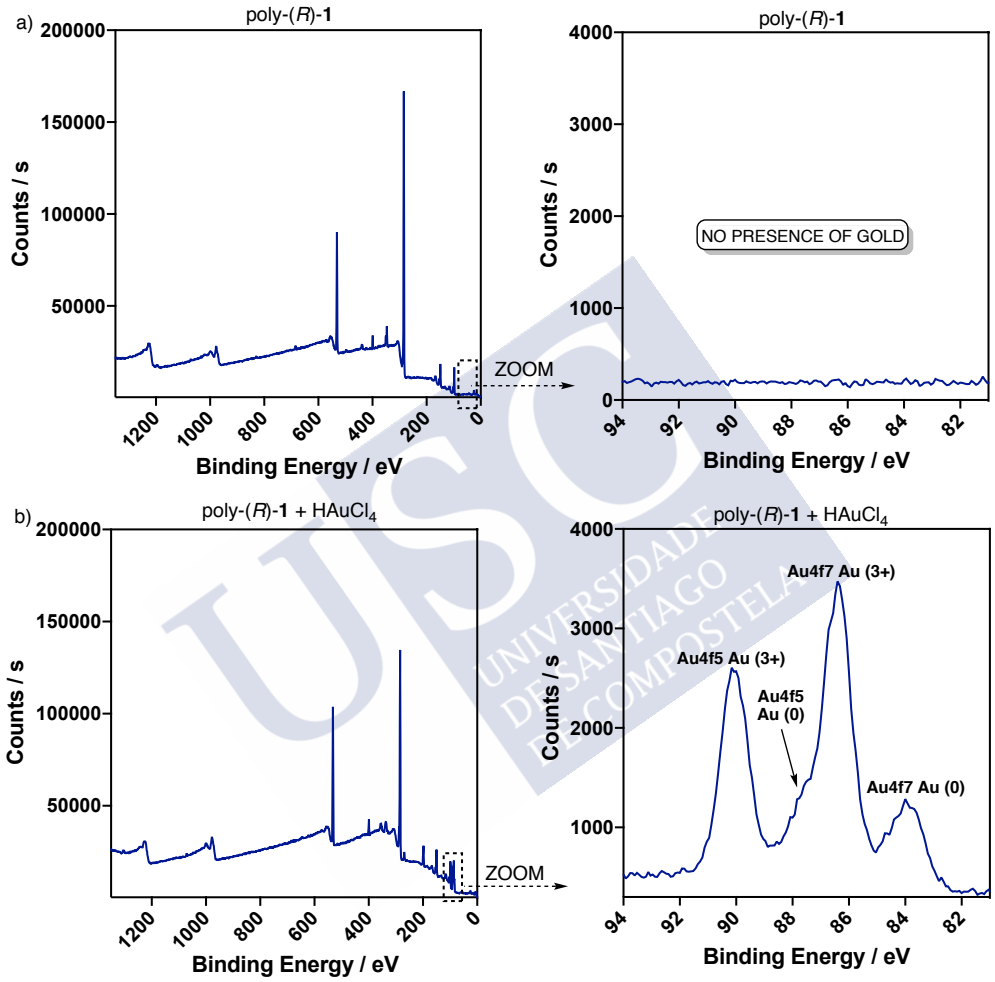

Figure S4. XPS studies of a) poly-(*R*)-**1** and b) poly-(*R*)-**1** in presence of $HAuCl_4$.

5. TEM images of poly-(*R*)-1 after addition of $HAuCl_4$

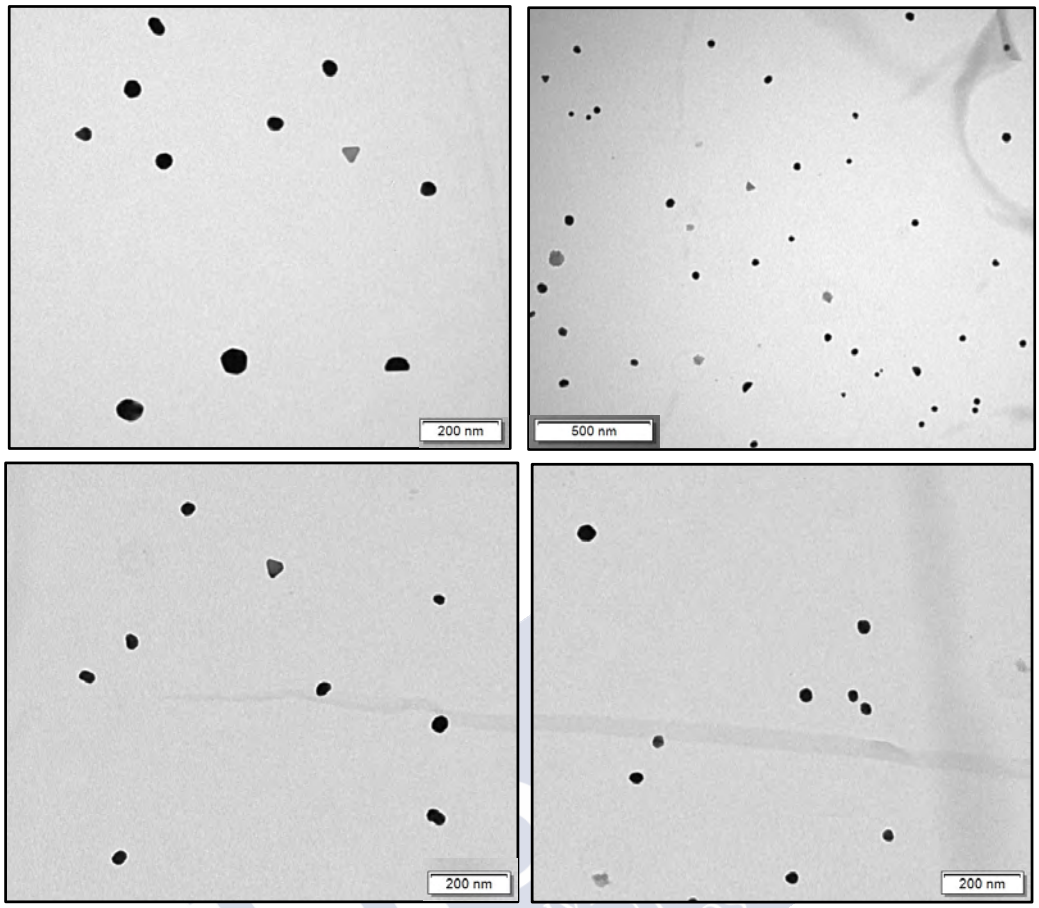

Figure S5. TEM images of poly-(*R*)-**1** after addition of $HAuCl_4$.

6. CD and UV-Vis for poly-(*R*)-1 in presence of $N(C_8H_{17})_4^+AuCl_4^-$

A solution of poly-(*R*)-**1** (0.3 mg mL^{-1}) in $CHCl_3$ was titrated with different amounts of $N(C_8H_{17})_4^+AuCl_4^-$ (10 mg mL^{-1}) in MeOH. CD studies showed a null cotton effect in vinylic region (CD_{380} = 0) indicating the no interaction between poly-(*R*)-**1** and the $N(C_8H_{17})_4^+AuCl_4^-$.

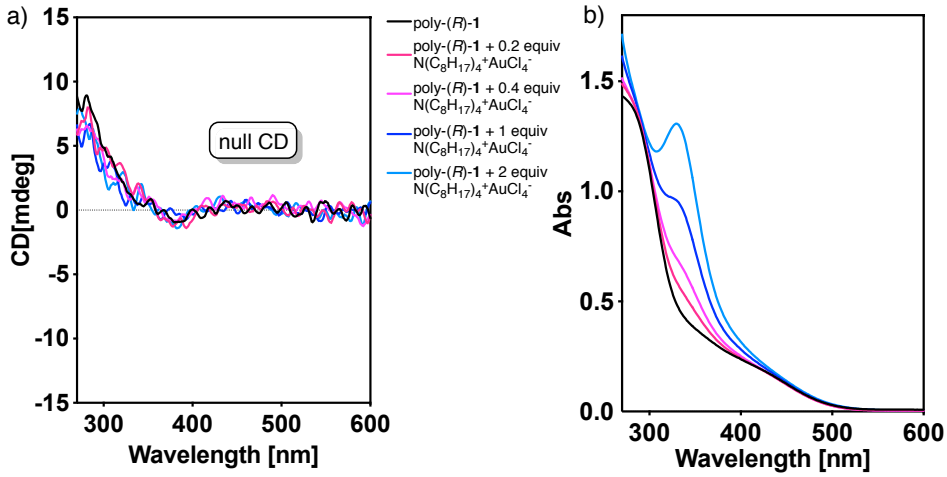

Figure S6. a) CD and b) UV-Vis measurements of poly-(*R*)-**1** and poly-(*R*)-**1** after addition of $N(C_8H_{17})_4^+AuCl_4^-$.

7. ^{1}H NMR spectra for poly-(*R*)-1 titrated with $HAuCl_4$

The *cis* stereoregularity of poly-(*R*)-**1** was determined by ^{1}H NMR spectroscopy where the vinyl proton resonates at 5.8 ppm. ^{1}H NMR spectra of poly-(*R*)-**1** after addition of $HAuCl_4$ (10 mg mL^{-1}, methanol-d_4) did not show the presence of the vinyl proton at 5.8 ppm.

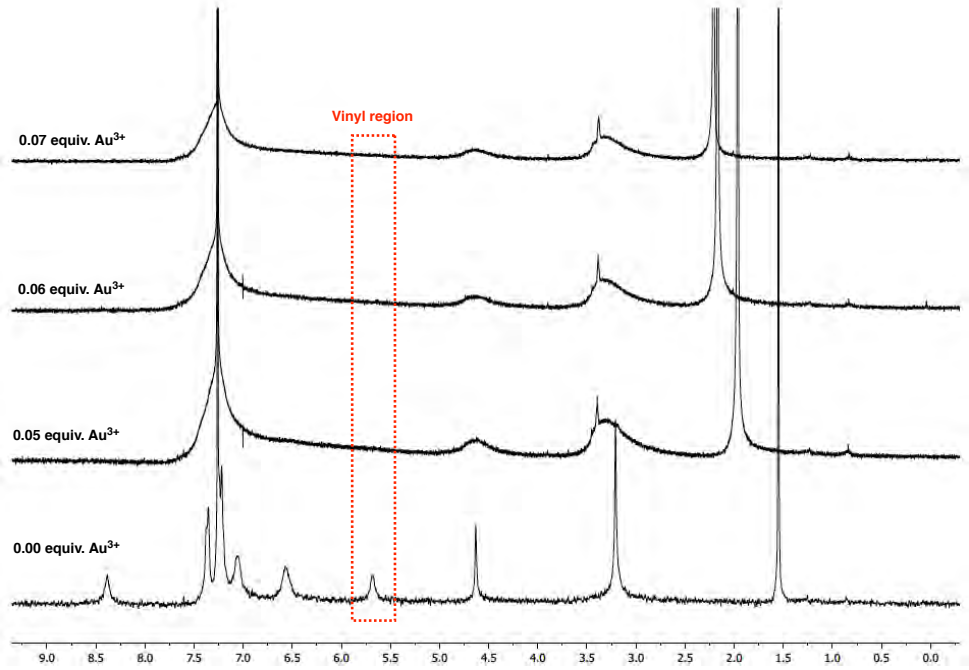

Figure S7. ^{1}H NMR for poly-(*R*)-**1** (3 mg mL^{-1}, $CDCl_3$) in presence of different amounts of $HAuCl_4$.

8. General procedure for the synthesis of poly-(*R*)-1-AuNPs nanocomposites

To a solution of tetraoctylamonium bromide (TOAB, 0.444 g, 0.812 mmol) into DCM (20mL) was added a solution of $HAuCl_4$ (0.080 g, 0.202 mmol) in distilled water (1.25 mL) and allowed to stir at rt. After some time the mixture was washed with DCM (20 mL x 3). Poly-(*R*)-**1** solution (0.020 g) in DCM (5 mL) and another solution of dodecanethiol (40 uL) in DCM (5 mL) were prepared, both solutions were added simultaneously to the reaction mixture and allowed to stir at -4°C for 30 min. After this time was added as a reducing agent, a solution of $NaBH_4$ (0.076 mg) in distilled water (2 mL). The reaction mixture turns a yellow-orange to brown–black. EtOH (HPLC grade, 50 mL) is added to the solution and left at -4°C for 18 h. After this time, the reaction mixture was filtered using a filter plate. The precipitate obtained was dissolved in $CHCl_3$ and a second process was conducted in toluene precipitation using centrifuge (1h, 11000 rpm) and obtaining poly-(*R*)-**1**-AuNPs/dodecanethiol. Extra purification was required for the nanocomposites. The peak corresponding to poly-(*R*)-**1**-AuNP/dodecanethiol was collected and further analyzed by means of UV, CD and TEM.

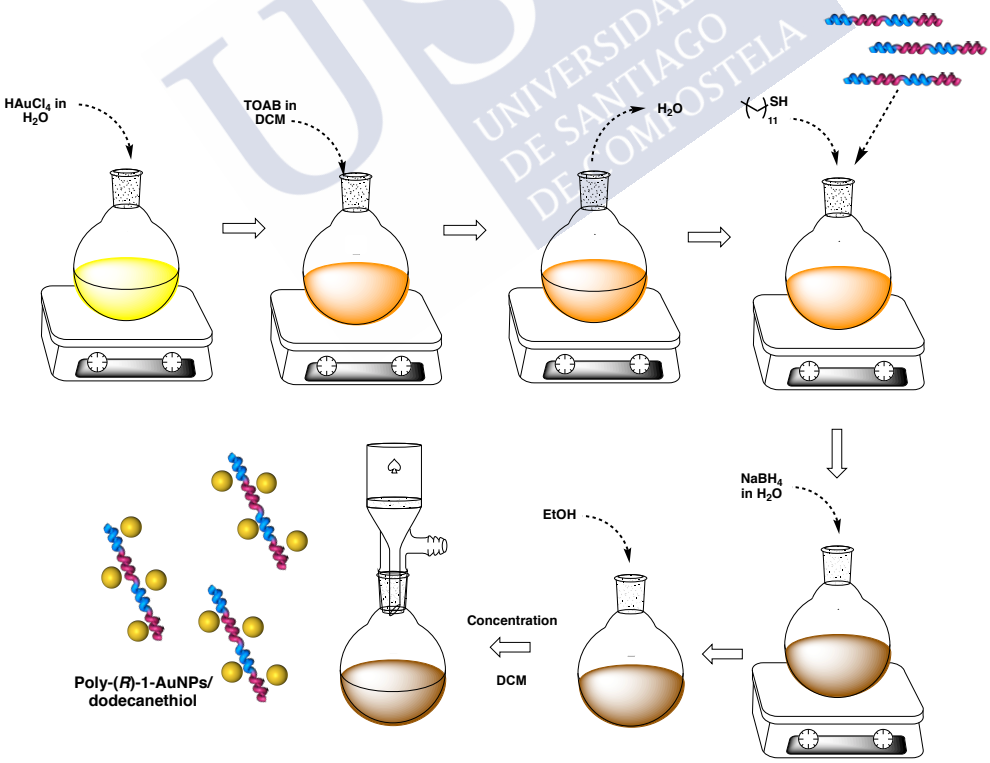

Figure S8. Schematic representation for the preparation of poly-(*R*)-**1**-AuNPs/dodecanethiol nanocomposites.

9. Characterization for poly-(*R*)-1-AuNPs/dodecanethiol nanocomposites

9.1 CD and UV-Vis studies

CD and UV-Vis studies from a solution of poly-(*R*)-**1**-AuNPs/dodecanethiol (0.1 mg mL^{-1}) in $CHCl_3$ show a null CD in the vinylic region due to the presence of an axially racemic nanocomposites.

Moreover, UV-Vis spectra showed the typical LSPR band corresponding to the formation of spherical AuNPs at 540 nm.

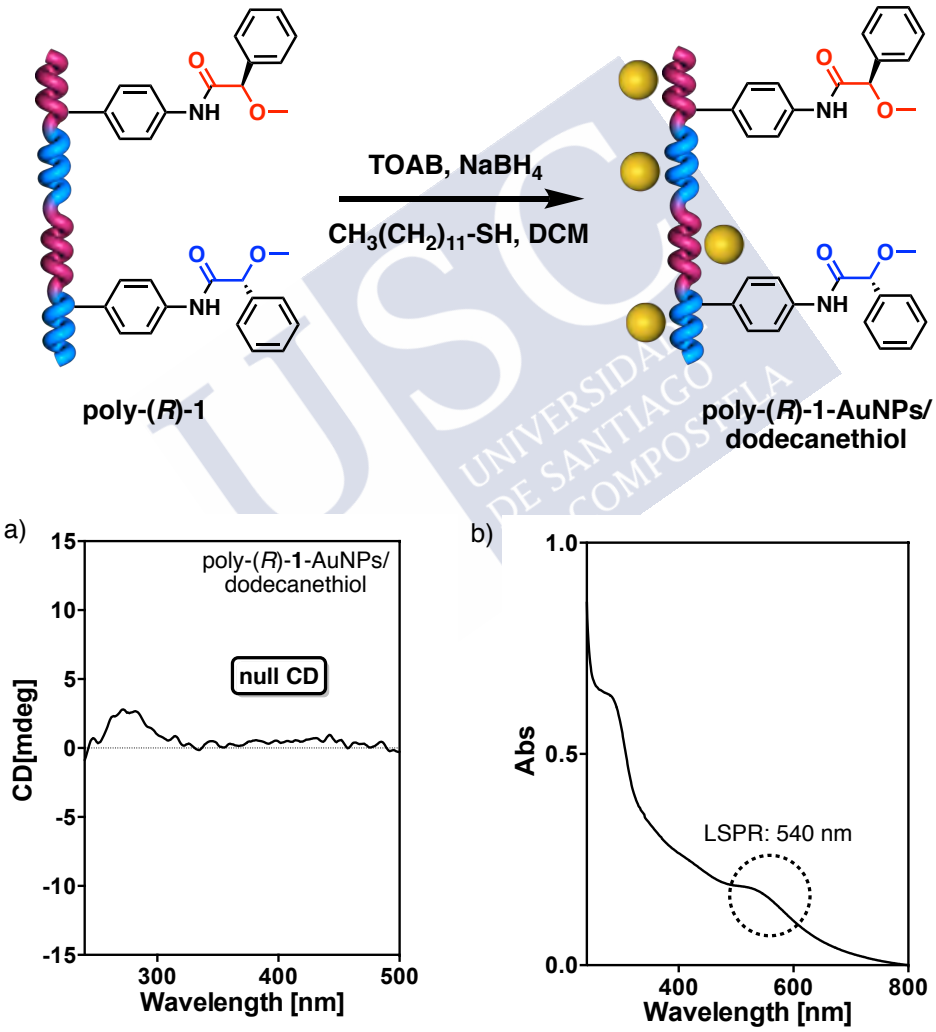

Figure S9. a) CD and b) UV-Vis spectra for poly-(*R*)-**1**-AuNPs/dodecanethiol.

The peak at 1568 cm^{-1} is assigned to C=C bond stretching in the *cis* poly(acetylene) and overlaps with that of the phenyl ring. The peak at 1340 cm^{-1} is assigned to the *cis* C-C bond

coupled with the single bond connecting the main chain and the phenyl ring. The peak at 1004 cm^{-1} is assigned to the C-H bond deformation of the *cis* form.

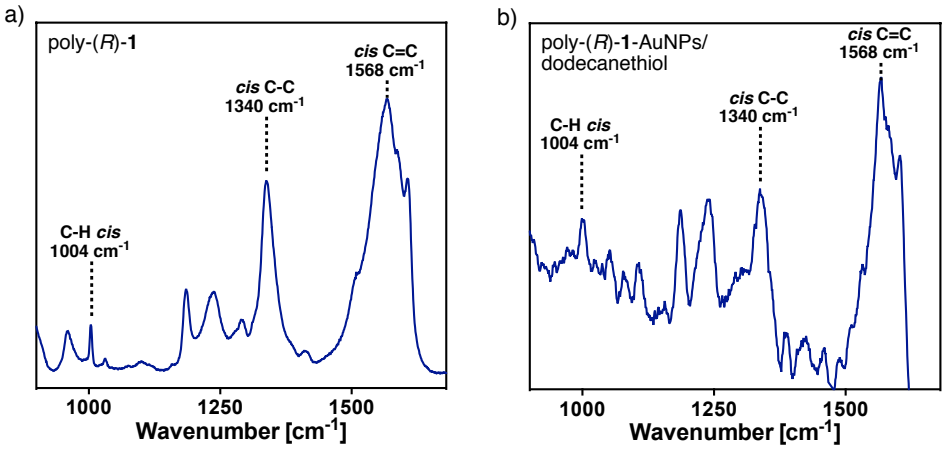

Figure S10. Raman spectra for a) poly-(*R*)-**1** and b) poly-(*R*)-**1**-AuNPs/dodecanethiol.

9.2 FT-IR studies for poly-(*R*)-1-AuNPs/dodecanethiol

FT-IR experiments of poly-(*R*)-**1** and poly-(*R*)-**1**-AuNPs/dodecanethiol nanocomposites were carried out to determine the interaction between poly-(*R*)-**1** and the AuNPs. These experiments confirmed the strong interaction between the anilide group of poly-(*R*)-**1** and the AuNPs —$D\tilde{\nu}_{CO}$ = 78 cm^{-1}; $D\tilde{\nu}_{NCO}$ = 16 cm^{-1}.

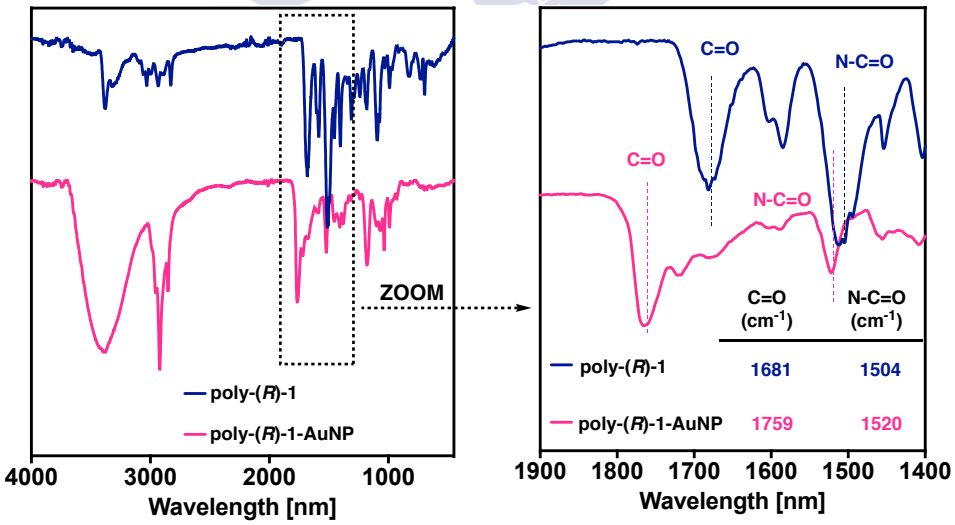

Figure S11. FT-IR spectra of poly-(*R*)-**1** and poly-(*R*)-**1**-AuNPs/dodecanethiol nanocomposites.

9.3 DLS studies of poly-(*R*)-1-AuNPs/dodecanethiol

DLS studies of poly-(*R*)-**1** (0.3 mg mL^{-1}, $CHCl_3$) and poly-(*R*)-**1**-AuNPs/dodecanethiol (0.3 mg mL^{-1}, $CHCl_3$) showed an increase in the size when the nanocomposite is formed.

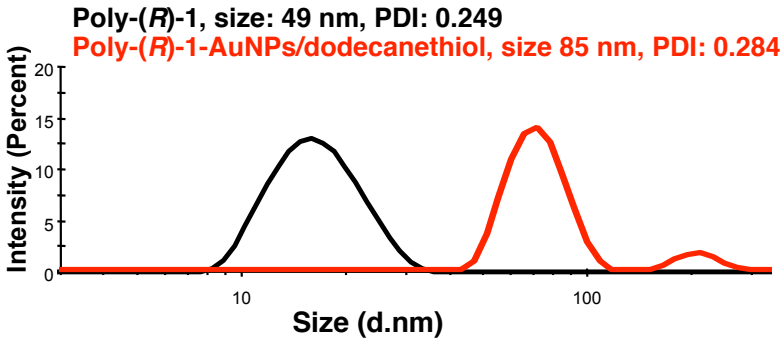

Figure S12. DLS measurements for poly-(*R*)-**1** and poly-(*R*)-**1**-AuNPs/dodecanethiol.

9.4 GPC characterization for poly-(*R*)-1-AuNPs/dodecanethiol

Size exclusion chromatography studies were performed on a Alliance 2695 HPLC System (Waters) liquid chromatography system equipped with a UV 2489 detector (Waters) using. The samples were eluted by two Phenogel columns connected to each other with stacionary phases of 10^3 and 10^5 Amstrong and packed with a solid support of a cross-linked stiyrene and *p*-divinylbenzene copolymer. To characterize the hybrid materials poly-(*R*)-**1**-AuNPs/dodecanethiol GPC chromatograms were recorded at 380 (polymer absorption) and 540 nm (gold nanoparticles absorption).

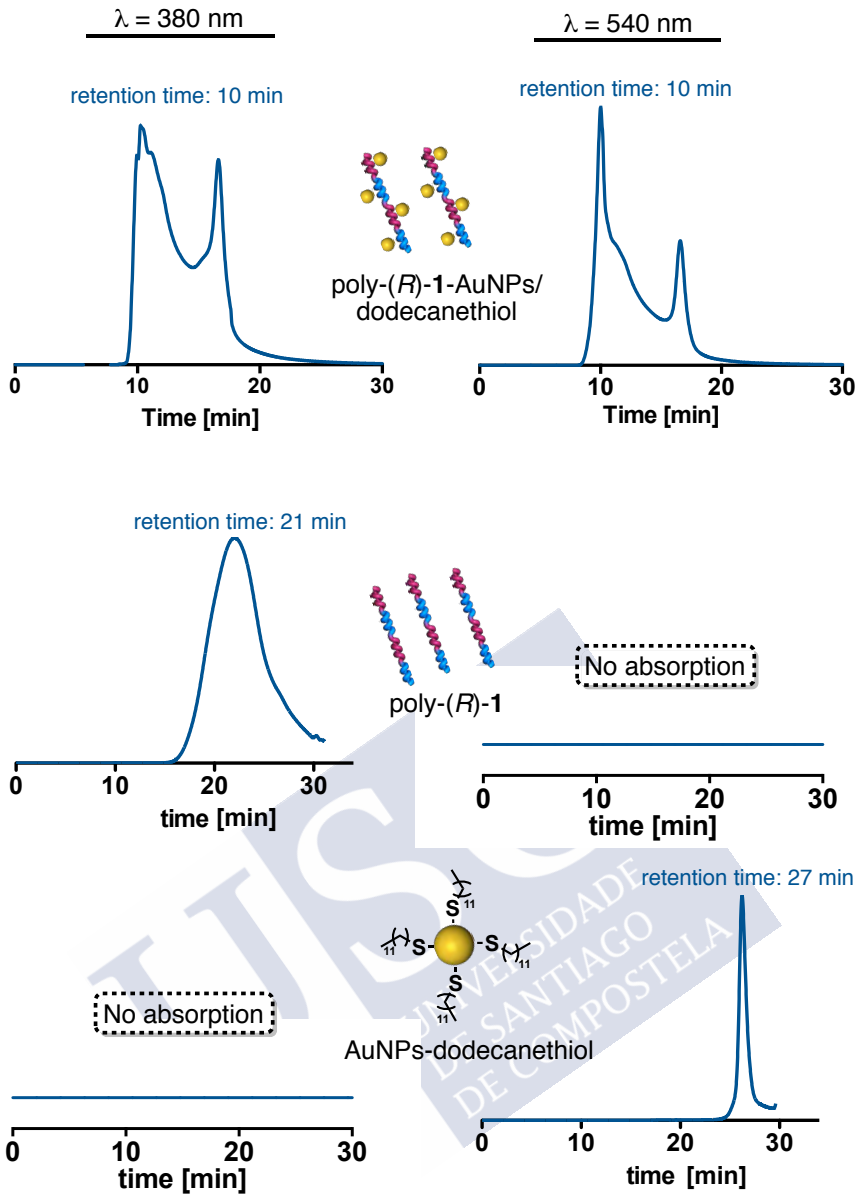

Figure S13. GPC chromatograms for solutions of poly-(*R*)-**1**, AuNPs@dodecanethiol and poly-(*R*)-**1**-AuNPs/dodecanethiol in THF at 380 and 540 nm.

10. Thermal studies for poly-(*R*)-1 and poly-(*R*)-1-AuNPs/dodecanethiol

10.1 DSC studies for poly-(*R*)-1 and poly-(*R*)-1-AuNPs/dodecanethiol

DSC studies were carried out in order to determine de geometry of the polymer backbone. As a general protocol, a polymer sample was kept in an aluminum pan and heated from 40 ºC to 350 ^{o}C with a heating rate of 10 ºC/min.

The thermograms showed the typical traces for a *cis-cisoidal* backbone for poly-(*R*)-**1** and poly-(*R*)-**1**-AuNPs/dodecanethiol.

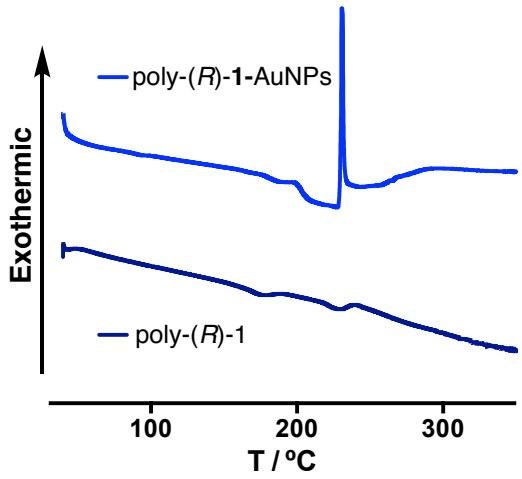

Figure S14. DSC thermograms for poly-(*R*)-**1** and poly-(*R*)-**1**-AuNPs/dodecanethiol.

10.2 TGA studies for poly-(*R*)-1 and poly-(*R*)-1-AuNPs/dodecanethiol

TGA Studies were carried out in order to determine the thermal stability of the copolymers. As a general protocol, a polymer sample was kept in a platinum pan and heated from 40 ^{o}C to 850 ^{o}C with a heating rate if 10 ^{o}C min^{-1}.

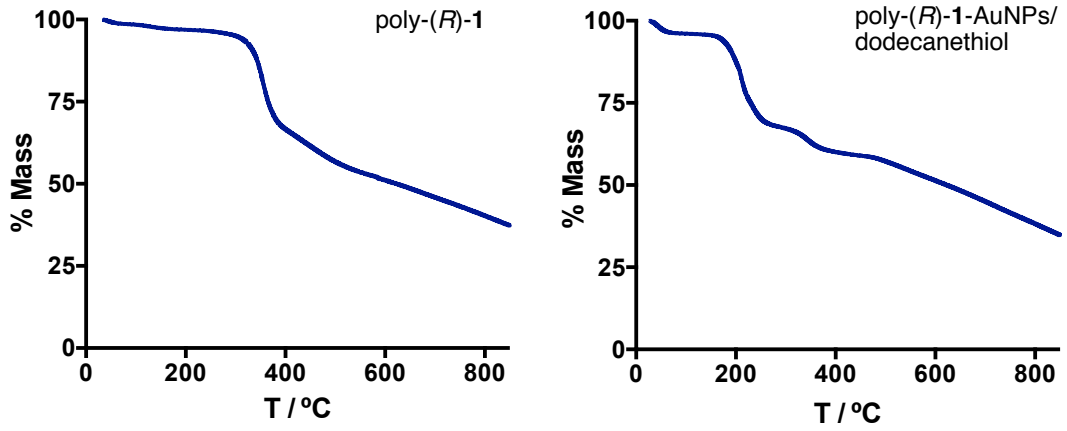

Figure S15. TGA studies for poly-(*R*)-**1** and poly-(*R*)-**1**-AuNPs/dodecanethiol.

11. ^{1}H NMR for poly-(*R*)-1-AuNPs/dodecanethiol

The *cis* stereoregularity of the poly-(*R*)-**1**-AuNPs/dodecanethiol (1 mg mL^{-1}, $CDCl_3$) was determined by ^{1}H NMR spectroscopy where the vinyl proton resonates around 5.8 ppm.

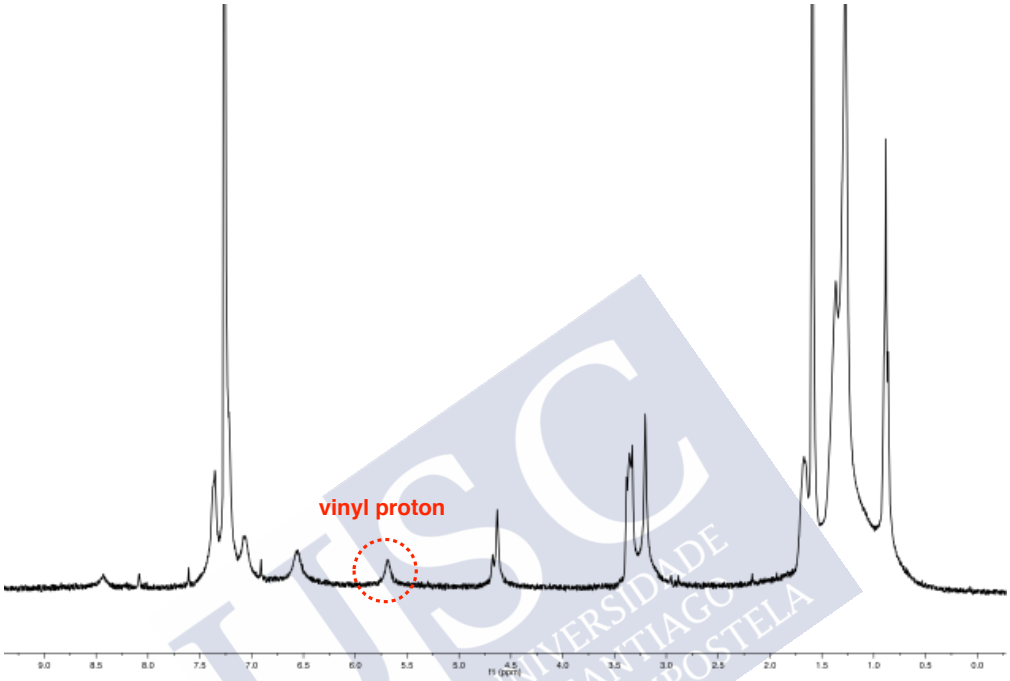

Figure S16. ^{1}H NMR for poly-(*R*)-**1**-AuNPs/dodecanethiol in $CDCl_3$.

12. TEM images for poly-(*R*)-1-AuNPs/dodecanethiol nanocomposites

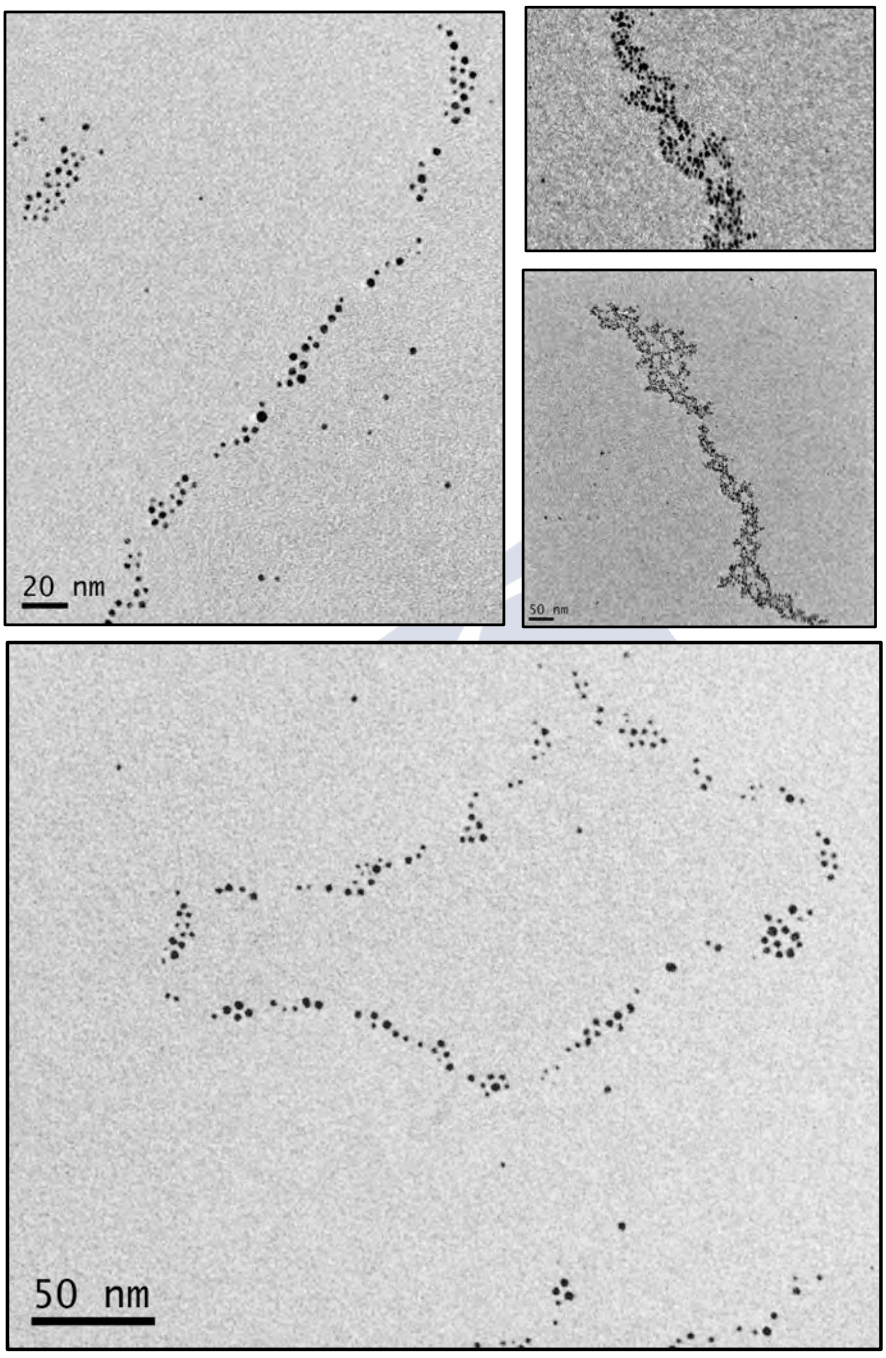

Figure S17. TEM images for poly-(*R*)-**1**-AuNPs/dodecanethiol nanocomposites.

13. Stimuli responsive studies for poly-(*R*)-1-AuNPs/dodecanethiol with metal ions

The addition of monovalent metal ions (Li^+) in THF to a solution of poly-(*R*)-**1**-AuNPs/dodecanethiol (0.1 mg mL^{-1}) in $CHCl_3$ produces *M* due to the chelation of the Li^+ ions to the carbonyl and the presence of the Li^+-p.

The addition of divalent metal ions (Ba^{2+}) in THF to a solution of poly-(*R*)-**1**-AuNPs/dodecanehtiol (0.1 mg mL^{-1}) in $CHCl_3$ produces *P* due to the chelation of the Ba^{2+} ions to the carbonyl and the methoxy groups.

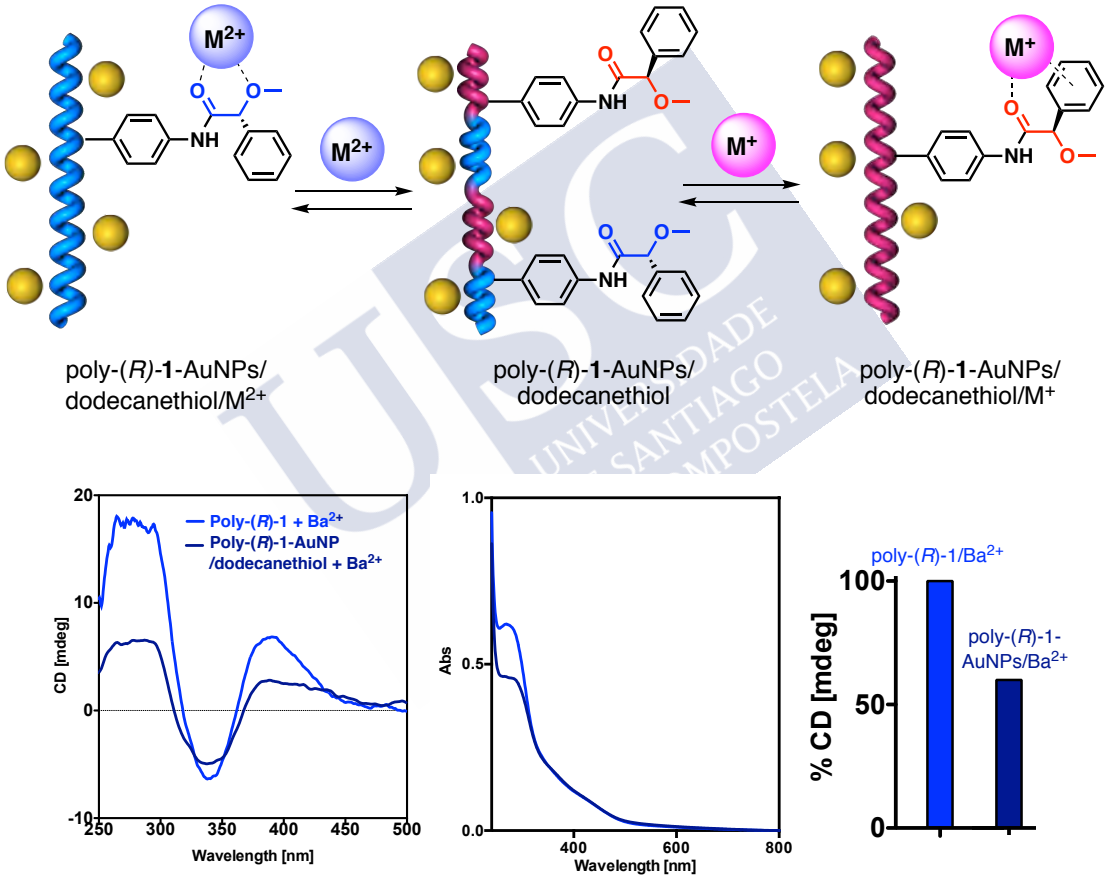

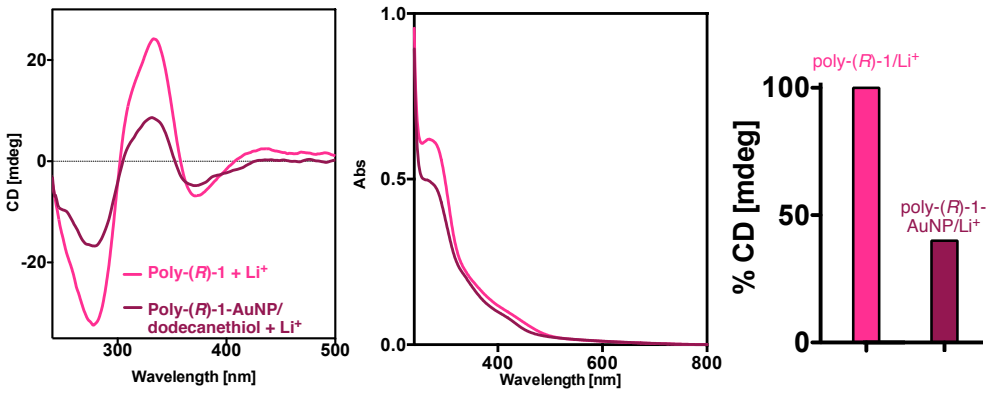

Figure S18. Dynamic behavior of poly-(*R*)-**1**-AuNPs/dodecanethiol with monovalent (Li^+) and divalent metal ions (Ba^{2+}).

14. Nanostructuration of poly-(*R*)-1-AuNPs/dodecanethiol using Ba^{2+} in polymeric nanospheres

The addition of divalent metal ions (Ba^{2+}) in THF to a solution of poly-(*R*)-**1**-AuNPs/dodecanehtiol (0.3 mg mL^{-1}) in $CHCl_3$ produces *P* due to the chelation of the Ba^{2+} ions to the carbonyl and the methoxy groups.

Moreover, the Ba^{2+} ions act as crosslinking agents between PPAs chains promoting the formation of nanospheres.

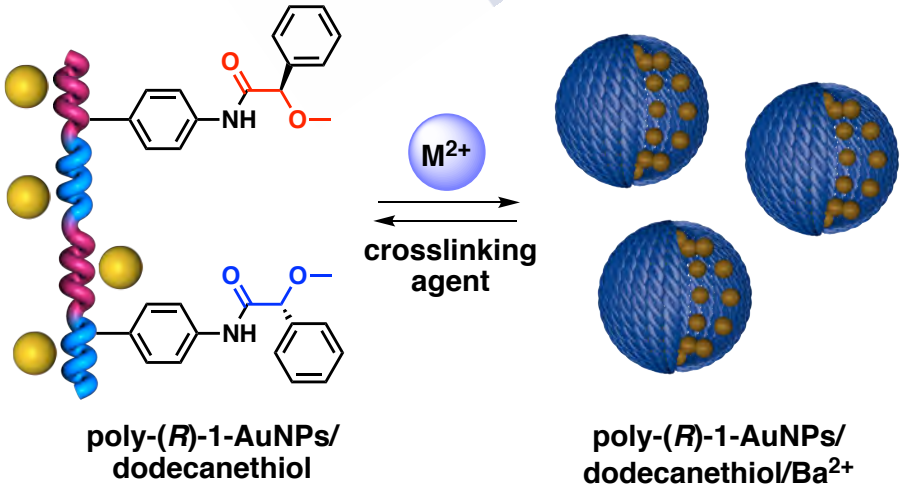

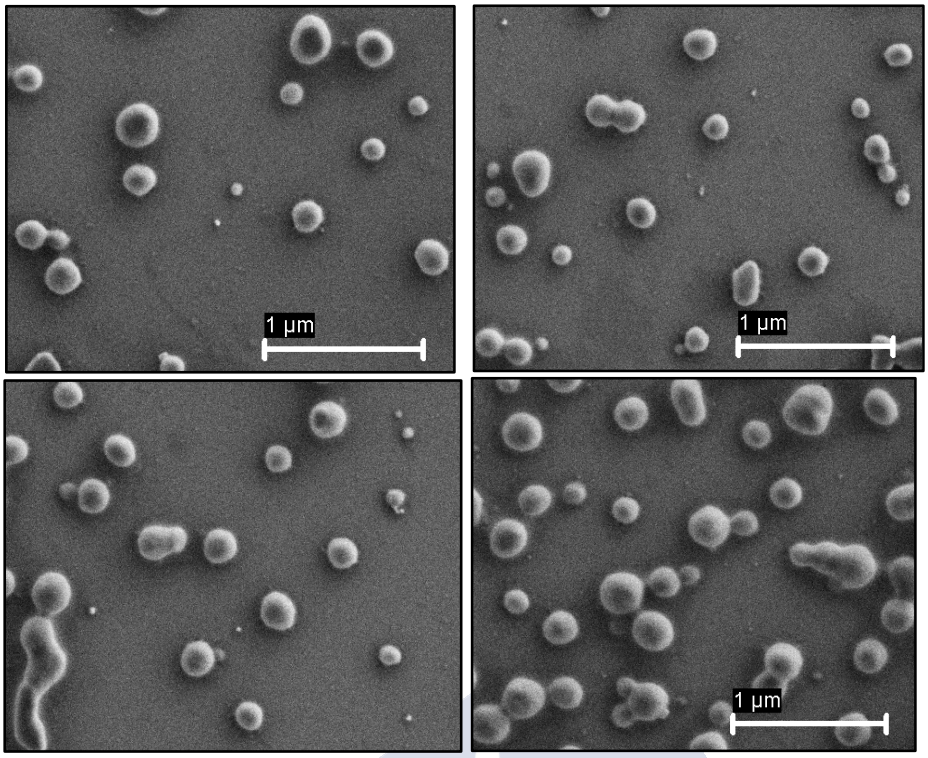

Figure S19. SEM images for poly-(*R*)-**1**-AuNPs/dodecanethiol/Ba^{2+} nanospheres.

15. References

S1. Freire, F.; Seco, J. M.; Quiñoá, E.; Riguera, R. Nanospheres with Tunable Size and Chirality from Helical Polymer–Metal Complexes. *J. Am. Chem. Soc.*, **2012**, *134*, 19374-19383.

S2. Bergueiro, J.; Núñez-Martínez, M.; Arias, S.; Quiñoá, E.; Riguera, R.; Freire, F.; Chiral Gold-PPA Nanocomposites with Tunable Helical Sense and Morphology. *Nanoscale Horiz.*, **2020**, *5*, 495-500.

S3. Núñez-Martínez, M.; Arias, S.; Quiñoá, E.; Riguera, R.; Freire, F.;. Dynamic Chiral PPA–AgNP Nanocomposites: Aligned Silver Nanoparticles Decorating Helical Polymers. *Chem. Mater.*, **2021**, *33*, 4805-4812.

USC
UNIVERSIDADE
DE SANTIAGO
DE COMPOSTELA

USC
UNIVERSIDADE
DE SANTIAGO
DE COMPOSTELA

Experimental Section Chapter VI:

1. Molecules and Codes

Monomers

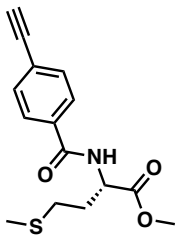

M-(*L*)-**1**

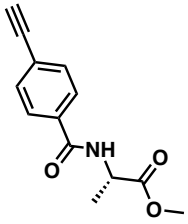

M-(*L*)-**2**

Homopolymers

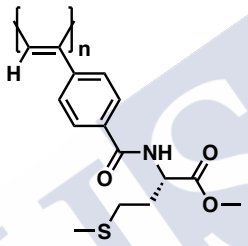

poly-(*L*)-**1**

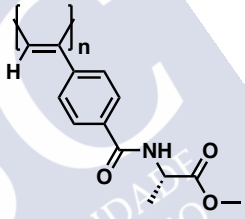

poly-(*L*)-**2**

Copolymer

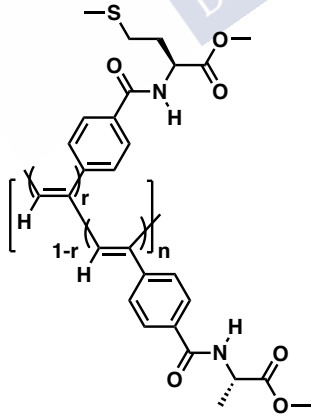

poly-[(*L*)-**1**$_r$-*co*-(*L*)-**2**$_{1-r}$]

2. Materials and methods

Chemicals. Commercially available chemicals have been used as delivered. Solvents were purchased as reagent grade and distilled if necessary. Anhydrous solvents were either purchased as ultra-dry solvent from Acros Organics® or received from solvent purification system. For the coupling and polymerization reactions, dry THF was obtained from MBRAUN SPS 800 solvent purification system. Water was purified by Millipore water purification system. Coupling reagents N-(3-Dimethylaminopropyl)-N'-ethylcarbodiimide hydrochloride (EDC·HCl), 1-Hydroxybenzotriazole hydrate (HOBt) and 4-ethynylbenzoic acid, were purchased from AnaSpec Inc. (*L*)-alanine methyl ester hydrochloride, (*L*)-methionine methyl ester hydrochloride, rhodium norbornadiene chloride dimer {$[Rh(nbd)Cl]_2$}, diisopropylethylamine (DIEA), triethylamine (TEA, 99%), sodium borohydride ($NaBH_4$), silver perchlorate ($AgClO_4$) and barium perchlorate [$(Ba(ClO_4)_2$], lithium perchlorate ($LiClO_4$) and gold(III) chloride hydrate ($HAuCl_4$) were purchased from Aldrich.

Instrumentations and Characterizations. NMR experiments were carried out in a Varian Inova 300 (300 MHz resonance 1H). Size exclusion chromatography studies were performed on Alliance 2695 HPLC System (Waters) liquid chromatography system equipped with a UV 2489 detector (Waters). The samples were eluted by three Phenogel columns connected to each other with stationary phases of 10^3, 10^4 and 10^5 Amstrong and packed with a solid support of a cross-linked styrene and *p*-divinylbenzene copolymer. CD and UV measurements were registered in a Jasco-720 spectropolarimeter and a Jasco-730 spectrophotometer respectively at a nanocomposite concentration of 0.3 mg mL^{-1}. FT-IR measurements were carried out on a Bruker IFS-66v. DLS studies were performed on a Nano-ZS 90 (Malvern) equipped with a He-Ne laser (l = 633 nm) under scattering angle of 173°. The samples were maintained at the designed temperature for 5 min before testing. DLS measurements were carried out in all cases at 0.3 mg·mL^{-1}. SEM measurements were performed on a LEO-435VP electron microscope equipped with an energy dispersive X-ray (EDX) spectrometer. TEM measurements were performed on a JEOL JEM 2010 and 200 KV as a voltage. To study the nanocomposite, or the nanospheres the same protocol was used. A dispersion of the nanocomposite or the nanospheres at a concentration of 0.3 mg mL^{-1} was drop casted onto of silicon wafer chip and allowed to dry at rt for 12h for SEM studies, while in case of TEM studies the dispersed materials were drop-casted onto carbon chip.

3. Synthesis of monomer M-(*L*)-1

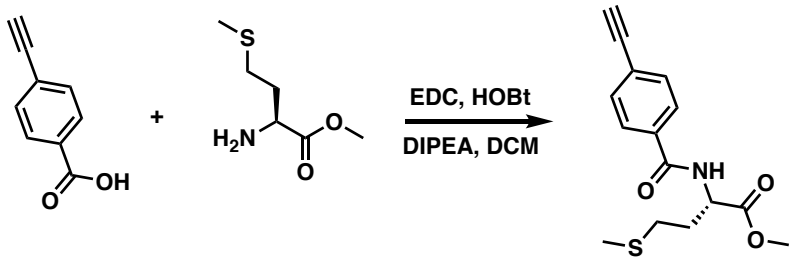

1-Ethyl-3-(3-dimethylaminopropyl)carbodiimide (EDC, 1.87 g, 1.2 equiv.), hydroxybenzotriazole (HOBt, 1.25 g, 1.2 equiv.), 4-ethynylbenzoic acid (1.0 g, 1.0 equiv) and diisopropyltriethylamine (DIPEA, 1.4 mL, 1.2 equiv.) were dissolved in 70 mL of CH_2Cl_2, and the mixture was stirred for 15 min to activate the acid. Then, *L*-methionine methyl ester hydrochloride (1.92 g, 1.2 equiv) was added and the reaction mixture was stirred overnight. The organic layer was washed with HCl 1M, saturated solution of $NaHCO_3$ and brine. The combined organic layers were dried over anhyd Na_2SO_4, filtered and the solvent was evaporated at reduced pressure. The crude product was chromatographed on silica gel (70-230 mesh) with hexane/ethyl acetate (7/3) as eluent [1.62 g M-(*L*)-**1**], 83% of pure product.

Spectroscopic data:

^{1}H NMR (300 MHz, $CDCl_3$) δ (ppm): 2.1 (s, 3H), 2.26 (m, 2H), 2.58 (t, 2H), 3.20 (s, 3H), 3.79 (s, 3H), 4.91 (q, 1H), 7.01 (d, 1H), 7.54 (2H, d), 7.77 (d, 2H).

^{13}C NMR (75 MHz, $CDCl_3$) δ (ppm): 15.7, 30.2, 31.6, 52.3, 52.8, 79.8, 82.8, 125.9, 127.2, 132.4, 133.8, 166.4, 172.6.

$[\alpha]_D^{20}$= = +42 (10 mg mL^{-1}, $CHCl_3$)

HRM (ESI) m/z calcd for $C_{15}H_{17}NO_3S$ $[M+Na]^+$: 314.0821, found: 314.0823.

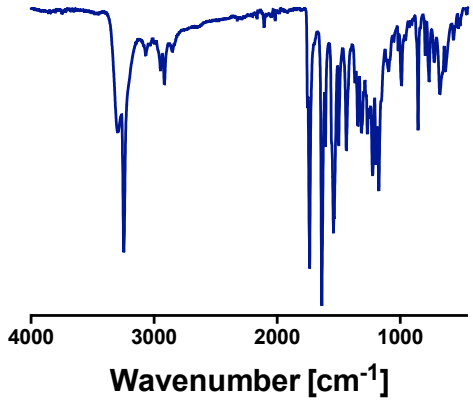

Figure S1. FT-IR spectrum of M-(*L*)-**1**.

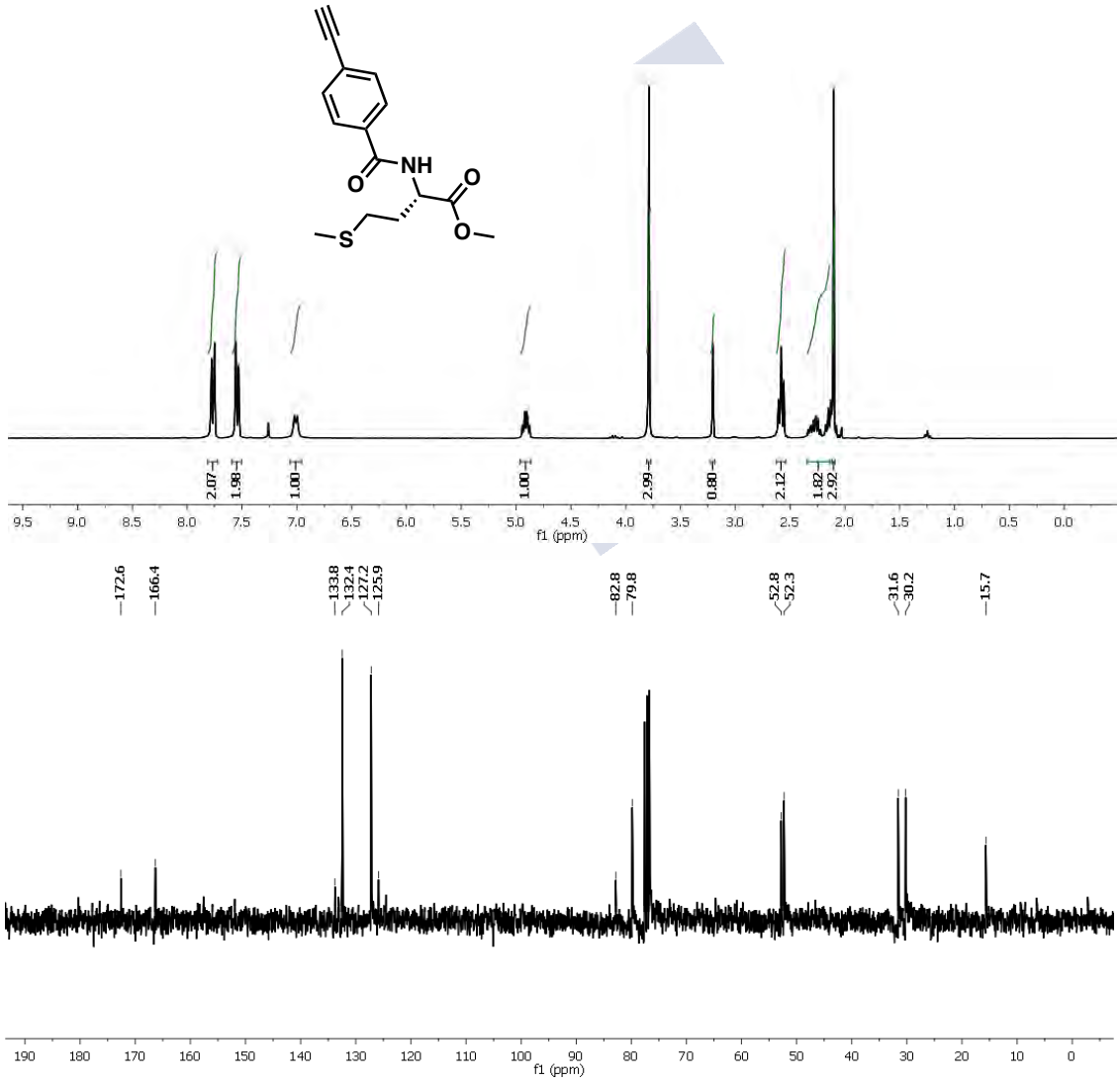

Figure S2. ^{1}H NMR and ^{13}C NMR spectra of M-(*L*)-**1** in $CDCl_3$.

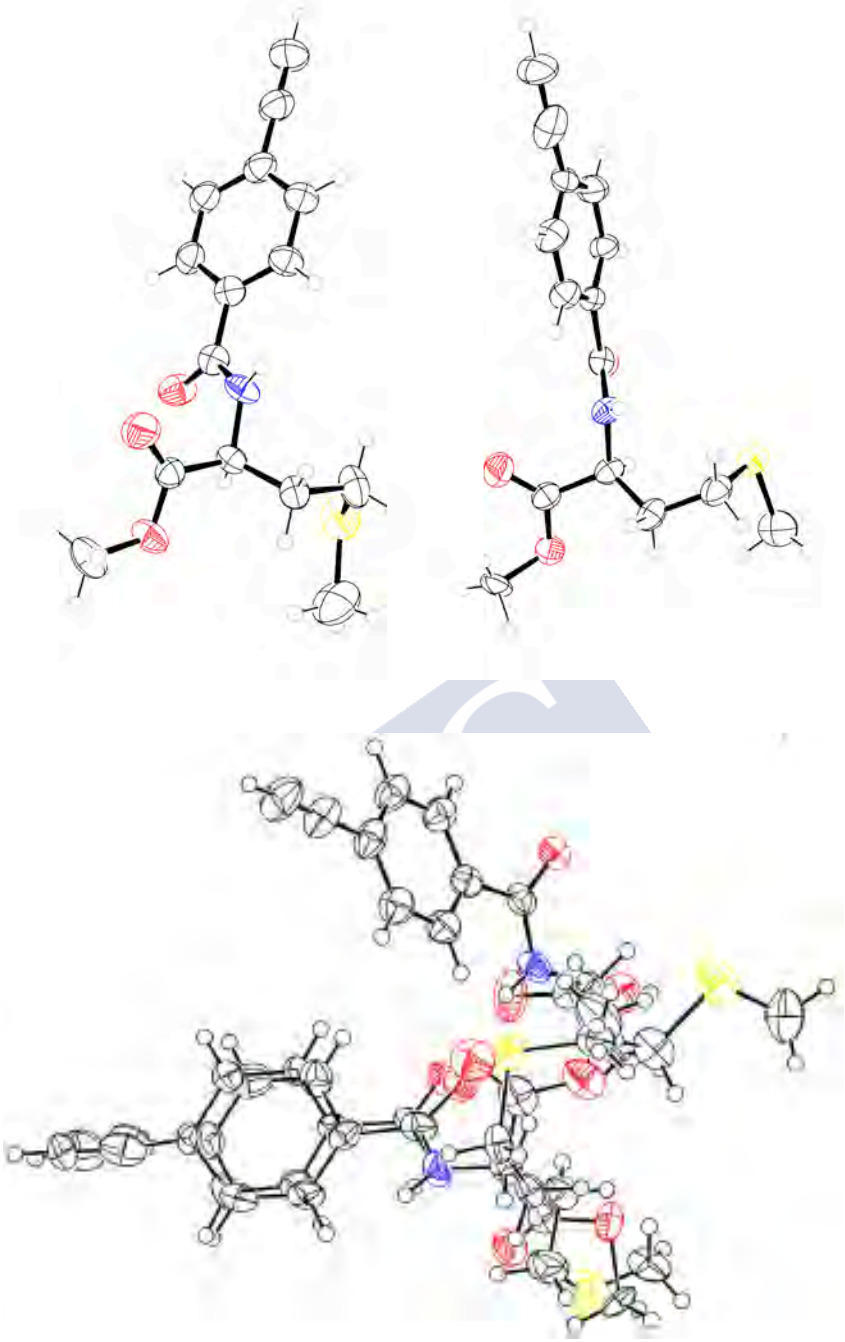

Figure S3. X-ray structure of monomer M-(*L*)-**1**.

Crystal data

$C_{15}H_{17}NO_3S$
$M_r = 291.35$
Monoclinic, $P2_1$
Hall symbol: P 2yb
$a = 9.5205\ (6)$ Å
$b = 16.2751\ (8)$ Å
$c = 10.6413\ (6)$ Å
$\beta = 109.997\ (3)°$
$V = 1549.43\ (15)$ Å^3
$Z = 4$
$F(000) = 616$
$D_x = 1.249$ Mg m^{-3}
Cu $K\alpha$ radiation, $\lambda = 1.54184$ Å
Cell parameters from 9919 reflections
$\theta = 4.9–79.0°$
$\mu = 1.91$ mm^{-1}
$T = 100$ K
Plate, colourless
0.22 × 0.16 × 0.08 mm

Data collection

Bruker D8 VENTURE PHOTON III-14 diffractometer
Radiation source: INCOATEC microfocus sealed tube, Incoatec IμS 3.0
Incoatec multilayer mirror monochromator
Detector resolution: 7.3910 pixels mm^{-1}
ω and phi scans
Absorption correction: multi-scan BRUKER *SADABS2016/2*
$T_{min} = 0.700$, $T_{max} = 0.818$
41097 measured reflections
6275 independent reflections
5904 reflections with $I > 2\sigma(I)$
$R_{int} = 0.044$
$\theta_{max} = 74.5°$, $\theta_{min} = 4.9°$
$h = -11 \rightarrow 11$
$k = -20 \rightarrow 20$
$l = -13 \rightarrow 13$

Refinement

Refinement on F^2
Least-squares matrix: full
$R[F^2 > 2\sigma(F^2)] = 0.052$
$wR(F^2) = 0.149$
$S = 1.05$
6275 reflections
548 parameters
20 restraints
0 constraints
Primary atom site location: dual
Secondary atom site location: dual
Hydrogen site location: mixed
H atoms treated by a mixture of independent and constrained refinement
$w = 1/[\sigma^2(F_o^2) + (0.0897P)^2 + 0.4876P]$ where $P = (F_o^2 + 2F_c^2)/3$
$(\Delta/\sigma)_{max} < 0.001$
$\Delta\rho_{max} = 0.55$ e Å^{-3}
$\Delta\rho_{min} = -0.55$ e Å^{-3}
Absolute structure: Flack x determined using 2599 quotients [(I+)-(I-)]/[(I+)+(I-)] (Parsons, Flack and Wagner, Acta Cryst. B69 (2013) 249-259).
Absolute structure parameter: 0.015 (7)

Figure S4. X-ray structure of monomer M-(*L*)-**1**.

4. Synthesis of monomer M-(*L*)-2

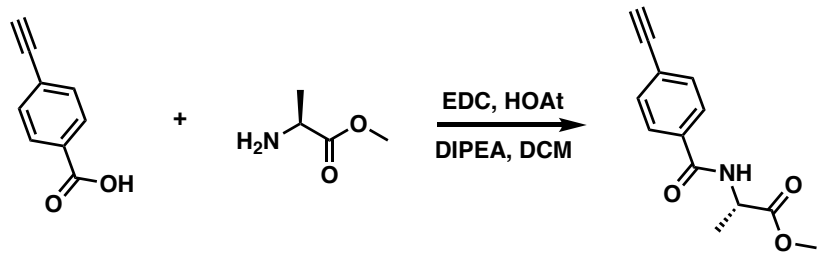

1-Ethyl-3-(3-dimethylaminopropyl)carbodiimide (EDC, 0.656 g, 1.2 equiv), hydroxybenzotriazole (HOBt, 0.465 g, 1.2 equiv), 4-ethynylbenzoic acid (0.500 g, 1.2 equiv) and diisopropyltriethylamine (DIPEA, 0.596 mL, 1.2 equiv) were dissolved in 70 mL of CH_2Cl_2, and the mixture was stirred for 15 min to activate the acid. Then, methyl *L*-Alaninate (0.388 g, 1.0 equiv) was added and the reaction mixture was stirred overnight. The organic layer was washed with HCl 1M, saturated solution of $NaHCO_3$ and brine. The combined organic layers were dried over anhyd Na_2SO_4, filtered and the solvent was evaporated at reduced pressure. The crude product was chromatographed on silica gel (70-230 mesh) with hexane/ethyl acetate (7/3) as eluent [0.503 g M-(*L*)-**2**], 76% of pure product.

Spectroscopic data:

^{1}H NMR (300 MHz, $CDCl_3$) δ (ppm): 1.49 (d, 3H), 3.25 (s, 1H), 3.74 (s, 3H), 4.75 (q, 1H), 7.29 (d, 1H), 7.48 (d, 2H), 7.76 (d, 2H).

^{13}C NMR (75 MHz, $CDCl_3$) δ (ppm): 18.0, 48.5, 52.4, 79.7, 82.7, 125.4, 127.1, 132.0, 133.6, 166.2, 173.5.

$[\alpha]_D^{20}$= +81 (15 mg mL^{-1}, $CHCl_3$).

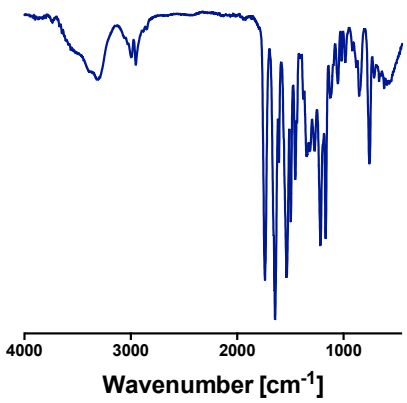

Figure S5. FT-IR spectrum for M-(*L*)-**2**.

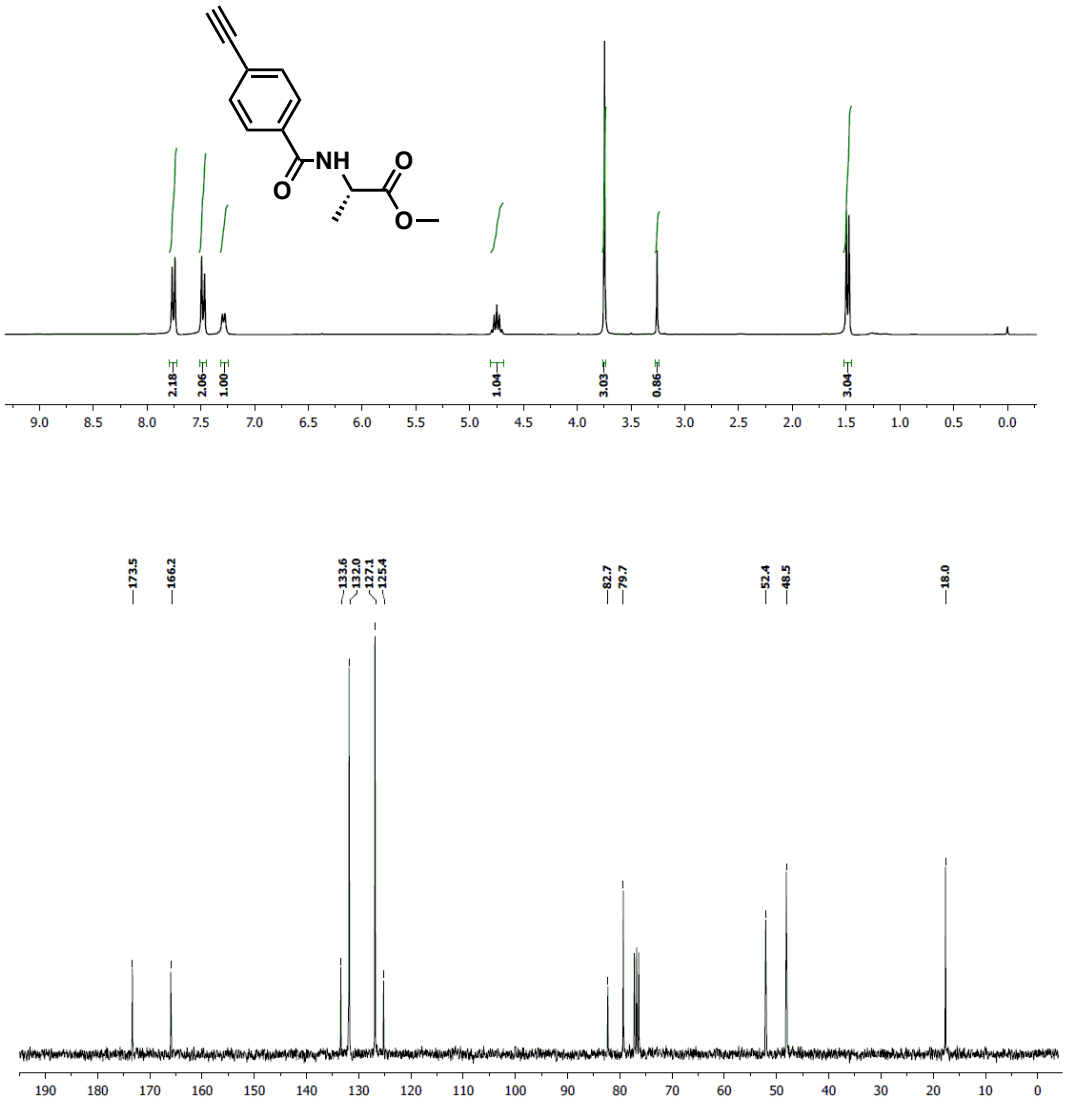

Figure S6. ^{1}H and ^{13}C NMR of monomer M-(*L*)-**2** in $CDCl_3$.

5. Synthesis of homopolymers

5.1 General procedure

The polymer was synthesized in a reaction flask (sealed ampoule) that was dried under vacuum and flushed with argon for three times before monomers were added as a solid. Then, the flask was evacuated on a vacuum line and flushed with dry argon (three times). Dry THF was added with a syringe and then, Et_3N dropwise. A solution of rhodium norbornadiene chloride dimer, $[Rh(nbd)Cl]_2$, in THF was added at 30 ^oC. The reaction mixture was stirred at 60 ^oC for 1 h. Next, the resulting polymer was diluted in CH_2Cl_2 and they were precipitated in a large amount of diethyl ether, centrifuged (twice) and re-precipitated in hexane and centrifuged again.

5.2 Synthesis of polymer poly-(*L*)-1

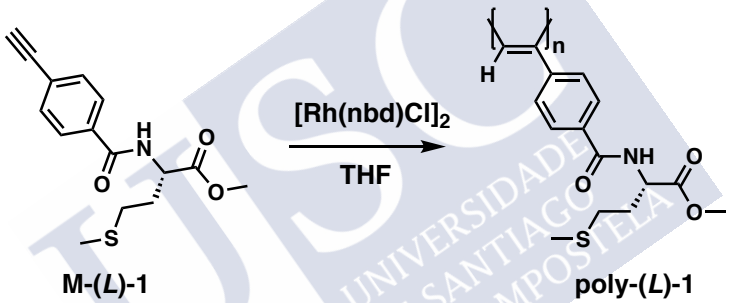

Following the general procedure, M-(*L*)-**1** (60 mg, 0.206 mmol), Et_3N (5 μL) and $[Rh(nbd)Cl]_2$ (0.94 mg) in THF (0.412 mL) yielded after centrifugation (88%) of poly-(*L*)-**1.**

GPC data: M_n = 13585, M_w = 33002, M_p = 12283, M_z = 93739, PDI = 2.42.

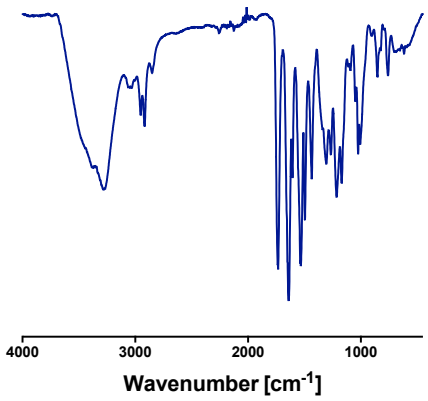

Figure S7. FT-IR spectrum of poly-(*L*)-**1**.

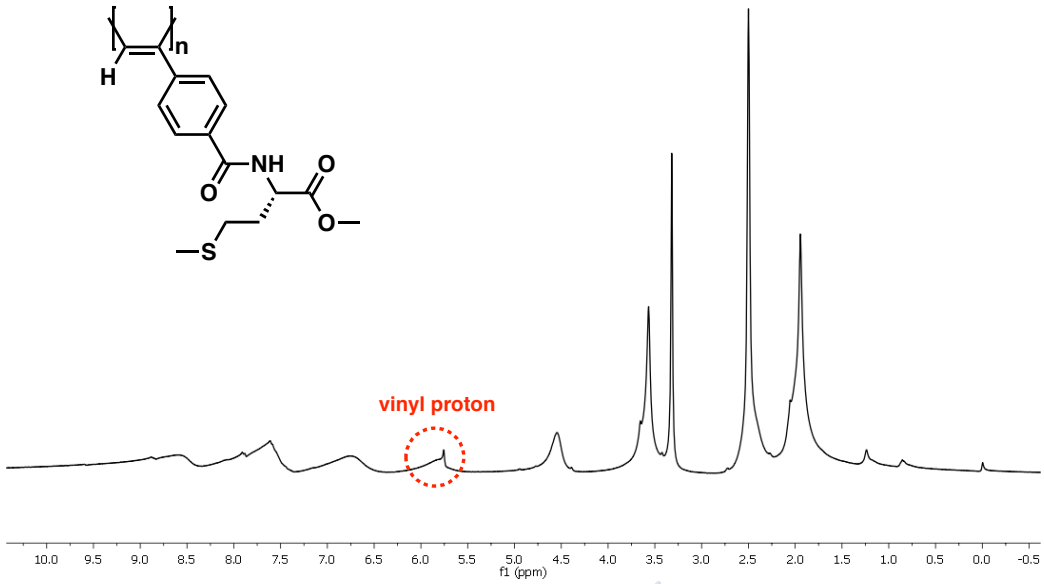

Figure S8. ^{1}H NMR spectrum of poly-(*L*)-**1** in DMSO-d_6.

5.3 Synthesis of polymer poly-(*L*)-2

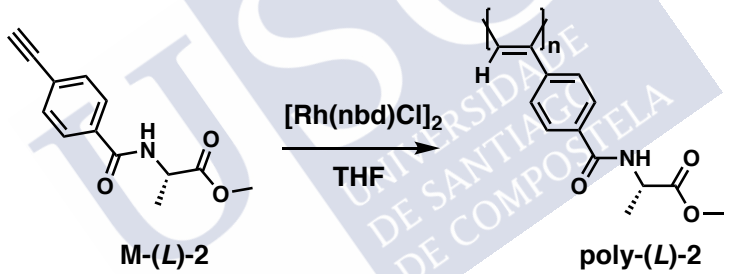

Following the general procedure, M-(*L*)-**2** (100 mg, 0.433 mmol), Et_3N (5 μL) and $[Rh(nbd)Cl]_2$ (1.98 mg) in THF (0.860 mL) yielded after centrifugation (91%) of poly-(*L*)-**2**. **GPC data**: M_n = 8989, M_w =35877, M_p = 8374, M_z = 250055, PDI = 3.99.

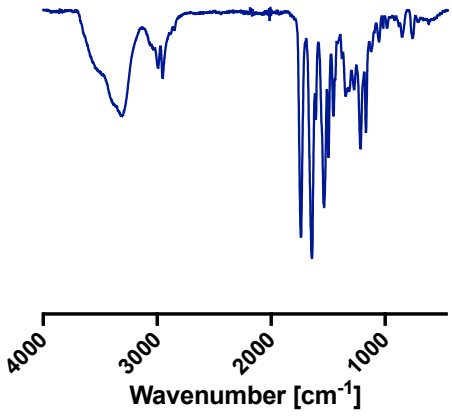

Figure S8. FT-IR spectrum of poly-(*L*)-**2.**

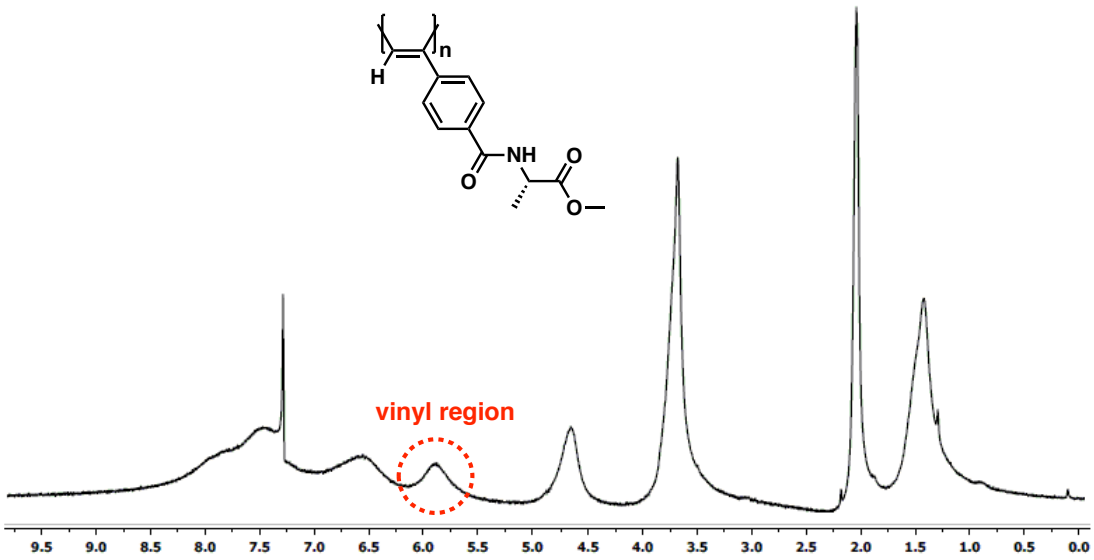

Figure S9. ^{1}H NMR spectrum of poly-(*L*)-**2** in $CDCl_3$.

7. Synthesis of copolymers poly-[(*L*)-1_r-*co*-(*L*)-2_{1-r}] series

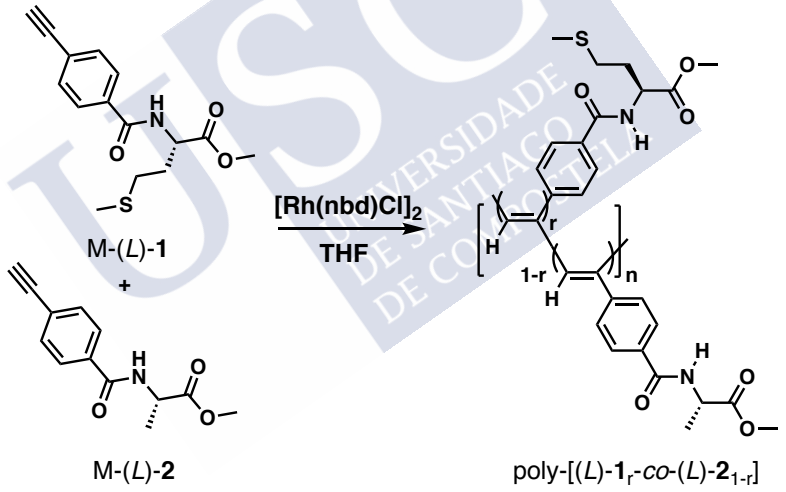

Following the general procedure, poly-[(*L*)-$\mathbf{1}_r$-*co*-(*L*)-$\mathbf{2}_{1-r}$] series was synthesized according to the different amounts of reagents M-(*L*)-**1** and M-(*L*)-**2**, Et_3N, $[Rh(nbd)Cl]_2$ and THF) reported in the table S1. The *cis* stereoregularity of the copolymers was determinated by ^{1}H NMR where the vynil proton resonance is between 5.6-5.9 ppm.

Table S1. Quantities of monomers, Et_3N, $[Rh(nbd)Cl]_2$ and THF.

Copolymer	**M1**	**M2**	**Et_3N (μL)**	**$[Rh(nbd)Cl]_2$ (mg)**	**THF (mL)**	**Yield (%)**
Poly-[(*L*)-**1**$_{0.8}$-*co*-(*L*)-**2**$_{0.2}$]	83	17	5	2	0.87	85
Poly-[(*L*)-**1**$_{0.6}$-*co*-(*L*)-**2**$_{0.4}$]	65	35	5	2	0.87	81
Poly-[(*L*)-**1**$_{0.4}$-*co*-(*L*)-**2**$_{0.6}$]	45	55	5	2	0.87	91
Poly-[(*L*)-**1**$_{0.2}$-*co*-(*L*)-**2**$_{0.8}$]	24	76	5	2	0.87	80

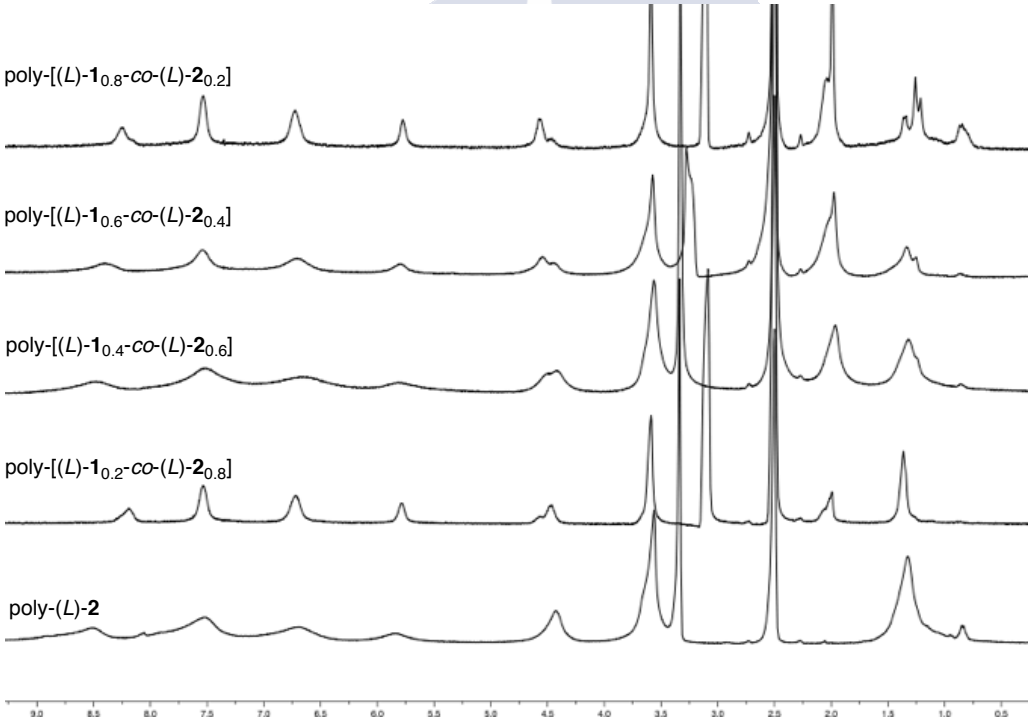

Figure S10. ^{1}H NMR of poly-[(*L*)-**1**$_r$-*co*-(*L*)-**2**$_{1-r}$] (r = 0.8-0.2) and poly-(*L*)-**2** series of copolymers (DMSO-d_6, 300 MHz).

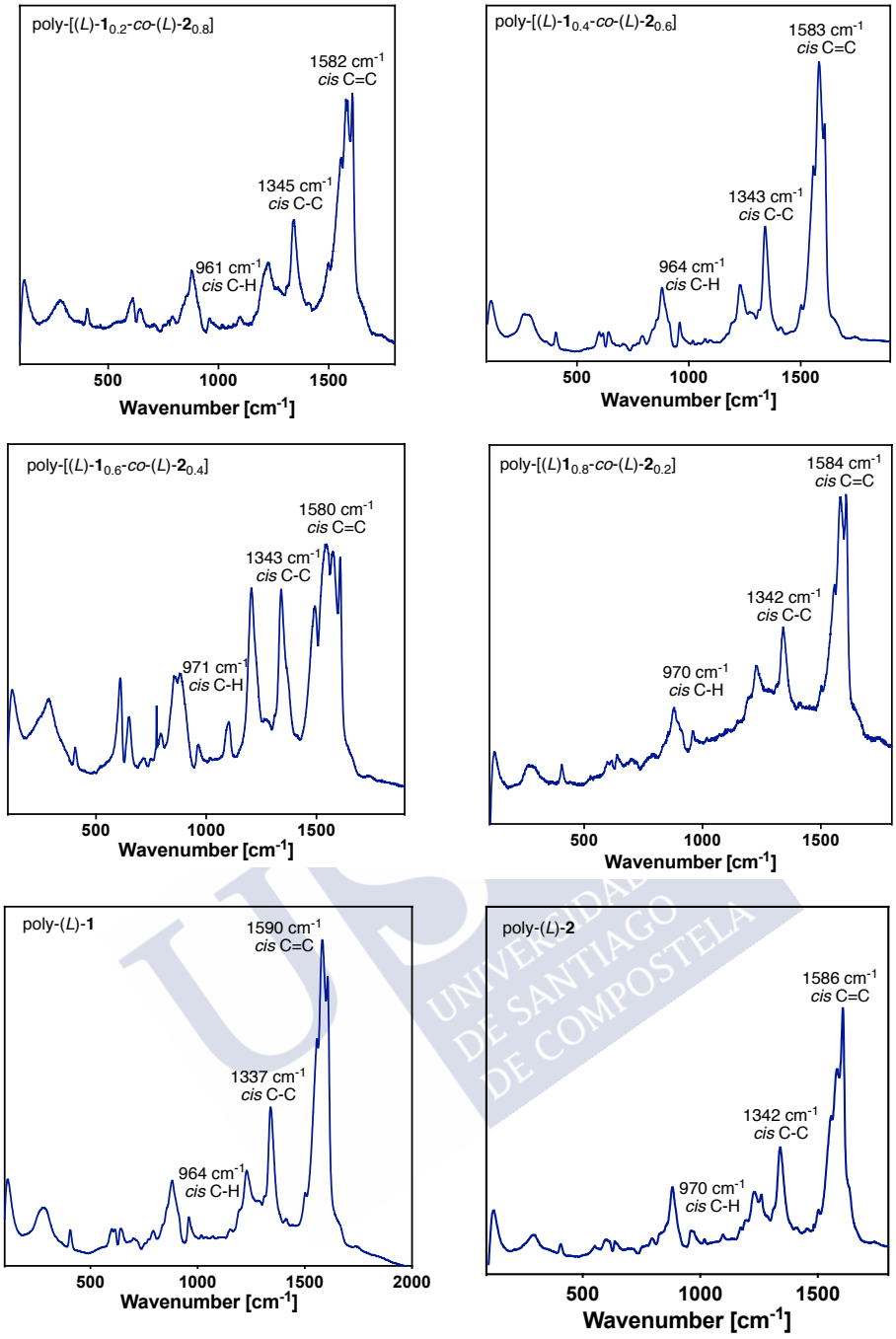

Figure S11. Raman spectra for copolymers poly-[(*L*)-**1**$_r$-*co*-(*L*)-**2**$_{1-r}$] (r = 0.8-0.2) (r = 0.8-0.2) series.

DSC studies were carried out in order to determine de geometry of the polymer backbone. As a general protocol, a polymer sample was kept in an aluminium pan and heated from 40°C to 350°C with a heating rate of 10°C min^{-1}.

- **DSC studies of poly-[(*L*)-$\mathbf{1}_r$-*co*-(*L*)-$\mathbf{2}_{1-r}$] (r = 0.8-0.2)**

The thermograms of the polymers showed typical traces for a *cis-trans* backbone, where two exothermal peaks corresponding to the *c-t* to *c-c* and the *c-c* to *t-t* were observed.

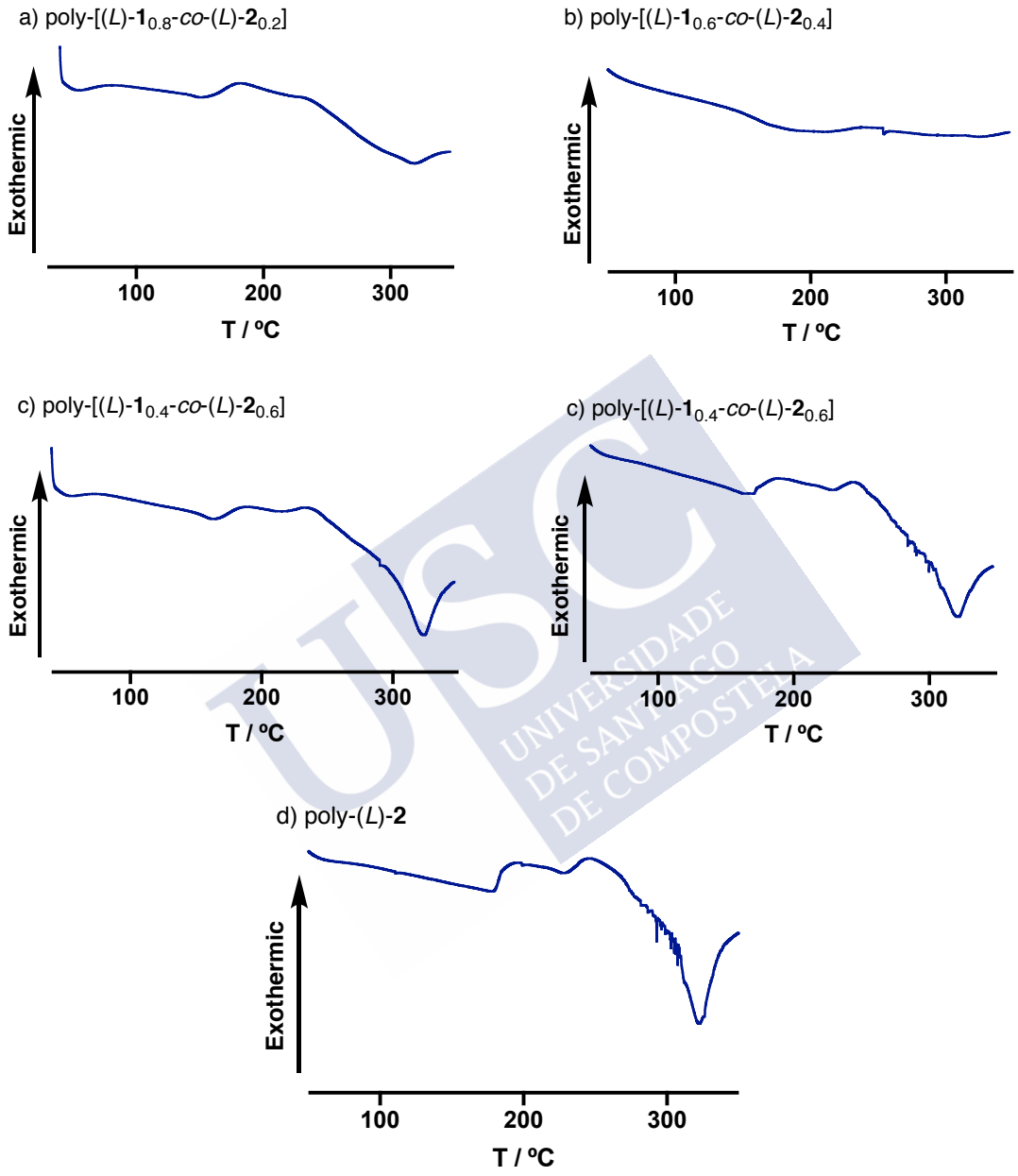

Figure S12. DSC studies of poly-[(*L*)-$\mathbf{1}_r$-*co*-(*L*)-$\mathbf{2}_{1-r}$] (r = 0.8-0.2) series of copolymers.

- **TGA studies of poly-[(*L*)-1_r-*co*-(*L*)-2_{1-r}] (r = 0.8-0.2) series**

TGA Studies were carried out in order to determine the thermal stability of the copolymers. As a general protocol, a copolymer sample was kept in a platinum pan and heated from 40 ^{o}C to 850 ^{o}C with a heating rate if 10 ^{o}C min^{-1}.

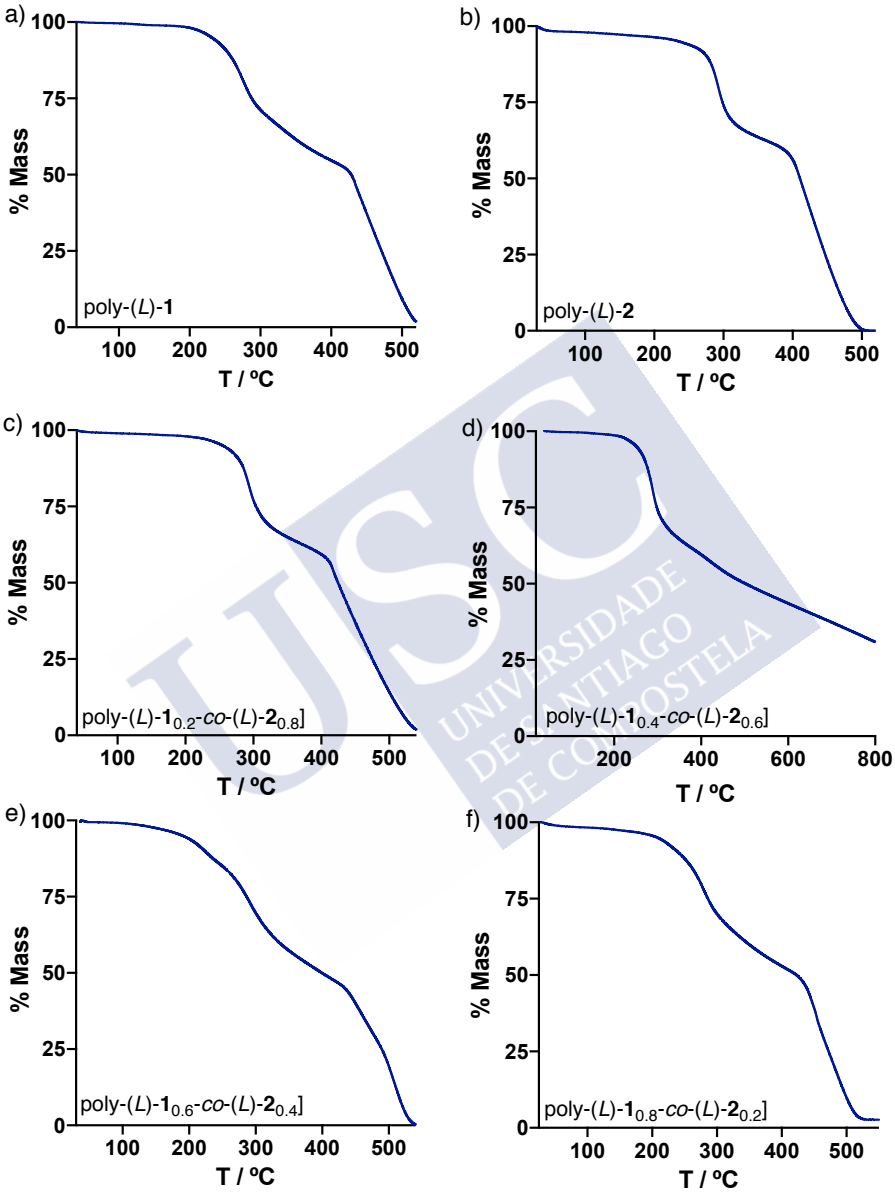

Figure S12. TGA studies of poly-[(*L*)-$\mathbf{1}_r$-*co*-(*L*)-$\mathbf{2}_{1-r}$] (r = 0.8-0.2) series of copolymers.

Table S2. GPC data of the copolymers.

Polymer	M_n	M_w	M_p	M_z	PDI
Poly-(*L*)-**2**	8989	35877	8374	250055	3.99
Poly-[(*L*)-$\mathbf{1}_{0.8}$-*co*-(*L*)-$\mathbf{2}_{0.2}$]	5281	23296	7395	129509	4.41
Poly-[(*L*)-$\mathbf{1}_{0.6}$-*co*-(*L*)-$\mathbf{2}_{0.4}$]	5186	19214	7939	78399	3.70
Poly-[(*L*)-$\mathbf{1}_{0.4}$-*co*-(*L*)-$\mathbf{2}_{0.6}$]	8780	40844	20269	157407	4.65
Poly-[(*L*)-$\mathbf{1}_{0.2}$-*co*-(*L*)-$\mathbf{2}_{0.8}$]	7690	9226	7759	11161	1.20

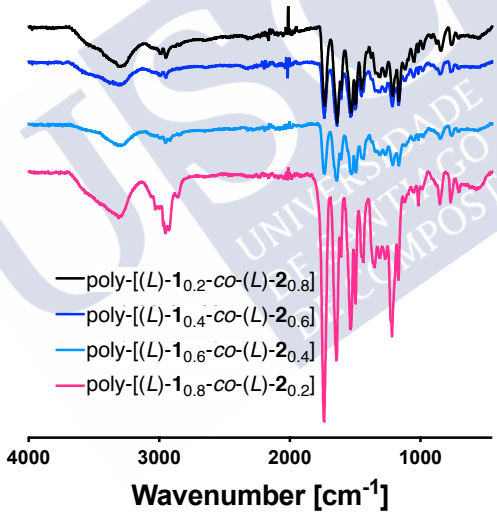

Figure S13. FT-IR spectra of poly-[(*L*)-$\mathbf{1}_r$-*co*-(*L*)-$\mathbf{2}_{1-r}$] (r = 0.8-0.2) series of copolymers.

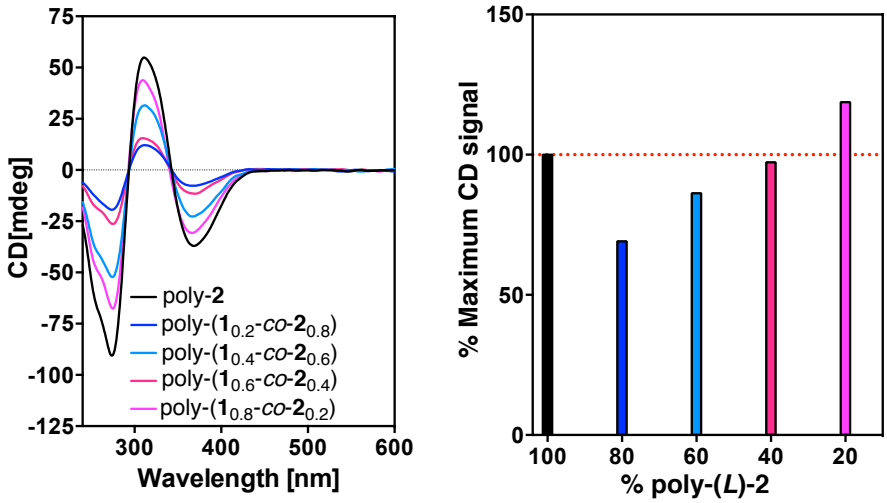

Figure S14. CD spectra and %Maximum CD signal for copolymers poly-[(*L*)-**1**$_r$-*co*-(*L*)-**2**$_{1-r}$) (r = 0.8-0.2) series.

8. Microscopy studies of poly-(*L*)-1

During the preparation of poly-(*L*)-**1**, it was observed formation of a gel structure if the the synthesis of the polymer is carried out at room temperature. SEM studies after sputtering with Ir during 5 s have shown the formation of a gel structure.

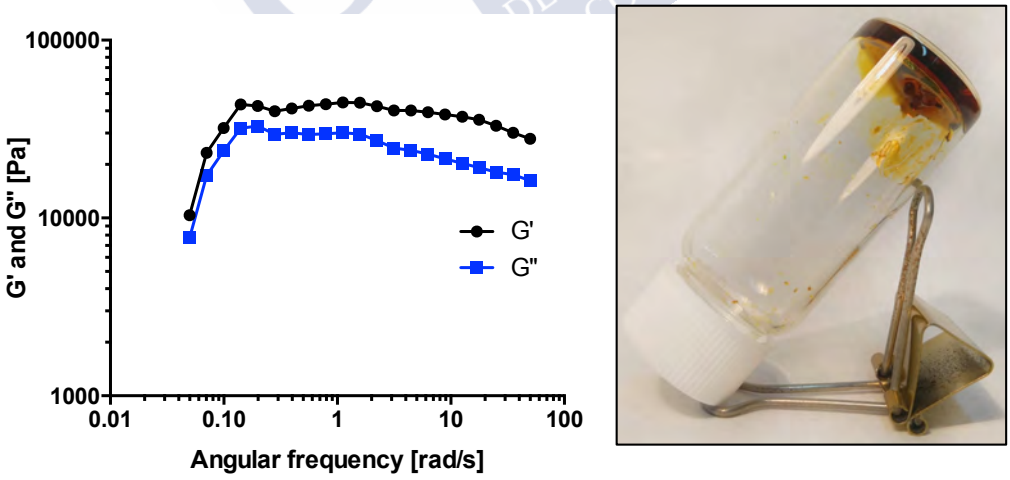

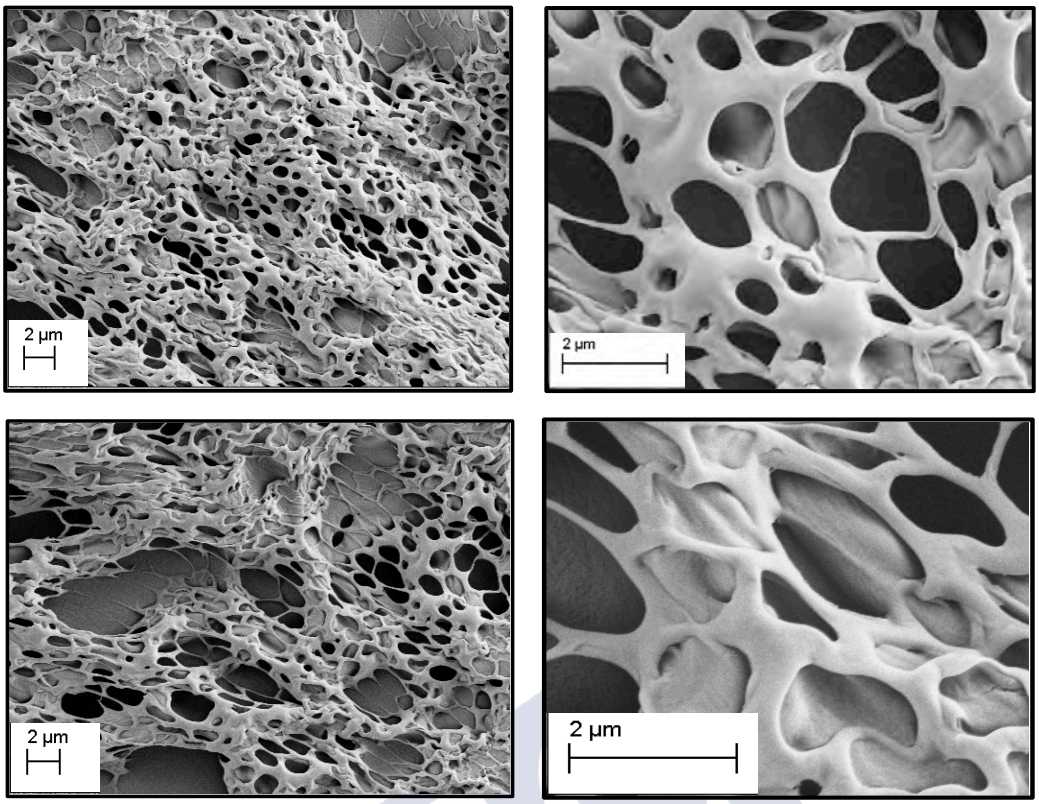

Figure S15. SEM images of gel structure in poly-(*L*)-**1**.

9. FT-IR studies of poly-(*L*)-1 in presence of Ba^{2+} ions

ATR/FT-IR spectra were recorded in a BRUKER IFS-66v spectrophotometer. A solution of $Ba(ClO_4)_2$ (0.5 equiv, 10.0 mg mL^{-1} in MeOH) was added to a solution of poly-(*L*)-**1** in $CHCl_3$ (0.3 mg mL^{-1}) and then the FT-IR spectrum were registred. The experiments confirmed the coordination of Ba^{2+} to both carbonyl groups in poly-(*L*)-**1**.

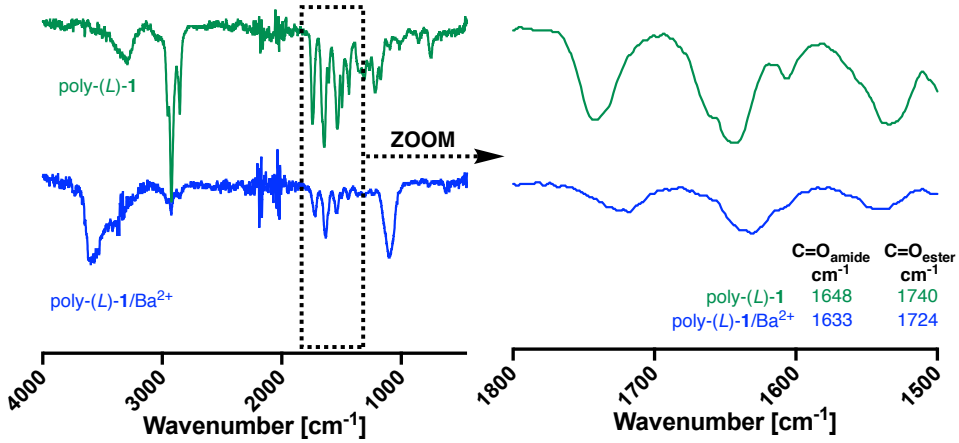

Figure S16. FT-IR spectra of poly-(*L*)-**1** and poly-(*L*)-**1**/Ba^{2+} complexes.

10. Stimuli responsive studies of poly-(*L*)-2 in presence of Au^{3+} ions and polar and low polar solvents

Stimuli-responsive studies in presence of Au^{3+} ions and polar and low polar solvents were carried out to determine the dynamic properties of poly-(*L*)-**2**. For that, CD studies were carried out with a solution of poly-(*L*)-**2** (0.3 mg mL^{-1}) in $CHCl_3$ in presence of $HAuCl_4$ (10 mg mL^{-1} in MeOH) as source of Au^{3+} ions.

Thus, poly-(*L*)-**2** dissolved in $CHCl_3$ showed the formation of *M* helices ($CD_{370} < 0$) corresponding to an *anti* conformation between carbonyl groups. On the other hand, the addition of 0.4 equiv of Au^{3+} ions to poly-(*L*)-**2** promoted an helical inversion (*P* helices, $CD_{370} > 0$) due to the coordination of the Au^{3+} ions to the carbonyl groups in an *anti* conformation.

Moreover, the solution of poly-(*L*)-**2** in low polar solvents ($CHCl_3$, DCM) lead to the formation of *M* helices ($CD_{370} < 0$, *anti* conformation) whereas the solution of poly-(*L*)-**2** in high polar solvents (DMF, DMSO) formed the opposite helical sense (*P* helices, $CD_{370} > 0$).

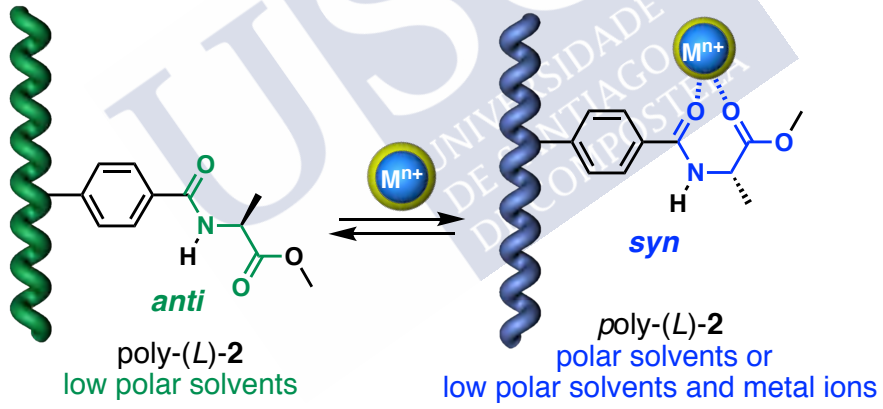

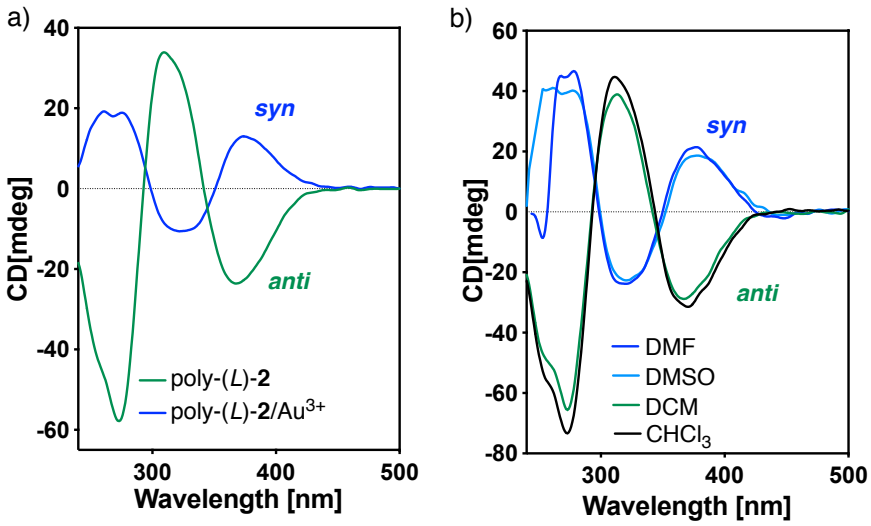

Figure S17. CD studies for the preparation of poly-(*L*)-**2** in presence of Au^{3+} ions and low poly and high polar solvents.

The coordination of Au^{3+} ions to poly-(*L*)-**2** was studied by FT-IR experiments. A solution of $HAuCl_4$ (0.5 equiv, 10.0 mg mL^{-1} in MeOH) was added to a solution of poly-(*L*)-**2** in $CHCl_3$ (0.3 mg mL^{-1}) and then the FT-IR spectrum were registered. The experiments confirmed the coordination of Au^{3+} to both carbonyl groups in poly-(*L*)-**2**.

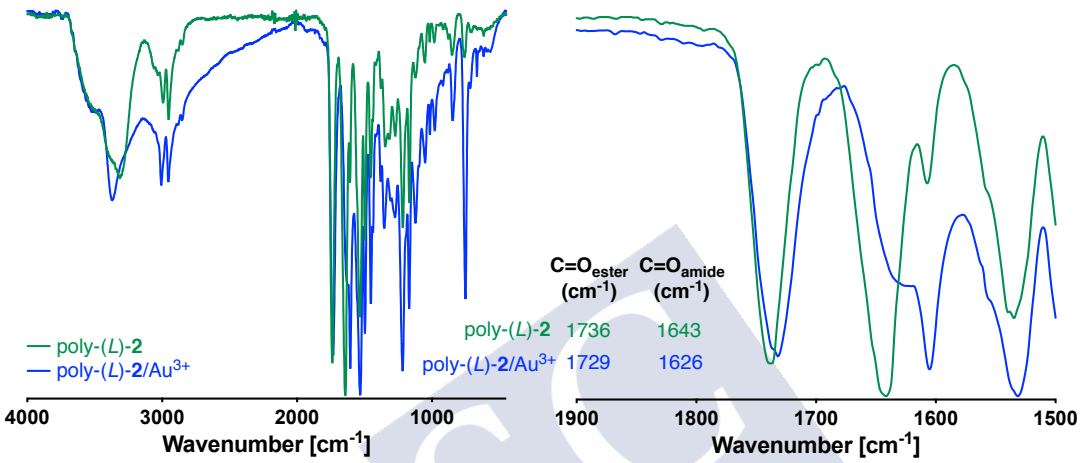

Figure S18. FT-IR spectra of poly-(*L*)-**2** and poly-(*L*)-**2**/Au^{3+} complexes.

11. Stimuli responsive studies of poly-[(*L*)-1_r-co-(*L*)-2_{1-r}] (r = 0.2-0.8) in presence of Ba^{2+} ions

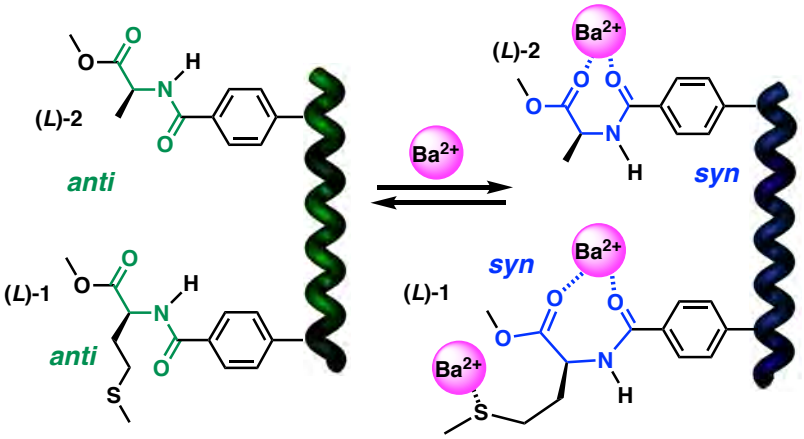

poly-[(*L*)-**1**$_r$-*co*-(*L*)-**2**$_{1-r}$] poly-[(*L*)-**1**$_r$-*co*-(*L*)-**2**$_{1-r}$]/Ba^{2+}

Stimuli-responsive studies of poly-[(*L*)-**1**$_r$-*co*-(*L*)-**2**$_{1-r}$] (r = 0.8-0.2) in presence of Ba^{2+} ions were carried out to determine the dynamic properties of the PPAs. For that, CD studies were carried out with a solution of poly-[(*L*)-**1**$_r$-*co*-(*L*)-**2**$_{1-r}$] (r = 0.2-0.8) (0.3 mg mL^{-1}) in $CHCl_3$ in presence of $BaClO_4$ (10 mg mL^{-1} in MeOH) as source of Ba^{2+} ions.

Thus, poly-[(*L*)-**1**$_r$-*co*-(*L*)-**2**$_{1-r}$] (r = 0.2-0.8) in $CHCl_3$ showed the formation of *M* helices (CD_{370} < 0) corresponding to an *anti* conformation between carbonyl groups. On the other hand, the addition 0.4 equiv of Ba^{2+} ions to poly-[(*L*)-**1**$_r$-*co*-(*L*)-**2**$_{1-r}$] (r = 0.2-0.8) promoted an helical inversion (*P* helices, CD_{370} > 0) due to the coordination of the Ba^{2+} ions to the carbonyl groups in a *syn* conformation.

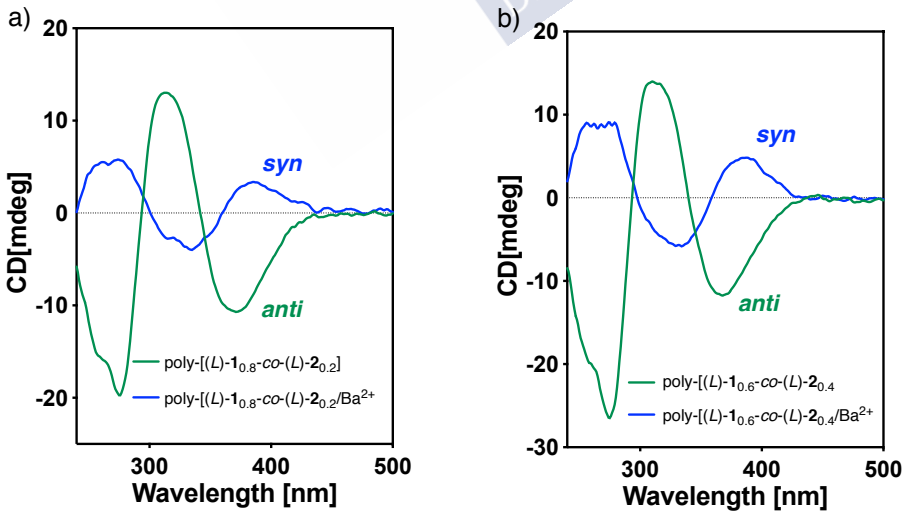

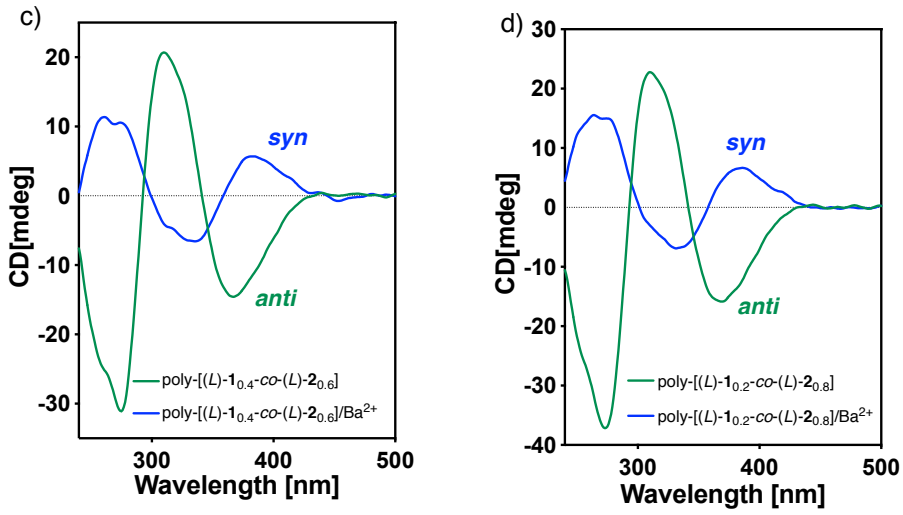

Figure S19. a) CD and UV studies of poly-[(*L*)-**1**$_{0.8}$-*co*-(*L*)-**2**$_{0.2}$] in presence of Ba^{2+} ions. b) CD and UV studies of poly-[(*L*)-**1**$_{0.6}$-*co*-(*L*)-**2**$_{0.4}$] in presence of Ba^{2+} ions. c) CD and UV studies of poly-[(*L*)-**1**$_{0.4}$-*co*-(*L*)-**2**$_{0.6}$] in presence of Ba^{2+} ions. d) CD and UV studies of poly-[(*L*)-**1**$_{0.2}$-*co*-(*L*)-**2**$_{0.8}$] in presence of Ba^{2+} ions.

12. Preparation of poly-(*L*)-2-AuNPs nanocomposites

A solution of poly-(*L*)-**2** (0.3 mg mL^{-1}) in $CHCl_3$ (CD_{370} < 0, *M* helices) is titrated with 0.5 equiv of $HAuCl_4$ (10 mg mL^{-1}, MeOH) to form a poly-(*L*)-**2**/Au^{3+} complexes resulting an helical inversion (CD_{370} > 0, *P* helices). Finally, the addition of 1.0 equiv of $NaBH_4$ (1 mg mL^{-1}, MeOH form poly-(*L*)-**2**-AuNPs.

UV-Vis showed the presence of a classical LSPR band corresponding to the formation of spherical AuNPs. TEM images confirm the formation of high polydisperse spherical AuNPs. Furthermore, the AuNPs have shown a poor stability in solution.

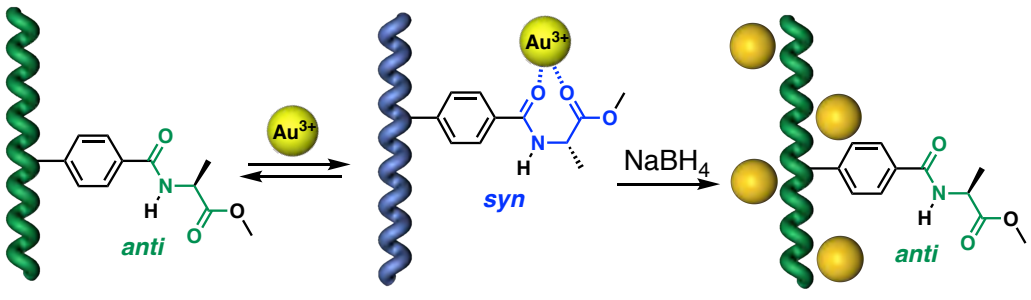

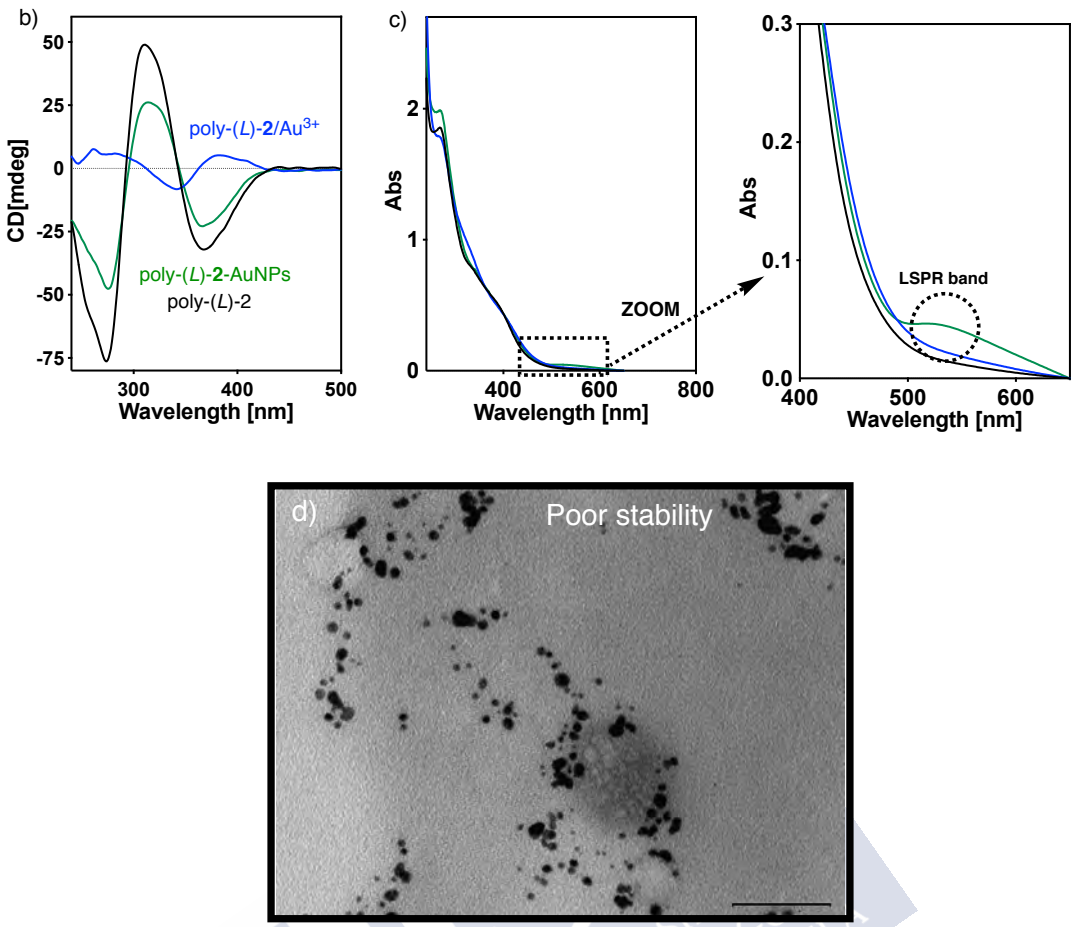

Figure S20. a) Schematic representation for the preparation for poly-(*L*)-**2**-AuNPs nanocomposites. b) CD traces for poly-(*L*)-**2**, poly-(*L*)-**2**/Au^{3+} complexes and poly-(*L*)-**2**-AuNPs nanocomposites. c) UV-Vis experiments for poly-(*L*)-**2**, poly-(*L*)-**2**/Au^{3+} complexes and poly-(*L*)-**2**-AuNPs nanocomposites. d) TEM image for poly-(*L*)-**2**-AuNPs nanocomposites.

13. Preparation of poly-(*L*)-2-AgNPs nanocomposites

A solution of poly-(*L*)-**2** (0.3 mg mL^{-1}) in $CHCl_3$ (CD_{370} < 0, *M* helices) is titrated with 0.5 equiv. of $AgClO_4$ (10 mg mL^{-1}, MeOH) to form a poly-(*L*)-**2**/Ag^+ complexes resulting an helical inversion (CD_{370} > 0, *P* helices). Finally, the addition of 1.0 equiv. of $NaBH_4$ (1 mg mL^{-1}, MeOH form poly-(*L*)-**2**-AgNPs.

UV-Vis showed the presence of the typical localized plasmon surface resonance (LSPR) band corresponding to the formation of spherical AgNPs. Interestilgy, UV-Vis spectrum after 24 hours showed a strong depletion in the LSPR band indicating a poor stability of the AgNPs.

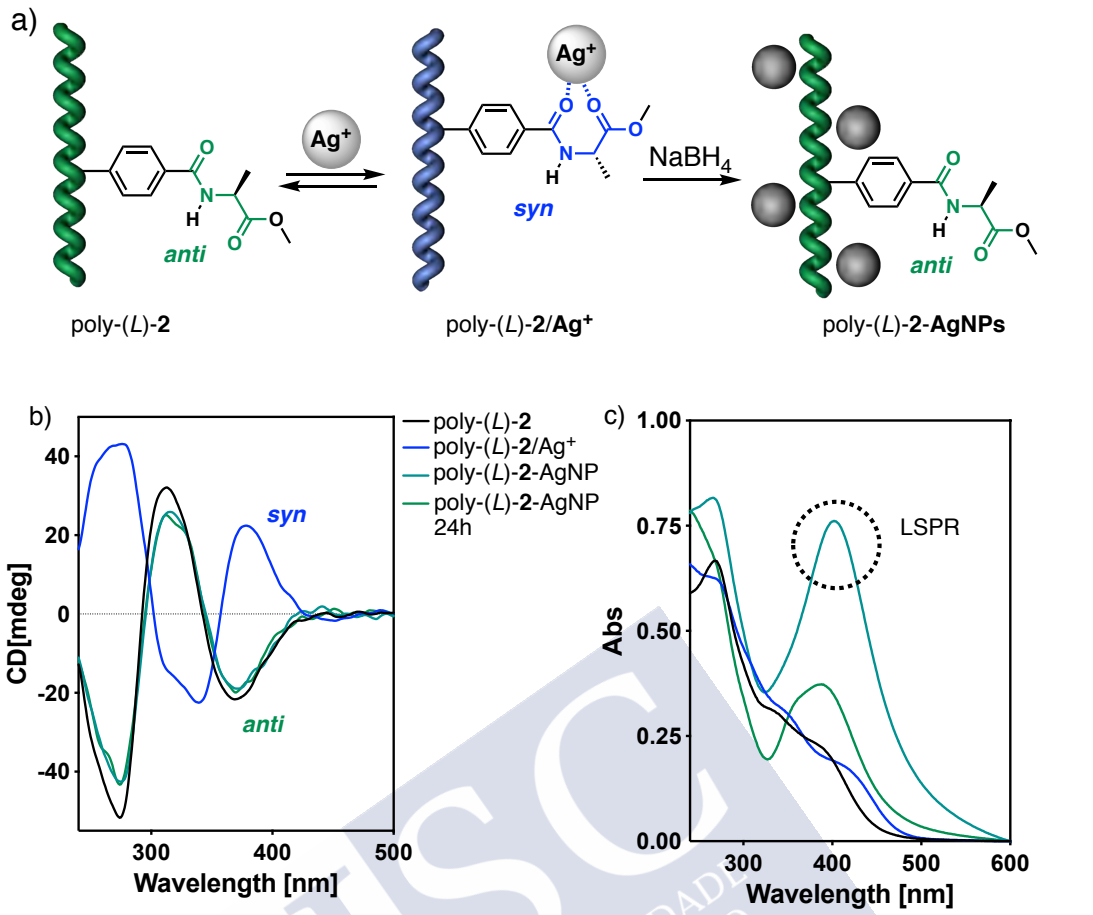

Figure S21. a) Schematic representation for the preparation for poly-(*L*)-**2**-AgNPs nanocomposites. b) CD traces for poly-(*L*)-**2**, poly-(*L*)-**2**/Ag^+ complexes, poly-(*L*)-**2**-AgNPs nanocomposites and poly-(*L*)-**2**-AgNPs at 24 hours. c) UV-Vis experiments CD traces for poly-(*L*)-**2**, poly-(*L*)-**2**/Ag^+ complexes, poly-(*L*)-**2**-AgNPs nanocomposites and poly-(*L*)-**2**-AgNPs at 24 hours.

14. Preparation of poly-(*L*)-1-AuNPs nanocomposites

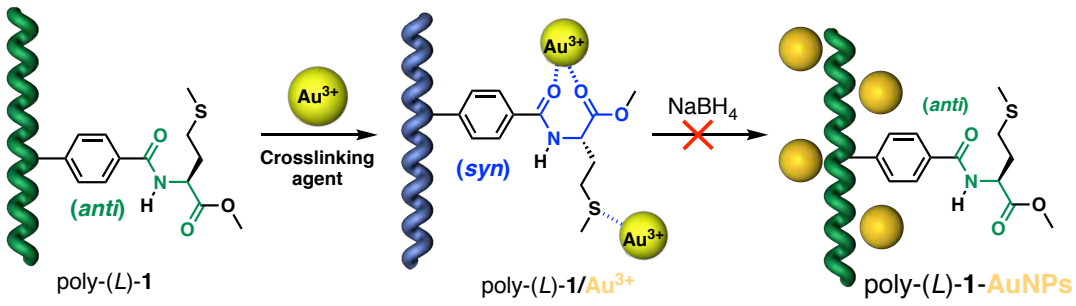

The general protocol to form the nanocomposites was employed to determine the ability of poly-(*L*)-**1** as stabilizing agent of AuNPs.

For that, CD studies of poly-(*L*)-**1** in $CHCl_3$ (0.3 mg mL^{-1}) showed the formation of *M* helices ($CD_{370} < 0$) corresponding an *anti* conformation between carbonyl groups. Interestingly, the addition of 0.5 equiv $HAuCl_4$ (10 mg mL^{-1}, MeOH) to poly-(*L*)-**1** showed the aggregation of the polymer chains leading to null CD in the vinylic region (370 nm). The aggregation of PPAs chains avoided the ulterior formation of the AuNPs.

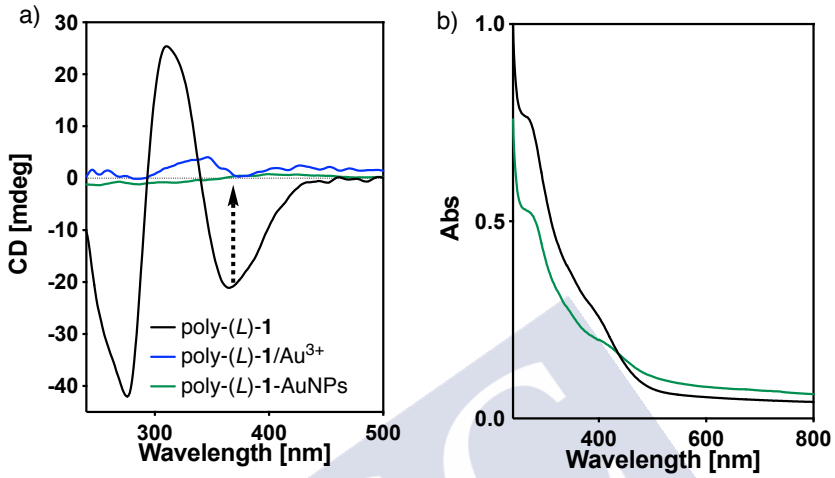

Figure S22. a) CD and b) UV studies for the preparation of poly-(*L*)-**1**-AuNPs nanocomposites.

13. Preparation of poly-(*L*)-1-AgNPs nanocomposites

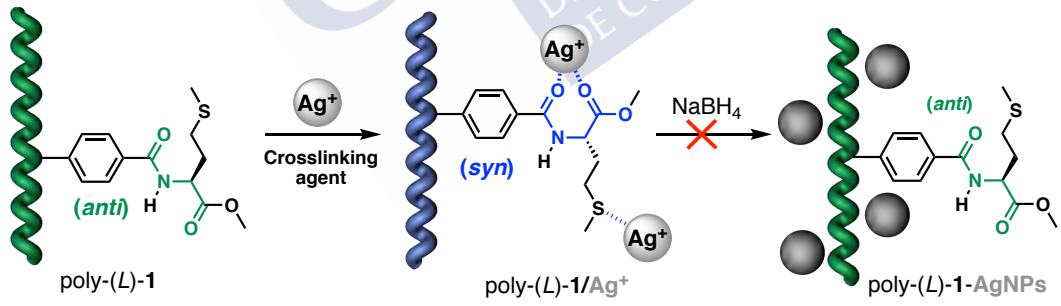

The general protocol to form the nanocomposites was employed to determine the ability of poly-(*L*)-**1** as stabilizing agent of AgNPs.

For that, CD studies of poly-(*L*)-**1** in $CHCl_3$ (0.3 mg mL^{-1}) showed the formation of *M* helices ($CD_{370} < 0$) corresponding an *anti* conformation between carbonyl groups. Interestingly, the addition of 0.5 equiv $AgClO_4$ (10 mg mL^{-1}, MeOH) to poly-(*L*)-**1** showed the aggregation of the polymer chains leading to null CD in the vinyl region ($CD_{370} = 0$). The aggregation of PPAs chaing avoided the ulterior formation of the AgNPs.

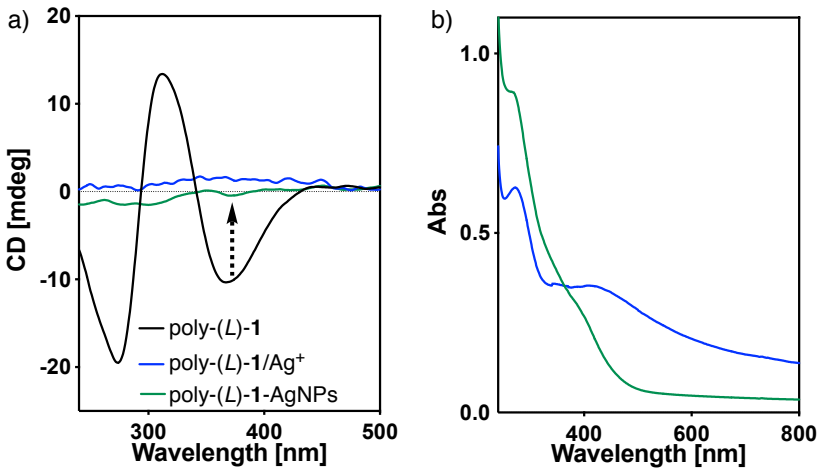

Figure S23. a) CD and b) UV studies for the preparation poly-(*L*)-**1**-AgNPs nanocomposites.

14. General procedure for the preparation of poly-[(*L*)-$\mathbf{1}_r$-*co*-(*L*)-$\mathbf{2}_{1-r}$)-MNPs (M = Ag or Au) nanocomposites

Poly-[(*L*)-$\mathbf{1}_{0.2}$-*co*-(*L*)-$\mathbf{2}_{0.8}$)-MNPs (M = Au, Ag) nanocomposites were prepared according to this procedure. First, all the glassware was washed with aqua regia, Milli Q water and acetone. The reaction was carried out at room temperature and using Ar atmosphere.

Poly-[(*L*)-$\mathbf{1}_{0.2}$-*co*-(*L*)-$\mathbf{2}_{0.8}$) was dissolved in $CHCl_3$ (0.3 mg mL^{-1}) and then, $HAuCl_4$ (10 mg mL^{-1}) as source of Au^{3+} ions or $AgClO_4$ (0.5 equiv.) as source of Ag^+ ions in MeOH were added to form the poly-($\mathbf{1}_r$-*co*-$\mathbf{2}_{1-r}$)/M^{n+} (M^{n+} = Au^{3+}, Ag^+) complexes. Next, $NaBH_4$ (1.0 equiv., 1.0 mg mL^{-1}) in MeOH was added to form Poly-[(*L*)-$\mathbf{1}_{0.2}$-*co*-(*L*)-$\mathbf{2}_{0.8}$)-MNPs (M = Ag or Au) nanocomposites.

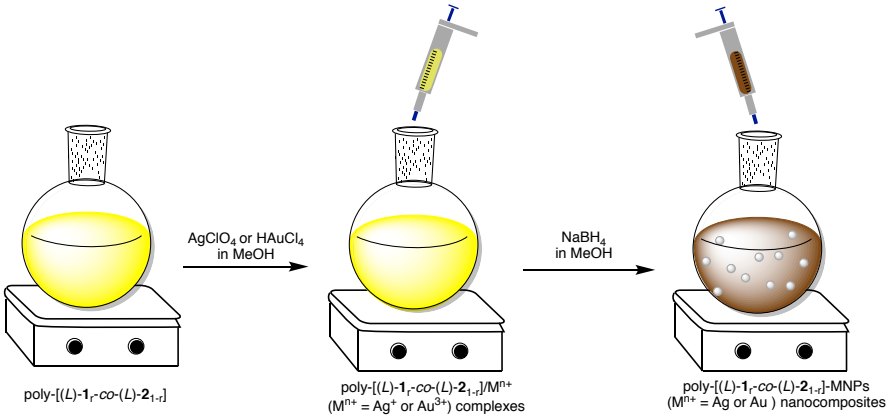

Figure S24. Conceptual representation for the preparation of poly-($\mathbf{1}_{0.2}$-*co*-$\mathbf{2}_{0.8}$)-MNPs (M = Au and Ag) nanocomposites.

15. TEM images for poly-[(*L*)-1_r-*co*-(*L*)-2_{1-r})-AuNPs (r = 0.8-0.2) nanocomposites

For TEM studies, a drop of poly-[(*L*)-$\mathbf{1}_{0.2}$-*co*-(*L*)-$\mathbf{2}_{0.8}$)-AuNPs (0.3 mg mL^{-1}) in $CHCl_3$ was settled onto a carbon film and allowed to dry 12 h. TEM images showed the presence of spherical and low polydisperse AuNPs coating by the helical polymer.

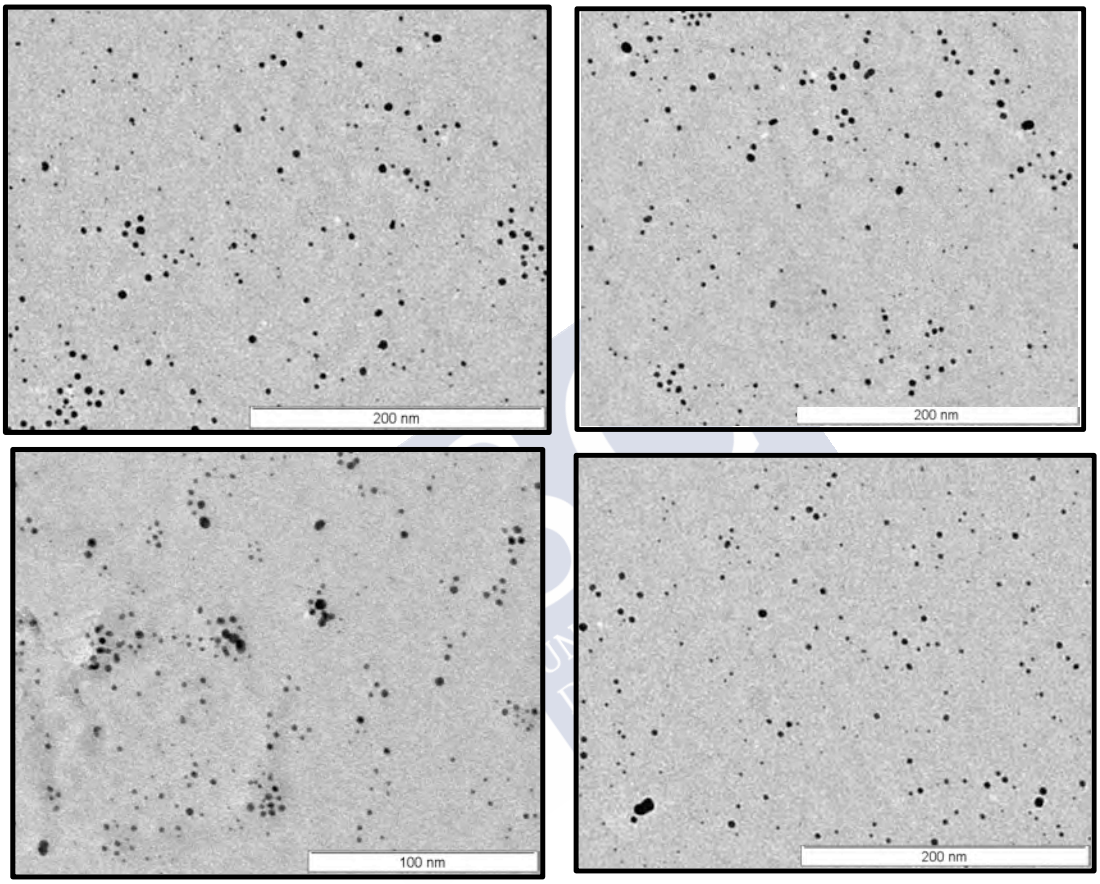

Figure S25. TEM images of poly-[(*L*)-$\mathbf{1}_{0.2}$-*co*-(*L*)-$\mathbf{2}_{0.8}$]-AuNPs.

16. Influence of the amount of AuNPs in the dynamic behaviour of poly-[(*L*)-$1_{0.2}$-*co*-(*L*)-$2_{0.8}$]

The influence of the gold nanoparticles (AuNPs) in the secondary structure of poly-[(*L*)-$\mathbf{1}_{0.2}$-*co*-(*L*)-$\mathbf{2}_{0.8}$] was studied by preparation of poly-[(*L*)-$\mathbf{1}_{0.2}$-*co*-(*L*)-$\mathbf{2}_{0.8}$]-AuNPs nanocomposites by addition of different amounts of $HAuCl_4$ as source of Au^{3+} ions.

For that, a solution of poly-[(*L*)-$\mathbf{1}_{0.2}$-*co*-(*L*)-$\mathbf{2}_{0.8}$] (0.3 mg mL^{-1}) in $CHCl_3$ was titrated by different amounts of $HAuCl_4$ (0.2, 0.5, 1.0 and 2.0 equiv., 10 mg mL^{-1}) in MeOH and next,

AuNPs were prepared following the general procedure. CD spectra registered for the poly-[(*L*)-**1**$_{0.2}$-*co*-(*L*)-**2**$_{0.8}$]-AuNPs have shown a decrease in the intensity of the Cotton Effect at 370 nm due to the presence of AuNPs in the polymer chain.

On the other hand, UV-Vis experiments have shown the typical traces for poly-(**1**$_{0.2}$-*co*-**2**$_{0.8}$) and LSPR bands have confirmed the formation of AuNPs. Moreover, LSPR bands increase its intensity when the amount of $HAuCl_4$ is higher.

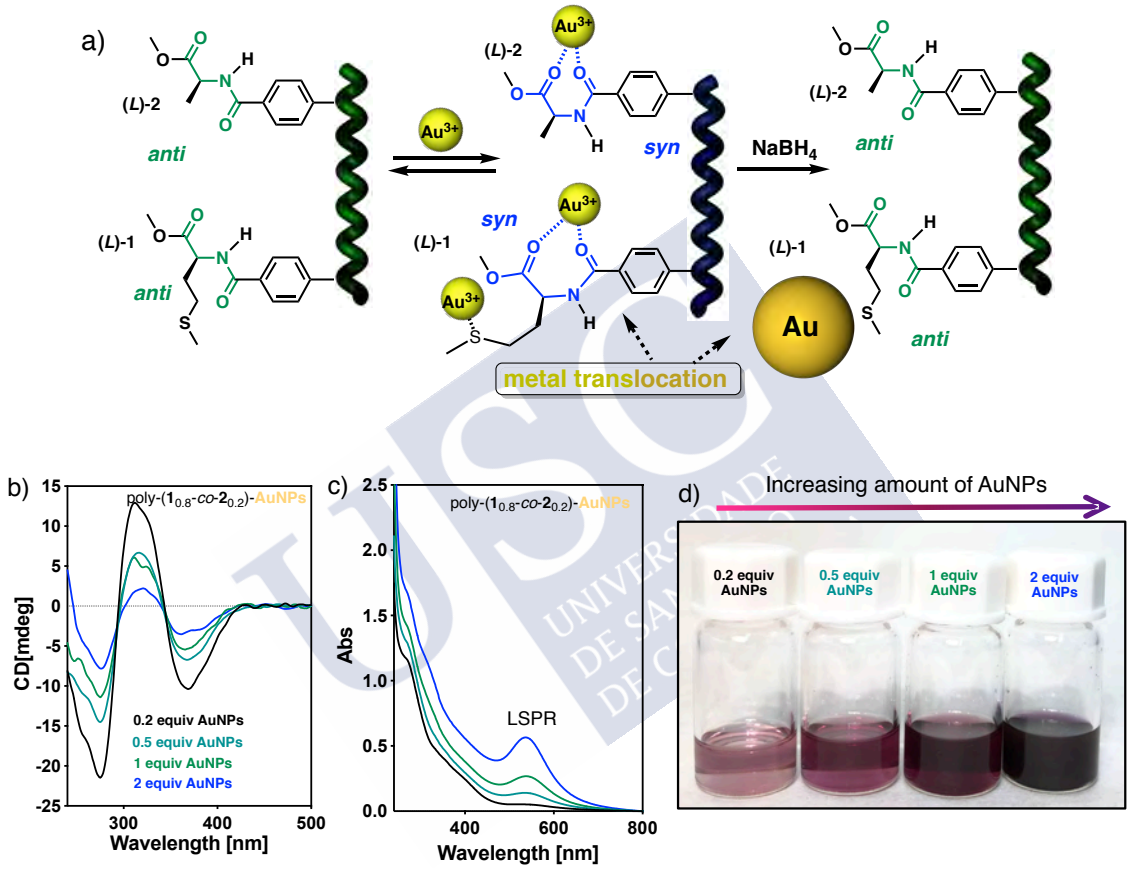

Figure S26. a) Schematic representation for the influence of the AuNPs in the secondary structure of poly-[(*L*)-**1**$_{0.2}$-*co*-(*L*)-**2**$_{0.8}$]. b) CD spectra for poly-[(*L*)-**1**$_{0.2}$-*co*-(*L*)-**2**$_{0.8}$]-AuNPs with different amount of AuNPs. c) UV-Vis spectra for poly-(**1**$_{0.2}$-*co*-**2**$_{0.8}$)-AuNPs with different amount of AuNPs. d) Images for the dispersions of poly-(**1**$_{0.2}$-*co*-**2**$_{0.8}$)-AuNPs nanocomposites in $CHCl_3$.

17. Influence of the amount of AgNPs in the dynamic behaviour of poly-[(*L*)-$\mathbf{1}_{0.2}$-*co*-(*L*)-$\mathbf{2}_{0.8}$]

The influence of the silver nanoparticles (AgNPs) in the secondary structure of poly-[(*L*)-$\mathbf{1}_{0.2}$-*co*-(*L*)-$\mathbf{2}_{0.8}$] was studied by preparation of poly-[(*L*)-$\mathbf{1}_{0.2}$-*co*-(*L*)-$\mathbf{2}_{0.8}$]-AgNPs nanocomposites by addition of different amounts of $AgClO_4$ as source of Ag^+ ions.

For that, a solution of poly-[(*L*)-$\mathbf{1}_{0.2}$-*co*-(*L*)-$\mathbf{2}_{0.8}$] (0.3 mg mL^{-1}) in $CHCl_3$ was titrated by different amounts of $AgClO_4$ (0.2, 0.5, 1.0 and 2.0 equiv., 10 mg mL^{-1}) in MeOH and nexy, AgNPs were prepared following the general protocol. CD spectra registered for the poly-[(*L*)-$\mathbf{1}_{0.2}$-*co*-(*L*)-$\mathbf{2}_{0.8}$]-AgNPs have shown a decrease in the intensity of the Cotton Effect at 370 nm due to the presence of AgNPs in the PPA chain.

On the other hand, the UV-Vis experiments showed the typical traces for poly-($\mathbf{1}_{0.2}$-*co*-$\mathbf{2}_{0.8}$) and the presence of LSPR band confirmed the formation of AgNPs. Moreover, LSPR bands increased their intensity when the amount of $AgClO_4$ is higher.

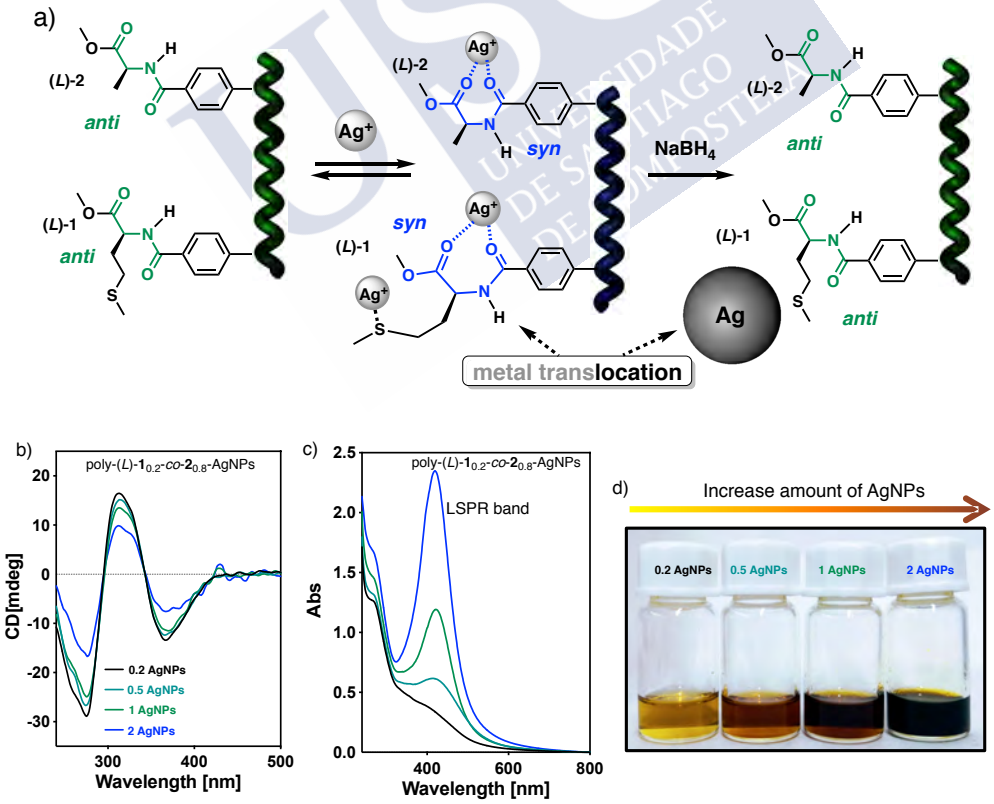

Figure S27. a) Schematic representation for the influence of the AgNPs in the secondary structure of poly-[(*L*)-$\mathbf{1}_{0.2}$-*co*-(*L*)-$\mathbf{2}_{0.8}$]. b) CD spectra for poly-[(*L*)-$\mathbf{1}_{0.2}$-*co*-(*L*)-$\mathbf{2}_{0.8}$]-AgNPs with different amount of

AgNPs. c) UV-Vis spectra for poly-(**1**$_r$-*co*-**2**$_{1-r}$)-AgNPs with different amount of AgNPs. d) Images for the dispersions of poly-(**1**$_r$-*co*-**2**$_{1-r}$)-AgNPs nanocomposites in $CHCl_3$.

18. TEM images for poly-(1$_r$-*co*-2$_{1-r}$)-AgNPs nanocomposites

For TEM studies, a drop of poly-[(*L*)-**1**$_{0.2}$-*co*-(*L*)-**2**$_{0.8}$]-AgNPs (0.3 mg mL^{-1}) in $CHCl_3$ was settled onto a carbon film and allowed to dry 12 h. TEM images showed the presence of spherical and low polydisperse AgNPs coating by poly-[(*L*)-**1**$_{0.2}$-*co*-(*L*)-**2**$_{0.8}$].

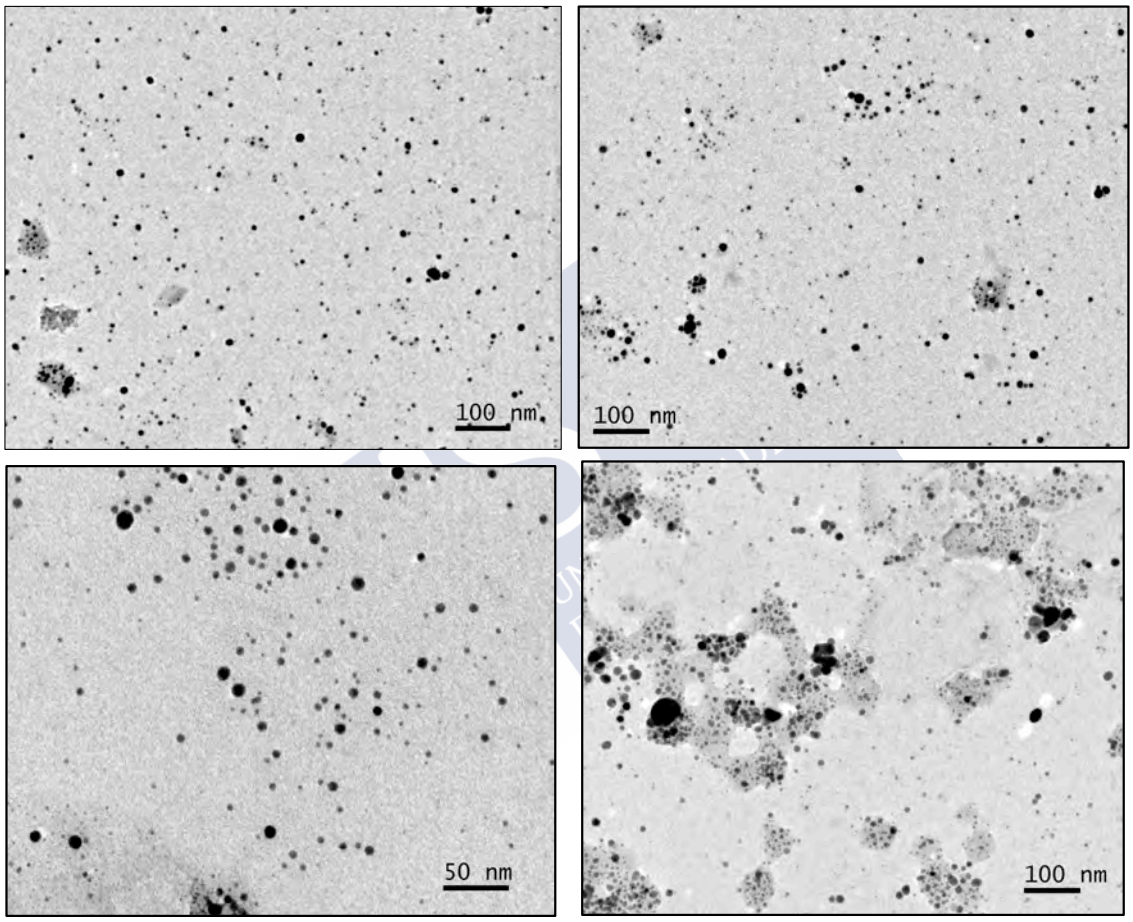

Figure S28. TEM images for poly-[(*L*)-**1**$_{0.2}$-*co*-(*L*)-**2**$_{0.8}$]-AgNPs.

19. TGA studies of poly-[(*L*)-1$_{0.2}$-*co*-(*L*)-2$_{0.8}$]-AuNPs and poly-[(*L*)-1$_{0.2}$-*co*-(*L*)-2$_{0.8}$]-AgNPs nanocomposites

TGA Studies were carried out in order to determine the thermal stability of the nanocomposites. As a general protocol, a nanocomposite sample was kept in a platinum pan and heated from 40 ^oC to 800 ^oC with a heating rate if 10 ^oC/min.

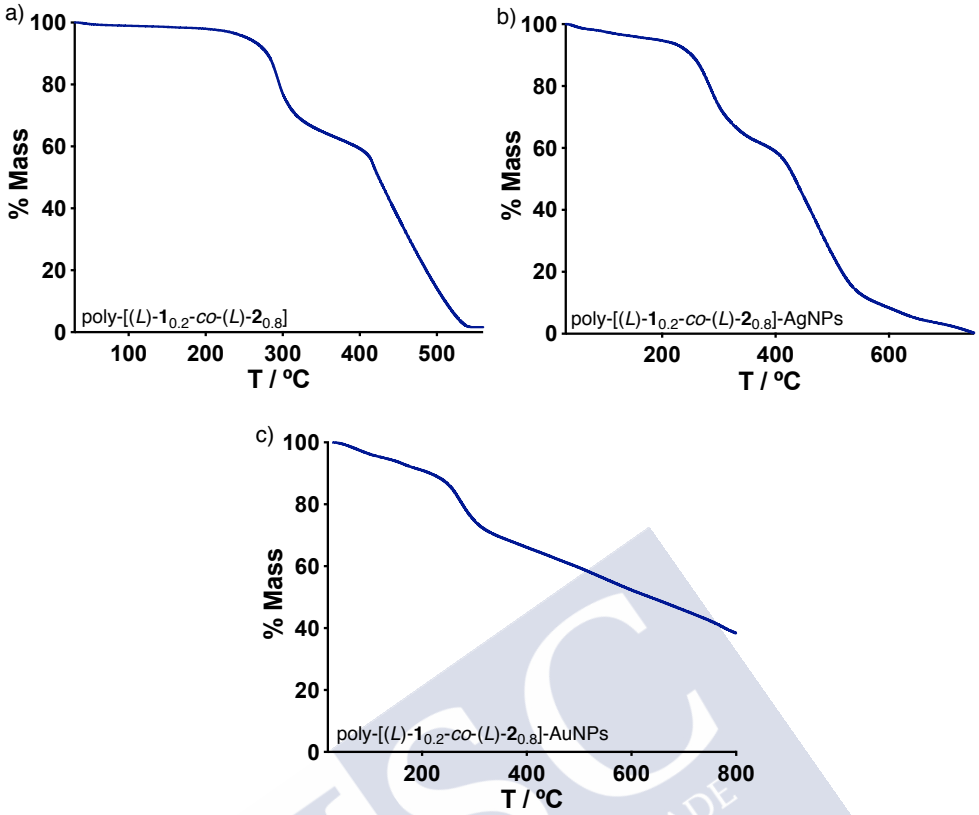

Figure S29. TGA studies for poly-[(*L*)-**1**$_{0.2}$-*co*-(*L*)-**2**$_{0.8}$], poly-[(*L*)-**1**$_{0.2}$-*co*-(*L*)-**2**$_{0.8}$]-AgNPs and poly-[(*L*)-**1**$_{0.2}$-*co*-(*L*)-**2**$_{0.8}$]-AuNPs.

20. Stability studies for poly-[(*L*)-1$_{0.2}$-*co*-(*L*)-2$_{0.8}$)-AuNPs nanocomposites

The stability of poly-[(*L*)-**1**$_{0.2}$-*co*-(*L*)-**2**$_{0.8}$]-AuNPs nanocomposites was determined by CD and UV-Vis measurements at different times.

CD studies for a dispersion of poly-[(*L*)-**1**$_{0.2}$-*co*-(*L*)-**2**$_{0.8}$]-AuNPs (0.3 mg mL^{-1}) nanocomposites in $CHCl_3$ at different times have shown the presence of *M* helices ($CD_{370} < 0$) confirming the stability of the chiral nanocomposites.

UV-Vis measurements for a dispersion of poly-[(*L*)-**1**$_{0.2}$-*co*-(*L*)-**2**$_{0.8}$]-AuNPs (0.3 mg mL^{-1}) in $CHCl_3$ have shown the presence of the same LSPR band at different times indicating that the nanocomposites present a good stability in solution.

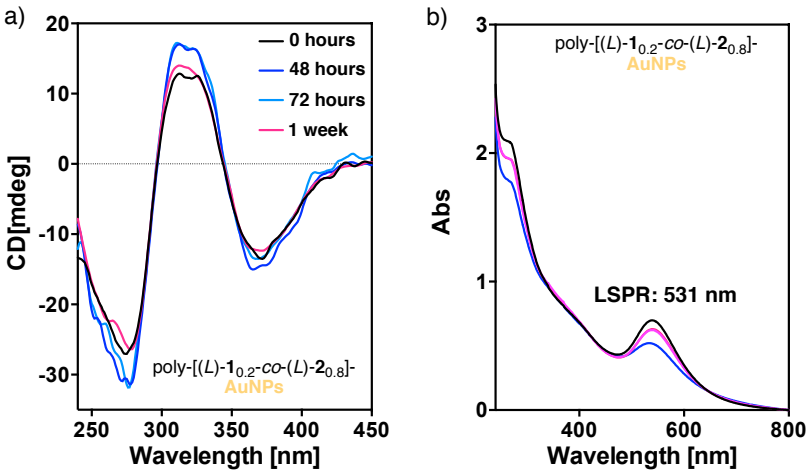

Figure S30. a) CD studies for a dispersion of poly-[(*L*)-**1**$_{0.2}$-*co*-(*L*)-**2**$_{0.8}$]-AuNPs at different times. b) UV-Vis measurements for a dispersion of poly-[(*L*)-**1**$_{0.2}$-*co*-(*L*)-**2**$_{0.8}$]-AuNPs a different times.

20. Stability studies for poly-[(*L*)-1$_{0.2}$-*co*-(*L*)-2$_{0.8}$)-AgNPs nanocomposites

The stability of poly-[(*L*)-**1**$_{0.2}$-*co*-(*L*)-**2**$_{0.8}$]-AgNPs nanocomposites was determined by CD and UV-Vis measurements at different times.

CD studies for a dispersion of poly-[(*L*)-**1**$_{0.2}$-*co*-(*L*)-**2**$_{0.8}$]-AgNPs (0.3 mg mL^{-1}) in $CHCl_3$ at different times have shown the presence of *M* helices (CD_{370} < 0) indicating that the nanocomposites preserve the helical sense of the parent PPA.

UV-Vis measurements for a dispersion poly-[(*L*)-**1**$_{0.2}$-*co*-(*L*)-**2**$_{0.8}$]-AgNPs (0.3 mg mL^{-1}) in $CHCl_3$ have shown the presence of the same LSPR band at different times indicating that the nanocomposites present a good stability in solution.

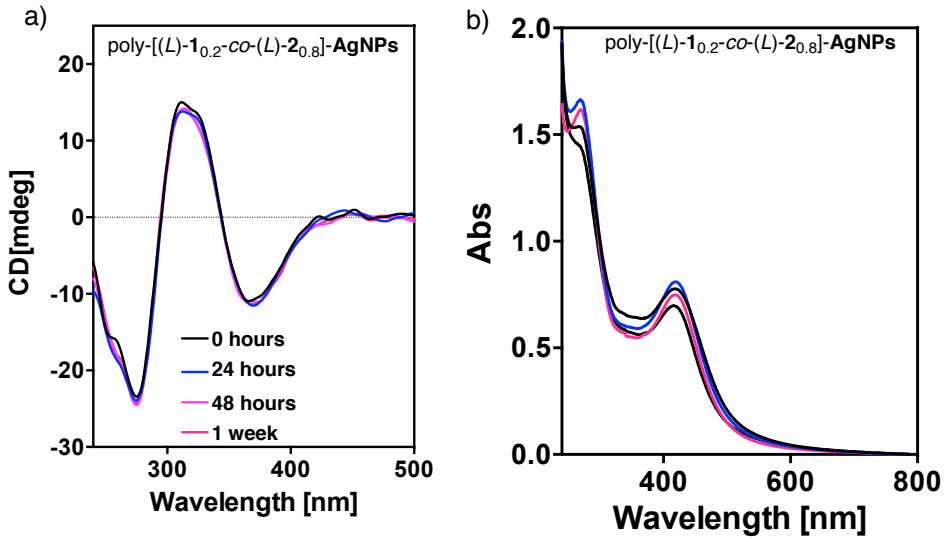

Figure S31. a) CD studies for a dispersion of poly-[(*L*)-**1**$_{0.2}$-*co*-(*L*)-**2**$_{0.8}$]-AgNPs at different times. b) UV-Vis measurements for a dispersion of poly-[(*L*)-**1**$_{0.2}$-*co*-(*L*)-**2**$_{0.8}$]-AgNPs a different times.

21. FT-IR experiments for poly-[(*L*)-1$_{0.2}$-*co*-(*L*)-2$_{0.8}$]-MNPs (M = Au and/or Ag)

A solution of $HAuCl_4$ or $AgClO_4$ (0.5 equiv., 10.0 mg mL^{-1} in MeOH) was added to a solution of poly-[(*L*)-**1**$_{0.2}$-*co*-(*L*)-**2**$_{0.8}$]-MNPs (M = Au^{3+} or Ag^{+}) (in $CHCl_3$ (0.3 mg mL^{-1}). Next, $NaBH_4$ (1 mg mL^{-1} in MeOH) was added to form poly-[(*L*)-**1**$_{0.2}$-*co*-(*L*)-**2**$_{0.8}$]-MNPs (M = Au or Ag) nanocomposites and the FT-IR spectra were recorded. The experiments have shown that the nanocomposites present a organic coating formed by poly-[(*L*)-**1**$_{0.2}$-*co*-(*L*)-**2**$_{0.8}$].

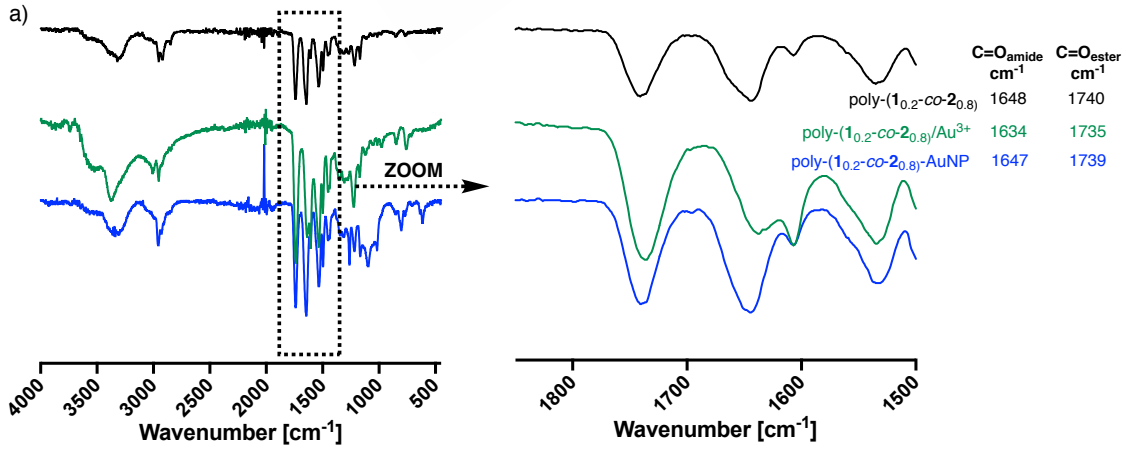

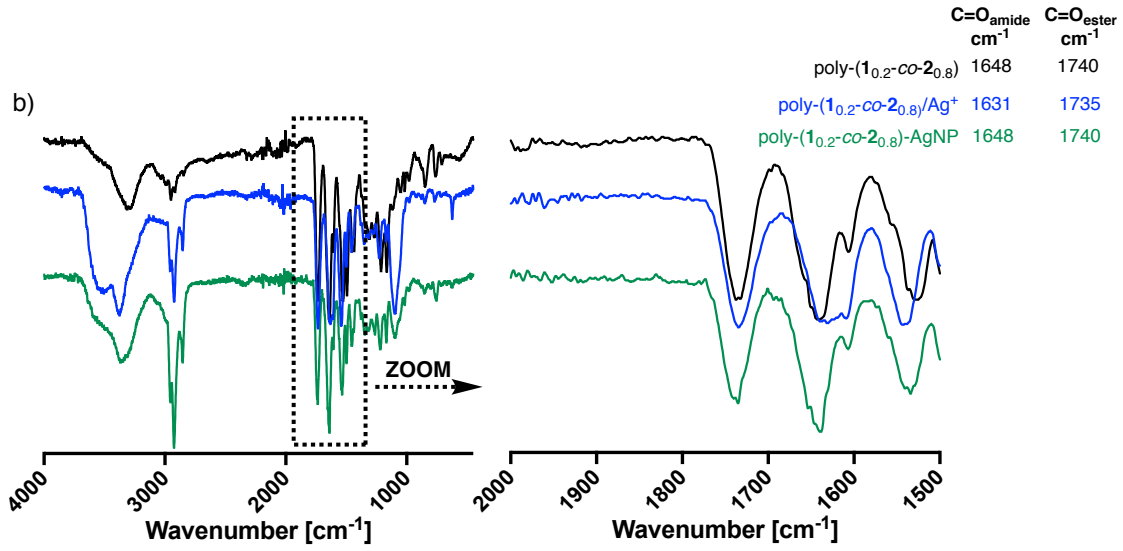

Figure S32. FT experiments for a) poly-(**1**$_r$-*co*-**2**$_{1-r}$)-AuNPs and b) poly-(**1**$_r$-*co*-**2**$_{1-r}$)-AgNPs.

22. Raman experiments for poly-(1$_r$-*co*-2$_{1-r}$)-MNPs (M = Au and/or Ag)

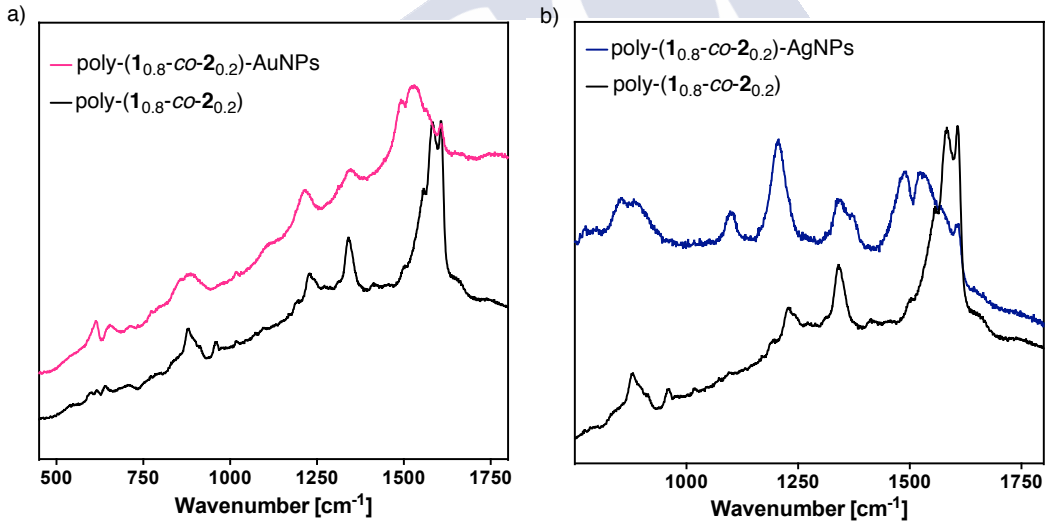

Figure S33: Raman experiments for a) poly-(**1**$_r$-*co*-**2**$_{1-r}$)-AuNPs and b) poly-(**1**$_r$-*co*-**2**$_{1-r}$)-AgNPs.

23. Stimuli-responsive studies: Preparation of poly-[(*L*)-1$_{0.2}$-*co*-(*L*)-2$_{0.8}$]-AgNPs in low polar and high polar solvents

Following the general procedure, poly-[(*L*)-**1**$_{0.2}$-*co*-(*L*)-**2**$_{0.8}$]-AgNPs nanocomposites were prepared using different high polar (DMSO, DMF) and low-polar (DCM) solvents.

- Preparation of poly-[(*L*)-**1**$_{0.2}$-*co*-(*L*)-**2**$_{0.8}$]-AgNPs in DCM

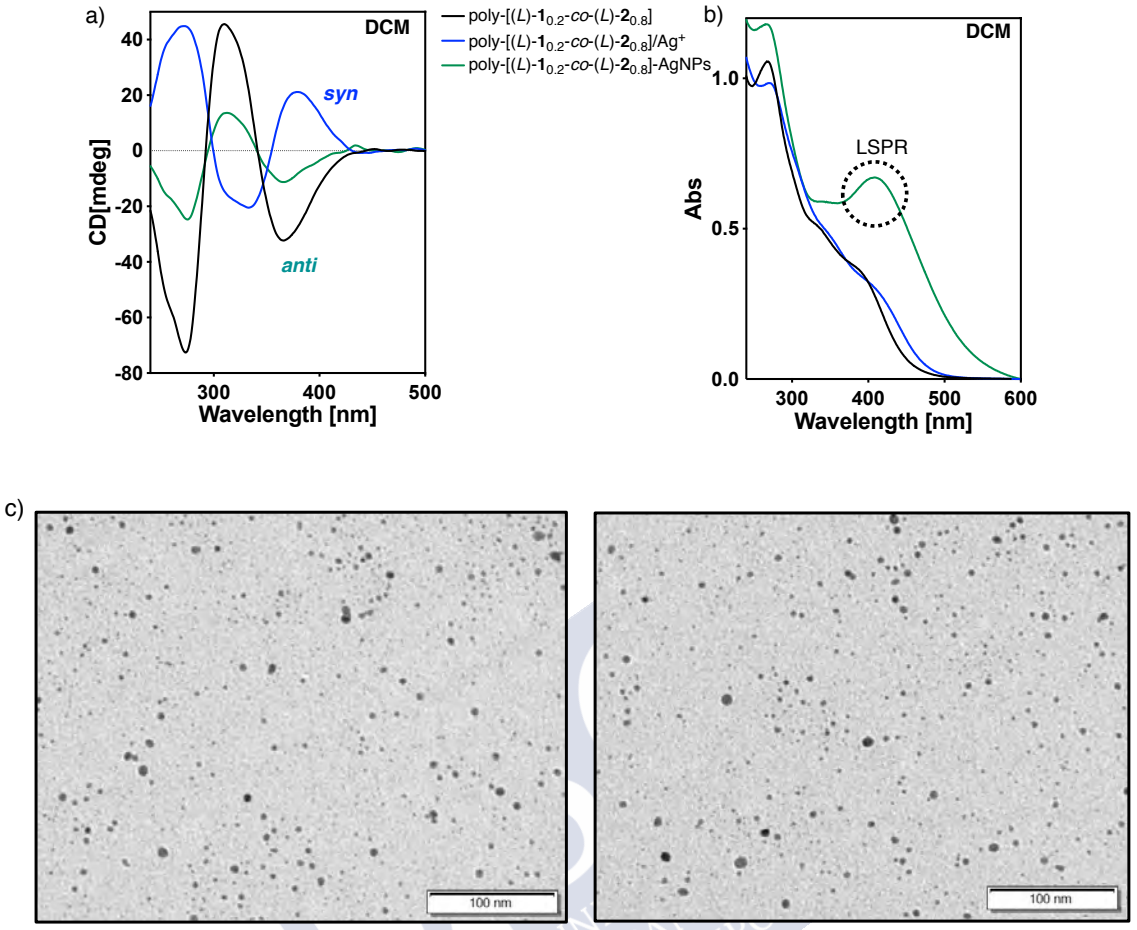

Figure S34. a) CD studies and b) UV-Vis studies of preparation of poly-[(*L*)-**1**$_{0.2}$-*co*-(*L*)-**2**$_{0.8}$]-AgNPs in and c) poly-[(*L*)-**1**$_{0.2}$-*co*-(*L*)-**2**$_{0.8}$]-AgNPs in DCM.

- Preparation of poly-[(*L*)-**1**$_{0.2}$-*co*-(*L*)-**2**$_{0.8}$]-AgNPs in DMF

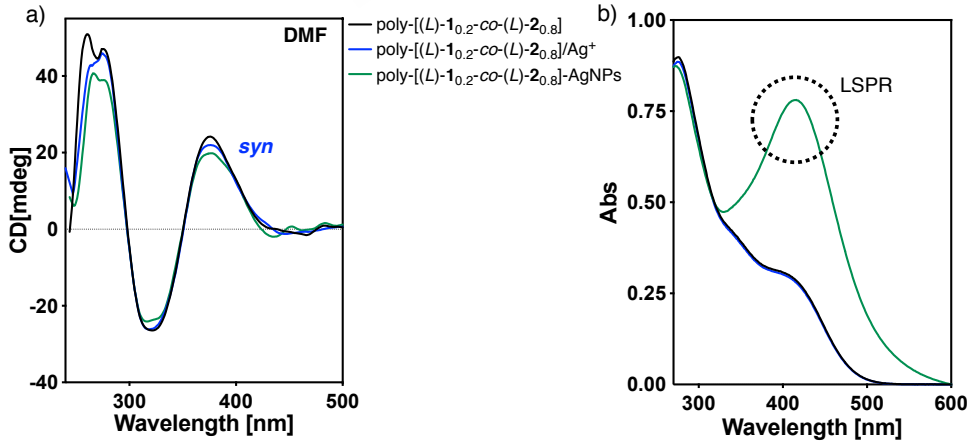

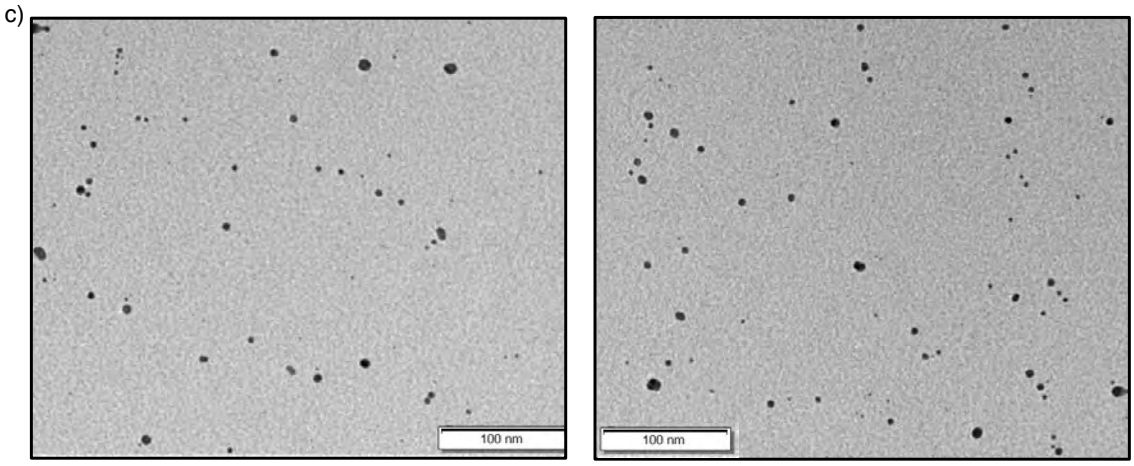

Figure S35. a) CD studies and b) UV-Vis studies of preparation of poly-[(*L*)-**1**$_{0.2}$-*co*-(*L*)-**2**$_{0.8}$]-AgNPs in and c) TEM images of poly-[(*L*)-**1**$_{0.2}$-*co*-(*L*)-**2**$_{0.8}$]-AgNPs in DMF.

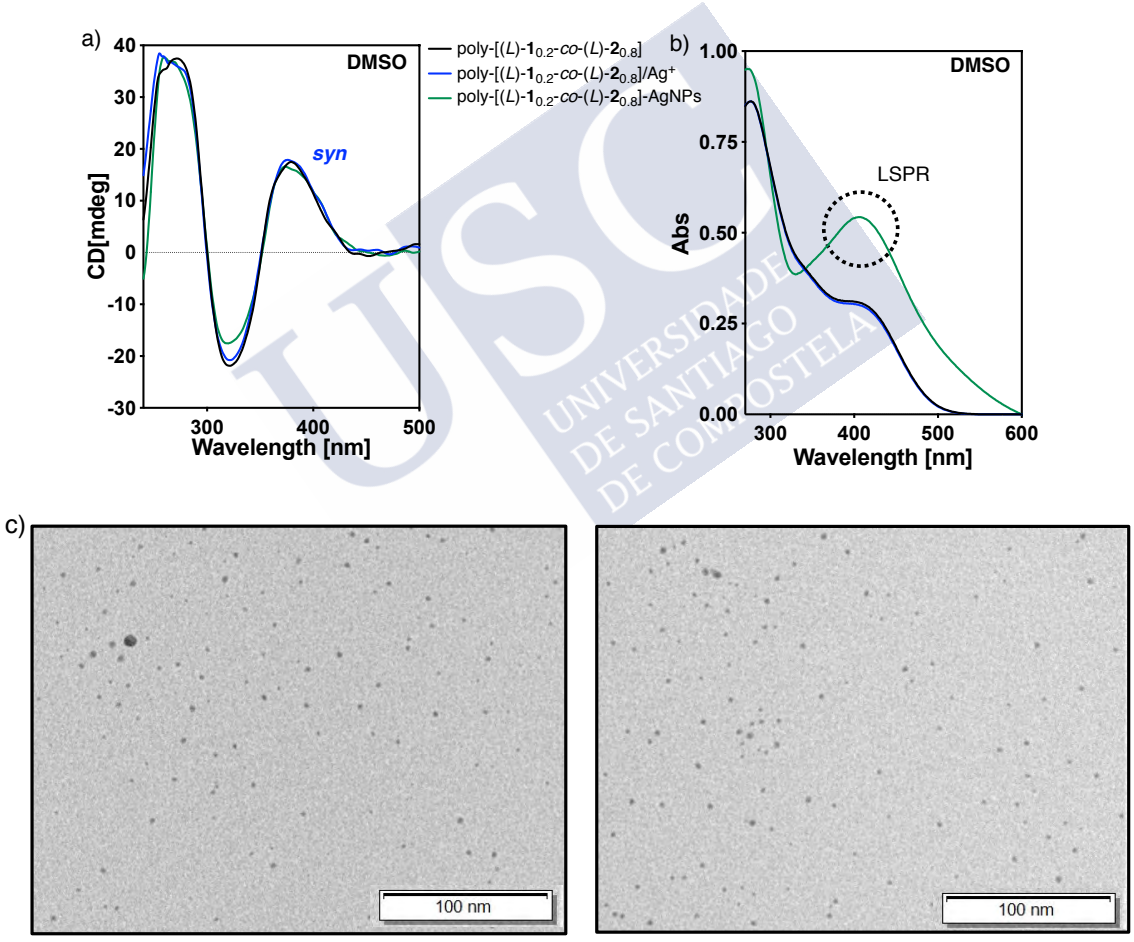

Figure S36. a) CD studies and b) UV-Vis studies of preparation of poly-[(*L*)-**1**$_{0.2}$-*co*-(*L*)-**2**$_{0.8}$]-AgNPs and c) TEM images of poly-[(*L*)-**1**$_{0.2}$-*co*-(*L*)-**2**$_{0.8}$]-AgNPs in DMSO.

24. Stimuli-responsive studies: Preparation of poly-[(*L*)-$\mathbf{1}_{0.2}$-*co*-(*L*)-$\mathbf{2}_{0.8}$]-AuNPs in low polar and high polar solvents

Following the general procedure, poly-[(*L*)-$\mathbf{1}_{0.2}$-*co*-(*L*)-$\mathbf{2}_{0.8}$]-AuNPs nanocomposites were prepared using different high polar (DMSO, DMF) and low-polar (DCM) solvents.

- Preparation of poly-[(*L*)-$\mathbf{1}_{0.2}$-*co*-(*L*)-$\mathbf{2}_{0.8}$]-AuNPs in DCM

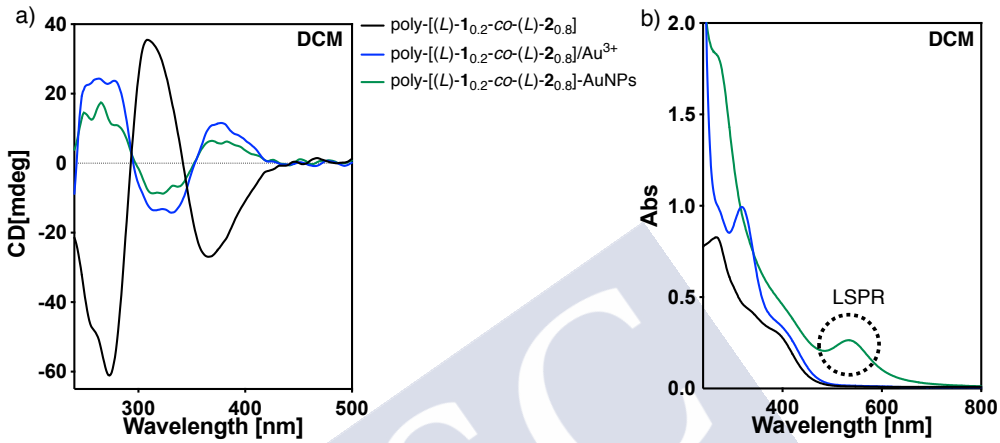

Figure S37. a) CD studies and b) UV-Vis studies of preparation of poly-[(*L*)-$\mathbf{1}_{0.2}$-*co*-(*L*)-$\mathbf{2}_{0.8}$]-AuNPs in DCM.

- Preparation of poly-[(*L*)-$\mathbf{1}_{0.2}$-*co*-(*L*)-$\mathbf{2}_{0.8}$]-AuNPs in DMF

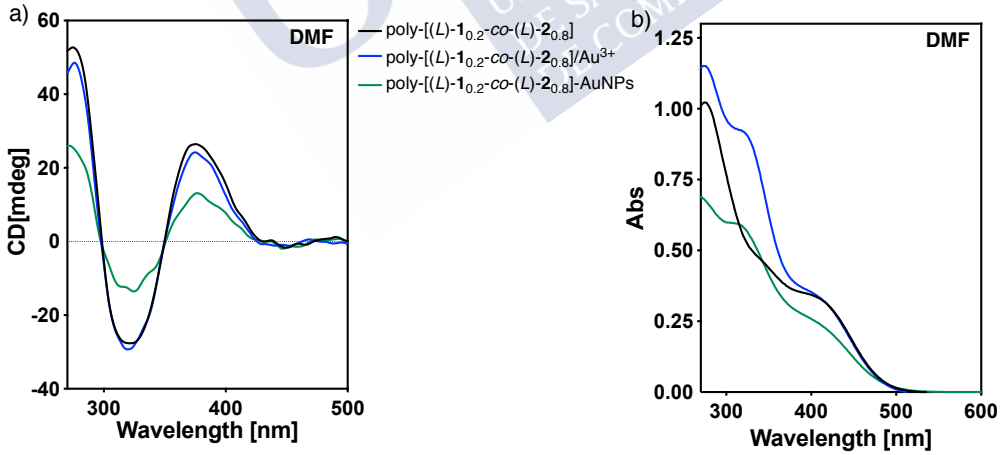

Figure S38. a) CD studies and b) UV-Vis studies of preparation of poly-[(*L*)-$\mathbf{1}_{0.2}$-*co*-(*L*)-$\mathbf{2}_{0.8}$]-AuNPs in DMF.

- Preparation of poly-[(*L*)-**1**$_{0.2}$-*co*-(*L*)-**2**$_{0.8}$]-AuNPs in DMSO.

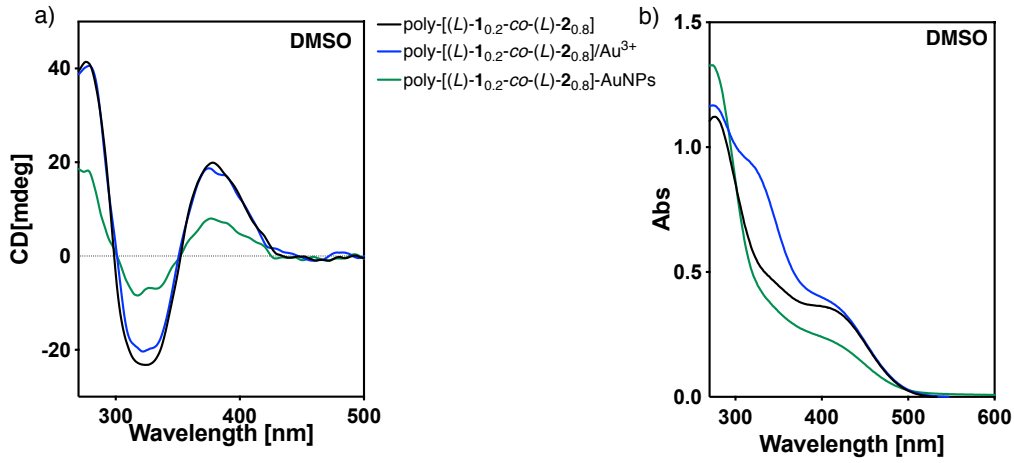

Figure S39. a) CD studies and b) UV-Vis studies of preparation of poly-[(*L*)-**1**$_{0.2}$-*co*-(*L*)-**2**$_{0.8}$]-AuNPs in DMSO.

25. Control of the helical sense in poly-(**1**$_r$-*co*-**2**$_{1-r}$)-AgNPs by addition of metal ions

CD studies and UV-Vis were performed with a dispersion of poly-[(*L*)-**1**$_{0.2}$-*co*-(*L*)-**2**$_{0.8}$]-AgNPs nanocomposites in $CHCl_3$ (0.3 mg mL^{-1}) using monovalent and divalent metal ions in MeOH (M^{n+}= Li^+, Ba^{2+}) which concentration was 10.0 mg mL^{-1}.

Thus, a dispersion of poly-[(*L*)-**1**$_{0.2}$-*co*-(*L*)-**2**$_{0.8}$]-AgNPs nanocomposites in $CHCl_3$ (0.3 mg mL^{-1}) showed the presence of *M* helices (CD_{370} < 0) corresponding to an *anti* conformation between carbonyl groups. The addition of different metal ions (10 mg mL^{-1}, MeOH) promotes a helical inversion (CD_{370} > 0) leading to the formation of *P* helices due to the coordination of the M^{n+} ions to both carbonyl groups.

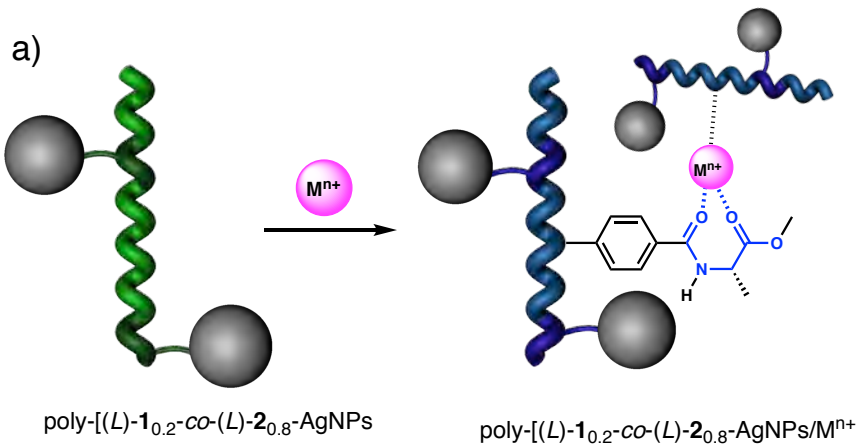

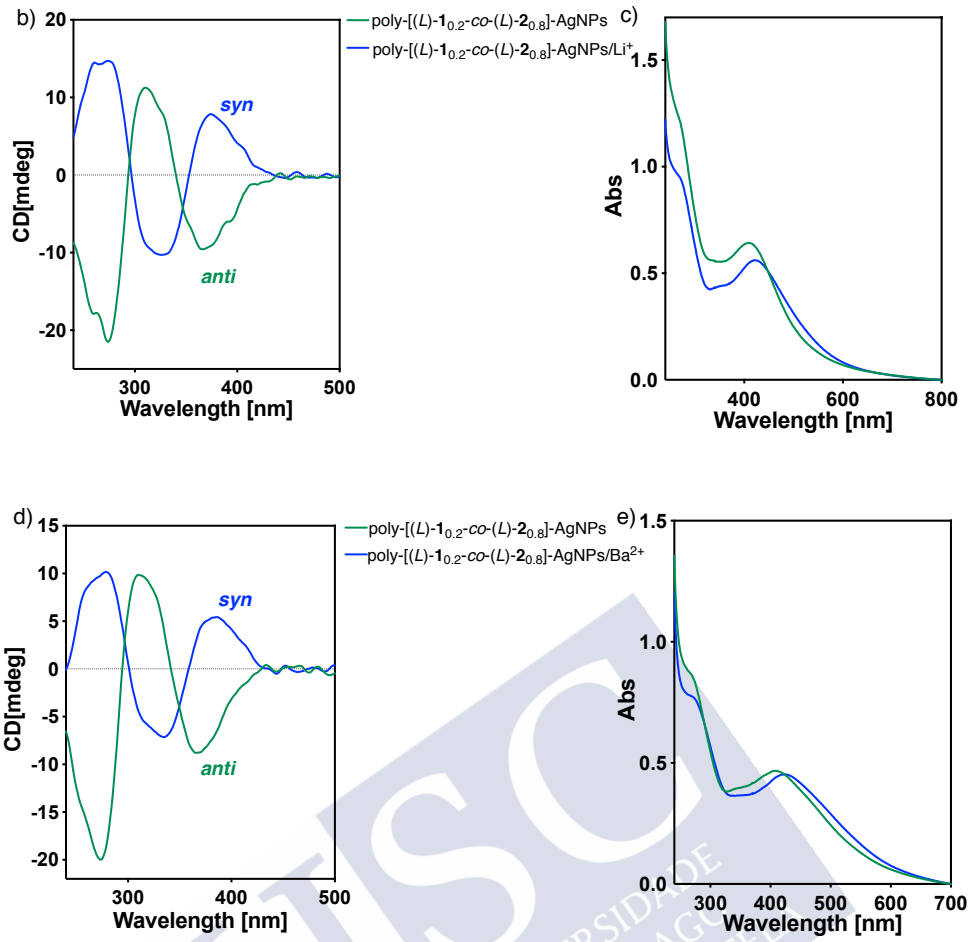

Figure S40. a) Schematic representation of helical sense control in poly-[(*L*)-**1**$_{0.2}$-*co*-(*L*)-**2**$_{0.8}$]-AgNPs nanocomposites by addition of metal ions. b) CD studies of poly-[(*L*)-**1**$_{0.2}$-*co*-(*L*)-**2**$_{0.8}$]-AgNPs in presence of Li^+ ions. c) UV-Viss tudies of poly-[(*L*)-**1**$_{0.2}$-*co*-(*L*)-**2**$_{0.8}$]-AgNPs in presence of Li^+ ions. d) CD studies of poly-[(*L*)-**1**$_{0.2}$-*co*-(*L*)-**2**$_{0.8}$]-AgNPs in presence of Ba^{2+} ions. e) UV-Vis studies of poly-[(*L*)-**1**$_{0.2}$-*co*-(*L*)-**2**$_{0.8}$]-AuNPs in presence of Ba^{2+} ions.

26. Stimuli-responsive studies: Helical sense control of poly-[(*L*)-1$_{0.2}$-*co*-(*L*)-2$_{0.8}$]-AuNPs by addition of metal ions

CD studies and UV-Vis were performed with a dispersion of poly-[(*L*)-**1**$_{0.2}$-*co*-(*L*)-**2**$_{0.8}$]-AuNPs nanocomposites in $CHCl_3$ (0.3 mg mL^{-1}) using monovalent and divalent metal ions in MeOH (M^{n+}= Li^+, Ba^{2+}) which concentration was 10.0 mg mL^{-1}.

Thus, a dispersion of poly-[(*L*)-**1**$_{0.2}$-*co*-(*L*)-**2**$_{0.8}$]-AuNPs nanocomposites in $CHCl_3$ (0.3 mg mL^{-1}) showed the presence of *M* helices (CD_{370} < 0) corresponding to an *anti* conformation between carbonyl groups. The addition of different metal ions (10 mg mL^{-1}, MeOH) promotes a

helical inversion (CD_{370} > 0) leading to the formation of *P* helices due to the coordination of the M^{n+} ions to both carbonyl groups.

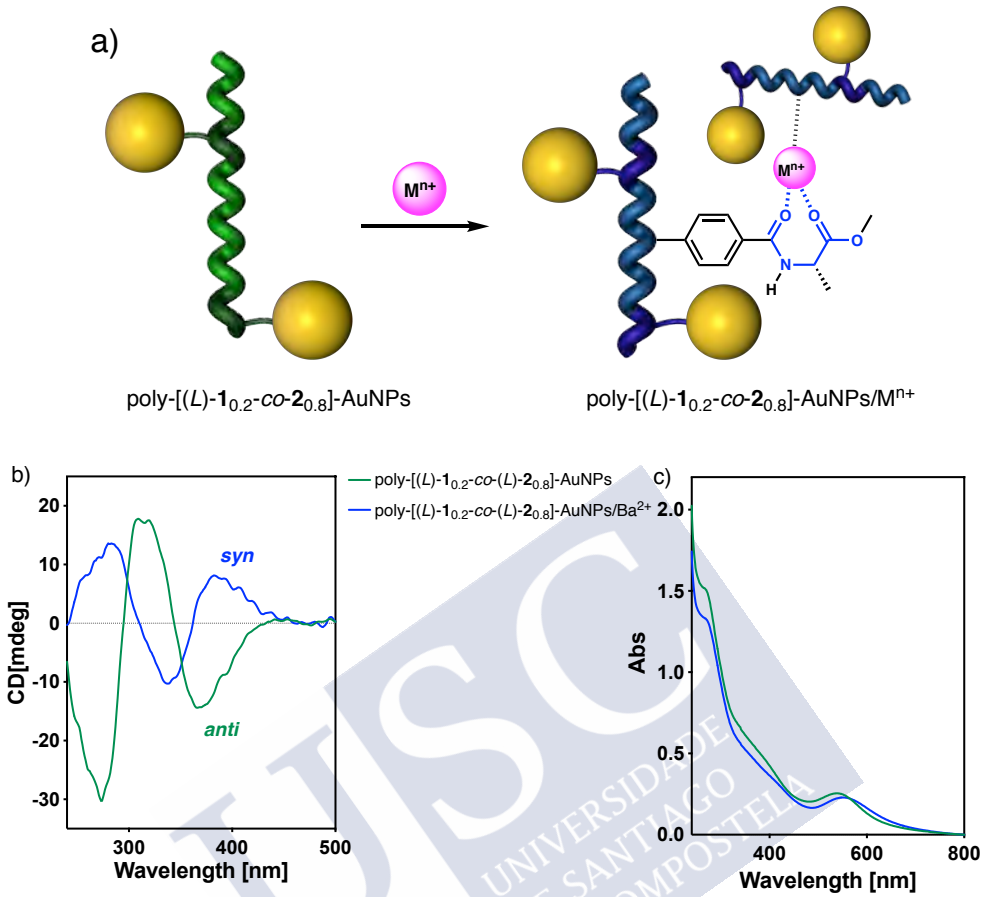

Figure S41. a) Schematic representation of helical sense control in poly-[(*L*)-**1**$_{0.2}$-*co*-(*L*)-**2**$_{0.8}$]-AuNPs nanocomposites by addition of metal ions. b) CD studies of poly-[(*L*)-**1**$_{0.2}$-*co*-(*L*)-**2**$_{0.8}$]-AuNPs in presence of Ba^{2+} ions. c) UV-Visstudies of poly-[(*L*)-**1**$_{0.2}$-*co*-(*L*)-**2**$_{0.8}$]-AuNPs in presence of Ba^{2+} ions.

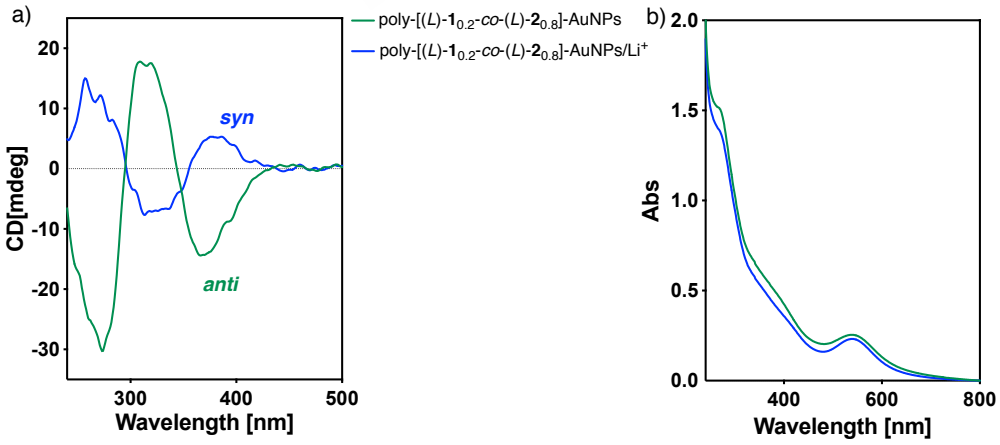

Figure S42. a) CD studies of poly-[(*L*)-**1**$_{0.2}$-*co*-(*L*)-**2**$_{0.8}$]-AuNPs in presence of Li^{+} ions and b) UV-Vis studies of poly-[(*L*)-**1**$_{0.2}$-*co*-(*L*)-**2**$_{0.8}$]-AuNPs in presence of Li^{+} ions.

27. SEM images for poly-[(*L*)-$\mathbf{1}_{0.2}$-*co*-(*L*)-$\mathbf{2}_{0.8}$]-AgNPs/Ag^+ nanospheres

A solution of $AgClO_4$ (10 mg mL^{-1}, MeOH) was added to a dispersion of poly-[(*L*)-$\mathbf{1}_{0.2}$-*co*-(*L*)-$\mathbf{2}_{0.8}$]-AgNPs or poly-[(*L*)-$\mathbf{1}_{0.2}$-*co*-(*L*)-$\mathbf{2}_{0.8}$]-AuNPs (0.3 mg mL^{-1}, $CHCl_3$) to form poly-[(*L*)-($\mathbf{1}_{0.2}$-*co*-(*L*)-$\mathbf{2}_{0.8}$]-AgNPs/Ag^+ or poly-[(*L*)-$\mathbf{1}_{0.2}$-*co*-(*L*)-$\mathbf{2}_{0.8}$]-AuNPs/Ag^+ complexes. The ability of the Ag^+ ions to act as crosslinking agents for polymer chains allow forming polymer nanospheres.

DLS studies confirmed the formation of low polidisperse poly-[(*L*)-$\mathbf{1}_{0.2}$-*co*-(*L*)-$\mathbf{2}_{0.8}$]-AgNPs/Ag^+ or poly-[(*L*)-$\mathbf{1}_{0.2}$-*co*-(*L*)-$\mathbf{2}_{0.8}$]-AuNPs/Ag^+ nanospheres in solution. Next, a drop of poly-[(*L*)-$\mathbf{1}_{0.2}$-*co*-(*L*)-$\mathbf{2}_{0.8}$]-AgNPs/Ag^+ or poly-[(*L*)-$\mathbf{1}_{0.2}$-*co*-(*L*)-$\mathbf{2}_{0.8}$]-AuNPs/Ag^+ was drop casted onto silicon wafer chip and SEM images were registered.

SEM images obtained have shown the formation of low polydisperse (PDI < 0.2) poly-[(*L*)-$\mathbf{1}_{0.2}$-*co*-(*L*)-$\mathbf{2}_{0.8}$]-AgNPs/Ag^+ or poly-[(*L*)-$\mathbf{1}_{0.2}$-*co*-(*L*)-$\mathbf{2}_{0.8}$]-AuNPs/Ag^+ nanospheres. Interestingly, be the presence of AgNPs or AuNPs can be observed on the surface of the nanospheres.

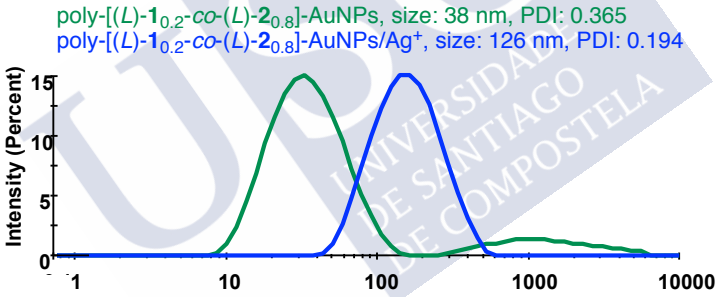

Figure S42. DLS studies of poly-[(*L*)-$\mathbf{1}_{0.2}$-*co*-(*L*)-$\mathbf{2}_{0.8}$]-AuNPs and poly-[(*L*)-$\mathbf{1}_{0.2}$-*co*-(*L*)-$\mathbf{2}_{0.8}$]-AuNPs/Ag^+ complexes.

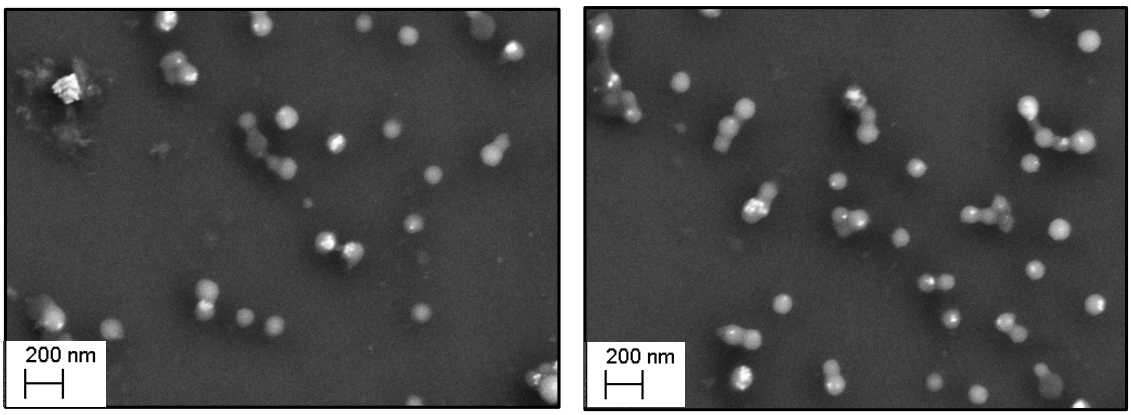

Figure S43. SEM images of poly-[(*L*)-$\mathbf{1}_{0.2}$-*co*-(*L*)-$\mathbf{2}_{0.8}$]-AuNPs/Ag^+ nanospheres (size: 98 ± 11 nm).

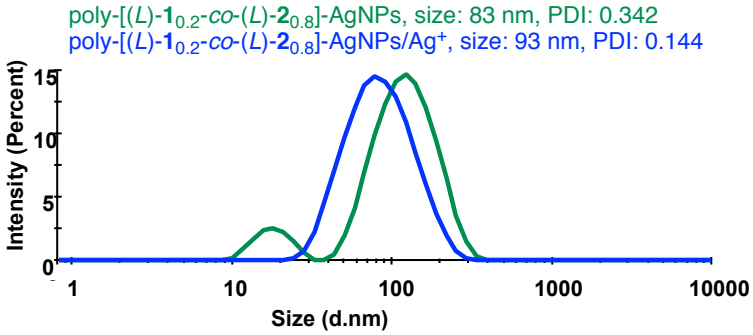

Figure S44. DLS studies of poly-[(*L*)-**1**$_{0.2}$-*co*-(*L*)-**2**$_{0.8}$]-AgNPs and poly-[(*L*)-**1**$_{0.2}$-*co*-(*L*)-**2**$_{0.8}$]-AgNPs/Ag$^+$ complexes.

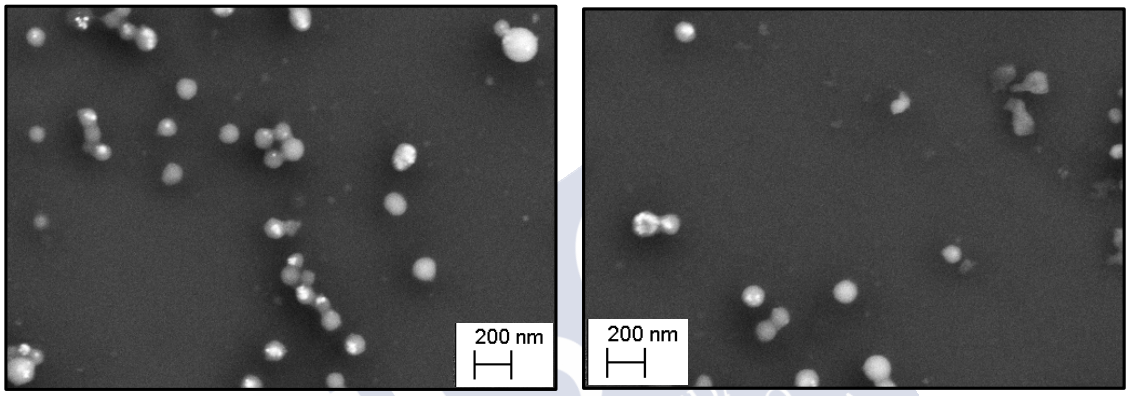

Figure S45. SEM images of poly-[(*L*)-**1**$_{0.2}$-*co*-(*L*)-**2**$_{0.8}$]-AgNPs/Ag$^+$ nanospheres (size: 90 ± 15 nm) nanospheres.

28. Experiments with metal scavenger resins

Commercially available Quadrapure™ (Aldrich) resin (TU) was employed as metal scavenger resin. The TU resin contains a thiourea functional group.

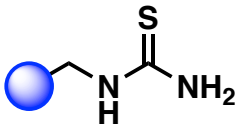

Quadrapure TU

Figure S46. Chemical structure of Quadrapure TU metal scavenger resin.

To carry out these experiments, the resins were swollen in $CHCl_3$ for 1h (0.05 g mL^{-1}). Next, 100 mg of resins were added to a solution of poly-[(*L*)-**1**$_{0.2}$-*co*-(*L*)-**2**$_{0.8}$]-MNPs/Ag$^+$ (M = Ag

or Au) (0.3 mg mL^{-1} in $CHCl_3$). After 30 min, CD measurements showed the spectra of poly-[(*L*)-**1**$_{0.2}$-*co*-(*L*)-**2**$_{0.8}$]-MNPs (CD_{370} < 0) confirming that Ag^+ ions were removed.

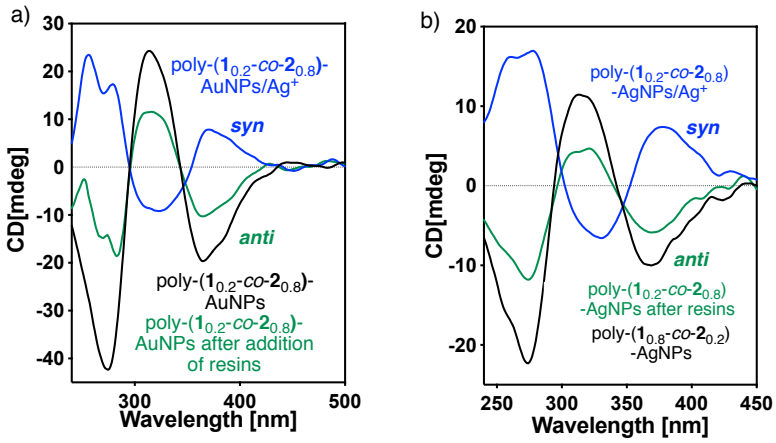

Figure S47. CD spectra of a) poly-[(*L*)-**1**$_{0.2}$-*co*-(*L*)-**2**$_{0.8}$]-AuNPs/Ag^+ and b) poly-[(*L*)-**1**$_{0.2}$-*co*-(*L*)-**2**$_{0.8}$]-AgNPs/Ag^+ after addition of metal scavenger resins.

29. References

S1. Arias, S.; Núñez-Martínez, M.; Quiñoá, E.; Riguera, R.; Freire, F.; A general route to chiral nanostructures from helical polymers: *P/M* switch via dynamic metal coordination. *Polym. Chem.*, **2017**, *8*, 3740-3745.

S2. Bergueiro, J.; Núñez-Martínez, M.; Arias, S.; Quiñoá, E.; Riguera, R.; Freire, F.; *Nanoscale Horiz.*, **2020**, *5*, 495-500**.**

S3. Arias, S.; Freire, F.; Quiñoá, E.; Riguera, R.; The leading role of cation–π interactions in polymer chemistry: the control of the helical sense in solution, *Polym. Chem.*, **2015**, *6*, 4725-4733.

USC
UNIVERSIDADE
DE SANTIAGO
DE COMPOSTELA

USC
UNIVERSIDADE
DE SANTIAGO
DE COMPOSTELA

Experimental Section Chapter VII:

1. Materials and Methods

Chemicals. Commercially available chemicals have been used as delivered. Solvents were purchased as reagent grade and distilled if necessary. Anhydrous solvents were either purchased as ultra-dry solvent from Acros Organics® or received from solvent purification system. For the coupling and polymerization reactions, dry THF was obtained from MBRAUN SPS 800 solvent purification system. Water was purified by Millipore water purification system. Coupling reagents (2-(7-Aza-1H-benzotriazole-1-yl)-1,1,3,3-tetramethyluronium hexafluorophosphate) (HATU), 4-ethynylbenzoic acid, and 4-ethynylaniline were purchased from AnaSpec Inc. (*R*)- (*S*)-α-methoxy-α-trifluoromethylphenylacetic acid, 11-mercaptoundecanoic acid, oxalyl choride, rhodium norbornadiene chloride dimer {$[Rh(nbd)Cl]_2$}, diisopropyltriethylamine (DIEA), triethylamine (TEA, 99%), 1-dodecanethiol, sodium borohydride ($NaBH_4$), gold(III) chloride trihydrate ($HAuCl_4$) and silver perchlorate ($AgClO_4$) were purchased from Aldrich.

Instrumentations and Characterizations. NMR experiments were carried out in a Varian Inova 300 (300 MHz resonance 1H). Size exclusion chromatography studies were performed on Alliance 2695 HPLC System (Waters) liquid chromatography system equipped with a UV 2489 detector (Waters). The samples were eluted by three Phenogel columns connected to each other with stationary phases of 10^3, 10^4 and 10^5 Amstrong and packed with a solid support of a cross-linked styrene and *p*-divinylbenzene copolymer. CD and UV measurements were registered in a Jasco-720 spectropolarimeter and a Jasco-730 spectrophotometer respectively at a nanocomposite concentration of 0.3 mg mL^{-1}. FT-IR measurements were carried out on a Bruker IFS-66v. DLS studies were performed on a Nano-ZS 90 (Malvern) equipped with a He-Ne laser (l = 633 nm) under scattering angle of 173°. The samples were maintained at the designed temperature for 5 min before testing. DLS measurements were carried out in all cases at 0.1 mg·mL^{-1}. SEM measurements were performed on a LEO-435VP electron microscope equipped with an energy dispersive X-ray (EDX) spectrometer. TEM measurements were performed on a JEOL JEM 2010 and 200 KV as a voltage. To study the nanocomposite, or the stereocomplexes the same protocol was used. A dispersion of the nanocomposite or the nanospheres at a concentration of 0.1 mg mL^{-1} was drop casted onto of silicon wafer chip and allowed to dry at rt for 12h for SEM studies, while in case of TEM studies the dispersed materials were drop-casted onto carbon chip and allowed to dry at rt for 12 h.

2. Synthesis of monomers

2.1 Synthesis of monomers (*R*)-1 and (*S*)-1

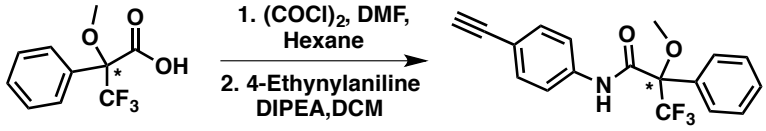

(*R*) or (*S*)-M2

Momomers (*R*)- and (*S*)-**1** was prepared according to reference [1]: Oxalyl chloride (260 mL, 1.4 equiv) was added dropwise to a solution of (*R*)- or (*S*)-α-methoxy-α-(trifluoromethyl)phenylacetic acid (500 mg, 1.0 equiv) in dry hexane and DMF (300 mL) at 0 ^{o}C under an Ar atm. After 4 h stirring at rt, the reaction mixture was filtered and the solution obtained dried under vacuum to give the acetyl chloride as colorless oil in quantitative yield.

The (*S*)- or (*R*)-α-methoxy-α-(trifluoromethyl)phenylacetyl chloride obtained, was disolved in DCM (40 mL) and diisopropyltriethylamine (DIPEA, 522 mL, 1.4 equiv) and 4-ethynilaniline (300 mg, 1.2 equiv) where added to the solution. The reaction mixture was stirred at rt overnight. The residue was diluted and the organic solution was washed with HCl 1M, saturated $NaHCO_3$ aq. solution and saturated NaCl aq solution; then the organic layer was dried over anhyd filtration, the solution was evaporated and the residue was chromatographed on silica gel with hexane-AcOEt (7/3, v/v) as the eluent [(*R*)-**1** 86% and (*S*)-**1** 90 % yield respectively of pure products].

Spectroscopic data:

^{1}H NMR (300 MHz, $CDCl_3$) δ (ppm): 3.06 (s, 1H), 3.49 (s, 3H), 7.41-7.49 (m, 5H), 7.55-7.59 (m, 4H), 8.61 (broad s, 1H).

^{13}C NMR (70 MHz, $CDCl_3$) δ (ppm): 55.2, 77.1, 83.1, 118.6, 119.5, 127.7, 128.8, 129.8, 131.9, 133.0, 137.1, 164.3.

^{19}F NMR (282.24 MHz, $CDCl_3$) δ (ppm): -68.7.

$[\alpha]_D^{20}$ for (*R*)-**1** = +68 (15 mg mL^{-1}, $CHCl_3$).

$[\alpha]_D^{20}$ for (*S*)-**1** = -72 (15 mg mL^{-1}, $CHCl_3$).

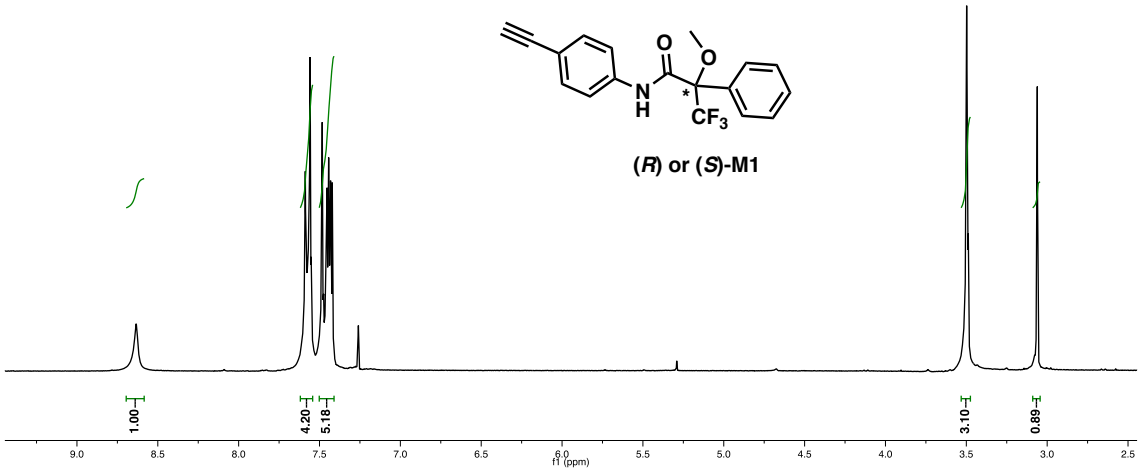

Figure S1. ^{1}H NMR for monomer **1** in $CDCl_3$.

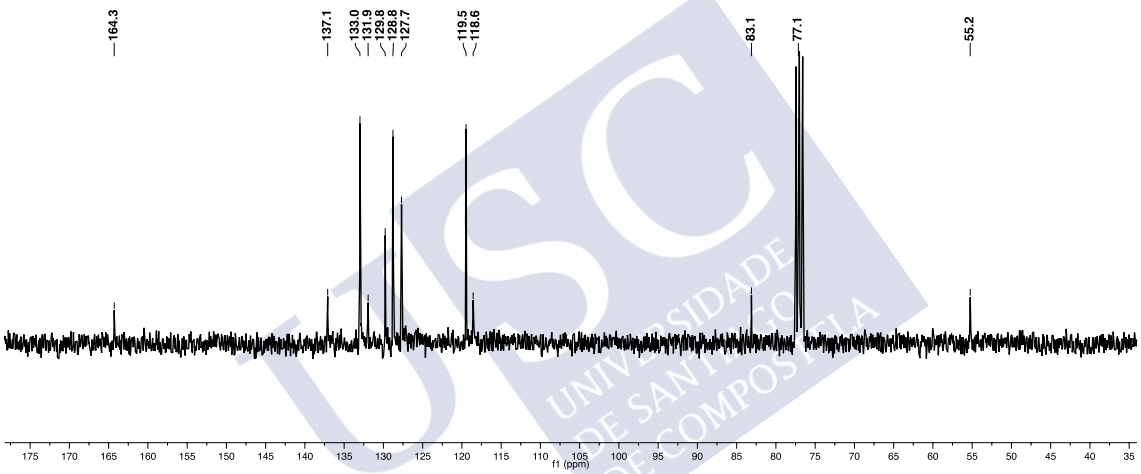

Figure S2. ^{13}C NMR for monomer **1** in $CDCl_3$.

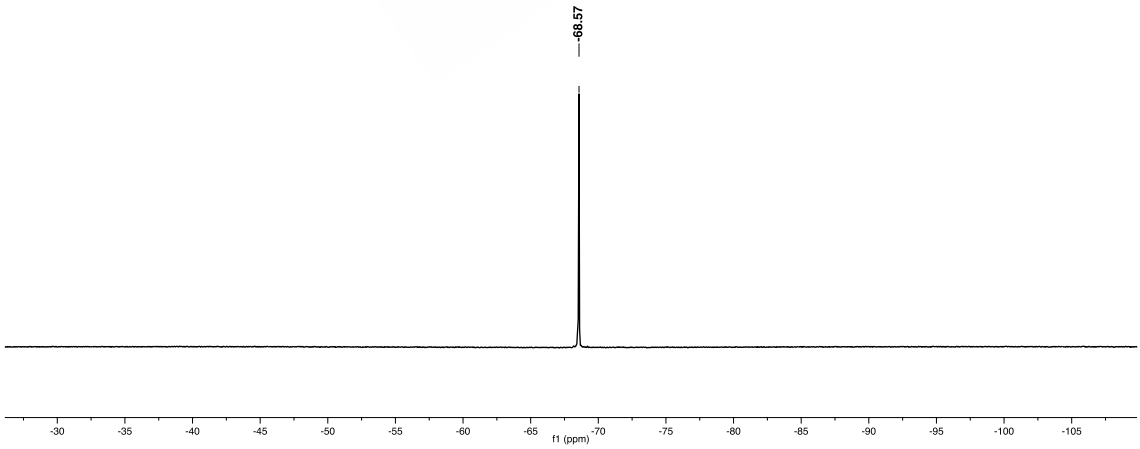

Figure S3. ^{19}F NMR for monomer **1** in $CDCl_3$.

2.2 Synthesis of Monomer M2

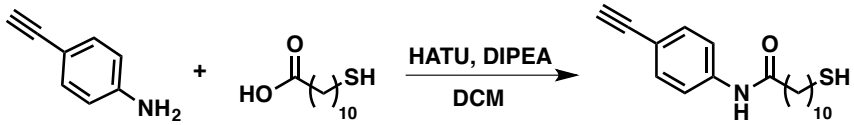

M1

(2-(7-Aza-1H-benzotriazole-1-yl)-1,1,3,3-tetramethyluronium hexafluorophosphate), (HATU, 2.11 g, 5.54 mmol), 1-hydroxy-7-azabenzotriazole (HOAt, 0.755 g, 5.54 mmol), 11-mercaptoundecanoic acid (1.211 g, 5.54 mmol) and diisopropyltriethylamine (DIPEA, 1 mL, 5.97 mmol) were dissolved in 50 mL of DCM, and the mixture was stirred for 30 min hour to activate the acid. Then, 4-ethynylaniline (0.500 g, 4.26 mmol) was added and the reaction mixture was stirred overnight. The organic layer was washed with HCl (1M) three times. The combined organic layers were dried over anhydrous Na_2SO_4, filtered and the solvent was evaporated at reduced pressure. The crude product was chromatographed on silica gel (70-230 mesh) with hexane/ethyl acetate (6/4) as eluent obtaining compound **2** in a 80% yield.

Spectroscopic data:

^{1}H NMR (300 MHz, $CDCl_3$) δ (ppm): 1.24 (m, 14H), 1.62 (m, 3H), 2.27 (t, 2H), 2.49 (m, 2H), 3.04 (s, 1H), 7.38 (d, 2H), 7.49 (d, 2H), 8.15 (s, 1H).

^{13}C NMR (70 MHz, $CDCl_3$) δ (ppm): 24.6, 25.5, 28.3, 29.0, 29.2, 29.3, 29.3, 29.4, 34.0, 37.7, 83.4, 119.3, 129.2, 132.9, 138.5, 171.7.

HRMS (ESI) m/z calculated for $C_{19}H_{28}NOS$ $[M + H]^+$: 318.1886, found: 318.1885.

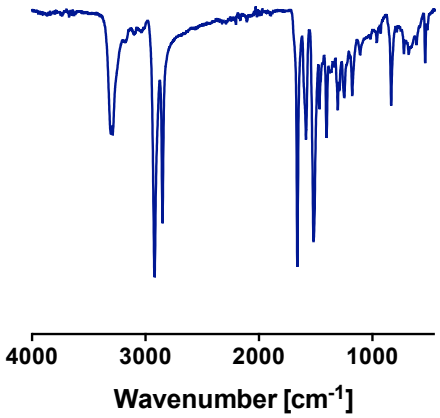

Figure S4. FT-IR spectrum for monomer **2**.

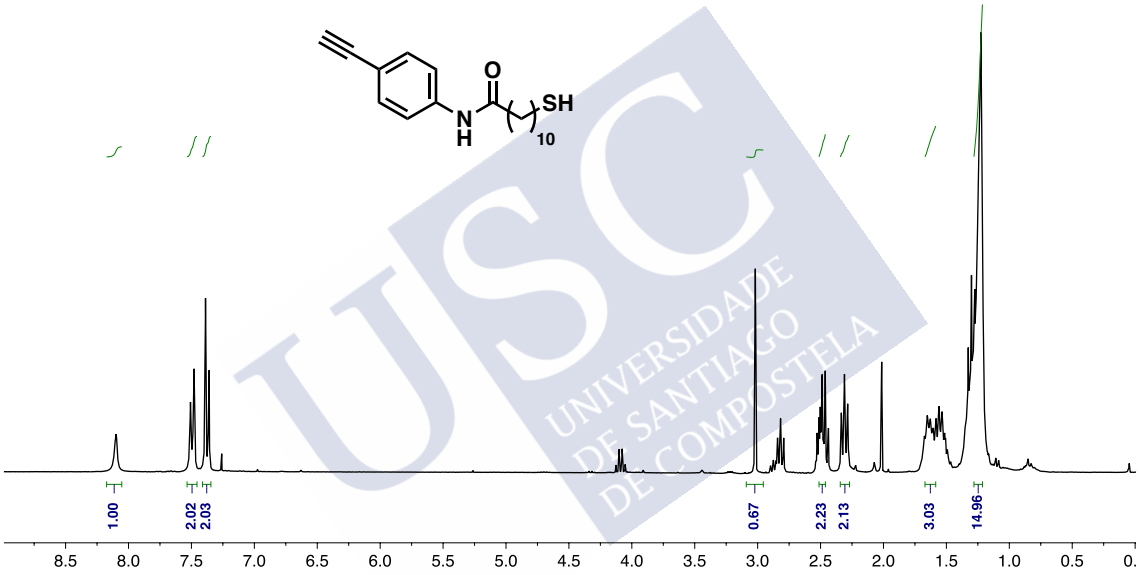

Figure S5. ^{1}H NMR for monomer **2** in $CDCl_3$.

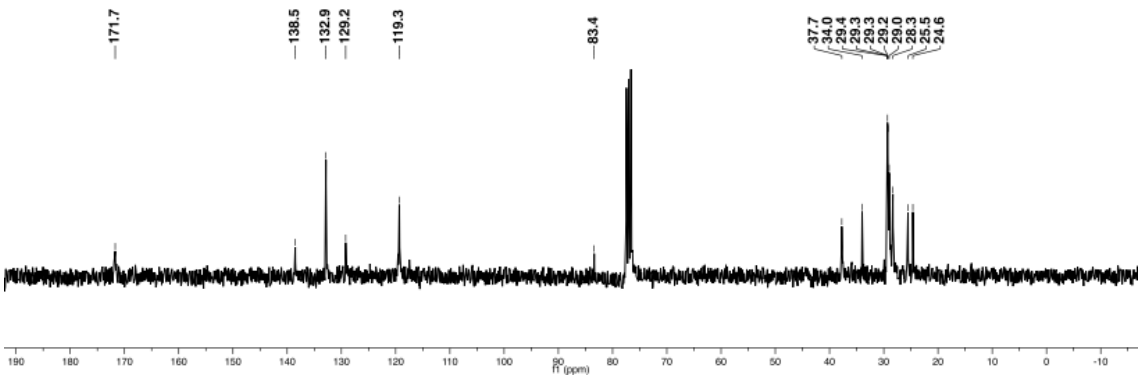

Figure S6. ^{13}C NMR for monomer **2** in $CDCl_3$.

3. Synthesis of copolymers

General procedure for polimerization: The reaction flask (sealed ampoule) was dried under vacuum and argon flushed for three times before a monomer amount was added as a solid. Then, the flask was evacuated on a vacuum line and flushed with dry argon (three times). Dry THF was added with a syringe and then triethylamine dropwise. A solution of rhodium norbornadiene chloride dimer {[Rh(nbd)Cl]$_2$} in THF was added at 30º C. The reaction mixture was stirred at 30ºC for 6 h. Then, the resulting polymer was diluted in DCM and it was precipitated in a large amount of methanol, centrifuged (2 times), reprecipitated in hexane and centrifuged again.

3.1 Synthesis of hompolymers poly-1

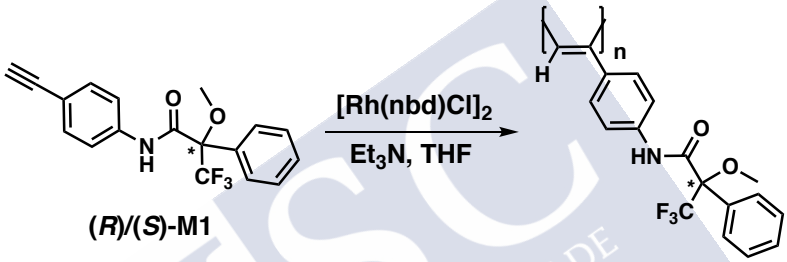

Following the general procedure: 60 mg (0.250 mmol) of M-(*R*)-**1** and M-(*S*)-**2**, 5 μL of Et_3N and 1.1 mg of [Rh(nbd)Cl]$_2$ were employed in 0.60 mL of THF to obtain after purification poly-(*R*)-**1** and poly-(*S*)-**1** (Yield: 92 and 85% respectively).[1]

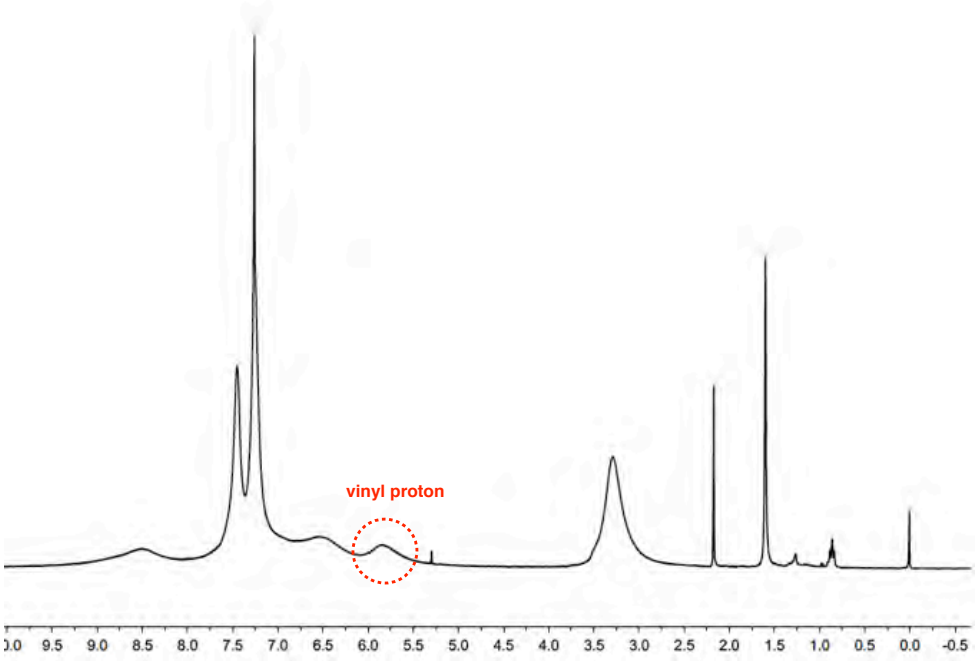

Figure S7. ^{1}H NMR spectra for poly-**1** in $CDCl_3$.

3.2 Synthesis for copolymers poly-(1_{1-r}-*co*-2_r) series (r = 0.01-0.03)

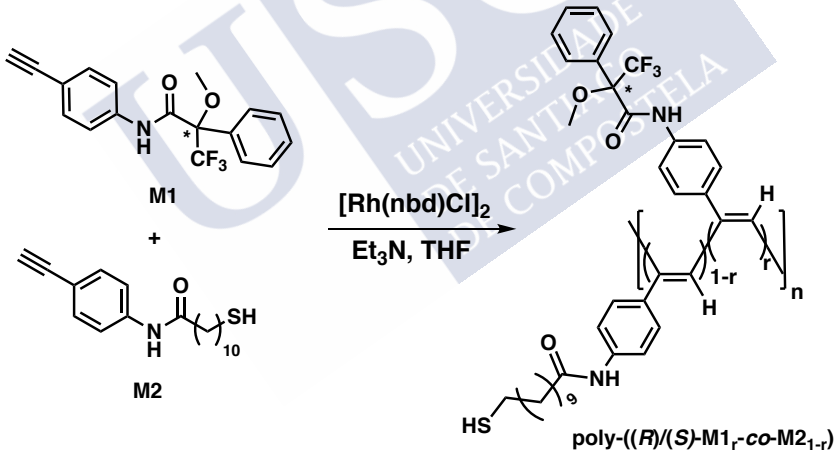

Table S1:

Copolymer	M1 mg	M1 (mmol	M2 (mg)	M2 (mmol)	Cat (mg)	THF (mL)	Et_3N (μL)	Poly (mg)	Yield (%)
Poly-M1									
Poly-($M1_{0.99}$-*co*-$M2_{0.01}$)	97.6	0.335	2.3	0.003	1.2	0.70	7	71	72
Poly-($M1_{0.98}$-*co*-$M2_{0.02}$)	95.1	0.327	4.6	0.006	1.2	0.70	7	65	66
Poly-($M1_{0.97}$-*co*-$M2_{0.03}$)	93.1	0.320	7.0	0.008	1.2	0.70	7	50	51

Table S2: GPC data for copolymers poly-$\mathbf{1}_{1\text{-}r}$-*co*-$\mathbf{2}_r$.

Polymer	M_n	M_w	M_p	M_z	PDI
Poly-1	84734	178058	182446	342353	2.10
Poly-$\mathbf{1}_{0.99}$-*co*-$\mathbf{2}_{0.01}$	72026	147633	116698	308708	2.04
Poly-$\mathbf{1}_{0.98}$-*co*-$\mathbf{2}_{0.02}$	55103	119220	74408	277477	2.16
Poly-$\mathbf{1}_{0.97}$-*co*-$\mathbf{2}_{0.03}$	65713	132212	88755	296729	2.01

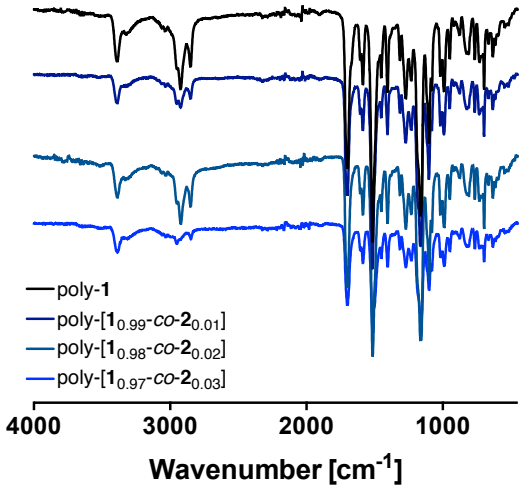

Figure S8. FT-IR spectra for poly-M**1** and copolymers poly-[$\mathbf{1}_{1\text{-}r}$-*co*-$\mathbf{2}_r$] (r = 0.01-0.03) series.

The *cis* stereoregularity of the copolymers was determined by ^{1}H NMR spectroscopy where the vinyl proton resonates at 5.8 ppm, and Raman resonances. The peak around 1570 cm^{-1} is assigned to C=C bond stretching in the *cis* poly(acetylene) and overlaps with that of the phenyl ring. The peak around 1340 cm^{-1} is assigned to the *cis* C-C bond coupled with the single bond connecting the main chain and the phenyl ring. The peak around 1004 cm^{-1} is assigned to the C-H bond deformation of the *cis* form.

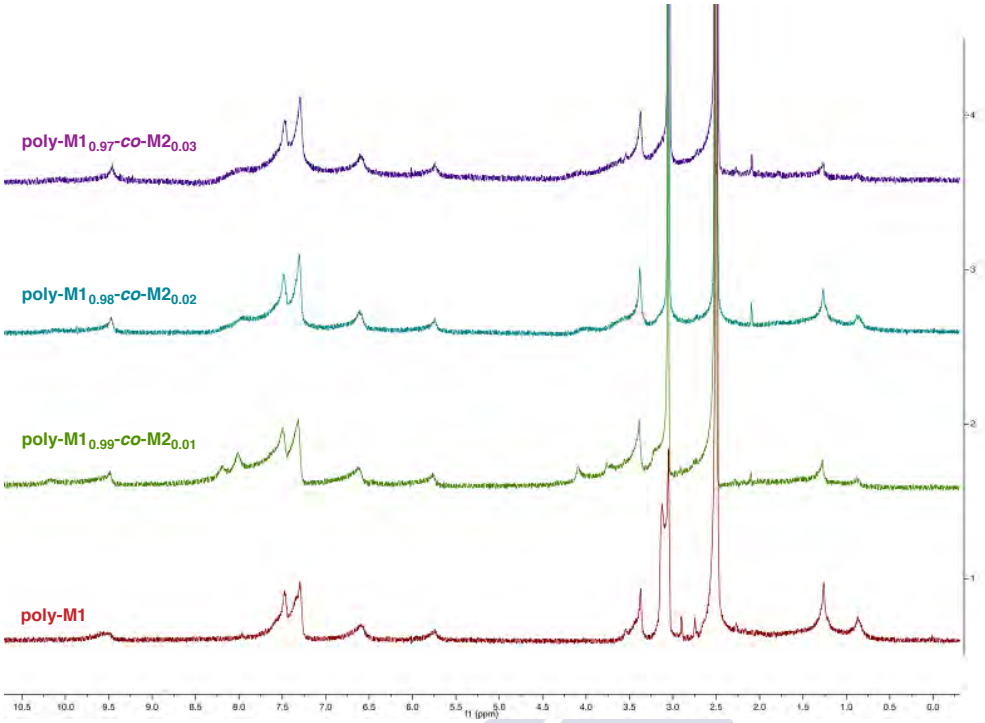

Figure S9. ^{1}H NMR spectra for poly-**1** and copolymers poly-[**1**$_{1-r}$-*co*-**2**$_{r}$] (r = 0.01-0.03) series (DMSO-d$_6$).

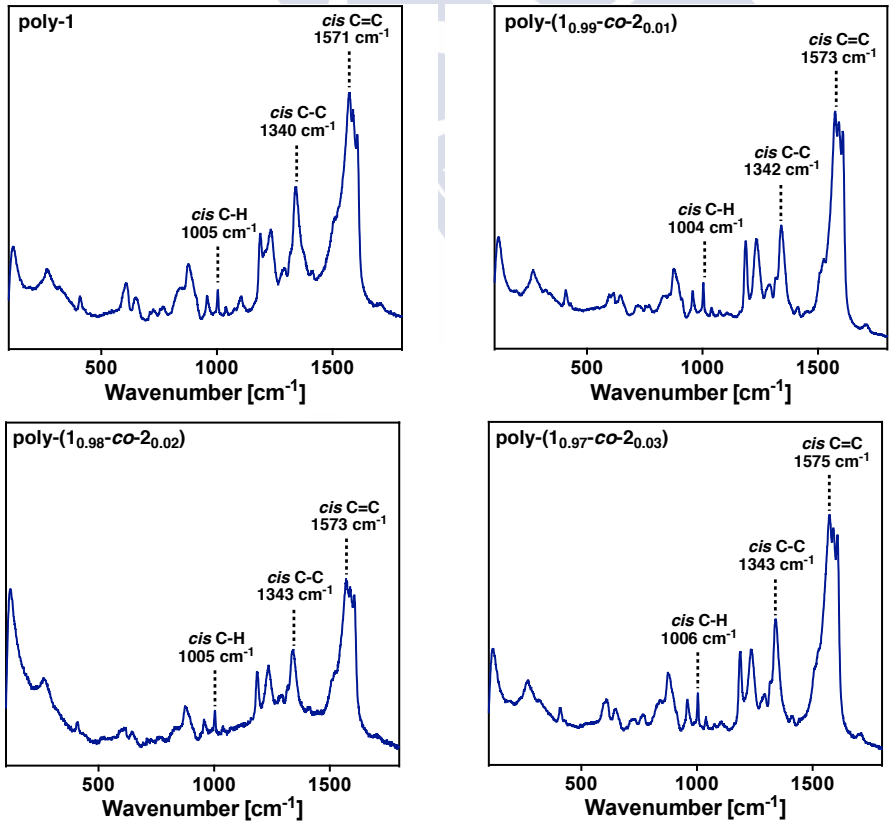

Figure S10. Raman spectra for poly-**1** and copolymers poly-[**1**$_{1-r}$-*co*-**2**$_{r}$] (r =0.01-0.03).

4. Thermal studies for copolymers

4.1 DSC studies

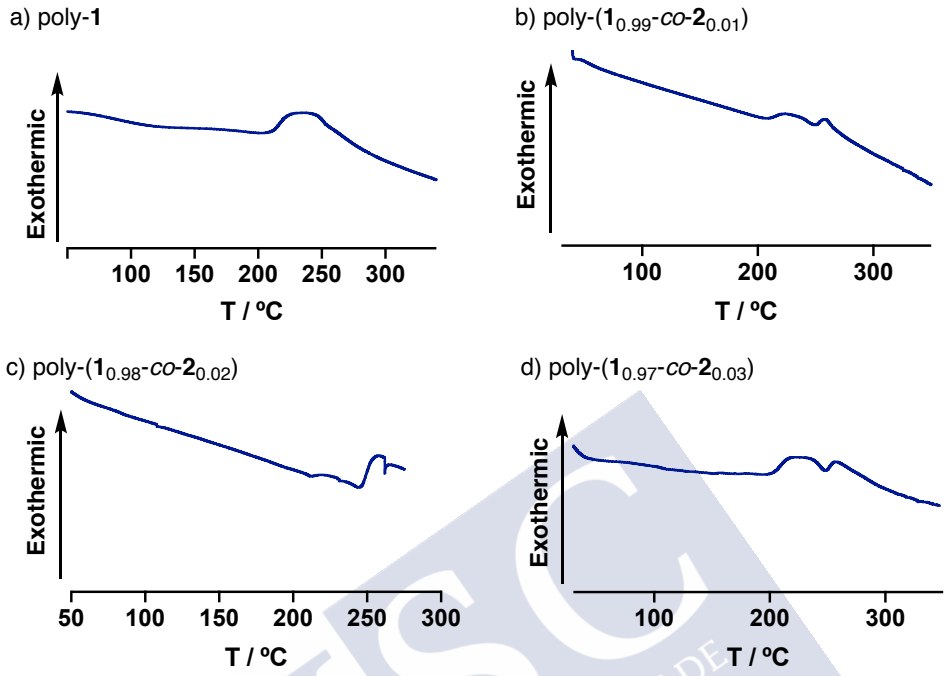

Figure S11. DSC thermograms for poly-**1** and copolymers poly-(**1**$_{1-r}$-*co*-**2**$_r$) (r = 0.01-0.03).

4.2 TGA studies

TGA Studies were carried out in order to determine the thermal stability of the copolymers. As a general protocol, a copolymer sample was kept in a platinum pan and heated from 40 ^{o}C to 850 ^{o}C with a heating rate if 10 ^{o}C min^{-1}.

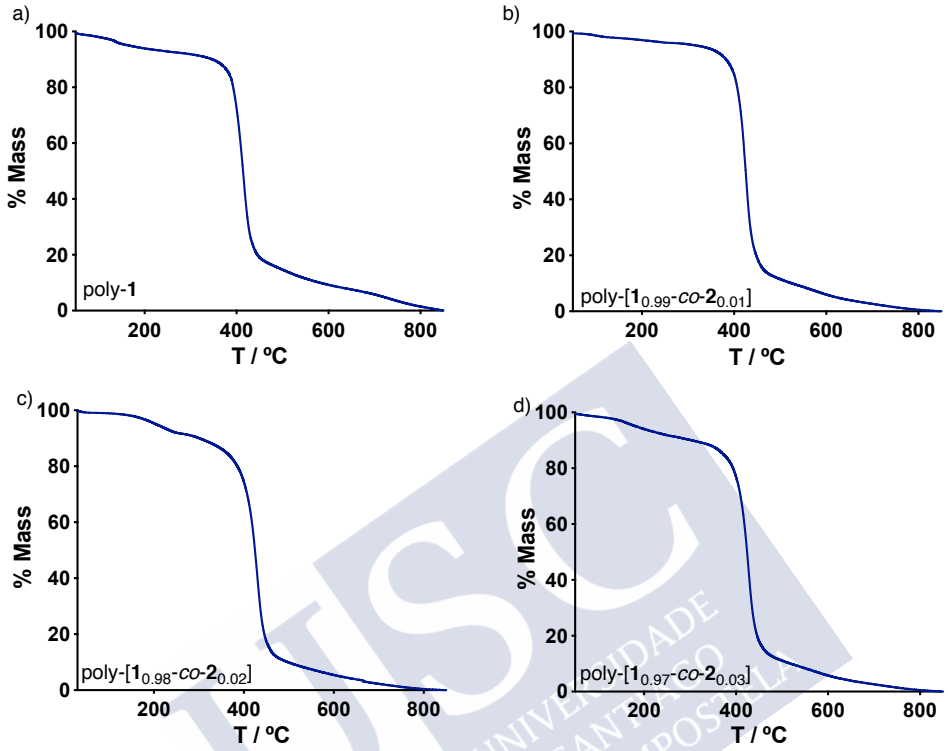

Figure S12. TGA experiments for poly-**1** and copolymers poly-(**1**$_{1-r}$-*co*-**2**$_r$) (r = 0.01-0.03).

5. CD studies of poly-(**1**$_{1-r}$-*co*-**2**$_r$) (r = 0.01-0.03) in different solvents

CD studies were carried out to determine the excess of helical sense in the poly-(**1**$_{1-r}$-*co*-**2**$_r$) (r = 0.01-0.03) series. For that, poly-(**1**$_{1-r}$-*co*-**2**$_r$) (r = 0.01-0.03) were dissolvent in different solvents (0.3 mg mL^{-1}) and then the CD spectra were recorded.

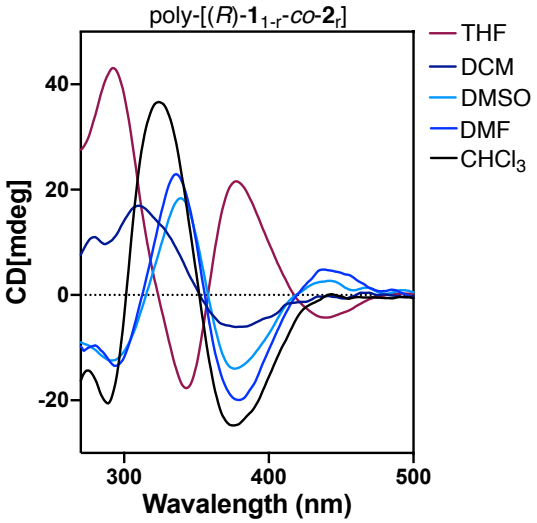

Figure S13. CD studies of poly-[(*R*)-**1**$_{1\text{-r}}$-*co*-**2**$_{r}$] (r = 0.01-0.03) in diferent solvents.

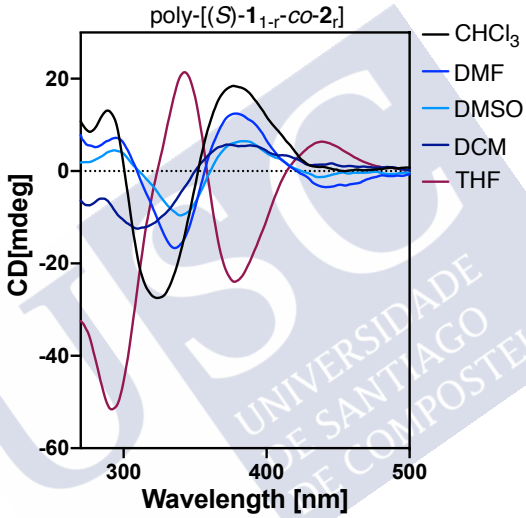

Figure S14. CD studies of poly-[(*S*)-**1**$_{1\text{-r}}$-*co*-**2**$_{r}$] (r = 0.01-0.03) in diferent solvents.

6. Aggregation studies for copolymers poly-(**1**$_{1\text{-r}}$-*co*-**2**$_{r}$) series

DLS traces for 50/50 (v/v) poly-[(*S*)-**1**$_{1\text{-r}}$-*co*-**2**$_{r}$]/poly-[(*R*)-**1**$_{1\text{-r}}$-*co*-**2**$_{r}$] (r = 0.01-0.03) mixture in THF shows the formation of large fiber-like aggregates. DLS comparison between 50/50 (v/v) poly-(*R*)-**1**/poly-(*S*)-**1** and 50/50 (v/v) poly-[(*S*)-**1**$_{1\text{-r}}$-*co*-**2**$_{r}$]/poly-[(*R*)-**1**$_{1\text{-r}}$-*co*-**2**$_{r}$] (r = 0.01-0.03) in THF shows a decrease in the size of the fiber-like aggregates due to the presence of M**2** in the copolymer chain.

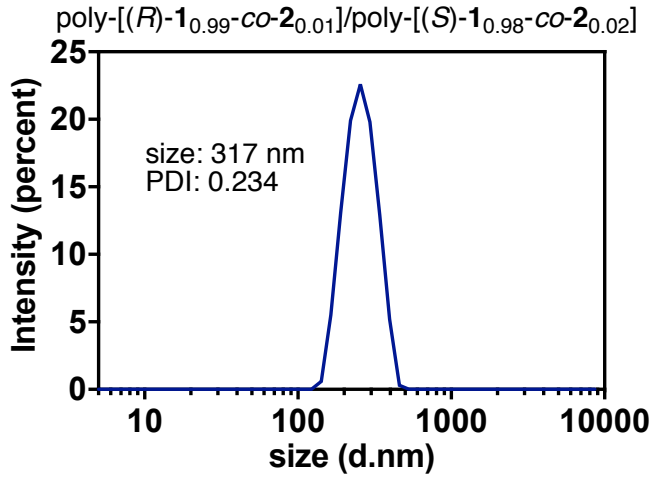

Figure S15. DLS traces of THF solutions of the stereocomplex (50/50) poly-[(*R*)-**1**$_{0.99}$-*co*-**2**$_{0.01}$]/ poly-[(*S*)-**1**$_{0.98}$-*co*-**2**$_{0.02}$].

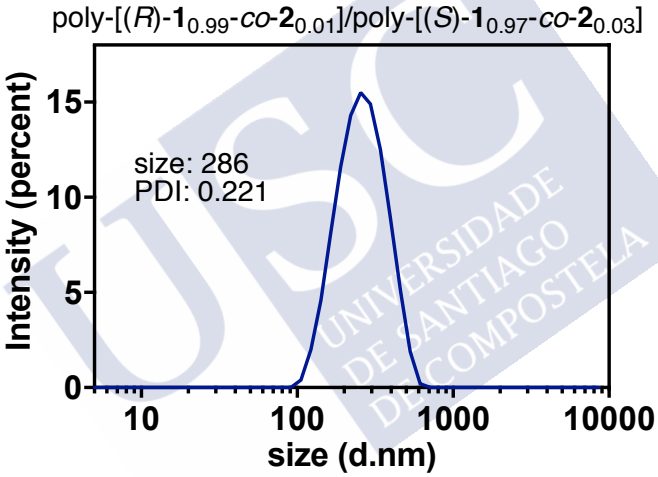

Figure S16. DLS traces of THF solutions of the stereocomplex (50/50) poly-[(*R*)-**1**$_{0.99}$-*co*-**2**$_{0.01}$]/ poly-[(*S*)-**1**$_{0.97}$-*co*-**2**$_{0.03}$].

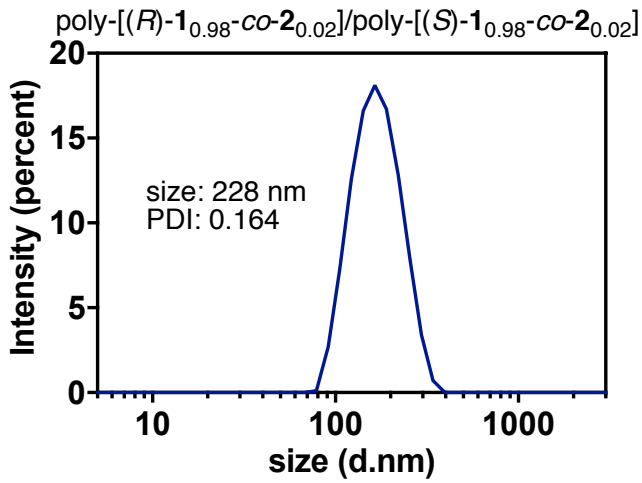

Figure S17. DLS traces of THF solutions of the stereocomplex (50/50) poly-[(*R*)-**1**$_{0.98}$-*co*-**2**$_{0.02}$]/ poly-[(*S*)-**1**$_{0.98}$-*co*-**2**$_{0.02}$].

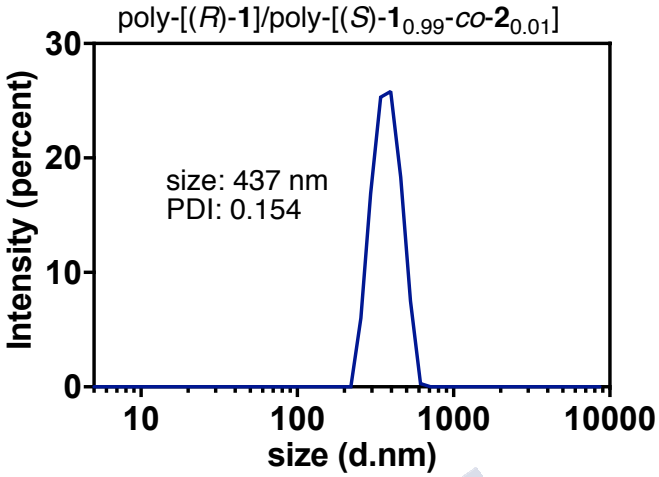

Figure S18. DLS traces of THF solutions of the stereocomplex (50/50) poly-(*R*)-**1**/ poly-[(*S*)-**1**$_{0.99}$-*co*-**2**$_{0.01}$].

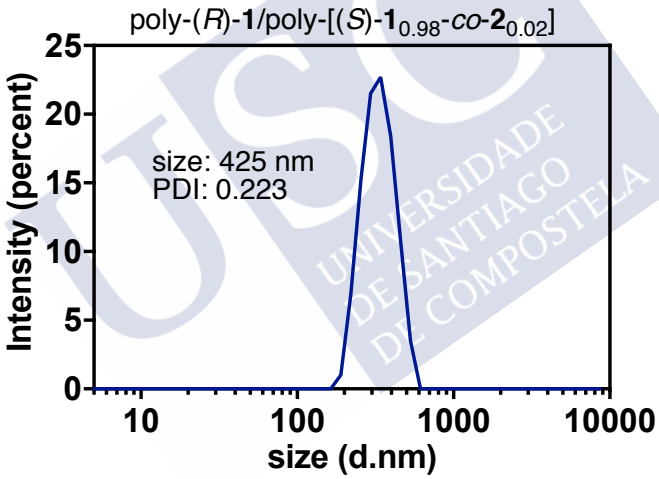

Figure S19. DLS traces of THF solutions of the stereocomplex (50/50) poly-(*R*)-**1**/ poly-[(*S*)-**1**$_{0.98}$-*co*-**2**$_{0.02}$].

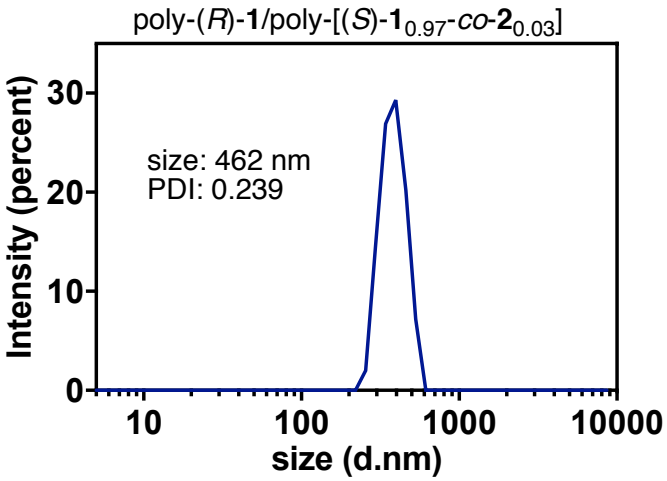

Figure S20. DLS traces of THF solutions of the stereocomplex (50/50) poly-(*R*)-**1**/ poly-[(*S*)-$\mathbf{1}_{0.97}$-*co*-$\mathbf{2}_{0.03}$].

7. SEM microscopy images for sterocomplexes formed by copolymers poly-[$\mathbf{1}_{1\text{-}r}$-*co*-$\mathbf{2}_r$] (r = 0.01-0.03)

- Control studies: poly-(*R*)-**1**/poly-(*S*)-**1** stereocomplexes

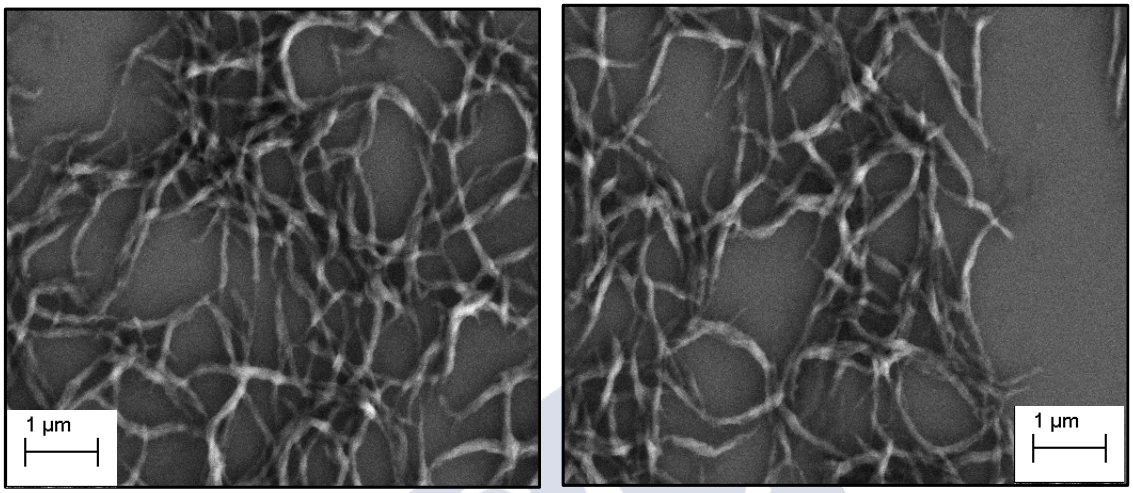

Figure S21. SEM images of THF solution of the stereocomplex (50/50) poly-(*R*)-**1**/poly-(*S*)-**1**.

- SEM studies of THF solutions of poly-[(*R*)-$\mathbf{1}_{1\text{-}r}$-*co*-$\mathbf{2}_r$]/ poly-[(*S*)-$\mathbf{1}_{1\text{-}r}$-*co*-$\mathbf{2}_r$] (r = 0.01-0.03)

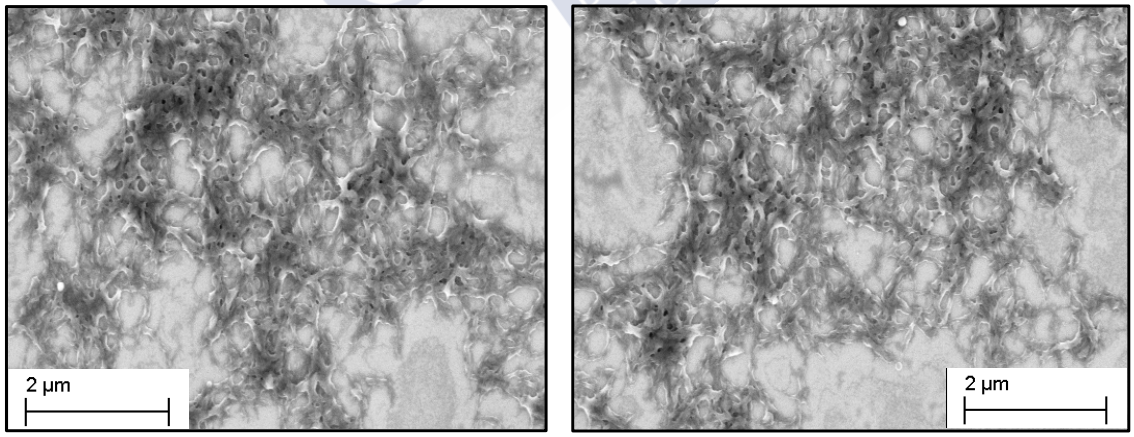

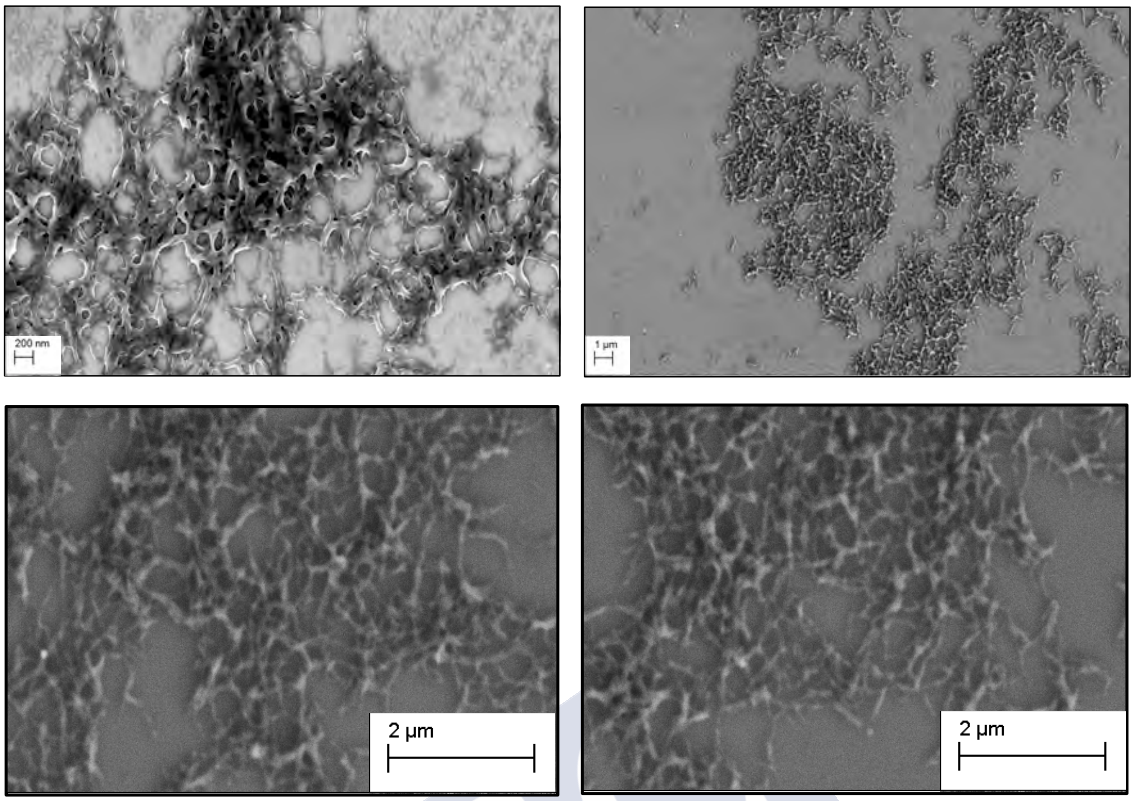

Figure S22. SEM images of THF solution of the stereocomplex (50/50) poly-[(*R*)-**1**$_{1\text{-r}}$-*co*-**2**$_r$]/ poly-[(*S*)-**1**$_{1\text{-r}}$-*co*-**2**$_r$] (r = 0.01-0.03)

8. Synthesis of poly-(**1**$_{1\text{-r}}$-*co*-**2**$_r$)-AuNPs and poly-(**1**$_{1\text{-r}}$-*co*-**2**$_r$)-AgNPs (r =0.01-0.03

- Synthesis of poly-(**1**$_{1\text{-r}}$-*co*-**2**$_r$)-AuNPs

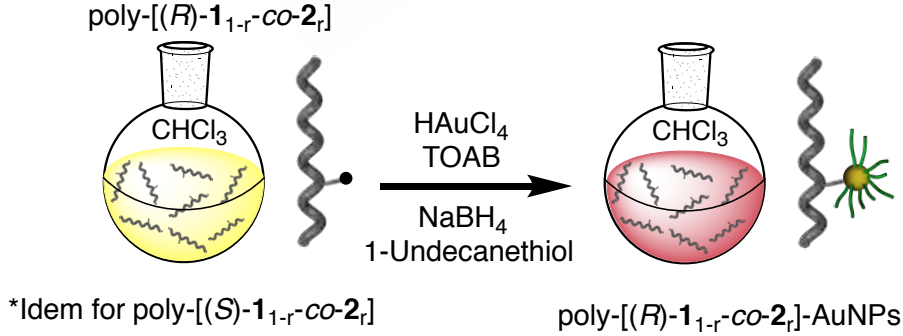

To a solution of tetraoctylamonium bromide (TOAB, 0.546 g, 0.942 mmol) into DCM (20mL) was added a solution of $HAuCl_4$ (0.080 g, 0.235 mmol) in distilled water (1.25 mL) and allowed to stir at rt. After some time, the mixture was washed with DCM (20 mL x 3). A solution of poly-(**1**$_{1\text{-r}}$-*co*-**2**$_r$] (r = 0.01-0.03) (20 mg) with dodecanethiol (40 µL) in DCM (5 mL) were prepared and both solutions were added simultaneously to the reaction mixture and

allowed to stir at -4°C for 30 min. After this time was added as a reducing agent, a solution of $NaBH_4$ (87 mg, 2.350) in distilled water (2 mL). The reaction mixture turns a yellow –orange to brown– black and EtOH (HPLC grade, 50 mL) is added to the solution and left at -4 ° C for 18 h. After this time, the reaction mixture was filtered using a filter plate. The precipitate obtained was dissolved in $CHCl_3$ and a second process was conducted in toluene precipitation using centrifuge (1h, 11000 rpm) and obtaining in a poly-(**1**$_{1\text{-r}}$-*co*-**2**$_r$]-AuNPs quantitative yield.

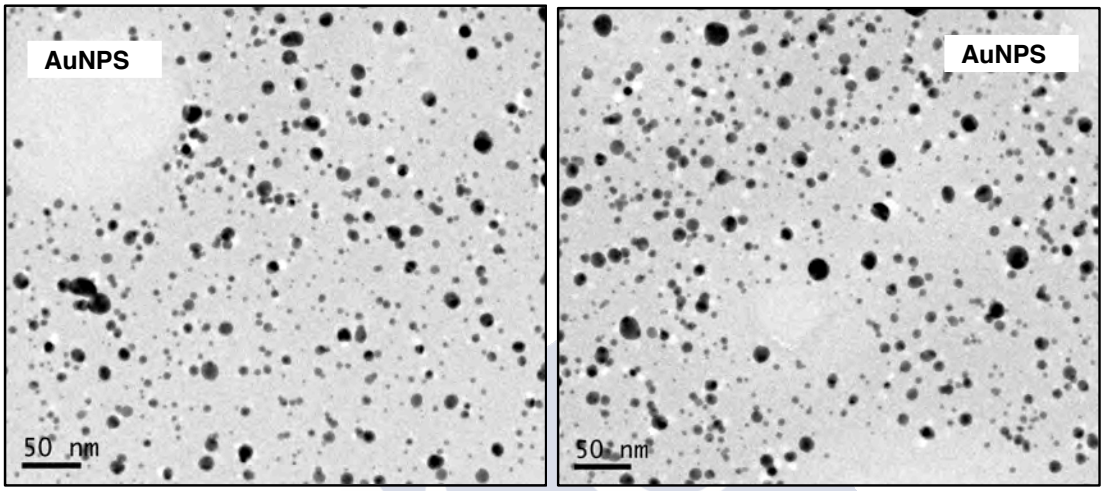

Figure S23. TEM images of poly- poly-(1$_{1\text{-r}}$-*co*-2$_r$)-AuNPs.

- Synthesis of poly-(**1**$_{1\text{-r}}$-*co*-**2**$_r$)-AgNPs

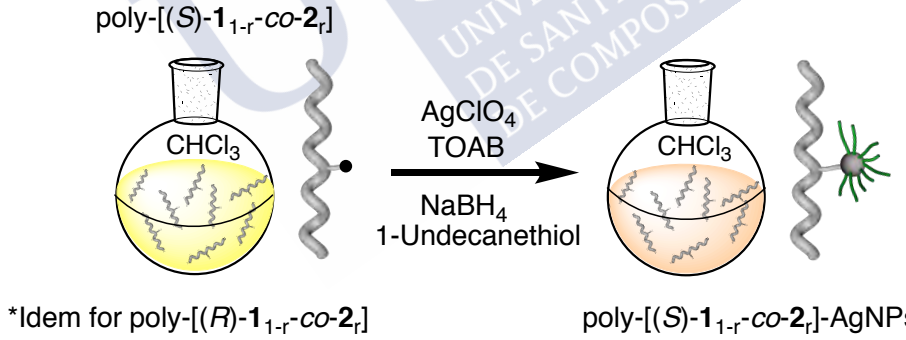

To a solution of tetraoctylamonium bromide (TOAB, 0.843 g, 0.1.544 mmol) into DCM (20mL) was added a solution of $AgClO_4$ (0.080 g, 0.386 mmol) in distilled water (1.25 mL) and allowed to stir at rt. After some time, the mixture was washed with DCM (20 mL x 3). A solution of poly-(**1**$_{1\text{-r}}$-*co*-**2**$_r$) (r = 0.01-0.03) (20 mg) with dodecanethiol (40 μL) in DCM (5 mL) were prepared and both solutions were added simultaneously to the reaction mixture and allowed to stir at -4°C for 30 min. After this time was added as a reducing agent, a solution of $NaBH_4$ (143 mg, 3.860) in distilled water (2 mL). The reaction mixture turns a yellow –orange to brown – black and EtOH (HPLC grade, 50 mL) is added to the solution and left at -4 ° C for 18 h. After this time, the reaction mixture was filtered using a filter plate. The precipitate obtained

was dissolved in $CHCl_3$ and a second process was conducted in toluene precipitation using centrifuge (1h, 11000 rpm) and obtaining in a poly-(**1**$_{1-r}$-*co*-**2**$_r$]-AgNPs quantitative yield.

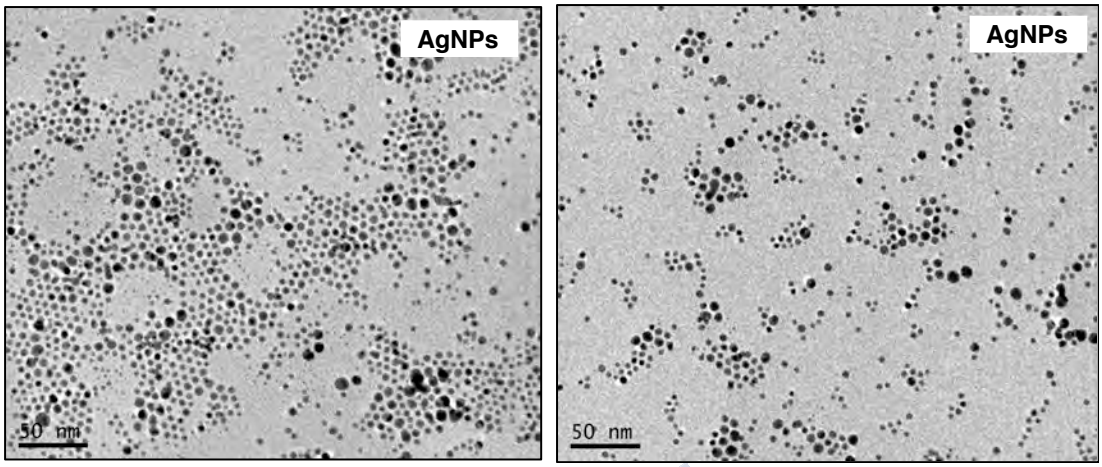

Figure S24. TEM images of poly- poly-(1$_{1-r}$-*co*-2$_r$)-AgNPs.

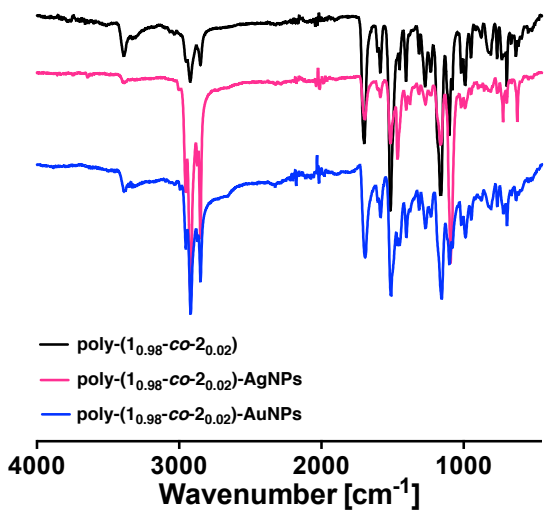

Figure S25. FT-IR spectra of poly-(**1**$_{0.98}$-*co*-**2**$_{0.02}$), poly-(**1**$_{0.98}$-*co*-**2**$_{0.02}$)-AgNPs and poly-(**1**$_{0.98}$-*co*-**2**$_{0.02}$)-AuNPs.

9. Stimuli-responsive studies of poly-(1$_{1-r}$-*co*-2$_r$)-MNPs (M = Au or Ag) in different solvents

CD and UV-Vis studies were performed with a solution of poly-[(*S*)-**1**$_{0.98}$-*co*-**2**$_{0.02}$)-AgNPs and poly-[(*R*)-**1**$_{0.98}$-*co*-**2**$_{0.02}$)-AuNPs in different solvents ($CHCl_3$, DMF, DMSO) which concentration was 0.3 mg mL^{-1}.

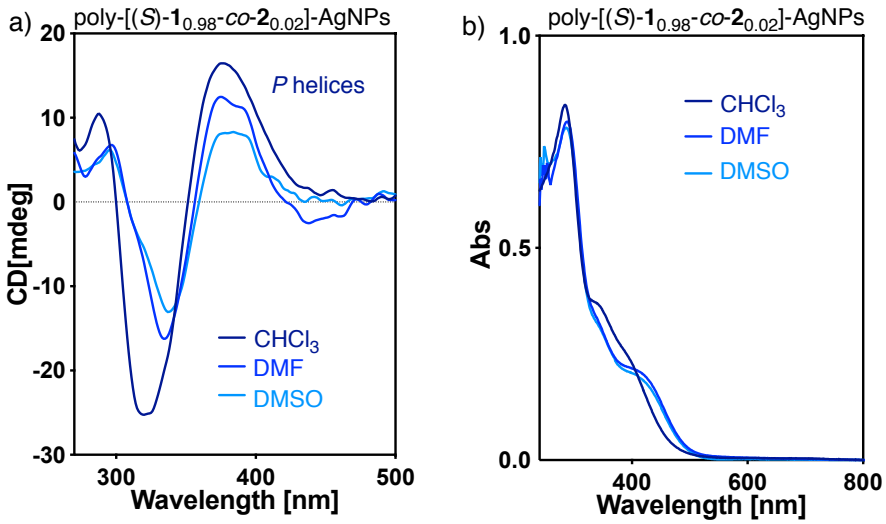

Figure S26. a) CD and b) UV-vis studies of poly-[(*S*)-$\mathbf{1}_{1\text{-r}}$-*co*-$\mathbf{2}_{r}$]-AgNPs in different solvents.

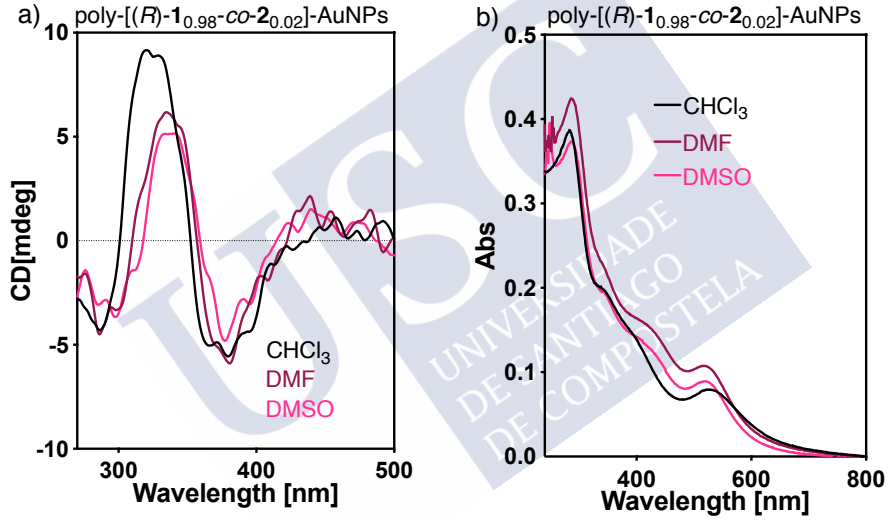

Figure S27. a) CD and b) UV-vis studies of poly-[(*R*)-$\mathbf{1}_{1\text{-r}}$-*co*-$\mathbf{2}_{r}$)-AuNPs in different solvents.

10. Raman studies of poly-($\mathbf{1}_{1\text{-r}}$-*co*-$\mathbf{2}_{r}$)-MNPs (Au or Ag)

FT-IR studies of poly-($\mathbf{1}_{1\text{-r}}$-*co*-$\mathbf{2}_{r}$)-MNPs (0.3 mg mL^{-1}) in THF showed the presence of the *cis*-amide at 1760 cm^{-1}.

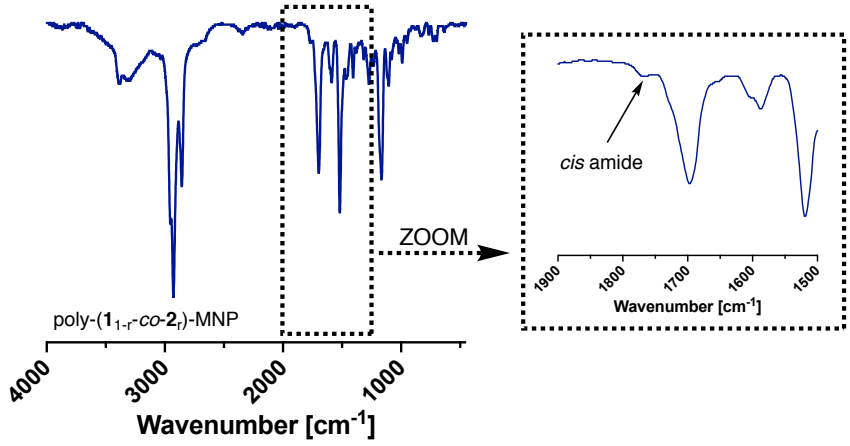

Figure S28. FT-IR studies of poly-($\mathbf{1}_{1\text{-}r}$-*co*-$\mathbf{2}_r$)-MNPs in THF showing the presence of *cis*-amide band.

11. Raman studies of poly-($\mathbf{1}_{1\text{-}r}$-*co*-$\mathbf{2}_r$)-MNPs (Au or Ag)

The *cis* stereoregularity of the nanocomposites poly-($\mathbf{1}_r$-*co*-$\mathbf{2}_{1\text{-}r}$)-AuNPs and poly-($\mathbf{1}_r$-*co*-$\mathbf{2}_{1\text{-}r}$)-AgNPs was determined by Raman resonances.

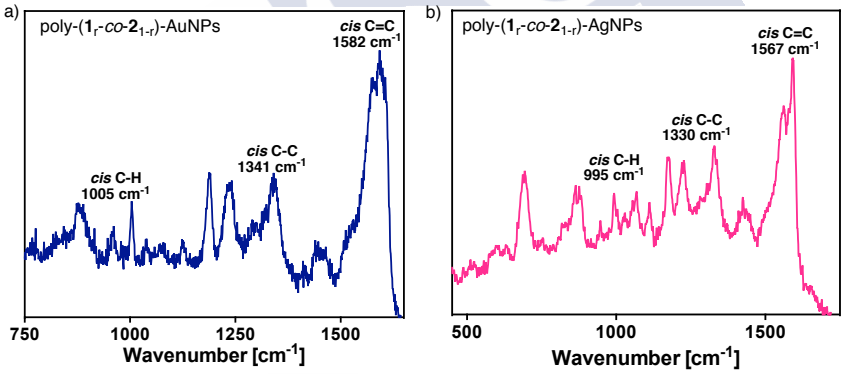

Figure S29. Raman spectra for a) poly-($\mathbf{1}_r$-*co*-$\mathbf{2}_{1\text{-}r}$)-AuNPs and b) poly-($\mathbf{1}_r$-*co*-$\mathbf{2}_{1\text{-}r}$)-AgNPs.

12. ON/OFF stereocomplexation studies of copolymers poly-[(*R*)-$\mathbf{1}_{1\text{-}r}$-*co*-$\mathbf{2}_r$)]/poly-[(*S*)-$\mathbf{1}_{1\text{-}r}$-*co*-$\mathbf{2}_r$)] and poly-($\mathbf{1}_{1\text{-}r}$-*co*-$\mathbf{2}_r$)/poly-1

- Effect of the temperature

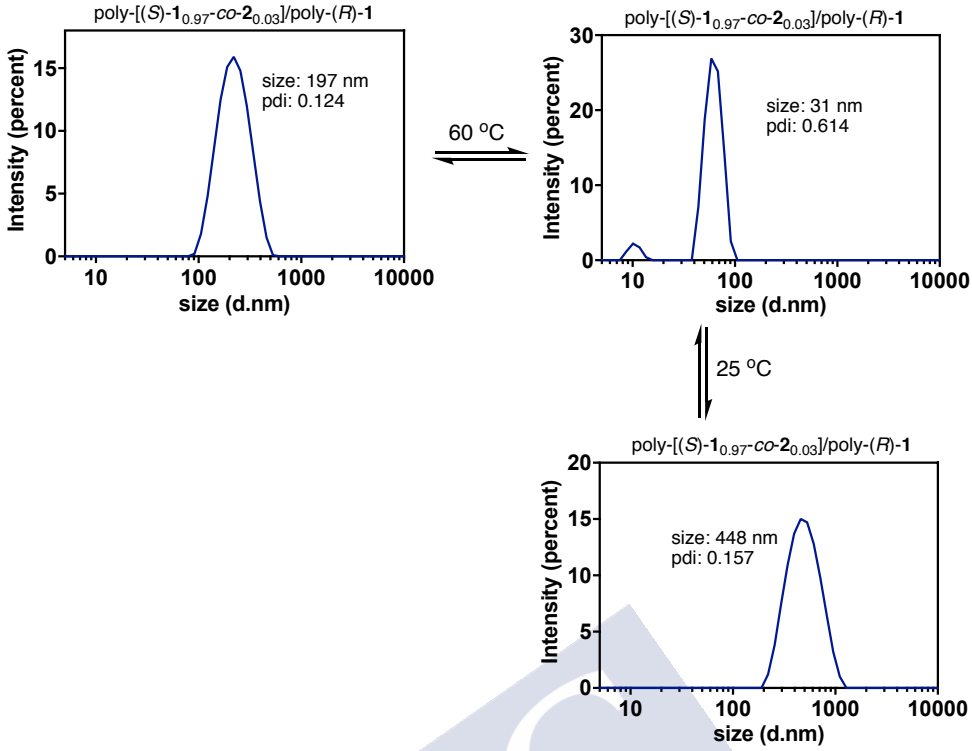

Figure S30. DLS traces of the sequential heating and cooling of THF solutions of the stereocomplex (50/50) poly-[(*S*)-**1**$_{0.97}$-*co*-**2**$_{0.03}$]/poly-(*R*)-**1**.

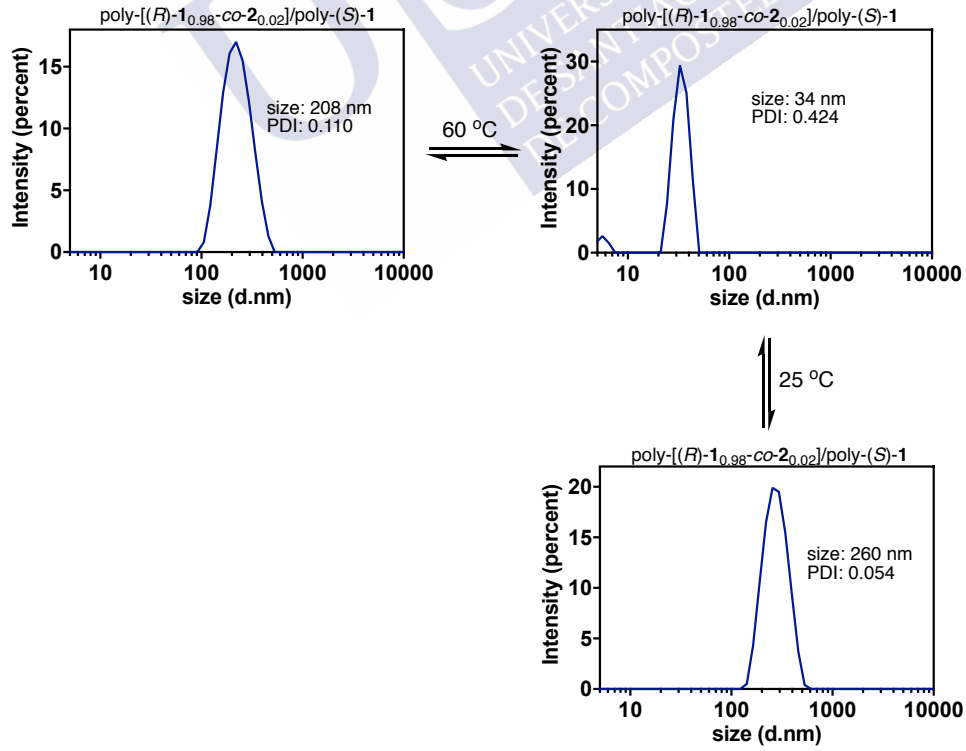

Figure S31. DLS traces of the sequential heating and cooling of THF solutions of the stereocomplex (50/50) poly-[(*R*)-**1**$_{0.98}$-*co*-**2**$_{0.02}$]/poly-(*S*)-**1**.

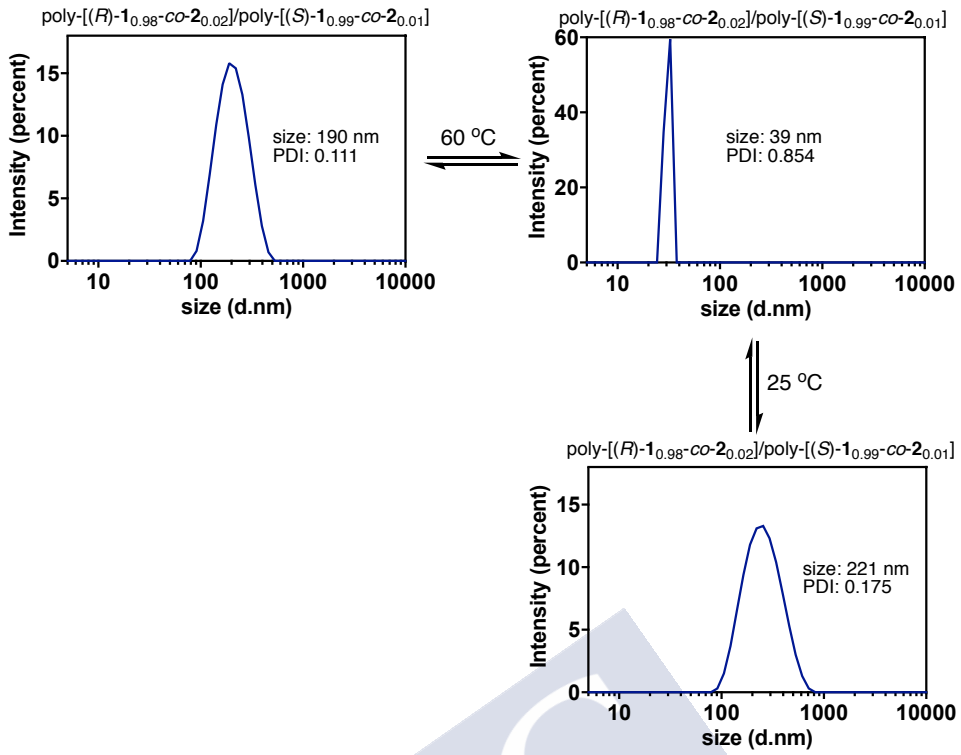

Figure S32. DLS traces of the sequential heating and cooling of THF solutions of the stereocomplex (50/50) poly-[(*R*)-**1**$_{0.98}$-*co*-**2**$_{0.02}$]/poly-[(*S*)-**1**$_{0.99}$-*co*-**2**$_{0.01}$].

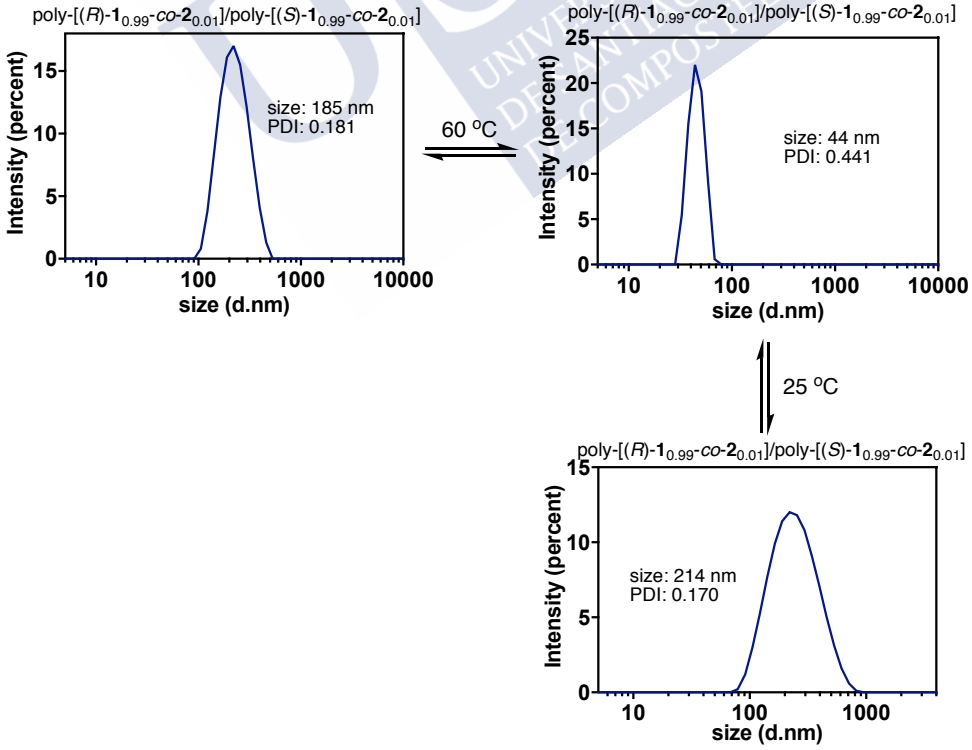

Figure S33. DLS traces of the sequential heating and cooling of THF solutions of the stereocomplex (50/50) poly-[(*R*)-**1**$_{0.99}$-*co*-**2**$_{0.01}$]/poly-[(*S*)-**1**$_{0.99}$-*co*-**2**$_{0.01}$].

- Effect of the MeOH addition

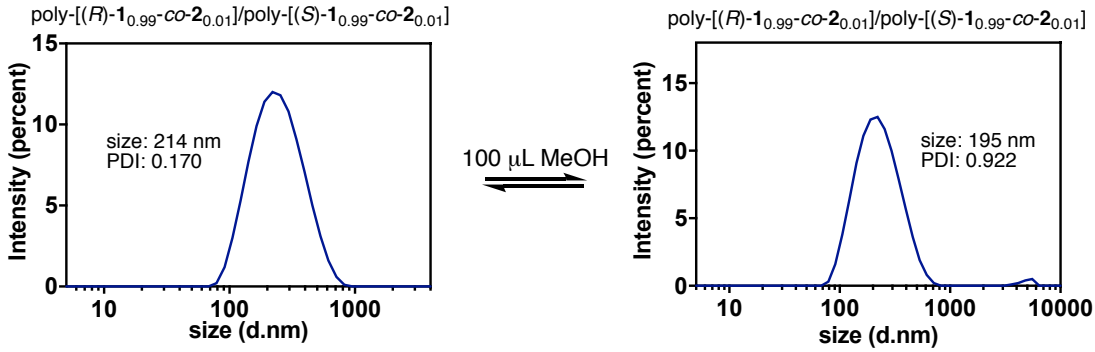

Figure S34. DLS traces of (50/50) poly-[(*R*)-**1**$_{0.99}$-*co*-**2**$_{0.01}$]/poly-[(*S*)-**1**$_{0.99}$-*co*-**2**$_{0.01}$] and poly-[(*R*)-**1**$_{0.99}$-*co*-**2**$_{0.01}$]/poly-[(*S*)-**1**$_{0.99}$-*co*-**2**$_{0.01}$] after addition of 100 mL of MeOH.

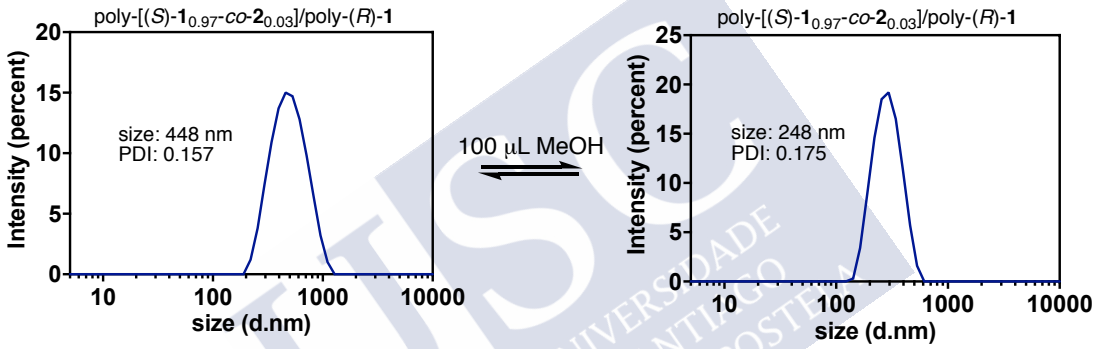

Figure S35. DLS traces of (50/50) poly-[(*S*)-**1**$_{0.97}$-*co*-**2**$_{0.03}$]/poly-[*R*)-**1** and poly-[(*S*)-**1**$_{0.97}$-*co*-**2**$_{0.01}$]/poly-(*R*)-**1**] after addition of 100 mL of MeOH

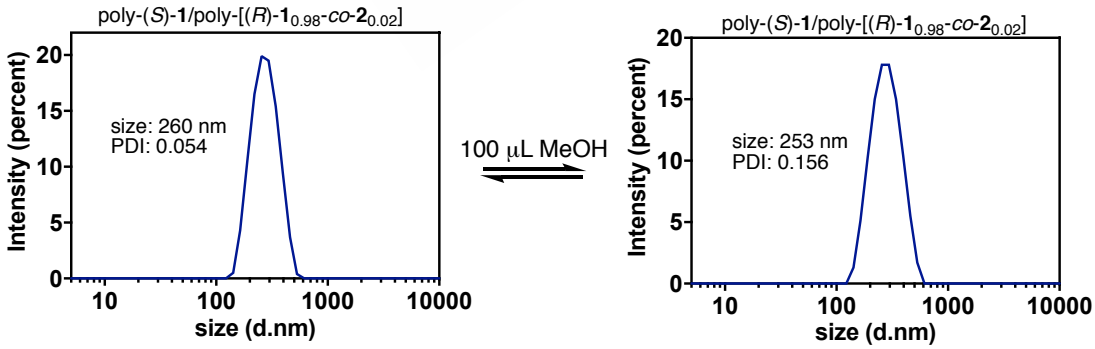

Figure S36. DLS traces of (50/50) poly-(*S*)-**1**/poly-[(*R*)-**1**$_{0.98}$-*co*-**2**$_{0.02}$] and poly-(*S*)-**1**/poly-[*R*)-**1**$_{0.98}$-*co*-**2**$_{0.02}$] after addition of 100 mL of MeOH.

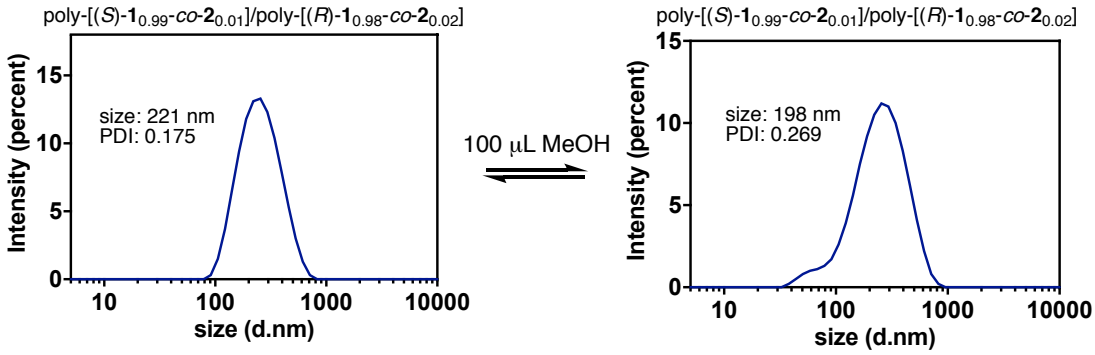

Figure S37. DLS traces of (50/50) poly-[(*S*)-**1**$_{0.99}$-*co*-**2**$_{0.01}$]/poly-[(*R*)-**1**$_{0.98}$-*co*-**2**$_{0.02}$] and poly-[(*S*)-**1**$_{0.99}$-*co*-**2**$_{0.01}$]/poly-[(*R*)-**1**$_{0.98}$-*co*-**2**$_{0.02}$]after addition of 100 mL of MeOH.

13. CD studies of copolymers poly-(**1**$_{1-r}$-*co*-**2**$_r$)-MPNs (M = Au or Ag)

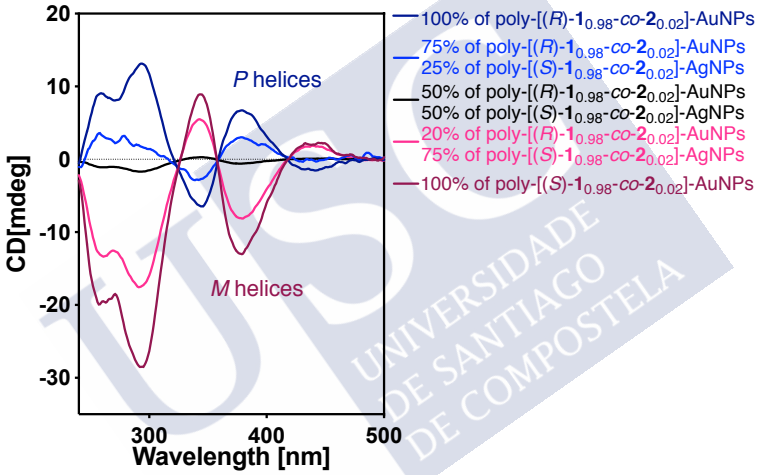

Figure S38. CD studies of poly-[(*R*)-**1**$_{0.98}$-*co*-**2**$_{0.02}$]-AuNPs + poly-[(*R*)-**1**$_{0.98}$-*co*-**2**$_{0.02}$]-AgNPs at different ratios in THF.

14. Aggregation studies for copolymers poly-($\mathbf{1}_{1\text{-}r}$-*co*-$\mathbf{2}_r$)-MPNs (M = Au or Ag)

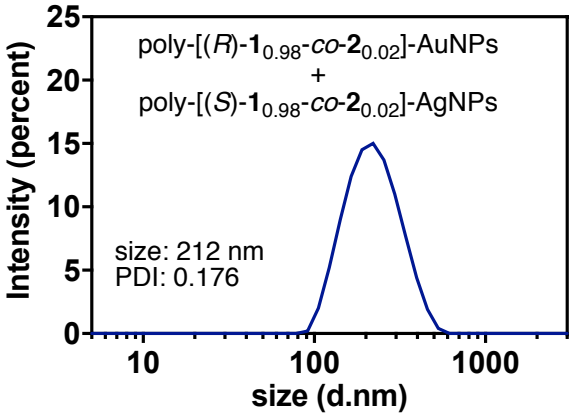

Figure S39. DLS traces of (50/50) of poly-[(*R*)-**1**$_{0.98}$-*co*-**2**$_{0.02}$]-AuNPs/poly-[(*S*)-**1**$_{0.98}$-*co*-**2**$_{0.02}$]-AgNPs stereocomplexes.

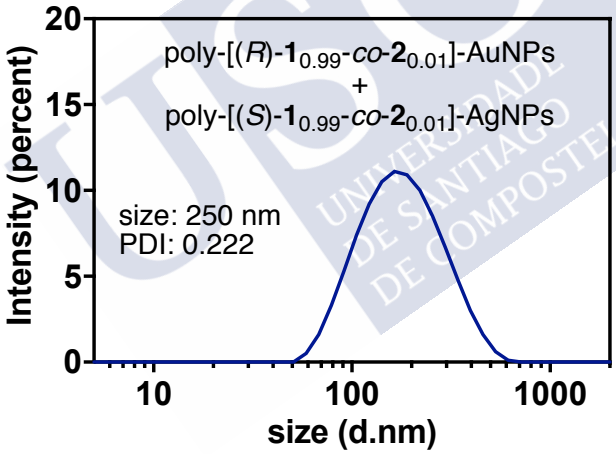

Figure S40. DLS traces of (50/50) of poly-[(*R*)-**1**$_{0.99}$-*co*-**2**$_{0.01}$]-AuNPs/poly-[(*S*)-**1**$_{0.99}$-*co*-**2**$_{0.01}$]-AgNPs stereocomplexes.

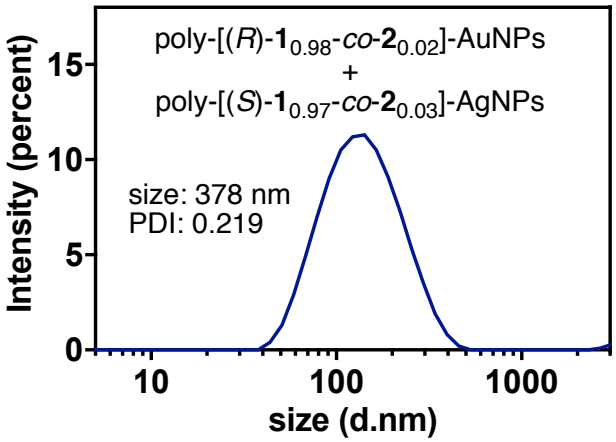

Figure S41. DLS traces of (50/50) of poly-[(*R*)-**1**$_{0.98}$-*co*-**2**$_{0.02}$]-AuNPs/poly-[(*S*)-**1**$_{0.97}$-*co*-**2**$_{0.03}$]-AgNPs stereocomplexes.

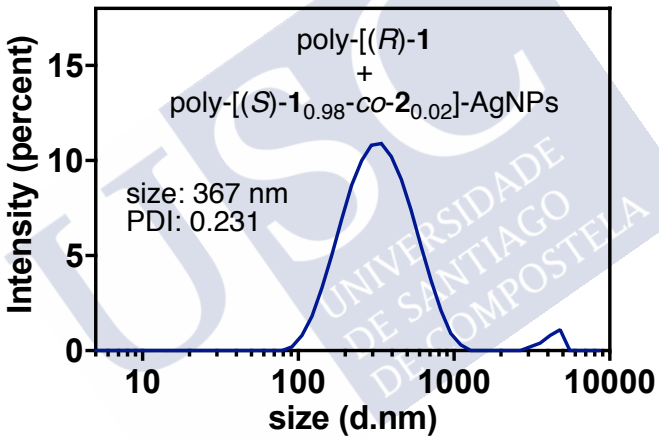

Figure S42. DLS traces of (50/50) of poly-[(*R*)-**1** /poly-[(*S*)-**1**$_{0.98}$-*co*-**2**$_{0.02}$]-AgNPs stereocomplexes.

15. SEM studies of poly-[(*R*)-1$_{1-r}$-*co*-2$_r$)]/poly-[(*S*)-1$_{1-r}$-*co*-2$_r$)]-MNPs mixtures

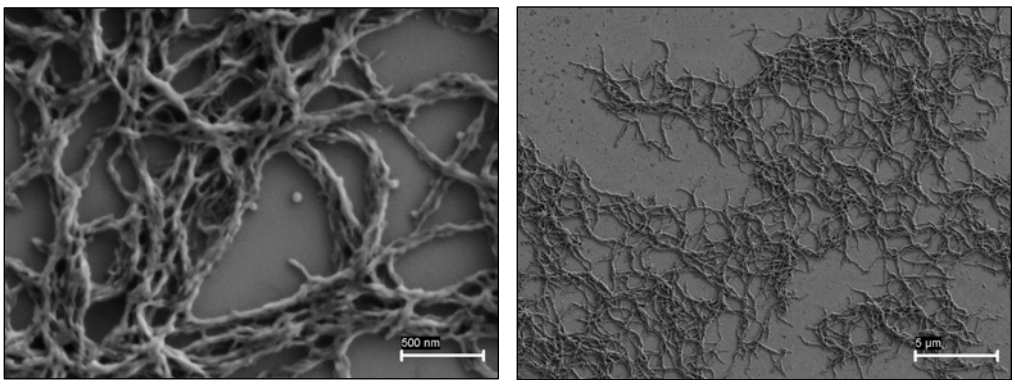

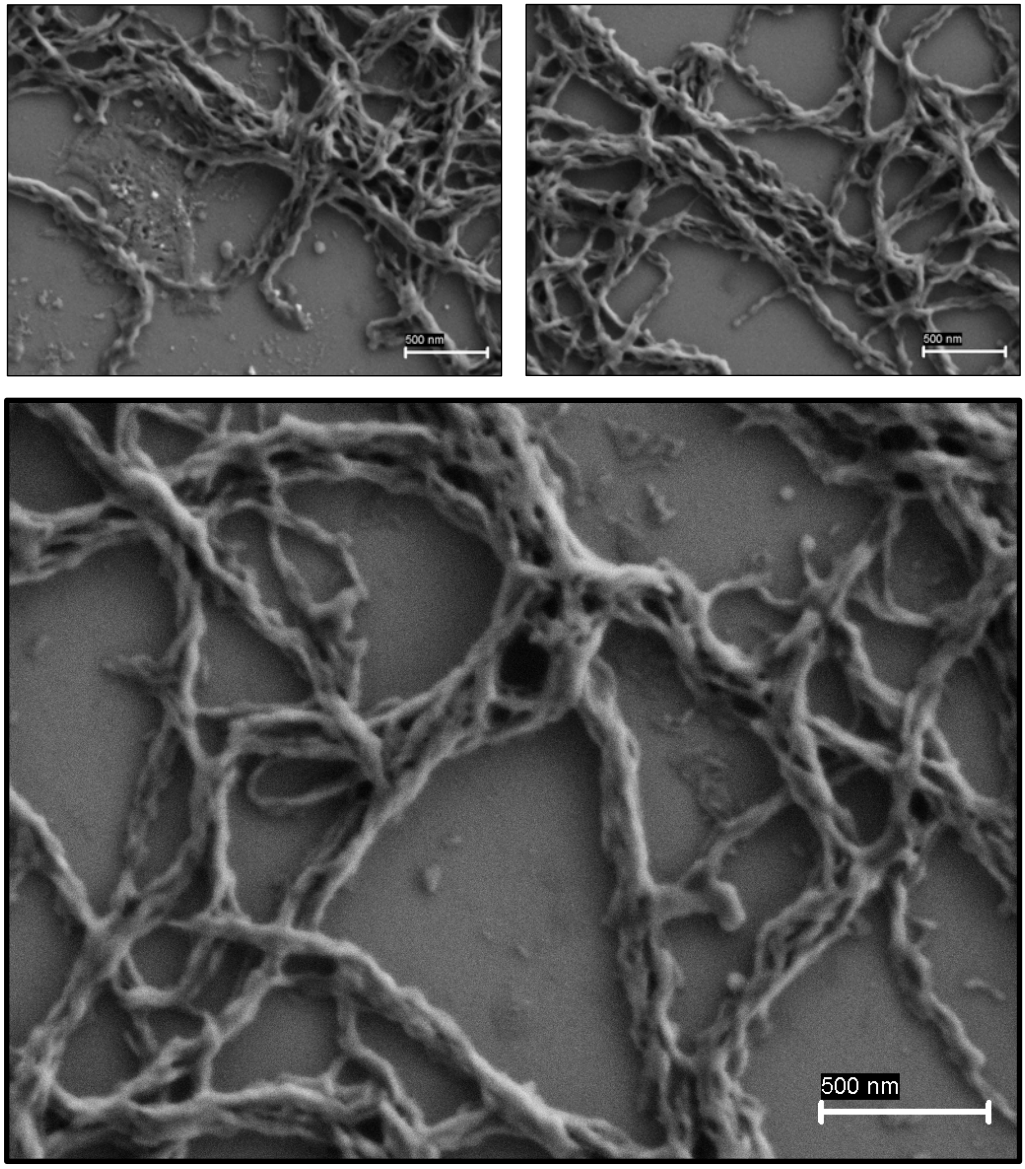

Figure S43. SEM images of poly-[(*R*)-**1**$_{1\text{-r}}$-*co*-**2**$_{r}$]/ poly-[(*R*)-**1**$_{1\text{-r}}$-*co*-**2**$_{r}$] stereocomplexes.

16. TEM studies of poly-[(*R*)-$\mathbf{1}_{1\text{-r}}$-*co*-$\mathbf{2}_{r}$)]/poly-[(*S*)-$\mathbf{1}_{1\text{-r}}$-*co*-$\mathbf{2}_{r}$)] mixtures

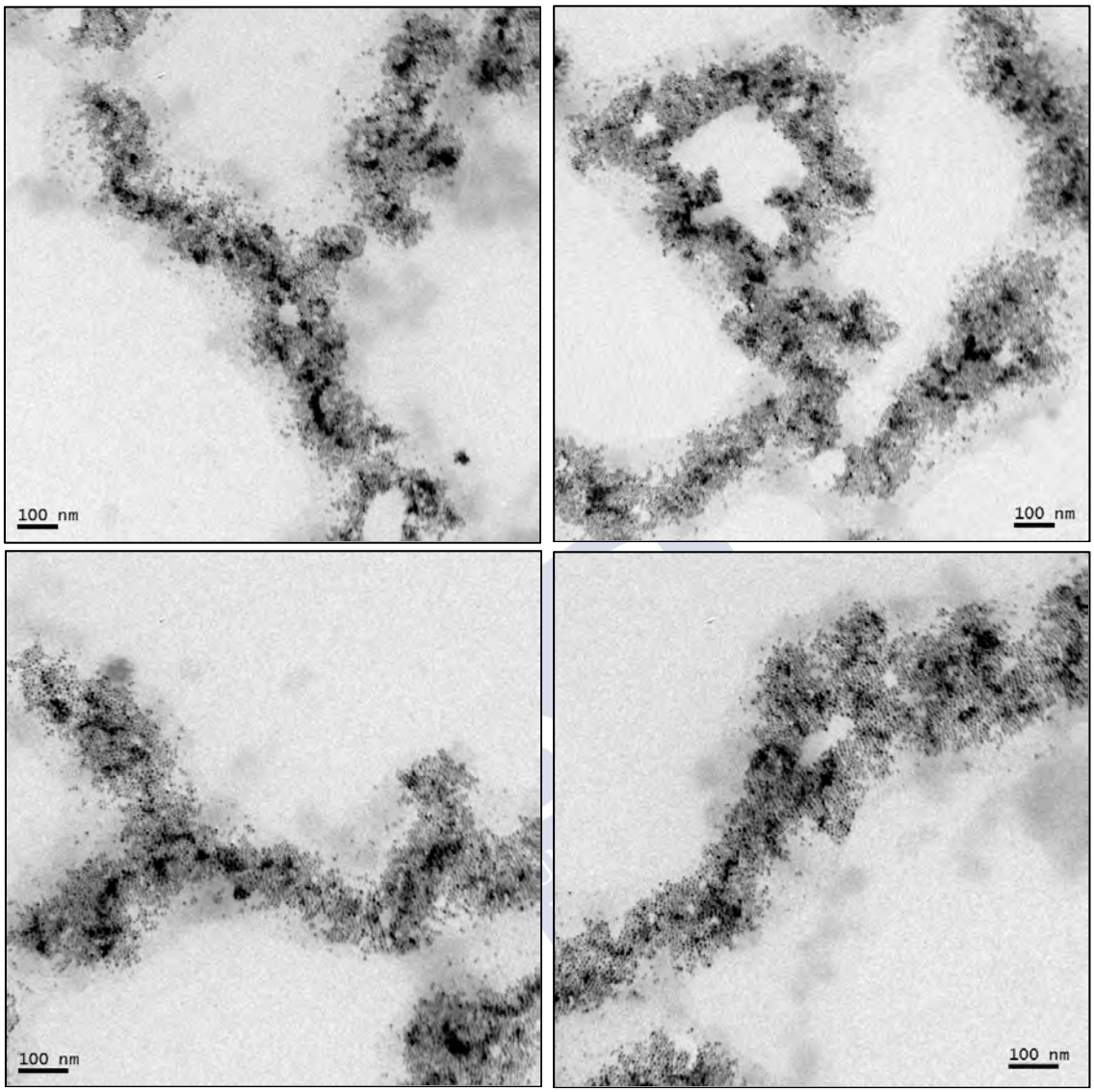

Figure S44. TEM images for stereocomplex formed by poly-([*R*)-$\mathbf{1}_{1\text{-r}}$-*co*-$\mathbf{2}_{r}$]/poly-[(*S*)-($\mathbf{1}_{1\text{-r}}$-*co*-$\mathbf{2}_{r}$].

17. Preparation of poly-1-AuNPs and poly-1-AgNPs

- Preparation of poly-(*R*)-**1**-AuNPs

0.5 equiv of $HAuCl_4$ (10 mg mL^{-1}) in MeOH was added to a solution of poly-(*R*)-**1** (0.3 mg mL^{-1}) in $CHCl_3$. Once the metal ion (Au^{3+}) is added, the solution turns from yellow to blue. Interestingly, CD spectra showed a null cotton Effect in the vinylic region (CD_{380} = 0) and the UV-Vis studies confirmed the absence of the vinylic band. All these experiments suggested the *cis-trans* isomerization of the polyene backbone.

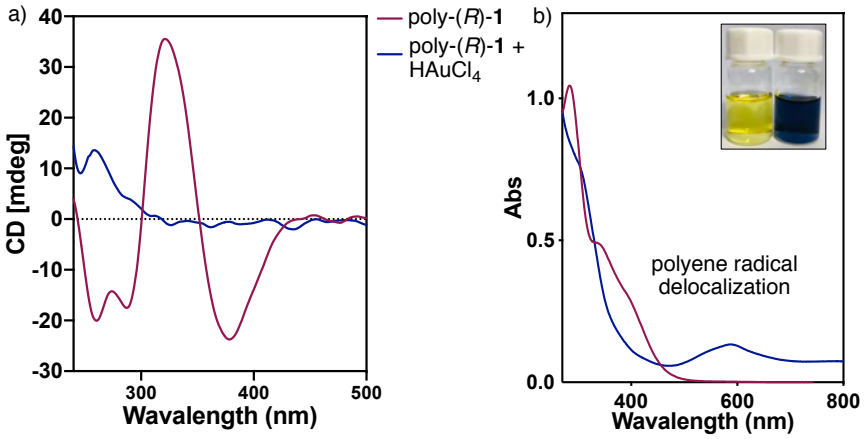

Figure S45. a) CD spectra of poly-(*R*)-**1** and poly-(*R*)-**1** + $HAuCl_4$ and b) UV-Vis spectra of poly-(*R*)-**1** and poly-(*R*)-**1** + $HAuCl_4$.

- Preparation of poly-(*R*)-**1**-AgNPs

Poly-(*R*)-**1**-AgNPs were prepared according to reference S4:

0.5 equiv of $AgClO_4$ (10 mg mL^{-1}, MeOH) was added to a solution of poly-(*R*)-**1** to form poly-(*R*)-**1**/Ag^+ complexes and the solution. Next, 1 equiv of $NaBH_4$ (1 mg mL^{-1}, MeOH) was added to poly-(*R*)-**1**/Ag^+ leading to the formation of poly-(*R*)-**1**-AgNPs. TEM images showed the formation of high polydisperse AgNPs with a poor stability in solution.

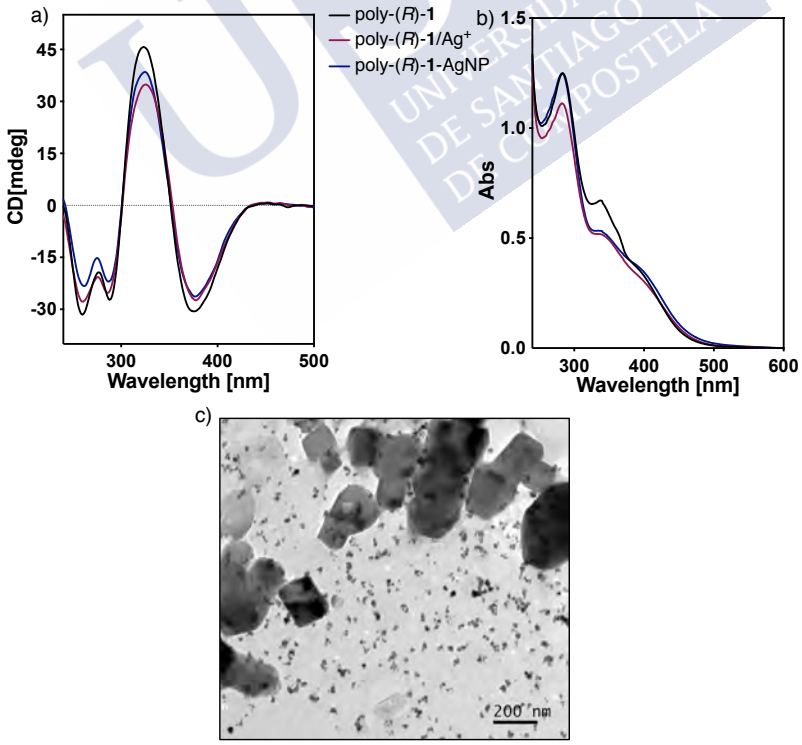

Figure S45. a) CD spectra of poly-(*R*)-**1** and poly-(*R*)-**1**/Ag^+ and poly-(*R*)-**1**-AgNPs. b) UV-Vis spectra of poly-(*R*)-**1** and poly-(*R*)-**1**/Ag^+ and poly-(*R*)-**1**-AgNPs. c) TEM image of poly-(*R*)-**1**-AgNPs.

18. References

S1. Leiras, S.; Freire, F.; Quiñoá, E.; Riguera, R. Reversible assembly of enantiomeric helical polymers: from fibers to gels. *Chem. Sci*., **2015**, *6*, 246–253.

S2. Leiras, S.; Freire, F.; Seco, J. M.; Quiñoá, E.; Riguera, R. Controlled modulation of the helical sense and the elongation of poly(phenylacetylene)s by polar and donor effect. *Chem. Sci*., **2013**, *4*, 2735-2743.

S3. Bergueiro, J.; Núñez-Martínez, M.; Arias, S.; Quiñoá, E.; Riguera, R.; Freire, F.; Chiral Gold-PPA Nanocomposites with Tunable Helical Sense and Morphology. *Nanoscale Horiz.,* **2020**, *5*, 495-500.

S4. Núñez-Martínez, M.; Arias, S.; Quiñoá, E.; Riguera, R.; Freire, F.; Dynamic Chiral PPA–AgNP Nanocomposites: Aligned Silver Nanoparticles Decorating Helical Polymers. *Chem. Mater.* **2021**, *33*, 4805–4812.

USC UNIVERSIDADE DE SANTIAGO DE COMPOSTELA

1. Names and codes

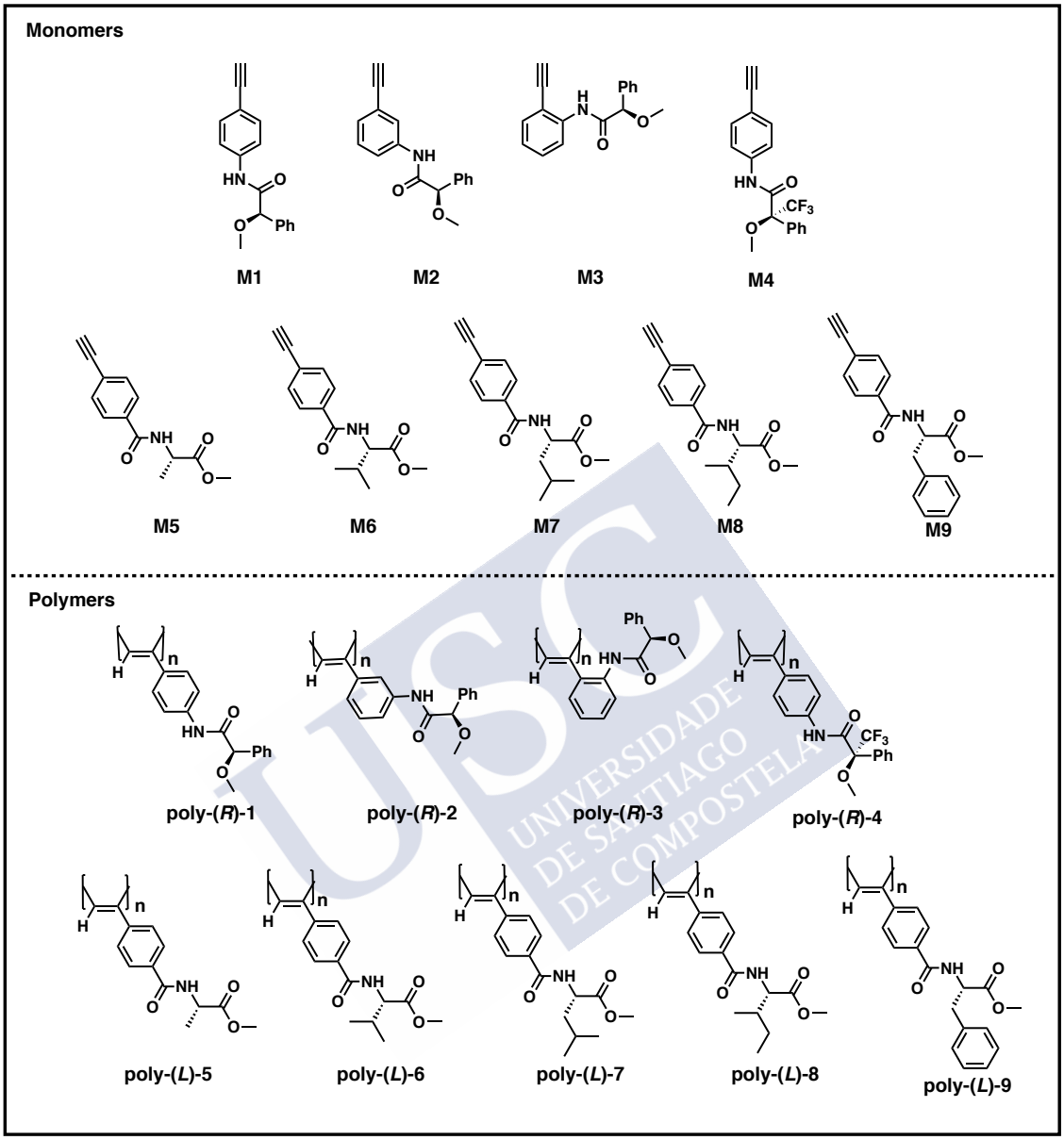

USC UNIVERSIDADE DE SANTIAGO DE COMPOSTELA

2. Materials and methods

Chemicals. Commercially available chemicals have been used as delivered. Solvents were purchased as reagent grade and distilled if necessary. Anhydrous solvents were either purchased as ultra-dry solvent from Acros Organics® or received from solvent purification system. For the coupling and polymerization reactions, dry THF was obtained from MBRAUN SPS 800 solvent purification system. Water was purified by Millipore water purification system. Coupling reagents (2-(7-Aza-1H-benzotriazole-1-yl)-1,1,3,3-tetramethyluronium hexafluorophosphate) (HATU), 4- ethynylbenzoic acid, 4-ethynylaniline, 3-ethynylaniline and 2-ethynylaniline were purchased from AnaSpec Inc. (*R*)-α-methoxy-α-trifluoromethylphenylacetic acid, oxalyl choride, 1-Ethyl-3-(3-dimethylaminopropyl)carbodiimide (EDC), hydroxybenzotriazole (HOBt), (*L*)-alanine methyl ester hydrochloride, (*L*)-valine methyl ester hydrochloride, (*L*)-isoleucine methyl ester hydrochloride, (*L*)-leucine methyl ester hydrochloride, (*L*)-phenylalanine methyl ester hydrochloride, rhodium norbornadiene chloride dimer {$[Rh(nbd)Cl]_2$}, diisopropyltriethylamine (DIPEA) and triethylamine (TEA, 99%) were purchased from Aldrich.

Instrumentations and Characterizations. NMR experiments were carried out in a Varian Inova 300 (300 MHz resonance 1H). Size exclusion chromatography studies were performed on Alliance 2695 HPLC System (Waters) liquid chromatography system equipped with a UV 2489 detector (Waters). The samples were eluted by three Phenogel columns connected to each other with stationary phases of 10^3, 10^4 and 10^5 Amstrong and packed with a solid support of a cross-linked styrene and *p*-divinylbenzene copolymer. CD and UV measurements were registered in a Jasco-720 spectropolarimeter and a Jasco-730 spectrophotometer respectively at a nanocomposite concentration of 0.3 mg mL^{-1}. FT-IR measurements were carried out on a Bruker IFS-66v. DLS studies were performed on a Nano-ZS 90 (Malvern) equipped with a He-Ne laser (l = 633 nm) under scattering angle of 173°. The samples were maintained at the designed temperature for 5 min before testing. DLS measurements were carried out in all cases at 0.1 mg·mL^{-1}. SEM measurements were performed on a LEO-435VP electron microscope equipped with an energy dispersive X-ray (EDX) spectrometer. TGA experiments were done in a TGA Q5000 (TA instruments, New Castle, UK) using a platinum pan. DSC traces were obtained in a DSC Q200 Tzero Technology (TA instruments, New Castle, UK) usinga platinum pan. TEM measurements were performed on a JEOL JEM 2010 and 200 KV as a voltage. To study the nanocomposite, or the stereocomplexes the same protocol was used. A dispersion of the nanocomposite or the nanospheres at a concentration of 0.1 mg mL^{-1} was

drop casted onto of silicon wafer chip and allowed to dry at rt for 12h for SEM studies, while in case of TEM studies the dispersed materials were drop-casted onto carbon chip and allowed to dry at rt for 12 h.

3. Synthesis of monomers

The general procedure for the procedure of monomers M**1**, M**4** and polymer poly-(*R*)-**1** and poly-(*R*)-**4** can be found in references **[S1]** and **[S2]**.

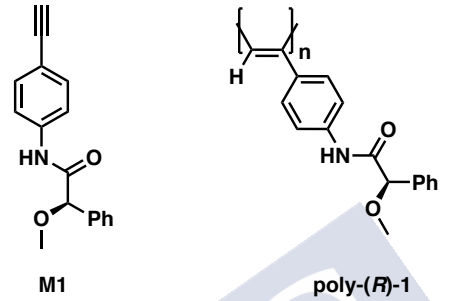

Figure S1. Structure of monomer M**1** and poly-(*R*)-**1**.

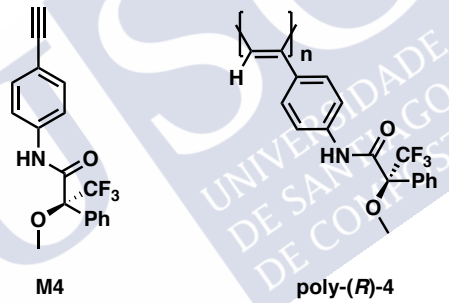

Figure S2. Structure of monomer M**4** and poly-(*R*)-**4**.

3.1 Synthesis of monomer M2

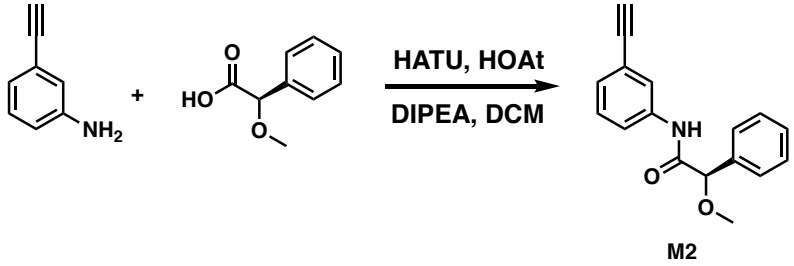

M2

(2-(7-Aza-1H-benzotriazole-1-yl)-1,1,3,3-tetramethyluronium hexafluorophosphate) (HATU, 2.3 g, 1.4 equiv), 1-hydroxy-7-azabenzotriazole (HOAt, 820 mg, 1.4 equiv), (*R*)-α-methoxy-α-phenylacetic acid ((*R*)-MPA, 1 g, 1.4 equiv), disiisopropyehtylamine (DIPEA) (1 mL, 1.4 equiv) were dissolved in CH_2Cl_2 and the mixture was stirred 15 min to activate the acid. Then, 3-ethynilaniline (500 mg, 1 equiv) was added and the mixture was stirred 24 h. The mixture was washed twice with HCl 1M, next with saturated $NaHCO_3$ solution (twice) and finally with saturated NaCl solution. The crude was chromatographed on silica gel (70-230 mesh) with hexane/ethyl acetate (7/3) as eluent (85 % of yield).

Spectroscopic data:

^{1}H NMR (300 MHz, $CDCl_3$) δ (ppm): 3.05 (s, 1H), 3.44 (s, 3H), 4.73 (s, 1H), 7.20-7.45 (m, 7H), 7.63 (d, 1H), 7.72 (s, 1H), 8.55 (s, 1H).

^{13}C NMR (75 MHz, $CDCl_3$) δ (ppm): 57.3, 83.1, 83.8, 120.2, 122.8, 123.1, 127.0, 128.1, 128.7, 129.0, 136.4, 137.4, 168.5.

$[\alpha]_D^{20}$= +75 (15 mg mL^{-1}, $CHCl_3$)

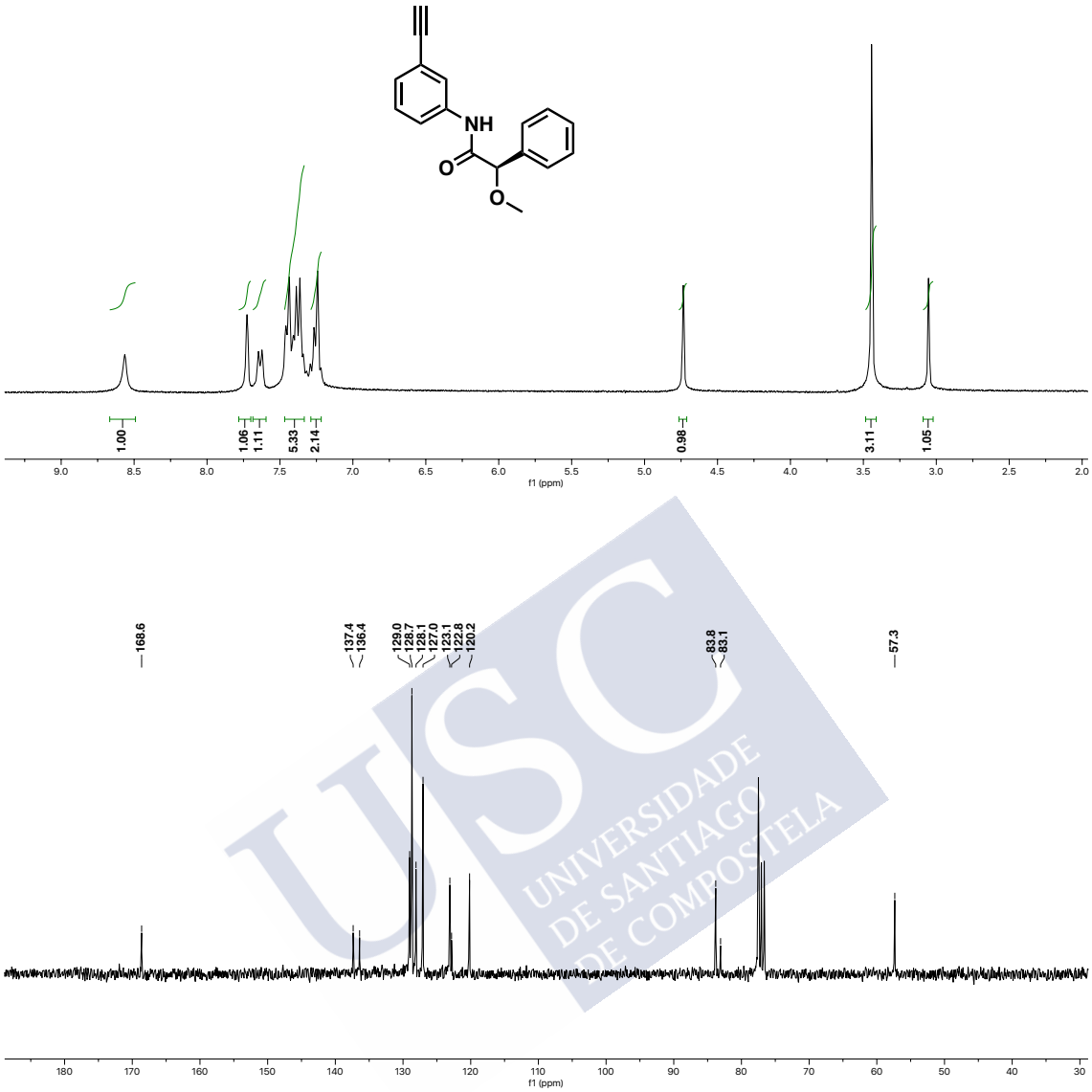

Figure S3. ^{1}H and ^{13}C NMR of poly-(*R*)-**1** in $CDCl_3$.

3.1 Synthesis of monomer M3

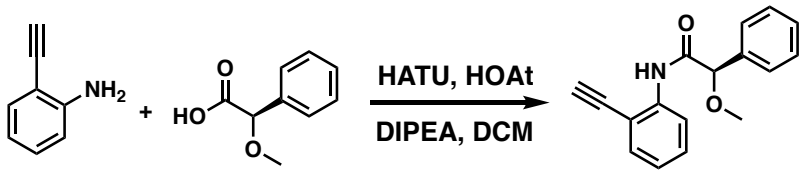

M3

(2-(7-Aza-1H-benzotriazole-1-yl)-1,1,3,3-tetramethyluronium hexafluorophosphate) (HATU, 2.3 g, 1.4 equiv), 1-hydroxy-7-azabenzotriazole (HOAt, 850 mg, 1.4 equiv), (*R*)-α-methoxy-α-phenylacetic acid ((*R*)-MPA, 1000 mg , 1.4 equiv), disiisopropyehtylamine (DIPEA) (1 mL, 2.55 mmol) were dissolved in CH_2Cl_2 and the mixture was stirred 15 min to activate the acid. Then, 2-ethynilaniline (500 mg, 1 equiv) was added and the mixture was stirred 24 h. The mixture was washed twice with HCl 1M, next with saturated $NaHCO_3$ solution (twice) and finally with saturated NaCl solution. The crude was chromatographed on silica gel (70-230 mesh) with hexane/ethyl acetate (7/3) as eluent (80% of yield).

Spectroscopic data:

^{1}H NMR (300 MHz, $CDCl_3$) δ (ppm): 3.49 (s, 3H), 3.61 (s, 1H), 4.82 (s, 1H), 7.03 (t, 1H), 7.35 (m, 4H), 7.47 (m, 3H), 8.39 (dd, 1H), 9.45 (s, 1H).

^{13}C NMR (75 MHz, $CDCl_3$) δ (ppm): 57.8, 79.1, 84.4, 84.5, 111.4, 119.4, 123.6, 127.1, 128.8, 130.3, 132.2, 136.8, 139.3, 168.9

$[\alpha]_D^{20}$= +193 (15 mg mL^{-1}, $CHCl_3$)

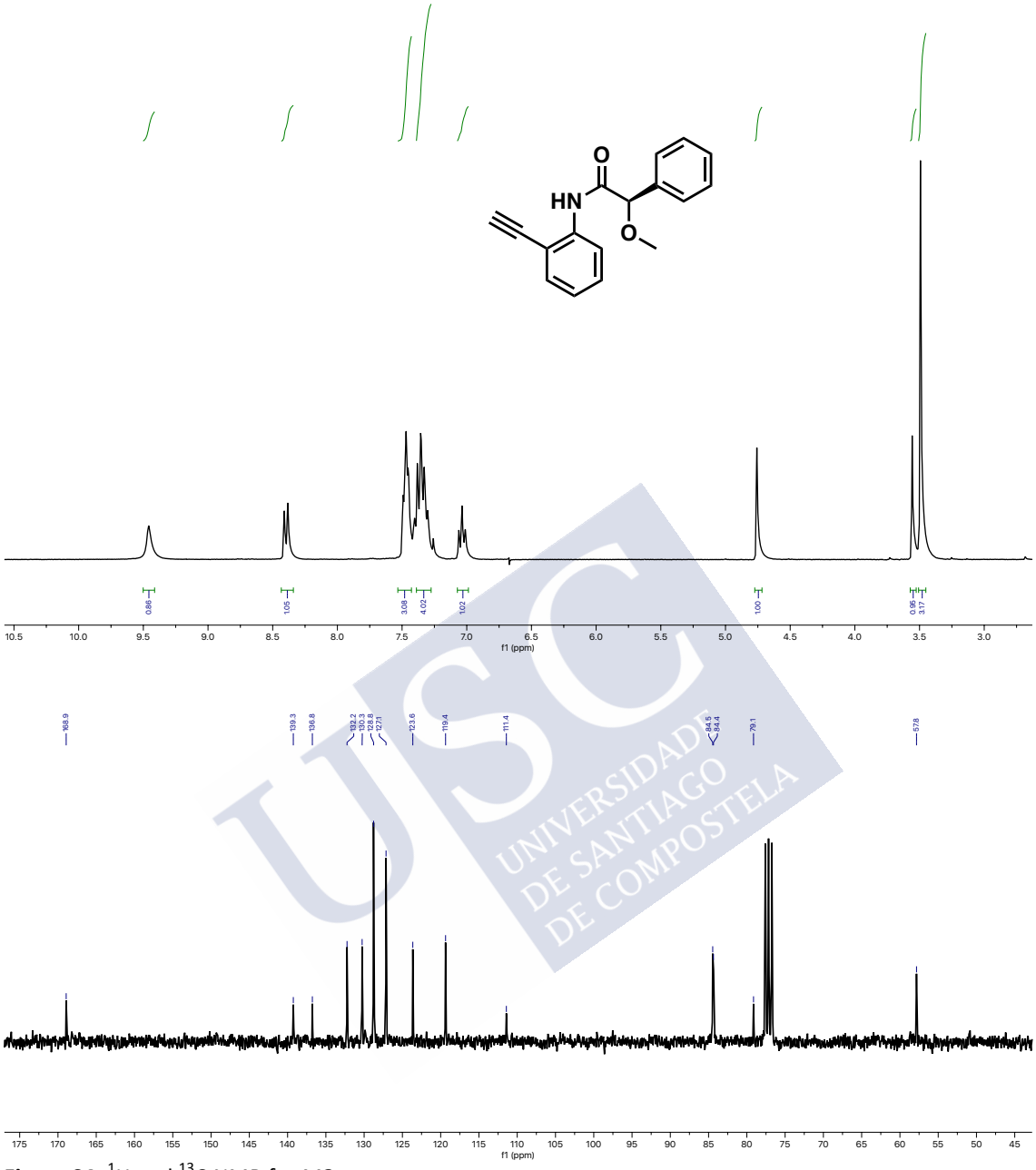

Figure S4. ^{1}H and ^{13}C NMR for M**3**.

3.1 Synthesis of monomer M5

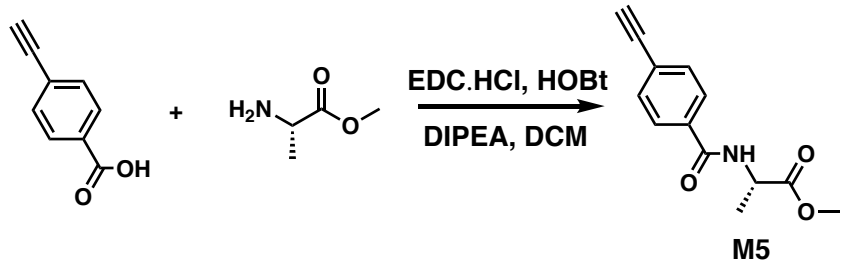

M5

1-Ethyl-3-(3-dimethylaminopropyl)carbodiimide (EDC, 1.350 g, 1.2 equiv.), hydroxybenzotriazole (HOBt, 1.400 g, 1.2 equiv.), 4-ethynylbenzoic acid (1.700 g, 1.2 equiv.) and diisopropyltriethylamine (DIPEA, 0.7 mL, 1.4 equiv.) were dissolved in 70 mL of CH_2Cl_2, and the mixture was stirred for 15 min to activate the acid. Then, (*L*)-alanine methyl ester (1.151 g, 1.0 equiv.) was added and the reaction mixture was stirred overnight. The organic layer was washed with HCl 1M, saturated solution of $NaHCO_3$ and brine. The combined organic layers were dried over anhyd. Na_2SO_4, filtered and the solvent was evaporated at reduced pressure. The crude product was chromatographed on silica gel (70-230 mesh) with hexane/ethyl acetate (7/3) as eluent, 82% of pure product.

Spectroscopic data:

^{1}H NMR (300 MHz, $CDCl_3$) δ (ppm): 1.49 (d, 3H), 3.25 (s, 1H), 3.74 (s, 3H), 4.75 (q, 1H), 7.29 (d, 1H), 7.48 (d, 2H), 7.76 (d, 2H).

^{13}C NMR (75 MHz, $CDCl_3$) δ (ppm): 18.0, 48.5, 52.4, 79.7, 82.7, 125.4, 127.1, 132.0, 133.6, 166.2, 173.5.

$[\alpha]_D^{20}$= +81 (15 mg mL^{-1}, $CHCl_3$)

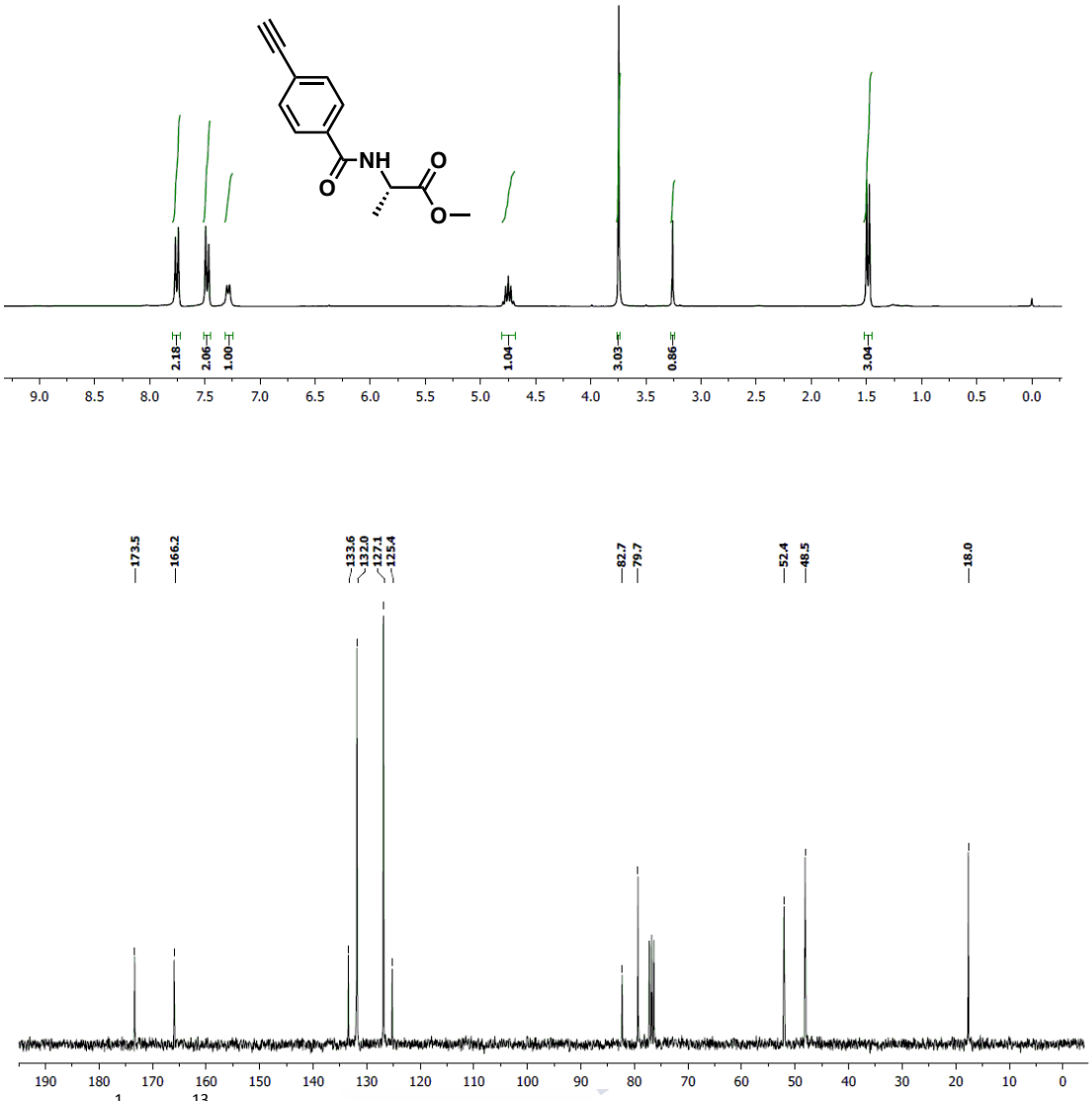

Figure S5: ^{1}H and ^{13}C NMR for M**5**.

3.2 Synthesis of monomer M6

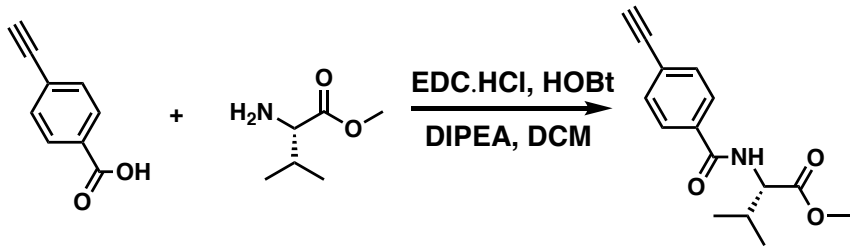

M6

1-Ethyl-3-(3-dimethylaminopropyl)carbodiimide (EDC, 0.656, 1.2 equiv.), hydroxybenzotriazole (HOBt, 0.465 g, 1.2 equiv), 4-ethynylbenzoic acid (0.500 g, 1.2 equiv) and diisopropyltriethylamine (DIPEA, 0.495 mL, 1.4 equiv) were dissolved in 50 mL of CH_2Cl_2, and the mixture was stirred for 15 min to activate the acid. Then, (*L*)-valine methyl ester (0.398 g, 1.0 equiv) was added and the reaction mixture was stirred overnight. The organic layer was washed with HCl 1M, saturated solution of $NaHCO_3$ and brine. The combined organic layers were dried over anhyd. Na_2SO_4, filtered and the solvent was evaporated at reduced pressure. The crude product was chromatographed on silica gel (70-230 mesh) with hexane/ethyl acetate (7/3) as eluent, 76% of pure product.

Spectroscopic data:

^{1}H NMR (300 MHz, $CDCl_3$) δ (ppm): 0.96 (m, 6H), 2.24 (m, 1H), 3.19 (1H, s), 3.73 (3H, s), 4.72 (q, 1H), 6.73 (d, 1H), 7.50 (d, 2H), 7.73 (d, 2H).

^{13}C NMR (75 MHz, $CDCl_3$) δ (ppm): 18.1, 19.0, 31.6, 52.3, 71.3, 79.7, 82.8, 125.6, 127.1, 132.3, 134.1, 166.5, 172.6

$[\alpha]_D^{20}$= +36 (15 mg mL^{-1}, $CHCl_3$)

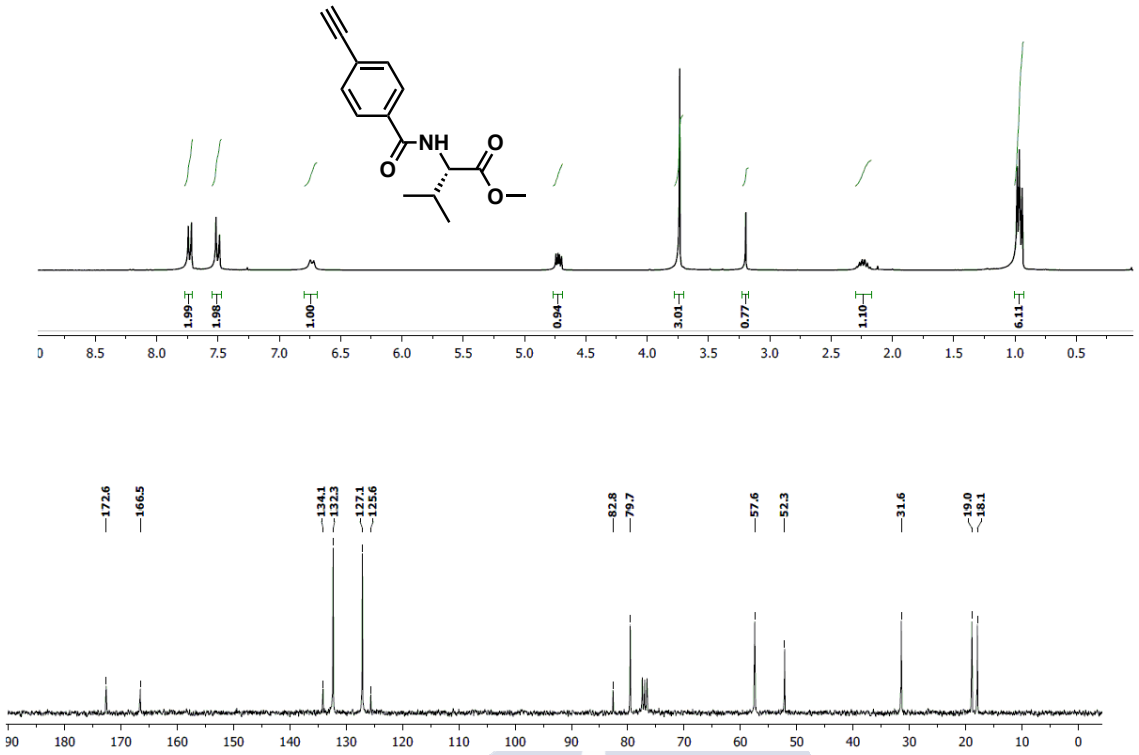

Figure S6. ^{1}H and ^{13}C NMR for M**6**.

3.3 Synthesis of monomer M7

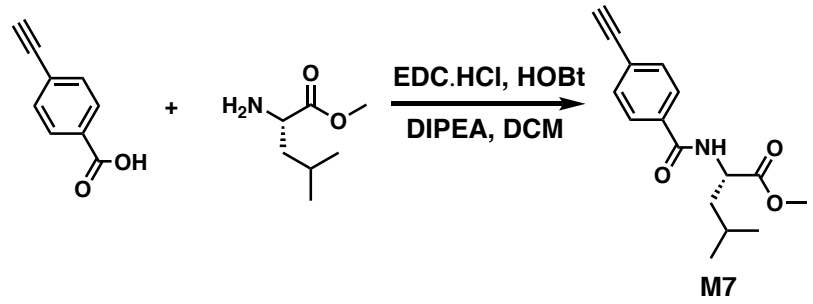

M7

1-Ethyl-3-(3-dimethylaminopropyl)carbodiimide (EDC, 0.122 g, 1.2 equiv.), hydroxybenzotriazole (HOBt, 0.087 g, 1.2 equiv), 4-ethynylbenzoic acid (1.7 g, 1.2 equiv) and diisopropyltriethylamine (DIPEA, 0.080 mL, 1.4 equiv) were dissolved in 30 mL of CH_2Cl_2, and the mixture was stirred for 15 min to activate the acid. Then, (*L*)-leucine methyl ester (0.771 g, 1.0 equiv) was added and the reaction mixture was stirred overnight. The organic layer was washed with HCl 1M, saturated solution of $NaHCO_3$ and brine. The combined organic layers were dried over anhyd Na_2SO_4, filtered and the solvent was evaporated at reduced pressure. The crude product was chromatographed on silica gel (70-230 mesh) with hexane/ethyl acetate (7/3) as eluent, 69% of pure product.

Spectroscopic data:

^{1}H NMR (300 MHz, $CDCl_3$) δ (ppm): 0.94 (d, 6H), 1.73 (m, 3H), 3.29 (s, 1H), 3.73 (s, 3H), 4.81 (q, 1H), 7.43 (d, 2H), 7.58 (d, 1H), 7.74 (d, 2H).

^{13}C NMR (75 MHz, $CDCl_3$) δ (ppm): 21.6, 22.8, 24.9, 29.5, 40.8, 51.2, 52.2, 70.8, 82.7, 125.5, 127.1, 131.9, 133.5, 166.6, 173.8.

$[\alpha]_D^{20}$= +44 (15 mg mL^{-1}, $CHCl_3$)

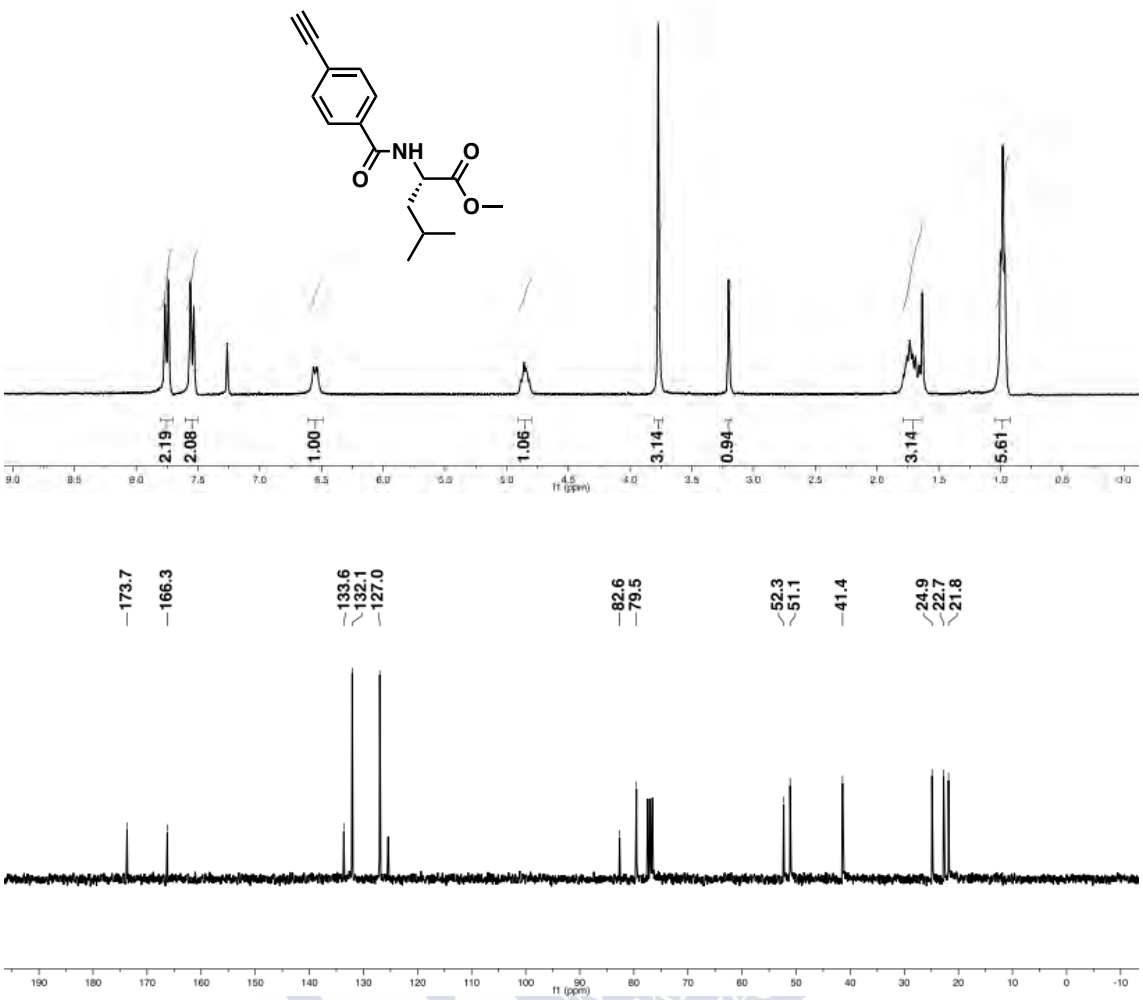

Figure S7. ^{1}H and ^{13}C NMR for M**7**.

3.4 Synthesis of monomer M8

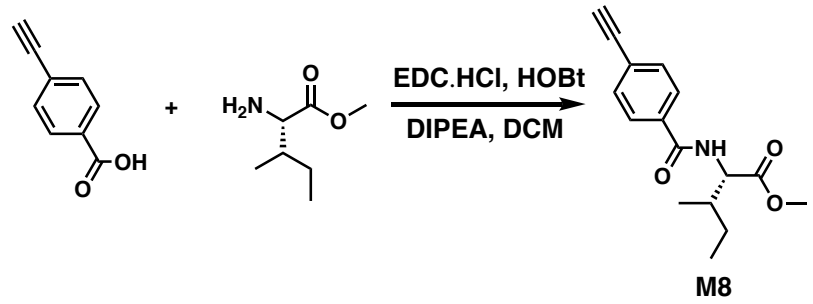

M8

1-Ethyl-3-(3-dimethylaminopropyl)carbodiimide (EDC, 1.350 g, 1.2 equiv.), hydroxybenzotriazole (HOBt, 1.400 g, 1.2 equiv), 4-ethynylbenzoic acid (1.700 g, 1.2 equiv) and diisopropyltriethylamine (DIPEA, 0.71 mL, 1.4 equiv) were dissolved in 70 mL of CH_2Cl_2, and the mixture was stirred for 15 min to activate the acid. Then, (*L*)-isoleucine methyl ester (1.151 g, 1.0 equiv) was added and the reaction mixture was stirred overnight. The organic layer was washed with HCl 1M, saturated solution of $NaHCO_3$ and brine. The combined organic layers were dried over anhyd. Na_2SO_4, filtered and the solvent was evaporated at reduced pressure. The crude product was chromatographed on silica gel (70-230 mesh) with hexane/ethyl acetate (7/3) as eluent, 72% of pure product

Spectroscopic data:

^{1}H NMR (300 MHz, $CDCl_3$) δ (ppm): 0.87 (d, 6H), 1.18 (m, 2H), 1.44 (m, 1H), 1.92 (m, 1H), 3.18 (s, 1H), 3.67 (s, 3H), 4.68 (t, 1H), 6.91 (d, 1H), 7.40 (d, 2H), 7.66 (d, 2H).

^{13}C NMR (75 MHz, $CDCl_3$) δ (ppm): 11.3, 15.3, 25.2, 37.8, 51.9, 56.8, 79.6, 82.5, 125.3, 126.9, 131.9, 133.8, 166.2, 172.4.

$[\alpha]_D^{20}$= +74 (15 mg mL^{-1}, $CHCl_3$).

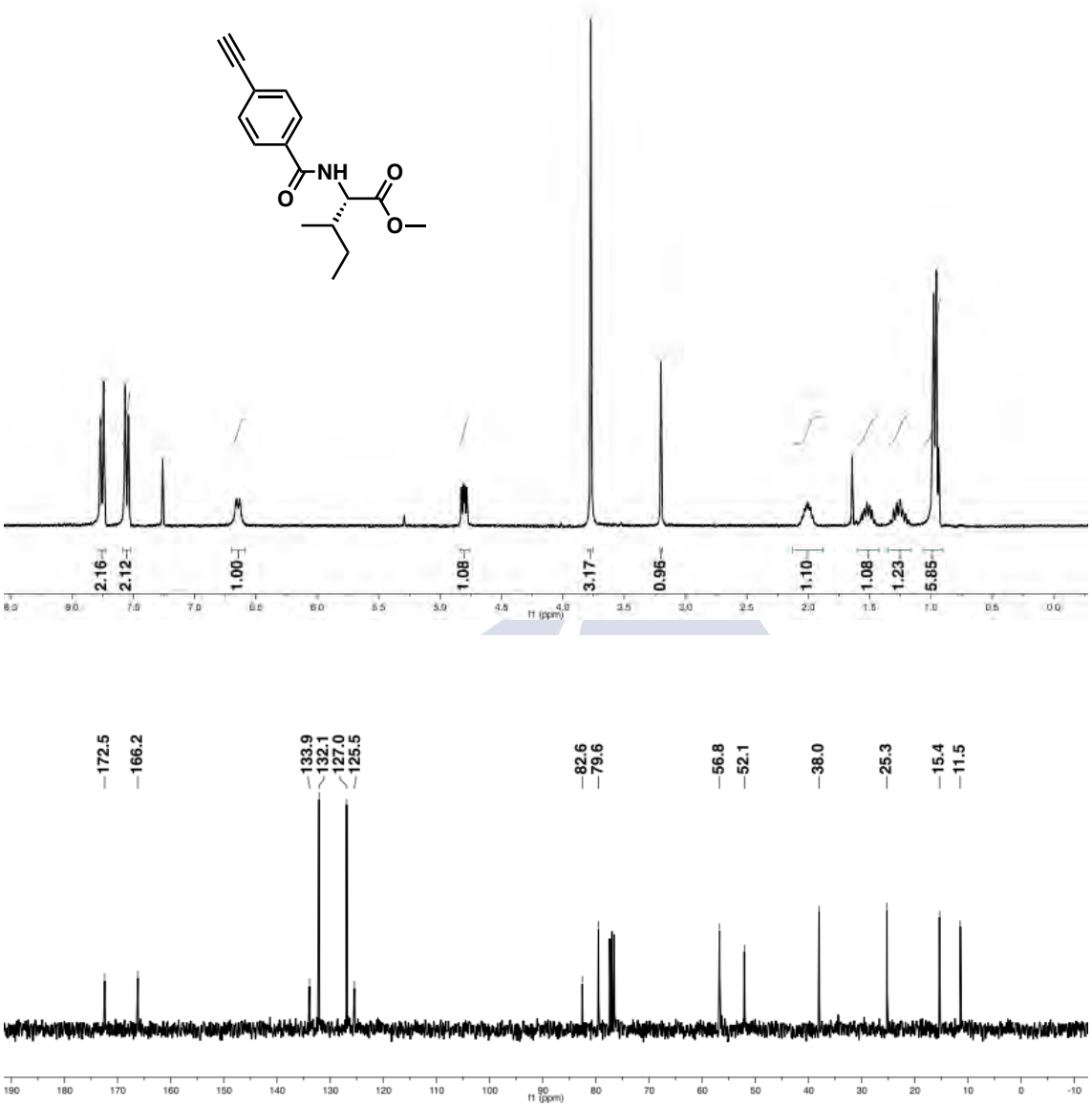

Figure S8. ^{1}H and ^{13}C NMR for M**8**.

.

3.4 Synthesis of monomer M9

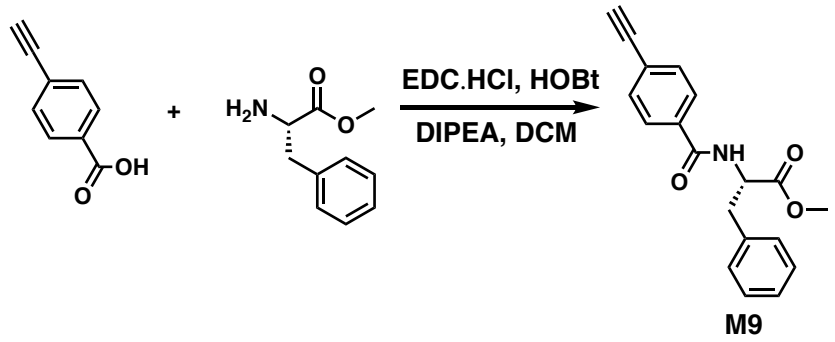

M9

1-Ethyl-3-(3-dimethylaminopropyl)carbodiimide (EDC, 0.656 g, 1.2 equiv.), hydroxybenzotriazole (HOBt, 0.465 g, 1.2 equiv), 4- ethynylbenzoic acid (1.7 g, 1.2 equiv) and diisopropyltriethylamine (DIPEA, 0.5 mL, 1.4 equiv) were dissolved in 30 mL of CH_2Cl_2, and the mixture was stirred for 15 min to activate the acid. Then, methyl *L*-phenylalanine methyl ester (0.500 g, 1.0 equiv) was added and the reaction mixture was stirred overnight. The organic layer was washed with HCl 1M, saturated solution of $NaHCO_3$ and brine. The combined organic layers were dried over anhyd Na_2SO_4, filtered and the solvent was evaporated at reduced pressure. The crude product was chromatographed on silica gel (70-230 mesh) with hexane/ethyl acetate (7/3) as eluent, 84% of pure product.

Spectroscopic data:

^{1}H NMR (300 MHz, $CDCl_3$) δ (ppm): 3.22 (s, 1H), 3.31 (m, 2H), 3.81 (s, 3H), 5.13 (q, 1H), 6.76 (d, 1H), 7.22 (d, 2H), 7.31 (m, 3H), 7.57 (d, 2H), 7.71 (d, 2H).

^{13}C NMR (75 MHz, $CDCl_3$) δ (ppm): 37.8, 52.4, 53.5, 79.5, 82.7, 125.6, 127.0, 128.7, 129.2, 129.4, 132.3, 133.8, 135.8, 166.0, 172.0.

$[\alpha]_D^{20}$= +50 (15 mg mL^{-1}, $CHCl_3$).

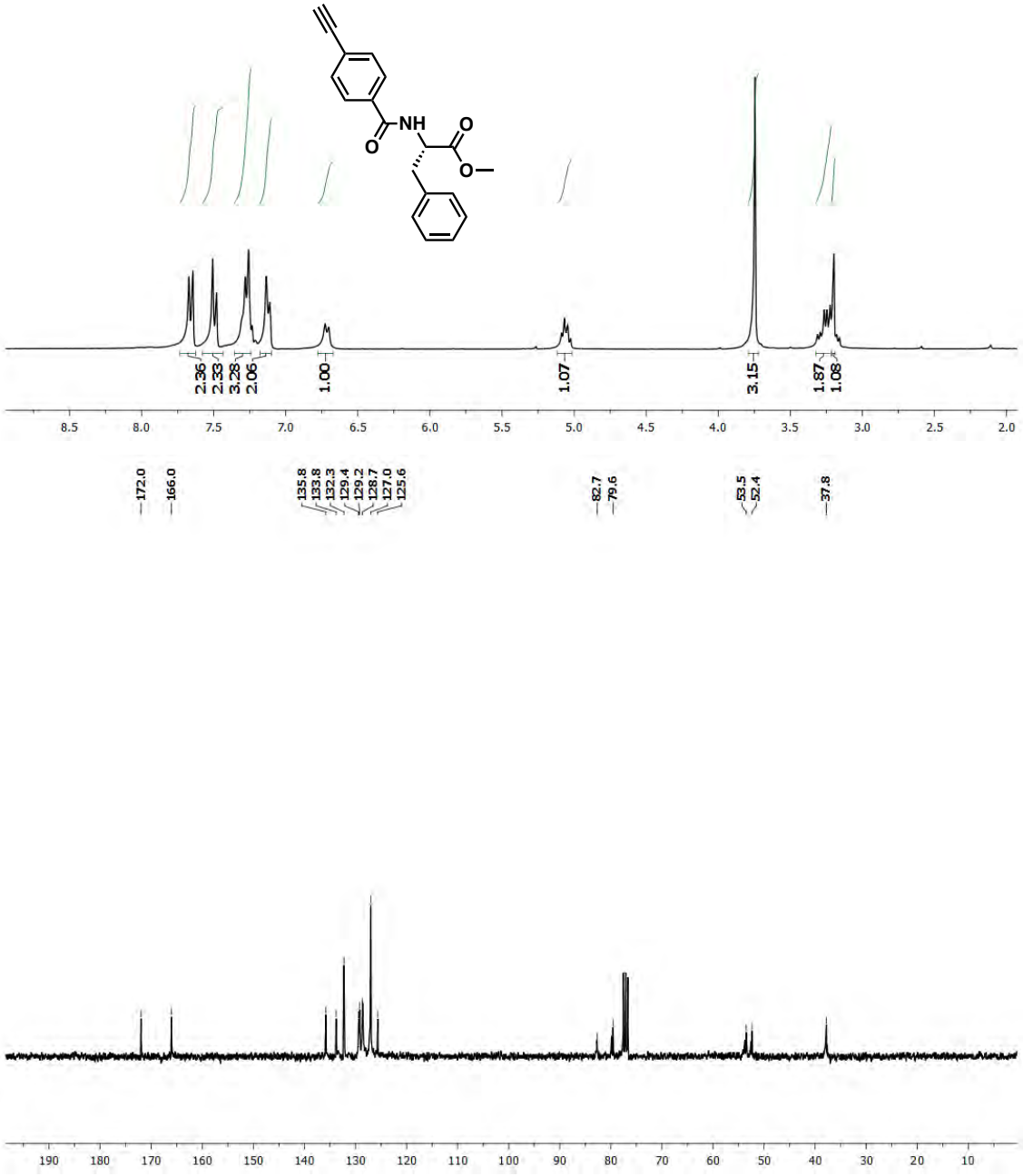

Figure S9. ^{1}H and ^{13}C NMR for M**9**

3. Synthesis of polymers

The general procedure to obtain the polymer can be found in the reference [S2].

The polymers were synthesized in a reaction flask (sealed ampoule) that was dried under vacuum and flushed with argon for three times before monomers were added as a solid. Then, the flask was evacuated on a vacuum line and flushed with dry argon (three times). Dry THF was added with a syringe and then, Et_3N dropwise. A solution of rhodium norbornadiene chloride dimer, $[Rh(nbd)Cl]_2$, in THF was added at 30 ºC. The reaction mixture was stirred at 30 ºC for 24 h. Next, the resulting polymers were diluted in CH_2Cl_2 and they were precipitated in a large amount of diethyl ether, centrifuged (twice) and re-precipitated in hexane and centrifuged again.

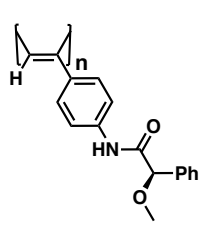

poly-(*R*)-1

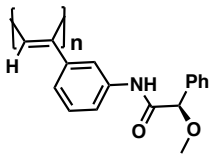

poly-(*R*)-2

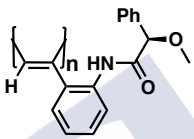

poly-(*R*)-3

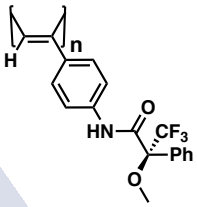

poly-(*R*)-4

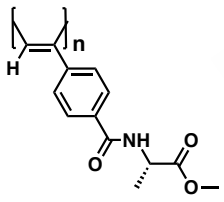

poly-(*L*)-5

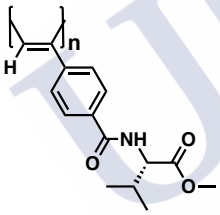

poly-(*L*)-6

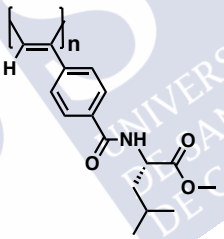

poly-(*L*)-7

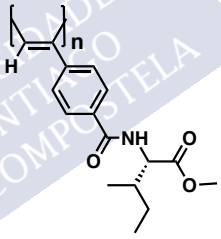

poly-(*L*)-8

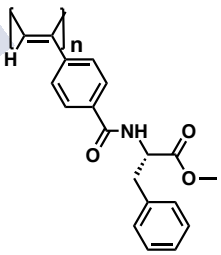

poly-(*L*)-9

Table S1.

Monomer	Mass /mg	THF / mL	Et_3N / mL	Catalyst/ mg	Yield %
Poly-(*R*)-**1**	100	1000	5	2	92
Poly-(*R*)-**2**	100	1000	5	2	88
Poly-(*R*)-**3**	100	1000	5	2	75
Poly-(*R*)-**4**	100	1000	5	2	95
Poly-(*L*)-**5**	100	1000	5	2	82
Poly-(*L*)-**6**	100	1000	5	2	89
Poly-(*L*)-**7**	100	1000	5	2	90
Poly-(*L*)-**8**	100	1000	5	2	98
Poly-(*L*)-**9**	100	1000	5	2	93

Table S2. GPC studies

Monomer	M_n	M_w	M_p	M_z	PDI
Poly-(*R*)-**1**	65563	150744	150264	273851	2.29
Poly-(*R*)-**2**	84737	178058	182446	342353	2.10
Poly-(*R*)-**3**	64843	151505	138784	328120	2.33
Poly-(*R*)-**4**	7339	10750	10731	14105	1.40
Poly-(*L*)-**5**	20823	54320	84477	106053	1.95
Poly-(*L*)-**6**	45297	170013	172184	374847	2.20
Poly-(*L*)-**7**	30902	247118	449082	588863	2.38
Poly-(*L*)-**8**	45377	129203	162848	261554	2.02
Poly-(*L*)-**9**	22000	120000	170000	340000	3.44

5. ^{1}H NMR of PPAs

The *cis* stereoregularity of the copolymers was determined by ^{1}H NMR spectroscopy where the vinyl proton resonates at 5.8 ppm.

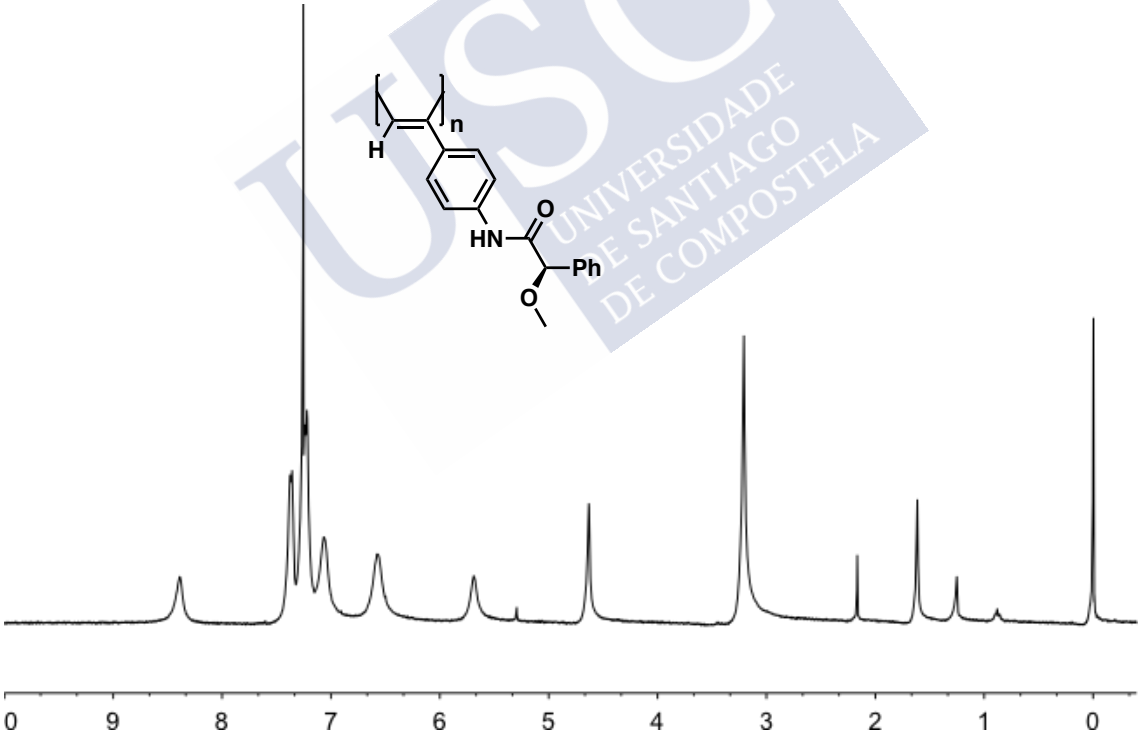

Figure S10: ^{1}H NMR for poly-(*R*)-**1** in $CDCl_3$.

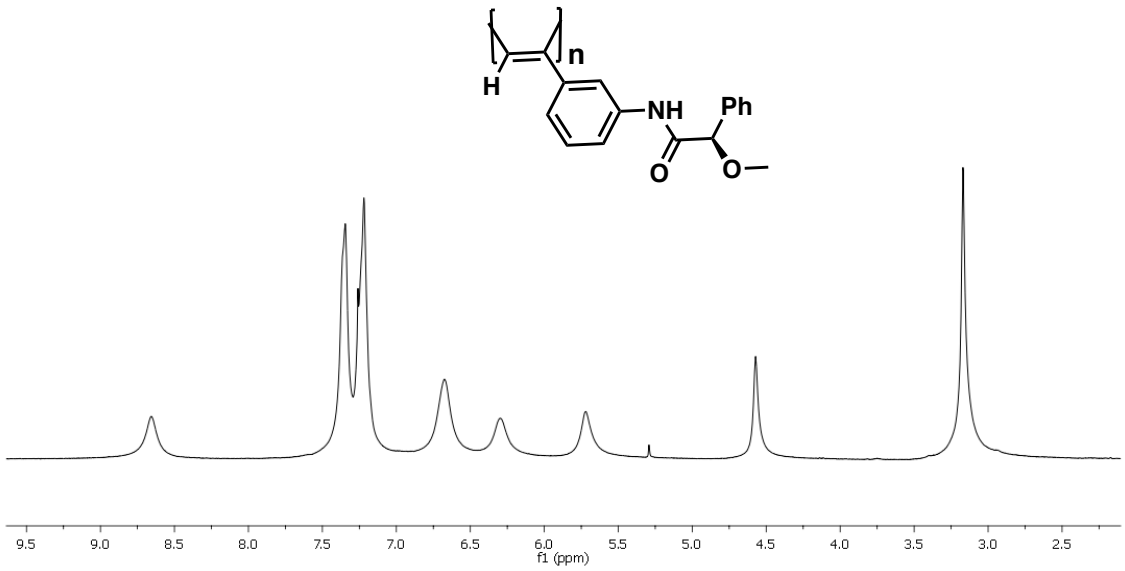

Figure S11. ^{1}H NMR for poly-(*R*)-**2** in $CDCl_3$.

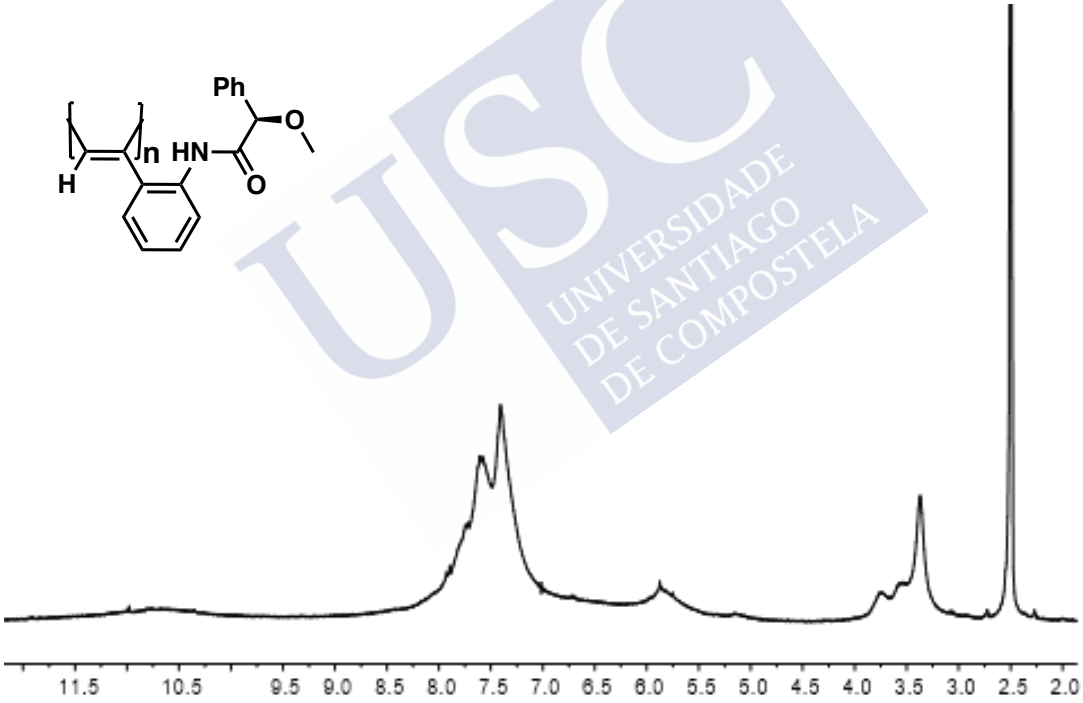

Figure S12. ^{1}H NMR for poly-(*R*)-**3** in $CDCl_3$.

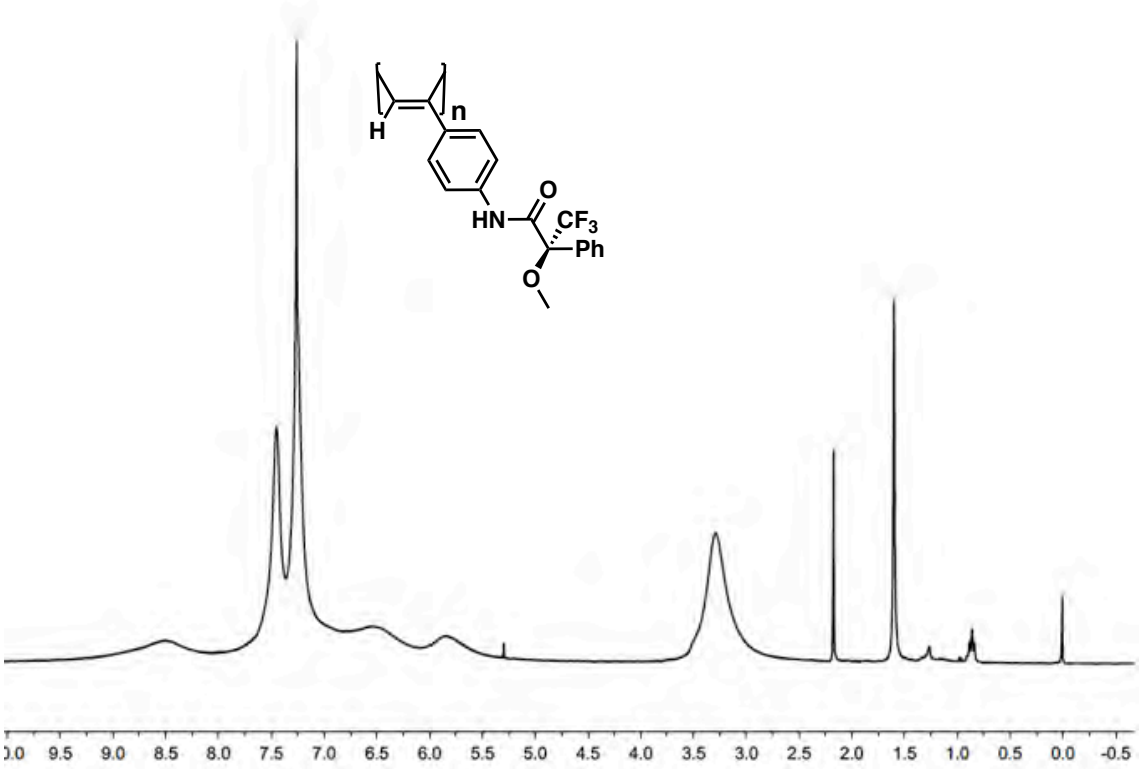

Figure S13. ^{1}H NMR for poly-(*R*)-**4** in $CDCl_3$.

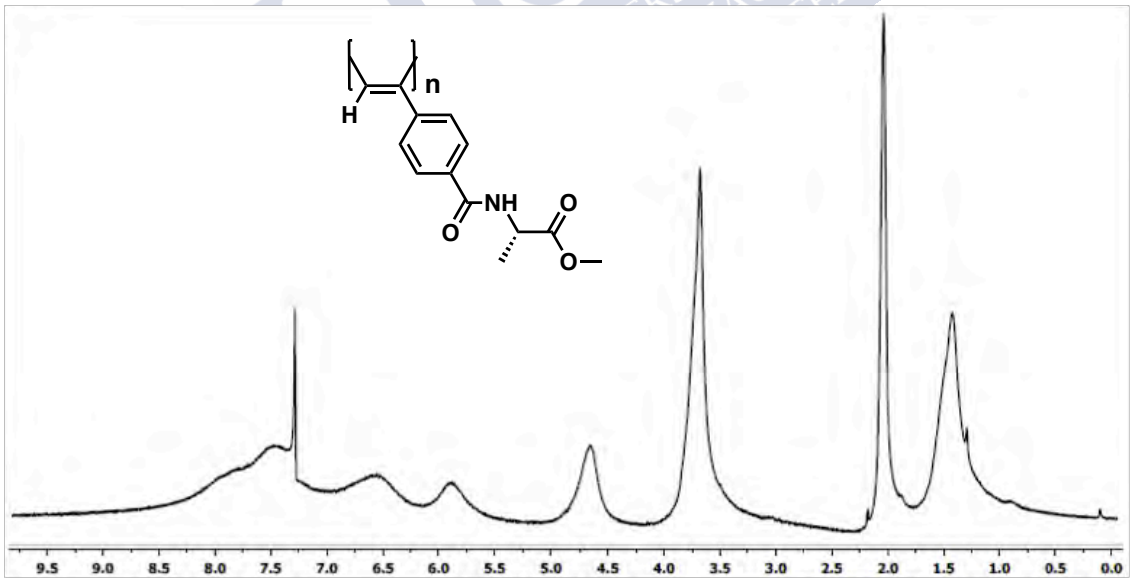

Figure S14. ^{1}H NMR for poly-(*L*)-**5** in $CDCl_3$.

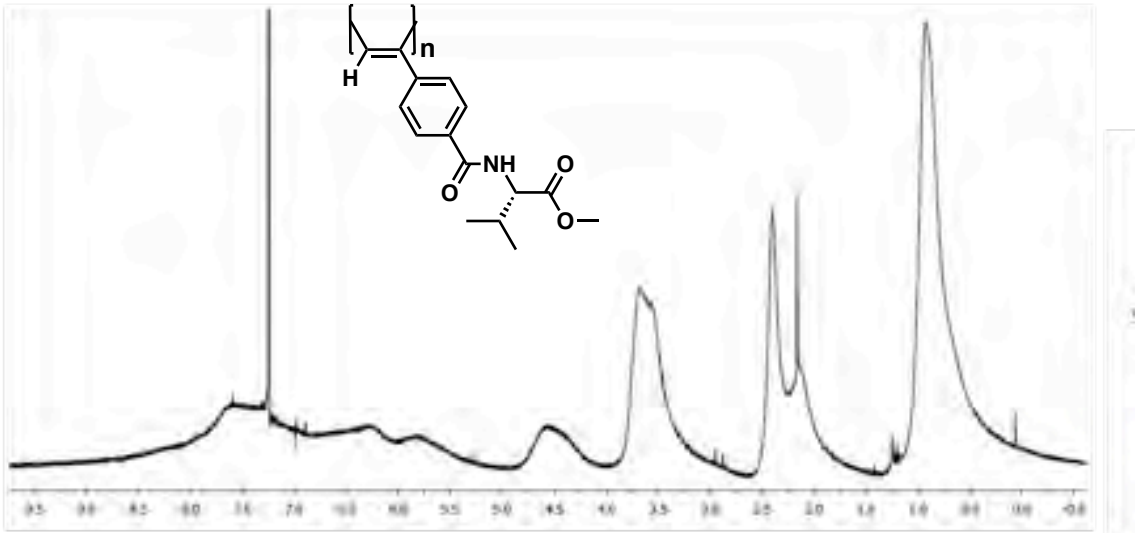

Figure S15. ^{1}H NMR for poly-**5** in $CDCl_3$.

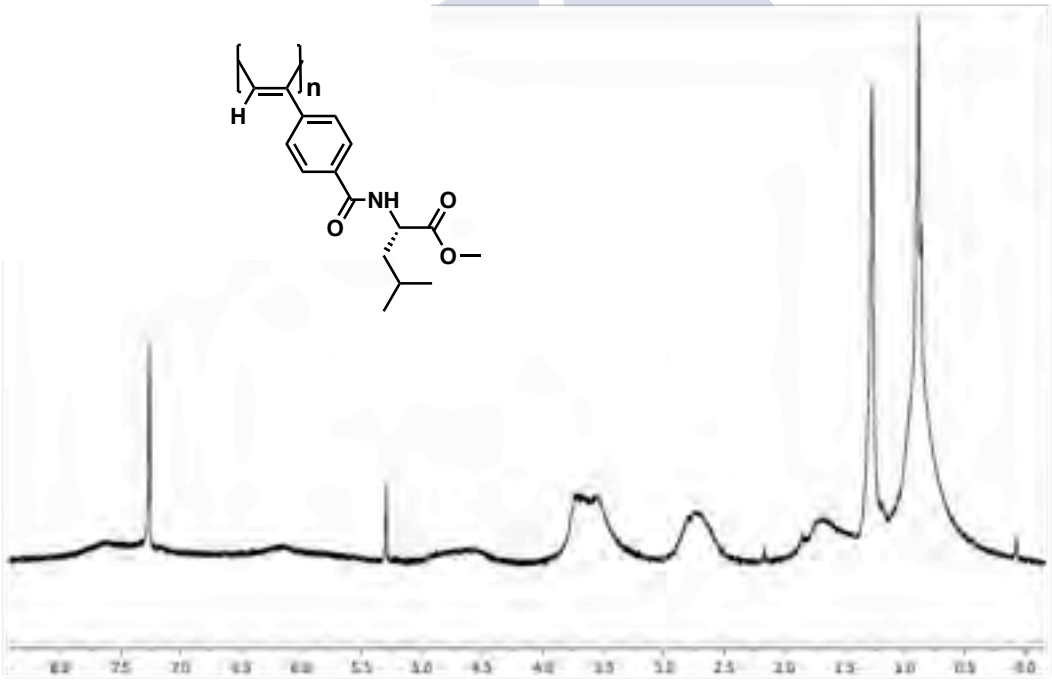

Figure S16. ^{1}H NMR for poly-**6** in $CDCl_3$.

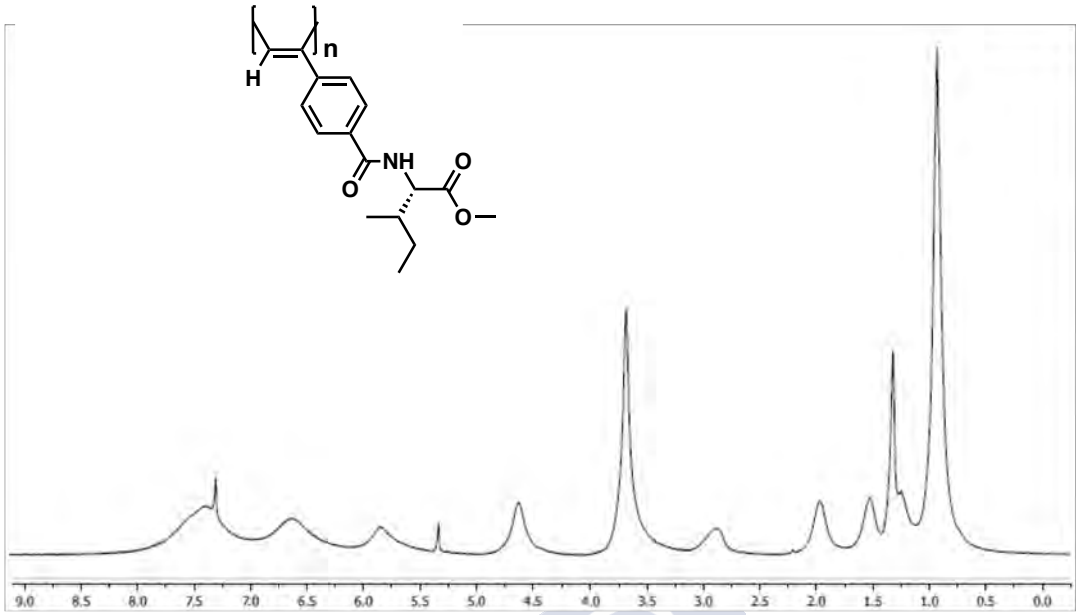

Figure S17. ^{1}H NMR for poly-(L)-**7** in $CDCl_3$.

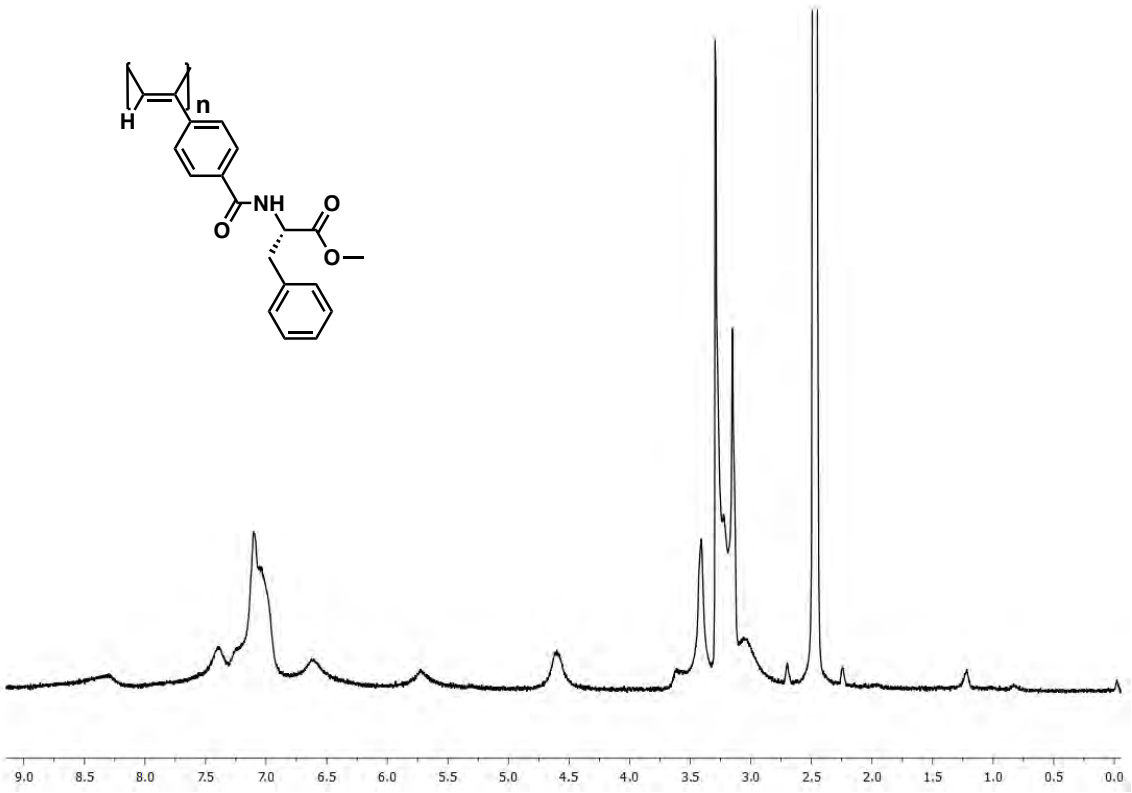

Figure S18: ^{1}H NMR for poly-(*L*)-**9** in dmso-d_8.

6. Raman studies

The *cis* stereoregularity of the copolymers was determined by Raman resonances. The peak around 1585 cm^{-1} is assigned to C=C bond stretching in the *cis* poly(acetylene) and overlaps with that of the phenyl ring. The peak around 1340 cm^{-1} is assigned to the *cis* C-C bond coupled with the single bond connecting the main chain and the phenyl ring. The peak around 970 cm^{-1} is assigned to the C-H bond deformation of the *cis* form.

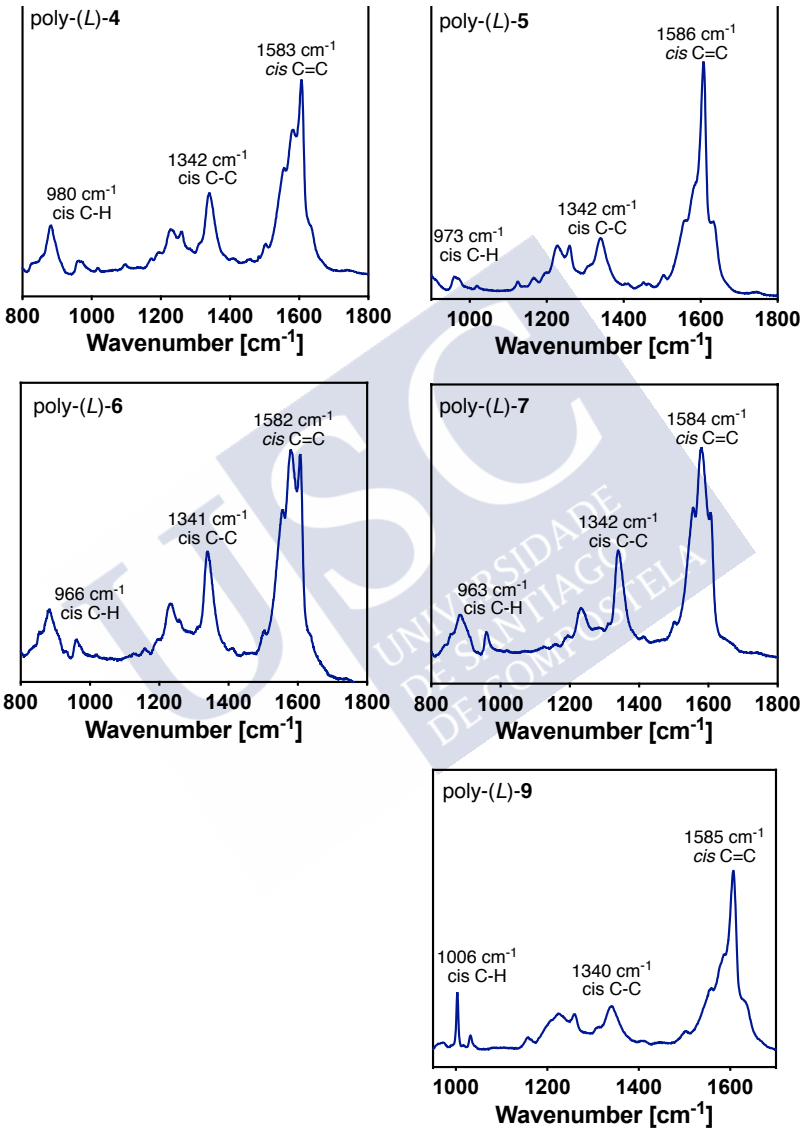

Figure S19. Raman studies of PPAs.

7. Thermal studies of PPAs

- **DSC studies**

DSC studies were carried out in order to determine de geometry of the polymer backbone. As a general protocol, a polymer sample was kept in an aluminum pan and heated from 40 ^{o}C to 350 ^{o}C with a heating rate of 10 ^{o}C min^{-1}. The thermograms of the polymers show typical traces for a *cis-trans* backbone, where two exothermal peaks corresponding to the *c-t* to *c-c* and the *c-c* to *t-t* were observed.

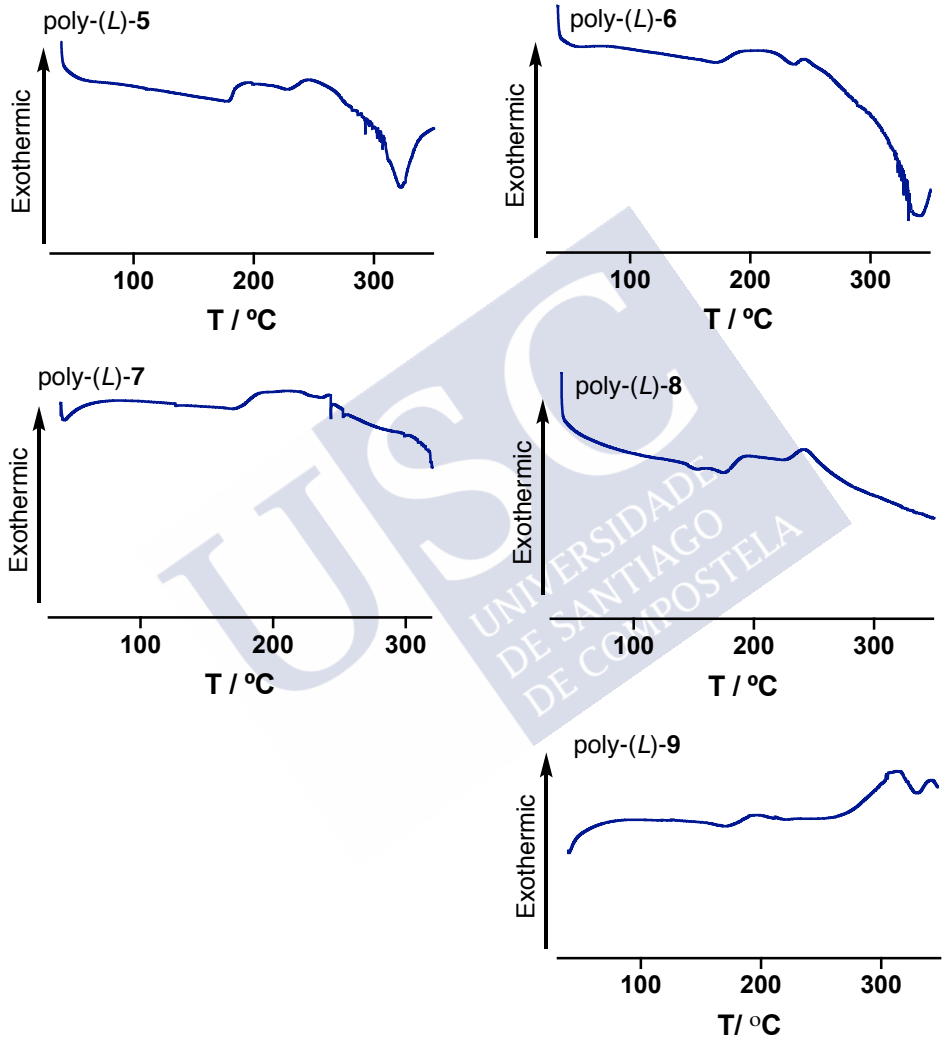

Figure S21. DSC thermograms of PPAs.

- **TGA studies**

TGA Studies were carried out in order to determine the thermal stability of the copolymers. As a general protocol, a polymer sample was kept in a platinum pan and heated from 40 to 850 ^{o}C with a heating rate if 10 ^{o}C min^{-1}.

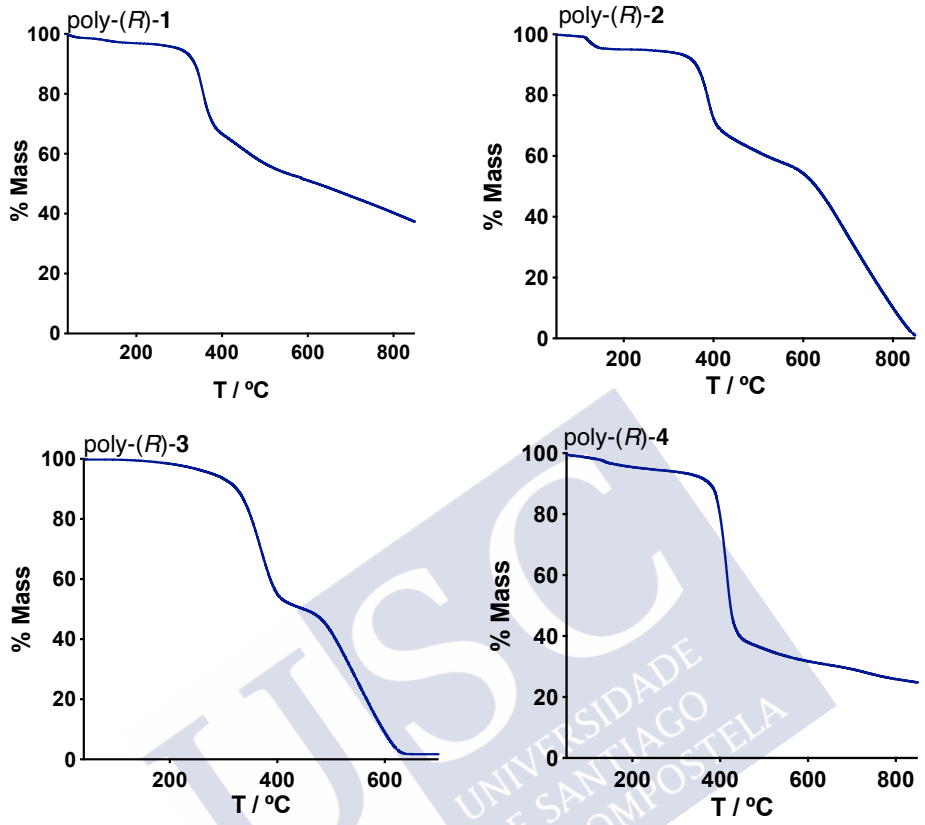

Figure S22. TGA thermograms of poly-(*R*)-**1**, poly-(*R*)-**2**, poly-(*R*)-**3** and poly-(*R*)-**4**.

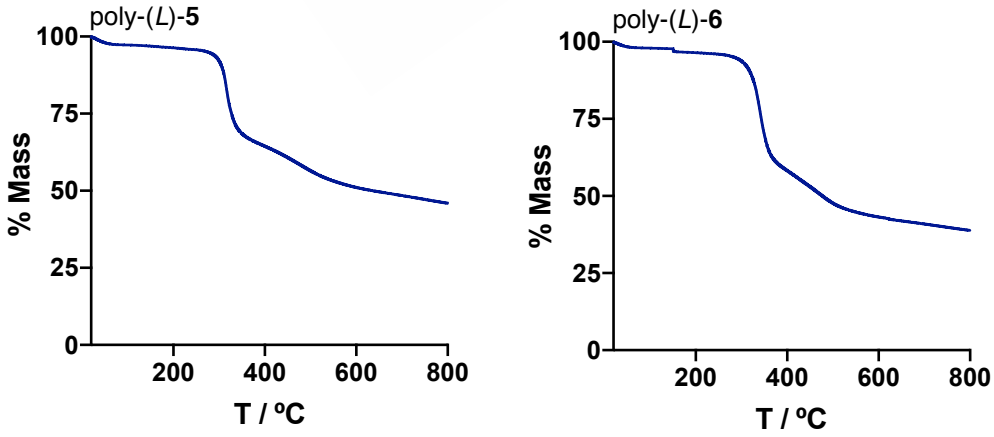

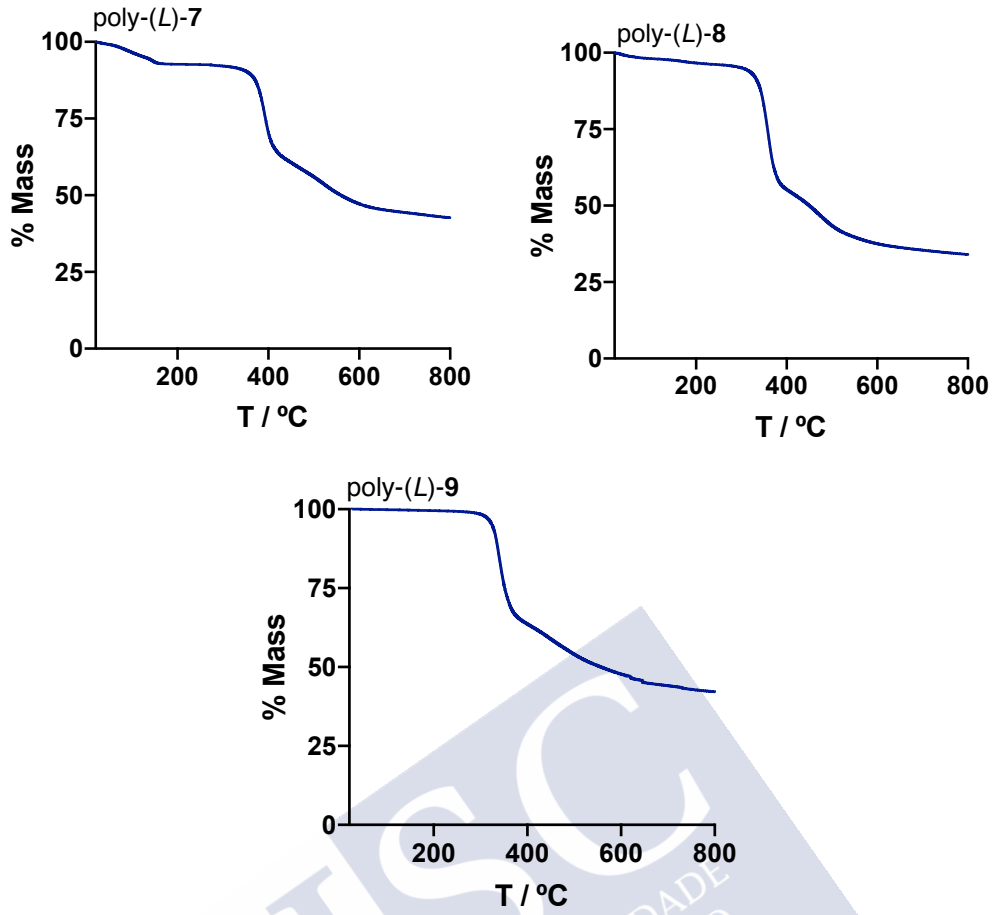

Figure S23. TGA thermograms of poly-(*L*)-**5**, poly-(*L*)-**6**, poly-(*L*)-**7**, poly-(*L*)-**8** and poly-(*L*)-**9**.

5. CD studies

5.1 CD studies in high polar and low polar solvents

The different responses of poly-(*R*)-**1**, poly-(*R*)-**2**, poly-(*R*)-**3**, poly-(*R*)-**4,** poly-(*L*)-**5**, poly-(*L*)-**6**, poly-(*L*)-**7**, poly-(*L*)-**8** and poly-(*L*)-**9** to a range of external stimuli such as solvents with different donor/acceptor/polarity characteristics were tested.

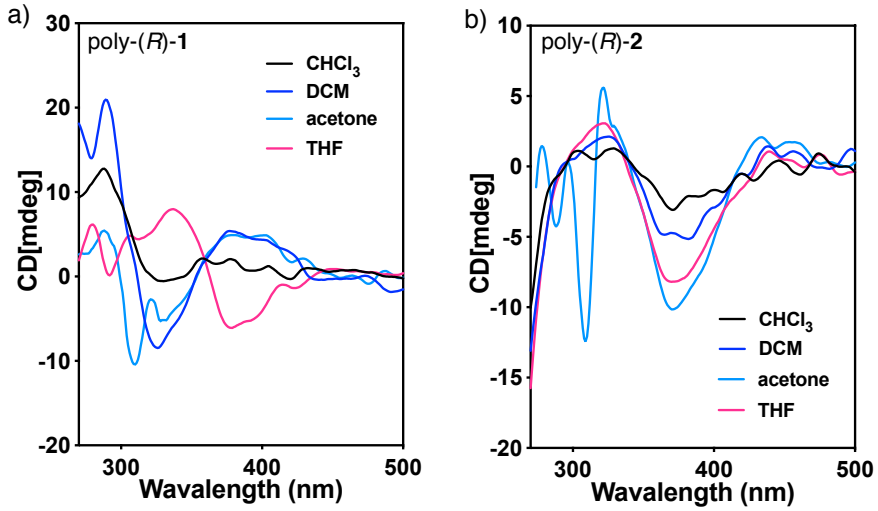

Figure S24. CD studies for poly-(*R*)-**1** and poly-(*R*)-**2** in different solvents.

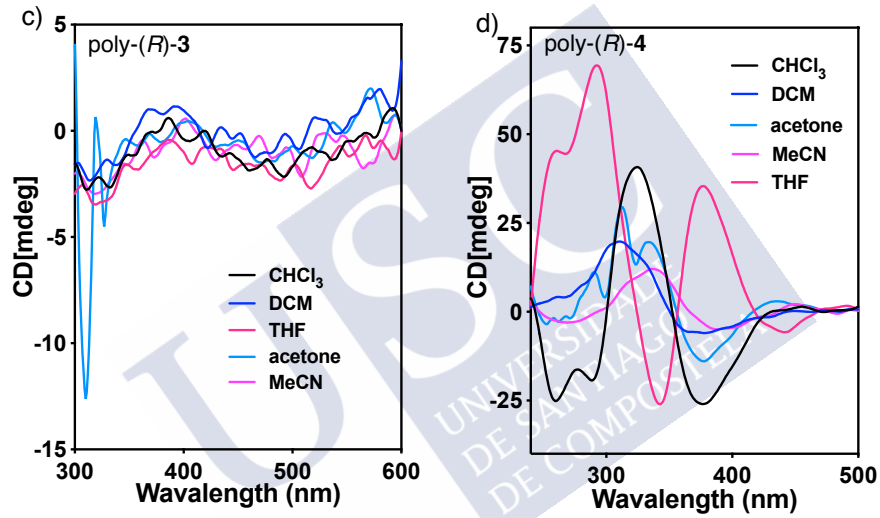

Figure S25. CD studies for poly-(*R*)-**3** and poly-(*R*)-**4** in different solvents.

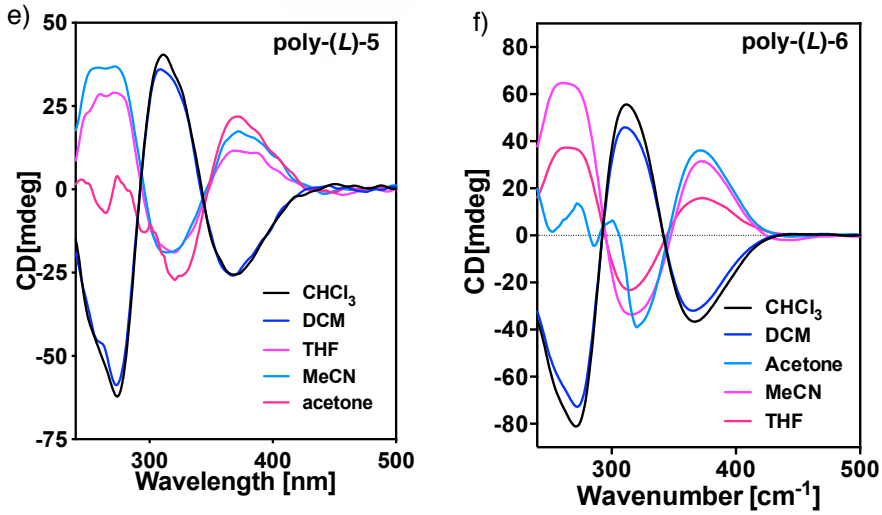

Figure S26. CD studies for poly-(*L*)-**5** and poly-(*L*)-**6** in different solvents.

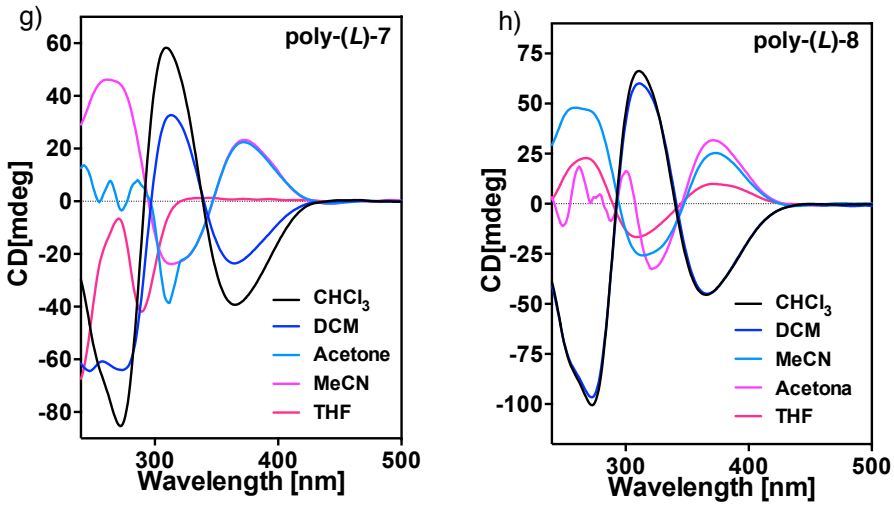

Figure S27. CD studies for poly-(*L*)-**7** and poly-(*L*)-**8** in different solvents.

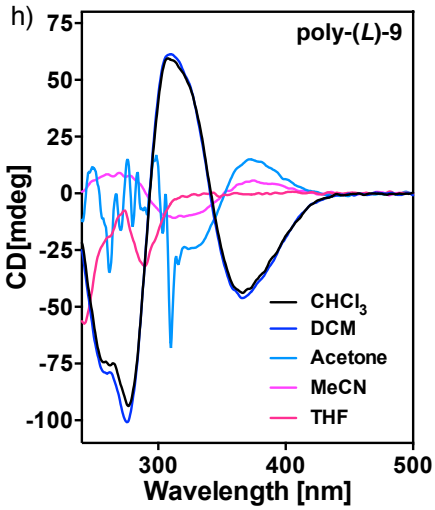

Figure S28. CD studies for poly-(*L*)-**9** in different solvents.

5.1 Acetone/water system

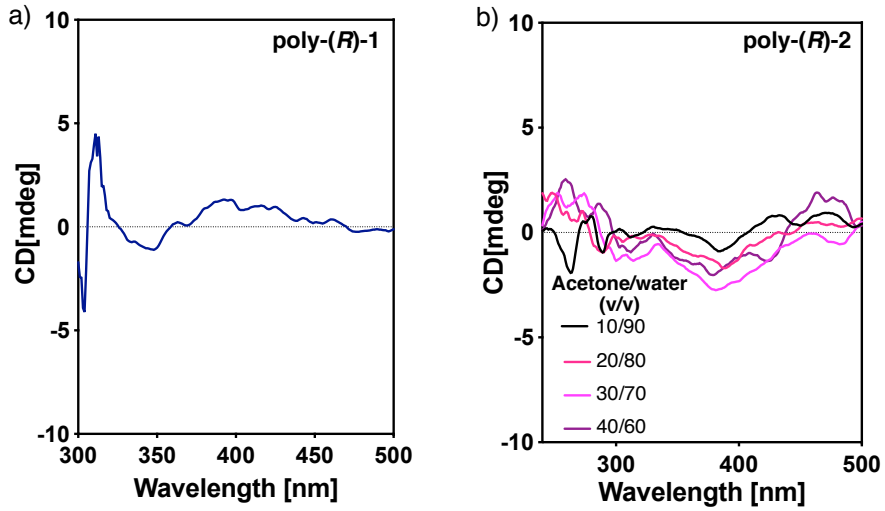

Figure S29. CD studies of poly-(*R*)-**1** and poly-(*R*)-**2** in acetone/ water mixtures-

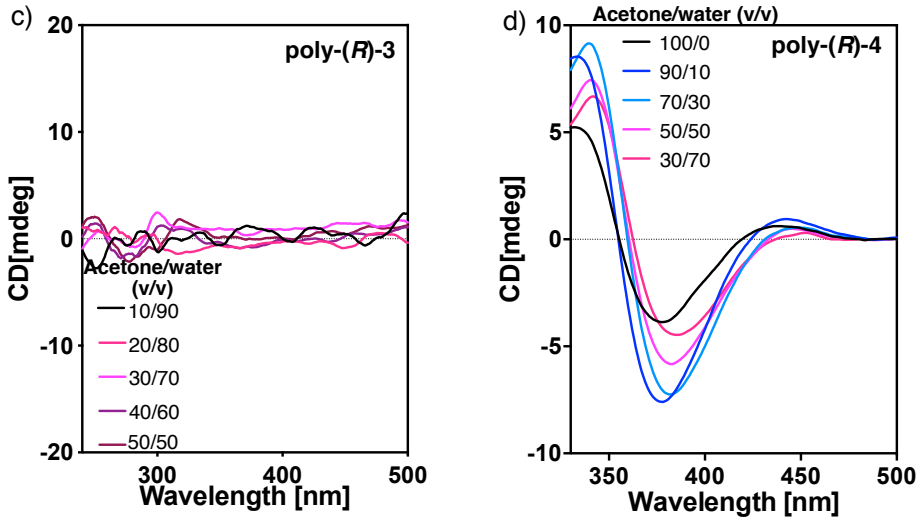

Figure S30. CD studies of poly-(*R*)-**3** and poly-(*R*)-**4** in acetone/H_2O mixtures.

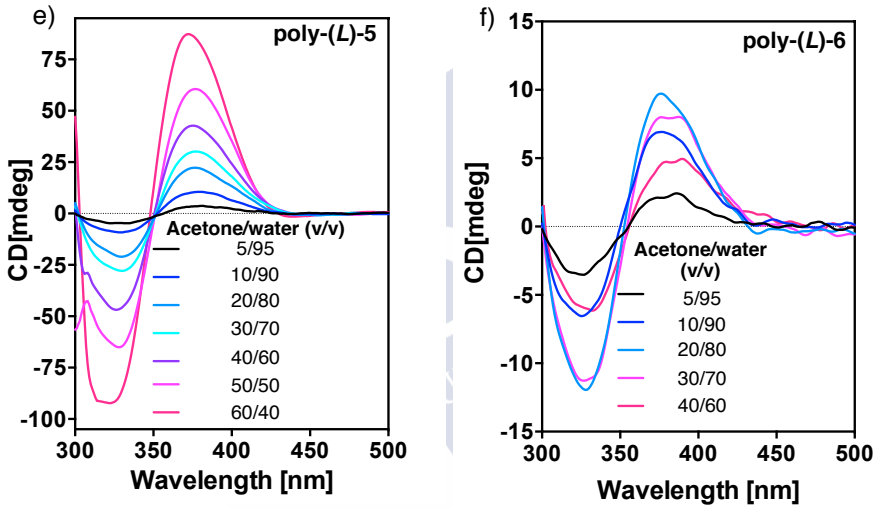

Figure S31. CD studies of poly-(*L*)-**5** and poly-(*L*)-**6** in acetone/H_2O mixtures.

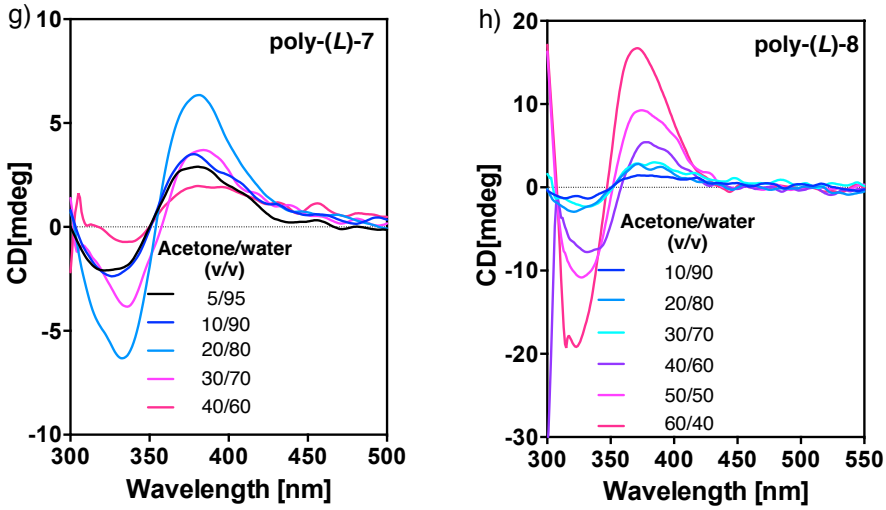

Figure S32. CD studies of poly-(*L*)-**7** and poly-(*L*)-**8** in acetone/H_2O mixtures.

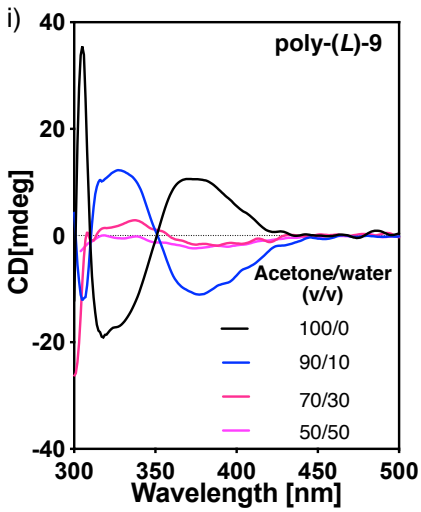

Figure S33. CD studies of poly-(*L*)-**9** in acetone/water mixtures.

5.2 THF/water system

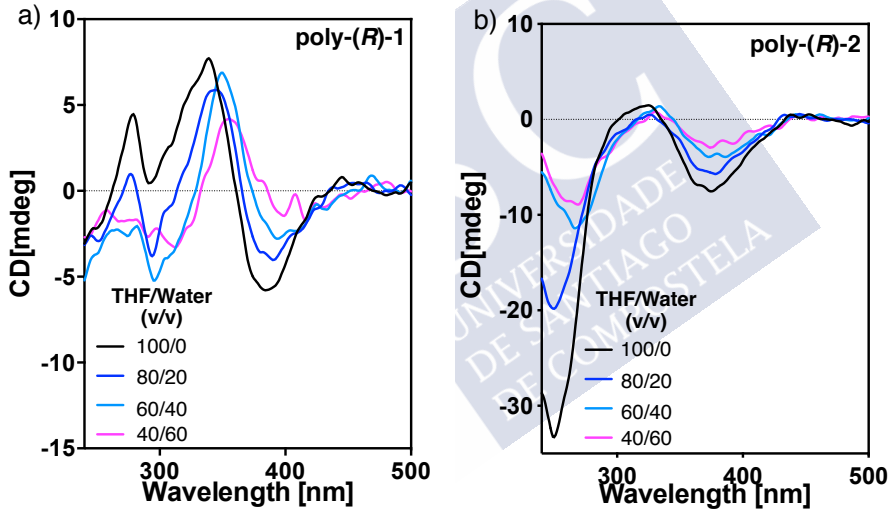

Figure S34.CD studies of poly-(*R*)-**1** and poly-(*R*)-**2** in THF/H_2O mixtures.

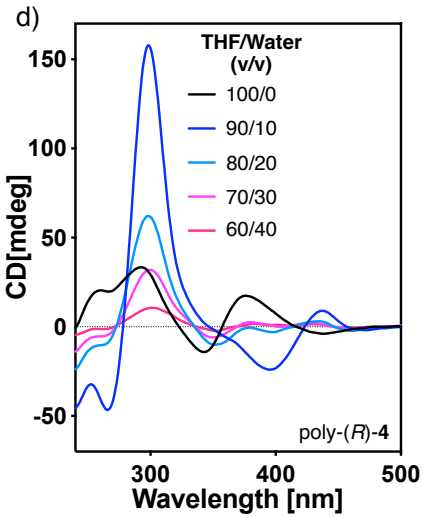

Figure S35. CD studies of poly-(*R*)-**1** and poly-(*R*)-**2** in THF/H_2O mixtures.

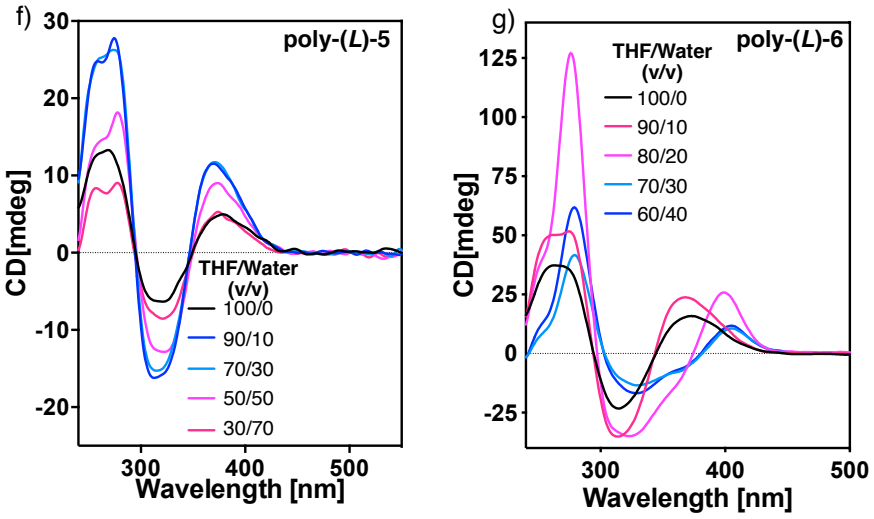

Figure S36. CD and UV-Vis studies for poly-(*L*)-**5** and poly-(*L*)-**6** in THF/H_2O mixtures.

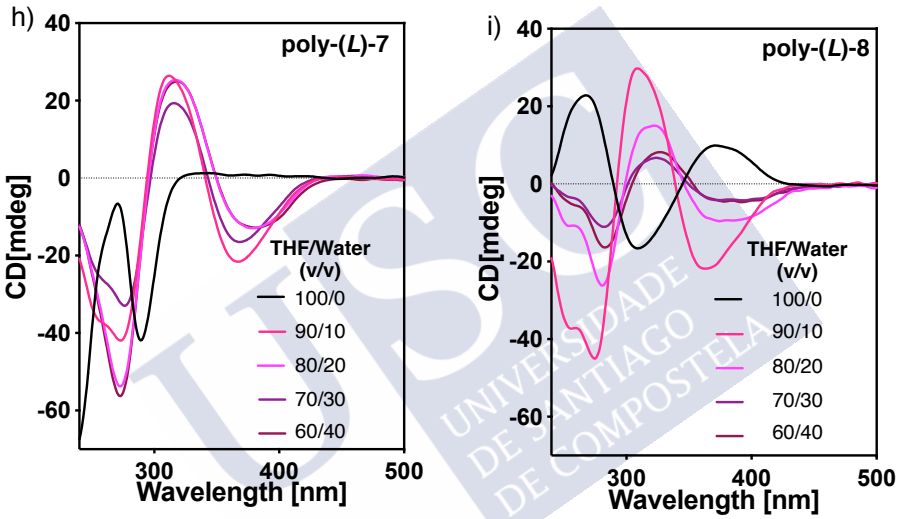

Figure S37. CD studies of poly-(*L*)-**7** and poly-(*L*)-**8** in THF/water mixtures.

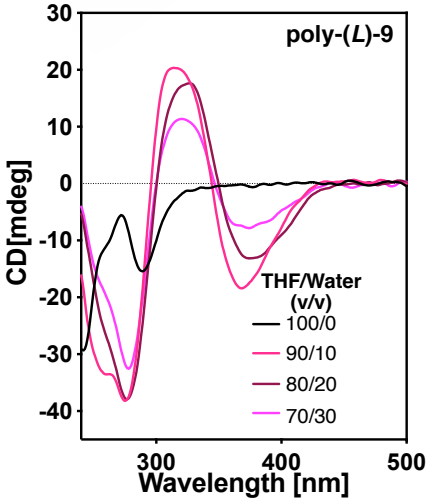

Figure S38. CD and UV studies for poly-**9** in THF/H_2O mixtures.

6. Nanostructuration studies

6.1 Acetone/H_2O mixtures

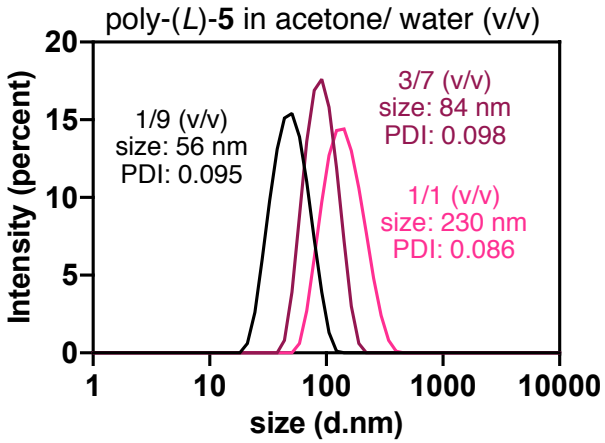

Figure S39. DLS measurements for poly-**5** in acetone/water mixtures

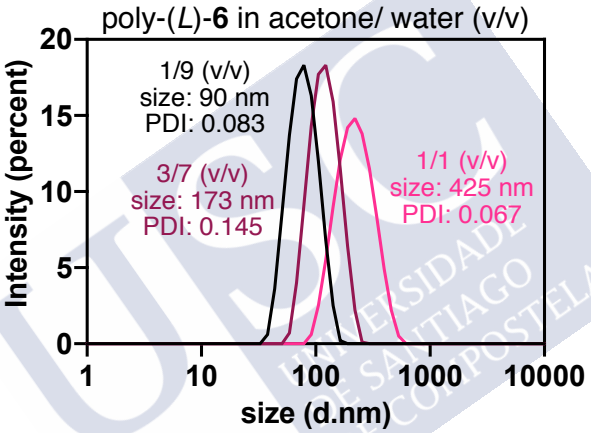

Figure S40. DLS measurements for poly-(*L*)-**6** in acetone/water mixtures.

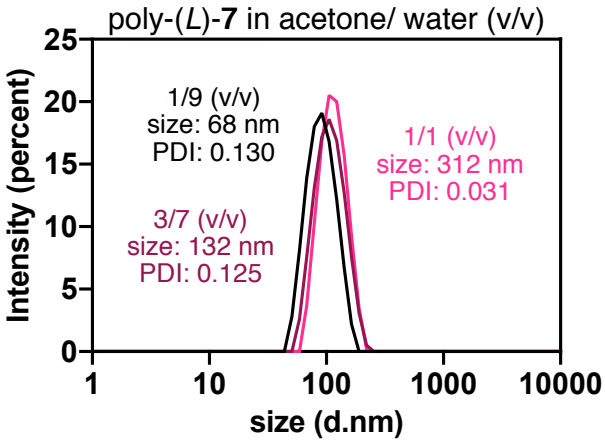

Figure S41. DLS measurements for poly-(*L*)-**7** in acetone/water mixtures.

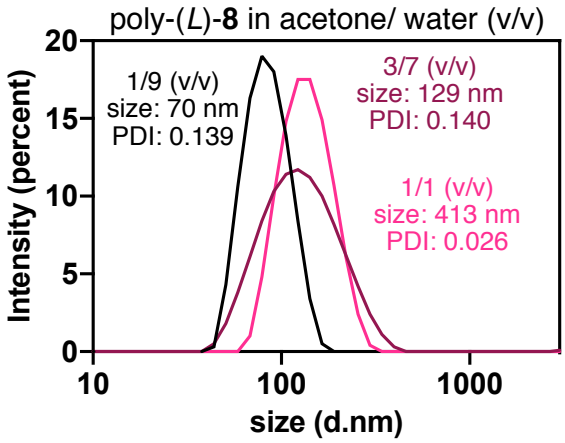

Figure S42: DLS measurements for poly-(*L*)-**8** in acetone/water mixtures.

6.2 THF/H_2O mixtures

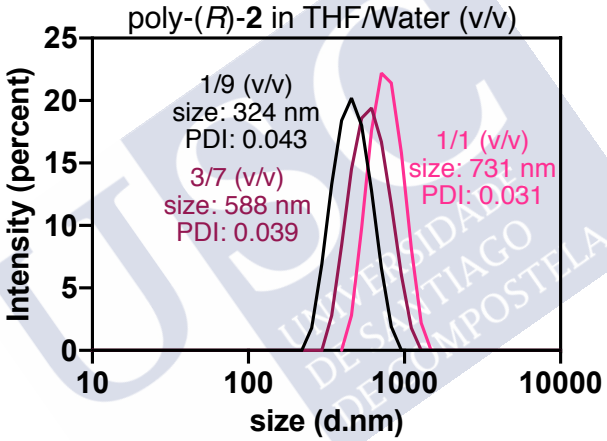

Figure S43. DLS measurements for poly-(*R*)-**2** in THF/water mixtures.

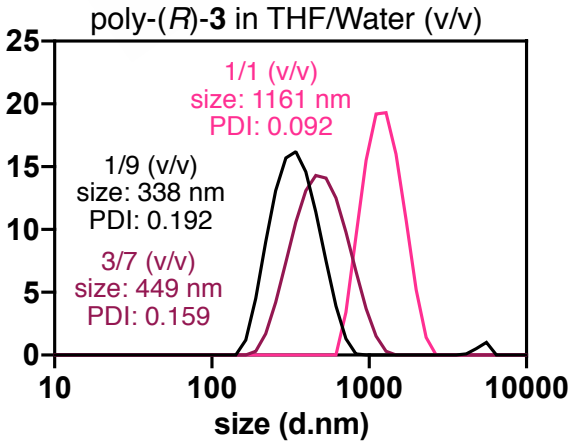

Figure S44. DLS measurements for poly-(*R*)-**3** in THF/water mixtures.

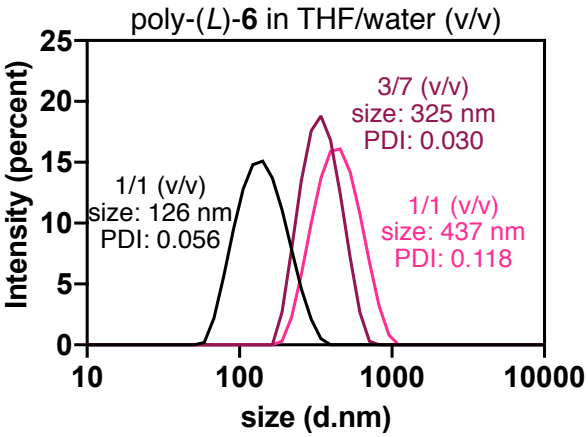

Figure S45. DLS measurements for poly-(*L*)-**6** in THF/water mixtures.

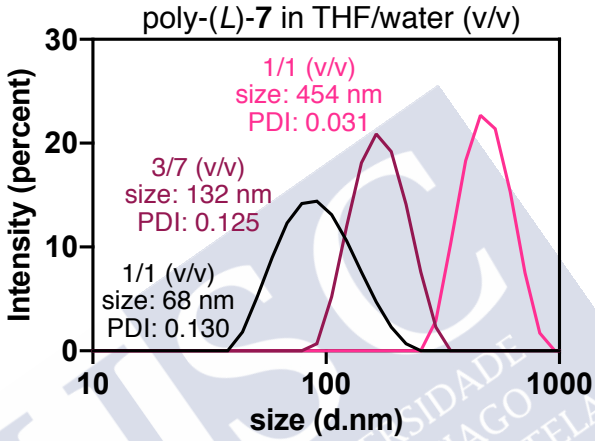

Figure S46. DLS measurements for poly-(*L*)-**7** in THF/water mixtures.

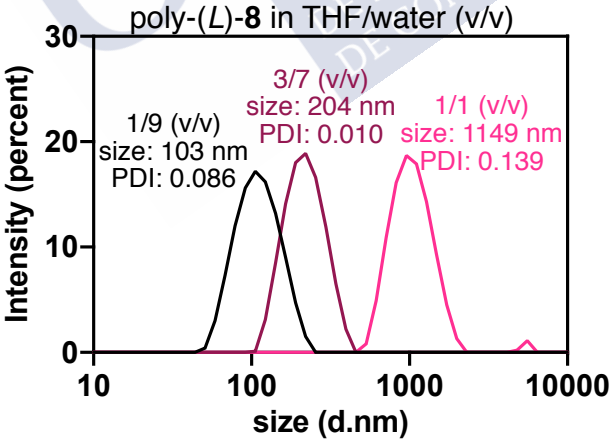

Figure S47. DLS measurements for poly-(*L*)-**8** in THF/water mixtures.

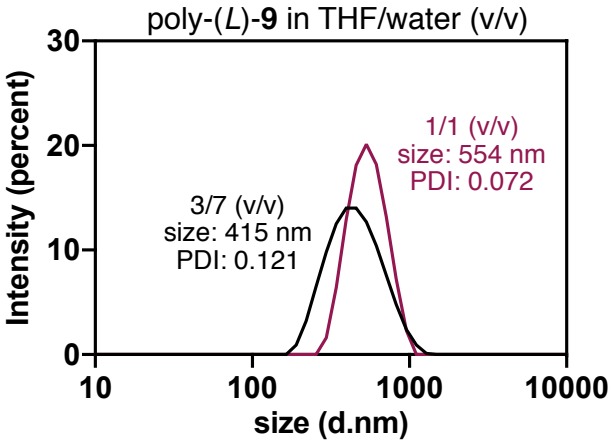

Figure S48. DLS measurements for poly-(*L*)-**9** in THF/water mixtures.

7. Microscopy studies: Acetone/water mixtures

7.1 SEM images for poly-(*R*)-1 in acetone/water mixtures

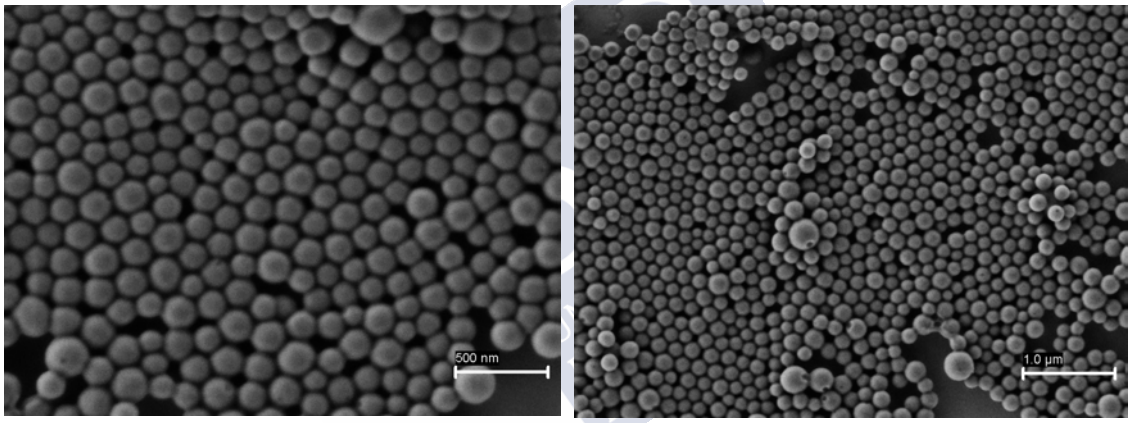

Figure S49. Nanospheres formed by poly-**1** in acetone/water .

7.2 SEM images for poly-(*R*)-2 in acetone/water mixtures

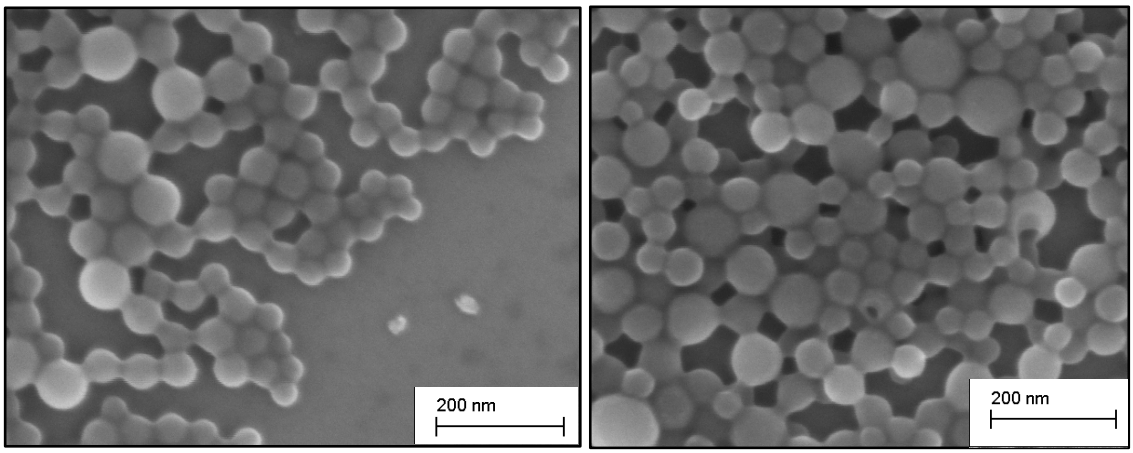

Figure S50. Nanospheres formed by poly-**2** in acetone/water (v/v).

7.3 SEM images for poly-3 in acetone/water

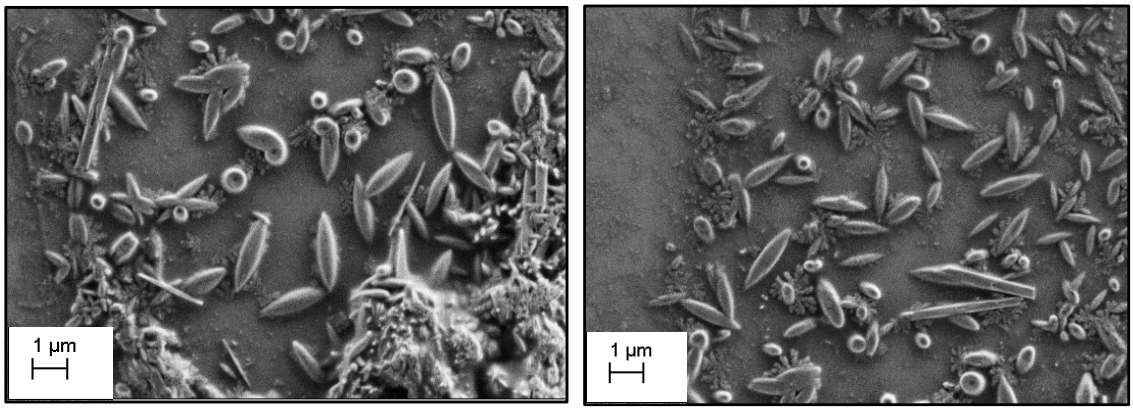

Figure S51. Nanospheres formed by poly-**3** in acetone/water (1:1 v/v).

4.4 SEM images for poly-(*R*)-4 in acetone/water mixtures

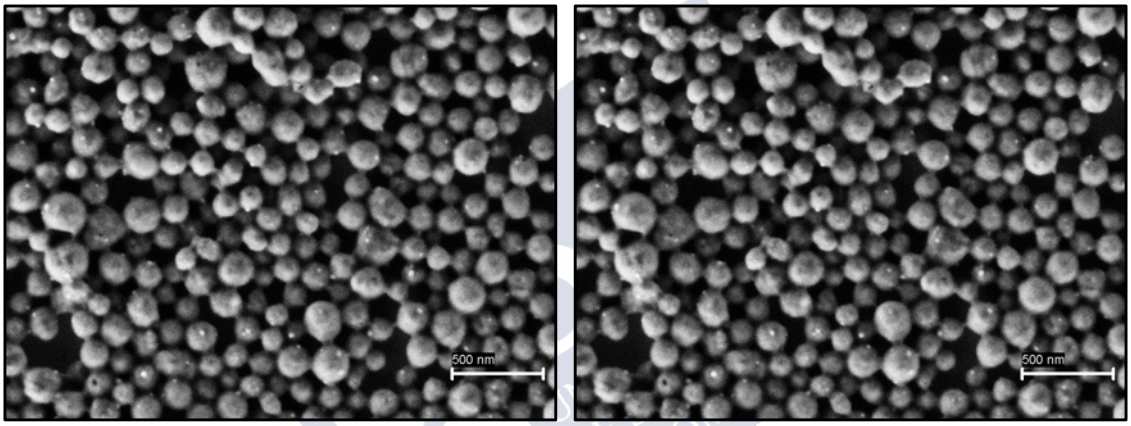

Figure S52. Nanospheres formed by poly-**4** in acetone/water.

4.5 SEM images for poly-(*L*)-5 in acetone/water mixtures

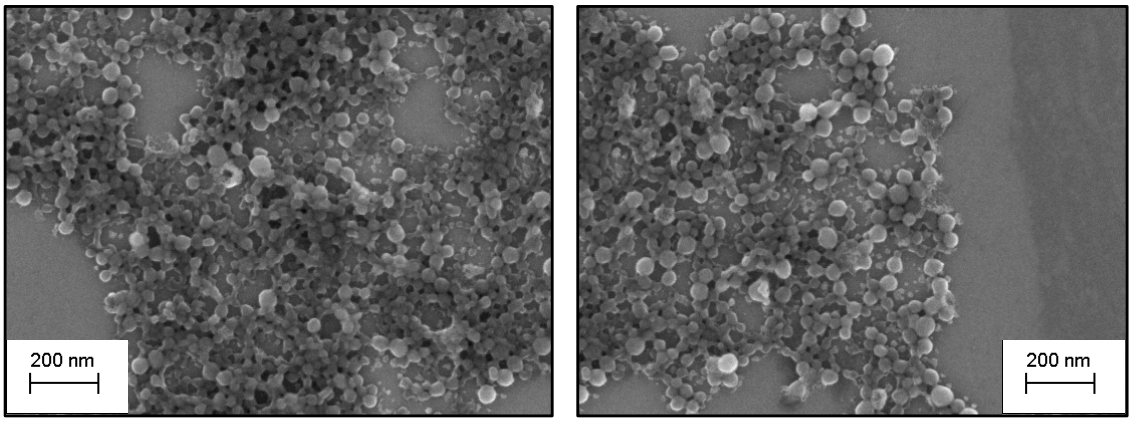

Figure S53. Nanospheres formed by poly-**5** in acetone/water.

4.6 SEM images for poly-(*L*)-6 in acetone/water mixtures

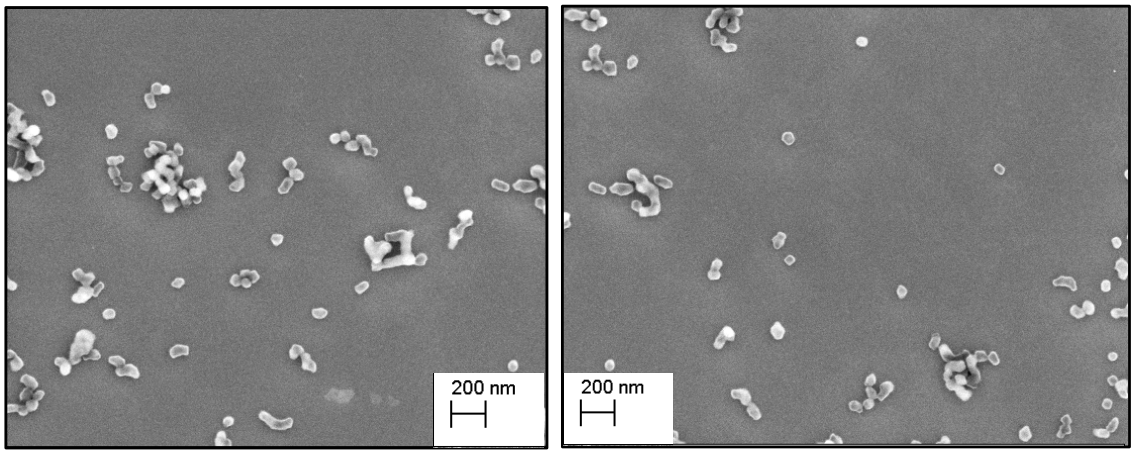

Figure S54. Nanospheres formed by poly-**6** in acetone/water.

4.7 SEM images for poly-(*L*)-7 in acetone/water mixtures

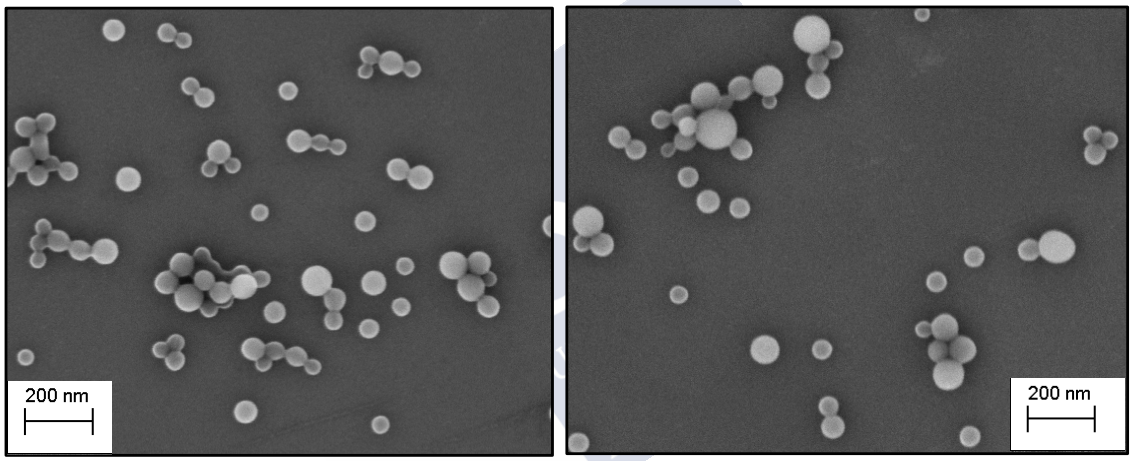

Figure S55. Nanospheres formed by poly-**7** in acetone/water.

4.8 SEM images for poly-(*L*)-8 in acetone/water mixtures

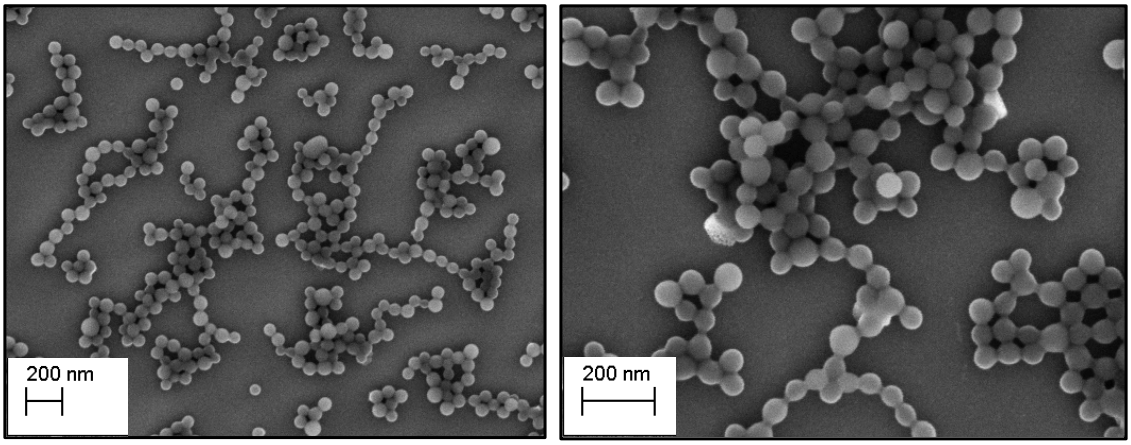

Figure S56. Nanospheres formed by poly-**8** in acetone/water.

4.9 SEM images for poly-(*L*)-8 in acetone/water mixtures

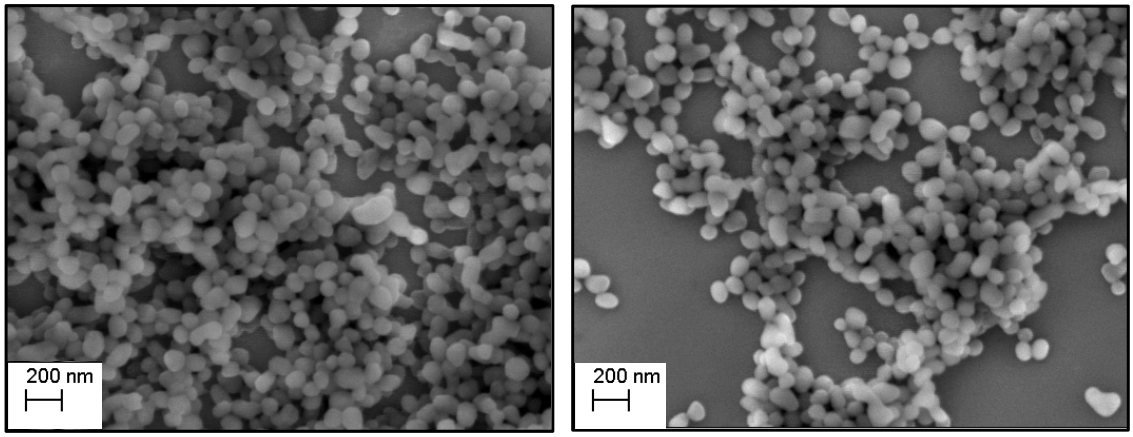

Figure S57. Nanospheres formed by poly-(*L*)-**9** in acetone/water.

8. Microscopy studies: THF/water mixtures

8.1 SEM images for poly-(*R*)-1 in THF/water mixtures

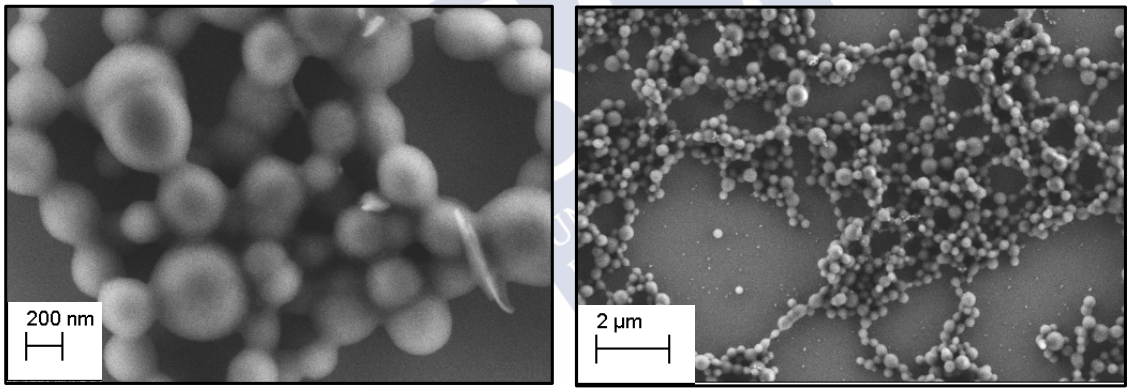

Figure S58. Nanospheres formed by poly-(*R*)-**1** in THF/water.

8.2 SEM images for poly-(*R*)-2 in THF/water mixtures

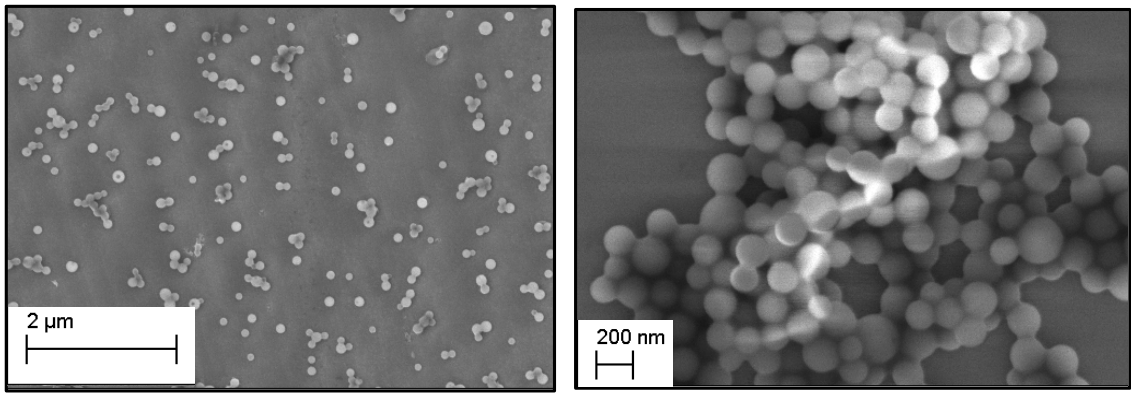

Figure S59. Nanospheres formed by poly-(*R*)-**2** in THF/water.

8.3 SEM images for poly-(*R*)-3 in THF/water mixtures

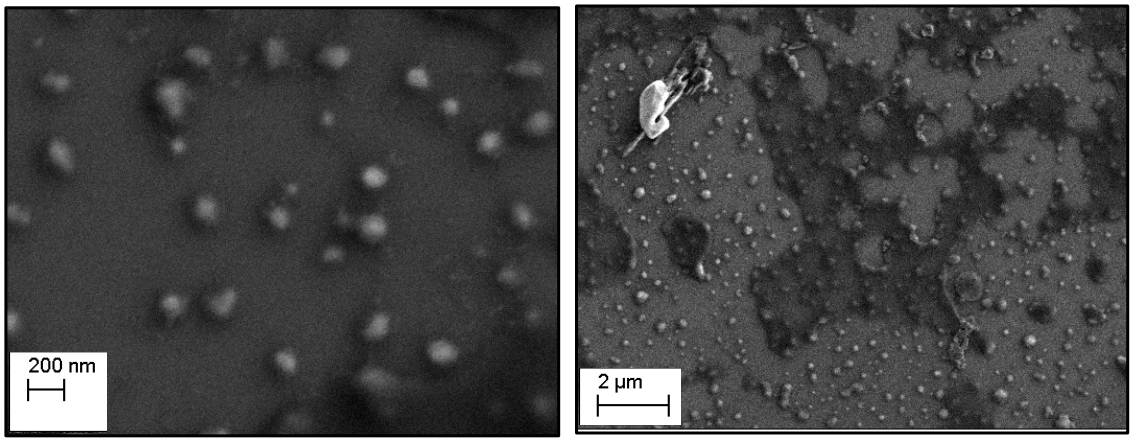

Figure S60. Nanospheres formed by poly-(*R*)-**3** in THF/water.

8.4 SEM images for poly-(*R*)-3 in THF/water mixtures

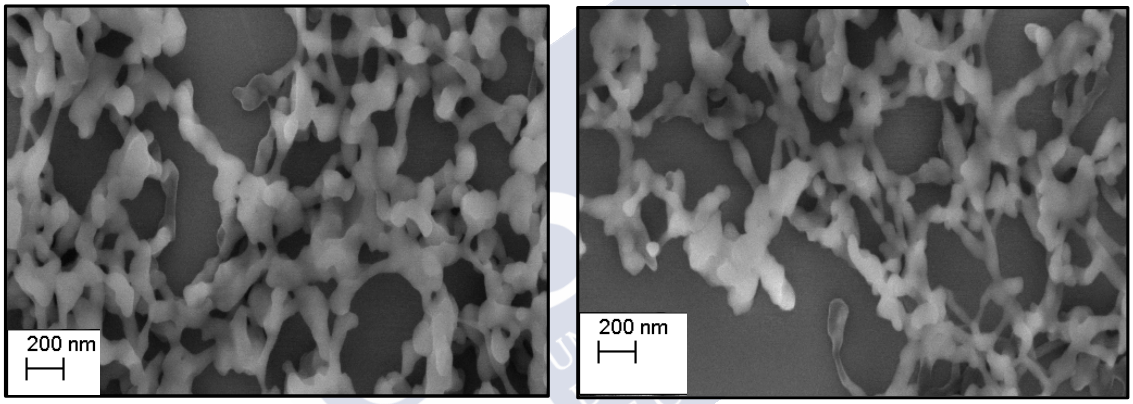

Figure S61. Nanospheres formed by poly-(*R*)-**4** in THF/water.

8.5 SEM images for poly-(*L*)-5 to poly-(*L*)-9 in THF/water mixtures

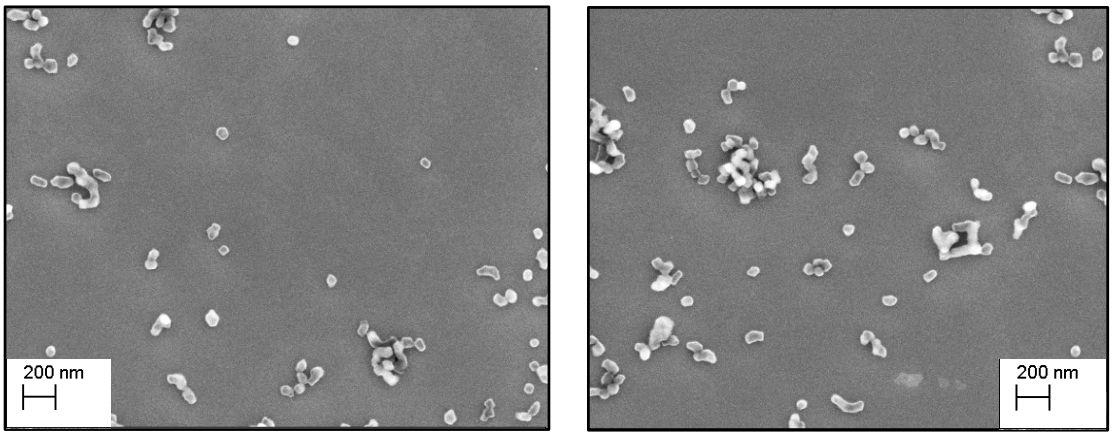

Figure S62. Nanospheres formed by poly-(*L*)-**5** and poly-(*L*)-**9** in THF/water.

5.TEM images for poly-(*R*)-1@PVA

To improve the stability of the nanospheres in solution, poly(vinylalcohol) (PVA) were added as surfactant to a solution of nanospheres.

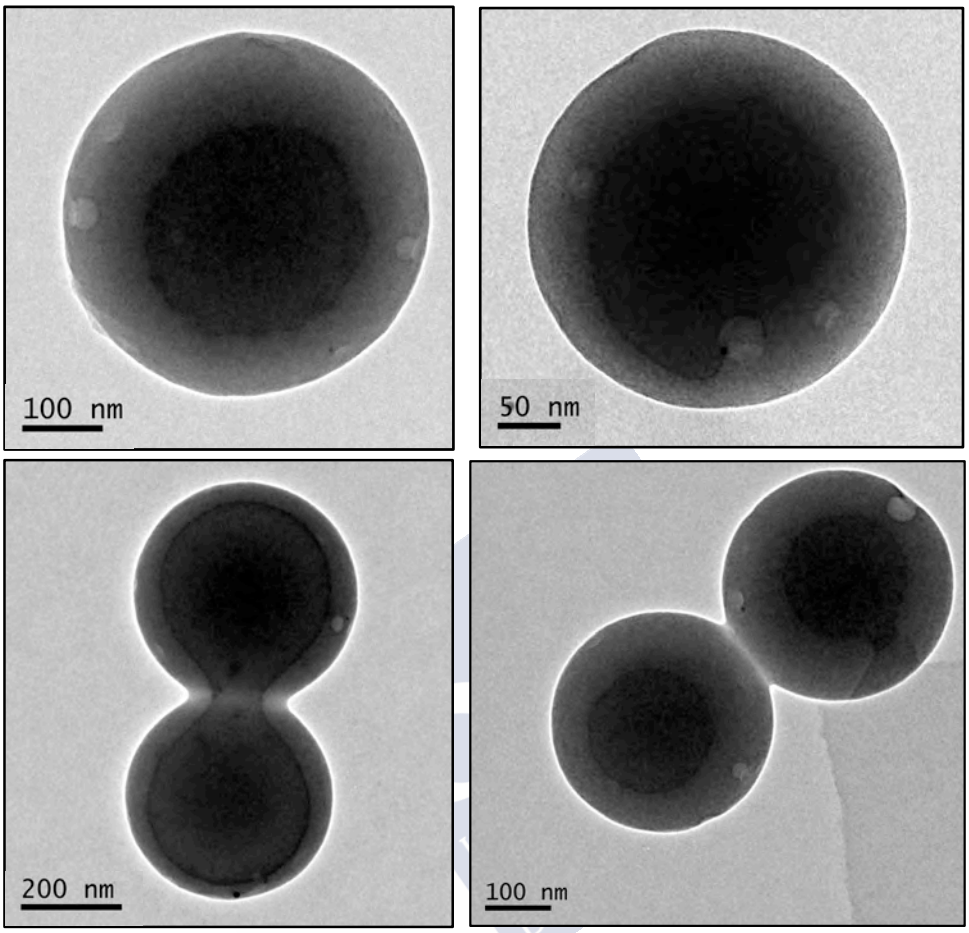

Figure S63. Nanospheres formed by poly-**1**@PVP in THF/water.

6.AFM images

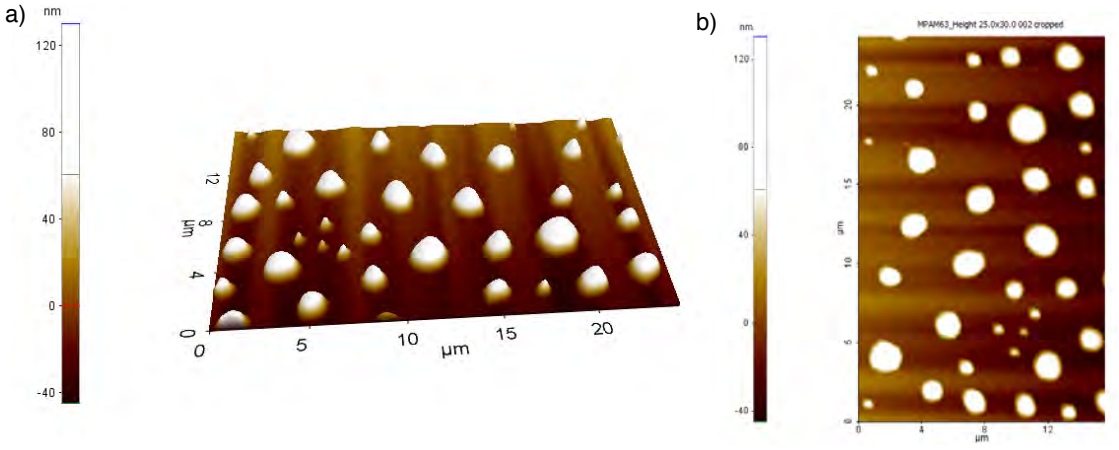

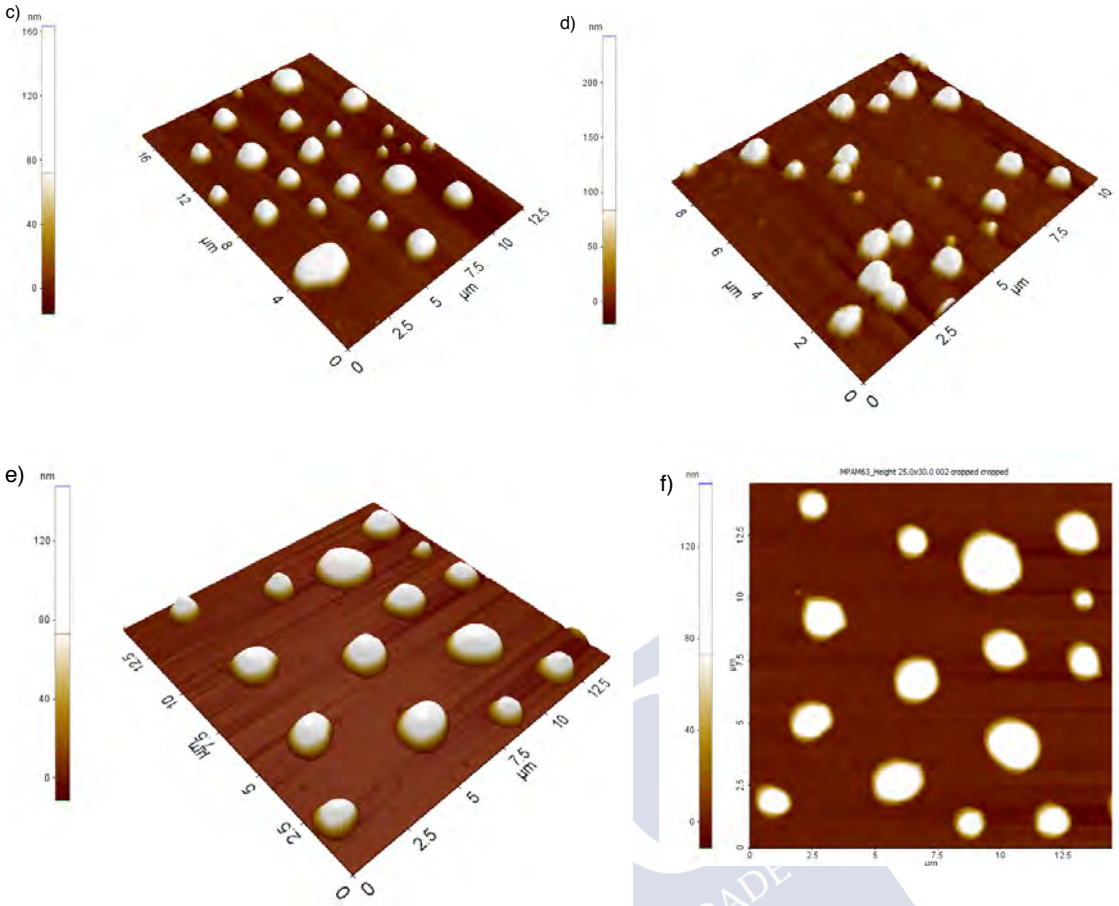

Figure S64. AFM images of poly-(*R*)-**1** nanospheres in acetone/water mixtures.

5. Confocal Microscopy: Encapsulation studies

Images were performed on a Leica TSC-SP2 microscope. Polymer (0.5 mg mL^{-1}) in THF/water or acetone/water mixtures with the correspondent fluorescent dyes (5,6-carboxyfluorescein, rhodamine B isothiocyanate) or Quantum Dots [Lumidot CdSe/ZnS (590 nm QD)] solution (10 mg mL^{-1}).

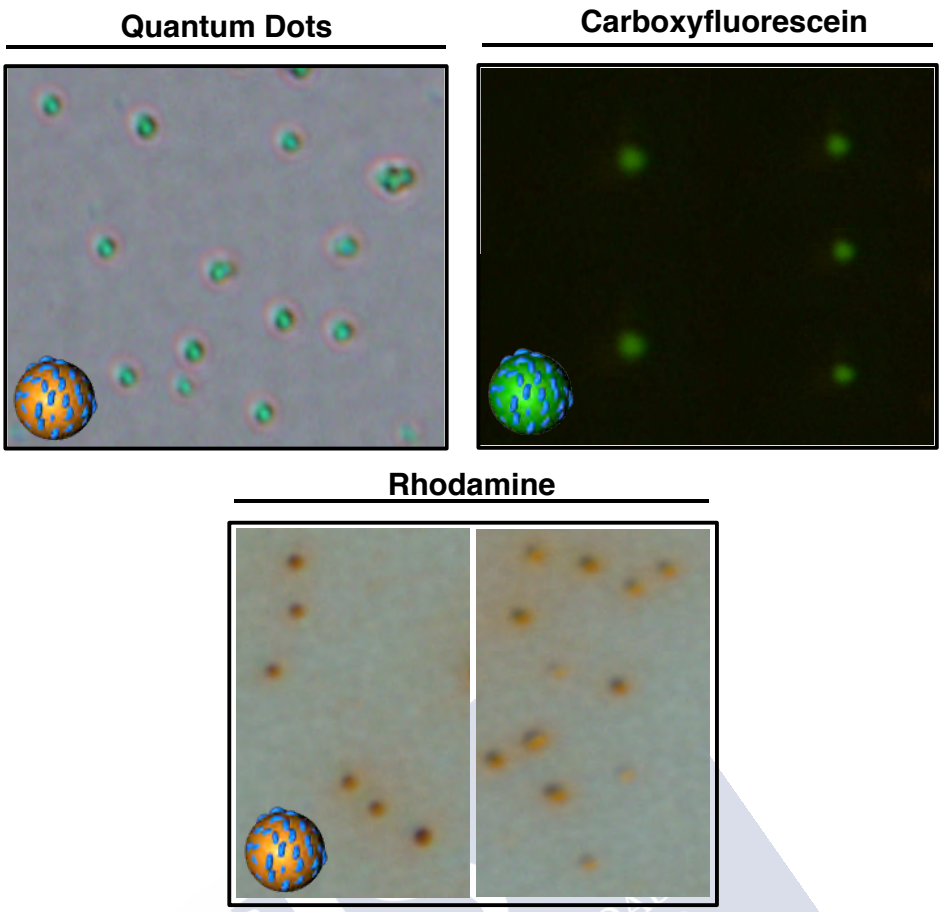

Figure S65. Representative confocal images of nanospheres formed by poly-**1** in THF/water (1:1 v/v) encapsulating Quantum Dots, 5,6-carboxyfluorescein and rhodamine B isothiocyanate.

6. Supporting references

S1) Rodríguez, R.; Quiñoá, E.; Riguera, R.; Freire, F.; Architecture of Chiral Poly(phenyl acetylene)s: From Compressed/Highly Dynamic to Stretched/Quasi-Static Helices. *J. Am. Chem. Soc.,* **2016**, *138,* 9260-9268.

S2) Leiras, S.; Freire, F.; Seco, J. M.; Quiñoá, E.; Riguera, R. Controlled modulation of the helical sense and the elongation of poly(phenylacetylene)s by polar and donor effect. *Chem. Sci*., **2013**, *4*, 2735-2743.

S3) Arias, S.; Núñez-Martínez, M.; Quiñoá, E.; Riguera, R.; Freire, F.; A general route to chiral nanostructures from helical polymers: *P/M* switch via dynamic metal coordination. *Polym. Chem.*, **2017**, *8*, 3740-3745.

USC
UNIVERSIDADE
DE SANTIAGO
DE COMPOSTELA

USC
UNIVERSIDADE
DE SANTIAGO
DE COMPOSTELA